

# **SYNTHESIS AND REACTIVITY OF Pincer-ligated metal complexes**

**By**

**NICHOLAS MATHEW LEASE**

A dissertation submitted to the

School of Graduate Studies

Rutgers, The State University of New Jersey

In partial fulfillment of the requirements

For the degree of

Doctor of Philosophy

Graduate Program in Chemistry and Chemical Biology

Written under the direction of

Alan S. Goldman

And approved by

---

---

---

---

New Brunswick, New Jersey

May, 2018

**ABSTRACT OF THE DISSERTATION**  
**SYNTHESIS AND REACTIVITY OF PINCER-LIGATED METAL COMPLEXES**

**By**  
**NICHOLAS MATHEW LEASE**

**Dissertation Director: Alan S. Goldman**

The understanding of small molecule activation by transition metal complexes is key for many fields of study such as organic and inorganic chemistry. Since their initial report in the 1960's, pincer-ligated (meridional bound tridentate ligands) complexes have demonstrated a rich chemistry for the activation of small molecules. This thesis will focus on new reactivity of known pincer-ligated complexes as well as the synthesis and reactivity of novel pincer-ligated transition metal complexes.

The addition of aryl O-H bonds to olefins (hydroaryloxylation) and cleavage of those C-O bonds (dehydroaryloxylation) have been examined using pincer-ligated iridium complexes. The mechanism of this reaction was determined by experimental (kinetic studies, KIE expt, competition and resting state studies etc.) and computational DFT analysis. The addition of aryl N-H bonds to olefins was not successful catalytically and was determined to have an overall larger energetic barrier by DFT computations.

Novel pincer-ligated osmium complexes were synthesized. These complexes are isoelectronic to (<sup>t</sup>BuPCP)Ir, one of the most active alkane dehydrogenation catalysts known. The reactivity of these complexes was examined to see how they compared to

their isoelectronic iridium analogues. These complexes were treated with olefins, carbon monoxide and nitrogen. Additionally they were tested for the dehydrogenation of alkanes and alcohols and the hydrogenation of olefins and ketones.

Recent reports have shown that pincer ligated metal complexes are capable of cleaving dinitrogen to form metal nitrides. Novel pincer-ligated rhenium and molybdenum complexes were synthesized in order to study their activity for dinitrogen cleavage. Synthesis of the pincer-ligated metal chlorides was achieved with further study required to test their reactivity with dinitrogen.

Finally new pincer complexes were developed to improve or demonstrate new reactivity. Three approaches were taken when examining new ligands. The first was incorporation of a positive charge away from the metal center in the ligand structure. The second was use of a PPP ligand with the potential for metal-ligand cooperativity. The third was using established ligand frameworks with metals not traditionally used for alkane dehydrogenation. Complexes for each of these strategies were synthesized and characterized.

## Acknowledgement

I would first like to thank my adviser, Professor Alan Goldman for his unwavering support throughout my work for this dissertation. Through my PhD. studies his insight and guidance have allowed me to learn so much about chemistry and how to be a scientist. Alan has helped me greatly and I appreciate all of the opportunities he has afforded me by working in his lab.

I would also like to thank my committee members Professor Charles Dismukes, Professor John Brennan and Dr. Bob Ianniello for serving on my thesis committee. I would also like to thank Professors Daniel Seidel, Kai Hultzsich and Karsten Krogh-Jespersen for serving on my original committee and giving me guidance in my first years as a graduate student.

I would also like to thank Dr. Tom Emge for all his help with X-Ray crystallographic analysis as well as Dr. Nagarajan Murali for all his guidance and help with NMR experimentation.

I am very thankful for all my time with former and current members of the Goldman Group. The group provided a supportive and fun environment to work in for the last five and a half years. I would like to thank specifically Dr. Michael Haibach, Dr. Thomas Dugan and Professor Akshai Kumar who were all great mentors and teachers in the lab. I must also thank former students Dr. Tian Zhou and Dr. Changjian Guan for all their computational analysis help. I also want to thank all the current and former members of

the Goldman group (Andrew Steffens, Benjamin Gordon, Tariq Bhatti, Yang Gao, Bo Li, Andrea Casuras, Arun Shada) whose discussions aided in this thesis

I am also extremely thankful to Professor Maria Contel at Brooklyn College for allowing me to work in her lab as an undergraduate. At the time of joining her lab I was unsure of what I wanted to do after my undergraduate studies and though her guidance I was able to focus on chemistry and decide to pursue a PhD.

I would like to thank my parents David and Joan Lease for all of their support throughout my PhD and my entire life shaping me into the person I am today. Also I would like to thank all my friends who have made these past five years fun even during the difficult periods of my research. I want to thank Anthony Spinella, Nancy Hernandez, Kristin Blacklock, Marissa Ringgold and Dean Chueng.

Finally I would like to thank my girlfriend Shayla Fray for all of the support thought the tough last two years of my PhD. Her kind words and cheerful attitude help motivate me through this difficult process and for that I am thankful she is in my life.

## **Dedication**

To Shayla, Mom, and Dad,

for all the love and support

## Table of Contents

<b>Abstract</b>	<b>ii</b>
<b>Acknowledgments</b>	<b>iv</b>
<b>Dedication</b>	<b>vi</b>
<b>Table of Contents</b>	<b>vii</b>
<b>List of Figures</b>	<b>xi</b>
<b>List of Schemes</b>	<b>xx</b>
<b>List of Tables</b>	<b>xxvi</b>
<b>Chapter 1      Introduction</b>	<b>1</b>
1.2      Research Goals of this thesis	11
1.3      References	13
<b>Chapter 2      Catalytic addition of N-H and O-H bonds to olefinic double                      bonds (hydroamination and hydroaryloxylation) using                      iridium pincer complexes</b>	<b>16</b>
2.1      Hydroamination introduction	17
2.2      Hydroamination reactions using iridium pincer catalysts	19
2.2.1 <i>Hydroamination of simple olefins (C<sub>2</sub>H<sub>4</sub>, C<sub>3</sub>H<sub>6</sub>, TBE)</i>	19
2.2.2 <i>Hydroamination of norbornene</i>	21
2.2.3 <i>Hydroamination of 1-phenyl-1-propyne</i>	22
2.3      Hydroaryloxylation using pincer iridium catalysts	23
and mechanistic analysis	
2.3.1 <i>Alkyl aryl ether formation</i>	23

2.3.2	<i>Pincer ligated iridium catalytic formation of alkyl aryl ether (hydroaryloxylation)</i>	25
2.3.3	<i>Mechanistic analysis of hydroaryloxylation</i>	29
2.4	Catalytic ether cleavage using pincer-ligated iridium catalysts (dehydroaryloxylation)	42
2.5	Summary	49
2.6	Experimental	49
2.7	References	58
<b>Chapter 3</b>	<b>Synthesis and reactivity of pincer-ligated osmium complexes</b>	<b>60</b>
3.1	Introduction	61
3.2	PNP-Pincer complexes of osmium, comparison with isoelectronic (PCP)Ir and (PNP)Ir <sup>+</sup> units	65
3.2.1	<i>Synthesis and structural characterization of precursors (<sup>t</sup>BuPNP)OsCl<sub>3</sub> and (<sup>t</sup>BuPNP)OsH<sub>4</sub></i>	65
3.2.2	<i>Dissociation of H<sub>2</sub> from (<sup>t</sup>BuPNP)OsH<sub>4</sub></i>	71
3.2.3	<i>Reactions with olefins</i>	72
3.2.4	<i>DFT calculations and explanation of the observed reactivity of (<sup>t</sup>BuPNP)Os complexes</i>	77
3.2.5	<i>DFT calculations and an underlying explanation of the thermodynamics in comparison with isoelectronic species</i>	83
3.2.6	<i>Cyclometalation and C-H addition to (<sup>t</sup>BuPNP)Os(II)</i>	92



	<i>complexes</i>	
	3.2.7 Summary of alkane dehydrogenation using ( <i>t</i> BuPNP)Os	94
	3.3 Hydrogenation of TBE and NBE using ( <i>t</i> BuPNP)OsH <sub>4</sub>	96
	3.4 Dehydrogenation and hydrogenation of 2-propanol and acetone	97
	3.5 Synthesis of ( <i>i</i> PrPNP)Os complexes	100
	3.5.1 Synthesis of ( <i>t</i> BuPNP)OsCl <sub>3</sub> and ( <i>t</i> BuPNP)OsH <sub>4</sub>	100
	3.5.2 Reactivity with olefins	103
	3.6 Dehydrogenative C-C coupling of styrene	104
	3.7 Reaction of ( <i>i</i> PrPNP)OsH <sub>4</sub> with N <sub>2</sub>	106
	3.8 Reactivity of ( <i>t</i> BuPNP)OsH <sub>4</sub> with carbon monoxide	109
	3.9 Metal Effects on the dearomatization of ( <i>t</i> BuPNP)M complexes	116
	3.10 Experimental	124
	3.11 References	184
<b>Chapter 4</b>	<b>Synthesis of pincer-ligated metal complexes for nitrogen reduction to ammonia</b>	<b>188</b>
	4.1 Introduction	189
	4.2 Synthesis of pincer-ligated rhenium complexes	194
	4.3 Synthesis of pincer-ligated molybdenum complexes	211
	4.4 Experimental	216
	4.5 References	235
<b>Chapter 5</b>	<b>Synthesis of pincer-ligated metal complexes for alkane dehydrogenation</b>	<b>238</b>

5.1	Introduction	239
5.2	Para-nitrogen ( <sup>t</sup> BuPCP)Ir synthesis and activity	244
	5.2.1 Computational analysis	244
	5.2.2 Synthesis of para-nitrogen ( <sup>t</sup> BuPCP)Ir	250
	5.2.3 Formation of the cationic para-nitrogen ( <sup>t</sup> BuPCP)Ir complex	260
5.3	Synthesis of triphosphine pincer-ligated iridium complexes	266
	5.3.1 Synthesis of ( <sup>i</sup> PrPPP)Ir complexes	266
	5.3.2 Synthesis of ( <sup>t</sup> BuPPP)Ir complexes	275
5.4	Pincer-ligated osmium complexes	280
5.5	Experimental	286
5.6	References	307

## List of Figures

Figure 1.1	Mechanism for H <sub>2</sub> addition to Wilkinson's complex	2
Figure 1.2	Photochemical alkane dehydrogenation using RhCl(PMe <sub>3</sub> ) <sub>2</sub> (CO) mechanism	6
Figure 1.3	Protonated ( <sup>t</sup> BuPCP) ligand	7
Figure 1.4	Variations of pincer ligands	7
Figure 1.5	Mechanism of transfer dehydrogenation of n-octane using ( <sup>t</sup> BuPCP)IrH <sub>2</sub>	9
Figure 1.6	Small molecule activation using pincer ligands	11
Figure 2.1	Actinide complexes for intramolecular hydroamination	18
Figure 2.2	Pincer iridium complexes used for hydroaryloxylation	26
Figure 2.3	Hydroaryloxylation 3,5 dimethyl phenol and simple olefins	26
Figure 2.4	Pincer iridium complexes used for hydroaryloxylation	27
Figure 2.5	Evaluation of potential acid based mechanism	28
Figure 2.6	Computationally derived mechanism for hydroaryloxylation (Free energy (ΔG) kcal/mol)	31
Figure 2.7	Plot of phenol concentration (mM) vs. rate of reaction (h <sup>-1</sup> ). order of 0.8 was calculated dependence for phenol	35
Figure 2.8	Plot of propylene pressure (atm) vs. rate of reaction (h <sup>-1</sup> ). Zero order propylene dependence was observed at catalytic conditions	37
Figure 2.9	Free energy comparison between addition of water and	41

	ammonia to ethylene ( $\Delta G$ kcal/mol)	
Figure 2.10	Substrate scope of cleavage of alkyl aryl ethers	46
Figure 2.11	Substrate scope of cleavage of alkyl aryl ethers at 200°C	47
Figure 2.12	Mechanism of C-O cleavage of alkyl aryl ethers	48
Figure 2.13	$^{31}\text{P}$ -NMR of resting state experiment. Temperature gradually increased from 40 to 80°C	52
Figure 3.1	Monodentate and bidentate osmium complexes	62
Figure 3.2	Pincer osmium complexes for alcohol and ketone and hydrogenation	63
Figure 3.3	( $^t\text{BuPNP}$ ) ligand and isoelectronic structures of ( $^t\text{BuPCP}$ )Ir and ( $^t\text{BuPNP}$ )Os	64
Figure 3.4	ORTEP representation (50% probability ellipsoids) of the structure of 1-Cl <sub>3</sub> determined by X-ray diffraction; hydrogen atoms omitted for clarity. Calculated structure of 1-Cl <sub>3</sub> possesses C <sub>2</sub> symmetry	66
Figure 3.5	(a) Structure of 1-H <sub>4</sub> determined by X-ray diffraction. H atoms other than hydrides omitted. (b) Residual electron-density map of the plane containing the four hydrido H atoms before placing them in the model (left) and after (right), with contours drawn at 0.05 e-/Å <sup>3</sup> increments, and using data out to 0.95 Å resolution. Dashed lines are negative contours.	69
Figure 3.6	ORTEP representation (50% probability ellipsoids) of the	74

	structures of (a) 1-H <sub>2</sub> (C <sub>2</sub> H <sub>4</sub> ) and (b) 1-H(Et)(CO), determined by X-ray diffraction. Hydrogen atoms other than hydrides and osmium-bound ethylene and ethyl hydrogen atoms omitted	
Figure 3.7	Free energy diagram (kcal/mol) for species involved in and to the hydrogenation of ethylene by 1. Enthalpies in italics and parentheses. Energy values (kcal/mol) are referenced to T = 298 K (5 °C) and a partial pressure P = 1 atm for each species participating in the reaction.	78
Figure 3.8	Free energy diagram (kcal/mol) for isomerization of 1-hexene. Energy values (kcal/mol) are referenced to T = 298 K (25 °C) and a partial pressure P = 1 atm for each species.	81
Figure 3.9	( <sup>t</sup> BuPNP) ligated complexes with charge distributed throughout the ligand	83
Figure 3.10	Calculated free energies (kcal/mol) of interconversion between various complexes of ( <sup>t</sup> Bu <sup>4</sup> PNP)Ir <sup>+</sup> (4), ( <sup>t</sup> Bu <sup>4</sup> PNP)Os (1), and ( <sup>t</sup> Bu <sup>4</sup> PCP)Ir (2) (indicated as N-Ir <sup>+</sup> , N-Os, and C-Ir respectively)	85
Figure 3.11	ORTEP representation (50% probability ellipsoids) of the structure of 5-Cl <sub>3</sub> determined by X-ray diffraction. H atoms other than hydrides omitted.	102
Figure 3.12	<sup>1</sup> H-NMR of dehydrogenative coupling of styrene using (5-H <sub>4</sub> )	105
Figure 3.13	<sup>31</sup> P-NMR of (5-H <sub>2</sub> (N <sub>2</sub> ))	107
Figure 3.14	<sup>1</sup> H-NMR of (5-H <sub>2</sub> (N <sub>2</sub> ))	108

Figure 3.15	IR spectra of (5-H <sub>2</sub> (N <sub>2</sub> ))	109
Figure 3.16	<sup>31</sup> P-NMR of reaction of (1-H <sub>4</sub> ) with CO	110
Figure 3.17	<sup>1</sup> H-NMR: Hydride region of reaction of (1-H <sub>4</sub> )	111
Figure 3.18	<sup>31</sup> P-NMR of (6-H(CO) <sub>2</sub> )	112
Figure 3.19	<sup>1</sup> H-NMR of (6-H(CO) <sub>2</sub> )	113
Figure 3.20	MALDI TOF spectra for (6-H(CO) <sub>2</sub> )	114
Figure 3.21	Mass Spec simulation of (6-H(CO) <sub>2</sub> ) minus one carbon monoxide ligand	114
Figure 3.22	ORTEP representation (50% probability ellipsoids) of the structure of 6-H(CO) <sub>2</sub> determined by X-ray diffraction; hydrogen atoms omitted for clarity.	115
Figure 3.23	<sup>31</sup> P NMR spectrum of 7-H(CO) <sub>2</sub>	118
Figure 3.24	<sup>1</sup> H NMR spectrum of 7-H(CO) <sub>2</sub>	118
Figure 3.25	MALDI TOF spectra for (7-H(CO) <sub>2</sub> )	119
Figure 3.26	Mass Spec simulation of 7-H(CO) <sub>2</sub> minus one carbon monoxide ligand	120
Figure 3.27	ORTEP representation (50% probability ellipsoids) of the structure of 7-H(CO) <sub>2</sub> determined by X-ray diffraction; hydrogen atoms omitted for clarity.	121
Figure 3.28	Computational thermodynamics for dearomatization	123
Figure 3.29	<sup>1</sup> H NMR spectrum of 1-Cl <sub>3</sub>	130
Figure 3.30	<sup>1</sup> H NMR spectrum of 1-H <sub>4</sub>	131

Figure 3.31	$^1\text{H}$ NMR spectrum of 1- $\text{H}_4$ at 60 °C	132
Figure 3.32	$^1\text{H}$ NMR spectrum of 1- $\text{H}_4$ at -80 °C	133
Figure 3.33	$^{31}\text{P}\{^1\text{H}\}$ NMR spectrum of 1- $\text{H}_4$	134
Figure 3.34	$^{31}\text{P}\{^1\text{H}\}$ -decoupled ca. {0 – 10 pp } NMR spectrum of 1- $\text{H}_4$	135
Figure 3.35	$^1\text{H}$ NMR spectrum of 1- $\text{H}_2(\text{C}_2\text{H}_4)$	136
Figure 3.36	$^{31}\text{P}\{^1\text{H}\}$ NMR spectrum of 1- $\text{H}_2(\text{C}_2\text{H}_4)$	137
Figure 3.37	$^1\text{H}$ NMR spectrum of 1- $\text{H}(\text{Et})(\text{CO})$	138
Figure 3.38	$^{31}\text{P}\{^1\text{H}\}$ NMR spectrum of 1- $\text{H}(\text{Et})(\text{CO})$	139
Figure 3.39	Plot of disappearance of hydride signal after addition of $\text{D}_2$ . Rate Constant = $0.542 \text{ hr}^{-1}$	143
Figure 3.40	$^2\text{D}$ NMR spectrum of reaction after 10 hours	144
Figure 3.41	Plot-Deuterium incorporation into ligand t-butyl groups vs. time	144
Figure 3.42	Plot-Deuterium incorporation into ligand signals vs. time	145
Figure 3.43	Kinetics Plot-Addition of $\text{H}_2$ to 1- $\text{H}_2(\text{C}_2\text{H}_4)$	146
Figure 3.44	Kinetics Plot-Addition of $\text{CO}$ to 1- $\text{H}_2(\text{C}_2\text{H}_4)$	147
Figure 3.45	Plot-Decomposition of 1- $\text{H}_2(\text{C}_2\text{H}_4)$ . Rate constant = $0.0048 \text{ min}^{-1}$ , $\Delta G^\ddagger = 25.25 \text{ kcal/mol}$	148
Figure 3.46	$T_1$ measurement plot	149
Figure 3.47	Structural data for complex $(^t\text{BuPNP})\text{OsCl}_3$ (1- $\text{Cl}_3$ )	157
Figure 3.48	Structural data for complex $(^t\text{BuPNP})\text{OsH}_4$ (1- $\text{H}_4$ )	158
Figure 3.49	Structural data for complex $(^t\text{BuPNP})\text{OsH}_2(\text{C}_2\text{H}_4)$ (1- $\text{H}_2(\text{C}_2\text{H}_4)$ )	159
Figure 3.50	Structural data for complex $(^t\text{BuPNP})\text{Os}(\text{H})(\text{Et})(\text{CO})$ (1- $\text{H}(\text{Et})(\text{CO})$ )	160

Figure 3.51	Structural data for complex (MeO- <sup>t</sup> BuPCP)IrH <sub>4</sub>	161
Figure 3.52	Structural data for complex (MeO- <sup>i</sup> PrPCP)IrH <sub>4</sub> (monoclinic)	162
Figure 3.53	Structural data for complex (MeO- <sup>i</sup> PrPCP)IrH <sub>4</sub> (triclinic)	163
Figure 3.54	Structural data for complex ( <sup>t</sup> BuPNP)Os(H)(CO) <sub>2</sub> (6-(H)(CO) <sub>2</sub> )	164
Figure 3.55	Structural data for complex ( <sup>t</sup> BuPNP)RuH(CO) <sub>2</sub> (7-(H)(CO) <sub>2</sub> )	174
Figure 4.1	Alternative pathways for dinitrogen reduction to ammonia	191
Figure 4.2	Reduction of dinitrogen by iron based complexes (Peters)	192
Figure 4.3	Electrochemical N <sub>2</sub> splitting approach	194
Figure 4.4	<sup>31</sup> P-NMR: Attempted synthesis of ( <sup>i</sup> PrPNP)ReCl <sub>2</sub> (4-1)	198
Figure 4.5	<sup>1</sup> H-NMR: Attempted synthesis of ( <sup>i</sup> PrPNP)ReCl <sub>2</sub> (4-1)	199
Figure 4.6	<sup>1</sup> H-NMR: Attempted synthesis of ( <sup>i</sup> PrPNP)ReCl <sub>2</sub> (4-1)	201
Figure 4.7	<sup>1</sup> H-NMR: Attempted synthesis of ( <sup>i</sup> PrPPP)ReCl <sub>2</sub> (4-2)	201
Figure 4.8	ORTEP representation (50% probability ellipsoids) of the structure of (4-3) determined by X-ray diffraction; hydrogen atoms omitted for clarity.	203
Figure 4.9	Mass spectroscopy simulation data for (4-3)	204
Figure 4.10	Mass spectroscopy data for (4-3)	204
Figure 4.11	<sup>1</sup> H-NMR spectra of ( <sup>t</sup> BuPNP)ReCl <sub>3</sub> (4-3)	205
Figure 4.12	<sup>1</sup> H-NMR spectra of ( <sup>t</sup> BuPNP)ReCl <sub>3</sub> (4-4)	207
Figure 4.13	<sup>31</sup> P-NMR: spectra of (4-5)	209
Figure 4.14	<sup>1</sup> H-NMR spectra (4-5)	209
Figure 4.15	<sup>31</sup> P-NMR spectra of (4-6)	213



Figure 4.16	$^1\text{H}$ -NMR spectra of (4-6)	214
Figure 4.17	ORTEP representation (50% probability ellipsoids) of the structure of (4-6) determined by X-ray diffraction; hydrogen atoms omitted for clarity.	215
Figure 4.18	Structural data for complex ( $^t\text{BuPNP}$ ) $\text{ReCl}_3$ (4-3)	224
Figure 4.19	Structural data for complex Ozerov-( $^t\text{BuPNP}$ ) $\text{MoCl}_3$ (4-6)	231
Figure 5.1	Modified ligand complexes	240
Figure 5.2	Tuning the trans-influence of pincer ligands	241
Figure 5.3	Outer sphere hydrogenation of ketone using MLC mechanism	242
Figure 5.4	Mechanism of transfer alkane dehydrogenation	245
Figure 5.5	Free energy diagram for alkane dehydrogenation by ( $^t\text{uPCP}$ )Ir	246
Figure 5.6	Free energy diagram for alkane dehydrogenation by ( $^t\text{uPOCOP}$ )Ir	246
Figure 5.7	Mechanisms for alkene isomerization by pincer iridium complexes	247
Figure 5.8	Model catalysts for charge incorporation into pincer ligand	248
Figure 5.9	Free energy diagram for alkane dehydrogenation by para-nitrogen ( $^t\text{uPCP}$ )Ir	249
Figure 5.10	Free energy diagram- alkane dehydrogenation by alkylated para-nitrogen ( $^t\text{uPCP}$ )Ir	249
Figure 5.11	Comparative free energy diagram for alkane dehydrogenation	250
Figure 5.12	$^1\text{H}$ -NMR spectra of (5-3)	253
Figure 5.13	$^1\text{H}$ -NMR spectra of (5-4)	254

Figure 5.14	$^{31}\text{P}$ -NMR spectra of (5-5)	255
Figure 5.15	$^1\text{H}$ -NMR spectra of (5-5)	255
Figure 5.16	$^{31}\text{P}$ -NMR spectra of (5-6)	256
Figure 5.17	$^1\text{H}$ -NMR spectra of (5-6)	257
Figure 5.18	$^{31}\text{P}$ -NMR spectra of (5-7)	258
Figure 5.19	$^{31}\text{P}$ -NMR spectra of (5-8, 5-9)	259
Figure 5.20	$^1\text{H}$ -NMR spectra of (5-8, 5-9)	259
Figure 5.21	$^{31}\text{P}$ -NMR of reaction of (5-8) with methyl iodide	262
Figure 5.22	$^1\text{H}$ -NMR of reaction of (5-8) with methyl iodide	262
Figure 5.23	$^{31}\text{P}$ -NMR of reaction of (5-8) with 3,5 dimethylbenzyl bromide	264
Figure 5.24	$^1\text{H}$ -NMR of reaction of (5-8) with 3,5 dimethylbenzyl bromide	264
Figure 5.25	$^1\text{H}$ -NMR: hydride shift upon reaction with trimethylsilyl triflate	266
Figure 5.26	$^{31}\text{P}$ -NMR of ( $i\text{PrPP}^{\text{H}}\text{P}$ )IrCl complex (5-10)	268
Figure 5.27	$^1\text{H}$ -NMR of ( $i\text{PrPP}^{\text{H}}\text{P}$ )IrCl complex (5-10)	269
Figure 5.28	$^1\text{H}$ -NMR of (5-10) heated to 100°C showing hydrogen migration	270
Figure 5.29	$^{31}\text{P}$ -NMR of (5-11, 5-12) heated to 70°C	272
Figure 5.30	$^1\text{H}$ -NMR of (5-11, 5-12) heated to 70°C	272
Figure 5.31	ORTEP representation (50% probability ellipsoids) of the structure of 5-11 determined by X-ray diffraction; hydrogen atoms omitted for clarity.	273
Figure 5.32	$^{31}\text{P}$ -NMR synthesis of ( $t\text{BuPPP}$ ) ligand	277
Figure 5.33	$^{31}\text{P}$ -NMR synthesis of ( $t\text{BuPP}^{\text{H}}\text{P}$ ) ligand	278

Figure 5.34	$^{31}\text{P}$ -NMR of $[\text{Ir}(\text{COE})\text{Cl}]_2$ reacted with ( $^{\text{tBu}}\text{PP}^{\text{H}}\text{P}$ ) ligand	279
Figure 5.35	$^{31}\text{P}$ -NMR spectra of (5-16)	282
Figure 5.36	$^1\text{H}$ -NMR spectra of (5-16)	282
Figure 5.37	ORTEP representation (50% probability ellipsoids) of the structure of (5-16) determined by X-ray diffraction; hydrogen atoms omitted for clarity.	283
Figure 5.38	$^{31}\text{P}$ -NMR spectra of (5-17)	285
Figure 5.39	$^{31}\text{P}$ -NMR spectra of (5-17)	285
Figure 5.40	Structural data for complex ( $^{\text{iPr}}\text{PPP}$ )IrHCl(CO) (5-11)	298
Figure 5.41	Structural data for complex Ozerov-( $^{\text{iPr}}\text{PNP}$ )OsCl <sub>3</sub> (5-13)	303

## List of Schemes

Scheme 1.1	Addition of H <sub>2</sub> to Vaska's complex	1
Scheme 1.2	Oxidative addition of H <sub>2</sub> to Wilkinson's complex	2
Scheme 1.3	C-H oxidative addition of naphthalene to Ru(0)(dmpe) <sub>2</sub>	3
Scheme 1.4	C-H oxidative addition of benzene to Cp <sub>2</sub> WH <sub>2</sub>	3
Scheme 1.5	C-H oxidative addition of cyclohexane to Cp*Ir(PMe <sub>3</sub> )(H) <sub>2</sub>	4
Scheme 1.6	C-H oxidative addition of neopentane to Cp*Ir(CO) <sub>2</sub>	4
Scheme 1.7	Transfer dehydrogenation using TBE using [IrH <sub>2</sub> (acetone) <sub>2</sub> (PPh <sub>3</sub> ) <sub>2</sub> ] [BF <sub>4</sub> ]	6
Scheme 1.8	Transfer dehydrogenation of cyclooctane using (t <sup>Bu</sup> PCP)IrH <sub>2</sub>	8
Scheme 1.9	Transfer dehydrogenation of n-octane using (t <sup>Bu</sup> PCP)IrH <sub>2</sub>	8
Scheme 2.1	NCN zirconium pincer catalyzed intramolecular hydroamination	18
Scheme 2.2	PNP palladium pincer catalyzed intramolecular hydroamination	19
Scheme 2.3	NCN rhodium pincer catalyzed intermolecular hydroamination	19
Scheme 2.4	Attempted hydroamination of simple olefins with 3,5 dimethylaniline	20
Scheme 2.5	Attempted hydroamination of simple olefins with 4-fluoroaniline	21
Scheme 2.6	Hydroamination of NBE with anilines	22
Scheme 2.7	Hydroamination of 1-phenyl-1-propyne with anilines	23
Scheme 2.8	Ether formation: Classical synthesis vs. hydroaryloxylation	24
Scheme 2.9	Stoichiometric C-O cleavage of alkyl phenyl ether	25
Scheme 2.10	Product determination: kinetic or thermodynamic	29

Scheme 2.11	Resting state of the catalyst under catalytic conditions at room temperature	32
Scheme 2.12	Resting state of the catalyst under catalytic conditions at elevated temperatures	32
Scheme 2.13	H/D scrambling between phenol (OD) and propylene	33
Scheme 2.14	KIE competition reactions	34
Scheme 2.15	Standard kinetic hydroaryloxylation run: phenol or propylene was varied	34
Scheme 2.16	Hydroaryloxylation reaction in the presence of hydrogen bond acceptor	38
Scheme 2.17	Competition reactions between electronically different alkyl aryl ethers	39
Scheme 2.18	Comparison between the addition of phenol and aniline to NBE	42
Scheme 2.19	Examples of common synthetic C-O bond cleavage reactions	43
Scheme 2.20	Examples of transition metal based catalytic C-O bond cleavages	44
Scheme 2.21	Cleavage of isopropyl phenyl ether using various pincer iridium complexes	45
Scheme 3.1	Alkene oxidation using OsO <sub>4</sub>	61
Scheme 3.2	Cyclooctane dehydrogenation using (CF <sub>3</sub> PCP)OsH(COD)	63
Scheme 3.3	Synthesis of (tBuPNP)OsCl <sub>3</sub> (1-Cl <sub>3</sub> )	65
Scheme 3.4	Synthesis of (tBuPNP)OsH <sub>4</sub> (1-H <sub>4</sub> )	68
Scheme 3.5	Synthesis of (tBuPNP)OsH <sub>2</sub> (C <sub>2</sub> H <sub>4</sub> ) (1-H <sub>2</sub> (C <sub>2</sub> H <sub>4</sub> ))	73

Scheme 3.6	Reaction of (1-H <sub>2</sub> (C <sub>2</sub> H <sub>4</sub> ) with H <sub>2</sub>	74
Scheme 3.7	Synthesis of (t <sup>Bu</sup> PNP)Os(H)(Et)(CO) (1-(H)(Et)(CO)	75
Scheme 3.8	Kinetics of ethylene insertion into Os-H bond	77
Scheme 3.9	Free Energy for H <sub>2</sub> addition to (PXP)M(olefin) and (PXP)MH <sub>2</sub>	88
Scheme 3.10	NBO Analysis of H <sub>2</sub> addition to (PXP)M and (PXP)MH <sub>2</sub>	89
Scheme 3.11	NBO analysis of ethylene addition to (PXP)MH <sub>2</sub> and H <sub>2</sub> addition to (PXP)M(C <sub>2</sub> H <sub>4</sub> )	91
Scheme 3.12	(t <sup>Bu</sup> PNP)OsH <sub>4</sub> hydrogenation of TBE	97
Scheme 3.13	(t <sup>Bu</sup> PNP)OsH <sub>4</sub> hydrogenation of NBE	97
Scheme 3.14	(t <sup>Bu</sup> PNP)Os(C <sub>2</sub> H <sub>4</sub> ) transfer dehydrogenation of 2-propanol	98
Scheme 3.15	(t <sup>Bu</sup> PNP)OsH <sub>4</sub> hydrogenation of acetone	99
Scheme 3.16	(t <sup>Bu</sup> PNP)OsH <sub>4</sub> hydrogenation of methyl acetate	100
Scheme 3.17	Synthesis of (i <sup>Pr</sup> PNP)OsCl <sub>3</sub> (5-Cl <sub>3</sub> )	101
Scheme 3.18	Synthesis of (i <sup>Pr</sup> PNP)OsH <sub>4</sub> (5-H <sub>4</sub> )	102
Scheme 3.19	Reaction of (5-H <sub>4</sub> ) with Ethylene	104
Scheme 3.20	Dehydrogenative coupling of styrene using (i <sup>Pr</sup> PCP)Ir	105
Scheme 3.21	Formation of four coordinate (t <sup>Bu</sup> PCP)IrN <sub>2</sub> complex	106
Scheme 3.22	Formation of (5-H <sub>2</sub> (N <sub>2</sub> ))	107
Scheme 3.23	Synthesis of (t <sup>Bu</sup> PNP)OsH(CO) <sub>2</sub> (5-H(CO) <sub>2</sub> )	112
Scheme 3.24	Mechanism for formation of (6-H(CO) <sub>2</sub> )	116
Scheme 3.25	Synthesis of (7-H(CO) <sub>2</sub> )	117
Scheme 3.26	Synthesis of 7-H(CO) <sub>2</sub>	122

Scheme 3.27	Synthesis of (7-H(CO) <sub>2</sub> )	122
Scheme 4.1	Reduction of dinitrogen to ammonia using PNPMo complexes	192
Scheme 4.2	Synthesis of MACHO rhenium pincer complex (Schneider)	195
Scheme 4.3	Reduction of MACHO Re complex followed by N <sub>2</sub> cleavage	195
Scheme 4.4	Synthesis of ( <sup>i</sup> PrPNP) ligand (Ozerov ligand)	197
Scheme 4.5	Attempted synthesis of ( <sup>i</sup> PrPNP)ReCl <sub>2</sub> (4-1)	198
Scheme 4.6	Synthesis of PPP ligand arm	199
Scheme 4.7	Synthesis of PPP ligand	200
Scheme 4.8	Attempted synthesis of ( <sup>i</sup> PrPPP)ReCl <sub>2</sub> (4-2)	200
Scheme 4.9	Synthesis of ( <sup>t</sup> BuPNP)ReCl <sub>3</sub> (4-3)	202
Scheme 4.10	Synthesis of dearomatized ( <sup>t</sup> BuPNP)ReCl <sub>2</sub> (4-4)	206
Scheme 4.11	Synthesis of 2-bromo-1,3-bis(bromomethyl)benzene	208
Scheme 4.12	Synthesis of ((2-bromo-1,3-phenylene)bis(methylene))bis (di-tert-butylphosphane) (4-5)	208
Scheme 4.13	Lithiation optimization reaction	210
Scheme 4.14	Lithiation of (4-5) followed by treatment with rhenium precursor	210
Scheme 4.15	Synthesis of ( <sup>i</sup> PrPNP)MoCl <sub>3</sub> (4-6)	213
Scheme 5.1	Transfer dehydrogenation of n-octane by ( <sup>i</sup> PrPNP)IrH <sub>2</sub>	240
Scheme 5.2	Loss of H <sub>2</sub> to form enamine pincer complex	242
Scheme 5.3	Addition of HX across metal-ligand bond	243
Scheme 5.4	Dearomatization of PNP ligand followed by HX addition across metal/ligand	244

Scheme 5.5	Synthesis of diethyl 2,6-dimethyl-1,4-dihydropyridine-3,5-dicarboxylate (5-1)	251
Scheme 5.6	Synthesis of diethyl 2,6-dimethylpyridine-3,5-dicarboxylate (5-2)	251
Scheme 5.7	Synthesis of (2,6-dimethylpyridine-3,5-diyl)dimethanol (5-3)	252
Scheme 5.8	Synthesis of 3,5-bis(bromomethyl)-2,6-dimethylpyridine (5-4)	253
Scheme 5.9	Synthesis of 3,5-bis((di-tert-butylphosphanyl)methyl)-2,6-dimethylpyridine (5-5)	254
Scheme 5.10	Synthesis of para-nitrogen ( <sup>t</sup> BuPCP)IrHCl complex (5-6)	256
Scheme 5.11	Synthesis of para-nitrogen ( <sup>t</sup> BuPCP)Ir(C <sub>2</sub> H <sub>4</sub> ) complex (5-7)	257
Scheme 5.12	Synthesis of para-nitrogen ( <sup>t</sup> BuPCP)IrH <sub>4</sub> /H <sub>2</sub> complexes (5-8, 5-9)	258
Scheme 5.13	Transfer dehydrogenation of n-octane using (5-9)	260
Scheme 5.14	Reaction of (5-8) with methyl iodide	261
Scheme 5.15	Reaction of (5-8) with 3,5 dimethylbenzyl bromide	263
Scheme 5.16	Reaction of (5-6) with trimethylsilyl triflate	267
Scheme 5.17	Synthesis of ligand arm ((2-bromophenyl)diisopropylphosphane)	267
Scheme 5.18	Synthesis of ( <sup>i</sup> PrPPP) ligand	267
Scheme 5.19	Synthesis of ( <sup>i</sup> PrPP <sup>H</sup> P)IrCl complex (5-10)	268
Scheme 5.20	Treatment of (5-10) with carbon monoxide to form cis/trans ( <sup>i</sup> PrPPP)IrHCl(CO) complexes	271
Scheme 5.21	COA transfer dehydrogenation using (5-10)	275
Scheme 5.22	Buchwald type phosphine coupling to form ligand arm	276
Scheme 5.23	Synthesis of ( <sup>t</sup> BuPP <sup>Cl</sup> P) ligand	276



Scheme 5.24	Synthesis of ( <sup>t</sup> BuPP <sup>H</sup> P) ligand	277
Scheme 5.25	( <sup>t</sup> BuPP <sup>H</sup> P) ligand reacted with [Ir(COE)Cl] <sub>2</sub>	279
Scheme 5.26	Synthesis of Ozerov ( <sup>i</sup> PrPNP)OsCl <sub>3</sub> (5-16)	281
Scheme 5.27	Synthesis of Ozerov ( <sup>i</sup> PrPNP)OsH <sub>4</sub> (5-17)	284

## List of Tables

Table 2.1	Hydroamination attempts of anilines using various pincer ligated iridium complexes	21
Table 2.2	Hydroamination attempts of 1-phenyl-1-propyne using various pincer ligated iridium complexes	23
Table 3.1	Selected Experimental and Computed Bond Distances (Å) and angles (Deg) for 1-Cl <sub>3</sub>	67
Table 3.2	Selected Experimental and Computed Bond Lengths (Å) and angles (Deg) for 1-H <sub>4</sub>	69
Table 3.3	Comparison of Crystallographic Data for 1-H <sub>4</sub> with (R <sup>4</sup> PCP)IrH <sub>4</sub> complexes	70
Table 3.4	Calculated Free Energies (kcal/mol) of Some Elementary Addition reactions	86
Table 3.5	Kinetics of TBE Hydrogenation	97
Table 3.6	Kinetics of transfer isopropanol dehydrogenation	98
Table 3.7	Kinetics of hydrogenation of acetone (Reaction temperature 70°C)	99
Table 3.8	Kinetics of Ethylene Hydrogenation	142
Table 3.9	Kinetics of 1-hexene isomerization	143
Table 3.10	Crystal data and structure refinement for (t <sup>Bu</sup> PNP)OsH(CO) <sub>2</sub> .	165
Table 3.11	Bond lengths [Å] and angles [°] for (t <sup>Bu</sup> PNP)OsH(CO) <sub>2</sub> .	166
Table 3.12	Crystal data and structure refinement for (t <sup>Bu</sup> PNP)RuH(CO) <sub>2</sub>	175

Table 3.13	Bond lengths [Å] and angles [°] for ( <sup>t</sup> BuPNP)RuH(CO) <sub>2</sub>	176
Table 4.1	Computational analysis for the N <sub>2</sub> cleavage using various pincer ligands and metals	196
Table 4.2	Full table for computational analysis for N <sub>2</sub> cleavage	217
Table 4.3	Crystal data and structure refinement for ( <sup>t</sup> BuPNP)ReCl <sub>3</sub> (4-3)	225
Table 4.4	Bond lengths [Å] and angles [°] for ( <sup>t</sup> BuPNP)ReCl <sub>3</sub> (4-3)	226
Table 4.5	Crystal data and structure refinement for ( <sup>i</sup> PrPNP)MoCl <sub>3</sub> (4-6)	232
Table 4.6	Bond lengths [Å] and angles [°] for ( <sup>i</sup> PrPNP)MoCl <sub>3</sub>	233
Table 5.1	Selected Bond Lengths (Å) and angles (°) for ( <sup>i</sup> PrPPP)IrHCl(CO)	274
Table 5.2	Selected Bond Lengths (Å) and angles (°) for ( <sup>i</sup> PrPNP)OsCl <sub>3</sub> (5-13)	283
Table 5.3	Crystal data and structure refinement for ( <sup>i</sup> PrPPP)IrHCl(CO)	299
Table 5.4	Bond lengths [Å] and angles [°] for ( <sup>i</sup> PrPPP)IrHCl(CO)	300
Table 5.5	Crystal data and structure refinement for ( <sup>i</sup> PrPNP)OsCl <sub>3</sub>	304
Table 5.6	Bond lengths [Å] and angles [°] for ( <sup>i</sup> PrPNP)OsCl <sub>3</sub>	305

## Chapter 1

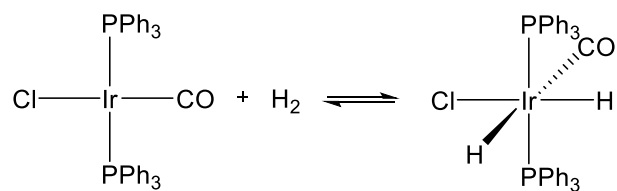
### Introduction

The selective activation of small molecules using transition metal complexes has been one of the main goals of organometallic chemistry for over 60 years. The activation of these bonds is key to many metal catalyzed reactions. Two key steps in many of these reactions are oxidative addition and the reverse reaction reductive elimination.

Oxidative addition of a substrate to a metal complex involves breaking an X-Y bond forming both an M-X and M-Y bond with a formal  $2 e^-$  oxidation of the metal center.<sup>1</sup>

Understanding of these elementary reactions is key to the development of new catalysts for activation and functionalization of small molecules.

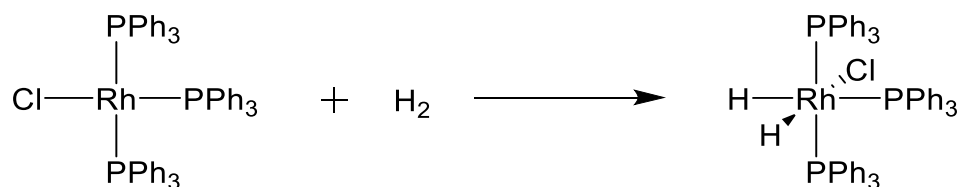
The first reported oxidative addition was reported by Vaska in 1962, wherein, he reported the addition of  $H_2$  to  $Ir(PPh_3)_2Cl(CO)$  also known as Vaska's complex.<sup>2</sup> Addition of  $H_2$  to the  $16 e^-$  iridium (I) species yielded a two  $e^-$  oxidation of the metal center to form the  $18 e^-$  iridium (III) complex.



**Scheme 1.1:** Addition of  $H_2$  to Vaska's complex

Following this report, Vaska demonstrated that his complex was able to perform the hydrogenation of ethylene and acetylene catalytically<sup>3</sup>. In 1965 Wilkinson reported the

oxidative addition of  $\text{H}_2$  to  $\text{RhCl}(\text{PPh}_3)_3$  better known as Wilkinson's catalyst.<sup>4,5</sup> He too showed that using his complex, catalytic hydrogenation of ethylene and acetylene could be performed. Mechanistic studies of the  $\text{H}_2$  oxidative addition revealed that the addition of hydrogen occurs predominantly after the loss of the triphenylphosphine ligand yielding a highly reactive  $14\text{ e}^-$  intermediate.



**Scheme 1.2:** Oxidative addition of  $\text{H}_2$  to Wilkinson's complex

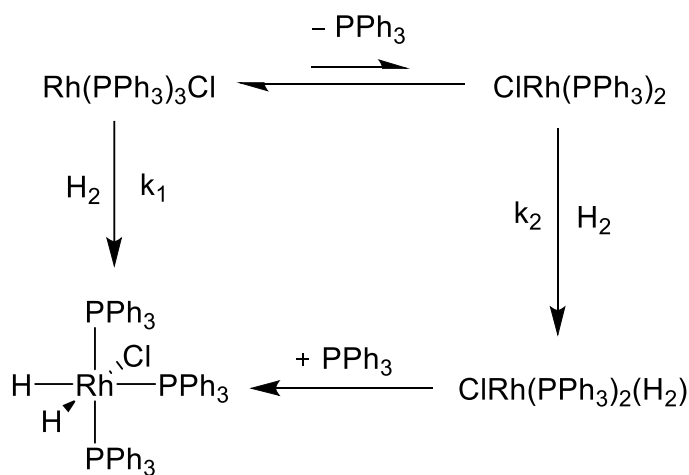
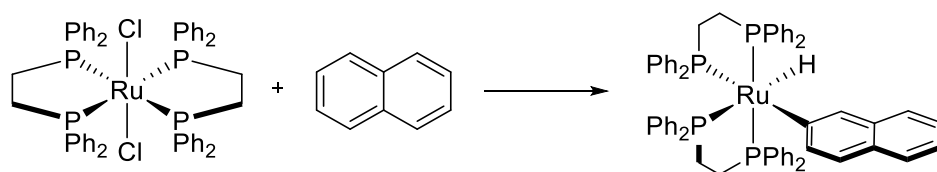


**Figure 1.1:** Mechanism for  $\text{H}_2$  addition to Wilkinson's complex

The pioneering work done by both Vaska and Wilkinson in understanding the activation of hydrogen and examination of the mechanism for hydrogenation and reductive elimination of olefins set the stage for further studies of small molecule

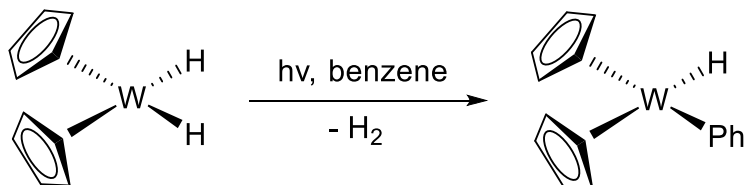
activation. Activation of the H-H bond was shown to be successful leading many to pursue the activation of stronger bonds such as the C-H bond.<sup>6-8</sup>

The ability to activate C-H bonds selectively is one of the most sought after transformations in chemistry. Breaking of the C-H bond can lead to easily functionalized products with synthetic value. The challenge, however, is with the strength of the C-H bond which is relatively inert and hard to activate. The first activation of C-H bonds using transition metals was reported by Chatt and Davidson in 1965. They reported that  $\text{Ru(0)(dmpe)}_2$  (dmpe = 1,2- bis(dimethylphosphino)ethane) could break the C-H bond in naphthalene to form a naphthyl hydride complex.<sup>9</sup>



**Scheme 1.3:** C-H oxidative addition of naphthalene to  $\text{Ru(0)(dmpe)}_2$

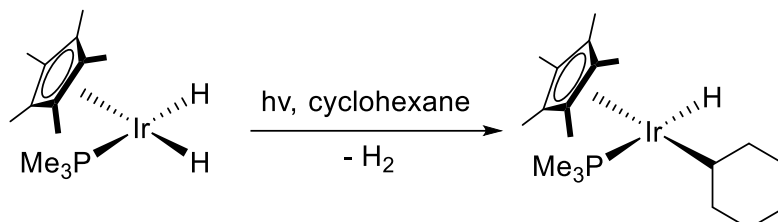
A few years after this initial report, Green and Knowles reported the oxidative addition of the C-H bond of benzene to  $\text{Cp}_2\text{WH}_2$  following the photolytic loss of  $\text{H}_2$ .<sup>10,11</sup>



**Scheme 1.4:** C-H oxidative addition of benzene to  $\text{Cp}_2\text{WH}_2$

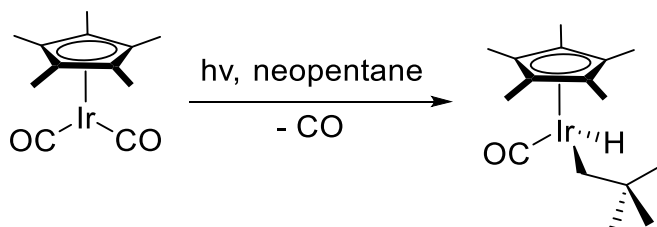
It was not until 1982 that the first alkyl C-H activation using transition metals was reported. Both Bergman and Graham independently reported the activation of the alkyl

C-H bond forming iridium alkyl hydride species. Bergman reported that irradiation of  $\text{Cp}^*\text{Ir}(\text{PMe}_3)(\text{H})_2$  lead to loss of  $\text{H}_2$  which when in cyclohexane or neopentane lead to the formation of the iridium alkyl hydride species.<sup>12</sup>



**Scheme 1.5:** C-H oxidative addition of cyclohexane to  $\text{Cp}^*\text{Ir}(\text{PMe}_3)(\text{H})_2$

Similarly Graham reported that irradiation of  $\text{Cp}^*\text{Ir}(\text{CO})_2$  lead to the loss of carbon monoxide which could then activate neopentane to form a iridium neopentyl hydride complex.<sup>13</sup> A few years after these initial reports, Jones<sup>14</sup> reported the same activation using complexes analogous to Bergman's using rhodium.



**Scheme 1.6:** C-H oxidative addition of neopentane to  $\text{Cp}^*\text{Ir}(\text{CO})_2$

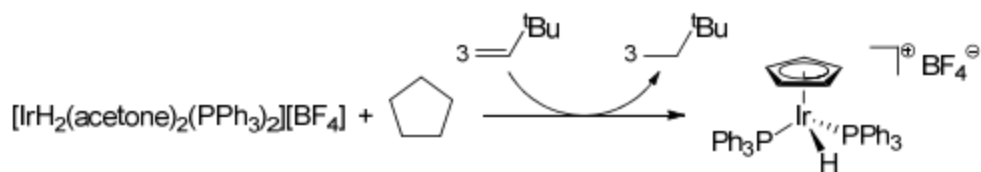
Selectivity studies for C-H activation were conducted by Bergman<sup>15</sup>, Jones<sup>16</sup> and Bercaw<sup>17</sup> independently. All found that selectivity for activation of the strongest C-H bond ( $1^\circ > 2^\circ > 3^\circ$ ) was most favorable despite using metal complexes with very different ligands and metals. Radical studies using hydrogen abstraction methods showed the inverse selectivity, preference for the more substituted position.<sup>18</sup>

Additionally, despite arene C-H bonds being stronger than alkyl C-H bonds, the studies showed the activation of arene C-H bonds to be more favorable.<sup>19,20</sup> While initial reports suggested this activity was determined by steric effects, more recent studies suggest that the electronic effects are more influential.<sup>19,20, 21-24</sup>

The activation of C-H bonds is incredibly important for many catalytic processes especially for alkane dehydrogenation, the conversion of alkanes to olefins. The conversion of abundant alkane feedstocks to valuable olefins is an important reaction as olefins are commonly used synthetic precursors. The process of alkane dehydrogenation is enthalpically unfavorable ( $\Delta H \sim 30$  kcal/mol)<sup>25,26</sup>, however it is favorable entropically due to the loss of H<sub>2</sub>. Some systems have been shown to be able to overcome the high enthalpy barrier to achieve catalytic turnover. One way to lower the overall barrier of this reaction is to couple the dehydrogenation process with a more favorable downhill reaction, such as using a sacrificial hydrogen acceptor such as tert-butylethylene (TBE) or norbornene (NBE). This would enable the reaction to be run under milder conditions.

This transfer dehydrogenation process (dehydrogenation using hydrogen acceptor) was first reported by Crabtree in 1979.<sup>27</sup> He reported that cycloalkanes could be dehydrogenated in the presence of TBE using  $[\text{IrH}_2(\text{acetone})_2(\text{PPh}_3)_2] [\text{BF}_4]$  to yield the cyclic iridium diene complexes. Then in 1987 Crabtree reported alkane dehydrogenation using *trans*-( $\text{P}(\text{p-C}_6\text{H}_5\text{F})_3$ )<sub>2</sub>Ir(H)<sub>2</sub>( $\kappa^2$ -O<sub>2</sub>CCF<sub>3</sub>) under both thermal transfer conditions and photochemical conditions.<sup>28</sup> Following this report, our group in 1989 reported the first efficient example of alkane dehydrogenation using photochemical dehydrogenation of alkanes catalyzed by  $\text{RhCl}(\text{PMe}_3)_2(\text{CO})$ .<sup>29, 30</sup>





**Scheme 1.7:** Transfer dehydrogenation using TBE using  $[\text{IrH}_2(\text{acetone})_2(\text{PPh}_3)_2][\text{BF}_4]$

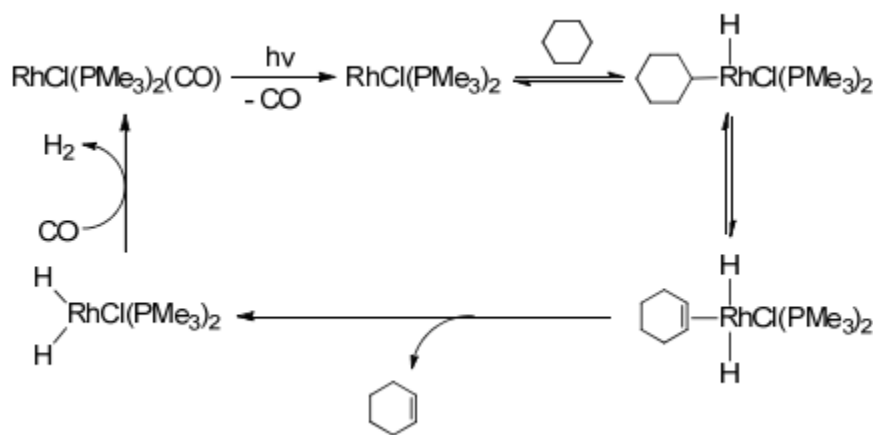


**Figure 1.2:** Photochemical alkane dehydrogenation using  $\text{RhCl}(\text{PMe}_3)_2(\text{CO})$  mechanism

Recently there have been advancements in the area of alkane dehydrogenation using a class of ligands referred to as “pincer ligands”. The first pincer ligand was reported by Moulton and Shaw in 1976<sup>31</sup>, wherein they describe complexes bearing  $\kappa^3$ -2,6- $(^t\text{Bu}_2\text{PCH}_2)_2\text{C}_6\text{H}_3$  referred to as  $(^t\text{BuPCP})$  a tridentate, meridional bound benzene based ligand. Since this initial report the term “pincer ligand” has been used to describe a ligand that is tridentate that binds in a predominately meridional bound fashion. Pincer ligated metal complexes are known for their high thermal stability and easy

tunability and have been used with metals such as Ir<sup>32</sup>, Ru<sup>33</sup>, Os<sup>34</sup>, Rh<sup>35</sup> as well as many others.<sup>36,37</sup>

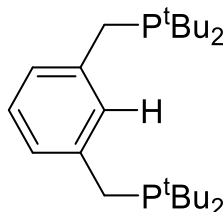
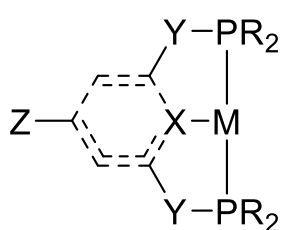


**Figure 1.3:** Protonated (<sup>t</sup>BuPCP) ligand

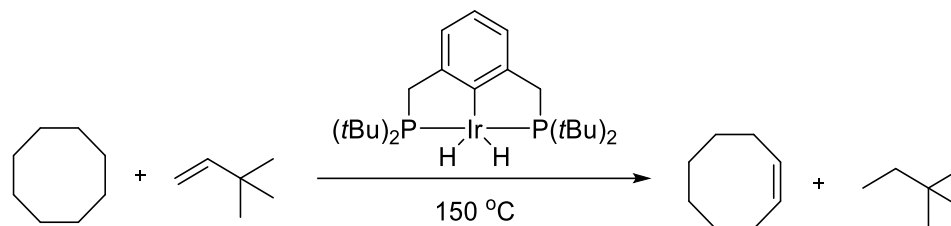
The ability to tune the pincer ligand sterically and electronically enables unique reactivity for certain ligands. Altering the substituents on the phosphorus donors (t-butyl, isopropyl, adamantly or trimethylfluoro) can alter the sterics and electronics of the pincer complex. Bulkier complexes have been shown to be more stable with higher selectivity for formation of terminal olefins, less bulky catalysts though have shown greater overall catalytic activity.<sup>38</sup> Adjusting the electronics of pincer ligands can be done through functionalizing the para position of the benzene ring (MeO, NH<sub>2</sub>, CO<sub>2</sub>Me)<sup>39-41</sup> or by altering the linker arm adjacent to the phosphorus donor atom (O, N, CH<sub>2</sub>).<sup>42-44</sup> Finally adjustment of the center position of the pincer framework allows for tuning the trans influence (N, O, Si, C)<sup>45,46,47,44</sup> of the pincer ligand.



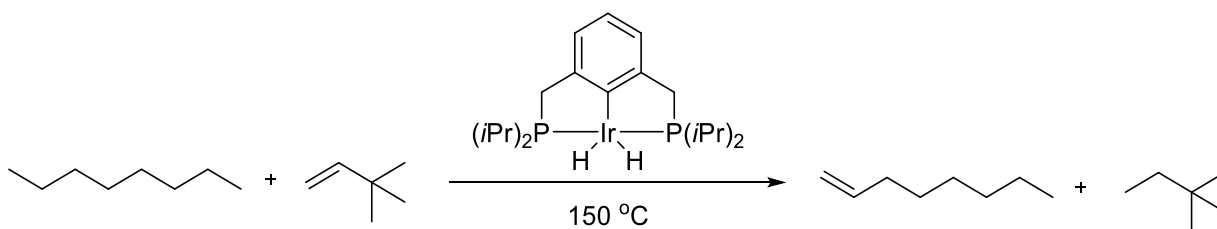
M: Ir, Ru, Os, Rh, Pd, Ni  
 R: <sup>t</sup>Bu, <sup>i</sup>Pr, Ad, CF<sub>3</sub>  
 X: C, N, O, Si  
 Y: N, O, CH<sub>2</sub>  
 Z: NH<sub>2</sub>, NMe<sub>2</sub>, OMe

**Figure 1.4:** Variations of pincer ligands

The first reported use of pincer ligated metal complexes for transfer dehydrogenation was reported by Kaska and Jensen in 1996.<sup>44</sup> They reported that  $(^t\text{BuPCP})\text{IrH}_2$  complex could dehydrogenate cyclooctane using TBE as a sacrificial hydrogen acceptor. A few years later our group reported the dehydrogenation of n-octane using  $(^i\text{PrPCP})\text{IrH}_2$  and TBE as the acceptor.<sup>48</sup> A key finding that our group reported was that these iridium complexes are regioselective for formation of the  $\alpha$ -olefins rather than the thermodynamically more stable internal ones. Pincer ligated rhodium analogues of these complexes were synthesized but were much less reactive for alkane dehydrogenation than their iridium counterparts.



**Scheme 1.8:** Transfer dehydrogenation of cyclooctane using  $(^t\text{BuPCP})\text{IrH}_2$



**Scheme 1.9:** Transfer dehydrogenation of n-octane using  $(^t\text{BuPCP})\text{IrH}_2$

These catalysts have shown high activity for alkane dehydrogenation and selectivity for terminal olefins, however they have also been shown to be very good

isomerization catalysts resulting in mixtures of internal and terminal olefins. While the terminal olefin is the kinetic product isomerization to the thermodynamically more favored internal olefins occurs readily.<sup>49,50</sup> Mechanistic studies of the dehydrogenation reaction suggest initial coordination of the sacrificial hydrogen acceptor to the  $(^t\text{BuPCP})\text{IrH}_2$  followed by a 1,2 insertion into the Ir-H bond. The accepted path follows reductive elimination of the alkane generates the 14 e<sup>-</sup>  $(^t\text{BuPCP})\text{Ir}$  species that can oxidatively add the C-H bond of the alkane.  $\beta$ -hydride elimination followed by olefin dissociation generates the olefin product and the starting catalyst  $(^t\text{BuPCP})\text{IrH}_2$ .<sup>51,52</sup>

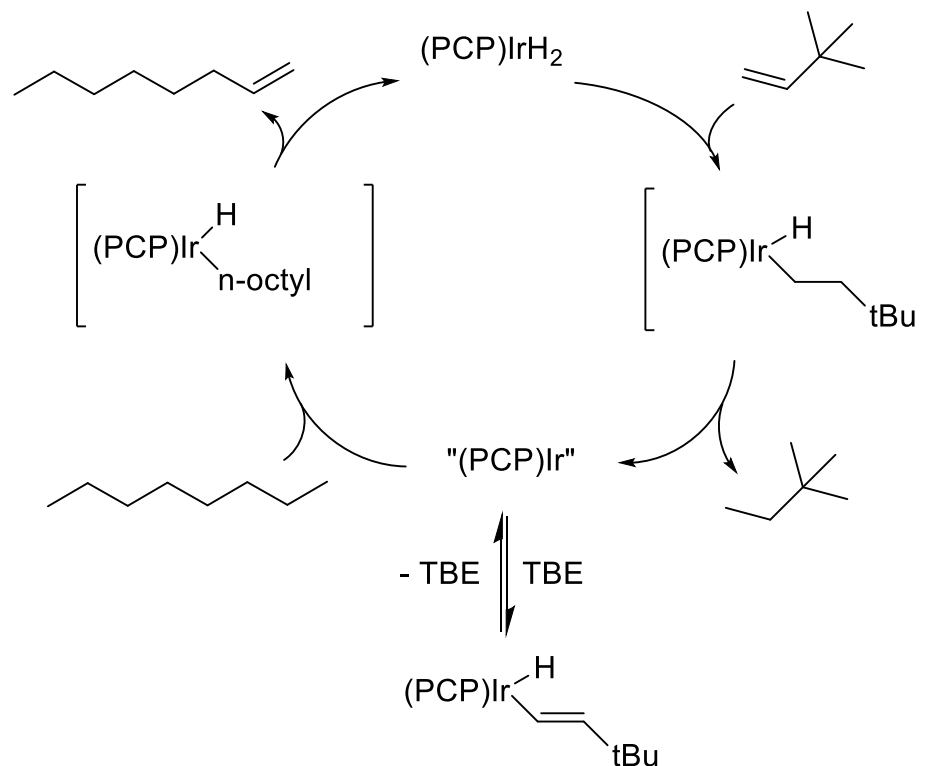


**Figure 1.5:** Mechanism of transfer dehydrogenation of n-octane using  $(^t\text{BuPCP})\text{IrH}_2$

In addition to C-H bonds, pincer-ligated complexes have been shown to activate other bonds such as O-H, O-O and C-O type bonds. The addition of water to  $(^t\text{BuPCP})\text{Ir}$

was reported by Morales-Morales yielding the  $(^t\text{BuPCP})\text{IrH}(\text{OH})$  species.<sup>53</sup> The O-H bonds of alcohols can undergo a similar O-H addition to the metal center followed by  $\beta$ -hydride elimination to form ketones and aldehydes. In the presence of sacrificial hydrogen acceptor these processes can be catalytic.<sup>54</sup>  $(^t\text{BuPCP})\text{Ir}$  was also shown to be reactive in the presence of oxygen resulting in the formation of either the bis or mono-dioxygen complex.<sup>55,56</sup>

The activation of N-H bonds using pincer ligated metal complexes has also been reported. Oxidative addition of N-H bonds to metal complexes is key to the functionalization of these bonds in either hydroamination or dehydrogenation reactions. Simple amines such as ammonia have been reported to undergo oxidative addition with  $(^t\text{BuPCP})\text{Ir}$  at low temperatures.<sup>57</sup> Utilizing this N-H activation, a rich amount of chemistry has been reported. This includes dehydrogenation of tertiary amines to enamines as well as hydrogenation of amides to give amines and alcohols as reported by Milstein.<sup>58</sup>

Pincer ligated metal complexes have also shown the ability to bind dinitrogen. With many pincer complexes this binding is inhibitory for catalytic processes. However certain pincer complexes using molybdenum have shown the ability to cleave dinitrogen to form metal nitrides.<sup>59,60</sup> More recently, rhenium<sup>61</sup> and osmium<sup>62</sup> complexes using an aliphatic PNP ligand framework have also demonstrated the ability to cleave dinitrogen. The cleavage of dinitrogen to form metal nitrides is a potential pathway for the reduction of dinitrogen to ammonia one of the most sought after reactions in chemistry today.

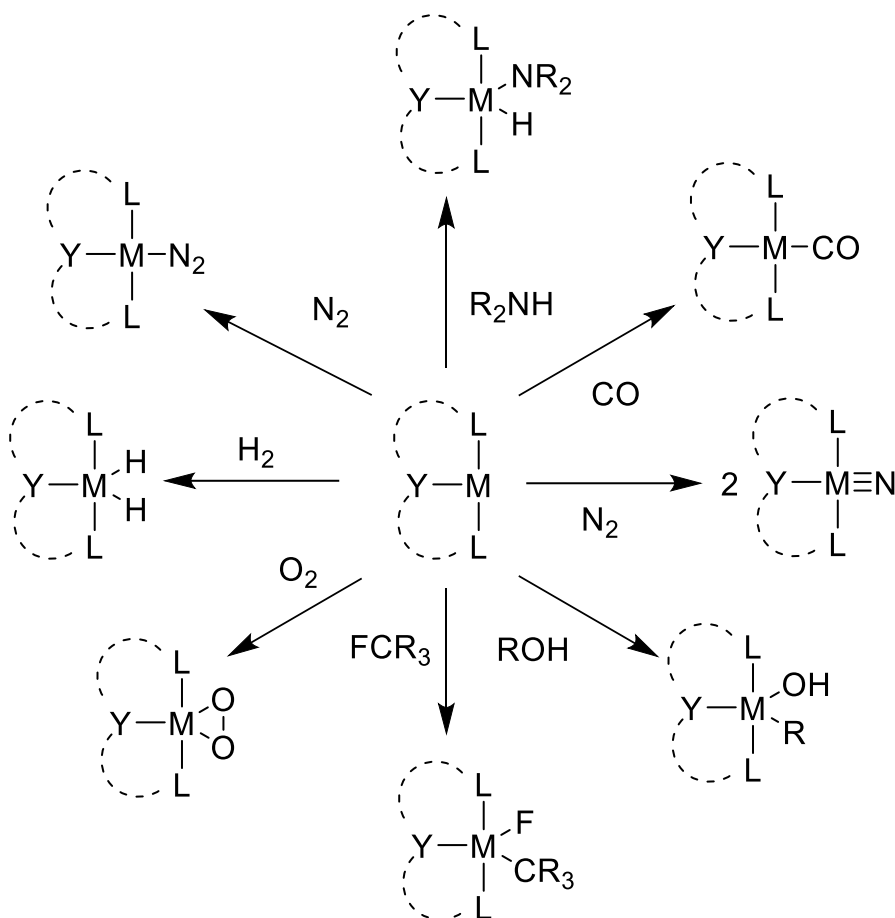


**Figure 1.6:** Small molecule activation using pincer ligands

## 1.2 Research Goals of this thesis

The search for new small molecule activations using established pincer-ligated metal complexes as well as the design and synthesis of new pincer-ligated metal complexes are two of the main goals of the Goldman lab. The aim of this thesis is to expand the known reactivity of pincer-ligated iridium catalysts and synthesize new pincer ligands with iridium and alternative metals while studying their reactivity. This thesis is separated into two main parts. The first is the use of iridium pincer-ligated complexes for catalytic O-H and N-H bond formation. The second part focuses on the

synthesis and reactivity of new pincer ligated complexes of osmium, iridium, rhenium and molybdenum for various applications.

Chapter 2 discusses the O-H and N-H addition of simple olefins to phenols and anilines, respectively, using iridium pincer complexes (ex. (<sup>i</sup>PrPCOP)IrH<sub>4</sub>). Mechanistic and catalytic studies show that the addition of O-H bonds to olefins is much more favorable using these catalysts. In addition, this chapter demonstrates the use of these catalysts in the reverse reaction i.e. ether cleavage (breaking C-O bonds).

Chapter 3 focuses on the synthesis and reactivity of pincer-ligated osmium complexes and the study of their activity for primarily alkane dehydrogenation. In this chapter we discuss the potential of the (<sup>t</sup>BuPNP)Os fragment, an isoelectronic fragment to the well-studied (<sup>t</sup>BuPCP)Ir system. In addition, other reactions with potential catalytic properties were examined as well.

Chapter 4 discusses the potential electrocatalytic reduction of nitrogen to form ammonia. Herein we focus on the synthesis of new rhenium and molybdenum based pincer complexes for the study of N<sub>2</sub> cleavage to form metal nitrides.

Chapter 5 discusses the synthesis of new iridium and osmium pincer complexes as potential catalysts for alkane dehydrogenation. This chapter focuses on the use of alternative ligands not used with iridium or osmium which have potential for unusual reactivity.

### 1.3 References

1. Hartwig, J.F. *Organotransition Metal Chemistry: From Bonding to Catalysis*; University Science Books: Sausalito, CA, 2010.
2. Vaska, L.; DiLuzio, J. W.; *J. Am. Chem. Soc.* **1962**, *84*, 679.
3. Vaska, L.; Rhodes, R. E. *J. Am. Chem. Soc.* **1965**, *87*, 4970.
4. Young, J. F.; Osborn, J. A.; Jardine, F. H.; Wilkinson, G. *Chem. Commun.* **1965**, 131.
5. Osborn, J. A.; Jardine, F. H.; Young, J. F.; Wilkinson, G. *J. Chem. Soc., A* **1966**, 1711.
6. Chock, P. B.; Halpern, J. *J. Am. Chem. Soc.* **1966**, *88*, 3511.
7. Eberhardt, G. G.; Vaska, L. *J. Catal.* **1967**, *8*, 183.
8. Halpern, J.; Wong, C. S. *J. Chem. Soc., Chem. Commun.* **1973**, 629.
9. Chatt, J.; Davidson, J. M. *J. Chem. Soc.* **1965**, 843.
10. Green, M. L. H.; Knowles, P. J. *J. Chem. Soc. D* **1970**, 1677.
11. Green, M. L. H.; Knowles, P. J. *J. Chem. Soc. A* **1971**, 1508.
12. Janowicz, J. A.; Bergman, R. G. *J. Am. Chem. Soc.* **1982**, *104*, 352.
13. Hoyano, J. K.; Graham, W. A. G. *J. Am. Chem. Soc.* **1982**, *104*, 3723.
14. Jones, W. D.; Feher, F.J. *J. Am. Chem. Soc.* **1984**, *106*, 1650.
15. Buchanan, J. M.; Stryker, J.M.; Bergman, R. G. *J. Am. Chem. Soc.* **1986**, *108*, 1537.
16. Northcutt, T. O.; Wick, D.D.; Vetter, A. J.; Jones, W. D. *J. Am. Chem. Soc.* **2001**, *123*, 7257.
17. Bryndza, H. E.; Fong, L. K.; Paciello, R.A.; Tam, W.; Bercaw, J.E. *J. Am. Chem. Soc.* **1987**, *109*, 1444.
18. Hass, H. B.; McBee, E. T.; Weber, P. *Ind. Eng. Chem.* **1936**, *28*, 333.
19. Janowicz, A. H.; Periana, R. A.; Buchanan, J. M.; Kovac, C. A.; Stryker, J. M.; Wax, M. J.; Bergman, R. G. *Pure and Appl. Chem.* **1984**, *56*, 13.
20. Jones, W. D.; Feher, F. J. *J. Am. Chem. Soc.* **1984**, *106*, 1650.
21. Jones, W. D.; Hessell, E. T. *J. Am. Chem. Soc.* **1993**, *115*, 554.
22. Bennett, J. L.; Wolczanski, P. T. *J. Am. Chem. Soc.* **1994**, *116*, 2179.
23. Wick, D. D.; Jones, W. D. *Organometallics* **1999**, *18*, 495.
24. Choi, G.; Morris, J.; Brennessel, W. W.; Jones, W. D. *J. Am. Chem. Soc.* **2012**, *134*, 9276.
25. Crabtree, R.H.; Mellea, M. F.; Mihelcic, J. M.; Quirk, J. M. *J. Am. Chem. Soc.* **2012**, *134*, 9276.
26. Afeefy, H. Y.; Liebman, J. F.; Stein, S. E., "Neutral Thermochemical Data" In *NIST Chemistry Webbook, NIST Standard Reference Database Number 69*; Linstrom, P. J., Mallard, W. G., Eds. Gaithersburg, MD, <http://webbook.nist.gov/chemistry/>, (retrieved September 28, 2012).
27. Crabtree, R. H.; Mihelcic, J. M.; Quirk, J. M. *J. Am. Chem. Soc.* **1979**, *101*, 7738.
28. Burk, M. J.; Crabtree, R. H. *J. Am. Chem. Soc.* **1987**, *109*, 8025.
29. Maguire, J. A.; Boese, W. T.; Goldman, A.S. *J. Am. Chem. Soc.* **1989**, *111*, 7088.
30. Rosini, G. P.; Soubra, S.; Vixamar, M.; Wang, S.; Goldman, A. S. *J. Organomet. Chem.* **1998**, *554*, 41.
31. Moulton, C. J.; Shaw, B. L. *J. Chem. Soc., Dalton Trans.* **1976**, 1020.



32. Gupta, M.; Hagen, C.; Flesher, R. J.; Kaska, W. C.; Jensen, C. M. *Chem. Commun.* **1996**, 2083.
33. Zhang, J.; Gunnoe, T.B.; Boyle, P.D. *Organometallics*. **2004**, *23*, 3094.
34. Gauvin, R.M.; Rozenberg, H.; Shimon, L.J.W.; Milstein, D. *Organometallics*. **2001**, *20*, 1719.
35. Montag, M.; Efremenko, I.; Cohen, R.; Shimon, L.J.W.; Leitus, G.; Diskin-Posner, Y.; Ben-David, Y.; Salem, H.; Jan. M.L.; Milstein, D. *Chemistry- A European Journal*. **2010**, *16*, 328.
36. Aydin, J.; Larsson, J.M.; Selander, N.; Szabo, K.J. *Organic Letters*. **2009**, *11*, 2852
37. Perez, G.; Pablo, M.; Di Franco, T.; Epenoy, A.; Scopelliti, R.; Hu, X.; *ACS Catalysis*. **2016**, *6*, 258.
38. Choi, J.; MacArthur, A. H. R.; Brookhart, M.; Goldman, A. S. *Chem. Rev.* **2011**, *111*, 1761.
39. Keming, Z.; Achord, P.D.; Zhang, X.; Krogh-Jespersen, K.; Goldman, A.S.; *J. Am. Chem. Soc.* **2004**, *126*, 13044
40. Bergbreiter, D.E.; Frels, J.D.; Rawson, J.; Li, J.; Reibenspies, J.H. *Inorganica Chimica Acta*. **2006**, *359*, 1912
41. Krogh-Jespersen, K.; Czerw, M.; Zhu, K.; Singh, B.; Kanzelberger, M.; Darji, N.; Achord, P.D.; Renkema, K.B.; Goldman, A.S. *J. Am. Chem. Soc.* **2002**, *124*, 10797
42. Morales-Morales, D.; Redon, R.; Yung, C; Jensen, C.M. *Inorganica Chimica Acta*. **2004**, *357*, 2953
43. Gorgas, N.; Alves, L.G.; Stoeger, B.; Martins, A.M.; Veiros, L.F.; Kirchner, K. *J. Am. Chem. Soc.* **2017**, *139*, 8130.
44. Gupta, M.; Hagen, C.; Flesher, R. J.; Kaska, W. C.; Jensen, C. M. *Chem. Commun.* **1996**, 2083.
45. Hermann, D.; Gandelman, M.; Rozenberg, H.; Shimon, L.J.W.; Milstein, D. *Organometallics*, **2002**, *21*, 812.
46. Haibach, M.C.; Wang, D.Y.; Emge, T.J.; Krogh-Jespersen, K.; Goldman, A.S.; *Chem. Sci.* **2013**, *4*, 3683
47. MacInnis, M.C.; MacLean, D.F.; Lundgren, R.J.; McDonald, R.; Turculet, L. *Organometallics*, **2007**, *26*, 6522
48. Liu, F.; Pak, E. B.; Singh, B.; Jensen, C. M.; Goldman, A. S. *J. Am. Chem. Soc.* **1999**, *121*, 4086.
49. Xu, W.; Rosini, G. P.; Gupta, M.; Jensen, C. M.; Kaska, W. C.; Krogh-Jespersen, K.; Goldman, A. S. *Chem. Commun.* **1997**, 2273.
50. Liu, F.; Goldman, A. S. *Chem. Commun.* **1999**, 655.
51. Renkema, K. B.; Kissin, Y. V.; Goldman, A. S. *J. Am. Chem. Soc.* **2003**, *125*, 7770.
52. Kanzelberger, M.; Singh, B.; Czerw, M.; Krogh-Jespersen, K.; Goldman, A. S. *J. Am. Chem. Soc.* **2000**, *122*, 11017.
53. Morales-Morales, D.; Jensen, C; *Organometallics* **2001**, *20*, 1144
54. Kundu, S.; Choi, J.; Wang, D. Y.; Choliy, Y.; Emge, T. J.; Krogh-Jespersen, K.; Goldman, A. S. *J. Am. Chem. Soc.* **2013**, *135*, 5127.
55. Boisvert, L.; Goldberg, K. I. *Acc. Chem. Res.* **2012**, *45*, 899.

56. Denney, M. C.; Smythe, N. A.; Cetto, K. L.; Kemp, R. A.; Goldberg, K. I. *J. Am. Chem. Soc.* **2006**, *128*, 2508.
57. Kanzelberger, M.; Zhang, X.; Emge, T. J.; Goldman, A. S.; Zhao, J.; Incarvito, C.; Hartwig, J. F. *J. Am. Chem. Soc.* **2003**, *125*, 13644.
58. Balaraman, E.; Gnanaprakasam, B.; Shimon, L. J. W.; Milstein, D. *J. Am. Chem. Soc.* **2010**, *132*, 16756.
59. Silantyev, G.A.; Förster, M.; Schluschaß, B.; Abbenseth, J.; Würtele, C.V.; Holthausen, M.C.; Schneider, S. *Angewandte Chemie*. **2017**, *56*, 5872.
60. Hebden, T.J.; Schrock, R.R.; Takase, M.K.; Müller, P. *Chem Commun.* 2012, *48*, 1851.
61. Klopsch, I.; Finger, M.; Würtele, C.; Milde, B.; Werz, D.B.; Schneider, S. *J. Am. Chem. Soc.* 2014, *136*, 6881.
62. Schendzielorz, F.S.; Finger, M.; Volkmann, C.; Wurtele, C.; Schneider, S. *Angewandte Chemie*. **2016**, *55*, 11417.

## Chapter 2

### Catalytic addition of N-H and O-H bonds to olefinic double bonds (Hydroamination and Hydroaryloxylation) using iridium pincer complexes

#### Abstract:

The catalytic addition of O-H bonds of phenols to simple olefins such as ethylene, propylene and isobutene (hydroaryloxylation) was performed using pincer ligated iridium catalysts ( $(^i\text{PrPCOP})\text{IrH}_4$ ). Mechanistic studies of this reaction suggest formation of the six coordinate  $(^i\text{PrPCOP})\text{Ir}(\text{OR})(\text{H})(\text{olefin})$  complex followed by insertion of the olefin into the Ir-O bond with C-H reductive elimination of the ether product. Studies suggest the olefin insertion to be the rate determining step. The addition of N-H bonds to olefins using analogous reactions with aniline showed no reactivity except for the stoichiometric addition to norbornene (NBE). Computational analysis determined the overall barrier for insertion of the olefin into the Ir-N bond to be 12 kcal/mol higher in energy than for the analogous Ir-O insertion. The reverse reaction of hydroaryloxylation, the cleavage of C-O bonds was performed catalytically using  $(^i\text{PrPCOP})\text{IrH}_4$ .

**Portions of this chapter are reproduced with permission form the following articles.**

Michael C. Haibach, Changjian Guan, David Y. Wang, Bo Li, Nicholas Lease, Andrew M. Steffens, Karsten Krogh-Jespersen, and Alan S. Goldman. *J. Am. Chem. Soc.* **2013** 135, 15062. Copyright 2013 American Chemical Society

Michael C. Haibach, Nicholas Lease, Alan S. Goldman. *Angew. Chem., Int. Ed.* **2014**, 53, 10160. Copyright 2014 Wiley publishing

## 2.1 Hydroamination introduction

The intermolecular addition of X-H bonds across olefinic double bonds catalyzed by transition metal complexes is a key reaction in organic synthesis.<sup>1</sup> Extensive work has been done studying and advancing transition metal catalyzed intramolecular and intermolecular hydroamination reactions, the addition of N-H bonds to alkynes and alkenes.<sup>2</sup> The synthesis of amines, enamines and imines are very valuable as bulk chemicals, specialty chemicals and pharmaceuticals.<sup>3</sup> Formation of these organic products can be done through various organic chemistry preparations such as reductive amination reactions or substitution reactions.<sup>4</sup>

Direct hydroamination using transition metal based catalysts can be seen as an improved atom-economical way to make amines, enamines and imines. This process does not generate the waste associated with other synthetic pathways as the N-H bond is directly added to the olefin. Extensive research has been reported for the metal catalyzed hydroamination of alkene and alkynes.

Alkaline and rare earth metals as well as actinide metals have shown to be highly efficient catalysts for the intramolecular hydroamination of unsaturated C-C bonds. These complexes have also been reported to have high regioselectivity's, however they do not catalyze intermolecular hydroamination reactions very efficiently. Complexes using Cp\* bound Sm<sup>5</sup>, Eu<sup>5</sup>, Nd<sup>5</sup> and Yb<sup>6</sup> metals have all been reported active catalysts for intramolecular hydroaminations.

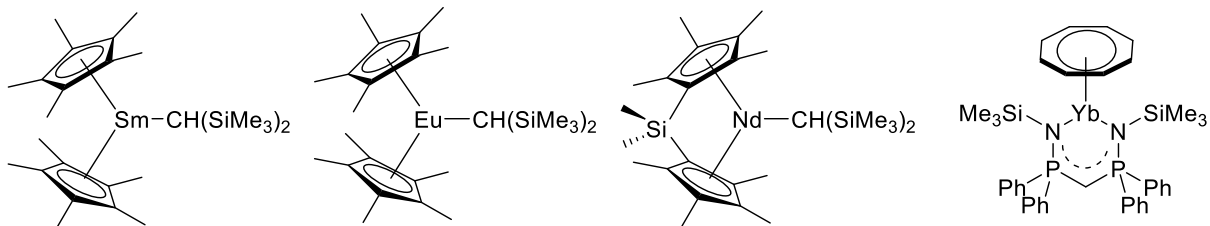
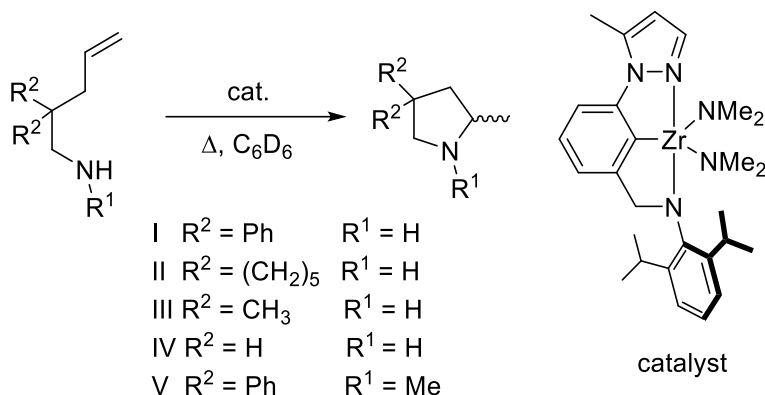


**Figure 2.1:** Actinide complexes for intramolecular hydroamination

Transition metals have also been reported to be active for hydroaminations.

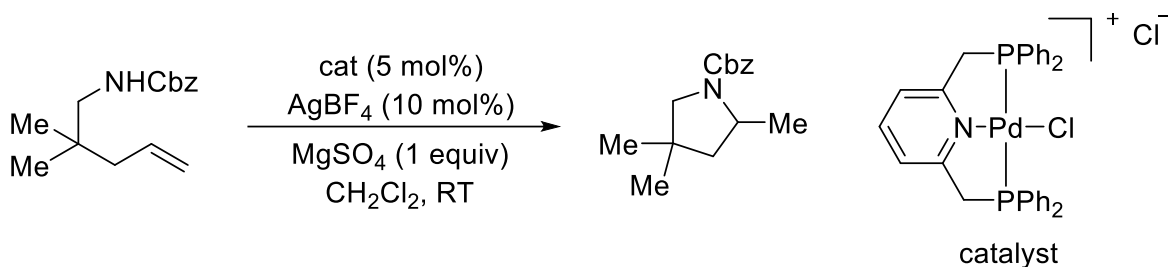
Lewis acidic metals with electron configurations of  $d^8$  and  $d^{10}$  have been reported to be very good catalysts for hydroamination reactions.<sup>7</sup> Additionally early transition metals in groups 4 and 5 have also found much success in hydroamination reactions, especially complexes containing Zr and Ti.<sup>8, 9</sup>

Pincer ligated metal complexes have also been reported for hydroaminations, primarily intramolecular reactions or reactions involving activated olefins. Giambastiani reported the hydroamination/cyclization of primary and secondary amines tethered to monoalkenes using pincer ligated zirconium complexes.<sup>10</sup>



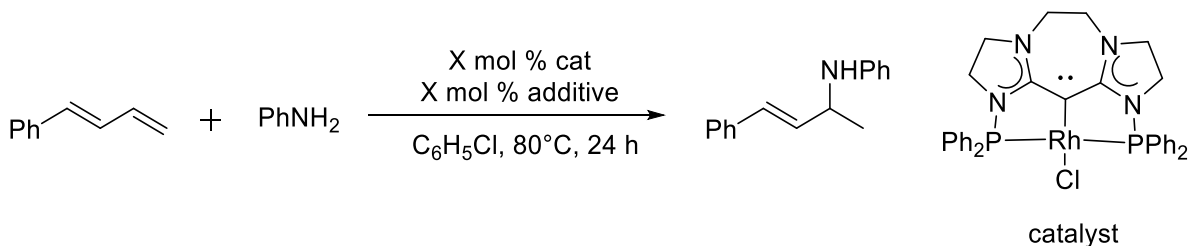
**Scheme 2.1:** NCN zirconium pincer catalyzed intramolecular hydroamination

Zhang et.al. reported the use of a PNP palladium complexes for intramolecular hydroamination of amino-1,3-dienes achieving high yields of cyclized product.<sup>11</sup>



**Scheme 2.2:** PNP palladium pincer catalyzed intramolecular hydroamination

In 2014 the Meek group reported the intermolecular addition of aniline and other secondary amines to activated 1,3 dienes in high yield.<sup>12</sup>



**Scheme 2.3:** NCN rhodium pincer catalyzed intermolecular hydroamination

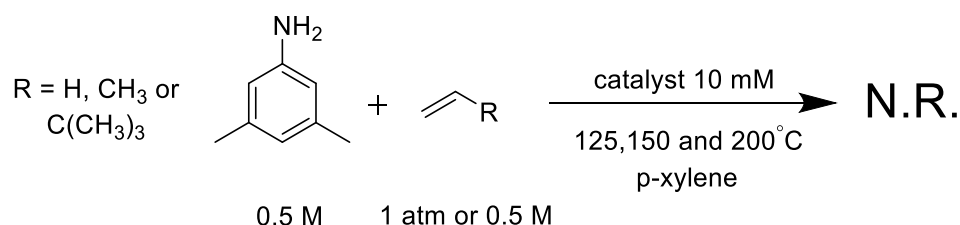
The addition of amines to PCP iridium complexes has been reported using amines such as aniline<sup>13</sup> and ammonia<sup>14</sup> demonstrating pincer iridium complexes can perform initial steps for hydroaminations reactions. Here in we report our attempts to perform hydroamination reactions using pincer ligated iridium complexes and unactivated olefins.

## 2.2 Hydroamination reactions using iridium pincer catalysts

### 2.2.1 Hydroamination of simple olefins (ethylene, propylene, tert-butyl ethylene)

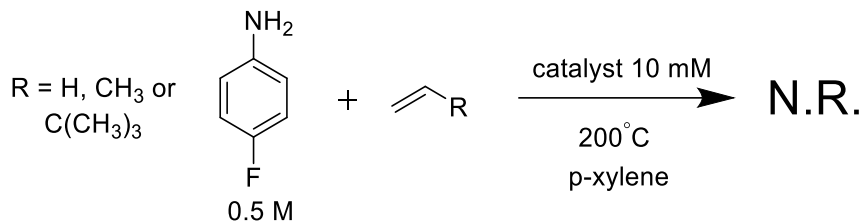
We began our study of hydroamination by focusing on aniline substrates similar to the phenol substrates used in the hydroaryloxylation report by our group<sup>15</sup>. The first catalyst studied was  $^t\text{BuPCPIrH}_2$  which was prepared according to literature precedent.<sup>16</sup>

The reactions were run in sealed ampoules with a total volume of 1.2 mL which when charged with gaseous olefin gave approximately 1.8 eq of olefin vs. aniline. In the case of TBE, olefin was added directly to the stock solution which was then separated into 5 ampoules per reaction. Reaction of  $^t\text{BuPClIrH}_2$  with simple olefins such as ethylene, propylene and TBE at multiple temperatures (125, 150 and 200°C) yielded no hydroamination products. Next less sterically hindered catalysts ( $^i\text{PrPClIrH}_4$  and  $\text{MeO-}^i\text{PrPClIrH}_4$ ) were used to see if the steric bulk of the previous catalyst was limiting the reactivity. Reaction of  $^i\text{PrPClIrH}_4$  or  $\text{MeO-}^i\text{PrPClIrH}_4$  with either ethylene or propylene yielded no hydroamination products even at 200°C.



**Scheme 2.4:** Attempted hydroamination of simple olefins with 3,5 dimethylaniline

Next, we examined the reactivity of 4-fluoroaniline for hydroamination. 4-fluoroaniline was chosen because it is more acidic than 3,5 dimethylaniline due to the inductive effect of the para fluorine. This increase in acidity would bring the pka of the aniline closer to that of phenol used for hydroaryloxylation which we hypothesized could be a factor for reactivity. A variety of pincer ligated iridium complexes were used with ethylene, propylene and TBE and in all cases no hydroamination was observed.



**Scheme 2.5:** Attempted hydroamination of simple olefins with 4-fluoroaniline

**Table 2.1:** Hydroamination attempts of anilines using various pincer ligated iridium complexes

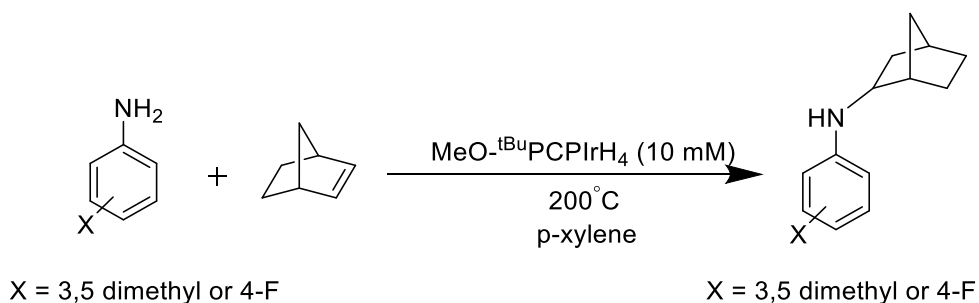
Catalyst/olefin	Ethylene	Propylene	TBE
$(^{tBu}PCP)IrH_2$	N.R.	N.R.	N.R.
$(^{iPr}PCP)IrH_4$	N.R.	N.R.	N.R.
$MeO-(^{iPr}PCP)IrH_4$		N.R.	
$MeO-(^{tBu}PCP)IrH_4$		N.R.	
$(^{tBu}PCP)Ir(\eta^2-C_2H_4)$	N.R.		
$(^{iPr}PCP)Ir(\eta^2-C_2H_4)$		N.R.	N.R.
$(^{tBu}POCOP)IrH_4$		N.R.	N.R.
$(^{iPr}PCOP)Ir(\eta^2-C_2H_4)$		N.R.*	
$(^{iPr}NCOP^{tBu})IrHCl$		N.R.*	

### 2.2.2 Hydroamination of norbornene (NBE)

The next olefin studied for hydroamination was norbornene (NBE). NBE was thought to be a promising candidate for hydroamination as the bicyclic olefin's strained structure could lead to higher reactivity at the olefin position. Additionally, the Milstein group had reported a bis-phosphine octahedral iridium complex was capable of insertion of the NBE double bond into an Ir-N bond stoichiometrically.<sup>17</sup>



Using  $\text{MeO-}^t\text{BuPCP IrH}_4$  (10 mM) as the catalyst NBE was reacted with both 3,5 dimethylaniline and 4-fluoroaniline at 125, 150 and 200°C. In both cases, two new peaks were observed by GC with a retention times a few minutes (about 8.5 and 11.5 min) after the starting materials. Control experiments showed that the peak observed at 8.5 min (observed in runs with both 3,5 dimethylaniline and 4-fluoroaniline) was a product of norbornene polymerization as this peak appeared even in the case of no catalyst. The other new peak at approximately 11.5 was hypothesized to be the hydroamination product. In both cases the peak was calculated to be slightly lower than 10 mM (even after 5 days of heating at 200°C) suggesting that at most 1 turnover occurred. GC/MS confirmed the product (parent peak of 204 in the case of 4-fluoroaniline) as the hydroamination addition product of NBE to the corresponding aniline.

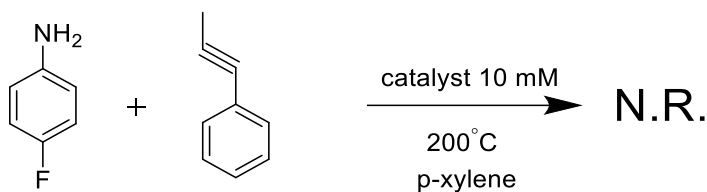


**Scheme 2.6:** Hydroamination of NBE with anilines

### 2.2.3 Hydroamination of 1-phenyl-1-propyne

After not being very successful adding N-H bonds to alkenes our next goal was to look at slightly more reactive starting materials such as alkynes. Literature reports have shown that hydroamination is easier when using activated olefins (conjugated or electron rich) or alkynes.<sup>18</sup> We chose to start looking at 1-phenyl-1-propyne as our alkyne source. Multiple pincer ligated iridium complexes were reacted with 4-

fluoroaniline and 1-phenyl-1-propyne. In all cases no hydroamination product was observed.



**Scheme 2.7:** Hydroamination of 1-phenyl-1-propyne with anilines

**Table 2.2:** Hydroamination attempts of 1-phenyl-1-propyne using various pincer ligated iridium complexes

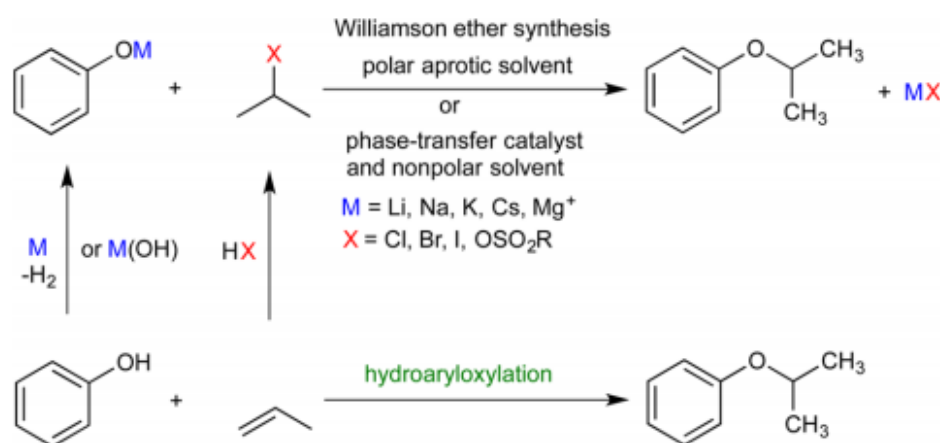
Catalyst/olefin	Phenyl Acetylene
( <sup>t</sup> BuPCP)IrH <sub>2</sub>	N.R.
( <sup>i</sup> PrPCP)IrH <sub>4</sub>	N.R.
MeO-( <sup>i</sup> PrPCP)IrH <sub>4</sub>	N.R.
( <sup>t</sup> BuPOCOP)IrH <sub>4</sub>	N.R.

## 2.3 Hydroaryloxylation using pincer-ligated iridium catalysts and mechanistic analysis

### 2.3.1 Alkyl aryl ether formation

Alkyl aryl ethers are important industrial chemicals as they have value as fragrance and pharmaceutical building blocks.<sup>19</sup> These ethers are still currently produced both industrially and on small scale applications by using the classical Williamson ether synthesis reaction.<sup>20</sup> This is done by reacting an alkali salt of the appropriate phenol with an alkyl halide or alkyl sulfonate ester, typically in polar aprotic

solvent. When performed industrially, the Williamson ether synthesis generates 1 equivalent alkali halide or alkali sulfonate waste in addition to the waste generated preparing the alkali phenol salt and alkyl halide which is synthesized from the corresponding olefin.



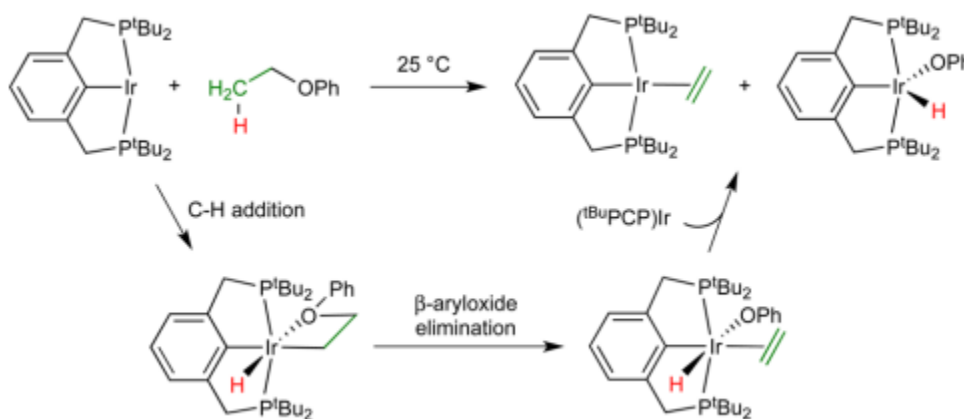
**Scheme 2.8:** Ether formation: Classical synthesis vs. hydroaryloxylation

A more atom economically way to synthesize ethers would be through the hydroaryloxylation pathway shown in (Scheme 2.8). However despite the advantages of the hydroaryloxylation pathway the Williamson ether synthesis is still used both industrially and on small scale applications. This can be explained in part by the fact that the main catalysts for O-H addition to olefins are Brønsted and Lewis acids such as H<sub>2</sub>SO<sub>4</sub> and BF<sub>3</sub>·OEt<sub>2</sub>. These catalysts, while highly active, suffer from poor chemoselectivity and competing Friedel-Crafts alkylations.<sup>21</sup> Following He's report in 2005<sup>22</sup> focus had shifted towards transition metal pre-catalysts for hydroaryloxylation such as (PPh<sub>3</sub>)Au(OTf). Hintermann reported that many of these transition metal catalysts were simply Brønsted acid delivery systems with Ag(OTf) in chlorinated

solvents serving as the most common source.<sup>23,24</sup> At the start of this work no knowledge of a true transition metal catalyzed route for hydroaryloxylation had been shown.

### 2.3.2 Pincer ligated iridium catalytic formation of alkyl aryl ethers (hydroaryloxylation)

Work previously reported by coworkers in the Goldman lab<sup>25</sup> showed precursors of the fragment (tBuPCP)Ir (RPCP =  $\kappa^3$ -C<sub>6</sub>H<sub>3</sub>-2,6-(CH<sub>2</sub>PR<sub>2</sub>)<sub>2</sub>) were able to cleave sp<sup>3</sup> C-O bonds via initial C-H activation. The complexes then underwent a dehydroaryloxylation to form the iridium olefin and O-H addition products. The kinetically facile olefin loss and phenol elimination suggested the possibility that the thermodynamically more favorable reverse reaction (hydroaryloxylation) could be done catalytically.



**Scheme 2.9:** Stoichiometric C-O cleavage of alkyl phenyl ether

Their initial attempts to perform hydroaryloxylation using (tBuPCP)IrH<sub>4</sub> were done using phenol and ethylene or propylene. When ethylene was used no O-H addition products were observed. In the case of propylene stoichiometric O-H addition was observed forming the isopropyl phenyl ether. Testing some less sterically hindered PCP derivatives they identified several catalysts active for the hydroaryloxylation of 3,5 dimethylphenol with propylene. The three catalysts that performed the best were

(<sup>t</sup>Bu<sup>3</sup>MePCP)Ir, (MeO-<sup>i</sup>PrPCP)Ir, and (<sup>i</sup>PrPCOP)Ir with the corresponding tetrahydrides reacting slightly better than the corresponding ethylene complexes. This was attributed to the binding strength of ethylene.

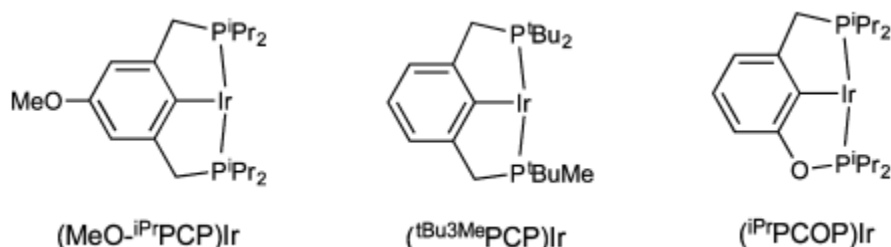


**Figure 2.2:** Pincer iridium complexes used for hydroaryloxylation

Reaction of 3,5-dimethyl phenol (500 mM) with propylene (2 atm) using (<sup>i</sup>PrPCOP)IrH<sub>4</sub> (10 mM) as the catalyst resulted in the formation of 400 mM of isopropyl aryl ether (40 TON) in 24 hours. Neither the n-propyl aryl ether nor any other alkyl phenols were found by GC. When ethylene was used instead of propylene the only product observed was the ethyl aryl ether. In the case of 1-butene the reaction proceeded slower and needed about 4 atm for comparable rates and only the iso-butyl aryl ether was observed by GC. In all cases, the iso-product was the only species generated demonstrating that the reaction is fully regio- and chemoselective.

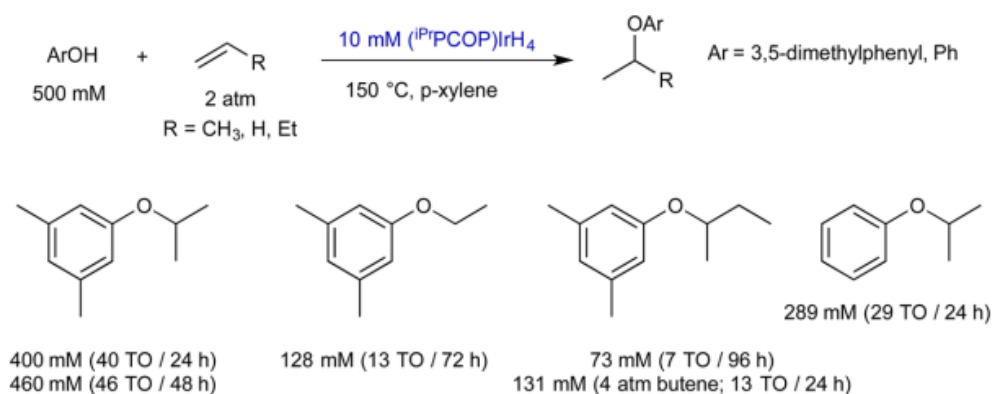


**Figure 2.3:** Hydroaryloxylation 3,5 dimethyl phenol and simple olefins

Based on the good regio- and chemoselectivity of our catalysts without the associated Friedel Crafts alkylation side products it was believed that this was a purely transition metal catalyzed reaction and operated under a different mechanism than Hintermann's "hidden" Bronsted acid catalysts. In order to test this the hydroaryloxylation reaction was run using Hintermann's Bronsted acid catalyst (10 mM AgOTf and 40 mM  $t$ BuCl) and no isopropyl aryl ether was observed. Instead ten different alkylation products of both the phenol ring and p-xylene solvent were observed for this reaction.

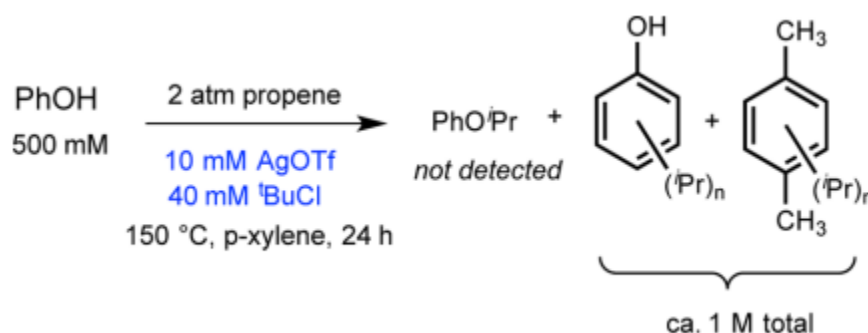


**Figure 2.4:** Pincer iridium complexes used for hydroaryloxylation

In order to further rule out the possibility of an acid based mechanism, a competition reaction was run between propylene and isobutene. Under acid catalyzed conditions the protonated isobutene would form a more stable tertiary carbocation and should yield the tert-butyl phenol ether as the major product. When hydroaryloxylation was performed with equal parts isobutene and propylene the isopropyl aryl ether was formed in a greater than 40:1 ratio compared to the t-butyl aryl ether. A control reaction using Hintermann's catalyst (10 mM AgOTf and 40 mM  $t$ BuCl) yielded no isopropyl aryl ether and a small amount of t-butyl aryl ether. The majority of the

products were Friedel Crafts side products. Additional evidence against the carbocation based mechanism can be seen by the reactivity of propylene vs. ethylene. Propylene will react with 3,5 dimethylphenol faster than ethylene in independent runs, however when in direct competition of each other the ethylene will react 3 times faster than propylene.

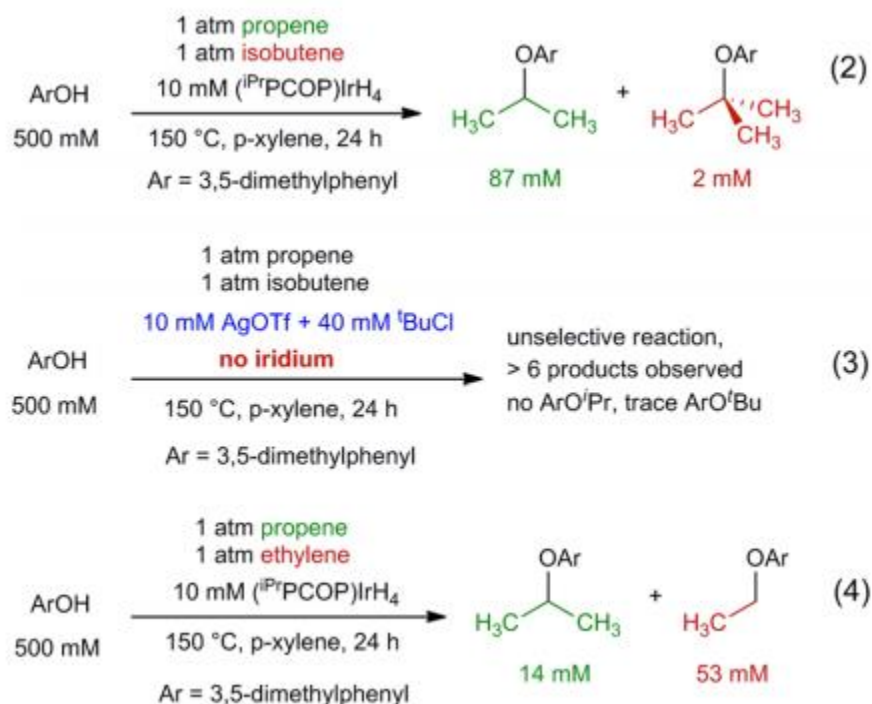
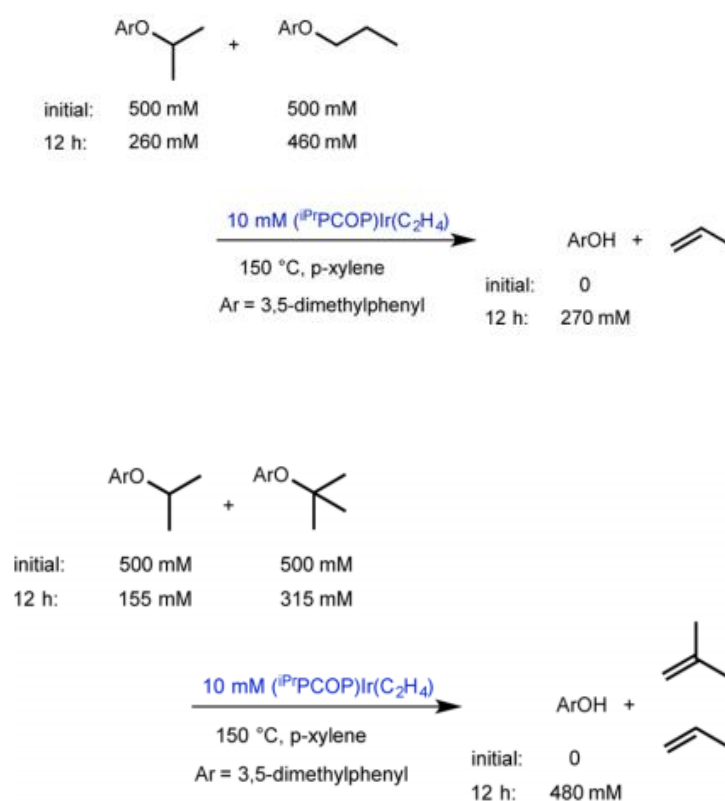


**Figure 2.5:** Evaluation of potential acid based mechanism

Our group next studied the preferential formation of the isopropyl ether versus the n-propyl isomer and the high chemoselectivity for the isopropyl ether vs. isobutyl ether. The preferential formation of the isopropyl vs. the isobutyl product might be attributed to thermodynamics rather than kinetics. This would suggest that the back reaction (ether cleavage) would be even faster. A competition reaction between n-propyl vs. isopropyl aryl ethers was conducted and the rate of cleavage was much higher for the isopropyl vs. the n-propyl aryl ether. This higher rate of reaction for both the O-H

bond addition and C-O bond cleavage suggests that the reaction is kinetically controlled not thermodynamically. The same type of competition reaction using isopropyl vs. isobutyl aryl ethers also showed higher rates of cleavage for the isopropyl ether over the isobutyl analogue. This then implies that, much like the regioselectivity for the isopropyl aryl ether, the chemoselectivity is also a kinetic phenomenon.



**Scheme 2.10:** Product determination: kinetic or thermodynamic

### 2.3.3 Mechanistic analysis of hydroaryloxylation

The work done by my coworkers showed that hydroaryloxylation of phenols with olefins such as ethylene, propylene and 1-butene to form ethers were very successful when using pincer ligated iridium complexes ((<sup>i</sup>PrPCOP)Ir(C<sub>2</sub>H<sub>2</sub>), (MeO-<sup>i</sup>PrPCP)IrH<sub>4</sub> and



(<sup>t</sup>Bu<sub>3</sub>MePCP)IrH<sub>4</sub>).<sup>15</sup> The proceeding work focused on the mechanism of this reaction to understand what factors and intermediates provide this interesting reactivity. This mechanistic approach used both experimental methods as well as computational methods in its analysis.

### 2.3.3.1 Computational mechanism

Building upon the proposed computationally derived mechanism reported in the initial hydroaryloxylation paper<sup>15</sup>, a slightly modified mechanism was proposed. As was reported, the computed mechanism shows formation of the isopropyl aryl ether to be the thermodynamically favorable isomer agreeing with experimental results. The computational mechanism in Figure 2.6 (work done by Changjian Guan) details the three key steps of this reaction. The initial step of the mechanism is the addition of olefin (propylene) to the five coordinate (<sup>i</sup>PrPCOP)Ir(H)(OH) species. This six coordinate (<sup>i</sup>PrPCOP)Ir(η<sup>2</sup>-propene)(OPh)(H) complex then undergoes olefin insertion into the Ir-O bond. This step was calculated to be the rate determining step. Finally C-H reductive elimination generates the free alkyl aryl ether and 14 e<sup>-</sup> (<sup>i</sup>PrPCOP)Ir fragment that then reacts with phenol to restart the cycle.

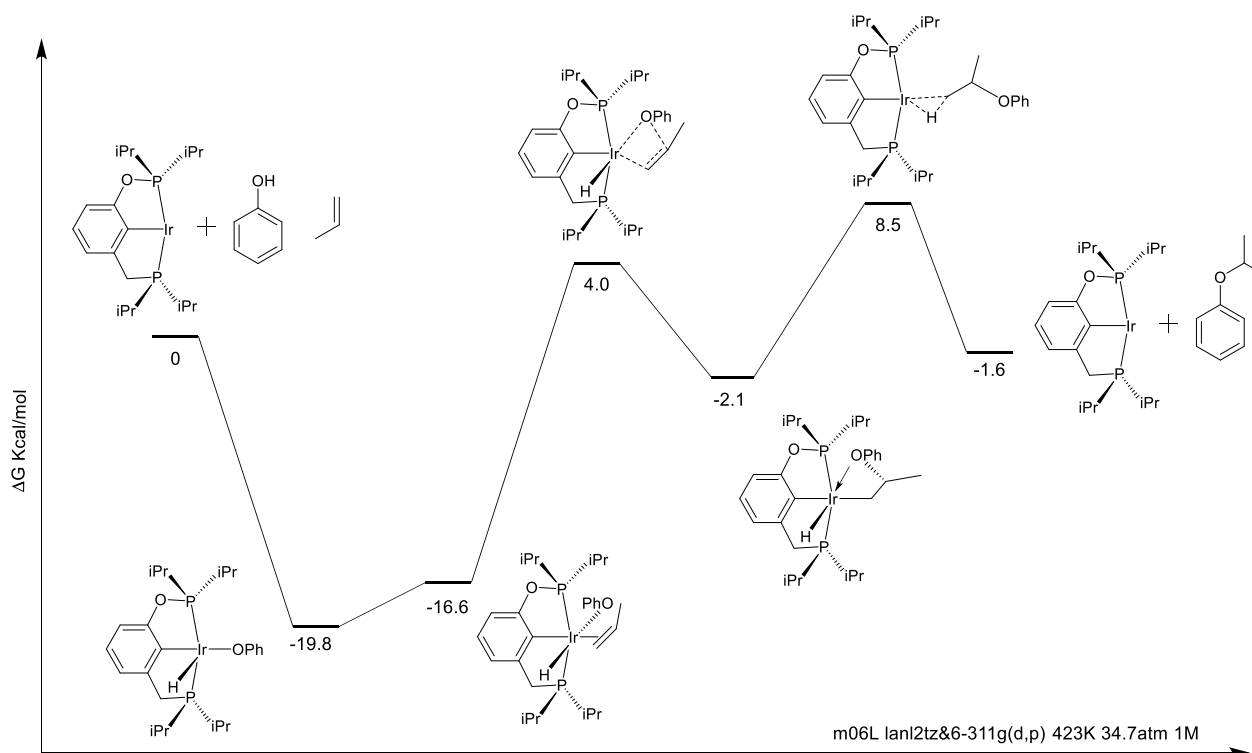
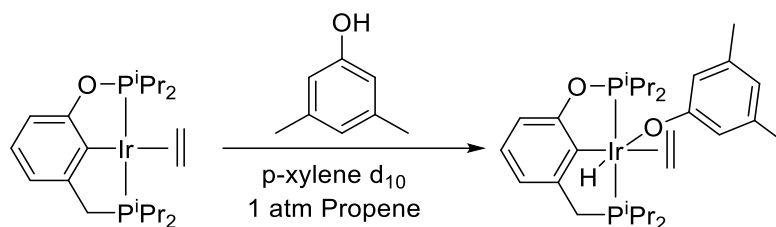


**Figure 2.6:** Computationally derived mechanism for hydroaryloxylation (Free energy ( $\Delta G$ ) kcal/mol)

### 2.3.3.2 Resting State Experiments

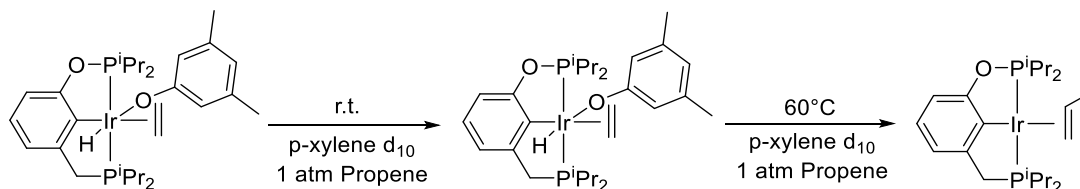
In order to determine the resting state of the catalyst, a stock solution of  $(iPrPCOP)Ir(C_2H_2)$  and 3,5 dimethylphenol in *p*-xylene  $d_{10}$  was charged with 1 atm of propylene. Upon treating  $(iPrPCOP)Ir(C_2H_2)$  with 3,5 dimethylphenol (0.5 M) at room temperature a single new species was observed by NMR.  $^{31}P$ -NMR showed a two doublets at 167 and 46 ppm and the  $^1H$ -NMR showed a new triplet hydride signal at -29.4 ppm ( $J = 16.8$  Hz). The product was initially believed to be the five coordinated O-H addition product  $(iPrPCOP)Ir(H)(OPh)$ , however independent synthesis of the five coordinated species showed a hydride peak that was further upfield than the one observed..

The product was identified as the six coordinate ( $i^{\text{Pr}}\text{PCOP})\text{Ir}(\text{H})(\text{OPh})(\text{C}_2\text{H}_4)$  species by NMR. This was unusual as 1 atmosphere of propylene was added to the solution suggesting displacement of bound ethylene with propylene. However the hydride signal did not match what was previously assigned to the ( $i^{\text{Pr}}\text{PCOP})\text{Ir}(\text{H})(\text{OPh})(\eta^2\text{-C}_3\text{H}_6)$  species.



**Scheme 2.11:** Resting state of the catalyst under catalytic conditions at room temperature

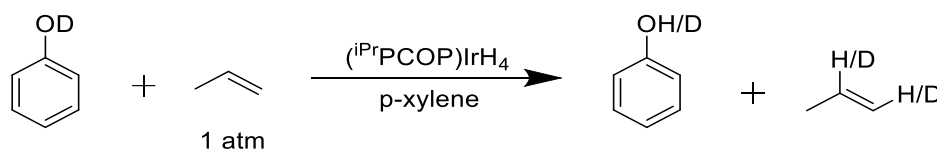
In order to observe the resting state under catalytic conditions VT NMR was performed heating the solution gradually to 100°C.  $^{31}\text{P}$ -NMR indicated that as the solution was heated the signals corresponding to the six coordinate ( $i^{\text{Pr}}\text{PCOP})\text{Ir}(\text{H})(\text{OPh})(\text{C}_2\text{H}_4)$  gradually disappeared until they were no longer visible at 60°C. Two new doublets could be seen growing in as the solution was heated and above 60°C, this was the only product in solution. The signals observed correspond with the four coordinate ( $i^{\text{Pr}}\text{PCOP})\text{Ir}(\eta^2\text{-C}_3\text{H}_6)$  species. This result suggests that under reaction conditions near reaction temperatures the resting state of the catalyst is the four coordinate propylene complex.



**Scheme 2.12:** Resting state of the catalyst under catalytic conditions at elevated temperatures

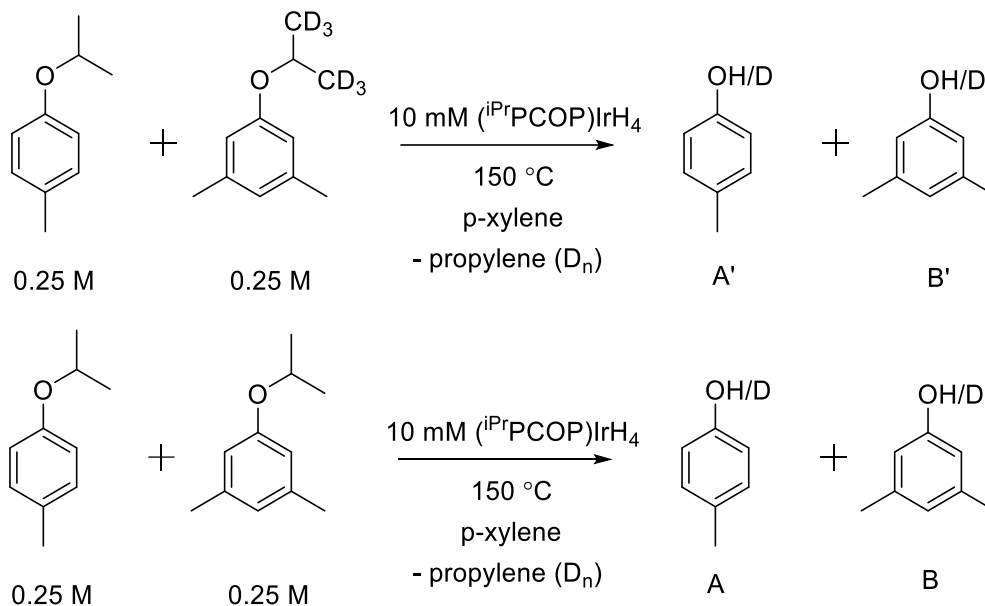
### 2.3.3.3 Kinetic isotope studies

In order to help determine the rate limiting step of the reaction, KIE (kinetic isotope effect) studies were conducted. Initially the KIE was going to be calculated using the hydroaryloxylation reaction of deuterated phenol with propylene. However upon reacting the deuterated phenol with propylene a small amount of H/D scrambling into the propylene was observed in a few minutes even at room temperature.



**Scheme 2.13:** H/D scrambling between phenol (OD) and propylene

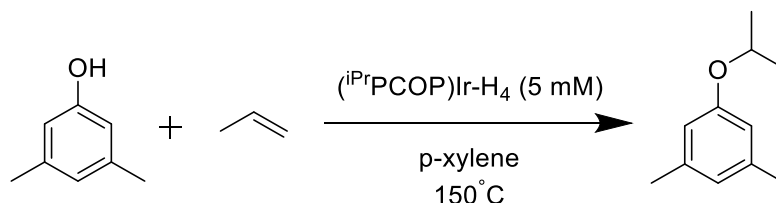
To go around this problem the KIE was calculated using the back reaction i.e. ether cleavage. However one other issue that we envisioned was once the phenol was generated it could also undergo H/D exchange. To resolve this issue the KIE was run as a competition reaction between two different isopropyl aryl ethers. One would have the standard 3,5 dimethyl phenyl group and the other would have 4-para methyl phenyl group.



**Scheme 2.14:** KIE competition reactions

The rate of ether cleavage in both competition reactions was determined by GC analysis of the product and concentrations calculated vs. an internal standard. The KIE was calculated using the formula  $KIE = [B']/[A'] \cdot [A]/[B]$  which gave a value of 1.7. This value was consistent with computational analysis done by our group and is not consistent with a primary KIE. This suggests that C-H bond activation for ether cleavage or C-H bond reductive elimination in hydroaryloxylation is not the rate determining step.

#### 2.3.3.4 Kinetic analysis of phenol addition to propylene



**Scheme 2.15:** Standard kinetic hydroaryloxylation run: phenol or propylene was varied

Another step to analyze the hydroaryloxylation mechanism was to study the kinetic dependence of phenol and propylene in the reaction. To study the kinetics the reactions were run in sealable NMR tubes using stock solutions of ( $i^{\text{Pr}}$ PCOP)IrH<sub>4</sub> in p-xylene d<sub>10</sub> which were then heated in a GC oven equipped with a stirring mechanism to mix the reaction while heating. Reactions for phenol dependence were run using 2 atm of propylene with varying concentrations of 3,5 dimethylphenol (0.5, 0.25, 0.125 and 0.0625 M). Propylene dependence reactions were run using a stock solution of 0.5 M 3,5 dimethylphenol and charging the tubes with various propylene pressures (4, 2, 1, 0.5 atm).

Varying the dependence of the 3,5 dimethylphenol showed a linear dependence on phenol concentration. It was hypothesized that 3,5 dimethylphenol should have a 1<sup>st</sup> order dependence however a non-integer dependence of 0.8 was calculated.

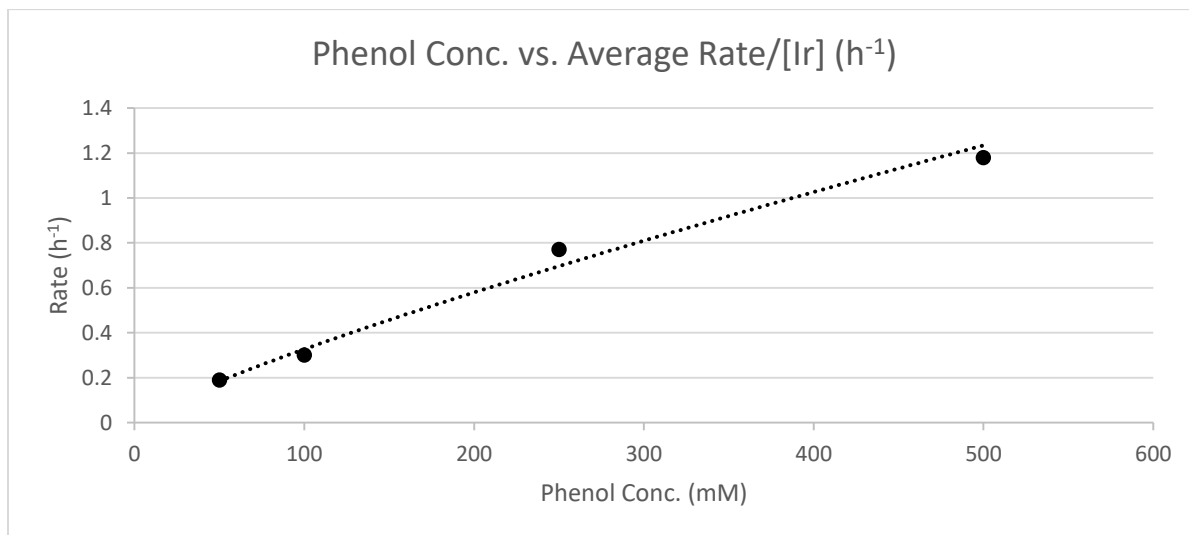


**Figure 2.7:** Plot of phenol concentration (mM) vs. rate of reaction (h<sup>-1</sup>). Order of 0.8 was calculated dependence for phenol

The non-integer value calculated was attributed to possible intermolecular hydrogen bonding interactions between two phenol molecules. Hepler et al. have observed the formation of hydrogen bonded pairs, trimers and tetramers of phenol in non-polar solvents.<sup>26</sup> Equilibrium reactions of forming and breaking hydrogen bonds prior to the O-H oxidative addition of phenol could alter the ideal 1<sup>st</sup> order kinetics giving a non-integer value.

Varying the propylene concentration showed a zero order dependence at higher propylene concentrations but as the propylene concentration decreased a more linear dependence was observed. As seen in the data below (Figure 2.8) the rate of reaction of propylene is very consistent at 4, 2 and 1 atmospheres. Upon lowering the propylene pressure to 0.5 atmospheres the rate is cut to about half. Decreasing the propylene concentration below 0.5 atmospheres continued this linear trend. Based on the proposed mechanism as well as the determination of the resting state as  $(^{iPr}PCOP)Ir(\eta^2\text{-propene})$  it would be hypothesized that propylene would have a zero order.

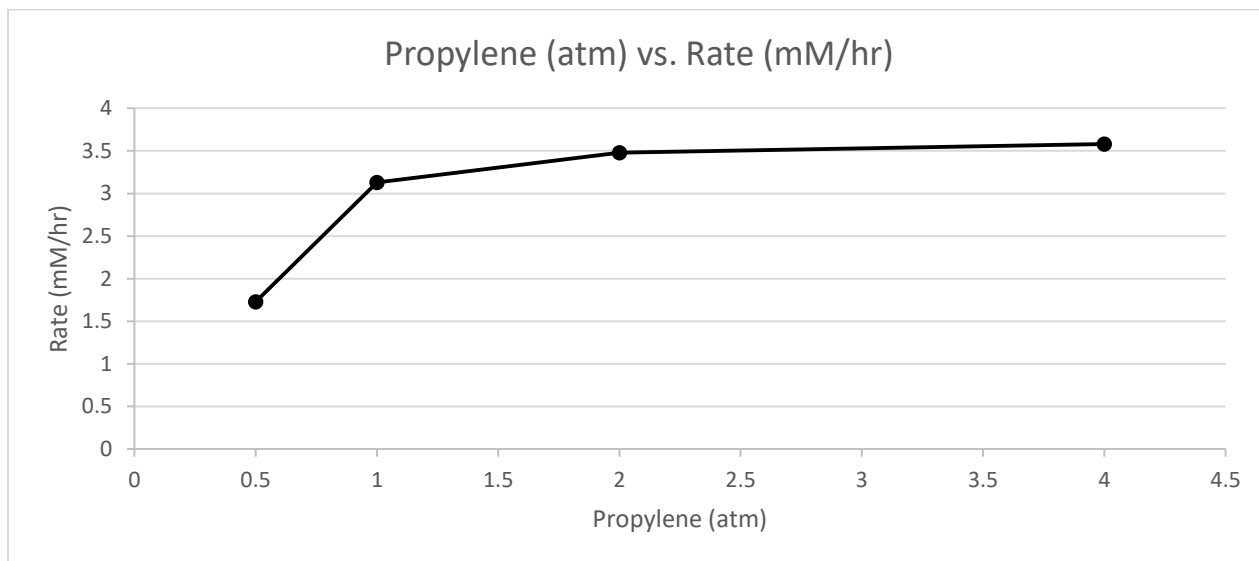


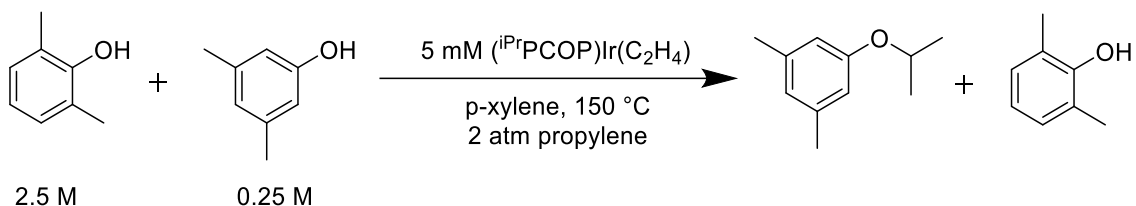
**Figure 2.8:** Plot of propylene pressure (atm) vs. rate of reaction ( $\text{h}^{-1}$ ). Zero order propylene dependence was observed at catalytic conditions

One possible explanation for this change in kinetic order would be a change in the resting state of the catalyst. Computational analysis showed that the five coordinate  $(^{\text{iPr}}\text{PCOP})\text{Ir}(\text{H})(\text{OPh})$  species and the four coordinate  $(^{\text{iPr}}\text{PCOP})\text{Ir}(\eta^2\text{-propene})$  species have a difference in energy of only 2.4 kcal/mol. While the resting state of the reaction was determined to be  $(^{\text{iPr}}\text{PCOP})\text{Ir}(\eta^2\text{-propene})$ , this was only determined at high propylene pressures. At low propylene pressures the five coordinate  $(^{\text{iPr}}\text{PCOP})\text{Ir}(\text{H})(\text{OPh})$  species could become the new resting state. This would explain the apparent first order kinetics observed at low pressures of propylene.

#### 2.3.3.5 Hydrogen bonding studies of phenol

Kinetic dependence of 3,5 dimethylphenol was determined to be a non-integer with a value of 0.8. We hypothesized this non-integer order could be the result of formation of hydrogen bonded dimers of phenol prior to addition to the iridium metal center. To test this theory, hydroaryloxylation reactions were run in the presence of a large amount of hydrogen bonding substrate as a “pseudo solvent”. 2,6 dimethyl phenol was chosen as it was unreactive toward hydroaryloxylation reactions with propylene. This non-reactivity was determined to be caused by the increased steric bulk at the ortho positions to the phenol.





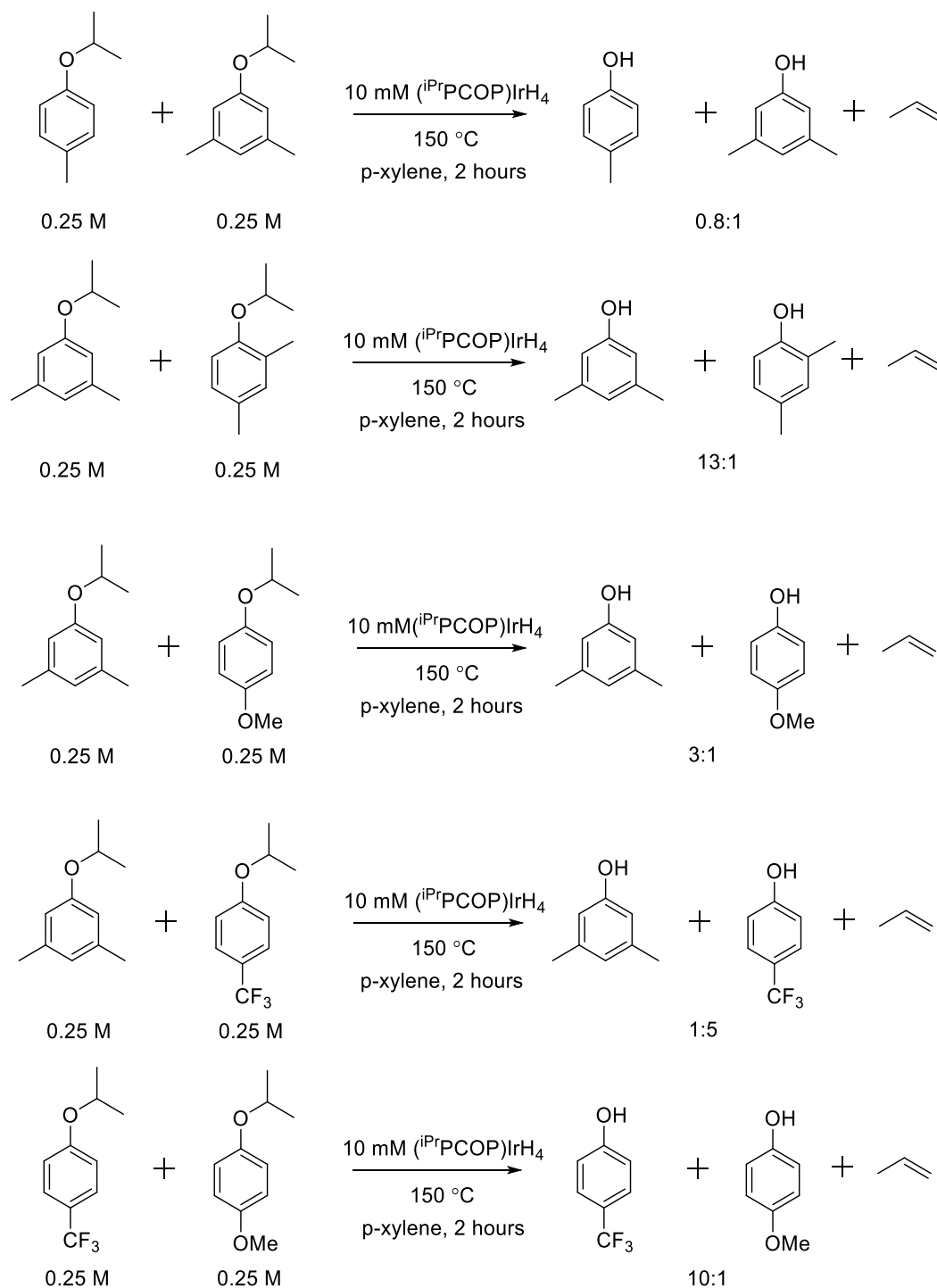
**Scheme 2.16:** Hydroaryloxylation reaction in the presence of hydrogen bond acceptor

Running the hydroaryloxylation of 3,5 dimethylphenol and propylene using (*i*PrPCOP)Ir(C<sub>2</sub>H<sub>4</sub>) and a large excess of 2,6 dimethylphenol showed a considerable decrease in the rate of alkyl aryl ether formation. In the absence of the hydrogen bonding substrate (2, 6 dimethylphenol) 80% conversion is observed after 24 hours. Upon addition of hydrogen bonding substrate the formation of the alkyl aryl ether product was negligible after 24 hours. These results clearly demonstrate that additionally hydrogen bonding partners does impede the reaction rate.

### 2.3.3.6 Competition reactions

The KIE calculated for the reverse reaction of hydroaryloxylation was experimental calculated to be 1.7 suggesting that C-H reductive elimination was not the rate determining step. The alternative step that could be rate determining would be the olefin insertion into the Ir-oxygen bond or de-insertion in the ether cleavage pathway. In order to test if olefin insertion was the rate determining step competition reactions were run. These competition reactions were performed using the ether cleavage reactions using ethers with varying electronic substituents on the aryl ring. If C-H activation was the rate determining step electronic effects on the ring would not have a large impact on reactivity. However the electronic substituents do in fact play a large

role in the rate of reaction. It can be proposed then that olefin insertion is the rate determining step.



**Scheme 2.17:** Competition reactions between electronically different alkyl aryl ethers

The results of the competition reactions showed that altering the electronic properties of the aryl ring had a significant effect on the rate of reaction. Ethers with electron withdrawing groups ( $\text{CF}_3$ ) on the ring showed much faster reaction rates compared to ethers with electron donating groups (10 times faster than the para methoxy substituted ether). Furthermore steric effects also had an effect on the rate of reaction demonstrated by the much slower reactivity of 4,6 dimethyl substituted phenol vs. 3,5 dimethyl substituted phenol. Based on the results of KIE measurements, computational analysis and the ether cleavage competition reactions the olefin insertion was shown to be the rate limiting step of this mechanism.

#### **2.3.3.7 Computational analysis of N-H vs O-H addition to olefins**

Computational and experimental insights have allowed us to elucidate the mechanism for O-H addition, however, we were also interested in explaining why O-H addition worked and N-H addition did not. Simple computational analysis of the addition of ammonia and water to ethylene were performed to help explain this reactivity (computational work done by Changjian Guan). When comparing the ammonia addition vs. the water addition some key observations can be made. First the formation of the key six coordinate intermediate ( $\text{Ir}(\text{H})(\text{OH})(\text{C}_2\text{H}_4)$  vs.  $\text{Ir}(\text{H})(\text{NH}_2)(\text{C}_2\text{H}_4)$ ) is much more energetically favorable by 10 kcal/mol. Secondly the overall barrier for N-H activation followed by olefin insertion is approximately 40 kcal/mol and is 10 kcal/mol higher than for the analogous O-H pathway. This difference in energetics could explain why pincer-ligated iridium catalysts show activity for O-H addition and not for N-H addition.

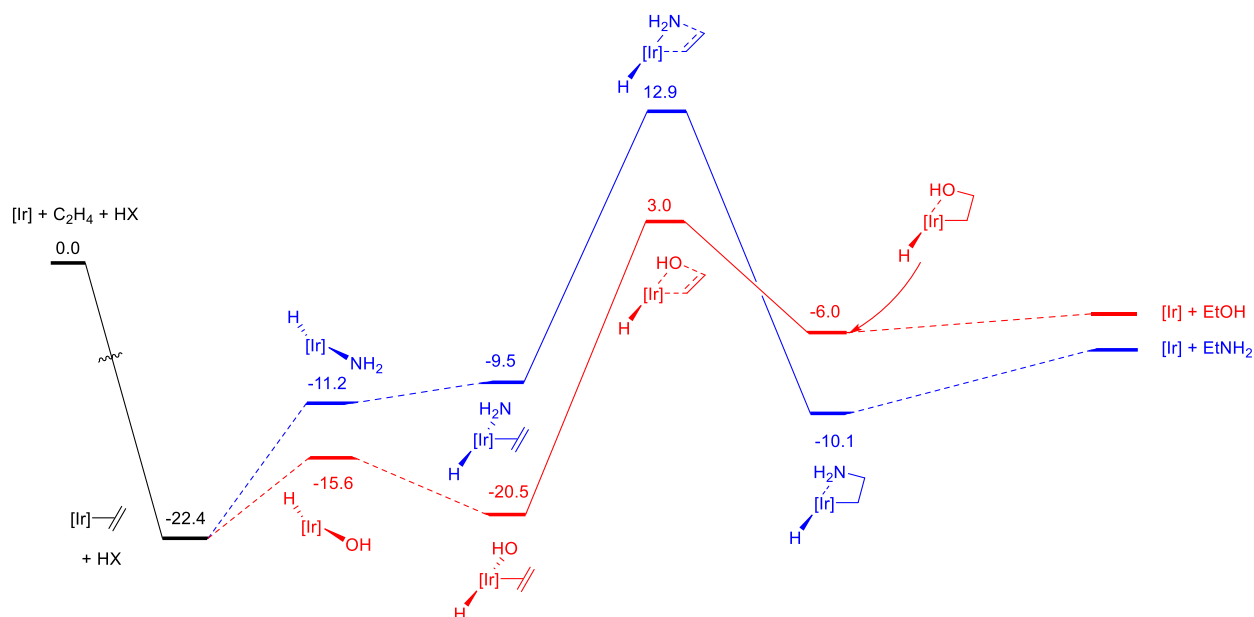
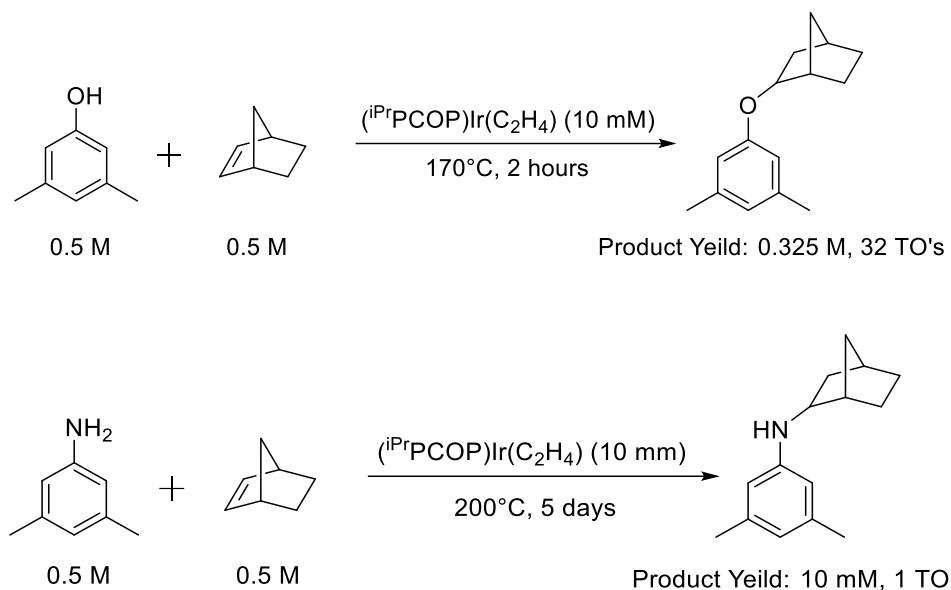


**Figure 2.9:** Free energy comparison between addition of water and ammonia to ethylene ( $\Delta G$  kcal/mol)

To further illustrate this point two identical reactions were run to directly compare N-H vs. O-H addition. (<sup>i</sup>PrPCOP)Ir(C<sub>2</sub>H<sub>4</sub>) catalyzed hydroamination and hydroaryloxylation of 3,5 dimethylaniline and 3,5 dimethylphenol with norbornene was conducted. As mentioned previously the hydroamination of 3,5 dimethylaniline with norbornene even at elevated temperatures of 200°C showed approximately 10 mM of product (1 turnover) even after 5 days. However hydroaryloxylation even at 170°C yielded 65% conversion (0.325 M) to the O-H addition product in 2 hours.

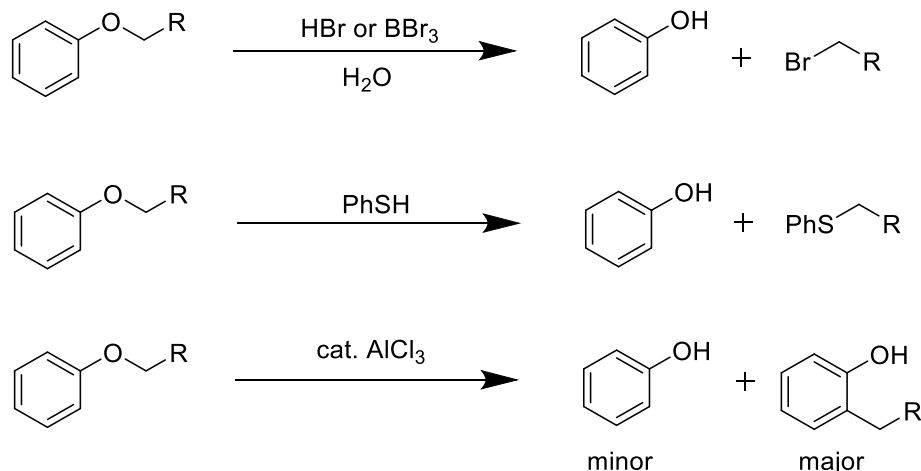


**Scheme 2.18:** Comparison between the addition of phenol and aniline to NBE

## 2.4 Catalytic ether cleavage using pincer-ligated iridium catalysts

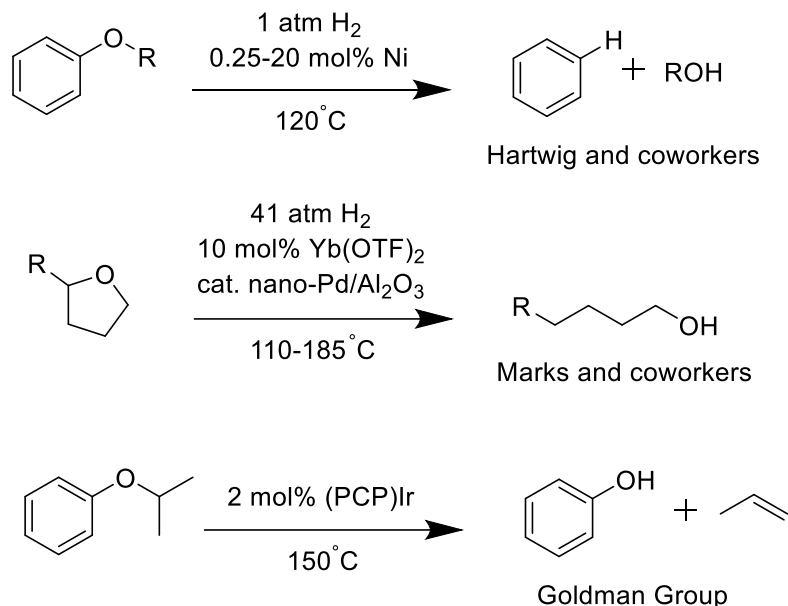
### (dehydroaryloxylation)

The cleavage of alkyl aryl ethers or dehydroaryloxylation also has many potential applications such as the reduction of biomass<sup>27</sup> and as a synthetic tool in organic chemistry.<sup>28</sup> The stability of lignocellulosic biomass can largely be attributed to the stability of its ether bonds. Alkyl aryl ethers are also commonly used in organic chemistry as protecting groups and in many cases harsh conditions are needed in order to remove them such as strong Lewis acids or stoichiometric amounts of strong nucleophiles.



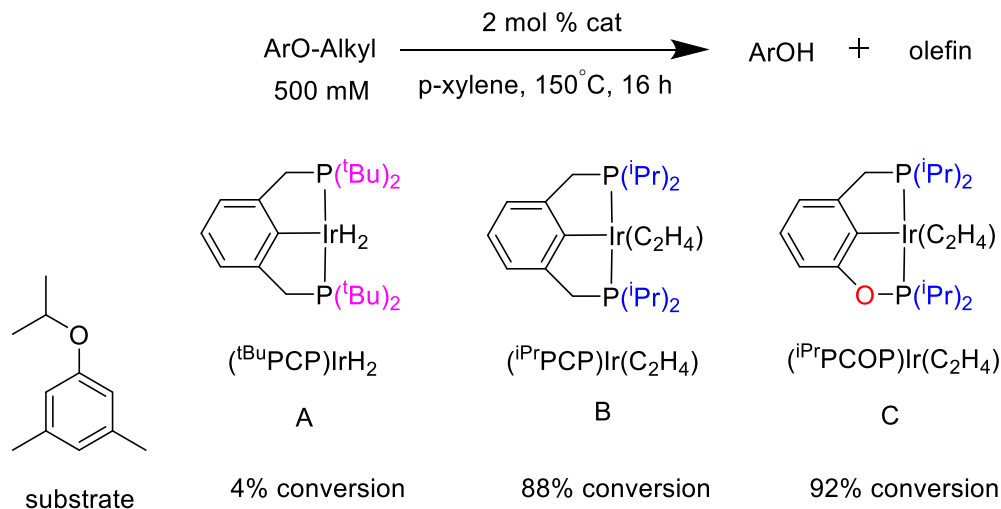
**Scheme 2.19:** Examples of common synthetic C-O bond cleavage reactions

Current methods for catalytic ether cleavage focus mainly on the use of hydrogen, a non-renewable carbon based input. In many cases the pressures and temperatures used for these reactions are far too high to be used in a laboratory setting. Recently, examples of dehydroaryloxylation reactions without the use of high pressures of hydrogen gas have been reported. Marks has reported the catalytic ring opening of cyclic ethers using  $\text{Yb}(\text{Otf})_3$  wherein he proposes the initial formation of alkenols protonated by palladium nanoparticles thus overcoming the energetics of the ring opening.<sup>29</sup> Additionally, Hartwig has reported Nickel based catalysts that are able to cleave alkyl aryl ethers at the aryl C-O bond under the use of 1 atmosphere of hydrogen.<sup>30</sup> To our knowledge we have reported the first known catalytic ether cleavage/dehydroaryloxylation that is atom economical in that no external reagents are needed included hydrogen gas.



**Scheme 2.20:** Examples of transition metal based catalytic C-O bond cleavages

During our study of hydroaryloxylation of phenols to simple olefins it was observed that the reverse reaction, the cleavage of C-O bonds was also catalytic. Our group previously showed that the reaction of (<sup>t</sup>BuPCP)Ir with ethyl phenyl ether or isopropyl phenyl ether resulted in the stoichiometric formation of (<sup>t</sup>BuPCP)Ir(H)(OH) and free olefin. When this reaction was run catalytically (2% (<sup>t</sup>BuPCP)IrH<sub>2</sub> and 0.5 M of 1-isopropoxy-3,5-dimethylbenzene) at 150°C only 4% conversion was observed. As was the case with the forward hydroaryloxylation reaction the use of less sterically hindered catalysts such as (<sup>i</sup>PrPCP)Ir(C<sub>2</sub>H<sub>4</sub>) or (<sup>i</sup>PrPOCP)Ir(C<sub>2</sub>H<sub>4</sub>) showed considerably better activity. After 16 hours ether cleavage with 88% and 92% conversion respectively was observed. The only products of the reaction were olefin and the corresponding phenol with no Friedel Crafts alkylation side products observed.



**Scheme 2.21:** Cleavage of isopropyl phenyl ether using various pincer iridium complexes

The scope of the dehydroaryloxylation reaction was explored by studying the cleavage of multiple alkyl aryl phenols (Figure 2.10) and functional group tolerance was observed in most cases. In general above 70% conversion was observed within 16-48 hours when using 2% catalyst loading at 150°C. In the case of p-methoxyphenyl isopropyl ether no cleavage of the para-methoxy group was observed. In the case 1-(sec-butoxy)-3,5-dimethylbenzene 99% conversion was acquired but longer reaction times (240 hours) were needed. Despite the slower initial reactivity when compared to the corresponding isopropyl ether (41% vs 72% after 4 hours), the 2-butyl ether reaction also proceeds to full conversion.



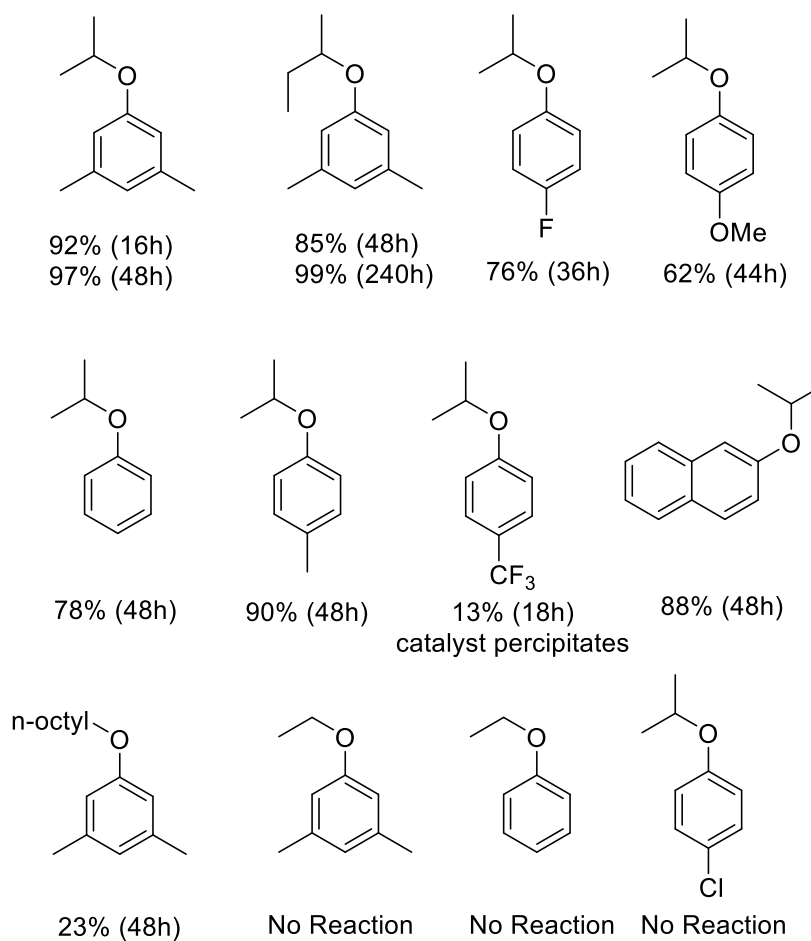
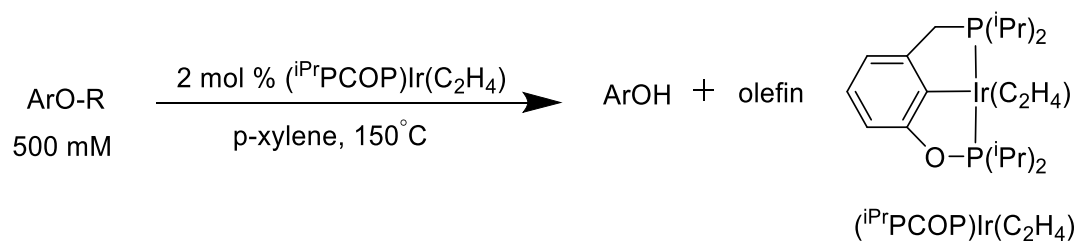


**Figure 2.10:** Substrate scope of cleavage of alkyl aryl ethers

Not all of the alkyl aryl ethers synthesized show activity for ether cleavage nor were all functional groups tolerated. Ethers with long alkyl chains such as n-octyl showed lower reactivity with only 23% conversion after 48 hours. Functional groups

including para CF<sub>3</sub> or chloro groups showed lower reactivity or none at all. In the para-chloro case we hypothesize C-Cl activation deactivates the catalyst. Ethyl aryl ethers showed no reactivity toward ether cleavage even after extended heating.

When these reactions were heated to 200°C the reactions ran at a much faster rate (Figure 2.11).

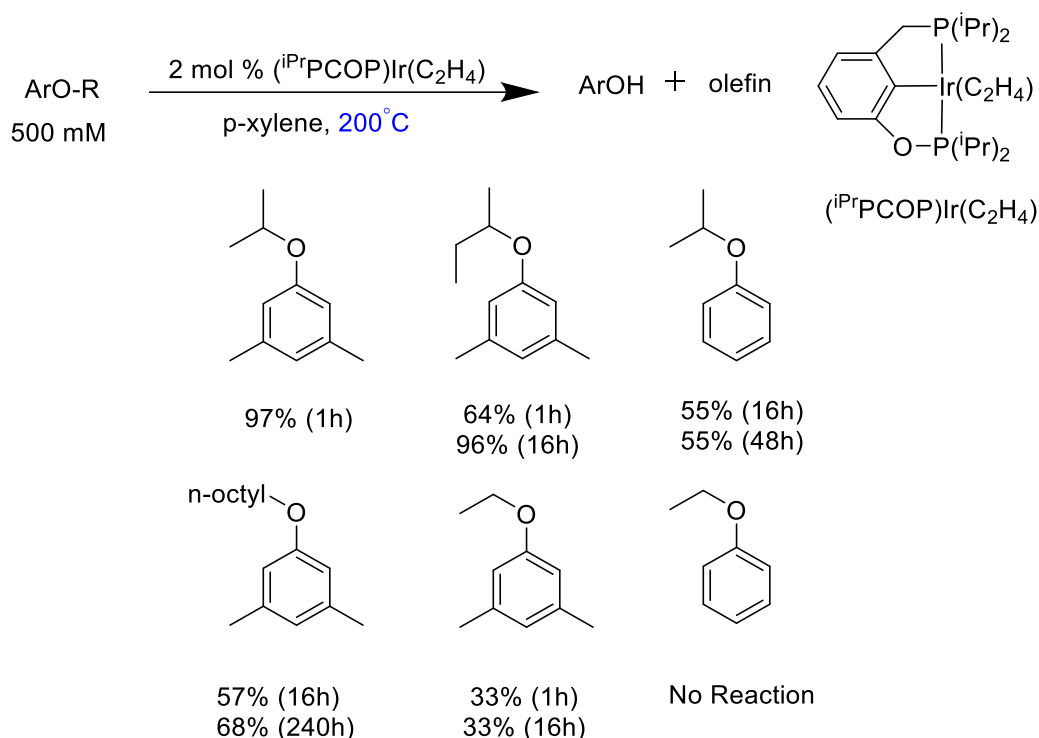


**Figure 2.11:** Substrate scope of cleavage of alkyl aryl ethers at 200°C

The rate of cleavage of 1-isopropoxy-3,5-dimethylbenzene increased from 72% conversion after 4 hours at 150 °C to 97% conversion after 1 hour at 200°C . This increased rate was also observed for the 2-butyl and n-octyl analogues.

The mechanism of ether cleavage is the reverse of the forward reaction (hydroaryloxylation). The various rates observed for ether cleavage with different aryl

substituents helped reinforce the previous data that would suggest the olefin de-insertion (olefin insertion for hydroaryloxylation) is the rate limiting step. Furthermore primary alkyl transition metal complexes are thermodynamically more favored than the corresponding secondary alkyls. This would explain the higher reactivity for  $i\text{PrOAr}$  and 2-BuOAr where  $R_2=\text{H}$  instead n-BuOAr and n-OctOAr where  $R_2 = \text{alkyl}$  (Figure 2.10). Additionally the binding energy of propene would be less sterically demanding than 1-butene contributing to greater reactivity of  $i\text{PrOAr}$  vs. 2-BuOAr. Finally  $i\text{PrOAr}$  would also have two different primary carbon positions that could be activated which should contribute to its higher reaction rate.

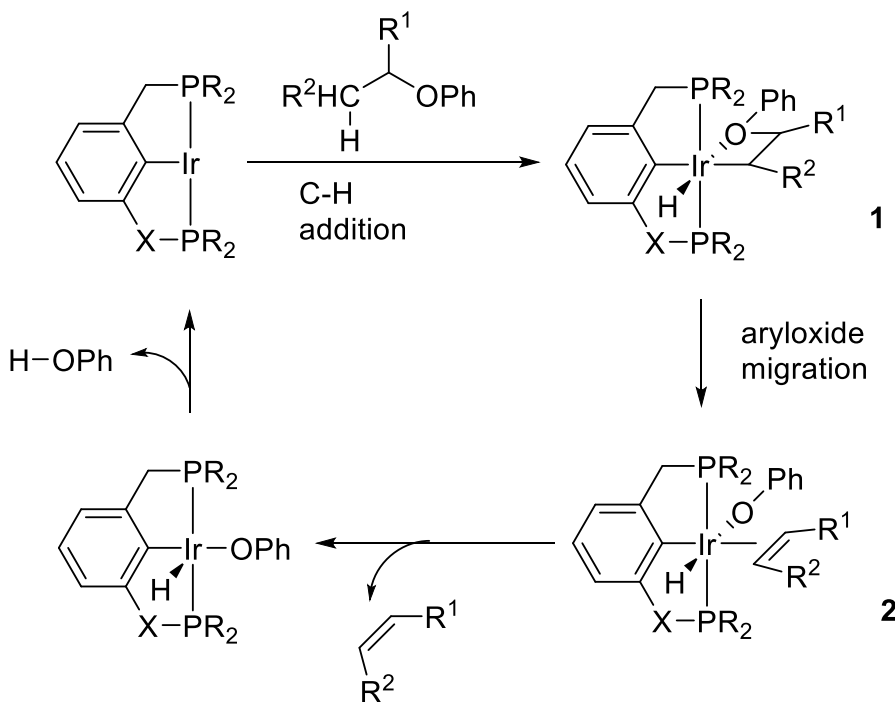


**Figure 2.12:** Mechanism of C-O cleavage of alkyl aryl ethers

## 2.5 Summary

The catalytic addition of phenols to simple olefins using (<sup>i</sup>PrPCOP)IrH<sub>4</sub> was reported. Mechanistic studies showed this reaction occurs via formation of the six coordinate intermediate (<sup>i</sup>PrPCOP)Ir(H)(OH)(olefin). Insertion of the olefin into the Ir-O bond was determined to be the rate limiting step for this reaction via KIE, competition reactions and computational analysis. Unusual non-integer kinetics were observed for phenol determined to be caused by initial intermolecular hydrogen bonding of phenol in nonpolar solvent. The reverse reaction i.e. cleavage of C-O bonds was also observed to be catalytic using (<sup>i</sup>PrPCOP)IrH<sub>4</sub>. Functional group tolerance was observed in most cases with increased reaction rates observed when run at 200°C. The analogous addition of anilines to simple olefins was not found to proceed except for stoichiometric addition of aniline to norbornene. Computational analysis predicts the addition of O-H bonds to be more favorable than N-H bonds by approximately 10 kcal/mol.

## 2.6 Experimental

All manipulations were carried out under argon using standard Schlenk or glovebox techniques. Anhydrous p-xylene was purchased from Sigma-Aldrich and purged with argon before use. Authentic samples of 3,5-dimethylphenol, 2-naphthol, 4-methoxyphenol, 4-methylphenol, 4-fluorophenol, and phenol were purchased from Sigma-Aldrich. 1-isopropoxy-3,5-dimethylbenzene, 1-ethoxy-3,5-dimethylbenzene, 1-(2-butoxy)-3,5-dimethylbenzene, isopropoxybenzene, 2-isopropoxynaphthalene, 4-isopropoxyanisole, 1-fluoro-4-isopropoxybenzene, 1-isopropoxy-4-methylbenzene,

(tBuPCP)IrH<sub>2</sub>, (iPrPCP)Ir(C<sub>2</sub>H<sub>4</sub>), and (iPrPCOP)Ir(C<sub>2</sub>H<sub>4</sub>) were prepared according to the literature, degassed via freeze-pump-thaw cycles, and dried over 4Å. <sup>1</sup>H, <sup>13</sup>C, and <sup>31</sup>P NMR were recorded on 300, 400, and 500 MHz Varian spectrometers and chemical shifts are reported in ppm. <sup>1</sup>H and <sup>13</sup>C NMR are referenced to the residual solvent signals, and <sup>31</sup>P NMR is referenced to an external standard of 85% H<sub>3</sub>PO<sub>4</sub>. GC analyses (FID detection) were conducted on a Varian 430 instrument equipped with a Varian FactorFour capillary column (stationary phase = VF-1ms, dimensions = 15 m x 0.25 mm, film thickness = 0.25 μm). The following method parameters were used:

**General procedure for hydroamination reactions:**

Procedure was run in the same manner as reaction for O-H addition to olefins described in the Goldman reported supporting information<sup>15</sup>. Inside the glovebox, a flame-dried glass vial was charged with 1.0 mL p-xylene solution 10 mM in catalyst, aniline (0.50 mmol, 500 mM), and 5.0 mg C<sub>6</sub>Me<sub>6</sub> (0.031 mmol, 31 mM) and olefin if a solid or liquid (0.5 mmol, 500 mM). The solution was stirred until homogeneous, then divided into 0.10 mL aliquots into sealable glass ampoules (sealed volume 2.3 mL). The ampoules were attached to Kontes valves (total headspace volume 4.6 mL) and removed from the glovebox. The Kontes valves were attached to a vacuum-gas manifold and the solutions inside were frozen with liquid N<sub>2</sub>. In the case where olefin was a liquid or solid the ampoule headspace was evacuated down to a pressure of 0.010 Torr and was sealed with an oxygen torch this decreased the volume by 50%. In the cases where olefin was a gas the headspace was evacuated down to a pressure of 0.010 Torr and then placed under 1 atm of olefin (ethylene or propylene). The ampoule was fully

immersed in liquid N<sub>2</sub>, allowing the olefin to condense. After 1 minute, the ampoule was sealed with an oxygen torch (this decreased the volume by 50% and brought the total pressure to 2 atm).

Each sealed ampoule was carefully allowed to reach room temperature and then placed in a GC oven and heated to the desired temperature. At the desired times, the GC oven was cooled to room temperature and an ampoule was removed and immersed in liquid N<sub>2</sub> to condense the olefin. The ampoule was then cracked open and analyzed by GC, using C<sub>6</sub>Me<sub>6</sub> as the internal standard.

#### **Resting state experiments:**

In an Argon filled glovebox a solution of 3,5 Dimethylphenol (0.5M) and (<sup>i</sup>PrPCOP)Ir(C<sub>2</sub>H<sub>4</sub>) (0.02 M) were prepared using p-xylene as the solvent and the solution was then added to a J. Young tube. This tube was then charged with propylene gas (1 or .4 atm). The solution was allowed to sit at room temperature for one hour. <sup>31</sup>P and <sup>1</sup>H-NMR of the sample were taken at 25 °C. The sample was then heated in the NMR and <sup>31</sup>P and <sup>1</sup>H-NMR spectrum were obtained at 40, 60, 80 and 100 °C respectively.

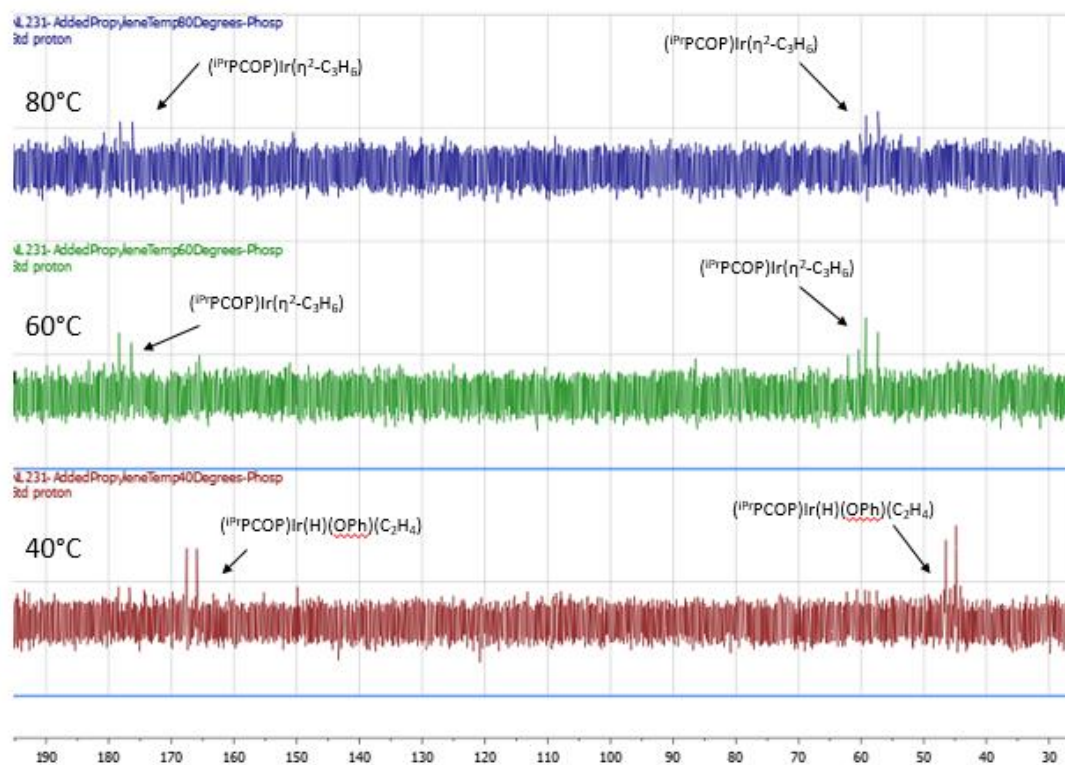


**Figure 2.13:**  $^{31}\text{P}$ -NMR of resting state experiment. Temperature gradually increased from 40 to 80°C

### Kinetic Isotope Effect Studies:

The kinetic isotope effect was studied using two competition reactions. The competition reactions were run in the same manner as the previously stated competition reactions. The first reaction studied was the dehydroaryloxylation of 1-isopropoxy-3,5-dimethylbenzene vs. 1-isopropoxy-4methylbenzene. The second reaction studied was the dehydroaryloxylation of 1,3-dimethyl-5-((propan-2yl-1,1,1,3,3,3- $d_6$ )oxy)benzene vs. 1-isopropoxy-4methylbenzene. The ampoules were cracked open and studied by GC analysis using hexamethylbenzene as the internal standard. The concentrations of the products was calculated by calculating the ratio of

the starting ethers vs. the internal standard and comparing this to the initial zero point measurement.

#### **Kinetic Studies General Procedure:**

Kinetic analysis of the hydroaryloxylation reaction of 3,5-Dimethylphenol and propylene was conducted using flame dried sealable NMR tubes. The reaction vessels used were commercially available NMR tubes with 2 inch glass extensions attached in order to flame seal the tubes. The extended NMR tubes have a volume of 4.5 mL leaving 4 mL of headspace when sample is added. The samples were added to the NMR tubes in an Argon filled glovebox and then connected to Kontes valves and removed from glovebox. The valves were then connected to a vacuum-gas manifold where the samples were frozen using liquid Nitrogen. The NMR tubes were evacuated down to a pressure of 0.011 Torr and then charged with the necessary amount of propylene (between .25 and 2 atm). The tubes were put in liquid Nitrogen to condense the propylene and after about 1 minute were sealed using an oxygen torch. When sealed the volume of the NMR tubes decreases approximately 50% thus doubling the pressure of propylene inside the tube. The NMR tubes were then allowed to reach room temperature and then put in a GC oven (at 150°C) equipped with a rotation device allowing the tube to be stirred while heating. Rotating the tube while in the oven was done in order to ensure good mixing of the propylene into solution. After 2, 4 and 6 hours the tubes were removed from the oven and allowed to reach room temperature. A  $^1\text{H}$ -NMR was taken of each sample which was then put back in the GC oven.



### Kinetic Procedure: Preparation of the Sample

In an Argon filled glovebox stock solutions of 3,5-Dimethylphenol (1 M) and  $(^i\text{PrPCOP})\text{Ir}(\text{C}_2\text{H}_4)$  (0.02 M) were prepared using deuterated p-xylene as the solvent.

Using these stock solutions the reaction samples were prepared. A reaction sample contained 3,5-Dimethylphenol, catalyst, standard and solvent. The standard and solvent used were diphenylmethane and p-xylene  $d_{10}$  respectively.

For the 3,5-Dimethylphenol dependence studies the molarities of the phenol used in the reaction sample were 0.05, 0.1, 0.25 or 0.5 M. In addition to the phenol the reaction samples contained 10  $\mu\text{L}$  of standard (diphenylmethane), catalyst (5 mM) and were charged with 2 atm of propylene.

For the propylene dependence studies the pressures of propylene used were 0.5, 1.0, 2.0 and 4.0 atms. The reaction sample also contained phenol (0.5 M), 10  $\mu\text{L}$  of standard (diphenylmethane) and catalyst (5 mM).

### Hydrogen Bonding Studies of Phenol:

The non-integer order dependence of phenol was hypothesized to be caused by the formation of hydrogen bonding dimers and trimers in non-polar solvent. In order to test this hypothesis a reaction was performed using 2,6-dimethylphenol as a “pseudo solvent”. To run this reaction a stock solution was prepared by weighting 0.153 grams of 2,6-dimethylphenol (2.5 M) and 0.0153 grams of 3,5-dimethylphenol (0.25 M) and dissolving them in 0.5 mL of p-xylene  $d_{10}$ . Additionally 1.35 mg of  $(^i\text{PrPCOP})\text{Ir}(\text{C}_2\text{H}_4)$  (5 mM) and 10  $\mu\text{L}$  of diphenylmethane (internal standard) were added to the stock

solution. The stock solution was transferred to a sealable NMR tube where it was sealed under propylene atmosphere (2 atm) in the same manner as the kinetic studies. The sealed tube was allowed to cool to room temperature and then was transferred to the GC oven (150°C) with the rotation apparatus. At desired times the tube was removed from the GC oven and allowed to cool to room temperature. A  $^1\text{H}$ -NMR was then taken of the sample which was then returned to the GC oven to heat and rotate.

#### **Dehydroaryloxylation General Information:**

3,5-dimethylphenol, 2-naphthol, 4-methoxyphenol, 4-methylphenol, 4-fluorophenol, and phenol were purchased from Sigma-Aldrich. 1-isopropoxy-3,5-dimethylbenzene<sup>31</sup>, 1-ethoxy-3,5-dimethylbenzene<sup>32</sup>, 1-(2-butoxy)-3,5-dimethylbenzene<sup>33</sup>, isopropoxybenzene<sup>34</sup>, 2-isopropoxynaphthalene<sup>35</sup>, 4-isopropoxyanisole<sup>36</sup>, 1-fluoro-4-isopropoxybenzene<sup>37</sup>, 1-isopropoxy-4-methylbenzene<sup>34</sup> were prepared according to the literature, degassed via freeze-pump-thaw cycles, and dried over 4Å.

#### **General Synthetic Procedure for aryl alkyl ether synthesis:**

Phenol (1.2 equivalents), 2-bromopropane (1 equivalent) and  $\text{K}_2\text{CO}_3$  (1.2 equivalents) were dissolved in 25 mL of acetone. The suspension was stirred for 24 hours at reflux. The solution was allowed to cool to room temperature then 25 mL of water and 25 mL of hexane were added to the suspension dissolving any solid in the solution. The organic layer is separated and then washed with 2 M solution of KOH three times, 7%  $\text{NH}_3$  aqueous solution three times, water, brine and is then dried over  $\text{MgSO}_4$ . The solution

was filtered and concentrated under vacuum leaving in most cases a clear liquid product.

#### **General Procedure for Competition Reactions:**

Inside an Argon filled glovebox, a stock solution is prepared in a flame dried vial. The stock solution is comprised of 0.5 mL p-xylene (solvent), hexamethylbenzene (standard, 30.4 mM), (<sup>i</sup>PrPCOP)Ir(C<sub>2</sub>H<sub>4</sub>) (catalyst, 10 mM) and the two ethers being studied (0.25 M each). Next the stock solution was divided into 4 sealable glass ampoules (0.1 mL of stock per ampoule) leaving 0.1 mL of stock for use as a zero time measurement. The ampoules were then attached to Kontes valves and removed from the glovebox. The valves were attached to a vacuum-gas manifold and the solutions were frozen with liquid Nitrogen. The headspace of the ampoules were evacuated to 0.011 torr and then sealed under vacuum using an oxygen torch. The headspace of the ampoule is 4.6 mL before sealing and approximately 2.3 mL after sealing. The sealed ampoules were allowed to cool to room temperature and then were heated in a GC at 150 °C for the desired amount of time. When removed from the GC the ampoules were allowed to cool to room temperature. Next the solution was cooled using liquid nitrogen to condense any gaseous products. The ampoules were cracked open and studied by GC analysis using hexamethylbenzene as the internal standard. The concentrations of the products was calculated by calculating the ratio of the starting ethers vs. the internal standard and comparing this to the initial zero point measurement.

**General Procedure for catalytic ether cleavage using (iPrPCOP)Ir**

Inside an argon glovebox, a stock solution of 500 mM ether, 10 mM (iPrPCOP)Ir(C<sub>2</sub>H<sub>4</sub>) and the C<sub>6</sub>Me<sub>6</sub> standard is prepared in p-xylene. 100  $\mu$ L of stock solution is added to a 5 mL sealable glass ampoule (Wheaton brand Vacules, Sigma-Aldrich), which is then connected to a Kontes high-vacuum adapter via a length of Tygon tubing. The adapter is attached to a vacuum line, the solution frozen in liquid N<sub>2</sub>, and the headspace of the ampoule is evacuated down to 10 mTorr. With the bottom of the ampoule still immersed in liquid N<sub>2</sub>, the neck of the ampoule is sealed using an oxygen torch. The sealed ampoule is allowed to reach room temperature, then heated inside a GC oven for the desired amount of time. Products were identified by comparison with authentic samples of the phenols and concentrations were calculated using the internal standard.

## 2.7 References:

1. Hartwig, J.F. *Organotransition Metal Chemistry: From Bonding to Catalysis*; University Science Books: Sausalito, CA, 2010.
2. Müller, T.E.; Hultsch, K.C.; Yus, M.; Foubelo, F.; Tada, M. *Chem. Rev.* **2008**, *108*, 3795.
3. Brunet, J.J.; Neibecker, D. In *Catalytic Heterofunctionalization from Hydroamination to Hydrozirconation*; Togni, A., Grützmaier, H. Eds, VCH, Weinheim, Germany, 2001, pp 99-141.
4. Wade Jr. L.G. *Organic Chemistry*, 7th ed.; Pearson. New Jersey, **2010**.
5. Tian, S.; Arredondo, V.M.; Stern, C.L.; Marks, T.J. *Organometallics* **1999**, *18*, 2568.
6. (a) Zulys, A.; Panda, T.K.; Gamer, M.T.; Roesky, P.W. *Chem. Commun.* **2004**, 2584-2585. (b) Panda, T.K.; Zulys, A.; Gamer, M.T.; Roesky, P.W. *Organometallics* **2005**, *24*, 2197-2202.
7. Müller, T.E.; Pleier, A-K. *J. Chem. Soc. Dalton Trans.* **1999**, 583-588
8. (a) Walsh, P.J.; Baranger, A.M.; Bergman, R.G. *J. Am. Chem. Soc.* **1992**, *114*, 1708-1719. (b) Baranger, A.M.; Walsh, P.J.; Bergman, R.G. *J. Am. Chem. Soc.* **1993**, *115*, 2753-2763. (c) Walsh, P.J.; Hollander, F.J.; Bergman, R.G. *Organometallics* **1993**, *12*, 3886, *Chemical Reviews*, **2008**, Vol. 108, No. 9 Müller et al. 3705-3723. (d) Lee, S.Y.; Bergman, R.G. *Tetrahedron* **1995**, *51*, 4255-4276. (e) Polse, J.L.; Andersen, R.A.; Bergman, R.G. *J. Am. Chem. Soc.* **1998**, *120*, 13405-13414.
9. Pohlki, F.; Dove, S. *Angew. Chem. Int. Ed.* **2001**, *40*, 2305-2308.
10. Luconi, L.; Rossin, A.; Motta, A.; Tuci, G.; Giambastiani, G. *Chem. Eur. J.* **2013**, *19*, 4906 – 4921.
11. Pierson, J.M.; Ingalls, E.L.; Vo, R.D.; Michael, F.E.; *Angew. Chem. Int. Ed.* **2013**, *52*, 13311 –13313.
12. Goldfogel, M.J.; Roberts, C.C.; Meek, S.J. *J. Am. Chem. Soc.* **2014**, *136*, 6227–6230.
13. Zhao, J.; Goldman, A.S.; Hartwig, J.F. *Science* **2005**, *307*, 1080-1082.
14. Kanzelberger, M.; Zhang, X.; Emge, T. J.; Goldman, A. S.; Zhao, J.; Incarvito, C.; Hartwig, J. F. *J. Am. Chem. Soc.* **2003**, *125*, 13644.
15. Haibach, M.C.; Guan, C.; Wang, D.Y.; Li, B.; Lease, N.; Steffens, A.; Krogh-Jespersen, K.; Goldman, A.S.; *J. Am. Chem. Soc.* **2013**, *135*, 15062-15070.
16. Moulton, C. J.; Shaw, B. L. *J. Chem. Soc., Dalton Trans.* **1976**, 1020.
17. A. L. Casalnuovo, J. C. Calabrese, D. Milstein, *J. Am. Chem.Soc.* **1988**, *110*, 6738
18. Haggins, J. *Chem. Eng. News* **1993**, *71* (22), 23–27.
19. Fiege, H.; Voges, H.-W.; Hamamoto, T.; Umemura, S.; Iwata, T.; Miki, H.; Fujita, Y.; Buysch, H.-J.; Garbe, D.; Paulus, W. In *Ullmann's Encyclopedia of Industrial Chemistry*; Wiley-VCH: Weinheim, Germany, 2000.
20. Williamson, A. *Philos. Mag.* **1850**, *37*, 350–356
21. Sowa, F. J.; Hinton, H. D.; Nieuwland, J. A. *J. Am. Chem. Soc.* **1932**, *54*, 3694–3698.
22. Yang, C.-G.; He, C. *J. Am. Chem. Soc.* **2005**, *127*, 6966–6967
23. Hintermann, L. In *C-X Bond Formation*; Vigalok, A., Ed.; Springer: Berlin, Heidelberg: 2010; Vol. 31, pp 123–155.

24. Dang, T. T.; Boeck, F.; Hintermann, L. *J. Org. Chem.* **2011**, *76*, 9353–9361.
25. Kundu, S.; Choi, J.; Wang, D. Y.; Choliy, Y.; Emge, T. J.; Krogh-Jespersen, K.; Goldman, A. S. *J. Am. Chem. Soc.* **2013**, *135*, 5127–5143.
26. Woolley, E.M.; Travers, J.G.; Erno, B.P.; Hepler, L.G. *J. Phys. Chem.*, Vol. 76, No. 93, **1971**, 3591.
27. a) J. Zakzeski, P. C. A. Bruijninx, A. L. Jongerius, B. M. Weckhuysen, *Chem. Rev.* **2010**, *110*, 3552 – 3599; b) A. M. Ruppert, K. Weinberg, R. Palkovits, *Angew. Chem.* **2012**, *124*, 2614 – 2654; *Angew. Chem. Int. Ed.* **2012**, *51*, 2564 – 2601; For recent examples of catalytic approaches to CO bond cleavage in lignin and model compounds, see: c) S. Son, F. D. Toste, *Angew. Chem.* **2010**, *122*, 3879 – 3882; *Angew. Chem. Int. Ed.* **2010**, *49*, 3791 – 3794; d) J. M. Nichols, L. M. Bishop, R. G. Bergman, J. A. Ellman, *J. Am. Chem. Soc.* **2010**, *132*, 12554 – 12555; e) S. K. Hanson, R. Wu, L. A. Silks, *Angew. Chem.* **2012**, *124*, 3466 – 3469; *Angew. Chem. Int. Ed.* **2012**, *51*, 3410 – 3413; f) J. M. W. Chan, S. Bauer, H. Sorek, S. Sreekumar, K. Wang, F. D. Toste, *ACS Catal.* **2013**, *3*, 1369 – 1377.
28. T. W. Greene, P. G. Wuts, J. Wiley, *Protective Groups in Organic Synthesis*, Vol. 168, Wiley, New York, 1999.
29. a) A. C. Atesin, N. A. Ray, P. C. Stair, T. J. Marks, *J. Am. Chem. Soc.* **2012**, *134*, 14682 – 14685; b) R. S. Assary, A. C. Atesin, Z. Li, L. A. Curtiss, T. J. Marks, *ACS Catal.* **2013**, *3*, 1908 – 1914; c) Z. Li, R. S. Assary, A. C. Atesin, L. A. Curtiss, T. J. Marks, *J. Am. Chem. Soc.* **2014**, *136*, 104 – 107.
30. a) A. G. Sergeev, J. F. Hartwig, *Science* **2011**, *332*, 439 – 443; b) A. G. Sergeev, J. D. Webb, J. F. Hartwig, *J. Am. Chem. Soc.* **2012**, *134*, 20226 – 20229; Other reports that may be mechanistically related.
31. Wolter, M.; Nordmann, G.; Job, G.E.; Buchwald, S. L. *Org. Lett.* **2002**, *4*, 973-976.
32. Naidu, A.B.; Jaseer, E.A.; Sekar, G. *J. Org. Chem.* **2009**, *74*, 3675-3679.
33. Tateiwa, J.-i.; Nishimura, T.; Horiuchi, H.; Uemura, S. *J. Chem. Soc., Perkin Trans. 1* **1994**, 3367-3371.
34. Olson, W.T.; Hipsher, H.F.; Buess, C.M.; Goodman, I.A.; Hart, I.; Lamneck, J.H.; Gibbons, L.C. *J. Am. Chem. Soc.* **1947**, *69*, 2451-2454.
35. Barbasiewicz, M.; Szadkowska, A.; Makal, A.; Jarzemska, K.; Woźniak, K.; Grela, K. *Chem–Eur. J.* **2008**, *14*, 9330-9337.
36. Siegman, J.R.; Houser, J.J. *J. Org. Chem.* **1982**, *47*, 2773-2779.
37. Jones, B. *J. Chem. Soc.* **1938**, 1414-1417.

### Chapter 3

#### Synthesis and Reactivity of pincer-ligated osmium complexes

##### Abstract:

The dehydrogenation of alkanes to olefins is a valuable commercial process as olefins are key precursors in many synthetic pathways. Pincer-ligated iridium catalysts such as ( $R^4$ PCP)Ir are some of the most active catalysts for alkane dehydrogenation with strong regioselectivity for formation of  $\alpha$  olefins. ( $R^4$ PNP)Os complexes are isoelectronic to ( $R^4$ PCP)Ir and have access to a greater number of oxidation states relative to iridium that could improve catalytic activity. Herein we report the synthesis and characterization of ( $R^4$ PNP)Os complexes and their unique properties compared to ( $R^4$ PCP)Ir. Alkane dehydrogenation using ( $R^4$ PNP)Os complexes were unsuccessful as decomposition of the catalyst occurs when heated in the presence of olefin. Computational analysis shows osmium binds hydrogen and olefins much stronger than iridium. This increased binding strength makes hydrogenation of sacrificial olefin difficult preventing alkane dehydrogenation. ( $R^4$ PNP)Os complexes have shown catalytic activity for hydrogenation of ketones and olefins, dehydrogenation of alcohols, dehydrogenative coupling of styrene as well as small molecule activations of carbon monoxide and dinitrogen.

**Portions of this chapter are reproduced with permission form the following articles.**

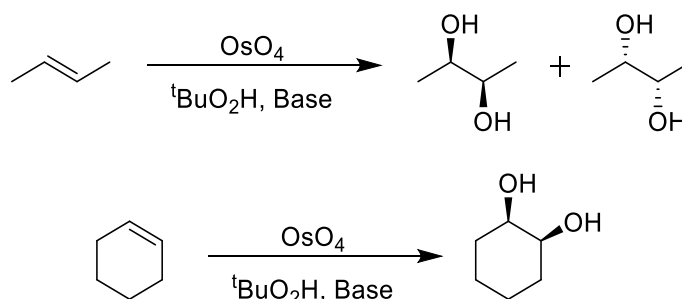
Nicholas Lease, Elizabeth M. Pelczar, Tian Zhou, Santanu Malakar, Thomas J. Emge, Faraj Hasanayn, Karsten Krogh-Jespersen and Alan S. Goldman. *Organometallics*. **2018**

37, 314. Copyright 2018 American Chemical Society

### 3.1 Introduction

Homogenous late transition metal catalysis has long been dominated by use of certain metals. Complexes containing palladium, platinum, ruthenium, rhodium and iridium are extensively explored in organometallic chemistry. Examples of homogenous catalysis using osmium metal complexes are far less reported than other late transition metals. Advantages of using osmium include access to multiple oxidation states as well as strong ligand binding as osmium is a third row transition metal.<sup>1</sup>

Perhaps the most famous example of homogenous osmium chemistry is the oxidation of alkenes to form diols using  $\text{OsO}_4$ . It has been reported by Sharpless that using potassium ferricyanide as a reoxidant, the oxidation of alkenes using  $\text{OsO}_4$  can be catalytic.<sup>2</sup>  $\text{OsO}_4$  however is a volatile liquid with high toxicity making it less than ideal to work with.



**Scheme 3.1:** Alkene oxidation using  $\text{OsO}_4$

The earliest report of monodentate homogenous osmium catalysis was reported by Vaska and Mitchell who demonstrated  $\text{OsHCl}(\text{CO})(\text{PPh}_3)_3$  was capable of hydrogenation of C=C bonds.<sup>3,4</sup> Chatt and coworkers were then able to demonstrate that complexes



$\text{OsH}_2(\text{PEtPh}_2)_4$ ,  $\text{OsH}_2(\text{CO})(\text{PEtPh}_2)_3$ , and  $\text{OsH}_4(\text{PEtPh}_2)_3$  were able to isomerize and hydrogenate octenes.<sup>5</sup>

More recent work has shown that homogenous osmium complexes are very effective catalysts for the dehydrogenation of alcohols and hydrogenation of ketones. Osmium complexes containing monophosphines<sup>6</sup>, bidentate phosphines<sup>7</sup>, and bidentate amines<sup>8</sup> have all been reported to undergo transfer hydrogenation of ketones and aldehydes.

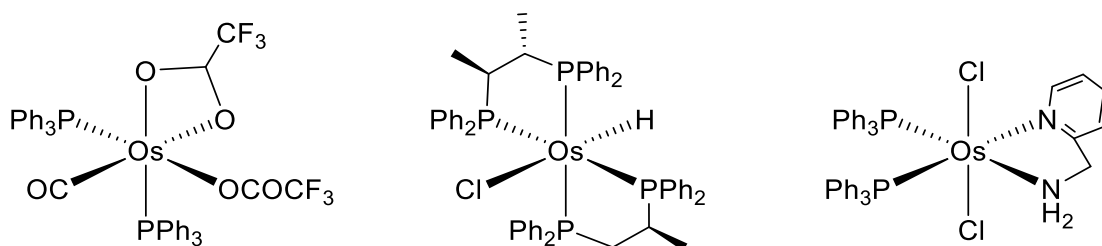
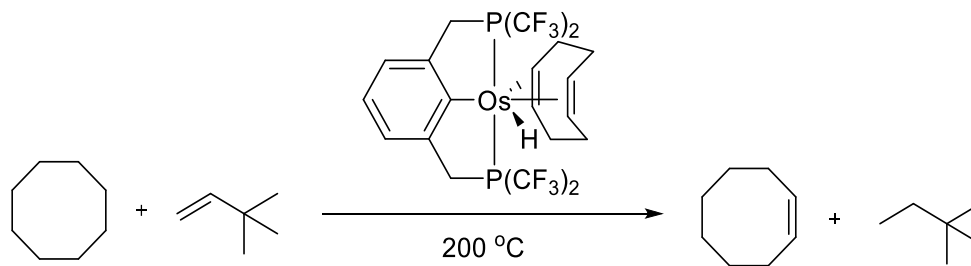


**Figure 3.1:** Monodentate and bidentate osmium complexes

Tridentate ligands including pincer ligands have also been reported with osmium for catalytic hydrogenation of ketones. Complexes containing pincer-ligated CNN ligands have been shown to be very effective in the hydrogenation of ketones (acetone, hex-5-en-2-one).<sup>9</sup> Additionally osmium complexes ligated with the <sup>i</sup>PrMACHO ligand demonstrated activity to hydrogenate acetophenone and 1-cyclohexylethan-1-one in polar solvents.<sup>10</sup> More recently pybox ((2,6-Bis[(4S)-4-isopropyl-2-oxazoliny]pyridine) ligated osmium complexes have been reported to hydrogenate acetophenone and benzophenone.<sup>11</sup> Osmium complexes containing (<sup>R4</sup>PCP)<sup>12</sup>, (PSiNSiP)<sup>13</sup> and (<sup>R4</sup>POP)<sup>14</sup> ligands have been reported.

While the dehydrogenation and hydrogenation of alcohols and ketones has been studied extensively using osmium complexes, there are few reports of alkane dehydrogenation. In 2013, Roddick reported the transfer dehydrogenation of cyclooctane using TBE by a ( $\text{CF}_3\text{PCP}$ )Os(II) complex.<sup>15</sup> He reported that while not as active as the ruthenium analogy the osmium complex provided better stability resulting in overall larger turnover numbers.



While osmium complexes using (<sup>Ph</sup>PNP) have been reported none have ever been reported using the (<sup>t</sup>BuPNP) ligand system. In 2002 Milstein introduced the <sup>t</sup>Bu<sup>4</sup>PNP ligand<sup>16</sup> (<sup>R</sup><sup>4</sup>PNP = η<sup>3</sup>-C<sub>5</sub>NH<sub>3</sub>-2,6-(CH<sub>2</sub>PR<sub>2</sub>)<sub>2</sub>) and subsequently reported an extraordinarily rich body of chemistry<sup>18</sup>, particularly with complexes of Ru<sup>17</sup> and Fe<sup>18</sup>, but also Rh<sup>19</sup>, Ir<sup>20</sup>,

Pd and Pt<sup>21</sup>. The chemistry of the fragment (<sup>R4</sup>PNP)Os<sup>22</sup> has been much less explored and is of particular interest based on its isoelectronic relationship to (<sup>R4</sup>PCP)Ir

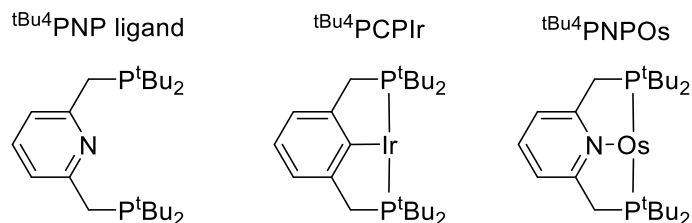


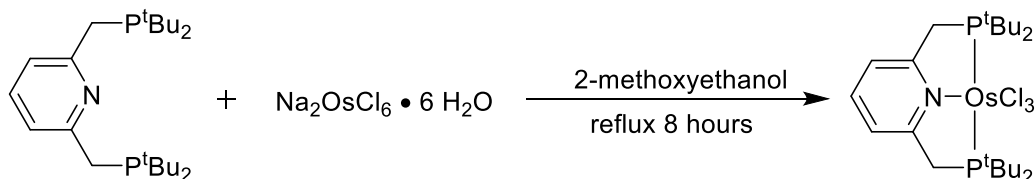
**Figure 3.3:** (<sup>tBu</sup>PNP) ligand and isoelectronic structures of (<sup>tBu</sup>PCP)Ir and (<sup>tBu</sup>PNP)Os

Many complexes with the tridentate "PCP" motif have been synthesized and extensively investigated.<sup>23</sup> Such complexes include the most effective catalysts reported to date for the dehydrogenation of alkanes<sup>24</sup> and they have been reported to effect numerous other stoichiometric and catalytic reactions involving the cleavage of C-H bonds.<sup>25</sup> The ability of (PCP)Ir(I) fragments to oxidatively add C-H bonds is clearly key to much of their C-H activation chemistry. (PNP)Os(0) fragments might be expected to add C-H bonds even more favorably, assuming that the C-H "oxidative additions" are oxidative in more than a purely formal sense.<sup>26</sup> Herein we report the synthesis and investigation of (<sup>tBu</sup>PNP)Os complexes. We focus in particular on the comparison with isoelectronic (<sup>tBu</sup>PCP)Ir and (<sup>tBu</sup>PNP)Ir<sup>+</sup> units, and we attempt to achieve an understanding of principles underlying the relationships between the chemistry of such isoelectronic ligand-metal units.

### 3.2 PNP-Pincer Complexes of Osmium. Comparison with Isoelectronic (PCP)Ir and (PNP)Ir<sup>+</sup> Units

### 3.2.1 Synthesis and structural characterization of precursors (<sup>t</sup>Bu<sup>4</sup>PNP)OsCl<sub>3</sub> and (<sup>t</sup>Bu<sup>4</sup>PNP)OsH<sub>4</sub>

We began our study with the metalation of <sup>t</sup>Bu<sup>4</sup>PNP by its reaction with Na<sub>2</sub>OsCl<sub>6</sub> • 6H<sub>2</sub>O in 2-methoxyethanol, following the work of Zaoying who reportedly synthesized (<sup>Ph</sup>4PNP)OsCl<sub>2</sub>.<sup>22a</sup>



**Scheme 3.3:** Synthesis of (<sup>t</sup>Bu<sup>4</sup>PNP)OsCl<sub>3</sub> (**1-Cl<sub>3</sub>**)

<sup>1</sup>H and <sup>31</sup>P NMR spectroscopy of the recrystallized product indicated it to be a paramagnetic <sup>t</sup>Bu<sup>4</sup>PNP complex (see Experimental). Elemental analysis was consistent with its formulation as (<sup>t</sup>Bu<sup>4</sup>PNP)OsCl<sub>3</sub> (Scheme 3.3), **1-Cl<sub>3</sub>**, which was confirmed by single crystal X-ray diffraction (Figure 3.4). The structure was found to be approximately octahedral, with inter-ligand angles between 89.4° and 90.8° in the plane perpendicular to the P-P axis and Os-Cl bond distances 2.36 Å to 2.38 Å, consistent with reported Os(III) chloride complexes,<sup>27</sup> including analogous (POP)OsCl<sub>3</sub> complexes reported by Asensio, Esteruelas and co-workers.<sup>28</sup> Electronic structure calculations (DFT method employing the PBE exchange-correlation functional, the SDD effective core potential and associated basis set for transition metal atoms Os and Ir, and all-electron 6-311G(d,p) basis sets for all other atoms; predict a doublet ground state for **1-Cl<sub>3</sub>** while the lowest quartet state is over 40 kcal/mol higher in energy.

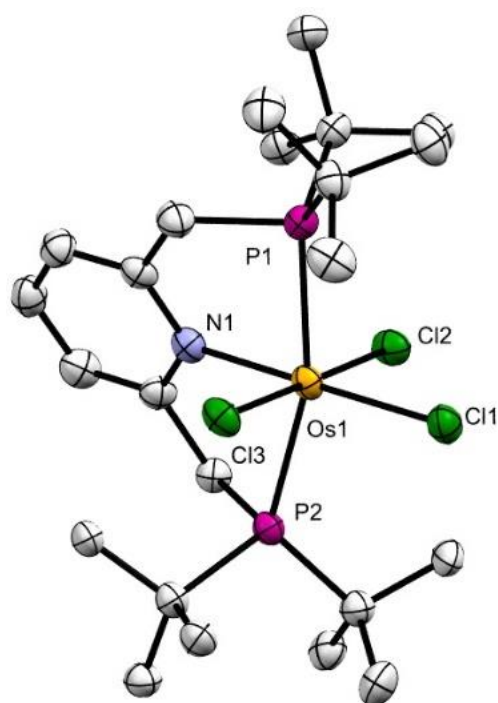


**Figure 3.4** ORTEP representation (50% probability ellipsoids) of the structure of **1-Cl<sub>3</sub>** determined by X-ray diffraction; hydrogen atoms omitted for clarity. Calculated structure of **1-Cl<sub>3</sub>** possesses  $C_2$  symmetry.

**Table 3.1** Selected Experimental and Computed Bond Distances (Å) and Angles (Deg) for **1-Cl<sub>3</sub>**

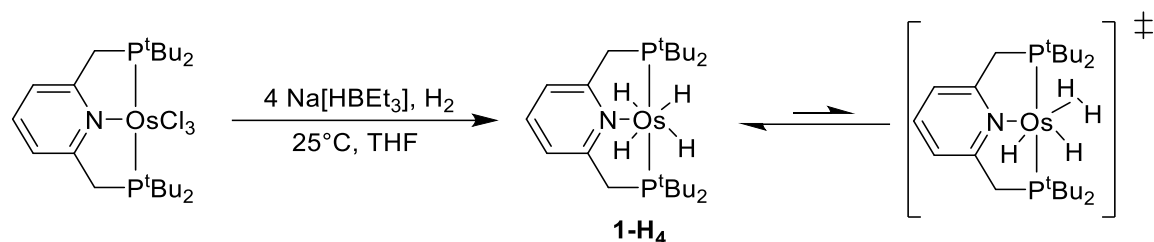
Parameter	Exp.	Calc.	Parameter	Exp.	Calc.
Os(1)-N(1)	2.067(7)	2.091	Os(1)-Cl(3)	2.3606(19)	2.416
Os(1)-Cl(2)	2.371(2)	2.481	Os(1)-Cl(1)	2.376(2)	2.381
Os(1)-P(2)	2.438(2)	2.427	Os(1)-P(1)	2.445(2)	2.427
N(1)-Os(1)-Cl(3)	89.3(2)	86.8	N(1)-Os(1)-Cl(2)	89.48(19)	86.8
Cl(3)-Os(1)-Cl(1)	90.82(5)	93.2	Cl(2)-Os(1)-Cl(1)	90.38(8)	93.2
N(1)-Os(1)-P(2)	80.8(2)	82.2	N(1)-Os(1)-P(1)	80.9(2)	82.2
Cl(3)-Os(1)-P(1)	87.71(8)	87.8	Cl(2)-Os(1)-P(1)	92.41(8)	87.8
Cl(1)-Os(1)-P(1)	98.62(8)	97.8	P(2)-Os(1)-P(1)	161.72(7)	164.5

**1-Cl<sub>3</sub>** was allowed to react with 4 equiv of sodium triethylborohydride in THF under hydrogen atmosphere. Removal of solvent gave a dark red solid which was dissolved in benzene to give a red solution. Addition of pentane precipitated a solid; filtration and

drying with an argon flow yielded yellow crystals. The  $^{31}\text{P}$  NMR spectrum of a toluene- $d_8$  solution of the sample showed one signal at  $\delta$  76.9 ppm. The  $^1\text{H}$  NMR spectrum, in addition to signals attributable to the coordinated  $^t\text{Bu}_4\text{PNP}$  ligand, at room temperature (r.t.) revealed a broad signal at -8.7 ppm. At 60 °C this signal appeared as a sharp triplet ( $J = 12$  Hz) which integrated to 4H. Additionally, at 60 °C the selectively (ca.  $\delta$  0 –  $\delta$  10 ppm)  $^1\text{H}$ -decoupled  $^{31}\text{P}$  NMR spectrum revealed a quintet at  $\delta$  77.2 ppm.

When the solution was cooled, the signal in the  $^1\text{H}$  NMR spectrum at  $\delta$ -8.7 ppm broadened, until it was fully lost in the baseline at -20°C. Upon further cooling to -80 °C, two broad but easily discernible signals at  $\delta$  -5.04 ppm and  $\delta$  -11.97 ppm were observed, which each integrated to 2H. The NMR data are all consistent with formulation of this complex as  $(^t\text{Bu}_4\text{PNP})\text{Os}(\text{H})_4$  (**1-H<sub>4</sub>**),<sup>29</sup> with rapid exchange between the two inequivalent sets of hydrides occurring at the higher temperatures, presumably via reversible formation of a transient species  $(^t\text{Bu}_4\text{PNP})\text{Os}(\text{H})_2(\text{H}_2)$  and rotation of the dihydrogen ligand about the Os-H<sub>2</sub> axis (Scheme 3.4). Determination of the exchange rates based on NMR line shapes (using the gNMR simulation program<sup>30</sup>) gives  $\Delta G^\ddagger = 9.0$  kcal/mol at 25 °C, while exchange rates from -65 °C to 25 °C yield activation parameters  $\Delta H^\ddagger = 10.2 \pm 1.6$  kcal/mol and  $\Delta S^\ddagger = -4 \pm 6$  eu.

$T_{1\text{ min}}$  measurements were conducted for the coalesced hydride peak in the  $^1\text{H}$  NMR spectrum in the temperature range from 25 °C to 0 °C and for the individual peaks at  $\delta$  -5.04 ppm and  $\delta$  -11.97 ppm from -40 °C to -65 °C. The respective  $T_{1\text{ min}}$  values for these peaks (determined on a 400-MHz NMR spectrometer) were 132 ms and 144 ms, consistent with formulation of **1-H<sub>4</sub>** as a classical tetrahydride.<sup>31</sup>



**Scheme 3.4:** Synthesis of (<sup>t</sup>BuPNP)OsH<sub>4</sub> (**1-H<sub>4</sub>**)

A single-crystal X-ray diffraction experiment confirmed the proposed structure of **1-H<sub>4</sub>** (Figure 3.5). The residual electron density map clearly shows the presence of the four hydride ligands and allows a determination of H-H distances of 1.75(5) Å (H(1)-H(2)) and 1.78(7) Å (H(1)⋯H(1A)). The Os-(H1) (endo) and Os-(H2) (exo) distances are determined to be 1.60(2) Å and 1.64(2) Å, respectively. These distances may be compared with the Os-H distances of 1.64 – 1.68 Å that were found by neutron diffraction for the four hydrides of Os(PMe<sub>2</sub>Ph)<sub>3</sub>H<sub>4</sub>.<sup>32</sup>

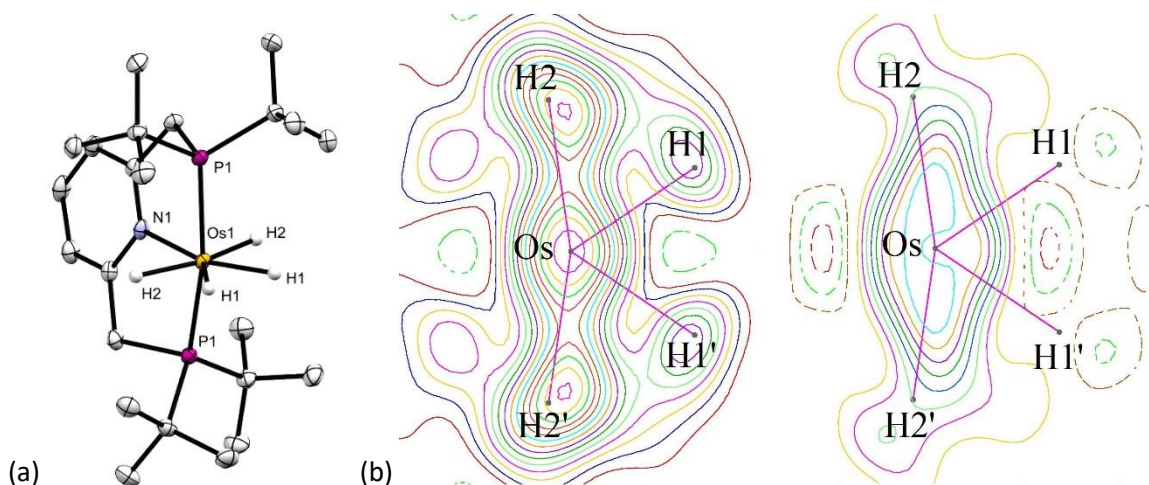


**Figure 3.5** (a) Structure of **1-H<sub>4</sub>** determined by X-ray diffraction. H atoms other than hydrides omitted. (b) Residual electron-density map of the plane containing the four hydrido H atoms before placing them in the model (left) and after (right), with contours drawn at 0.05 e<sup>-</sup>/Å<sup>3</sup> increments, and using data out to 0.95 Å resolution. Dashed lines are negative contours.

**Table 3.2 Selected Experimental and Computed Bond Lengths (Å) and Angles (Deg) for 1-H<sub>4</sub>**

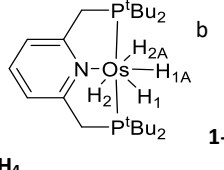
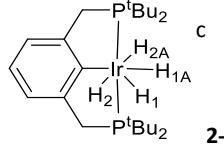
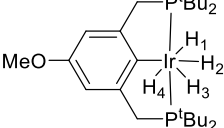
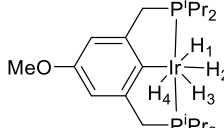
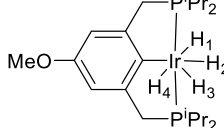
Parameter	Exp.	Calc.	Parameter	Exp.	Calc.
Os-N	2.153(4)	2.190	Os(1)-H(1)(endo)	1.60(2)	1.634
Os-P(1)	2.2877(6)	2.319	Os(1)-H(2)(exo)	1.64(2)	1.695
N-Os-P(1)	82.56(2)	82.3	H(1)-Os-H(1A)	67(3)	61.1
N-Os-H(1)	146.3(15)	149.4	H(1)-Os-H(2)	65(2)	68.2
N-Os-H(2)	81.1(15)	81.3			

The unambiguous tetrahydride character of **1-H<sub>4</sub>**, and the lack of fast exchange on the NMR timescale at -80 °C, contrasts<sup>33</sup> with (<sup>t</sup>BuPCP)IrH<sub>4</sub> (**2-H<sub>4</sub>**)<sup>34</sup> and derivatives.

Metric data from crystallographic studies (including the previously reported neutron diffraction structure of the parent complex<sup>33</sup>), shown in Table 3.3, clearly indicates at least some degree of dihydrogen complex character, or at least a compressed dihydride structure, for **2-H<sub>4</sub>** and derivatives (*p*-MeO-<sup>t</sup>BuPCP)IrH<sub>4</sub><sup>35</sup> and (*p*-MeO-<sup>i</sup>PrPCP)IrH<sub>4</sub>.<sup>36</sup> NMR studies (particularly H-D coupling) supported their assignment as dihydride dihydrogen complexes.<sup>33</sup>



**Table 3.3 Comparison of Crystallographic Data for 1-H<sub>4</sub> with (R<sup>4</sup>PCP)IrH<sub>4</sub> Complexes**

Pincer Complex	H...H Distances (Å) <sup>a</sup>	M-H Distance (Å)	H-M-H Angles (°)
 <b>1-</b> <b>H<sub>4</sub></b>	H(1)···H(2) 1.75(5) <b>H(1)···H(1A) 1.78(7)</b>	Os-H(2) 1.64(2) Os-H(1) 1.60(2)	H(1)-Os-H(2) 65(2) <b>H(1)-Os-H(1A) 67(3)</b>
 <b>2-H<sub>4</sub></b>	H(1)···H(2) 1.92(2) <b>H(1)···H(1A) 1.49(2)</b>	Ir-H(2) 1.697(8) Ir-H(1) 1.546(11)	H(1)-Ir-H(2) 72.4(6) <b>H(1)-Ir-H(1A) 57.5(9)</b>
 <b>b</b>	H(1)···H(2) 1.96(7) <b>H(2)···H(3) 1.47(4)</b> H(3)···H(4) 1.88(4)	Ir-H(1) 1.55(3) Ir-H(2) 1.59(3) Ir-H(3) 1.56(2) Ir-H(4) 1.56(3)	H(1)-Ir-H(2) 80(5) <b>H(2)-Ir-H(3) 55(3)</b> H(3)-Ir-H(4) 74(3)
 <b>b</b> monoclinic	H(1)···H(2) 1.98(6) <b>H(2)···H(3) 1.42(5)</b> H(3)···H(4) 1.70(5)	Ir-H(1) 1.57(2) Ir-H(2) 1.59(2) Ir-H(3) 1.58(2) Ir-H(4) 1.60(2)	H(1)-Ir-H(2) 77(3) <b>H(2)-Ir-H(3) 53(2)</b>
 <b>b</b> triclinic	H(1)···H(2) 1.80(5) <b>H(2)···H(3) 1.30(5)</b> H(3)···H(4) 1.99(4)	Ir-H(1) 1.57(2) Ir-H(2) 1.59(2) Ir-H(3) 1.60(2) Ir-H(4) 1.58(2)	H(1)-Ir-H(2) 69(2) <b>H(2)-Ir-H(3) 49(2)</b> H(3)-Ir-H(4) 77(2)

(a) Endo hydride (those trans to PNP N atom) H--H distances in bold. (b) Structure determined by X-ray diffraction (this work; see SI) (c) Structure determined by neutron diffraction, reference

19.

DFT calculations indicated that tetrahydride and dihydrogen/dihydride forms of **2-H<sub>4</sub>** and derivatives are very close in energy, with the tetrahydride electronic energy minimum slightly lower (1-3 kcal/mol). However, given that this value is small with respect to thermal energy available ( $\sim k_B T$ ) and, importantly, comparable to the zero-point energies, it was concluded that the iridium complexes are “not optimally

characterized in terms of individual well-defined structures [either tetrahydride or dihydrogen dihydride forms]".<sup>33</sup>

Consistent with the experimental data, DFT calculations of **1-H<sub>4</sub>** indicate, in contrast with the iridium complexes, a well-defined tetrahydride energy minimum with a calculated distance between endo hydrides (H1 and H1A in Table 3.3) of 1.66 Å, and an endo-exo distance of 1.87 Å. This minimum, however, is only 7.1 kcal mol lower in Gibbs free energy than a dihydrogen dihydride form (**1-(H<sub>2</sub>)H<sub>2</sub>**) in which the dihydrogen ligand is located cis to the PNP N atom (no energy minimum could be located with a dihydrogen ligand trans to N). The overall barrier to conversion between endo and exo hydride ligands, which proceeds via rotation of the H<sub>2</sub> ligand of **1-(H<sub>2</sub>)H<sub>2</sub>**, is calculated as  $\Delta G^\ddagger = 10.3$  kcal/mol ( $\Delta H^\ddagger = 10.3$  kcal/mol,  $\Delta S^\ddagger = -0.1$  eu) in excellent agreement with the values obtained by dynamic NMR spectroscopy as discussed above.

### 3.2.2 Dissociation of H<sub>2</sub> from **1-H<sub>4</sub>**.

Iridium complexes **2-H<sub>4</sub>** and derivatives readily lose H<sub>2</sub> to afford the corresponding dihydrides, even at room temperature (slowly) under vacuum. Indeed, **2-H<sub>4</sub>** can only be isolated in pure form under H<sub>2</sub> atmosphere; under argon a mixture of **2-H<sub>2</sub>** and **2-H<sub>4</sub>** is obtained.

In marked contrast with the iridium congener, **1-H<sub>4</sub>** reveals no tendency to lose H<sub>2</sub> under ambient conditions. Indeed, we have not been able to isolate or even observe the dihydride. At room temperature no change in the <sup>1</sup>H NMR spectrum of **1-H<sub>4</sub>** is observed upon addition of D<sub>2</sub> to a toluene-d<sub>8</sub> solution. Upon heating to 85 °C under D<sub>2</sub>, loss of the

$^1\text{H}$  NMR hydride signal occurred, following approximately first-order kinetics with a half-life of ca. 1.3 hours. No significant loss of the  $^1\text{H}$  NMR signals attributable to the  $^t\text{Bu}_4\text{PNP}$  ligand was observed under these conditions.

### 3.2.3. Reactions with olefins.

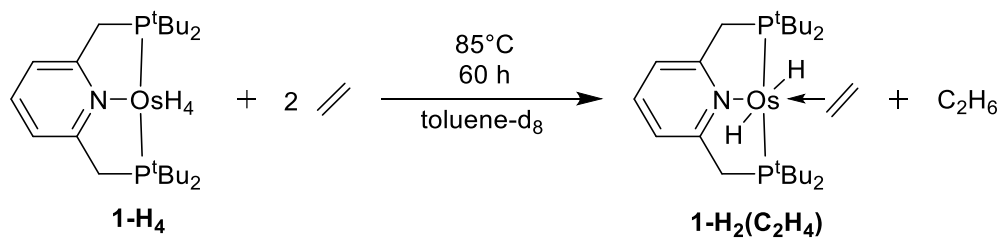
We attempted to catalyze alkane transfer-dehydrogenation with **1-H<sub>4</sub>**, in analogy with the behavior of iridium complex **2-H<sub>4</sub>**. Olefins such as NBE, TBE, or 1-hexene are readily hydrogenated by **2-H<sub>4</sub>** at relatively low temperatures ( $\leq 55\text{ }^\circ\text{C}$ ; in the absence of  $\text{H}_2$  atmosphere). These reactions yield the transient Ir(I) fragment **2** which can effect alkane dehydrogenation or add, reversibly, an additional olefin molecule to afford the corresponding adducts (in the case of TBE, the adduct with **2** is the product of  $\pi$ -vinyl C-H addition).<sup>37</sup>

In contrast with the iridium congener, the reaction of osmium complex **1-H<sub>4</sub>** with NBE or TBE (in the presence of either *n*-octane or cyclooctane) was quite slow, with no reaction observed at room temperature. After prolonged heating at  $100\text{ }^\circ\text{C}$ , loss of signals in both the  $^{31}\text{P}$  NMR and  $^1\text{H}$  NMR spectra were observed and the solution turned dark red. No solid was observed visually, nor was free ligand observed by NMR. Dehydrogenation of alkane was not observed.

Numerous PCP-type pincer iridium hydrides,<sup>38</sup> including **2-H<sub>4</sub>**, are well known to react with ethylene to effect hydrogenation and coordination to give complexes (pincer)Ir(ethylene), which can serve as precursors for the catalytically active 14e pincer-iridium species. In contrast, the reaction of **1-H<sub>4</sub>** with ethylene in toluene- $d_8$  at  $85\text{ }^\circ\text{C}$

afforded, after 60 hours, clean conversion to a single product by  $^{31}\text{P}$  NMR ( $\delta$  45.7 ppm).

The  $^1\text{H}$  NMR spectrum revealed the formation of ethane and signals attributable to a coordinated  $^t\text{Bu}_4\text{PNP}$  ligand, a hydride signal at  $\delta$  -5.39 ppm that integrated to 2 H per  $^t\text{Bu}_4\text{PNP}$ , and a signal ( $\delta$  1.97, 4H) attributable to coordinated ethylene; these data, as well as the  $^{13}\text{C}$  spectroscopic and HSQC data, are consistent with formulation of the product as *trans*-( $^t\text{Bu}_4\text{PNP}$ )Os(H) $_2$ (C $_2$ H $_4$ ) (**1-H $_2$ (C $_2$ H $_4$ )**, Scheme 3.5). Crystals of **1-H $_2$ (C $_2$ H $_4$ )** were obtained by slow evaporation of hexane from a saturated solution and the proposed structure was confirmed by single crystal X-ray diffraction (Figure 3.6).



**Scheme 3.5:** Synthesis of ( $^t\text{Bu}_4\text{PNP}$ )OsH $_2$ (C $_2$ H $_4$ ) (**1-H $_2$ (C $_2$ H $_4$ )**)

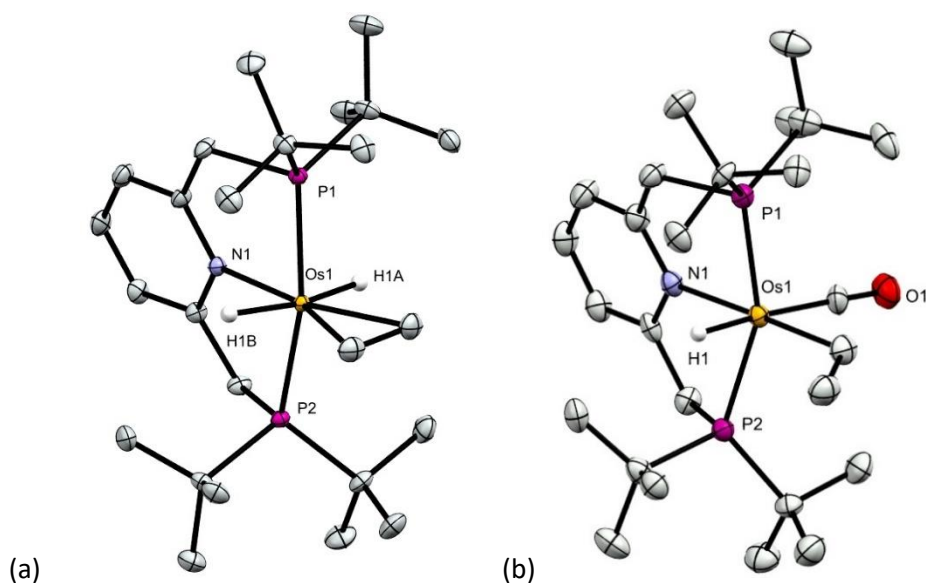
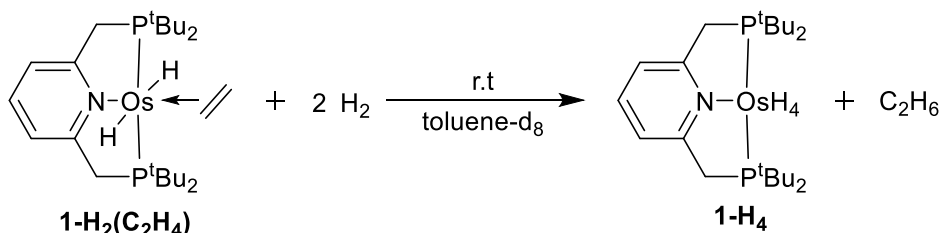


**Figure 3.6** ORTEP representation (50% probability ellipsoids) of the structures of (a) **1-H<sub>2</sub>(C<sub>2</sub>H<sub>4</sub>)** and (b) **1-H(Et)(CO)**, determined by X-ray diffraction. Hydrogen atoms other than hydrides and osmium-bound ethylene and ethyl hydrogen atoms omitted

**1-H<sub>2</sub>(C<sub>2</sub>H<sub>4</sub>)** is stable under argon atmosphere at ambient temperature. Under H<sub>2</sub> atmosphere in toluene, however, it reacts to give **1-H<sub>4</sub>** and ethane as determined by <sup>1</sup>H NMR spectroscopy (Scheme 3.6).



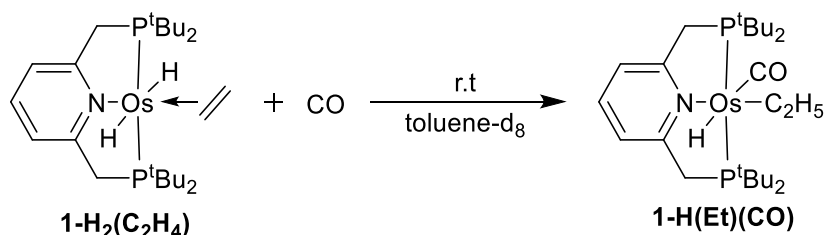
**Scheme 3.6:** Reaction of (**1-H<sub>2</sub>(C<sub>2</sub>H<sub>4</sub>)**) with H<sub>2</sub>

As might be predicted based upon Schemes 3.5 and 3.6 **1-H<sub>2</sub>(C<sub>2</sub>H<sub>4</sub>)** catalyzes the hydrogenation of ethylene under H<sub>2</sub> atmosphere. Within 15 min at 100 °C, a toluene solution of **1-H<sub>4</sub>** (8 mM) under 1 atm ethylene afforded 200 turnovers of ethane (63% conversion).

Kinetic measurements of the reaction in Scheme 3.6 were conducted at 25 °C. Loss of **1-H<sub>2</sub>(C<sub>2</sub>H<sub>4</sub>)** proceeded according to first-order kinetics. Varying the pressure of H<sub>2</sub> from 1 atm to 6 atm gave pseudo-first-order rate constants that were first order in P<sub>H<sub>2</sub></sub> according to eq 1, which corresponds to ΔG<sup>‡</sup> = 21.2 kcal/mol.

$$k_{4\text{-obs}} = 0.00166(6) \text{ s}^{-1} \text{ atm}^{-1} * P_{\text{H}_2} \quad (1)$$

Under 1 atm CO, a toluene solution of **1-H<sub>2</sub>(C<sub>2</sub>H<sub>4</sub>)** reacts at room temperature to give a complex with <sup>1</sup>H and <sup>31</sup>P NMR spectra indicative of the ethyl hydride carbonyl complex (<sup>t</sup>Bu<sup>4</sup>PNP)Os(CO)(H)(C<sub>2</sub>H<sub>5</sub>) (**1-H(Et)(CO)**); Scheme 3.7). Crystals of **1-H(Et)(CO)** were obtained by cooling a saturated hexane solution to -43°C and the proposed structure was confirmed by single crystal X-ray diffraction (Figure 3.6).



**Scheme 3.7:** Synthesis of (<sup>t</sup>Bu<sup>4</sup>PNP)Os(H)(Et)(CO) (**1-H(Et)(CO)**)

Kinetic measurements of the reaction in Scheme 3.7 were conducted at 25 °C, carried out analogously to the reactions of **1-H<sub>2</sub>(C<sub>2</sub>H<sub>4</sub>)** with dihydrogen (Scheme 3.6). As in that case the complex disappeared with first order kinetics, and *k*<sub>6-obs</sub> varied linearly with CO pressure, according to eq 2, which corresponds to a free energy of activation of Δ*G*<sup>‡</sup> = 21.4 kcal/mol. It should be noted that although the reaction rate depends linearly on CO pressure, the rates of reaction with CO and with H<sub>2</sub> are very similar (*k*<sub>6-obs</sub> ≈ 0.75 × *k*<sub>4-obs</sub>), suggestive of reactions that are nearly diffusion controlled.

$$k_{6\text{-obs}} = 0.00125(13) \text{ s}^{-1} \text{ atm}^{-1} * P_{\text{CO}} \quad (2)$$

In the absence of either CO or H<sub>2</sub>, **1-H<sub>2</sub>(C<sub>2</sub>H<sub>4</sub>)** is stable at 25 °C. At elevated temperatures, however, it decomposes to give approximately 1 equiv ethane and the solution turns to the same dark red color that is observed from the reaction of NBE or

TBE with **1-H<sub>4</sub>**. Also as in the case of the reactions of **1-H<sub>4</sub>** with these olefins, a complete loss of signal is observed in the <sup>31</sup>P NMR spectrum and the <sup>1</sup>H NMR spectrum shows only broad peaks; no free PNP ligand is observed in the NMR spectra. Thus the decomposition of **1-H<sub>2</sub>(C<sub>2</sub>H<sub>4</sub>)** appears to yield the same products as the reaction of **1-H<sub>4</sub>** with NBE or TBE, which would suggest the products are of the composition (<sup>t</sup>Bu<sup>4</sup>PNP)Os. Addition of 1 atm H<sub>2</sub> to the solution after decomposition does not generate **1-H<sub>4</sub>**, even upon heating. Kinetic measurements of the disappearance of **1-H<sub>2</sub>(C<sub>2</sub>H<sub>4</sub>)** at 90 °C in toluene reveal disappearance with first-order kinetics and a rate constant of  $(8.9 \pm 1.0) \times 10^{-5} \text{ s}^{-1}$ , corresponding to  $\Delta G^\ddagger = 28.1 \text{ kcal/mol}$ .

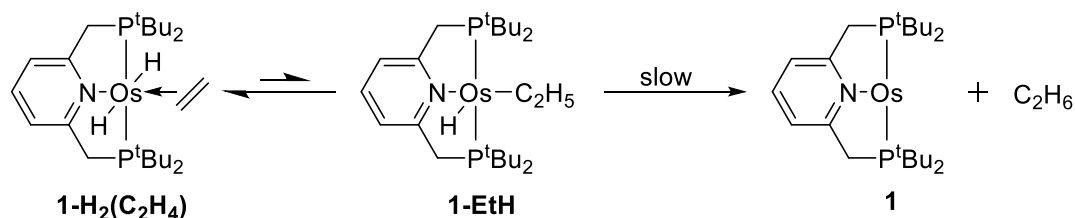
The reaction of 1-hexene with either **1-H<sub>4</sub>** or **1-H<sub>2</sub>(C<sub>2</sub>H<sub>4</sub>)** at 100 °C results in olefin isomerization rather than hydrogenation. Approximate kinetic data were obtained during an attempted transfer-dehydrogenation of cyclooctane. A stock solution of 5 mM **1-H<sub>2</sub>(C<sub>2</sub>H<sub>4</sub>)** in 5 mL of cyclooctane/1-hexene solution (3:2) was heated to 100 °C in sealed tubes. After 6 h and 26 h, approximately 15% (0.24 M, 48 TO) and (50% (0.82 M, 164 TO), respectively, of the 1-hexene was isomerized to internal hexenes.

### 3.2.4 DFT calculations and explanation of the observed reactivity of (<sup>t</sup>Bu<sup>4</sup>PNP)Os complexes.

Electronic structure calculations based on density functional theory (DFT) explain well the unusual reactivity described above. In particular, while **1-H<sub>2</sub>(C<sub>2</sub>H<sub>4</sub>)** does not readily undergo any observable reaction below ca. 60 °C, under H<sub>2</sub> atmosphere it readily eliminates ethane (Scheme 3.6 and eq 1), and under a CO atmosphere it yields the

product of ethylene insertion into an Os-H bond (Scheme 3.7 and eq 2). Relatedly, 1-hexene is much more readily isomerized than it is hydrogenated.

The reactivity of **1-H<sub>2</sub>(C<sub>2</sub>H<sub>4</sub>)** can be explained in terms of insertion of ethylene into an Os-H bond, occurring rapidly even at room temperature, followed by reaction of **1-EtH** with H<sub>2</sub> or CO. The fact that **1-H<sub>2</sub>(C<sub>2</sub>H<sub>4</sub>)** is stable in the absence of these species indicates that the insertion is reversible and the equilibrium lies far to the left (Scheme 3.8). Thus, although **1-EtH** is a five-coordinate d<sup>6</sup> species, representing a configuration known to favor very facile kinetics of C-H elimination,<sup>39</sup> unassisted elimination of ethane from **1-EtH** occurs very slowly, if at all.<sup>40</sup>



**Scheme 3.8:** Kinetics of ethylene insertion into Os-H bond



A full computed free energy profile (with enthalpies also shown) for **1**, **H<sub>2</sub>**, **C<sub>2</sub>H<sub>4</sub>** and related species is illustrated in Figure 3.6. Dihydrogen is calculated to bind quite strongly to the (tBu<sup>4</sup>PNP)Os fragment;  $\Delta H^\circ(\text{H}_2 \text{ addition to } \mathbf{1}) = -41 \text{ kcal/mol}$ . Addition of ethylene to (tBu<sup>4</sup>PNP)OsH<sub>2</sub> is also quite exothermic;  $\Delta H^\circ(\text{C}_2\text{H}_4 \text{ addition to } \mathbf{1}\text{-H}_2) = -32 \text{ kcal/mol}$ . Perhaps somewhat surprisingly, H<sub>2</sub> addition to the hypothetical 16e species

(<sup>t</sup>Bu<sup>4</sup>PNP)Os(C<sub>2</sub>H<sub>4</sub>) (the analogue of many stable reported (PCP)Ir complexes<sup>41</sup>) is also highly exothermic,  $\Delta H^\circ(\text{H}_2 \text{ addition to } \mathbf{1}\text{-C}_2\text{H}_4) = -34 \text{ kcal/mol}$ .

It follows from the thermodynamics of addition of H<sub>2</sub> and ethylene to **1** that loss of ethane from (<sup>t</sup>Bu<sup>4</sup>PNP)OsH<sub>2</sub>(C<sub>2</sub>H<sub>4</sub>) is endothermic by ca. 38 kcal/mol. The computed free energy of ethane loss is only 22.8 kcal/mol but this value reflects the favorable entropy of formation of a free ethane molecule. In the TS for loss of ethane, however, this entropy gain will be mostly unrealized. We were not able to locate a TS for ethane loss as a stationary point on the potential energy surface. However, a  $\sigma$ -ethane complex, **1-( $\sigma$ -EtH)**, is calculated to have an enthalpy and free energy of 28.6 kcal/mol and 24.6 kcal/mol, respectively, above **1-H<sub>2</sub>(C<sub>2</sub>H<sub>4</sub>)**. Assuming that loss of ethane from this complex has an activation enthalpy approximately equal to that of the reaction enthalpy (9.5 kcal/mol), and assuming that the activation entropy of this dissociation is between 0 and 20 eu, we can estimate that the barrier to loss of ethane from **1-( $\sigma$ -EtH)** is  $6.5 \pm 3.0 \text{ kcal/mol}$ , which implies that the TS for ethane loss has a free energy  $31.1 \pm 3.0 \text{ kcal/mol}$  above **1-H<sub>2</sub>(C<sub>2</sub>H<sub>4</sub>)**.

The barrier for ethylene insertion into an Os-H bond of **1-H<sub>2</sub>(C<sub>2</sub>H<sub>4</sub>)** is calculated to be fairly low,  $\Delta G^\ddagger = 13.1 \text{ kcal/mol}$  to give **1-EtH** which has a calculated free energy 8.7 kcal/mol above **1-H<sub>2</sub>(C<sub>2</sub>H<sub>4</sub>)**. As discussed above, the TS for elimination of ethane is much higher in free energy. In contrast, the barrier to H<sub>2</sub> addition to **1-EtH** is quite low, with a nearly negligible activation enthalpy,  $\Delta H^\ddagger = 2.1 \text{ kcal/mol}$ , and  $\Delta G^\ddagger = 9.3 \text{ kcal/mol}$  (Figure 3.6, pathway in blue). The initial product of this addition of H<sub>2</sub> is a dihydrogen complex, **1-(H<sub>2</sub>)EtH**, which is calculated to readily undergo oxidative addition of H<sub>2</sub> to yield an

Os(IV) complex, **1-H<sub>3</sub>Et**, which in turn readily eliminates ethane to give **1-H<sub>2</sub>**. The overall barrier to reaction in scheme 3.6, attributable to the TS for H<sub>2</sub> addition to **1-EtH**, is calculated to be only 18.0 kcal/mol, which is in reasonably good agreement with the experimental kinetics which indicate  $\Delta G^\ddagger_4 = 21.2$  kcal/mol.

Given that the activation enthalpy for addition of H<sub>2</sub> to **1-EtH** is nearly zero, we would expect that CO would also add without any significant enthalpic barrier. This is of course very consistent with the kinetics determined for the reaction in scheme 3.7 and the strong similarity with the kinetics of the reaction in scheme 3.6. The overall barrier implied by the kinetics of eq 2 is  $\Delta G^\ddagger = 21.4$  kcal/mol.

As indicated in Figure 3.6, the barrier to  $\beta$ -H-elimination from **1-EtH** is calculated to be far lower than that for ethyl-H elimination. This explains the kinetics of scheme 3.6 and scheme 3.7, and also underlies the observation of isomerization rather than hydrogenation of 1-hexene. Insertion of 1-hexene into an Os-H bond to give **1-H(2-hexyl)** is calculated to have a very low barrier, only 9.9 kcal/mol above the 1-hexene complexes **1-H<sub>2</sub>(1-hexene)**. This is significantly lower than the barrier for olefin insertion by **1-H<sub>2</sub>(C<sub>2</sub>H<sub>4</sub>)** largely reflecting that the binding energy of 1-hexene to **1-H<sub>2</sub>** is much less than that of ethylene.  $\beta$ -H elimination by **1-H(2-hexyl)** to give the 2-hexene complex also has a relatively low barrier, which is 11.0 kcal/mol less than that for reductive elimination to form the C-H bond (Figure 3.7). (The barrier to loss of hexane from the resulting *n*-hexane  $\sigma$ -bond complex is presumably even higher still.)

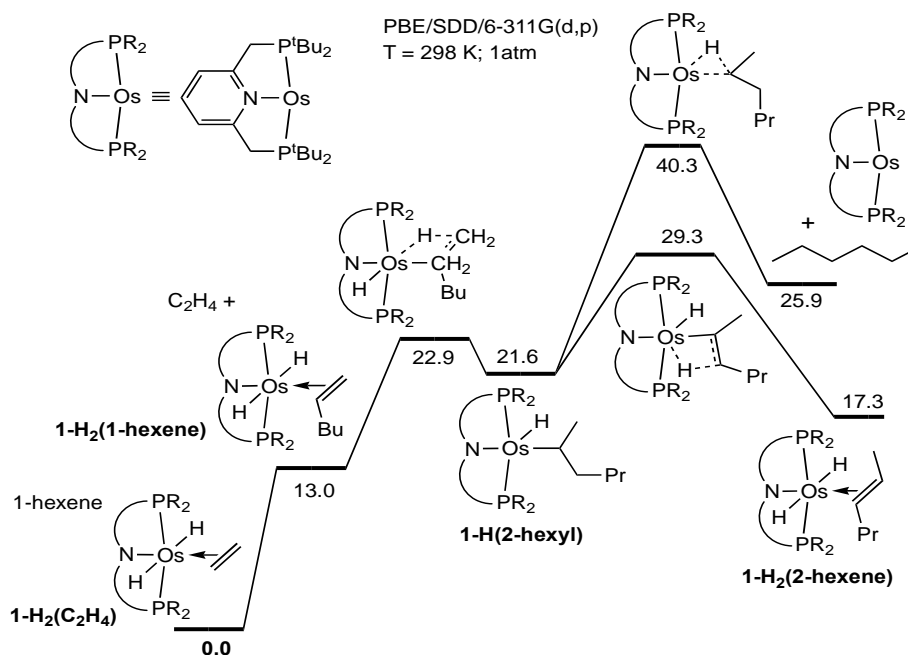


**Figure 3.8.** Free energy diagram (kcal/mol) for isomerization of 1-hexene. Energy values (kcal/mol) are referenced to T = 298 K (25 °C) and a partial pressure P = 1 atm for each species.

C-H activation and  $\beta$ -H elimination are often considered to be the “difficult” steps for alkane dehydrogenation.<sup>42</sup> However, the calculations illustrated in Figures 3.6 and 3.7, which are consistent with the observation discussed above, suggest that the failure of **1** to catalyze alkane transfer dehydrogenation may be attributable, in large part, to the very *favorable* thermodynamics of these steps which strongly contribute to a high barrier to the reverse reaction, the olefin-hydrogenation segment of a transfer dehydrogenation cycle. Viewed differently, formation of **1-(alkyl)H** does occur fairly readily but, unlike in the case of (PCP)Ir, the 16e alkyl hydride does not readily undergo C-H elimination. If alkane elimination did occur to generate the 14e fragment **1**, the calculations strongly indicate that **1** would be kinetically very competent for alkane dehydrogenation (although the calculations do not argue against the possibility that

other reactions, possibly leading to catalyst decomposition, would be even more facile as will be discussed in more detail below).

As noted in the Introduction, we were initially spurred to investigate the fragment **1** based in part on the hypothesis that it would add C-H bonds more favorably than (PCP)Ir complexes. This proposal is certainly supported by the results of the DFT calculations. Rather than favoring catalytic alkane dehydrogenation, however, the favorable thermodynamics of C-H addition (i.e. the unfavorable thermodynamics of C-H elimination) disfavor transfer-dehydrogenation. Likewise, the very favorable addition of H<sub>2</sub> to **1** would favor the dehydrogenation of alkanes if **1** could be generated but, instead, the strong binding of H<sub>2</sub> disfavors the generation of **1** by reaction with olefin. Of course this also disfavors simple loss of H<sub>2</sub> from **1-H<sub>2</sub>**; although we have not located a TS for this reaction, the enthalpy of H<sub>2</sub> loss from **1-H<sub>2</sub>** is calculated to be 41.1 kcal/mol. Moreover, the barrier to H<sub>2</sub> loss must be added to the free energy of **1-H<sub>2</sub>**, which will vary with reaction conditions (e.g. it is 16.9 kcal/mol above **1-H<sub>2</sub>(C<sub>2</sub>H<sub>4</sub>)** under 1 atm of ethylene as shown in Figure 4), but under no conditions studied does **1-H<sub>2</sub>** appear to be present in observable concentrations. Accordingly, all attempts to effect alkane acceptorless dehydrogenation by **1** have been unsuccessful.

The energy profile of **1** relevant to olefin hydrogenation is surprisingly similar to that of the Ir(I) fragment (carb-PNP)Ir (**3**, Figure 3.8) on which we have recently reported.<sup>43</sup> The ethylene dihydride adduct of **3** (**3-H<sub>2</sub>(C<sub>2</sub>H<sub>4</sub>)**), is also stable at ambient temperature but, like **1-H<sub>2</sub>(C<sub>2</sub>H<sub>4</sub>)**, reacts with H<sub>2</sub> to eliminate ethane, and catalyzes ethylene hydrogenation. **3-H<sub>2</sub>(C<sub>2</sub>H<sub>4</sub>)** undergoes reversible insertion of coordinated ethylene to

give **3-EtH**, in analogy with the behavior of **1-H<sub>2</sub>(C<sub>2</sub>H<sub>4</sub>)**, and the ethyl hydride reacts with H<sub>2</sub> leading to loss of ethane. Unassisted reductive elimination of ethane from **3-EtH** to form **3-(σ-EtH)** was calculated to be endergonic by 16.6 kcal/mol, nearly the same as the 17.4 kcal/mol for reductive elimination of ethane from **1-EtH**. Elimination of H<sub>2</sub> from **3-H<sub>2</sub>** was calculated to be highly endergonic, as found for **1-H<sub>2</sub>**, but surprisingly more so for the Ir(III) complex **3-H<sub>2</sub>**, 45.2 kcal/mol, as compared with 32.1 kcal/mol for Os(II) complex **1-H<sub>2</sub>**.<sup>43</sup>

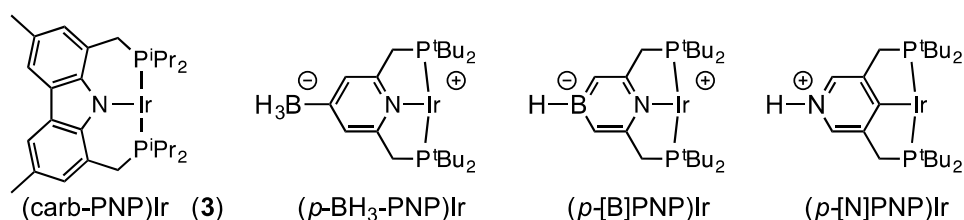


**Figure 3.9:** (<sup>t</sup>BuPNP) ligated complexes with charge distributed throughout the ligand

### 3.2.5 DFT calculations and an underlying explanation of the thermodynamics in comparison with isoelectronic species.

The very favorable addition of C-H bonds and H<sub>2</sub> to (<sup>t</sup>Bu<sup>4</sup>PNP)Os (**1**) as compared with addition to the isoelectronic Ir fragment, (<sup>t</sup>Bu<sup>4</sup>PCP)Ir (**2**), is one key factor underlying the different reactivity of these species. This difference would customarily be explained in terms of oxidation state: oxidative addition to Os(0) to give Os(II) is generally expected to be more favorable than oxidative addition to isoelectronic Ir(I) to give Ir(III). However, we have recently shown that a more electron-rich metal center does not necessarily undergo oxidative addition more favorably<sup>44</sup> in fact, more strongly electron-donating ancillary ligands can significantly disfavor oxidative addition. That observation, in

combination with the above noted similarities of **1** with the Ir(I) complex (carb-PNP)Ir (**3**), led us to consider if the differences between the thermodynamics of addition to isoelectronic fragments **1** and **2** are attributable to the difference in the metal centers and corresponding oxidation states (Os(0) vs. Ir(I)) or, alternatively, if they are better explained in terms of the difference in the coordinating atoms.

Our initial computational approach to the above question was a comparison of the reaction thermodynamics of the <sup>t</sup>Bu<sup>4</sup>PNP complexes of Os(0) (complex **1**) versus the <sup>t</sup>Bu<sup>4</sup>PNP complex of Ir(I), a cationic fragment reported by Milstein.<sup>5,31</sup> The first report of this iridium complex in fact provided some indication of the role of the PNP ligand in favoring addition thermodynamics compared with PCP; Milstein reported that (<sup>t</sup>Bu<sup>4</sup>PNP)IrPhH<sup>+</sup> is stable with respect to loss of benzene, in contrast with neutral **2-PhH** which undergoes rapid loss of benzene even on the NMR timescale at temperatures above ca. -30 °C.<sup>45</sup> Accordingly, we calculate (Figure 3.9) that the free energy for C-H addition of ethane to (<sup>t</sup>Bu<sup>4</sup>PNP)Ir<sup>+</sup> (**4**) is -7.2 kcal/mol, ca. 23 kcal/mol more favorable than addition to **2** ( $\Delta G = + 15.9$  kcal/mol). Ethane C-H addition to **1**, however, was calculated to be only 6.9 kcal/mol more favorable than addition to **4**. Moreover, in the case of H<sub>2</sub>, addition to Ir(I) cation **4**<sup>46</sup> was calculated to be slightly *more* exoergic than addition to Os(0) complex **1** (-34.5 kcal/mol vs. -32.1 kcal/mol), and 17.9 kcal/mol more favorable than addition to (<sup>t</sup>Bu<sup>4</sup>PCP)Ir. (Note that the geometry of the H<sub>2</sub> adducts is very different from that of the C-H adducts; whereas the former are distorted trigonal bipyramidal with axial P atoms and an acute H-Os-H angle, the latter are square pyramidal with H apical.)

For coordination of ethylene, the relationship between these three complexes is very similar to that for addition of  $\text{H}_2$ . Ethylene coordination to  $(^{\text{tBu}}_4\text{PNP})\text{Ir}^+$  was calculated to be slightly more favorable than addition to  $(^{\text{tBu}}_4\text{PNP})\text{Os}$  (-27.6 kcal/mol vs. -24.4 kcal/mol) which is 16.6 kcal/mol more favorable than addition to  $(^{\text{tBu}}_4\text{PCP})\text{Ir}$  (Figure 3.9).

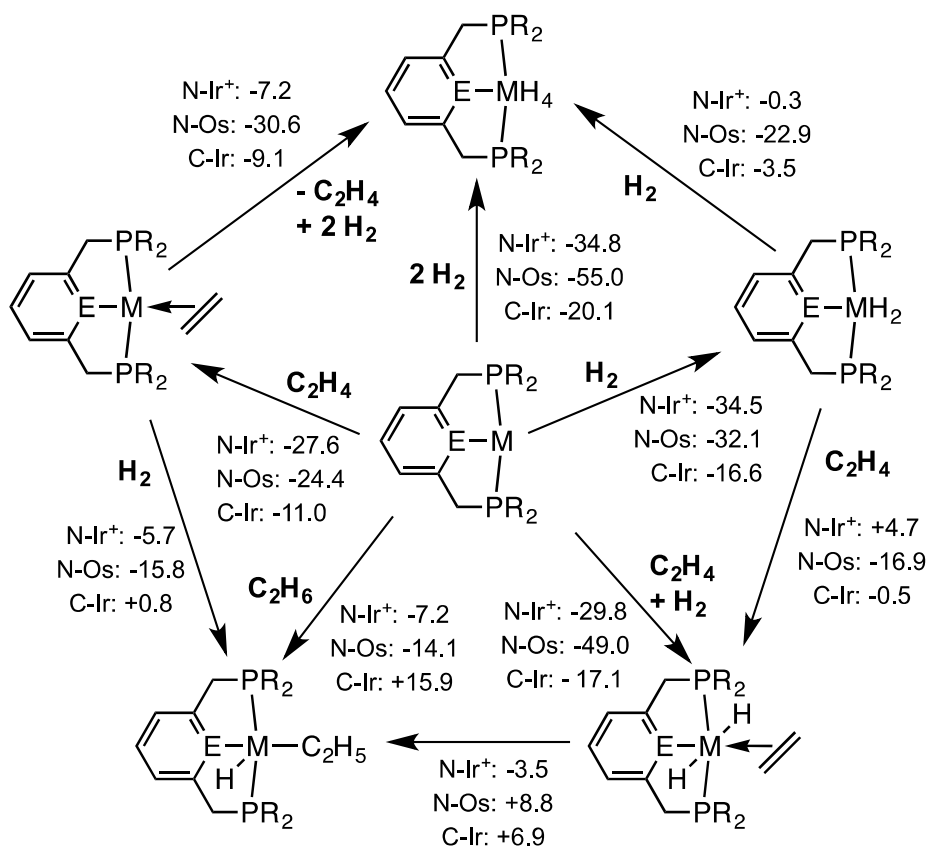


**Figure 3.10.** Calculated free energies (kcal/mol) of interconversion between various complexes of  $(^{\text{tBu}}_4\text{PNP})\text{Ir}^+$  (**4**),  $(^{\text{tBu}}_4\text{PNP})\text{Os}$  (**1**), and  $(^{\text{tBu}}_4\text{PCP})\text{Ir}$  (**2**) (indicated as N-Ir<sup>+</sup>, N-Os, and C-Ir respectively)



**Table 3.4** Calculated Free Energies (kcal/mol) of Some Elementary Addition Reactions

Complex (M)	$M + H_2 = MH_2$	$M + Et-H = M(Et)H$	$M + C_2H_4 = M(C_2H_4)$	$MH_2 + H_2 = MH_4$	$M(C_2H_4) + H_2 = \text{trans-}MH_2(C_2H_4)$
$(^{t}Bu^4PNP)Os$	-32.1	-14.1	-24.4	-22.9	-24.6
$(^{t}Bu^4PNP)Ir^+$	-34.5	-7.2	-27.6	-0.3	-2.2
$(^{t}Bu^4PCP)Ir$	-16.6	15.9	-11.0	-3.5	-6.1
$(p\text{-}BH_3\text{-}PNP)Ir$	-37.5	-6.6	-29.7	1.7	-0.5
$(p\text{-}[B]PNP)Ir$	-39.2	-6.1	-30.2	2.8	0.1
$(p\text{-}[N]PCP)Ir^+$	-14.2	17.0	-9.2	-4.4	-6.8

Given that  $(PNP)Ir^+$  is rigorously isoelectronic with both  $(PNP)Os$  and  $(PCP)Ir$  and yet contains a much less electron-rich metal center, its very favorable thermodynamics of C-H and H-H addition seemed sufficiently surprising to warrant further investigation. In particular we considered that the thermodynamics of addition of neutral species to  $(^{t}Bu^4PNP)Ir^+$  might be affected in ways that do not reflect the factors that we typically consider to affect bond strengths, or that perhaps the overall net charge would result in computational artifacts. We therefore investigated closely related neutral species. Firstly, a negatively charged substituent, a boryl group, was added to the para position of the PNP pyridine ring to give neutral (zwitterionic)  $(p\text{-}BH_3\text{-}^{t}Bu^4PNP)Ir$  (Table 3.4; Figure 3.8). The thermodynamics of addition of  $H_2$ , C-H bonds, or ethylene to this complex are not significantly different from those of the cationic parent  $(^{t}Bu^4PNP)Ir^+$ ; addition of  $H_2$  and addition of ethylene are more favorable, by only 3 kcal/mol and 2 kcal/mol, respectively, while addition of the ethane C-H bond is less favorable by 0.6 kcal/mol.

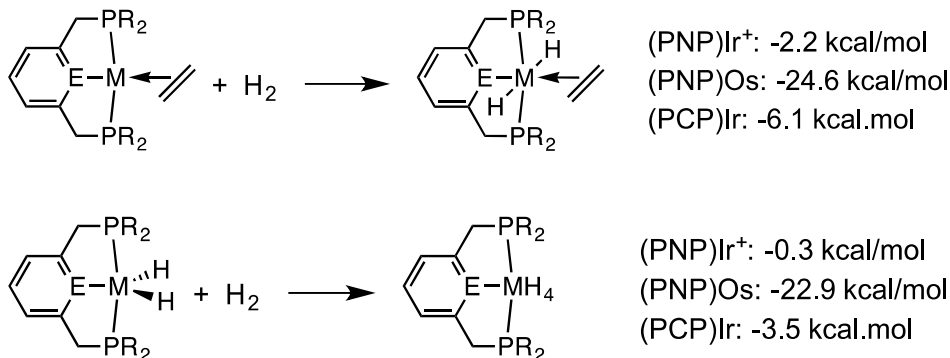
We then conducted calculations on a neutral derivative of  $(^{t}Bu^4PNP)Ir^+$  in which the added negative charge was more integrated into the molecule, an azaborinine derivative,  $(p\text{-}[B]PNP)Ir$  (Table 3.4, Figure 3.8). In this case also, substitution by the

negatively charged group was calculated to slightly favor addition of H<sub>2</sub> and ethylene, and to very slightly disfavor C-H addition of ethane. Finally, we did the converse experiment, introducing a positive charge to the neutral (PCP)Ir by substituting NH<sup>+</sup> for the C-H pair of atoms at the para position of (PCP)Ir to give (*p*-[N]PCP)Ir (Table 3.4, Figure 3.8). This also had no major affect on the thermodynamics of these addition reactions, disfavoring all three by only 1 - 2 kcal/mol.

Thus C-H addition, H<sub>2</sub> addition, and coordination of ethylene to (tBu<sup>4</sup>PNP)Ir<sup>+</sup> are thermodynamically similar to the corresponding additions to (tBu<sup>4</sup>PNP)Os. The overall charge on the (tBu<sup>4</sup>PNP)Ir<sup>+</sup> fragment does not play an important role in determining the thermodynamics, and for all three addenda the corresponding reactions with (PCP)Ir are much less favorable. The degree to which the metal center is electron-rich does not play a significant role in determining the addition thermodynamics (e.g. Os(0) vs. Ir(I)) but, in accord with our previous studies<sup>30b</sup>, increasing trans influence of the coordinating group of the pincer ligand strongly disfavors these additions.

In contrast with H<sub>2</sub> addition to the 14e (pincer)M species, further additions, to the 16e addition products, are much more favorable for (PNP)Os complexes than for complexes of (PCP)Ir or (PNP)Ir<sup>+</sup>. The addition of H<sub>2</sub> to (tBu<sup>4</sup>PEP)M(η<sup>2</sup>-C<sub>2</sub>H<sub>4</sub>) (E = N, C; M = Ir, Os) yielding *trans*-(tBu<sup>4</sup>PEP)M(H)<sub>2</sub>(η<sup>2</sup>-C<sub>2</sub>H<sub>4</sub>) is calculated to be only slightly exoergic for (PCP)Ir and (PNP)Ir<sup>+</sup> complexes (ΔG° = -6.1 kcal/mol and -2.2 kcal/mol respectively) but highly exoergic, ΔG° = -24.6 kcal/mol, for addition to (PNP)Os(ethylene) (Scheme 3.9). Likewise, addition of either ethylene or H<sub>2</sub> to the dihydride complexes is very similar for

the two Ir species (with absolute values of  $\Delta G^\circ$  close to zero), but significantly exoergic for  $(^t\text{Bu}^4\text{PNP})\text{OsH}_2$  ( $\Delta G^\circ = -22.9$  kcal/mol for  $\text{H}_2$  addition; Scheme 3.9 and Figure 3.9).<sup>47</sup>

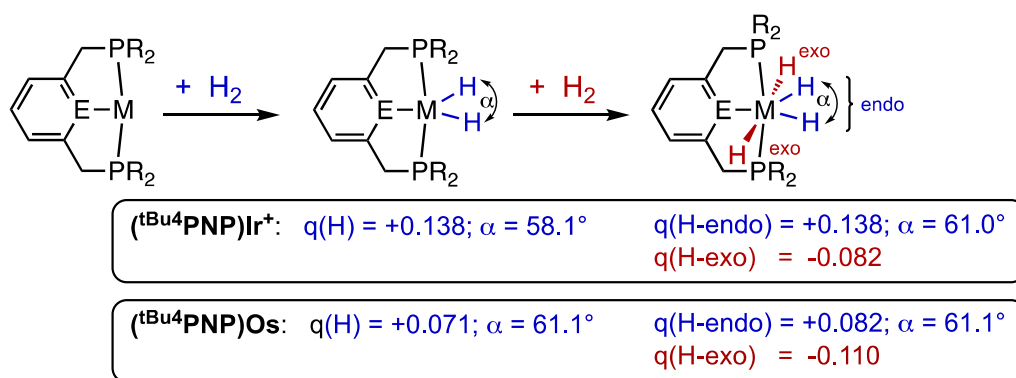


**Scheme 3.9:** Free Energy for  $\text{H}_2$  addition to  $(\text{PXP})\text{M}(\text{olefin})$  and  $(\text{PXP})\text{MH}_2$

Thus, quite unexpectedly,  $\text{H}_2$  addition to  $(^t\text{Bu}^4\text{PNP})\text{Ir}^+$  is slightly *more* favorable than addition to isoelectronic  $(^t\text{Bu}^4\text{PNP})\text{Os}(0)$  while  $\text{H}_2$  addition to  $(^t\text{Bu}^4\text{PNP})\text{IrH}_2^+$  is dramatically *less* favorable than to  $(\text{PNP})\text{OsH}_2$ , by 22.6 kcal/mol. These calculations are consistent with the results of experiments in the presence of  $\text{D}_2$ , showing that  $(^t\text{Bu}^4\text{PNP})\text{OsH}_4$  loses  $\text{H}_2$  slowly at ca. 85 °C (following roughly first-order kinetics with a half-life of ca. 1 hour). All efforts to generate and isolate or observe the corresponding dihydride, by reacting  $(^t\text{Bu}^4\text{PNP})\text{OsH}_4$  with olefin or by heating and applying vacuum, were unsuccessful. In contrast  $(^t\text{Bu}^4\text{PNP})\text{IrH}_4^+$  has been reported to rapidly exchange with  $\text{H}_2$  even at -20 °C.<sup>48</sup> Moreover, we find that removal of solvent from a methylene chloride (b.p. = 39.6 °C) solution of  $(^t\text{Bu}^4\text{PNP})\text{IrH}_4^+$  at room temperature results in loss of  $\text{H}_2$  to give complete conversion to  $(^t\text{Bu}^4\text{PNP})\text{IrH}_2^+$ . These observations indicate that  $\text{H}_2$  dissociates even more easily from  $(^t\text{Bu}^4\text{PNP})\text{IrH}_4^+$  than from  $(^t\text{Bu}^4\text{PCP})\text{IrH}_4$ , and strongly support the calculations

indicating that H<sub>2</sub> addition to either of the iridium dihydrides is only slightly exergonic (eq 2).

Clearly the differences noted above cannot be simply explained in terms of changes in formal oxidation states. NBO analysis<sup>49</sup> indicates, however, that different H<sub>2</sub> additions are accompanied by unexpectedly marked differences in transfer of charge to hydrogen. The hydride ligands resulting from H<sub>2</sub> addition to (tBu<sup>4</sup>PNP)M (M = Ir<sup>+</sup> and Os) are calculated to have a positive charge in both cases, +0.138 and +0.071 for M = Ir<sup>+</sup> and Os respectively (not surprisingly, the charge is somewhat more positive in the case of addition to the cation).<sup>50</sup> For purposes of thermodynamic analysis we will view the second H<sub>2</sub> addition as giving rise specifically to the exo hydride ligands of (PNP)MH<sub>4</sub> (Scheme 3.10). While this obviously does not reflect the actual mechanistic pathway, this partitioning is quite convenient for this analysis since the (tBu<sup>4</sup>PNP)M(H<sub>endo</sub>)<sub>2</sub> unit of (tBu<sup>4</sup>PNP)MH<sub>4</sub> has essentially the same geometry as the (tBu<sup>4</sup>PNP)MH<sub>2</sub> precursor and, most importantly, the endo hydrides of (tBu<sup>4</sup>PNP)MH<sub>4</sub> have calculated charges essentially identical to the hydrides of the respective (tBu<sup>4</sup>PNP)MH<sub>2</sub> complexes (Scheme 3.10).



**Scheme 3.10** NBO Analysis of H<sub>2</sub> addition to (PNP)M and (PNP)MH<sub>2</sub>

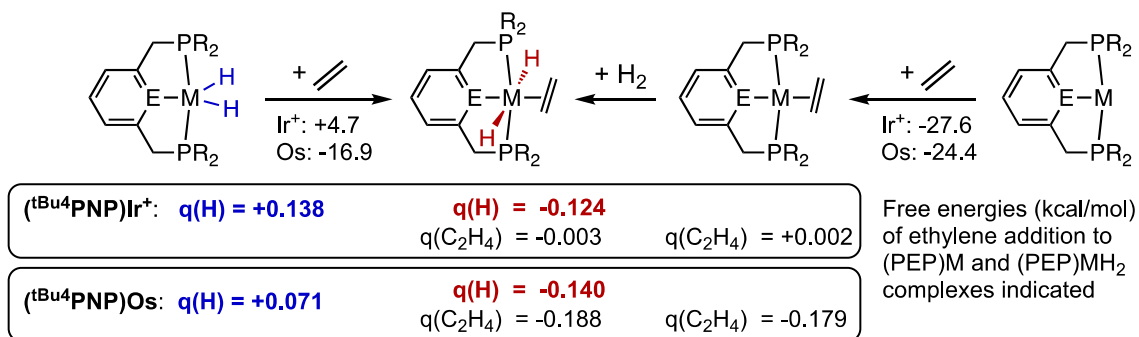
In contrast with the hydrides resulting from the first addition of H<sub>2</sub>, the exo hydrides have NBO-calculated charges that are distinctly negative, -0.082 and -0.110 for Ir<sup>+</sup> and Os(0) respectively. Thus the charges indicate that while the first "oxidative addition" of H<sub>2</sub> is actually reductive,<sup>50-51</sup> the second addition is physically oxidative. This provides a fairly straightforward explanation for the finding that the first addition of H<sub>2</sub> is more favorable for (tBu<sup>4</sup>PNP)Ir<sup>+</sup> while the second addition is more favorable for the much more electron-rich (tBu<sup>4</sup>PNP)Os(0) species.

The addition of H<sub>2</sub> to three-coordinate d<sup>8</sup> fragments, particularly Ir(I) has been studied in detail since the pioneering work by Eisenstein.<sup>52</sup> Addition of a second molecule of H<sub>2</sub>, or more generally addition to five-coordinate d<sup>6</sup> dihydrides, such as the (PNP)MH<sub>2</sub> complexes, has to our knowledge not been studied extensively. We find that the particularly oxidative nature of this addition can be rationalized in terms of a 3-center/4-electron bonding model. The doubly occupied H(exo)-Os-H(exo) bonding orbital of (PNP)OsH<sub>4</sub> has 72% Os character (sd<sup>6.8</sup> hybridization) and 28% H character, while the (also doubly occupied) non-bonding orbital has zero Os contribution by symmetry. In the case of (PNP)IrH<sub>4</sub><sup>+</sup>, the H(exo)-Ir-H(exo) bonding orbital has 77% Ir character (sd<sup>7.5</sup> hybridization) and 23% H character; again, the non-bonding orbital has zero Ir contribution. Hence, in both complexes, each of the exo hydrides receive 1.0 electron from the non-bonding orbital and are overall negatively charged, slightly more so in the osmium case, in accord with the composition of the bonding 3-center orbital.

As noted above addition of H<sub>2</sub> to (PEP)M(η<sup>2</sup>-C<sub>2</sub>H<sub>4</sub>) to give the trans dihydride is 22.4 kcal/mol more exoergic for (PNP)Os(η<sup>2</sup>-C<sub>2</sub>H<sub>4</sub>) than for (PNP)Ir(η<sup>2</sup>-C<sub>2</sub>H<sub>4</sub>)<sup>+</sup>. This difference,

and even the absolute values, are remarkably similar to those for  $\text{H}_2$  addition to the dihydrides  $(\text{PEP})\text{MH}_2$  discussed above. Accordingly, this  $\text{H}_2$  addition is also calculated to be oxidative and the charges on the resulting hydride ligands are each  $-0.124\text{ e}$  for Os and  $-0.140\text{ e}$  for Ir. The oxidative nature of this addition can be explained in terms of a 3-center/4-electron bonding model essentially no different from that used for the addition to  $(\text{PEP})\text{MH}_2$  above.

Although ethylene addition to  $(^{\text{tBu}}_4\text{PNP})\text{Ir}^+$  is slightly ( $3.2\text{ kcal/mol}$ ) more favorable than addition to  $(^{\text{tBu}}_4\text{PNP})\text{Os}$ , addition to  $(^{\text{tBu}}_4\text{PNP})\text{OsH}_2$  is  $21.6\text{ kcal/mol}$  more favorable than to  $(^{\text{tBu}}_4\text{PNP})\text{IrH}_2^+$  (Figure 3.9, Scheme 3.11). This large difference is not primarily due to differences in the nature of the metal-ethylene bonding; indeed the total charge on the coordinated ethylene units is essentially identical in  $(\text{PEP})\text{M}(\eta^2\text{-C}_2\text{H}_4)$  and *trans*- $(\text{PEP})\text{M}(\text{H})_2(\eta^2\text{-C}_2\text{H}_4)$  (Scheme 3.11). Instead the much more favorable ethylene addition to Os(0) vs. Ir(I) is due to the change in M-H bonding upon coordination of ethylene, from polarized strongly toward the metal center in  $(\text{PEP})\text{M}(\text{H})_2$  to strongly polarized toward H in *trans*- $(\text{PEP})\text{M}(\text{H})_2(\eta^2\text{-C}_2\text{H}_4)$ .



**Scheme 3.11:** NBO analysis of ethylene addition to  $(\text{PXP})\text{MH}_2$  and  $\text{H}_2$  addition to  $(\text{PXP})\text{M}(\text{C}_2\text{H}_4)$

### 3.2.6 Cyclometalation and C-H addition to (<sup>t</sup>Bu<sup>4</sup>PNP)Os(II) complexes.

The very favorable addition of H<sub>2</sub> to (<sup>t</sup>Bu<sup>4</sup>PNP)OsH<sub>2</sub>, as compared with addition to (<sup>t</sup>Bu<sup>4</sup>PCP)IrH<sub>2</sub> or (<sup>t</sup>Bu<sup>4</sup>PNP)IrH<sub>2</sub><sup>+</sup>, would suggest that C-H addition to (<sup>t</sup>Bu<sup>4</sup>PNP)OsH<sub>2</sub> would likewise be more favorable than to the Ir dihydrides. DFT calculations support this expectation; C-H addition of ethane to **1-H<sub>2</sub>** has a free energy barrier of only 17.9 kcal/mol (of which the enthalpic component is only 5.2 kcal/mol; Figure 3.6). A priori, this might seem promising with respect to possible alkane dehydrogenation cycles.<sup>12</sup> However, the relatively low barrier to C-H addition to Os(II) is also applicable to intramolecular C-H addition. Notably, **1-EtH** is calculated to undergo exergonic cyclometalation and loss of ethane with a barrier of  $\Delta G^\ddagger = 16.5$  kcal/mol (Figure 3.6), to give cyclometalated complex **cyclo-1**. The overall barrier for formation of **cyclo-1** from **1-H<sub>2</sub>(C<sub>2</sub>H<sub>4</sub>)** is  $\Delta G^\ddagger = 25.2$  kcal/mol which is in good agreement with the value determined experimentally for loss of **1-H<sub>2</sub>(C<sub>2</sub>H<sub>4</sub>)** and formation of ethane,  $\Delta G^\ddagger = 28.1$  kcal/mol.

The facile kinetics for formation of **cyclo-1** are accompanied by favorable thermodynamics. For cyclometalation and loss of ethane from **1-EtH**, the free energy of reaction is  $\Delta G^\circ = -9.3$  kcal/mol. Cyclometalation of the 14e (<sup>t</sup>Bu<sup>4</sup>PNP)Os fragment is even more exergonic,  $\Delta G^\circ = -23.4$  kcal/mol, with a kinetic barrier,  $\Delta G^\ddagger = 9.3$  kcal/mol, low enough that cyclometalation by this fragment would be extremely rapid. In combination with the thermodynamics, however, this translates to a very high barrier to the de-cyclometalation,  $\Delta G^\ddagger = 32.7$  kcal/mol. This markedly contrasts with the 14e (<sup>t</sup>Bu<sup>4</sup>PCP)Ir fragment for which cyclometalation is *endergonic* ( $\Delta G^\circ = 5.6$  kcal/mol).

Alkane dehydrogenation is generally favored by an extremely low  $H_2$  pressure and thus a free energy of  $H_2$  much lower than at the standard condition of  $P = 1$  atm used for the calculations in Figure 3.6. For example, in order to effect acceptorless alkane dehydrogenation (for which the free energy at standard states is ca. +22 kcal/mol), the partial pressure of  $H_2$  must be sufficiently low to render the free energy of  $H_2$  ca. 22 kcal/mol below that at 1 atm. Under such conditions, those states shown in Figure 3.6 that include free  $H_2$  would be relatively much lower in energy; **cyclo-1** plus  $H_2$  and  $C_2H_6$  would be the single lowest-free-energy state of those shown in Figure 3.6.<sup>53</sup> As noted above, elimination of ethane from **1-H<sub>2</sub>(C<sub>2</sub>H<sub>4</sub>)** (in the absence of a trap such as  $H_2$  or CO) at ca. 90 °C leads to loss of signals in the  $^{31}P$  NMR and  $^1H$  NMR spectra and the solution turning dark red. This appears to be the same uncharacterized mixture as obtained from the reaction of **1-H<sub>4</sub>** with other olefins (TBE or NBE), as discussed above, suggesting the composition of the 14e fragment **1**, which is the same as that of **cyclo-1**. The lack of well defined  $^{31}P$  or  $^1H$  NMR spectra, however, indicates that the product is not simply **cyclo-1** (for which the diamagnetic state is calculated to be far lower energy than any paramagnetic state). Confirming the conclusion that **cyclo-1** is not a major species present under these condition, addition of 1 atm  $H_2$  to the dark red solution does not generate **1-H<sub>4</sub>**, even upon heating (as would be expected, since the calculated barrier to hydrogenolysis of **cyclo-1** is very low,  $\Delta G^\ddagger = 9.9$  kcal/mol).

Although the fate of the (<sup>t</sup>Bu<sup>4</sup>PNP)Os unit in the reaction with olefins remains to be determined, we note that its degradation is *not* accompanied by loss of free PNP ligand. We believe this is consistent with a degradation pathway which likely proceeds via



cyclometalation to give **cyclo-1**. Like the related **1-EtH**, **cyclo-1** is expected to be susceptible to further inter- or intramolecular C-H additions.

### 3.2.7 Summary of alkane dehydrogenation using (<sup>t</sup>Bu<sup>4</sup>PNP)Os (**1**)

We report the synthesis of several complexes of (<sup>t</sup>Bu<sup>4</sup>PNP)Os. This species is isoelectronic with the (<sup>R</sup>PCP)Ir unit which has played the leading role in metal-complex-catalyzed alkane dehydrogenation to date. Olefins react under mild conditions to coordinate and insert into an Os-H bond to yield (<sup>t</sup>Bu<sup>4</sup>PNP)Os(alkyl)H which can be trapped with CO or undergo hydrogenolysis with H<sub>2</sub>. Experimental and computational results indicate that C-H and H<sub>2</sub> addition to (<sup>t</sup>Bu<sup>4</sup>PNP)Os are thermodynamically much more favorable than addition to (<sup>t</sup>Bu<sup>4</sup>PCP)Ir. A priori, the favorable thermodynamics of (<sup>t</sup>Bu<sup>4</sup>PNP)OsH<sub>2</sub> and especially (<sup>t</sup>Bu<sup>4</sup>PNP)Os(alkyl)(H) may seem promising in the context of alkane dehydrogenation, but they ultimately appear to disfavor catalytic activity. Elimination of alkane from the corresponding alkyl hydride is too unfavorable for the purposes of a catalytic cycle, specifically to allow formation of the corresponding three-coordinate d<sup>8</sup> pincer-metal species. C-H elimination from (<sup>t</sup>Bu<sup>4</sup>PNP)OsEtH is calculated to be 30.0 kcal/mol less favorable than elimination from (<sup>t</sup>Bu<sup>4</sup>PCP)IrEtH. Likewise, loss of H<sub>2</sub> from the corresponding metal dihydride is much more endoergic for (<sup>t</sup>Bu<sup>4</sup>PNP)OsH<sub>2</sub> than for (<sup>t</sup>Bu<sup>4</sup>PCP)IrH<sub>2</sub> (though "only" by 15.5 kcal/mol).

The thermodynamically very favorable addition of H<sub>2</sub> (or C-H bonds) to (<sup>t</sup>Bu<sup>4</sup>PNP)Os relative to (<sup>t</sup>Bu<sup>4</sup>PCP)Ir would generally be attributed to the Os(0) center being more electron-rich than Ir(I). However, we have previously demonstrated the critical role of

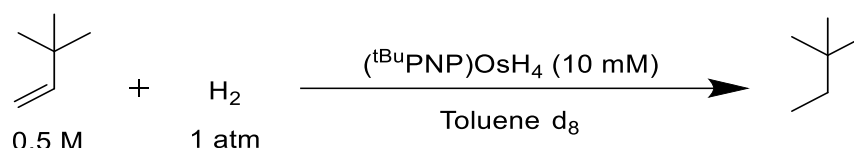
the ligand, specifically the coordinating group trans to the site of addition, in determining the thermodynamics of oxidative addition to three-coordinate  $d^8$  fragments. Accordingly, when we compare the thermodynamics of addition to the  $d^8$  metal centers Ir(I) and Os(0) coordinated to the same PNP pincer ligand, we find that  $H_2$  addition to the cationic Ir(I) complex is calculated to be slightly *more* favorable; thus the difference in the nature of the ligand, not the metal center, is responsible for the more favorable thermodynamics of  $H_2$  addition to  $(^{tBu_4}PNP)Os$  relative to  $(^{tBu_4}PCP)Ir$ . The calculated highly exoergic addition to  $(^{tBu_4}PNP)Ir^+$  is consistent with experimental observations of stable products of C-H addition to  $(^{tBu_4}PNP)Ir^+$ .<sup>5,31</sup> The fact that  $H_2$  addition is strongly favored by the less-electron donating PNP ligand vs. anionic PCP, and even slightly favored by the less electron-rich metal center Ir(I) vs. Os(0), suggests that  $H_2$  addition to these  $d^8$  pincer-M fragments cannot be considered oxidative in other than a formal sense. This conclusion is supported by the results of NBO analysis which indicate that the hydride ligands formed upon  $H_2$  addition to either  $(^{tBu_4}PNP)Os$  or  $(^{tBu_4}PNP)Ir^+$  have a slightly positive net charge. In contrast, calculations and experimental results reveal that  $H_2$  addition to the dihydrides to afford tetrahydrides, or  $H_2$  addition to the four-coordinate pincer-M ethylene complexes, is much more favorable for  $(^{tBu_4}PNP)Os$  than for either  $(^{tBu_4}PCP)Ir$  or  $(^{tBu_4}PNP)Ir^+$ . Accordingly, in these cases the NBO analysis indicates that the addition of  $H_2$  has a genuinely oxidative component.

Although  $(^{tBu_4}PNP)Os$  adds  $H_2$  or  $C_2H_4$  much more exoergically than does  $(^{tBu_4}PCP)Ir$ , ( $\Delta G^\circ = 15.5$  kcal/mol and 13.4 kcal/mol respectively), addition of C-H bonds enjoys an even greater advantage, e.g. 30.0 kcal/mol for addition of the C-H bond. As noted above

and illustrated in Figure 4, this contributes to a high overall barrier for a potential cycle for alkane dehydrogenation via an Os(0)/Os(II) cycle. Additionally, this also favors intramolecular C-H addition (cyclometalation) by 29 kcal/mol for (<sup>t</sup>Bu<sub>4</sub>PNP)Os vs. (<sup>t</sup>Bu<sub>4</sub>PCP)Ir. Moreover, further C-H addition to the cyclometalated species is presumably much more favorable for (<sup>t</sup>Bu<sub>4</sub>PNP)Os than for (<sup>t</sup>Bu<sub>4</sub>PCP)Ir, based on the calculation showing that additions to (<sup>t</sup>Bu<sub>4</sub>PNP)Os(II) complexes are much more favorable than additions to (<sup>t</sup>Bu<sub>4</sub>PCP)Ir(III). Thus the inability of **1** to effect alkane dehydrogenation catalysis may be viewed (perhaps counter-intuitively) in terms of the very favorable thermodynamics of C-H addition; the favorable thermodynamics contribute to a high barrier to catalysis (via an Os(0) intermediate), while probably also enabling undesirable pathways for ligand decomposition and cluster formation. Work is currently underway to design related pincer-Os complexes as catalysts that will exploit the favorable thermodynamics of additions, while circumventing the challenges, including cyclometalation, that have been identified in this work.

### 3.3 Hydrogenation of TBE and NBE using (<sup>t</sup>BuPNP)OsH<sub>4</sub>

**1-H<sub>4</sub>** was shown to hydrogenate ethylene in high yield. This hydrogenation is believed to occur through a Os(II)/Os(IV) type mechanism. This can likely be supported by osmium's stability at higher oxidation states and the inability of (<sup>t</sup>BuPNP)Os to access the Os(0) intermediate. TBE and NBE were used to see if this hydrogenation could be applied to other olefins such as NBE and TBE.

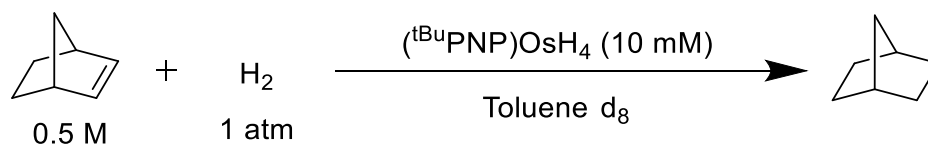


**Scheme 3.12:** (<sup>t</sup>BuPNP)OsH<sub>4</sub> hydrogenation of TBE

Hydrogenation reactions of TBE were prepared by adding a toluene d<sub>8</sub> stock solution of catalyst, TBE and standard (hexamethyldisiloxane) to a sealable NMR tube. Once the sample was charged with hydrogen gas and sealed it was heated to 85°C in a GC oven (rotating oven to stir the samples while heating). Results showed moderate reactivity for the hydrogenation of TBE to form TBA (tert-butyl ethane).

**Table 3.5:** Kinetics of TBE Hydrogenation

Time	TBE	TBA	Conversion	TO
0 min	500 mM	0	0%	0
1 hours	477.2mM	22.8 mM	4.5%	2.8
2 hours	464.7 mM	35.3 mM	7.1%	3.5
4 hours	385 mM	115 mM	23.0%	11.5



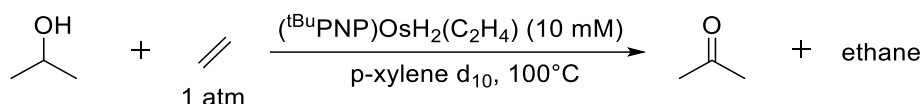
**Scheme 3.13** (<sup>t</sup>BuPNP)OsH<sub>4</sub> hydrogenation of NBE

The hydrogenation of NBE was carried out in the same fashion as the TBE reactions. NBE was also readily active for hydrogenation under H<sub>2</sub> atmosphere. After 2 hours of heating at 85°C approximately 125 mM of NBE (12.5 TO) was observed.

### 3.4 Dehydrogenation and Hydrogenation of 2-propanol and acetone

Both transfer and acceptor-less alkane dehydrogenation using **1-H<sub>4</sub>** were not successful. The dehydrogenation of alcohols has been reported to be much easier than dehydrogenation of alkanes. We next wanted to explore whether these substrates could be dehydrogenated using our pincer osmium complexes. The dehydrogenation of alcohols to ketones has been reported using osmium complexes including pincer-ligated osmium complexes.<sup>54</sup>

Alcohol dehydrogenation studies were performed using 2-propanol as the substrate and ethylene as the hydrogen acceptor. These reactions were run in sealable NMR tubes and then heated and stirred in a GC oven.



**Scheme 3.14:**  $(^t\text{BuPNP})\text{Os}(\text{C}_2\text{H}_4)$  transfer dehydrogenation of 2-propanol

**Table 3.6:** Kinetics of transfer isopropanol dehydrogenation

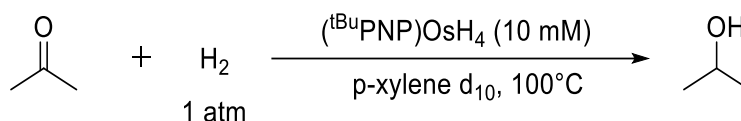
Time	2-Propanol	Acetone	Conversion	TO
0 min	523 mM	0	0%	0
2 hours	341 mM	182 mM	35%	14.0
4 hours	281 mM	242 mM	47%	18.6
7 hours	235 mM	288 mM	55%	22.2

Heating the 2-propanol/ethylene mixture to  $100^\circ\text{C}$  resulted in the formation of acetone and ethane, both of which were observed by  $^1\text{H}$ -NMR. The dehydrogenation of 2-propanol shows our osmium pincer complexes are active for dehydrogenation of more activated starting materials. This could also be explained by an alternative

mechanism for alcohol dehydrogenation going through a potential Os(II)/Os(IV) couple.

This would avoid the thermodynamically unfavorable formation of the Os(0) species.

Similar to alcohol dehydrogenation, the hydrogenation ketones using osmium based complexes including pincer-ligated osmium complexes has been reported.<sup>54</sup> We have demonstrated (<sup>t</sup>BuPNP)Os complexes can perform hydrogenations of alkanes such as ethylene, TBE and NBE. Next we attempted to hydrogenate ketones using acetone as the primary substrate.



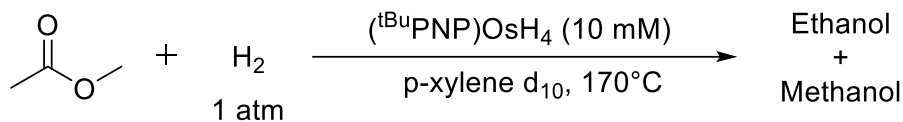
**Scheme 3.15:** (<sup>t</sup>BuPNP)OsH<sub>4</sub> hydrogenation of acetone

A reaction of acetone under one atmosphere of H<sub>2</sub> was heated to 100°C in a sealable NMR tube. After 2 hours 2-propanol was observed by NMR (86% conversion, 21 TO). Continued heating for another 2.5 hours pushed the overall conversion of 2-propanol to 94%. The hydrogenation of acetone was very fast at 100°C so this reaction was also run at 70°C to see if activity remained at lower temperature. At 70°C after six hour about 24% of acetone was hydrogenated to 2-propanol.

**Table 3.7:** Kinetics of hydrogenation of acetone (Reaction temperature 70°C)

Time	Acetone	2-Propanol	Conversion	TO
0 min	408.0 mM	0.0 mM	0.0%	0
1 hours	370.1 mM	37.1 mM	9.1%	3.9
3 hours	354.8 mM	53.2 mM	13.0%	5.54
6 hours	311.5 mM	96.5 mM	23.6%	10.1

In addition to hydrogenation of ketones, osmium complexes have been reported to hydrogenate esters to the corresponding alcohols.<sup>54</sup> We tested if (<sup>t</sup>BuPNP)Os complexes could also do this and using methyl acetate as our model substrate.



**Scheme 3.16:** (<sup>t</sup>BuPNP)OsH<sub>4</sub> hydrogenation of methyl acetate

A solution of methyl acetate with one atmosphere of H<sub>2</sub> was heated progressively to see if any hydrogenation would occur. Heating the reaction up to 150°C showed no reaction after two hours of heating. It was not until the solution was heated at 170°C for 14 hours was any reaction observed. Both ethanol and methanol could be seen in the proton NMR confirming hydrogenation of the substrate. However only a small amount of products was observed (approximately 2.7 turnovers). The multiple turnovers suggest a catalytic hydrogenation, however not a very active one.

### 3.5 Synthesis of (<sup>i</sup>PrPNP)Os complexes

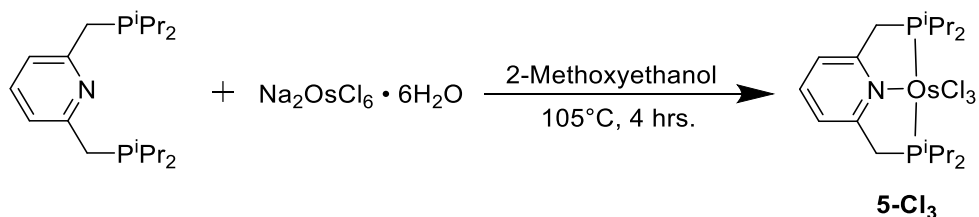
#### 3.5.1 Synthesis of (<sup>t</sup>BuPNP)OsCl<sub>3</sub> and (<sup>t</sup>BuPNP)OsH<sub>4</sub>

Alteration of the substituents on the phosphorus donor ligands of pincer based complexes is extremely common in order to adjust steric bulk and alter electronic properties of the ligand. In the case of the classic PCP ligand motif groups such as *t*-butyls, isopropyls, phenyls, trifluoromethyls have all been used as R groups on the phosphorus ligands. These alterations can have a great impact on the activity of the

catalyst. (<sup>i</sup>PrPCP)Ir is reported to have much higher activity for alkane dehydrogenation than the corresponding (<sup>t</sup>BuPCP)Ir complex. However loss of regioselectivity for terminal olefins was also obtained when switching from t-butyls to isopropyls.

The inability of **1-H<sub>4</sub>** to perform alkane dehydrogenation lead us to modify the catalyst in the hopes of improving the catalytic activity. The corresponding (PCP)Ir complexes have shown that changing the phosphorus substituents to less bulky isopropyl groups could lead to an increase in activity for alkane dehydrogenation. In light of this the (<sup>i</sup>PrPNP)OsH<sub>4</sub> complex was synthesized and studied for its reactivity towards alkane dehydrogenation.

Synthesis of the (<sup>i</sup>PrPNP) ligand was performed according to literature reports.<sup>55</sup> Metalation of the ligand was done analogous to **1-Cl<sub>3</sub>** by reacting the ligand with Na<sub>2</sub>OsCl<sub>6</sub> • 6H<sub>2</sub>O in 2-methoxyethanol.



**Scheme 3.17:** Synthesis of (<sup>i</sup>PrPNP)OsCl<sub>3</sub> (**5-Cl<sub>3</sub>**)

Just as in the case of (<sup>t</sup>BuPNP)OsCl<sub>3</sub>, <sup>1</sup>H and <sup>31</sup>P-NMR of the recrystallized product indicated the formation of a paramagnetic product. A single crystal of the product was obtained and a structure was determined, however the crystal was not of high enough quality for data to calculate the bond distances and angles.



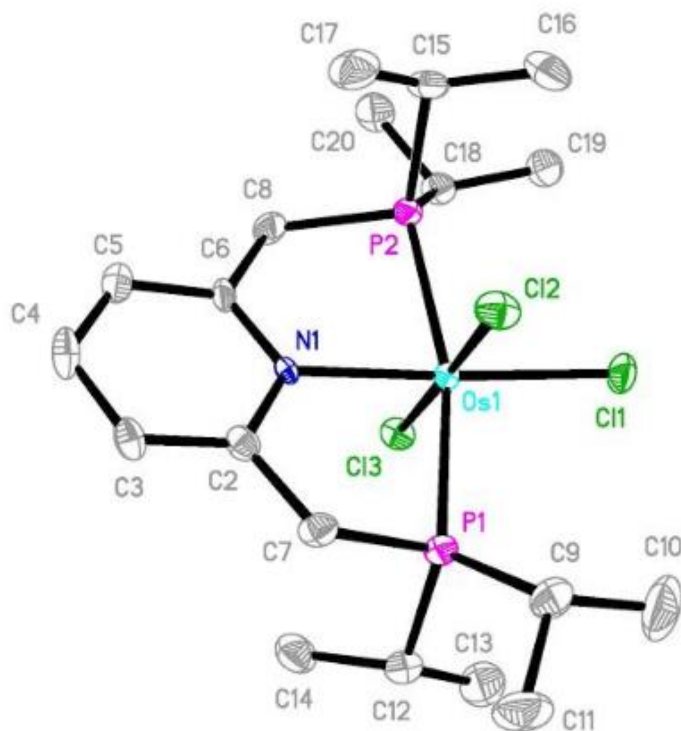
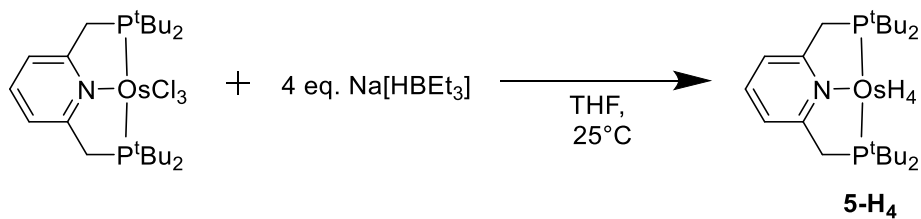


**Figure 3.11:** ORTEP representation (50% probability ellipsoids) of the structure of **5-Cl<sub>3</sub>** determined by X-ray diffraction. H atoms other than hydrides omitted.

**5-Cl<sub>3</sub>** was allowed to react with 4 equiv of sodium triethylborohydride in THF resulting in the formation of an orange/red sticky solid.



**Scheme 3.18:** Synthesis of (<sup>i</sup>PrPNP)OsH<sub>4</sub> (**5-H<sub>4</sub>**)

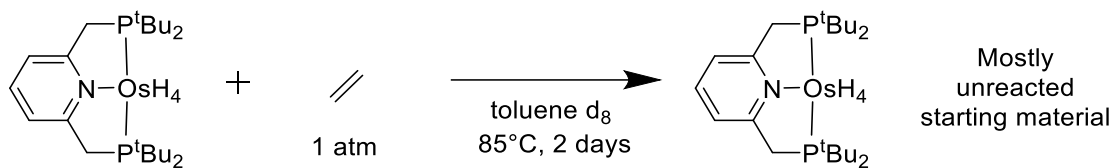
The <sup>31</sup>P NMR spectrum of the sample showed one main signal at δ 58.4 ppm with about 4 small signals between 56 and 58 ppm. The <sup>1</sup>H NMR spectrum, in addition to signals

attributable to the coordinated  $i^{\text{Pr}}\text{PNP}$  ligand revealed a broad signal at -8.95 ppm which integrates to 4 protons.

### 3.5.2 ( $i^{\text{Pr}}\text{PNP}$ )OsH<sub>4</sub> reactivity with olefins

As was stated previously olefins such as NBE, TBE, or 1-hexene are readily hydrogenated by (PCP)IrH<sub>4</sub> at relatively low temperatures. This was not the reactivity that was observed when **1-H<sub>4</sub>** was reacted with olefins as hydrogenation required higher temperatures and resulted in the loss of signals in both the <sup>1</sup>H and <sup>31</sup>P NMR. Next **5-H<sub>4</sub>** was reacted with olefins (NBE, TBE and ethylene) to see if the decreased steric bulk would have any effect on hydrogenation of the olefin.

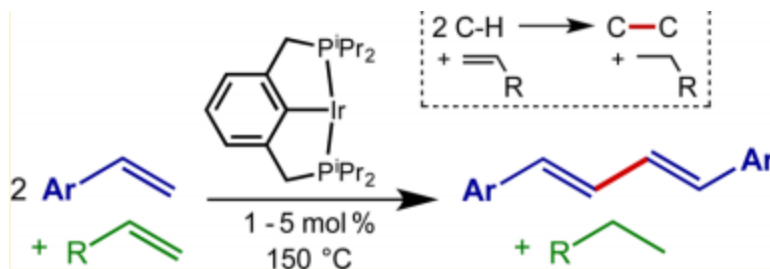
Reaction of **5-H<sub>4</sub>** with both TBE and NBE were resulted in no reaction. At room temperature no hydrogenated product was observed and even upon elevating the temperature to 100°C. Additionally no change in the signals in both the <sup>1</sup>H and <sup>31</sup>P NMR were observed. Reaction of **1-H<sub>4</sub>** with ethylene resulted in the formation of **1-H<sub>2</sub>(C<sub>2</sub>H<sub>4</sub>)** at elevated temperatures. Similar reactivity was expected with ( $i^{\text{Pr}}\text{PNP}$ )OsH<sub>4</sub> when reacted with ethylene, however no such product was observed. The mixture of **5-H<sub>4</sub>** and ethylene showed no reaction at room temperature. Upon heating to 85°C for 2 days slight loss of the ( $i^{\text{Pr}}\text{PNP}$ )OsH<sub>4</sub> signal was observed however much of the product remained the tetrahydride. The decreased steric bulk of the **5-H<sub>4</sub>** complex must make dissociation of H<sub>2</sub> less favorable hindering alkane hydrogenation.



**Scheme 3.19:** Reaction of (5-H<sub>4</sub>) with Ethylene

### 3.6 Dehydrogenative C-C coupling of styrene

The catalytic dehydrogenative C-C coupling of styrene using (<sup>i</sup>PrPCP)IrH<sub>4</sub> was recently reported by our group<sup>56</sup>. Using this catalyst it was reported that vinyl arenes could be coupled to form predominately (*E,E*)-1,4-diaryl-1,3 butadienes. Additionally the H<sub>2</sub> generated from this reaction could be used to hydrogenate one equivalent of arene to form the corresponding ethyl arene. DFT calculations of this reaction suggest a double C-H activation of styrene at both the ortho-aryl and β vinyl positions to form a Ir(III) intermediate. Addition of a second styrene through the β vinyl position leads to the formation of the C-C coupled product. The DFT calculations suggest that a transient Ir(V) species through a Ir(III)/Ir(V) couple is involved in this reaction and is the rate determining step. (PNP)OsH<sub>4</sub> under a similar mechanism would undergo a Os(II)/Os(IV) cycle for this reaction. The much easier accessibility of the Os(IV) oxidation state could allow accelerated rates for this reaction.



**Scheme 3.20:** Dehydrogenative coupling of styrene using (<sup>i</sup>PrPCP)Ir

Reaction of **1-H<sub>4</sub>** with styrene showed no reaction to form the 1,3 butadienes. At elevated temperatures (150°C) the only products observed were polymerized styrene. Control reactions showed polymerization was not caused by **1-H<sub>4</sub>**. Reaction of styrene with **5-H<sub>4</sub>** did show reactivity for dehydrogenative C-C coupling.

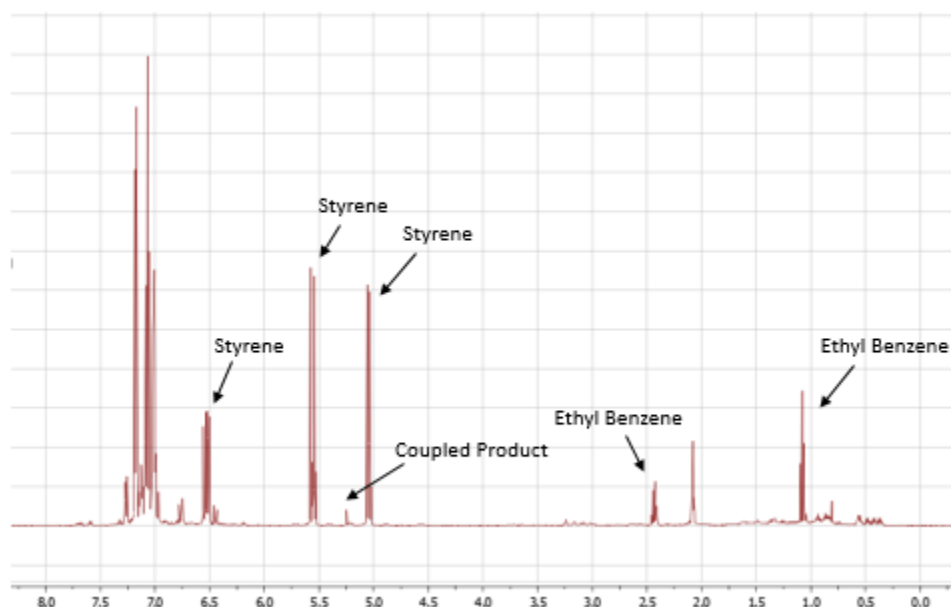


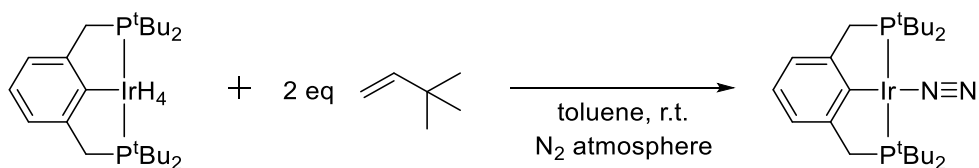
**Figure 3.12:** <sup>1</sup>H-NMR of dehydrogenative coupling of styrene using (**5-H<sub>4</sub>**)

Reactivity for dehydrogenative coupling of styrene using **5-H<sub>4</sub>** was observed and the overall activity was quite low. The reaction was run at 150°C for 30 hours and

concentration of coupling products were calculated by  $^1\text{H-NMR}$ . The spectra showed a total of 21 mM of product or about 1.33 turnovers (4.1% conversion). In comparison, reaction of  $(^i\text{PrPCP})\text{IrH}_4$  with styrene at  $150^\circ\text{C}$  produced 168 mM of product (92% conversion) after 30 hours. From the experimental data it is clear that PCPIr is still the superior catalyst for this reaction despite the possible advantages of using osmium.

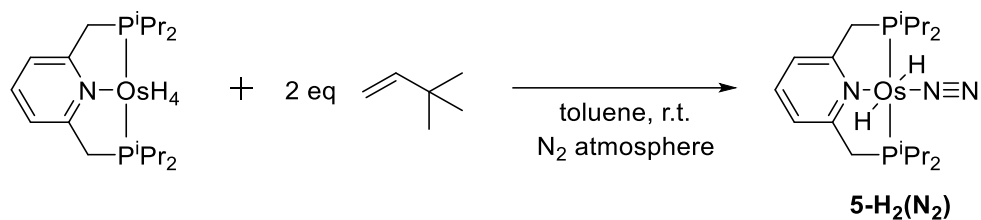
### 3.7 Reaction of $(^i\text{PrPNP})\text{OsH}_4$ (5-H<sub>4</sub>) with $\text{N}_2$

Pincer-ligated iridium complexes have been reported to form strong bonds to dinitrogen. In most cases reactions using these catalysts have to be performed under argon to avoid nitrogen binding to the  $14\text{ e}^-$  active species interfering with catalysis.<sup>57</sup> Synthesis of these dinitrogen bound complexes is done by treating the pincer-ligated iridium poly-hydride with hydrogen acceptor (TBE) under a nitrogen atmosphere. This will generate the four coordinate Ir(I) dinitrogen complex.<sup>57</sup>



**Scheme 3.21:** Formation of four coordinate  $(^t\text{BuPCP})\text{IrN}_2$  complex

$(^R\text{PNP})\text{Os}$  complexes are isoelectronic to  $(^R\text{PCP})\text{Ir}$  complexes that readily form dinitrogen complexes. We were interested to see if these pincer ligated osmium complexes would also form stable dinitrogen complexes.



**Scheme 3.22:** Formation of  $(5-H_2(N_2))$

Reaction of  $(iPrPNP)OsH_4$  with 2 equivalents of TBE under a nitrogen atmosphere yielded no new products at room temperature. Upon heating the solution to 105°C for 2 hours the color of the solution changed from orange to yellow. Two new phosphorus signals were visible in the  $^{31}P$ -NMR and upon continued heating at 105°C for another 5 hours full conversion to a single new species was observed.

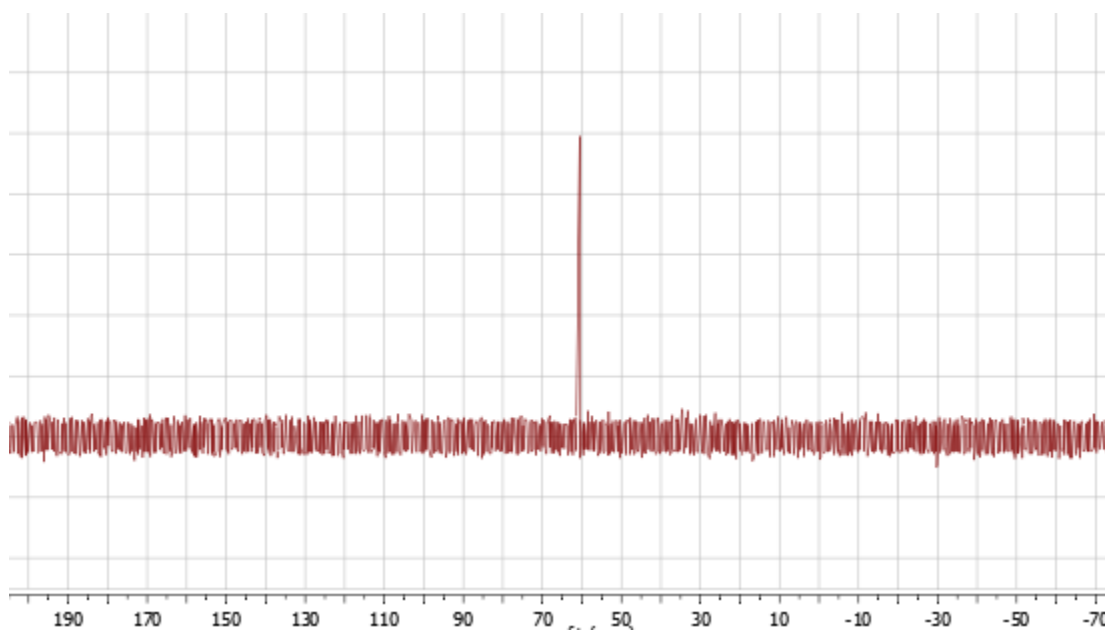


**Figure 3.13:**  $^{31}P$ -NMR of  $(5-H_2(N_2))$

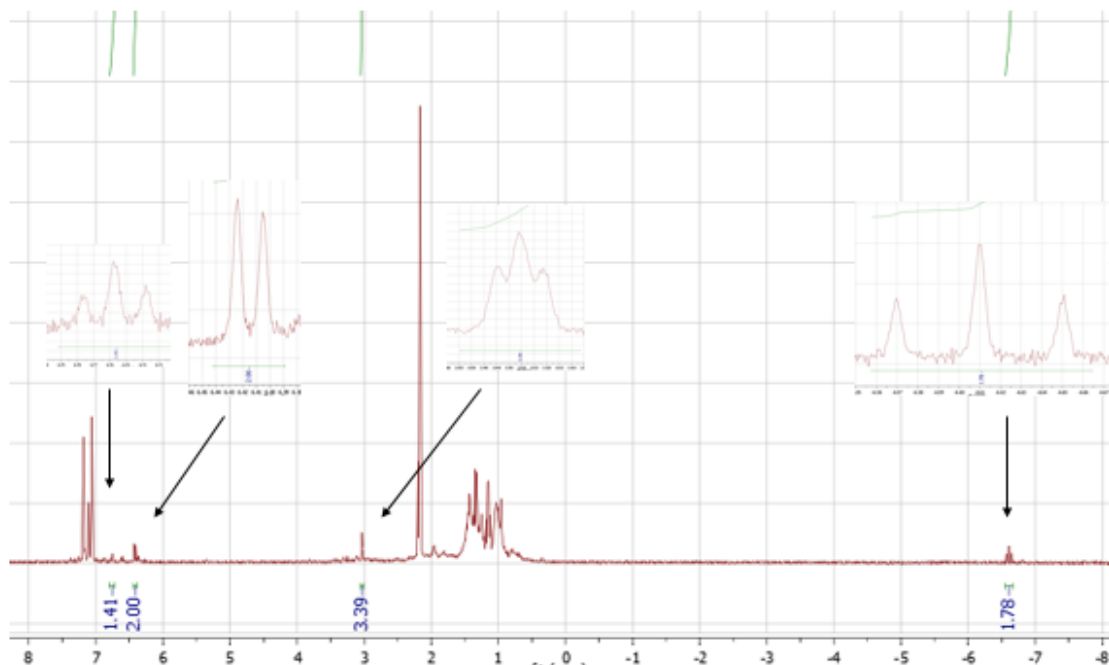


**Figure 3.14:**  $^1\text{H}$ -NMR of  $(5\text{-H}_2(\text{N}_2))$

$^{31}\text{P}$ -NMR showed a single product with a singlet at 60 ppm.  $^1\text{H}$ -NMR showed all the corresponding ligand signals with a triplet observed in the hydride region at -6.7 ppm. Integration of the hydride signal relative to the aryl protons correlates to 2 protons. This is consistent with formation of a (PNP)Os trans dihydride dinitrogen complex. IR spectroscopy of the complex revealed a large stretching frequency at  $2272\text{ cm}^{-1}$  consistent with osmium dinitrogen complexes.<sup>58</sup>

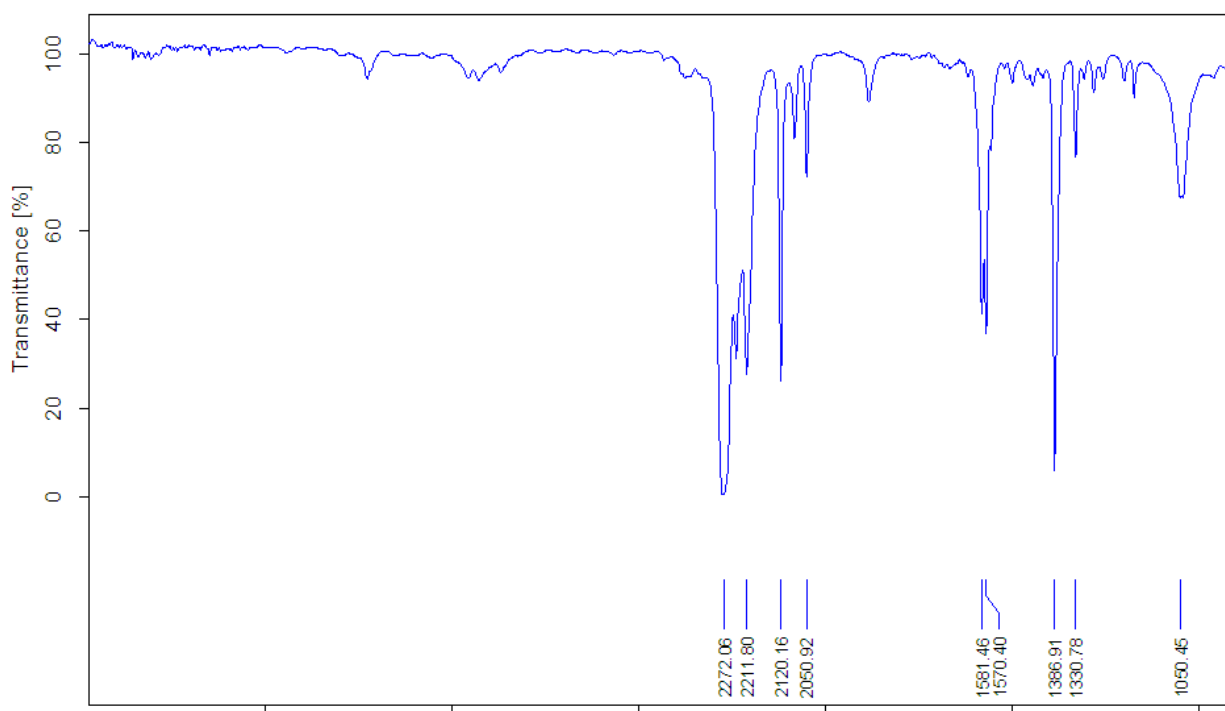


**Figure 3.15:** IR spectra of **(5-H<sub>2</sub>(N<sub>2</sub>))**

### 3.8 Reactivity of **1-H<sub>4</sub>** with carbon monoxide

Carbon monoxide is one of the most ubiquitous ligands present in transition metal chemistry. The back-bonding ability of carbon monoxide makes it a strongly bound ligand very useful for the trapping of intermediates. Reports using carbon monoxide to form stable pincer ligated iridium species are plentiful. Herein we report the reactivity of carbon monoxide with (<sup>t</sup>BuPNP)Os fragments discussed in this chapter.

Reactivity of **1-H<sub>2</sub>(C<sub>2</sub>H<sub>4</sub>)** with carbon monoxide was discussed earlier in this chapter, wherein the osmium bound ethylene under goes insertion into the osmium hydride bond reversibly at room temperature. Under a CO atmosphere coordination of CO to the osmium ethyl hydride complex is observed to form the **1-(H)(Et)(CO)** complex.



Reaction of **1-H<sub>4</sub>** with carbon monoxide at room temperature resulted in no formation of any new product. This was not unexpected as DFT calculations have suggest that the formation of (<sup>t</sup>BuPNP)OsH<sub>2</sub> by H<sub>2</sub> loss from **1-H<sub>4</sub>** has a  $\Delta G$  of 23 kcal/mol. Upon heating the solution to 80°C for 3 hours, 3 new products were visible in both the <sup>31</sup>P and <sup>1</sup>H-NMR with **1-H<sub>4</sub>** still remaining as the major species. In the <sup>31</sup>P-NMR two new singlets were observed in addition to four peaks that exhibited typical AB splitting pattern usually seen when pincer phosphorus atoms are inequivalent. The hydride region of the <sup>1</sup>H-NMR spectrum showed two new triplets (*J* = 20 Hz each), as well as two doublet of triplets (*J* = 5, 23 and 4, 13 Hz). The two doublet of triplets are consistent with formation of a cis-(PNP)Os(H)<sub>2</sub>CO complex. One of the new triplets observed is most likely then formation of the trans-dihydride carbonyl complex.

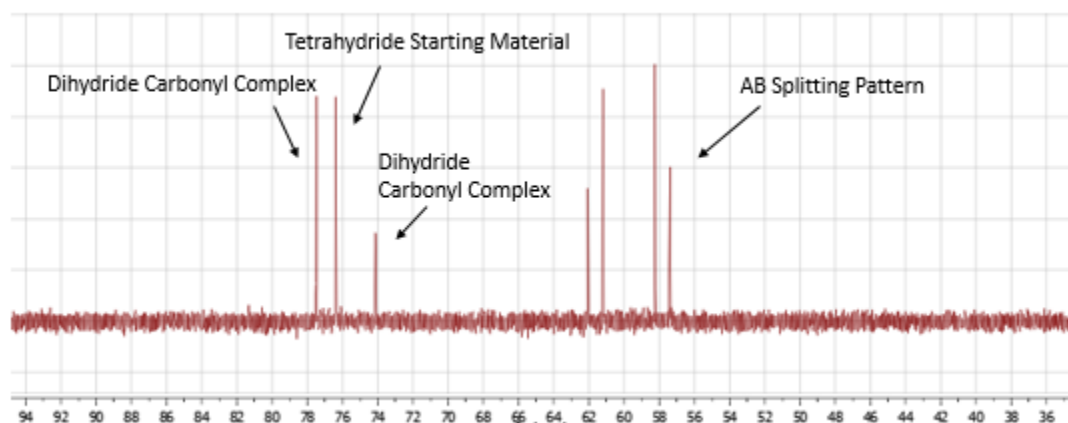


**Figure 3.16:** <sup>31</sup>P-NMR of reaction of (**1-H<sub>4</sub>**) with CO

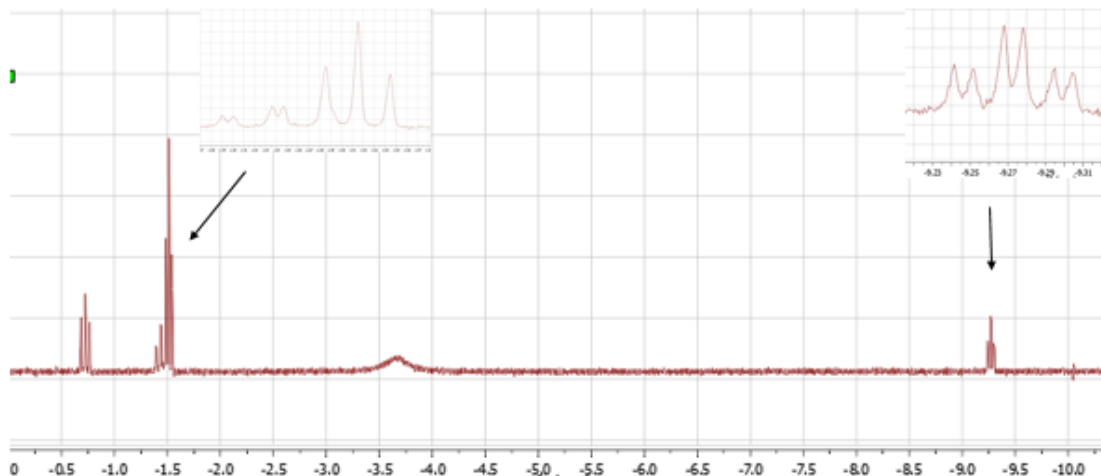
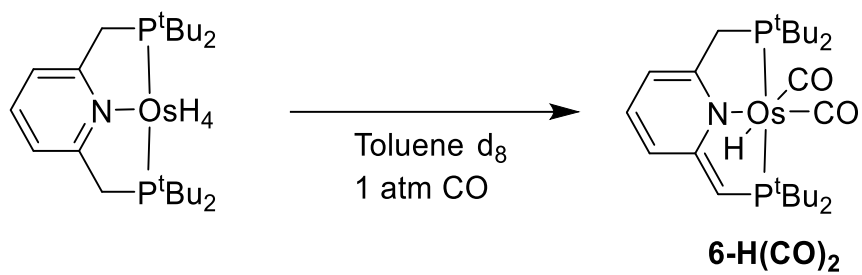


**Figure 3.17:**  $^1\text{H}$ -NMR: Hydride region of reaction of (**1-H<sub>4</sub>**)

Upon continued heating at 90°C for 16 hours full conversion was observed to the species with inequivalent phosphorus atoms.  $^{31}\text{P}$ -NMR showed four peaks with an AB splitting pattern with J values of 173 and 458 Hz. The  $^1\text{H}$ -NMR hydride region showed a single triplet which integrated to 1 proton when compared to the aryl backbone protons, which were now observed as three separate multiplet peaks. The loss of symmetry of the molecule was observed not only in the aryl peaks but in the t-butyl groups as well which are now split into two doublets of doublets. Additionally three new peaks (vt and 2 dd) were observed between 2.5 and 4 ppm all which integrated to 1 proton. The product was concluded to be the dearomatized ( $^t\text{BuPNP}$ )OsH(CO)<sub>2</sub> (**6-H(CO)-2**). Dearomatization of this ligand has been well documented by Milstein<sup>59</sup> and has been observed with many ( $^t\text{BuPNP}$ )M complexes.<sup>60</sup>



**Scheme 3.23:** Synthesis of (<sup>t</sup>BuPNP)OsH(CO)<sub>2</sub> (**5-H(CO)<sub>2</sub>**)

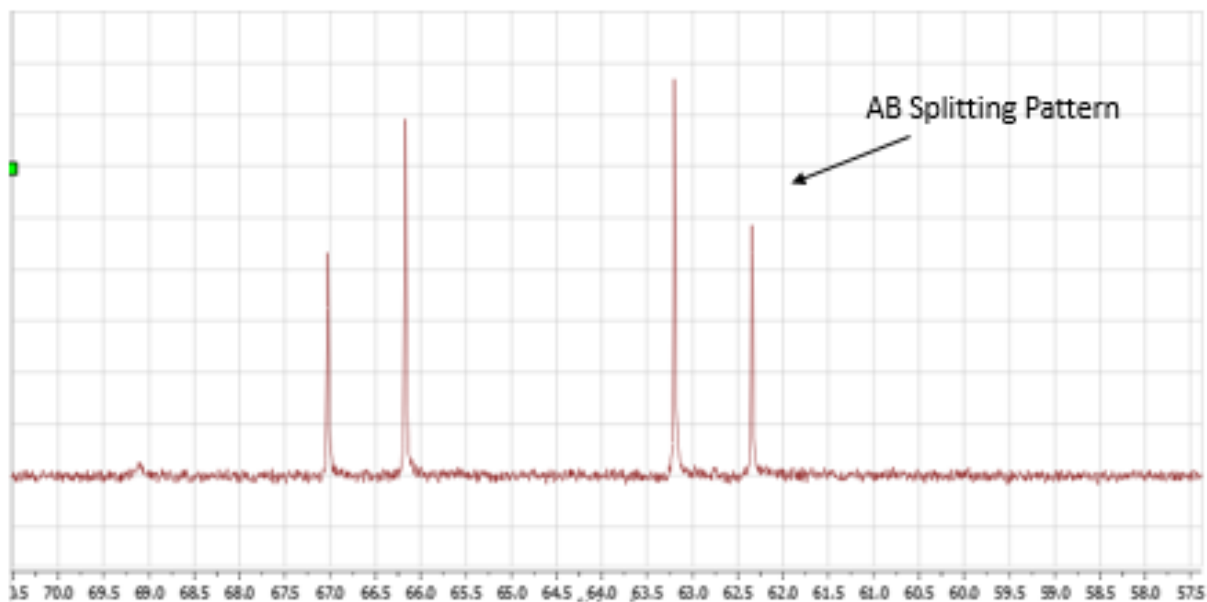


**Figure 3.18:** <sup>31</sup>P-NMR of (**6-H(CO)<sub>2</sub>**)

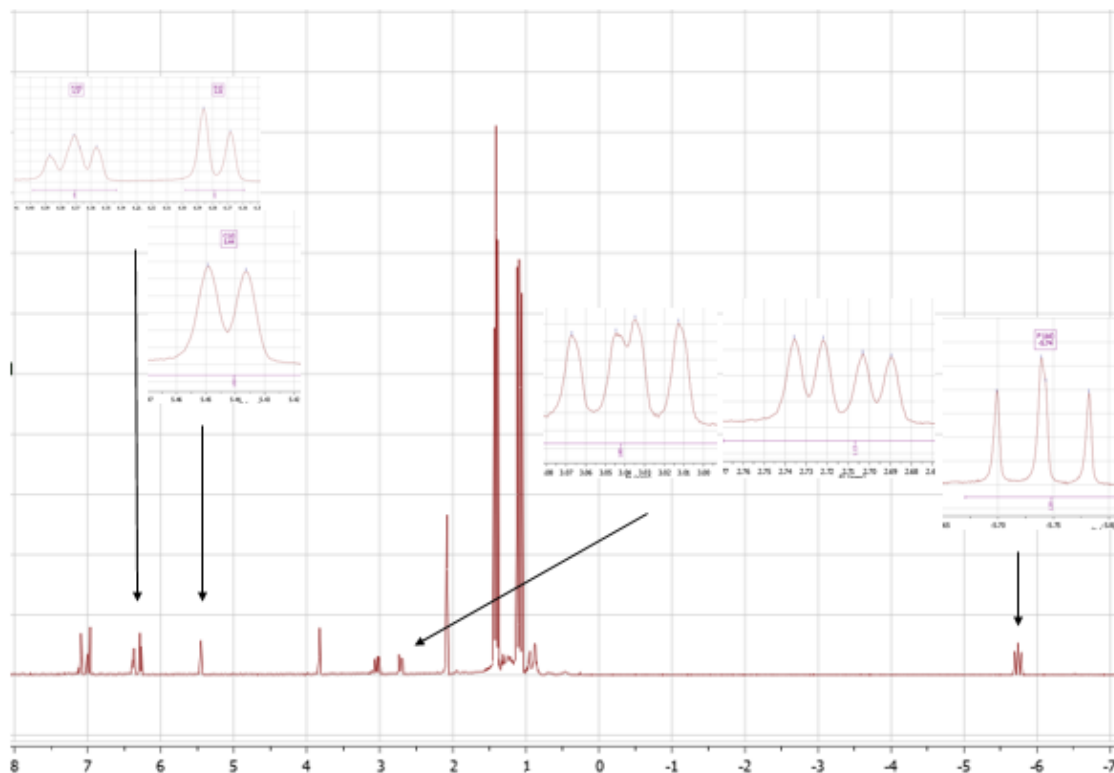


**Figure 3.19:**  $^1\text{H}$ -NMR of  $(6\text{-H}(\text{CO})_2)$

The NMR data is consistent with initial formation of 3 species the *trans*- $(^t\text{BuPNP})\text{Os}(\text{H})_2(\text{CO})$ , *cis*- $(^t\text{BuPNP})\text{Os}(\text{H})_2(\text{CO})$  and the dearomatized  $(^t\text{BuPNP})\text{OsH}(\text{CO})_2$  which upon continued heating all convert to the dearomatized product. MALDI TOF mass spectroscopy of the final product was conducted and confirmed the mass of the product. Parent peaks observed were consistent with standard osmium isotope splitting patterns and with the final products mass minus loss of one of the carbon monoxide ligands. Mass spec simulation showed an identical spectra providing more evidence for the product identification.

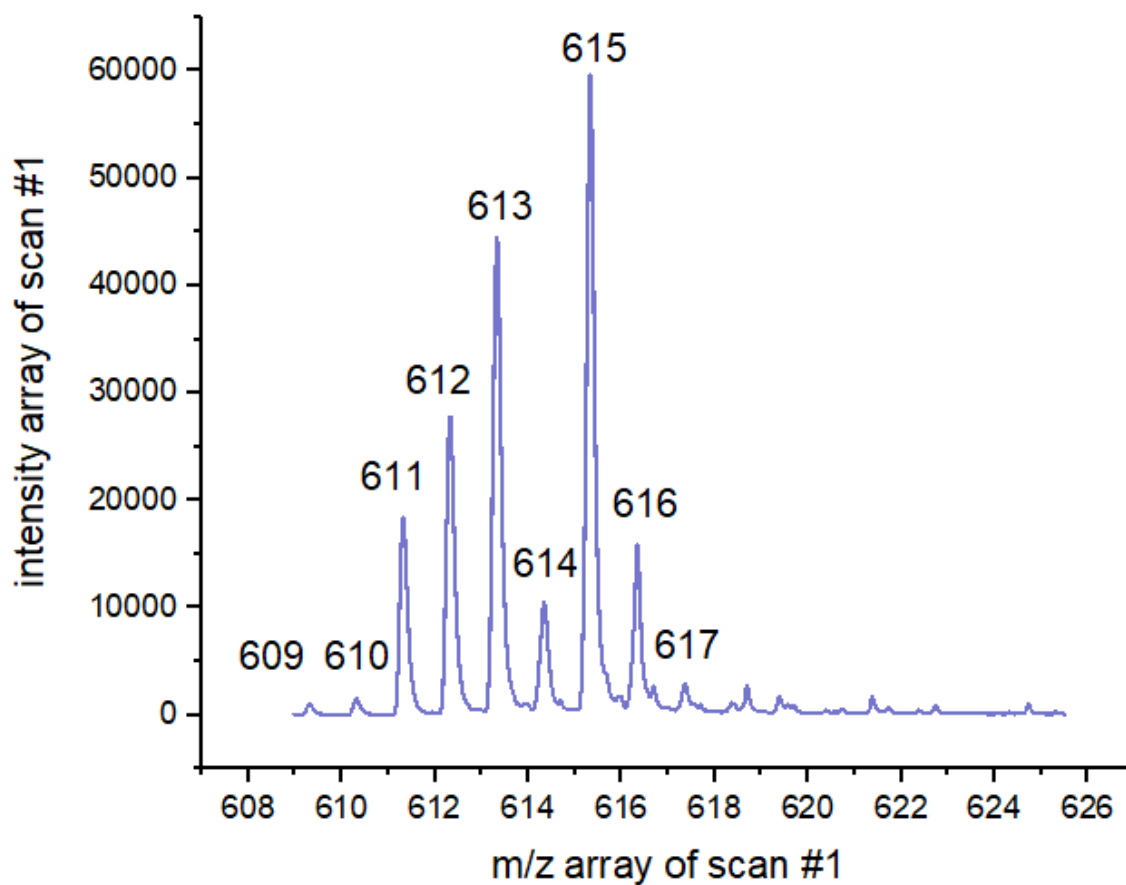


Figure 3.20: MALDI TOF spectra for (6-H(CO)<sub>2</sub>)

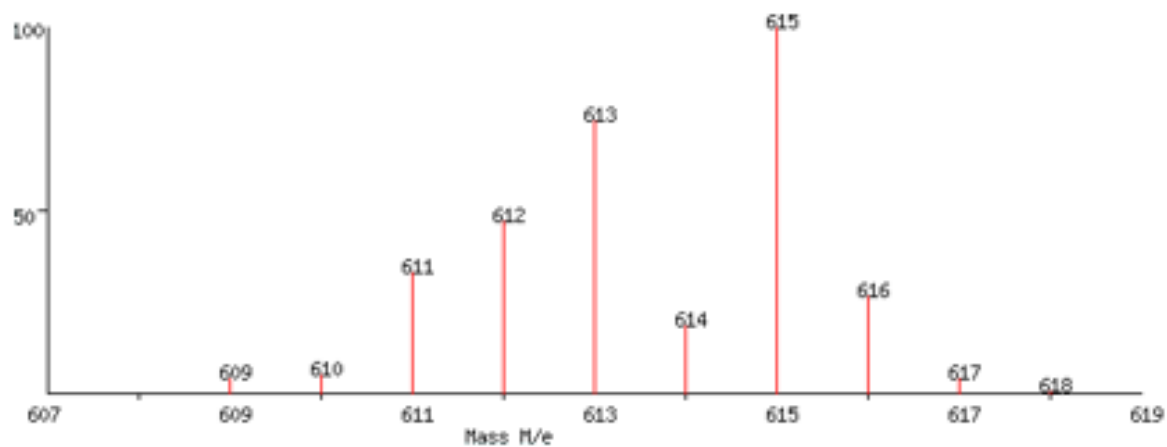
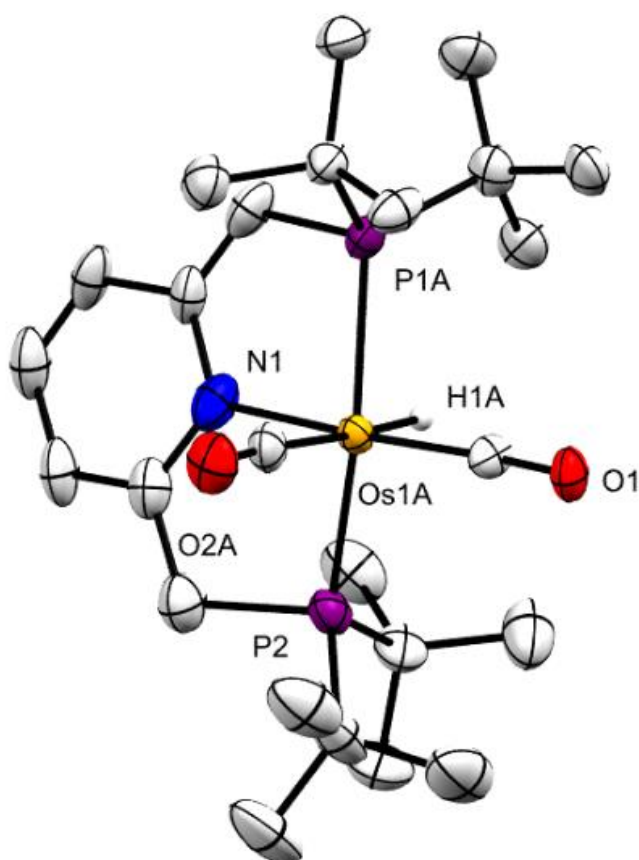


Figure 3.21: Mass Spec simulation of (6-H(CO)<sub>2</sub>) minus one carbon monoxide ligand

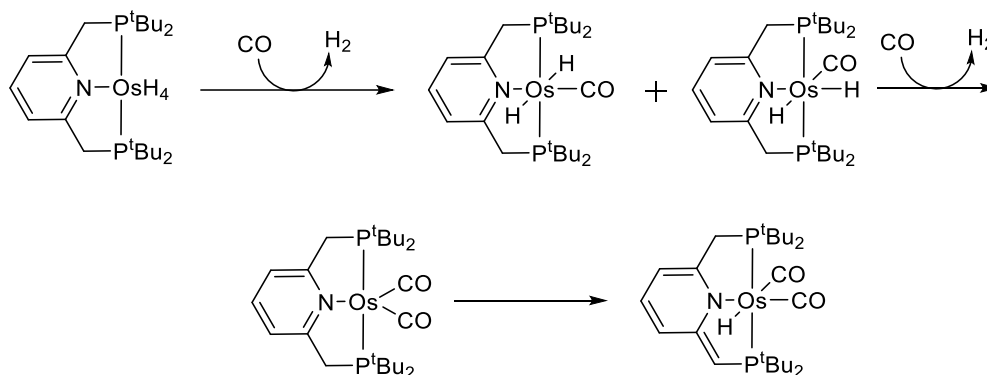
Single crystal X-ray analysis confirmed the structure as **6-H(CO)<sub>2</sub>** complex.

Twining of the crystal was observed however resolution of the crystal provided adequate crystal data. Bond distances between the pyridine ring and the CH<sub>2</sub> linker arms show distinct distances with one arm having a distance of 1.50 Å and the other 1.34 Å. The bond distance of 1.34 Å is consistent with a C-C double bond giving further evidence to the dearomatized structure.



**Figure 3.22** ORTEP representation (50% probability ellipsoids) of the structure of **6-H(CO)<sub>2</sub>** determined by X-ray diffraction; hydrogen atoms omitted for clarity.

The DFT calculated mechanism for this reaction was calculated to be initial loss of H<sub>2</sub> from **1-H<sub>4</sub>** followed by coordination of carbon monoxide to form the (t<sup>Bu</sup>PNP)(H)<sub>2</sub>(CO) complex. From there loss of another equivalent of H<sub>2</sub> followed by coordination of another equivalent of CO would give the (t<sup>Bu</sup>PNP)Os(CO)<sub>2</sub> complex. Dearomatization can then occur through transfer of a proton from the linker CH<sub>2</sub> arm to the metal center.



**Scheme 3.24:** Mechanism for formation of **(6-H(CO)<sub>2</sub>)**

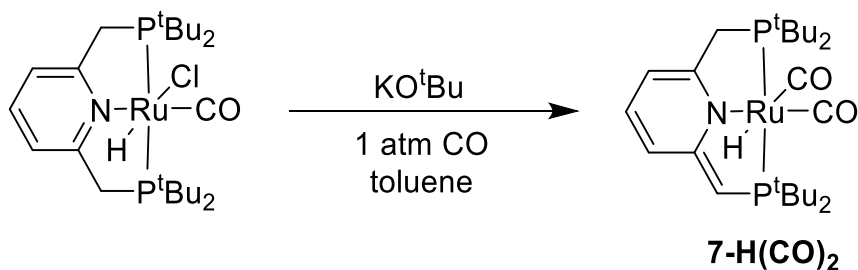
### 3.9 Metal effects on the dearomatization of (t<sup>Bu</sup>PNP)M complexes

The observation of the (t<sup>Bu</sup>PNP) ligand's dearomatization in complex **6-H(CO)<sub>2</sub>** was not surprising as this ligand has been reported to undergo such transformations. This however led us to hypothesize what factors influence this dearomatization. We chose to investigate what effects the metal in these complexes might have on this dearomatization and decided to focus on iron, ruthenium and osmium.

In 2008, our group reported the synthesis of (t<sup>Bu</sup>PNP)Fe(CO)<sub>2</sub>, the Fe analogue to the (t<sup>Bu</sup>PNP)Os(CO)<sub>2</sub> complex believed to occur in the formation of **6-H(CO)<sub>2</sub>**. It was reported that (t<sup>Bu</sup>PNP)Fe(CO)<sub>2</sub> was isolated as a stable blue solid. This suggest that this

complex favors the aromatized (<sup>t</sup>BuPNP)Fe(0) isomer. This observation was contrary to what we believe occurs with complex **6-H(CO)<sub>2</sub>** in which we do not isolate the Os(0) dicarbonyl intermediate. Instead in the case of osmium the complex favors the dearomatized (<sup>t</sup>BuPNP)Os(II) species.

In order to see how the metal effects the dearomatization of the ligand further we chose to look at the ruthenium analogues of these complexes in order to study the effects of moving down a group in the periodic table. (<sup>t</sup>BuPNP)Ru complexes and dearomatization of the PNP ligand framework have been studied extensively by the Milstein group. In 2010, the Milstein group<sup>61</sup> reported the synthesis of (<sup>t</sup>BuPNP)RuHCl(CO). This complex was prepared following literature procedure and treated with base under a carbon monoxide atmosphere. The resulting product was the dearomatized (<sup>t</sup>BuPNP)RuH(CO)<sub>2</sub> complex (**7-H(CO)<sub>2</sub>**).



**Scheme 3.25:** Synthesis of (**7-H(CO)<sub>2</sub>**)

The complex was identified by <sup>31</sup>P-NMR in which an AB splitting pattern of two doublets was observed at δ 93 ppm. The <sup>1</sup>H-NMR showed the same ligand pattern as **6-H(CO)<sub>2</sub>**, with a hydride signal (doublet of doublets) at δ -6.05 ppm.



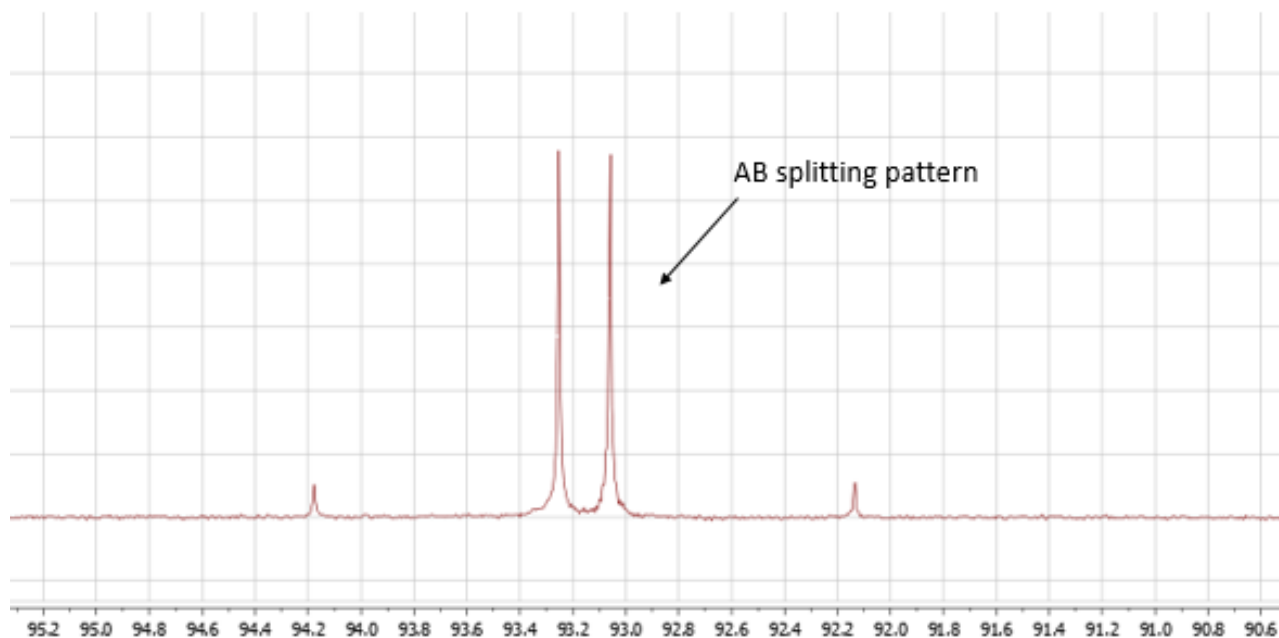


Figure 3.23.  $^{31}\text{P}$  NMR spectrum of 7-H(CO)<sub>2</sub>

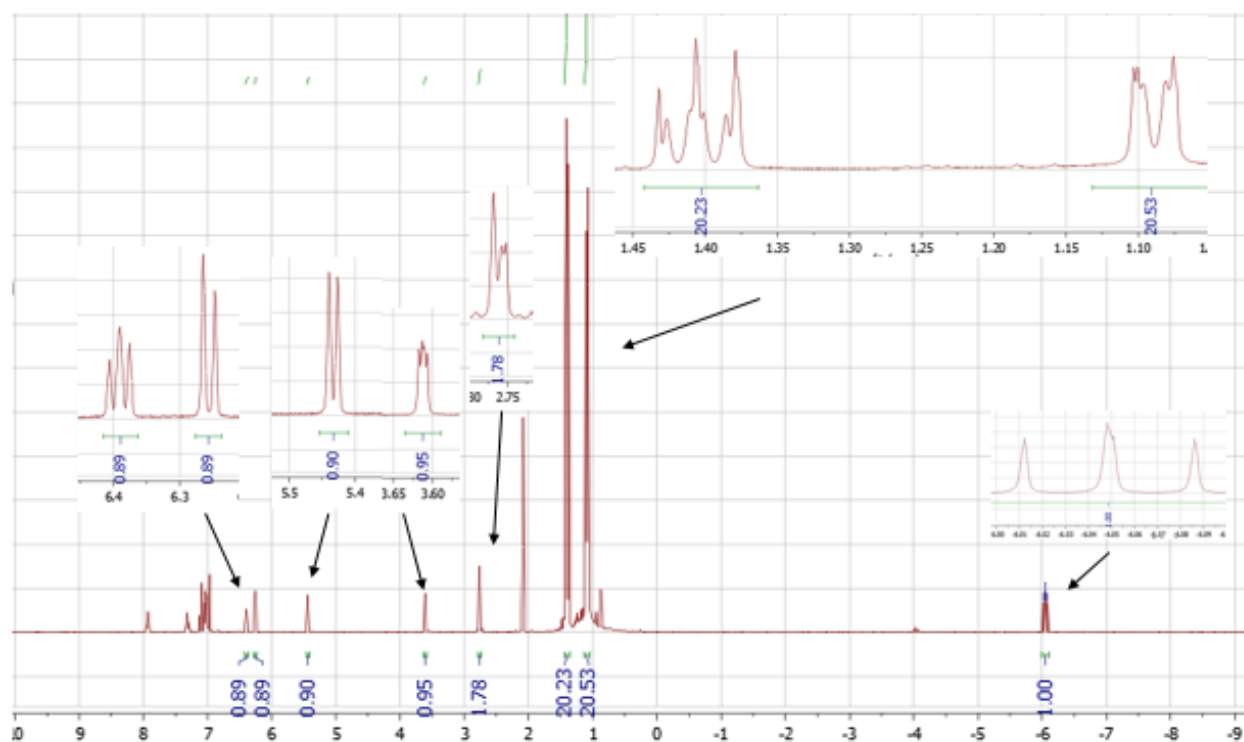
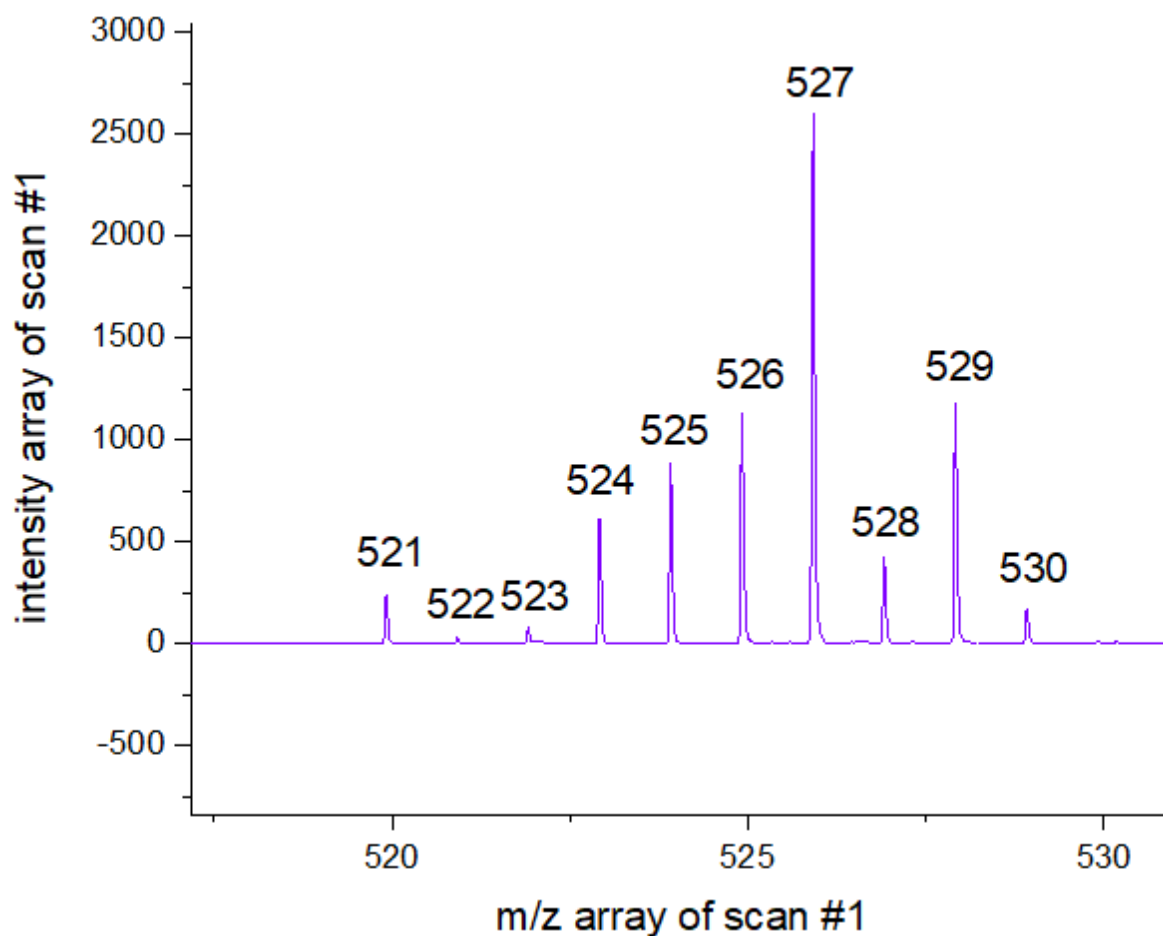
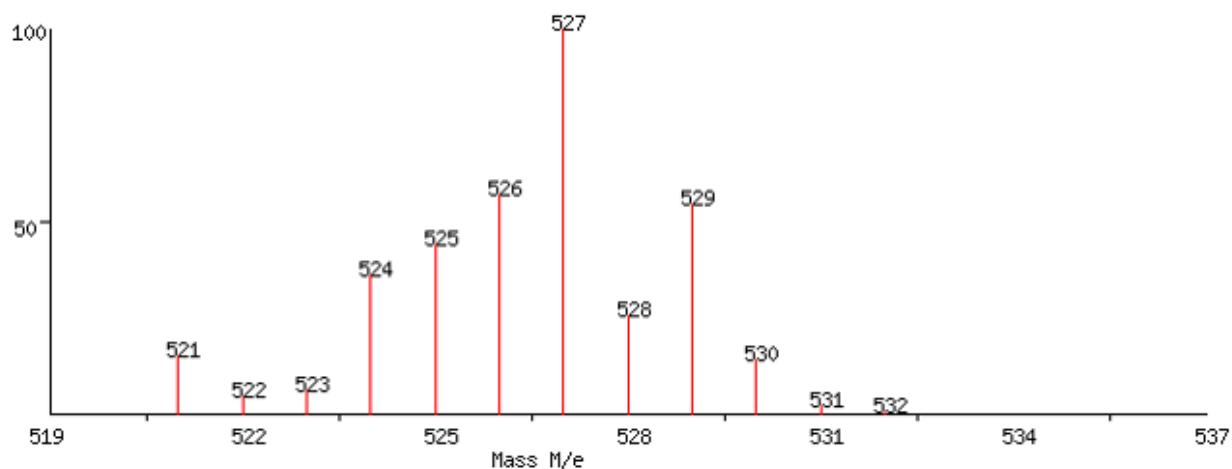


Figure 3.24.  $^1\text{H}$  NMR spectrum of 7-H(CO)<sub>2</sub>

In addition to NMR analysis, MALDI TOF mass spectroscopy of the product was conducted and confirmed the mass of the product. Parent peaks observed were consistent with standard ruthenium isotope splitting patterns and with the final products mass minus loss of one of the carbon monoxide ligands. Mass spec simulation showed an identical spectra providing more evidence for the product identification.



**Figure 3.25:** MALDI TOF spectra for (7-H(CO)<sub>2</sub>)



**Figure 3.26:** : Mass Spec simulation of **7-H(CO)<sub>2</sub>** minus one carbon monoxide ligand

Finally single crystal X-ray diffraction studies confirmed a isostructural product to the corresponding osmium analogue **6-H(CO)<sub>2</sub>**. Aryl-CH<sub>2</sub> bond distances of 1.51 and 1.39 are consistent with a double bond between one linker arm and the benzene ring.

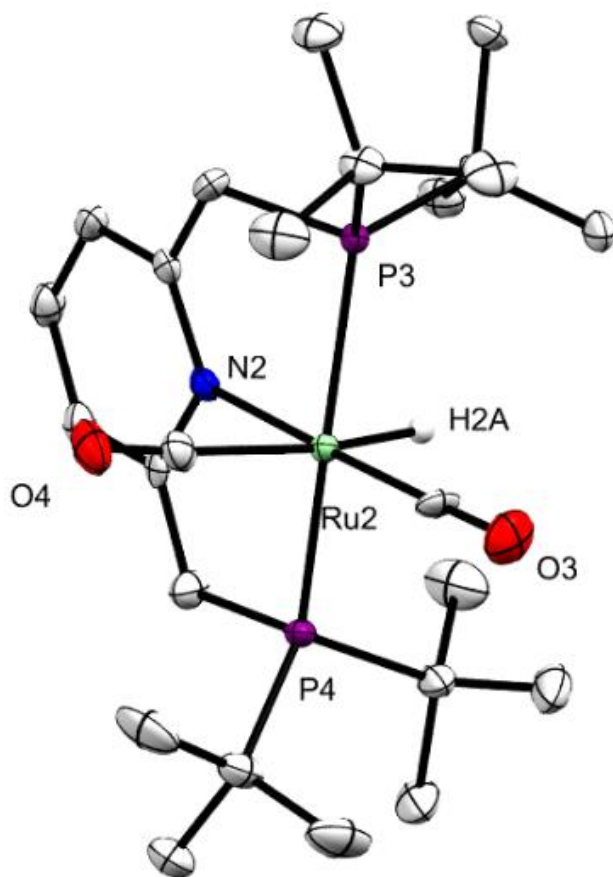
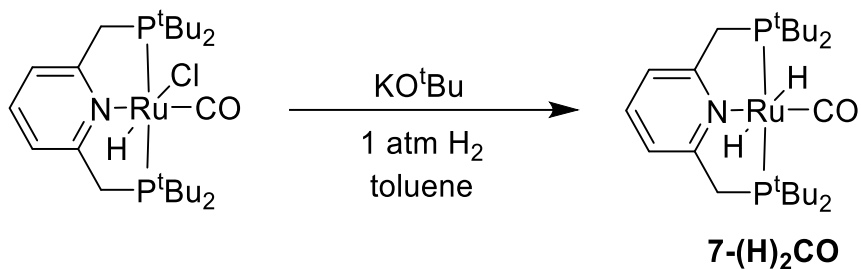


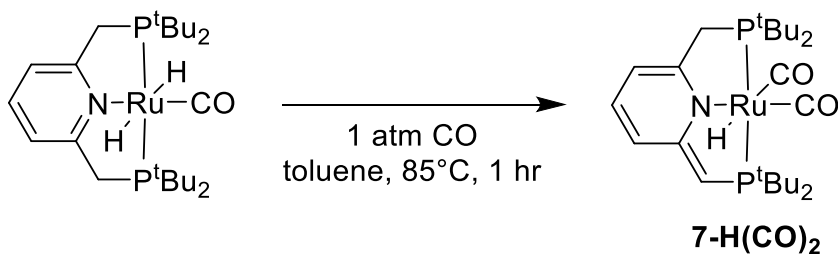
**Figure 3.27:** ORTEP representation (50% probability ellipsoids) of the structure of **7-H(CO)<sub>2</sub>** determined by X-ray diffraction; hydrogen atoms omitted for clarity.

One issue with synthesizing **7-H(CO)<sub>2</sub>** in this fashion is the possibility that the base could directly deprotonated the ligand yielding the dearomatized structure. In this scenario the preference of the ruthenium complex for the PNP Ru(0) complex vs. the PNP Ru(II) complex could not be determined. To remedy this situation the (<sup>t</sup>BuPNP)RuHCl(CO) complex was treated with base under a hydrogen atmosphere resulting in formation of the trans-(<sup>t</sup>BuPNP)Ru(H)<sub>2</sub>CO complex.



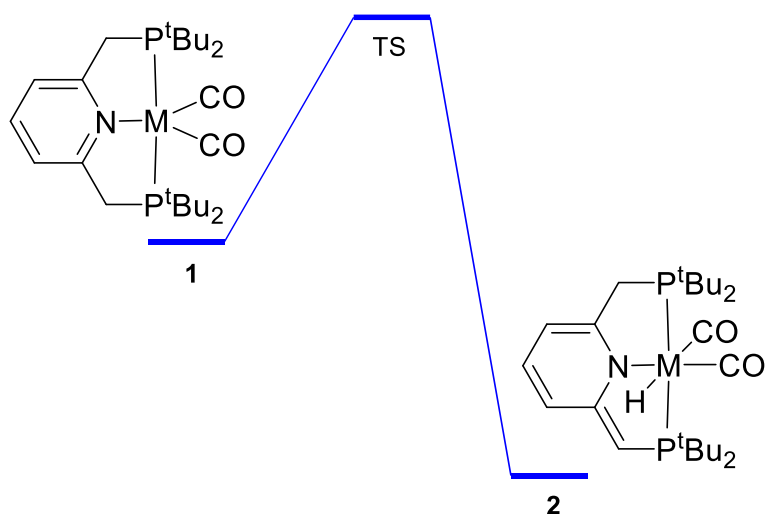
**Scheme 3.26:** Synthesis of **7-H(CO)<sub>2</sub>**

Complex **7-(H)<sub>2</sub>CO** is the ruthenium analogue of a species we identified in the osmium mechanism for formation of the dearomatized product. This product was then heated to 85°C under a carbon monoxide atmosphere upon which dearomatization to form complex **7-H(CO)<sub>2</sub>** occurred. This complex was then heated to 120°C showing no change to the Ru(0) isomer suggesting the dearomatized complex is the thermodynamic product.



**Scheme 3.27:** Synthesis of **(7-H(CO)<sub>2</sub>)**

Following these experiments, computational analysis was used to determine the thermodynamically stable species, the aromatized PNP metal (0) dicarbonyl or the dearomatized PNP metal (II) hydride dicarbonyl.



Metal	TS	Complex 2
Fe	37 kcal/mol	6 kcal/mol
Ru	34 kcal/mol	-0.5 kcal/mol
Os	30 kcal/mol	-10 kcal/mol

**Figure 3.28:** Computational thermodynamics for dearomatization

Computational analysis showed that conversion from the aromatized metal dicarbonyl complex to the dearomatized metal hydride dicarbonyl complex is thermodynamically favored for ruthenium and osmium but not iron. The analysis predicts high energy barriers for conversion to the dearomatized structure with iron being the most unfavorable. However only in the iron case is the dearomatized complex higher in energy than the aromatized complex. This agrees well with what was observed

in experimentation, wherein the  $(^t\text{BuPNP})\text{Fe}(\text{CO})_2$  complex was not observed to dearomatized. However, both the osmium and ruthenium  $(^t\text{BuPNP})$  complexes did dearomatized.

### 3.10 Experimental

#### 3.10.1 General Remarks

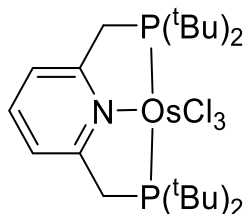
All procedures involving organometallic compounds were conducted under an argon atmosphere using standard glovebox and Schlenk techniques. Solvents were purchased as anhydrous grade and purged with argon before use. Deuterated solvents (*p*-xylene- $\text{d}_{10}$ , toluene- $\text{d}_8$ , benzene- $\text{d}_6$ , THF- $\text{d}_8$ ) were degassed via freeze-pump-thaw cycles and dried over activated  $\text{Al}_2\text{O}_3$  prior to use. Ethylene, Nitrogen and carbon monoxide was purchased from various suppliers in the highest purity available and used as received.  $^1\text{H}$  and  $^{31}\text{P}$  NMR spectra were recorded on 400 MHz and 500 MHz Varian spectrometers. Chemical shifts are reported in ppm.  $^1\text{H}$  NMR signals are referenced to the residual solvent signals, and  $^{31}\text{P}$  NMR signals are referenced to an external standard of 85%  $\text{H}_3\text{PO}_4$ . X-Ray diffraction was obtained from an oil coated crystal mounted on a glass fiber. X-Ray intensity measurements were made using a Bruker-AXS Smart APEX CCD diffractometer with graphite mono-chromatized  $\text{Mo K}\alpha$  radiation at 100 K or 120 K. The  $^t\text{Bu}_4\text{PNP}$  ligand was synthesized according to a method published by Milstein.<sup>62</sup>  $(^t\text{Bu}_4\text{PNP})\text{IrH}_2$  (**1-H<sub>2</sub>**) was synthesized by reaction of  $^t\text{Bu}_4\text{PNP}$  with  $\text{Ir}(\text{COE})_2(\text{acetone})_2$  following the procedure reported by Goldberg.<sup>63</sup>  $\text{Ir}(\text{COE})_2(\text{acetone})_2$  was prepared

following the procedure reported by Milstein.<sup>64</sup> Kinetic analyses were performed using the "COPASI: Biological System Simulator" program.

For all complexes, X-ray diffraction data were collected on a Bruker Smart APEX CCD diffractometer with graphite mono-chromatized MoK $\alpha$  radiation ( $\lambda = 0.71073\text{\AA}$ ) at a temperature of 100 K or 120 K. Crystals were immersed in Paratone oil and placed on a glass needle or nylon loop. The data were corrected for Lorentz effects, polarization, and absorption, the latter by a multiscan (SADABS) method.<sup>S1</sup> The structures were solved by direct methods (SHELXS86).<sup>S2</sup> All non-hydrogen atoms were refined (SHELXL97)<sup>3</sup> based upon  $F_{\text{obs}}$ .<sup>S3</sup> All hydrogen atom coordinates were calculated with idealized geometries (SHELXL97). Scattering factors ( $f_o$ ,  $f'$ ,  $f''$ ) are as described in SHELXL97.

### 3.10.2 Synthesis of (<sup>t</sup>Bu<sub>4</sub>PNP)Os pincer complexes

#### Synthesis of (<sup>t</sup>Bu<sub>4</sub>PNP)OsCl<sub>3</sub> (1-Cl<sub>3</sub>)



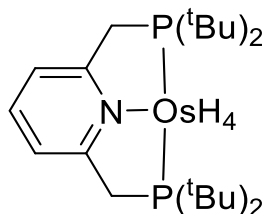
A mixture of (<sup>t</sup>Bu<sub>4</sub>PNP) (0.498 g, 1.11 mmol) and Na<sub>2</sub>OsCl<sub>6</sub>·6H<sub>2</sub>O (0.535 g, 1.3 mmol) was dissolved in 2-methoxyethanol (63 mL). Formation of a green solution was observed upon mixing. The solution was heated to reflux for 8 hours upon which the solution had turned a light orange color. The solution was filtered then concentrated until orange crystals began to precipitate. The solution was then stored at 0°C under argon overnight. The orange crystals were filtered from excess solvent through a frit and



washed with pentane (5 mL x 3). The filtrate was then further concentrated until precipitation was observed again. This process was repeated twice more to increase yield. Yield = 0.346 g (45%).

$^1\text{H-NMR}$  (400 MHz,  $\text{THF-d}_8$ ):  $\delta$  -2.19 (broad, 2H, m-py), -4.10 (broad, 1H, p-py), -4.81 (broad, 4H,  $\text{CH}_2$ ), -5 to -8 (very broad, 36H, tert-butyl). Anal. Calcd. for  $\text{OsP}_2\text{NCl}_3\text{C}_{23}\text{H}_{43}$ : C, 39.91; H, 6.26; N, 2.02; Cl, 15.36. Found: C, 39.75; H, 6.47; N, 1.94; Cl, 15.50.

#### Synthesis of ( $^t\text{Bu}^4\text{PNP}$ ) $\text{OsH}_4$ (**1-H<sub>4</sub>**)

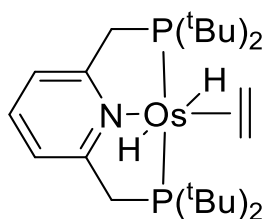


A sample of **1-Cl<sub>3</sub>** (0.8 grams, 1.15 mmol) was dissolved in dry and degassed THF (100 mL) resulting in an orange solution with some undissolved material. The solution was then bubbled with a flow of  $\text{H}_2$  gas for approximately ten minutes then allowed to remain under  $\text{H}_2$  atmosphere. A 1 M solution of sodium triethylborohydride was then added dropwise (4.62 mL). Immediately upon addition, the solution turned dark green but when all of the sodium triethylborohydride had been added the solution was dark with a red/orange tinge. The solution was stirred at room temperature for 24 hours upon which it turned light orange/brown with a white precipitate. All the solvent was removed leaving a brown solid. Addition of 25 mL of benzene followed by addition of 100 mL of pentane resulted in a brown solution with a white precipitate. The solution

was filtered, and the solvent was removed by vacuum leaving a light orange/brown solid. Yield = 0.358 g (42%).

$^1\text{H-NMR}$  (400 MHz, toluene- $\text{d}_8$ , room temperature):  $\delta$  6.84 (t,  $J = 8$ , 1H,  $p$ -py), 6.58 (d,  $J = 7$ , 2H,  $m$ -py), 3.33 (t,  $J = 3$ , 4H,  $\text{CH}_2$ ), 1.32 (t,  $J = 6$ , 36H, tert-butyl), -8.66 (broad, 3H, Os-H).  $^1\text{H-NMR}$  (300 MHz, toluene- $\text{d}_8$ , -80 °C):  $\delta$  6.77 (t,  $J = 8$ , 1H,  $p$ -py), 6.37 (d,  $J = 8$ , 2H,  $m$ -py), 3.17 (4H,  $\text{CH}_2$ ), 1.38 (36H, tert-butyl), -5.04 (broad, 2H, Os-H), -11.97 (broad, 2H, Os-H).  $^1\text{H-NMR}$  (300 MHz, toluene- $\text{d}_8$ , 60 °C):  $\delta$  6.97 (t,  $J = 7$ , 1H,  $p$ -py), 6.64 (d,  $J = 7$ , 2H,  $m$ -py), 3.38 (4H,  $\text{CH}_2$ ), 1.32 (t,  $J = 6$ , 36H, tert-butyl), -8.68 (t,  $J = 12$ , 4H, Os-H).  $^{13}\text{C-NMR}$  (126 MHz, toluene - $\text{d}_8$ )  $\delta$  166 (pyridine meta carbon), 134 (pyridine para carbon), 117 (pyridine meta carbon), 44 ( $\text{CH}_2$  linker), 35 (t-butyl- $\text{C}(\text{CH}_3)$ ), 29 (t-butyl  $\text{CH}_3$ ).  $^{31}\text{P-NMR}$   $\{^1\text{H}\}$  (121 MHz, toluene- $\text{d}_8$ ):  $\delta$  76.86. Anal. Calcd. for  $\text{OsP}_2\text{NCl}_3\text{C}_{23}\text{H}_{47}$ : C, 46.84; H, 8.03; N, 2.37. Found: C, 46.24; H, 7.67; N, 2.31.

#### Synthesis of $(\text{tBu}_4\text{PNP})\text{OsH}_2(\text{C}_2\text{H}_4)$ (**1-H<sub>2</sub>(C<sub>2</sub>H<sub>4</sub>)**)



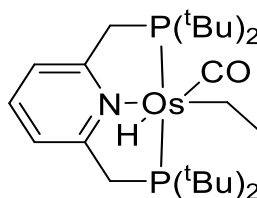
A sample of **1-H<sub>4</sub>** (0.13 grams, 0.22 mmol) was dissolved in toluene (15 mL) resulting in a yellowish solution with some undissolved material. The solution was then set to reflux at 85 °C under an ethylene atmosphere. After some time the solution began to turn orange. After 3 days the reaction was allowed to cool to room temperature, and the

solvent was removed by vacuum resulting in the formation of an orange/brown solid.

Yield = 0.136 g (80%).

$^1\text{H-NMR}$  (400 MHz, toluene- $d_8$ ):  $\delta$  6.7 (t,  $J = 7.3$ , 1H,  $p$ -py), 6.5 (d,  $J = 7.7$ , 2H,  $m$ -py), 3.1 (t,  $J = 3.1$ , 4H,  $\text{CH}_2$ ), 1.97 (t,  $J = 4$ , 4H,  $\text{CH}_2$  Ethylene), 1.2 (t,  $J = 6$ , 36H, tert-butyl), -5.4 (t,  $J = 14$ , 2H, Os-H).  $^{13}\text{C-NMR}$  (126 MHz, toluene- $d_8$ )  $\delta$  166 (pyridine meta carbon), 134 (pyridine para carbon), 117 (pyridine meta carbon), 44 ( $\text{CH}_2$  linker), 35 (t-butyl- $\text{C}(\text{CH}_3)$ ), 29 (t-butyl  $\text{CH}_3$ ), 8 ( $\text{CH}_2$  Ethylene).  $^{31}\text{P-NMR}\{^1\text{H}\}$  (121 MHz, toluene- $d_8$ ):  $\delta$  45.7 (s,  $\text{P}^t\text{Bu}_2$ )

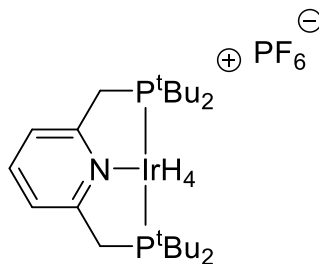
### Synthesis of $(^t\text{Bu}_4\text{PNP})\text{OsH}(\text{C}_2\text{H}_5)\text{CO}$ (**1-H(Et)(CO)**)



A sample of **1-H<sub>2</sub>(C<sub>2</sub>H<sub>4</sub>)** (5 mg, 0.008 mmol) was dissolved in toluene (0.5 mL) forming a light brown solution, which was transferred to a J. Young tube. The tube was then charged with 1 atm of carbon monoxide, and the sample was allowed to stir for 3 days at room temperature during which the solution turned reddish orange. Removal of solvent resulted in a reddish powder.

$^1\text{H-NMR}$  (400 MHz, toluene- $d_8$ ):  $\delta$  6.8 (t,  $J = 7$ , 1H,  $p$ -py), 6.5 (d,  $J = 7$ , 2H,  $m$ -py), 3.1 (m, 4H,  $\text{CH}_2$  ethylene), 1.34 (m, 18H, tert-butyl), 1.25 (m, 18H, tert-butyl), 1.09 (m, 2H, M- $\text{CH}_2$ ), 0.87 (t, 3H,  $\text{CH}_3$ ), -4.5 (t,  $J = 23$ , H, Os-H).  $^{13}\text{C-NMR}$  (126 MHz, toluene- $d_8$ )  $\delta$  185 (carbonyl), 164 (pyridine meta carbon), 133 (pyridine para carbon), 118 (pyridine meta carbon), 44 ( $\text{CH}_2$  linker), 37.5 (t-butyl- $\text{C}(\text{CH}_3)$ ), 35 (t-butyl- $\text{C}(\text{CH}_3)$ ), 30.1 (t-butyl  $\text{CH}_3$ ), 29.4 (t-butyl  $\text{CH}_3$ ), 29.8 (M- $\text{CH}_2$ ), 25.6 (M- $\text{CH}_2$ - $\text{CH}_3$ ).  $^{31}\text{P-NMR}\{^1\text{H}\}$  (121 MHz, toluene- $d_8$ ):  $\delta$  55.6 (s,  $\text{P}^t\text{Bu}_2$ )

### Synthesis of (<sup>t</sup>Bu<sup>4</sup>PNP)IrH<sub>4</sub> [PF<sub>6</sub>]



A sample of (<sup>t</sup>Bu<sup>4</sup>PNP)IrH<sub>2</sub> (PF<sub>6</sub>) (10 mg, 0.0136 mmol) prepared according to literature procedure was dissolved in 0.5 mL of CD<sub>2</sub>Cl<sub>2</sub> forming a pink/red solution. The solution was transferred to a J. Young tube, which was then charged with 1 atmosphere of H<sub>2</sub>. The NMR tube was rotated to promote gas-liquid mixing at room temperature for 1 hour during which the color of the solution lightened. NMR (<sup>1</sup>H and <sup>31</sup>P) spectra were taken. Upon removal of the solvent the complex had converted to (<sup>t</sup>Bu<sup>4</sup>PNP)IrH<sub>4</sub> (PF<sub>6</sub>).

<sup>1</sup>H-NMR (400 MHz, CD<sub>2</sub>Cl<sub>2</sub>): δ 7.8 (t, J = 7.8, 1H, p-py), 7.6 (d, J = 7.8, 2H, m-py), 3.8 (t, J = 3.8, 4H, CH<sub>2</sub>), 1.37 (dd, J = 7, 36H, tert-butyl), -9.3 (broad s, H, Ir-H). <sup>31</sup>P-NMR{<sup>1</sup>H} (121 MHz, toluene-d<sub>8</sub>): δ 65 (s, P<sup>t</sup>Bu<sub>2</sub>), -144 (hep, J = 700, PF<sub>6</sub>)

### 3.10.3 NMR Spectra

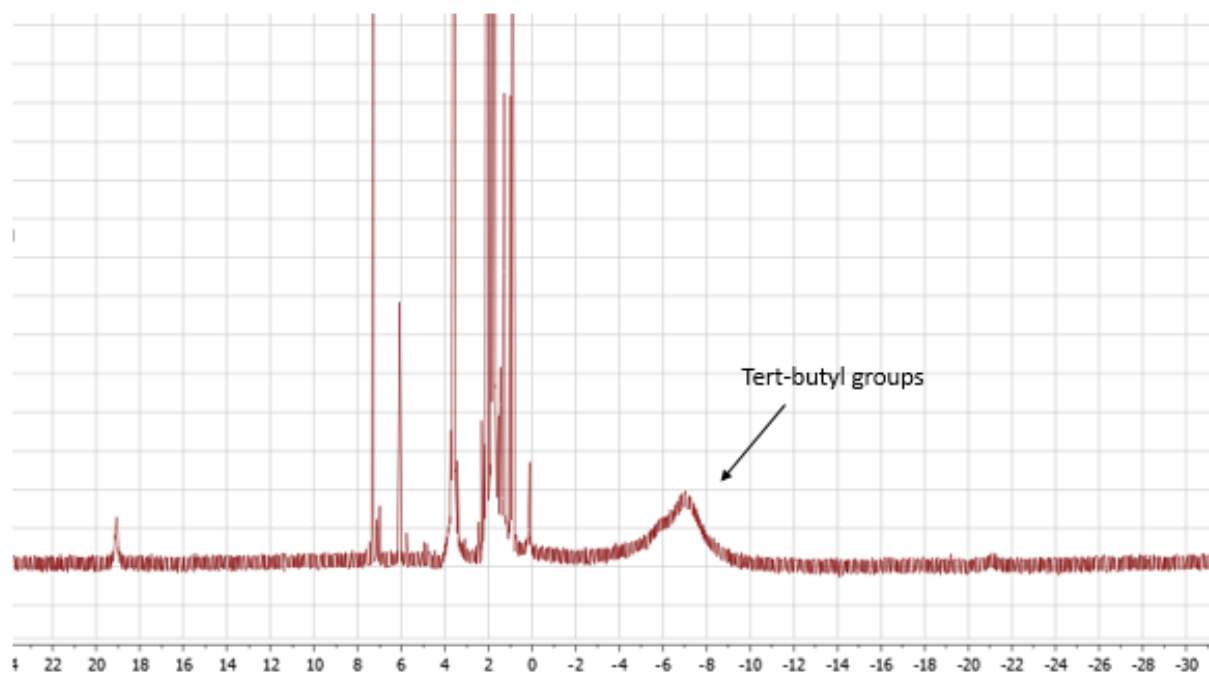


Figure 3.29.  $^1\text{H}$  NMR spectrum of 1- $\text{Cl}_3$

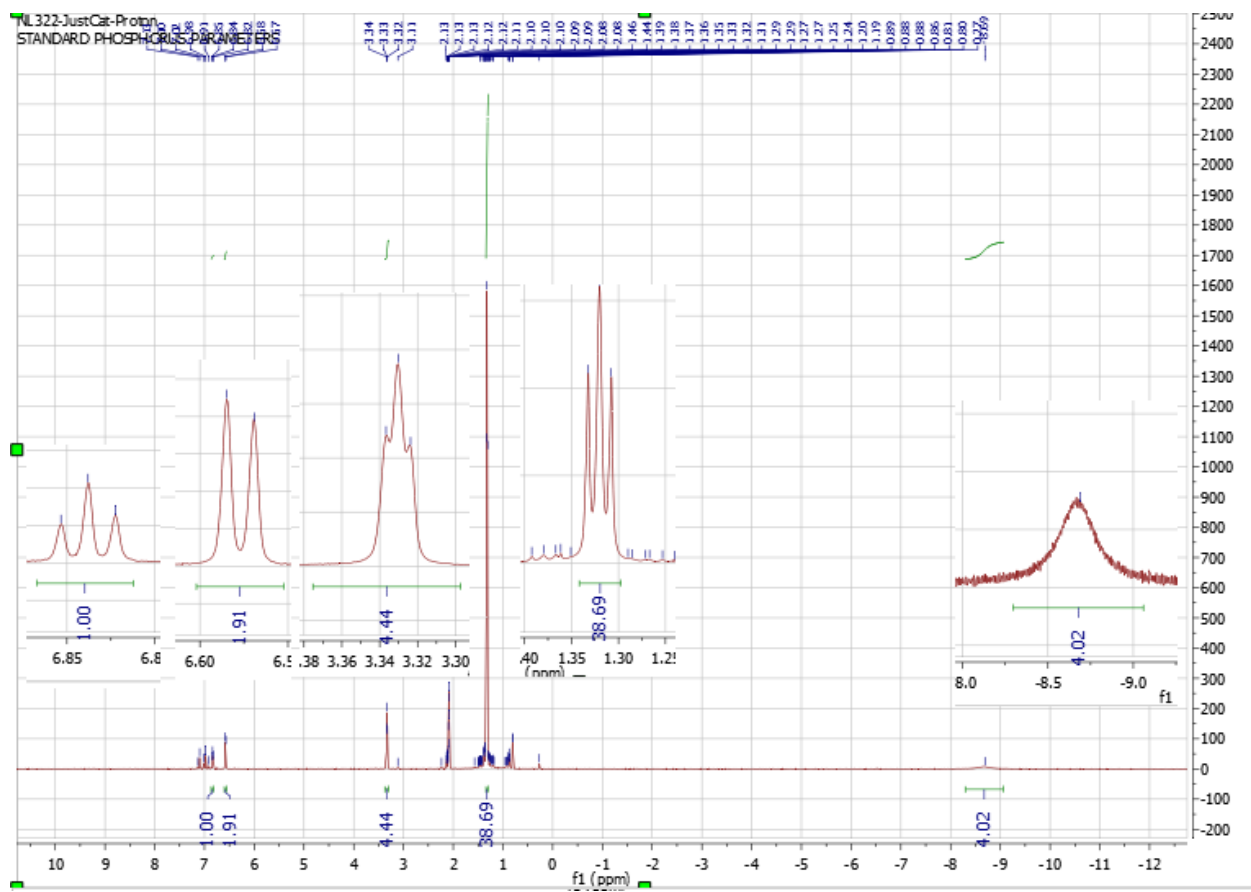
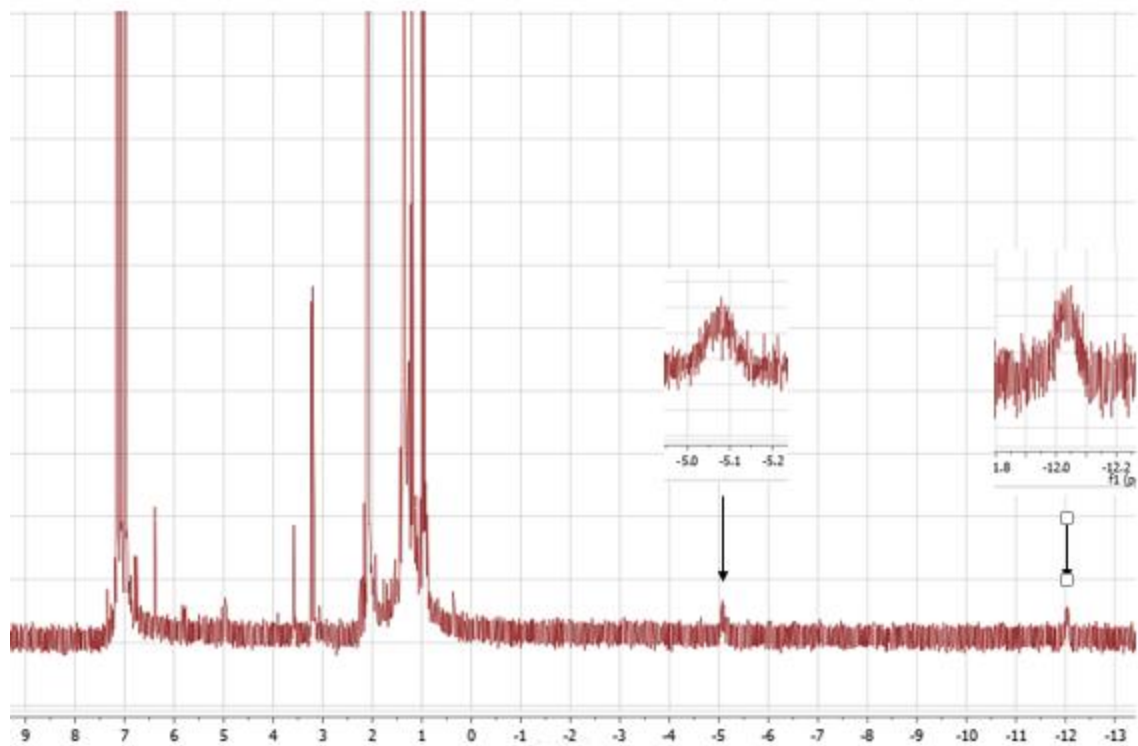


Figure 3.30.  $^1\text{H}$  NMR spectrum of **1-H<sub>4</sub>**

**Figure 3.31.**  $^1\text{H}$  NMR spectrum of **1-H<sub>4</sub>** at 60 °C



**Figure 3.32.**  $^1\text{H}$  NMR spectrum of **1-H<sub>4</sub>** at  $-80\text{ }^\circ\text{C}$



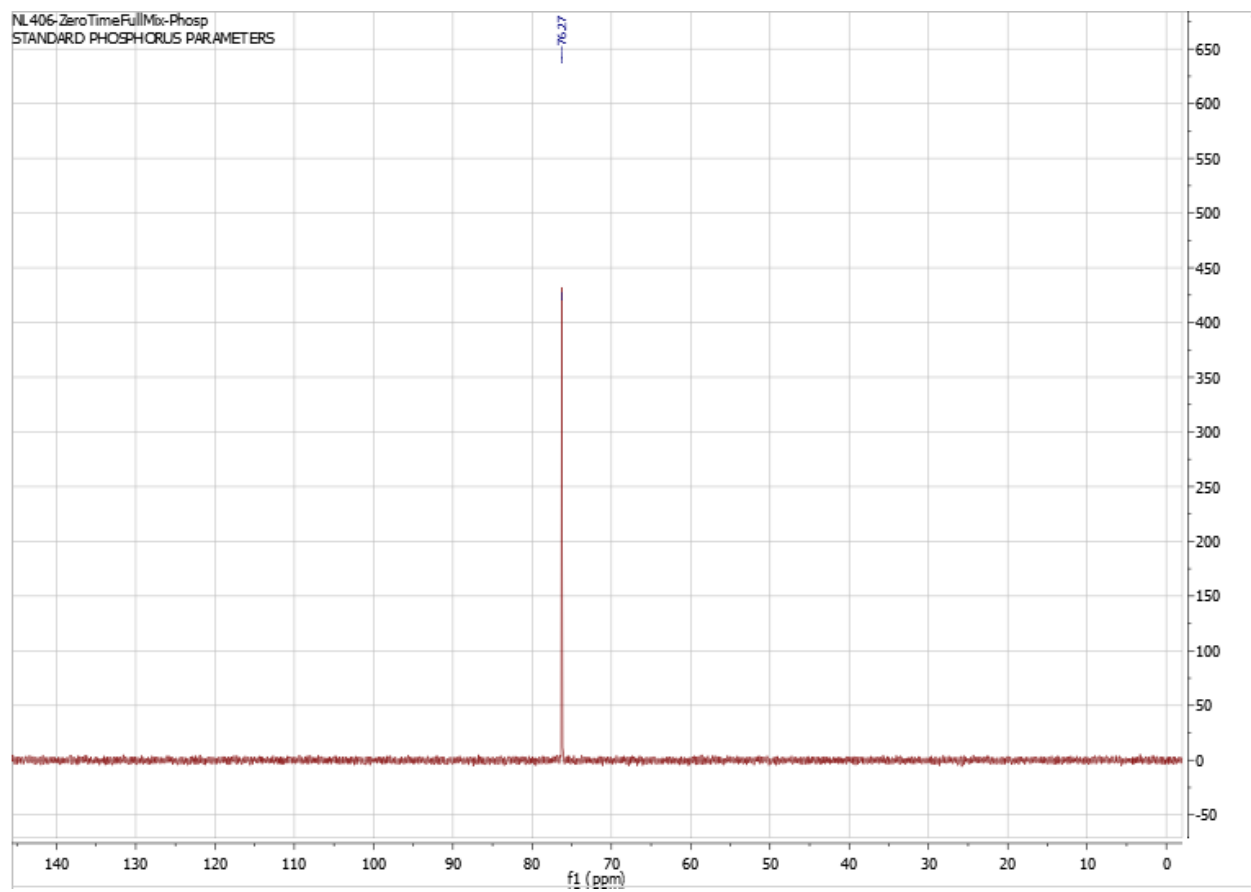


**Figure 3.33.**  $^{31}\text{P}\{^1\text{H}\}$  NMR spectrum of **1-H<sub>4</sub>**

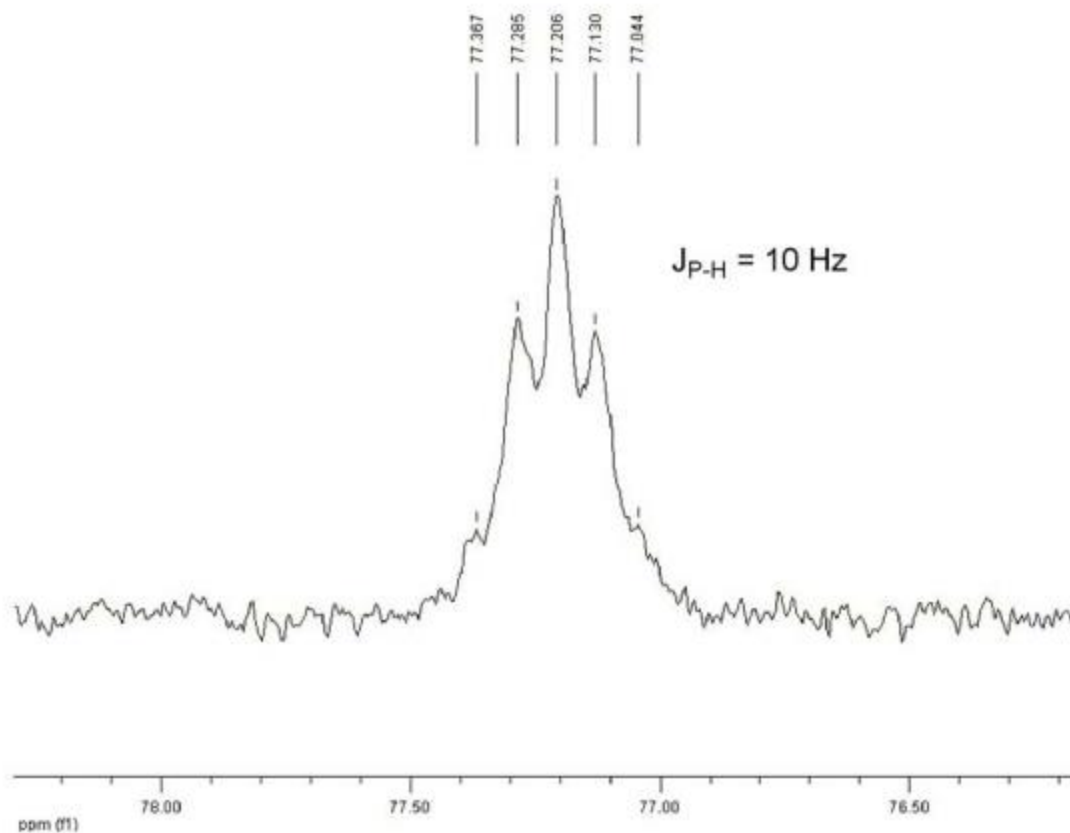


**Figure 3.34.**  $^{31}\text{P}\{^1\text{H-decoupled}$  ca.  $\delta$  0 –  $\delta$  10 ppm } NMR spectrum of **1-H<sub>4</sub>**

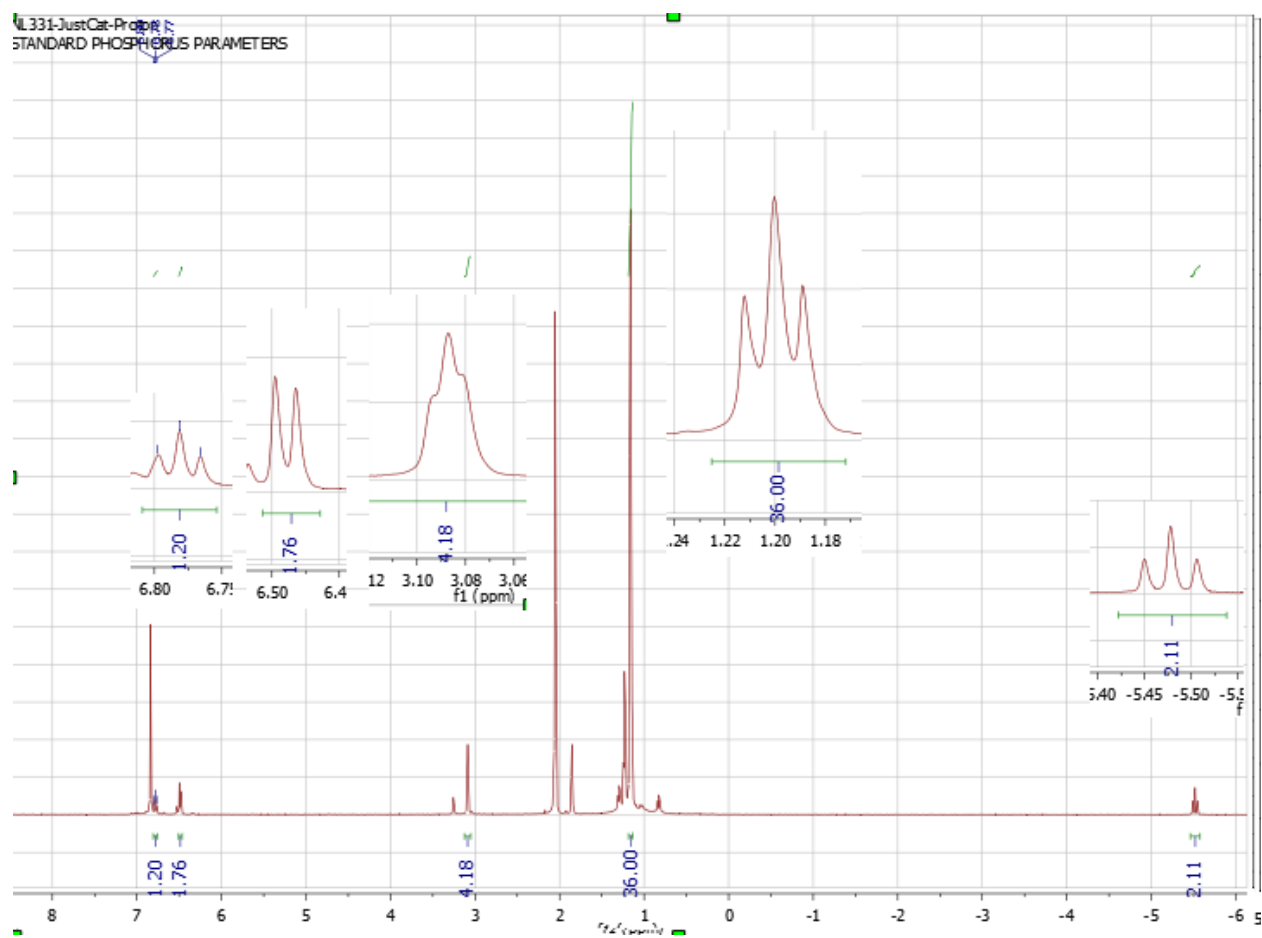


**Figure 3.35.**  $^1\text{H}$  NMR spectrum of  $1\text{-H}_2(\text{C}_2\text{H}_4)$



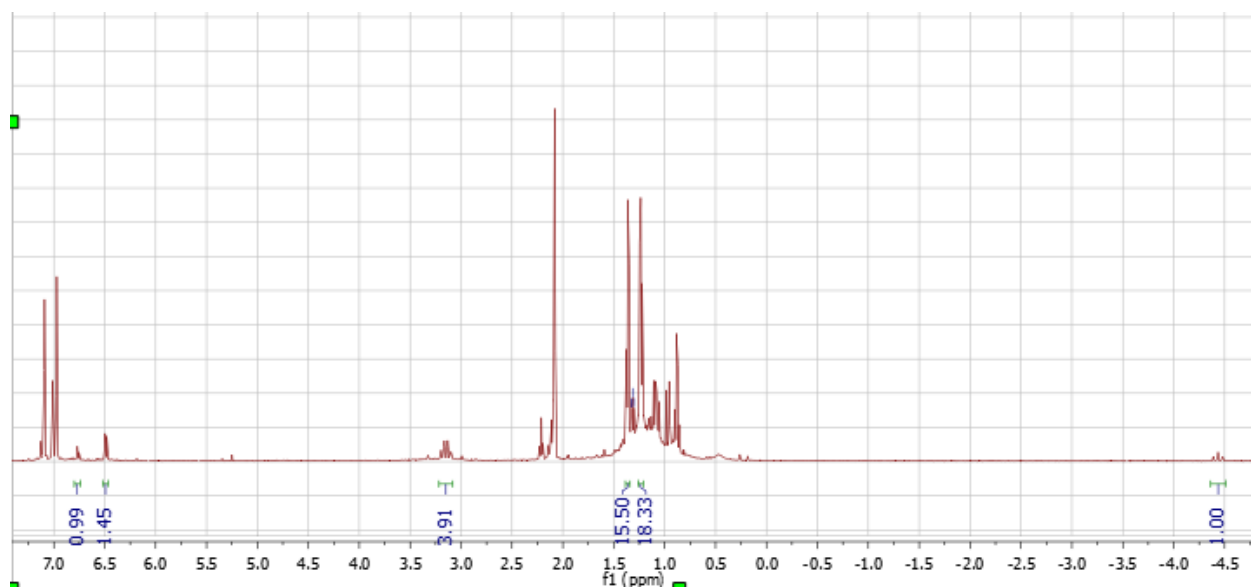
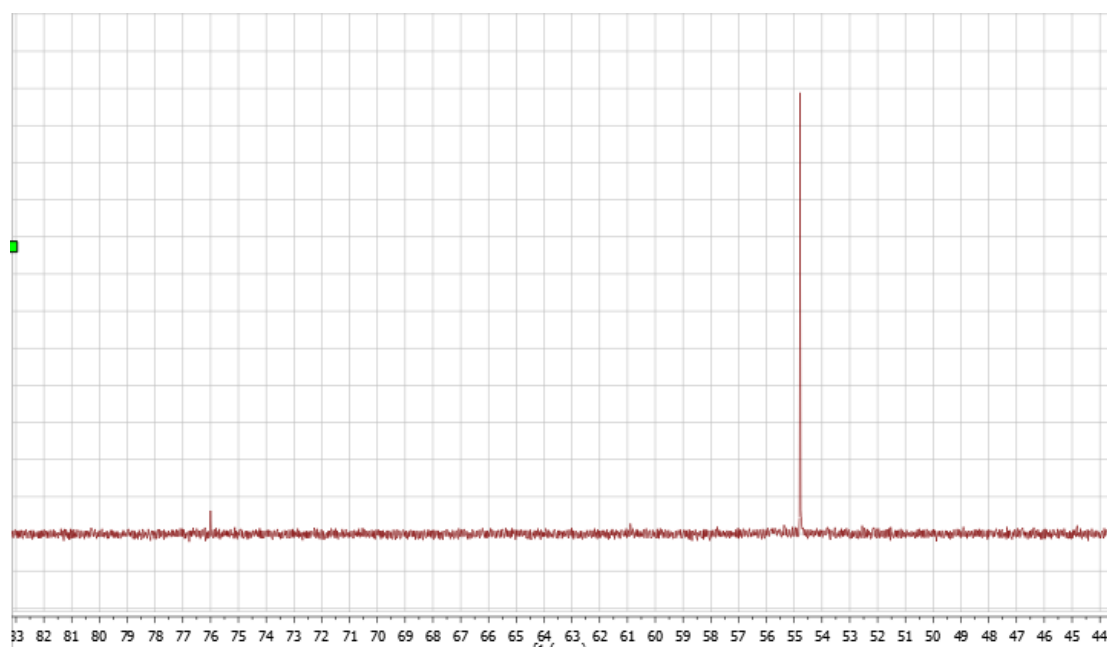


Figure 3.37.  $^1\text{H}$  NMR spectrum of  $1\text{-H(Et)(CO)}$



**Figure 3.38.**  $^{31}\text{P}\{^1\text{H}\}$  NMR spectrum of 1-H(Et)(CO)

### 3.10.4 Catalytic Reactions

#### General Procedures

Inside an argon filled glovebox, a stock solution was prepared from 0.5 mL cyclooctane (substrate), hexamethylbenzene (standard, 30.4 mM), **1-H<sub>2</sub>(C<sub>2</sub>H<sub>4</sub>)** or **1-H<sub>4</sub>** (catalyst, 10 mM), and hydrogen acceptor (0.5 M), in a flame-dried vial. The stock solution was then divided and placed into 5 sealable glass ampoules (0.1 mL of stock solution per ampoule), leaving one 0.1 mL ampoule for a zero-time measurement. The ampoules were then attached to Kontes valves with Tygon tubing and removed from the glovebox. The valves were attached to a vacuum-gas manifold, and the solutions were frozen with liquid nitrogen. The ampoules were evacuated to a pressure of 0.011 torr and then sealed under vacuum in the case of solid or liquid acceptors or charged with 1 atm of gas acceptor using an oxygen torch. The sealed ampoules were allowed to cool to room temperature, and then the ampoules were heated in an oven for the desired amount of time. After being removed from the oven the ampoules were allowed to cool to room temperature before being broken open. GC analysis of the product solution was performed. The concentrations of products were calculated based on the ratio of the starting cyclooctene vs. the internal standard and comparing this to the initial zero-time measurement.

#### Dehydrogenation Reactions in Sealed Tube

Inside the glovebox, an oven-dried NMR tube was charged with 0.5 mL *p*-xylene stock solution. The stock solution contained 200 mM alkane (cyclooctane or *n*-octane) and **1-H<sub>2</sub>(C<sub>2</sub>H<sub>4</sub>)** (0.008 mmol, 16 mM). The NMR tube was attached to a Kontes valve and

removed from the glovebox. The Kontes valve was attached to a vacuum-gas manifold, and the solution inside was frozen with liquid N<sub>2</sub>. The headspace was evacuated down to a pressure of 0.010 Torr and then placed under 1 atm of ethylene. The NMR tube was fully immersed in liquid N<sub>2</sub>, allowing the ethylene to condense. After ~1 minute, the NMR tube was sealed with an oxygen torch (this decreased the volume by 50% and brought the total pressure to 1.5 atm). The sealed NMR tube was allowed to warm to room temperature. The sample was then heated inside a GC oven equipped to stir the sample while inside the oven. The samples were heated in the oven stirring for set times; the oven is then returned to 25 °C and NMR spectra of the sample were taken.

#### **Hydrogenation of Ethylene Reactions in Sealed Tube**

Inside the glovebox, an oven-dried NMR tube was charged with 0.5 mL *p*-xylene solution of **1-H<sub>2</sub>(C<sub>2</sub>H<sub>4</sub>)** (0.008 mmol, 16 mM). The NMR tube was attached to a Kontes valve and removed from the glovebox. The Kontes valve was attached to a vacuum-gas manifold, and the solution inside was frozen with liquid N<sub>2</sub>. The headspace was evacuated down to a pressure of 0.010 Torr and then placed under 1 atm ethylene. The NMR tube was immersed in liquid N<sub>2</sub> slightly above the solvent line, allowing the ethylene to condense. Next the tube was charged with 1 atm of H<sub>2</sub> while the sample was still immersed in liquid N<sub>2</sub>. The sample was further immersed in liquid N<sub>2</sub> and after ~1 minute, the NMR tube was sealed with an oxygen torch (this decreased the volume by 50% and brought the total pressure to 2 atm). The sealed NMR tube was allowed to warm to room temperature. The sample was then heated inside a GC oven equipped to stir the sample



while inside the oven. The samples were heated in the oven, stirring for set times; the oven was then returned to 25 °C and NMR spectra were taken of the sample.

**Table 3.8.** Kinetics of Ethylene Hydrogenation

Time	Ethylene	Ethane	Conversion/Turnover
0 min	2.63 M	0 M	0% / 0 TO
15 min	0.97 M	1.66 M	63% / 208 TO
30 min	0.71 M	1.92 M	73% / 240 TO
45 min	0.47 M	2.16 M	82% / 270 TO

### Isomerization of 1-hexene

Inside an argon filled glovebox, a stock solution was prepared in a flame dried vial. The stock solution was comprised of 0.5 mL cyclooctane (substrate neat), hexamethylbenzene (standard, 30.4 mM), **1-H<sub>4</sub>** (catalyst, 5 mM) and 1-hexene (0.5 M). Next, the stock solution was divided into 5 sealable glass ampoules (0.1 mL of stock per ampoule) leaving one 0.1 mL ampoule for use as a zero-time measurement. The ampoules were then attached to Kontes valves and removed from the glovebox. The valves were attached to a vacuum-gas manifold, and the solutions were frozen with liquid N<sub>2</sub>. The headspace of the ampoules were evacuated to 0.011 torr and then sealed under vacuum in the case of solid or liquid acceptors or charged with 1 atm of ethylene using an oxygen torch. The sealed ampoules were allowed to cool to room temperature and then were heated in a GC oven at 100 °C. When removed from the GC the ampoules were allowed to cool to room temperature. The ampoules were cracked open and studied by GC analysis using hexamethylbenzene as the internal standard.

**Table 3.9:** Kinetics of 1-hexene isomerization

Time	1- hexene	Hexene isomers
0 min	1.6 M	0 M
6 hours	1.36 M	0.24 M
26 hours	0.78 M	0.82 M

### 3.10.5 H/D Exchange reactions

#### H/D Exchange of (<sup>t</sup>Bu<sup>4</sup>PNP)OsH<sub>4</sub> (1-H<sub>4</sub>) with D<sub>2</sub>

Inside the glovebox, an oven-dried NMR tube was charged with 0.5 mL toluene-d<sub>8</sub> solution of **1-H<sub>4</sub>** (0.008 mmol, 16 mM). The NMR tube was attached to a Kontes valve and removed from the glovebox. The Kontes valve was attached to a vacuum-gas manifold, and the solution inside was frozen with liquid N<sub>2</sub>. The headspace was evacuated down to a pressure of 0.010 Torr and then placed under 1 atm of D<sub>2</sub>. The sample was further immersed in liquid N<sub>2</sub> and after ~1 minute, the NMR tube was sealed with an oxygen torch (this decreased the volume by 50% and brought the total pressure to ~2 atm). Once sealed, zero- time NMR (<sup>1</sup>H and <sup>31</sup>P) spectra were taken. The sample was then stirred and heated inside a GC oven at 85 °C. NMR spectra were taken after 2, 4 and 6 hours.

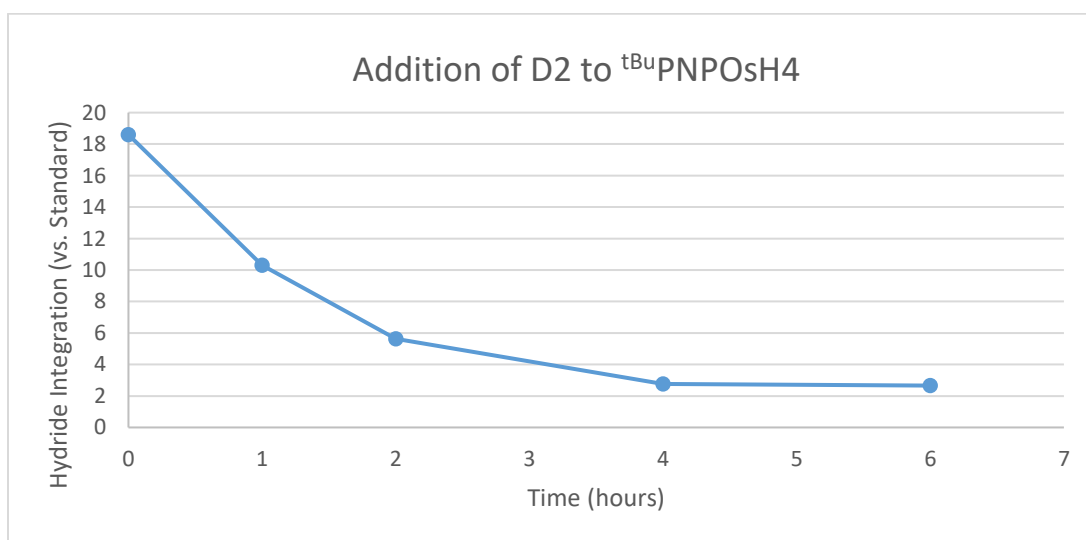


**Figure 3.39.** Plot of disappearance of hydride signal after addition of D<sub>2</sub>. Rate Constant = 0.542 hr<sup>-1</sup>

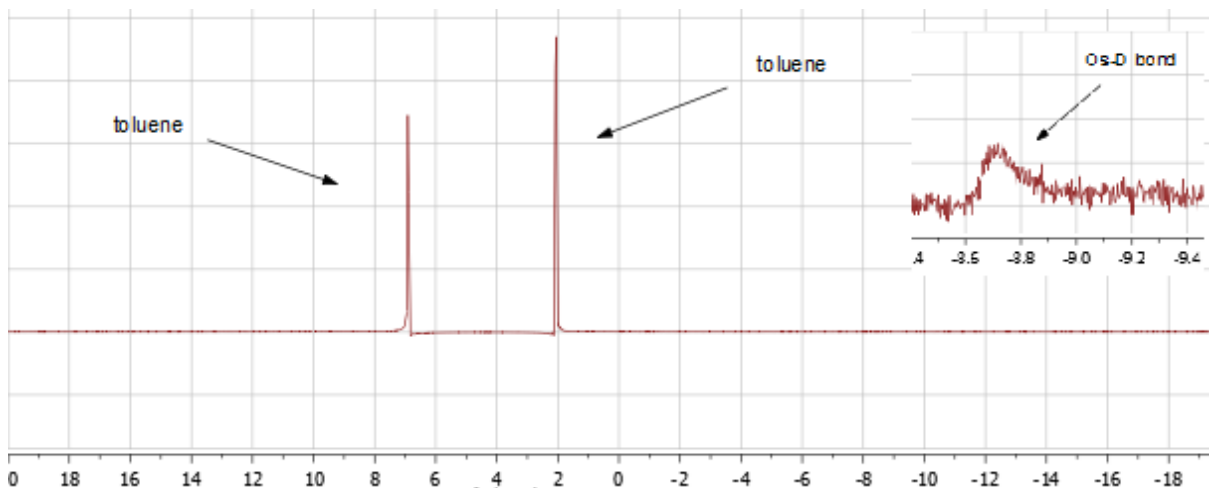


**Figure 3.40.**  $^2\text{D}$  NMR spectrum of reaction after 10 hours

### $(\text{tBu}^4\text{PNP})\text{OsH}_4$ ( $1\text{-H}_4$ ) exchange reaction with deuterated solvent

Inside the glovebox, an oven-dried J. Young NMR tube was charged with 0.5 mL toluene- $\text{d}_8$  solution of  $1\text{-H}_4$  (0.008 mmol, 16 mM). NMR of the sample ( $^1\text{H}$  and  $^{31}\text{P}$ ) was taken for a zero-time measurement. The J. Young tube was then heated in an oil bath at 95 °C. The tube was taken out of the oil bath after 2, 4, 6 and 10 hours, and NMR spectra were taken.

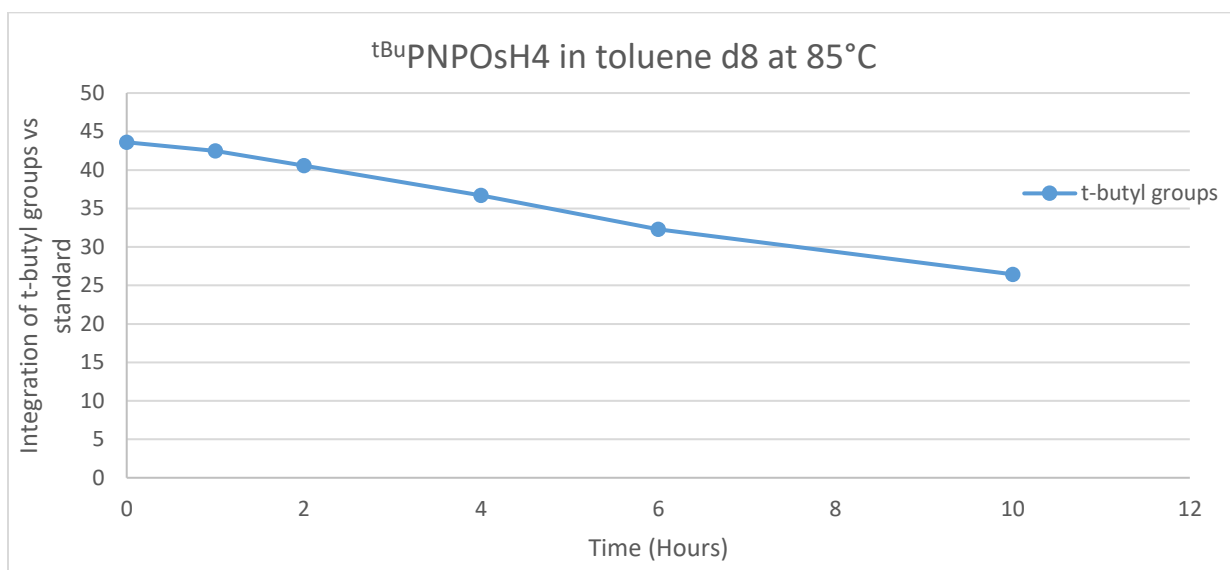


**Figure 3.41.** Plot-Deuterium incorporation into ligand t-butyl groups vs. time

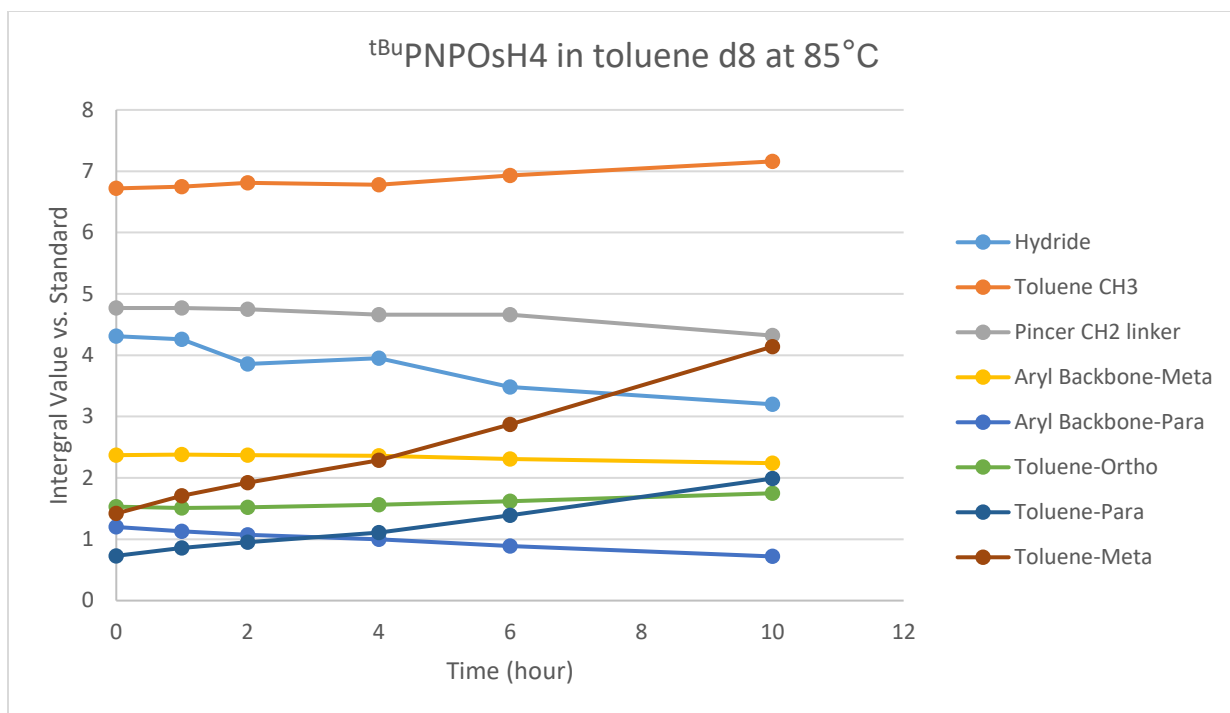


**Figure 3.42.** Plot-Deuterium incorporation into ligand signals vs. time

### H/D exchange reaction of **1-H<sub>2</sub>(C<sub>2</sub>D<sub>4</sub>)**

Inside the glovebox, a solution of **1-H<sub>4</sub>** (0.006 g, 0.01 mmol) in toluene-d<sub>8</sub> was added to an oven-dried J-Young NMR tube. The solution was then charged with 1 atmosphere of ethylene-d<sub>4</sub>(C<sub>2</sub>D<sub>4</sub>). The J. Young NMR tube was then heated in an oil bath to 85°C for 2, 4 and 10 hours. NMR (<sup>31</sup>P and <sup>1</sup>H) were taken at each time showing formation of deuterated isotopomers of **1-H<sub>2</sub>(C<sub>2</sub>H<sub>4</sub>)**. Extensive H/D exchange between the hydride and ethylene positions was observed. The ratio of fractional deuteration at hydride and ethylene positions (ca. 2:3) was found to be independent of time, indicating that H/D exchange was rapid relative to conversion of **1-H<sub>4</sub>** to the dihydride ethylene complex.

### 3.10.6 Kinetic Studies

A stock solution of **1-H<sub>2</sub>(C<sub>2</sub>H<sub>4</sub>)** (17.7 mM) and hexamethyldisiloxane (standard, 22.6 mM) in toluene-d<sub>8</sub> was prepared. This was used for all kinetics studies.

#### Addition of H<sub>2</sub> to 1-H<sub>2</sub>(C<sub>2</sub>H<sub>4</sub>)

Inside the glovebox 0.2 mL of **1-H<sub>2</sub>(C<sub>2</sub>H<sub>4</sub>)** stock solution was added to a high pressure rated J. Young tube (200 psi). The headspace of the tube was removed by freezing the solution in liquid nitrogen and vacuuming off the gas. The tube was then charged with H<sub>2</sub> gas (1, 2, 4 or 6 atm). NMR (<sup>1</sup>H and <sup>31</sup>P) spectra were taken as quickly as possible after addition of gas. Next, two consecutive NMR (<sup>1</sup>H and <sup>31</sup>P) spectra were taken. The sample was then ejected from the NMR spectrometer, and the tube was shaken three times and quickly put back into the NMR spectrometer. The process of taking two NMR spectra, followed by shaking of the tube was repeated three more times. The sample was then stored overnight to obtain a final NMR spectrum.

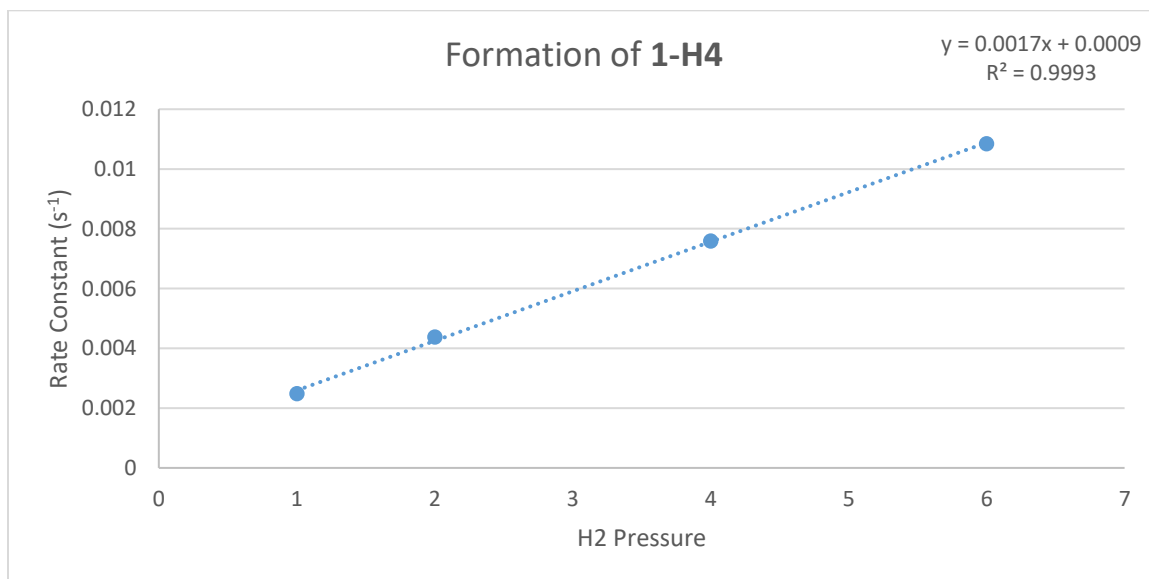


**Figure 3.43.** Kinetics Plot-Addition of H<sub>2</sub> to **1-H<sub>2</sub>(C<sub>2</sub>H<sub>4</sub>)**.

### Addition of CO to 1-H<sub>2</sub>(C<sub>2</sub>H<sub>4</sub>)

Inside the glovebox 0.2 mL of 1-H<sub>2</sub>(C<sub>2</sub>H<sub>4</sub>) stock solution was added to a high pressure rated J. Young tube (200 psi). The tube was then charged with CO gas (2, 4 or 6 atm). NMR (<sup>1</sup>H and <sup>31</sup>P) spectra were taken as quickly as possible after addition of gas. Next, two consecutive NMRs (<sup>1</sup>H and <sup>31</sup>P) were taken. The sample was then ejected from the NMR spectrometer, and the tube was shaken three times and quickly put back into the NMR spectrometer. The process of taking two NMR spectra, followed by shaking of the tube was repeated three more times. The sample was then stored overnight to obtain a final NMR spectrum.

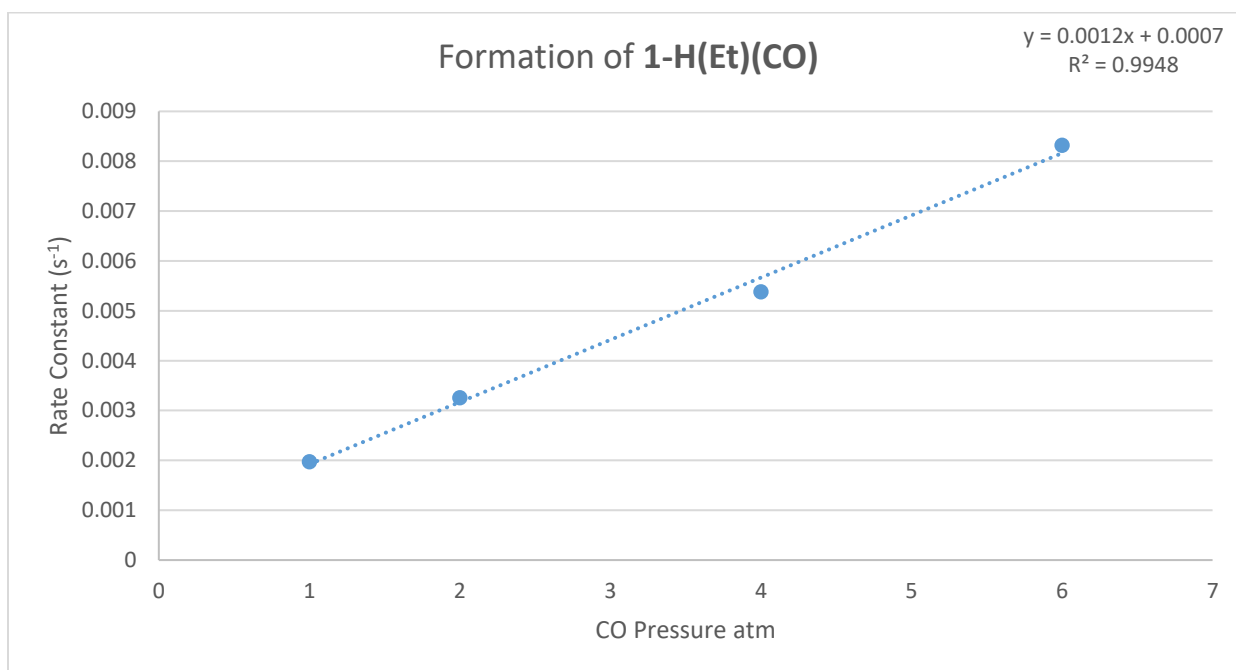


**Figure 3.44.** Kinetics Plot-Addition of CO to 1-H<sub>2</sub>(C<sub>2</sub>H<sub>4</sub>).

### Decomposition of 1-H<sub>2</sub>(C<sub>2</sub>H<sub>4</sub>)

Inside the glovebox 0.2 mL of 1-H<sub>2</sub>(C<sub>2</sub>H<sub>4</sub>) stock solution was added to a J. Young tube. NMR (<sup>1</sup>H and <sup>31</sup>P) spectra of the sample were taken. The sample was then heated to 85 °C, and NMR spectra were taken after 2, 4, 6 and 10 hours.

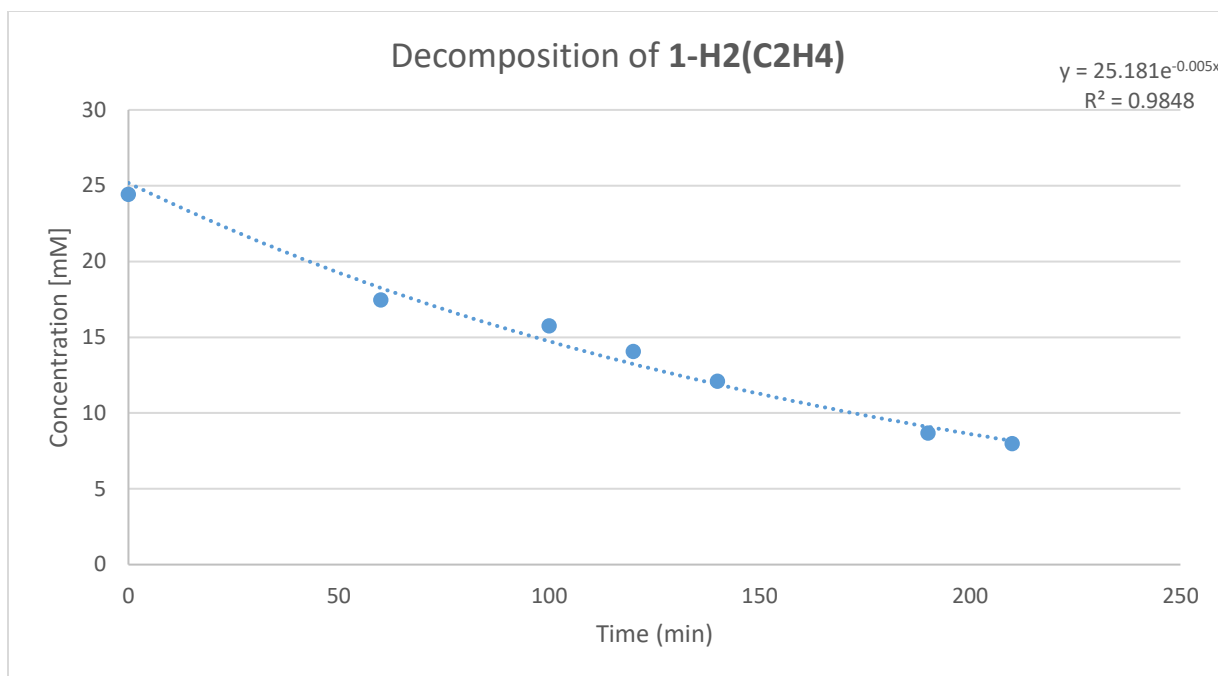


**Figure 3.45.** Plot-Decomposition of **1-H<sub>2</sub>(C<sub>2</sub>H<sub>4</sub>)**. Rate constant =  $0.0048 \text{ min}^{-1}$ ,  $\Delta G^\ddagger = 25.25 \text{ kcal/mol}$

### 3.10.7 T1 Measurements

A solution of **1-H<sub>4</sub>** (.008 g, 0.015 mmol) in toluene d<sub>8</sub> was transferred to a J. Young tube. T1 NMR measurements of the solution were taken at 25, 10, 0, -40, -50, -55, -60 and -65°C. Due to broadening of the hydride signals no visible signals are present between 0 and -40°C.

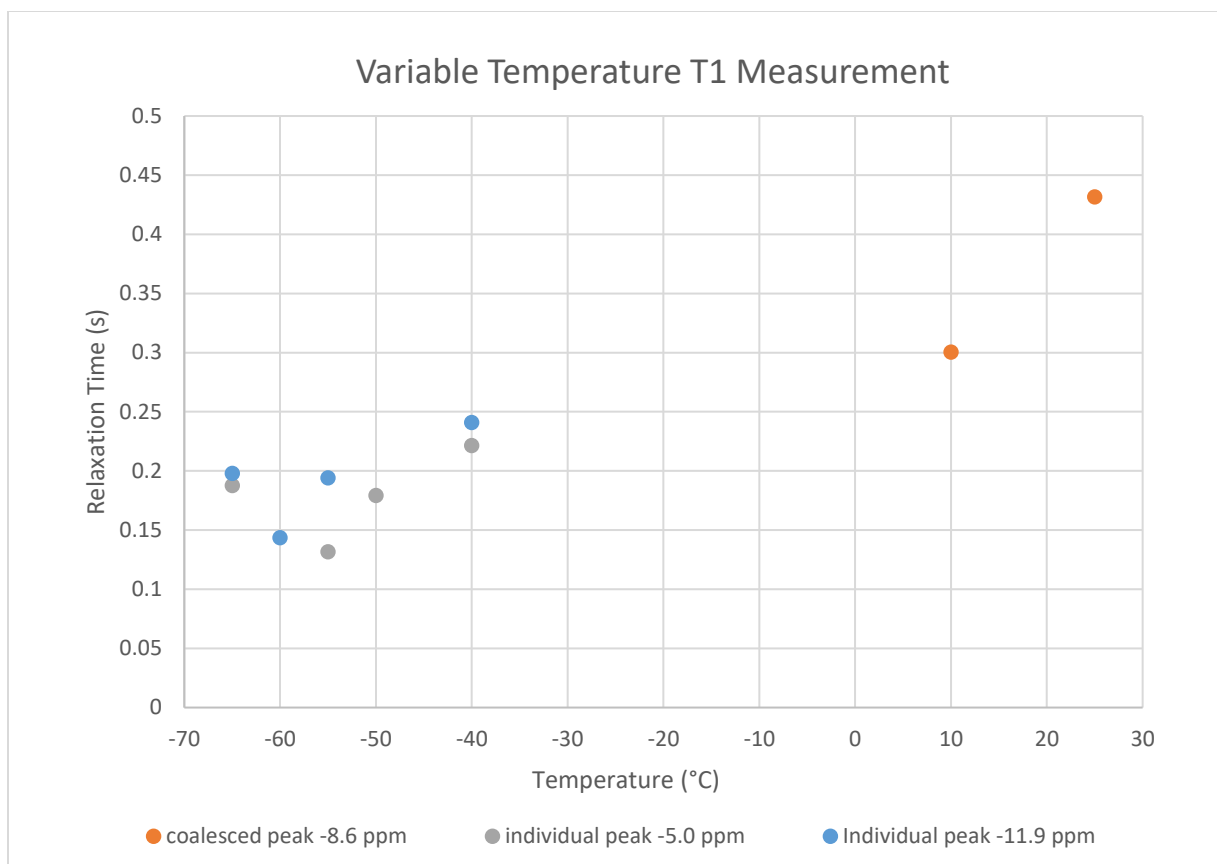


**Figure 3.46.** T1 measurement plot

### 3.10.8 Hydrogenation of TBE, NBE and Acetone Reactions in Sealed Tube

Inside the glovebox, an oven-dried NMR tube was charged with 0.5 mL *p*-xylene solution of **1-H<sub>2</sub>(C<sub>2</sub>H<sub>4</sub>)** (0.008 mmol, 16 mM) and substrate (0.5 M). The NMR tube was attached to a Kontes valve and removed from the glovebox. The Kontes valve was attached to a vacuum-gas manifold, and the solution inside was frozen with liquid N<sub>2</sub>. The headspace was evacuated down to a pressure of 0.010 Torr. Next the tube was charged with 1 atm of H<sub>2</sub>. The sample was further immersed in liquid N<sub>2</sub> and after ~1 minute, the NMR tube was sealed with an oxygen torch (this decreased the volume by 50% and brought the total pressure to 2 atm). The sealed NMR tube was allowed to warm to room



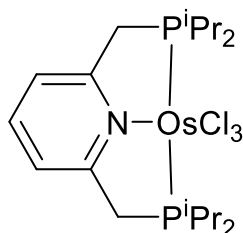
temperature. The sample was then heated inside a GC oven equipped to stir the sample while inside the oven. The samples were heated in the oven, stirring for set times; the oven was then returned to 25 °C and NMR spectra were taken of the sample.

### 3.10.9 Dehydrogenation of 2-Propanol

Inside the glovebox, an oven-dried NMR tube was charged with 0.5 mL *p*-xylene stock solution. The stock solution contained 500 mM isopropanol and **1-H<sub>2</sub>(C<sub>2</sub>H<sub>4</sub>)** (0.008 g, 16 mM). The NMR tube was attached to a Kontes valve and removed from the glovebox. The Kontes valve was attached to a vacuum-gas manifold, and the solution inside was frozen with liquid N<sub>2</sub>. The headspace was evacuated down to a pressure of 0.010 Torr and then placed under 1 atm of ethylene. The NMR tube was fully immersed in liquid N<sub>2</sub>, allowing the ethylene to condense. After ~1 minute, the NMR tube was sealed with an oxygen torch (this decreased the volume by 50% and brought the total pressure to 1.5 atm). The sealed NMR tube was allowed to warm to room temperature. The sample was then heated inside a GC oven equipped to stir the sample while inside the oven. The samples were heated in the oven stirring for set times; the oven is then returned to 25 °C and NMR spectra of the sample were taken.

### 3.10.10 Synthesis of (<sup>i</sup>PrPNP)Os complexes

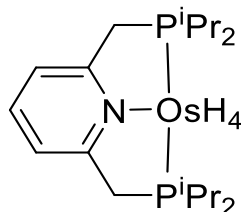
#### Synthesis of (<sup>i</sup>PrPNP)OsCl<sub>3</sub> (5-Cl<sub>3</sub>)



A mixture of (<sup>i</sup>PrPNP) ligand (0.150 g, 0.442 mmol) and Na<sub>2</sub>OsCl<sub>6</sub>·6H<sub>2</sub>O (0.535 g, 1.3 mmol) was dissolved in 2-methoxyethanol (20 mL). Formation of a green solution was observed upon mixing. The solution was heated to 105°C for 4 hours upon which the solution turned orange. The solution was filtered then concentrated until orange crystals began to precipitate. The solution was then stored at 0°C under argon overnight. The red crystals were filtered from excess solvent through a frit and washed with pentane (5 mL x 3). The filtrate was then further concentrated until precipitation was observed again. This process was repeated twice more to increase yield. Yield = 0.146 g (51%).

<sup>1</sup>H-NMR (400 MHz, THF-d<sub>8</sub>): δ -24.9 (broad, 1H, p-py), -17.4 (broad, 1H, m-py), -9.81 (broad, 12H, CH(CH<sub>3</sub>)), -8.9 (broad, 12H, CH(CH<sub>3</sub>)), -0.13 (broad, 4H, CH<sub>2</sub>), 14.7 (broad, 2H, CH(CH<sub>3</sub>)), 18.0 (broad, 2H, CH(CH<sub>3</sub>))

### Synthesis of (<sup>i</sup>PrPNP)OsH<sub>4</sub> (5-H<sub>4</sub>)



A sample of **5-Cl<sub>3</sub>** (0.118 grams, 0.185 mmol) was dissolved in dry and degassed THF (20 mL) resulting in a yellow solution with some undissolved material. The solution was then bubbled with H<sub>2</sub> gas for approximately ten minutes then allowed to remain under a H<sub>2</sub> atmosphere. A 1 M solution of sodium triethylborohydride was then added dropwise (0.735 mL). Immediately upon addition, the solution turned dark green but when all of the sodium triethylborohydride had been added to the solution the color was dark red/purple. The solution was stirred at room temperature overnight. The solution was filtered through a pad of celite to remove precipitate that formed. The solvent was removed by vacuum leaving a light orange/brown solid. Yield = 0.064 g (63.6%).

<sup>1</sup>H-NMR (400 MHz, toluene-d<sub>8</sub>): δ 6.79 (t, J = 7.8, 1H, *p*-py), 6.53 (d, J = 7.7, 2H, *m*-py), 3.18 (t, J = 3.6, 4H, CH<sub>2</sub>-P), 1.71 (m, 4H, isopropyl C-H), 1.18 (q, J = 7.0, 12H, isopropyl CH<sub>3</sub>), 0.88 (q, J = 7.0, 12H, isopropyl CH<sub>3</sub>), -8.96 (broad singlet, 4H, Os-H). <sup>31</sup>P-NMR{<sup>1</sup>H} (121 MHz, toluene-d<sub>8</sub>): δ 58.5 (s, P<sup>i</sup>Pr<sub>2</sub>)

### Reaction of (<sup>i</sup>PrPNP)OsH<sub>4</sub> with olefins (NBE, TBE, ethylene)

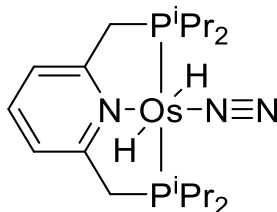
Inside the glovebox, an oven-dried J. Young NMR tube was charged with 0.5 mL toluene d<sub>8</sub> solution of (<sup>i</sup>PrPNP)OsH<sub>4</sub> (0.006 g, 0.011 mmol) and 0.5 M or 1 atm of olefin acceptor (NBE, TBE, ethylene). <sup>31</sup>P-NMR and <sup>1</sup>H-NMR were taken at room temperature. The

solutions were heated at 50, 65, 80 and 100°C for 3 hours at each corresponding temperature. NMR was taken after heating at each temperature.

### 3.10.11 Dehydrogenative coupling of styrene

A solution of (<sup>i</sup>PrPNP)OsH<sub>4</sub> (4.3 mg, 0.0067 mmol) and styrene (xx g, xx mmol) in toluene d<sub>8</sub> was added to a J. Young tube. The solution was heated at 150°C for 4, 19 and 52 hours with NMR's taken at each time point. Calculations of product concentration were based on styrene peaks and side product (ethyl benzene) peaks integration.

### 3.10.12 Synthesis of (<sup>i</sup>PrPNP)OsH<sub>2</sub>(N<sub>2</sub>) (5-(H)<sub>2</sub>N<sub>2</sub>)

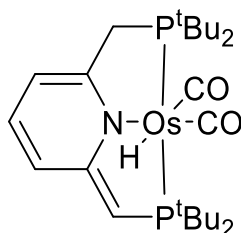


(<sup>i</sup>PrPNP)OsH<sub>4</sub> (5.0 mg, 0.009 mmol) and TBE (0.005 mL) were dissolved in toluene (0.5 mL) resulting in a yellow solution. The solution was then added to a J. Young tube which was then charged with N<sub>2</sub> (1 atm). The solution was heated at 105°C for 7 hours during which the solution became a more vibrant yellow color. The solution was filtered and solvent was removed leaving a yellow residue.

<sup>1</sup>H-NMR (400 MHz, toluene-d<sub>8</sub>): δ 6.67 (t, J = 7.7, 1H, *p*-py), 6.32 (d, J = 7.7, 2H, *m*-py), 2.94 (t, J = 3.8, 4H, CH<sub>2</sub>-P), 1.85 (m, 4H, isopropyl C-H), 1.25 (q, J = 7.4, 12H, isopropyl CH<sub>3</sub>), 1.06 (q, J = 6.9, 12H, isopropyl CH<sub>3</sub>), -6.70 (t, J = 16.1, 2H, Os-H). <sup>31</sup>P-NMR{<sup>1</sup>H} (121 MHz, toluene-d<sub>8</sub>): δ 60.56 (s, P<sup>i</sup>Pr<sub>2</sub>)

### 3.10.13 Synthesis of dearomatized (<sup>t</sup>BuPNP) complexes

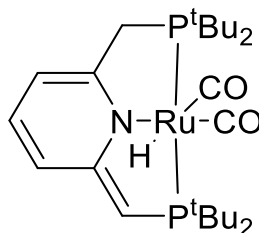
#### Synthesis of dearomatized (<sup>t</sup>BuPNP)OsH(CO)<sub>2</sub> (6- H(CO)<sub>2</sub>)



(<sup>t</sup>BuPNP)OsH<sub>4</sub> (0.005 g, 0.008 mol) and was dissolved in 0.5 mL of toluene forming a yellow/orange solution. The solution was then charged with 1 atm of carbon monoxide. The solution was then heated to 100°C for 8 hours under a CO atmosphere. Upon heating the solution turned a neon yellow/green color. The solution was cooled to r.t. and the solvent was removed by vacuum leaving a light brown solid.

<sup>1</sup>H-NMR (400 MHz, toluene-d<sub>8</sub>): δ 6.37 (dd, J = 8.7, 6.6, 1H, *p*-py), 6.28 (d, J = 8.8, 1H, *m*-py), 5.44 (d, J = 6.5, 1H, *m*-py), 3.82 (t, J = 3.3, 1H, CH-P), 3.04 (dd, J = 16.1, 11.2, 1H, CH<sub>2</sub>-P), 2.71 (dd, J = 16.2, 6.8, 1H, CH<sub>2</sub>-P), 1.41 (dd, J = 13.4, 11, 18H, tert-butyl), 1.08 (dd, J = 19.5, 13.5, 18H, tert-butyl), -5.74 (dd, J = 21.8, 19.7, 1H, Os-H). <sup>31</sup>P-NMR{<sup>1</sup>H} (121 MHz, toluene-d<sub>8</sub>): δ 59.6(dd (AB splitting pattern), P<sup>t</sup>Bu<sub>2</sub>)

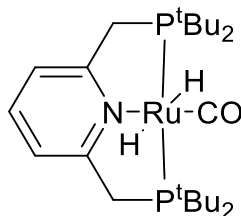
#### Synthesis of dearomatized (<sup>t</sup>BuPNP)RuH(CO)<sub>2</sub> (7- H(CO)<sub>2</sub>)



(<sup>t</sup>BuPNP)RuHCl(CO) (0.005 g, 0.012 mol) and was dissolved in 0.5 mL of toluene d<sub>8</sub> forming a neon yellow solution which was transferred to a J. Young tube. Next potassium tert-butoxide (0.001 g, 0.010 mol) was added turning the solution neon green/yellow immediately. The solution was then charged with 1 atm of carbon monoxide as quickly as possible. The solution was then allowed to stir at room temperature for one hour.

<sup>1</sup>H-NMR (400 MHz, toluene-d<sub>8</sub>): δ 6.48 (m, 1H, *p*-py), 6.37 (d, *J* = 8.8, 1H, *m*-py), 5.49 (d, *J* = 6.4, 1H, *m*-py), 3.71 (t, *J* = 3.3, 1H, CH-P), 2.79 (m, 1H, CH<sub>2</sub>-P), 1.45 (dt, *J* = 2.96, 10.2, 18H, tert-butyl), 1.09 (dt, *J* = 10.0, 3.3, 18H, tert-butyl), -5.95 (t, *J* = 18.4, 1H, Os-H). <sup>31</sup>P-NMR{<sup>1</sup>H} (121 MHz, toluene-d<sub>8</sub>): δ 88.2(dd (AB splitting pattern), P<sup>t</sup>Bu<sub>2</sub>)

#### Synthesis of dearomatized (<sup>t</sup>BuPNP)Ru(H)<sub>2</sub>CO (7- (H)<sub>2</sub>CO)

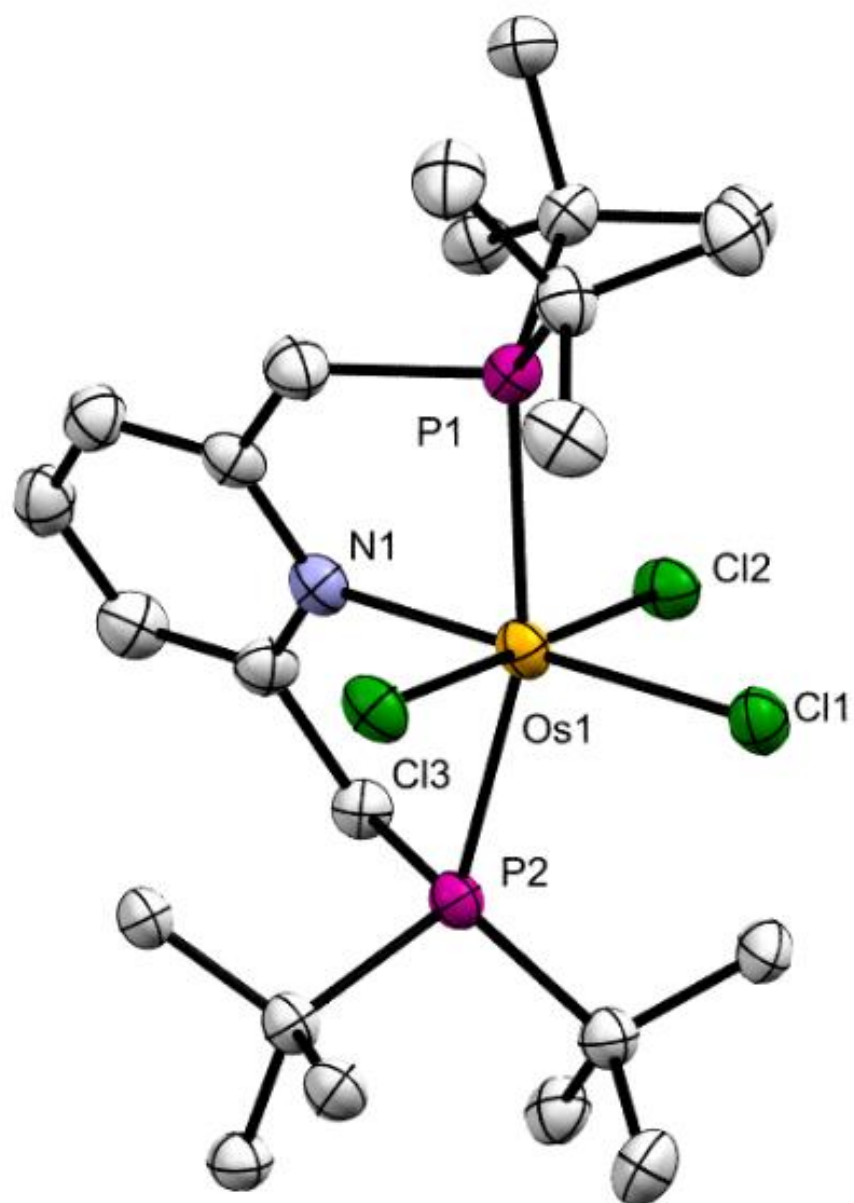


(<sup>t</sup>BuPNP)RuHCl(CO) (0.005 g, 0.012 mol) and was dissolved in 0.5 mL of toluene d<sub>8</sub> forming a neon yellow solution which was transferred to a J. Young tube. Next potassium tert-butoxide (0.001 g, 0.010 mol) was added turning the solution. The solution was then charged with 1 atm of hydrogen as quickly as possible and the solution turned light yellow. The solution was then allowed to stir at room temperature for one hour.

$^1\text{H}$ -NMR (400 MHz, benzene- $\text{d}_6$ ):  $\delta$  6.70 (t,  $J = 7.7$ , 1H,  $p$ -py), 6.37 (d,  $J = 7.7$ , 1H,  $m$ -py), 3.10 (t,  $J = 3.5$ , 4H,  $\text{CH}_2$  linkers), 1.43 (t,  $J = 6.3$ , 36H,  $\text{C}(\text{CH}_3)_3$ ), -4.88 (t,  $J = 17.1$ , 2H, Os-H).

$^{31}\text{P}$ -NMR $\{^1\text{H}\}$  (121 MHz, benzene- $\text{d}_6$ ):  $\delta$  106.3(s,  $\text{P}^t\text{Bu}_2$ )

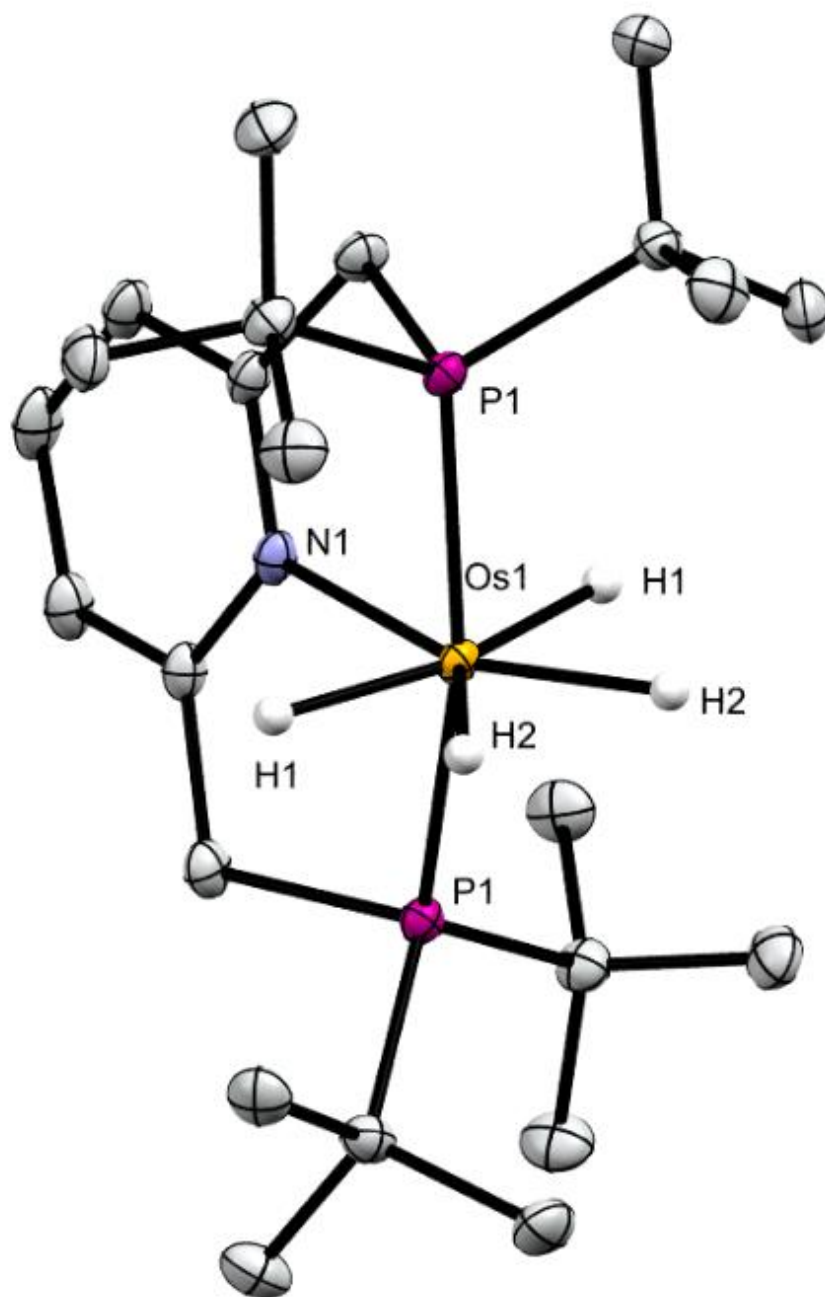
Figure 3.47: Structural data for complex (<sup>t</sup>BuPNP)OsCl<sub>3</sub> (**1-Cl<sub>3</sub>**)



ORTEP representation (50% probability ellipsoids) of structure (<sup>t</sup>BuPNP)OsCl<sub>3</sub> (**1-Cl<sub>3</sub>**) determined by X-ray diffraction; hydrogen atoms omitted for clarity. Crystal data can be found in the following reference.<sup>65</sup>

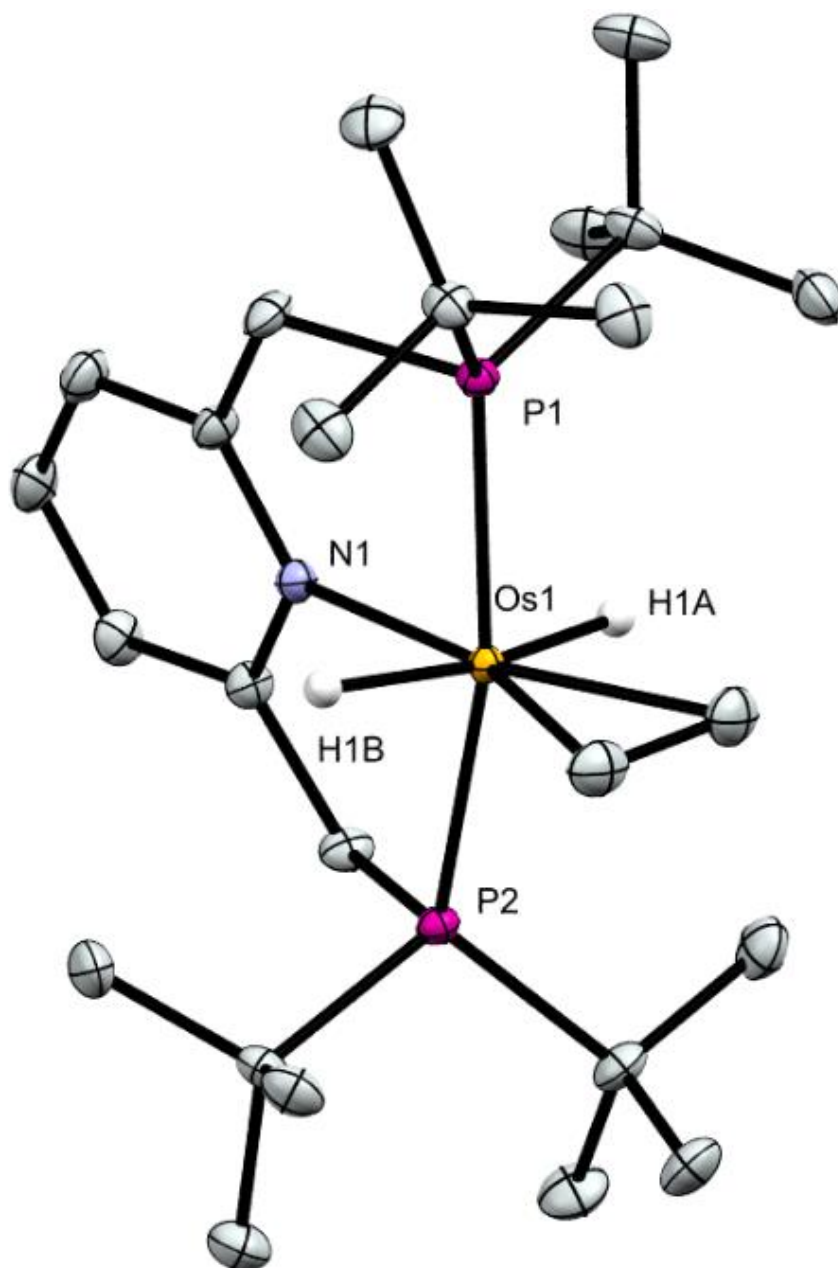


Figure 3.48: Structural data for complex (<sup>t</sup>BuPNP)OsH<sub>4</sub> (**1-H<sub>4</sub>**)



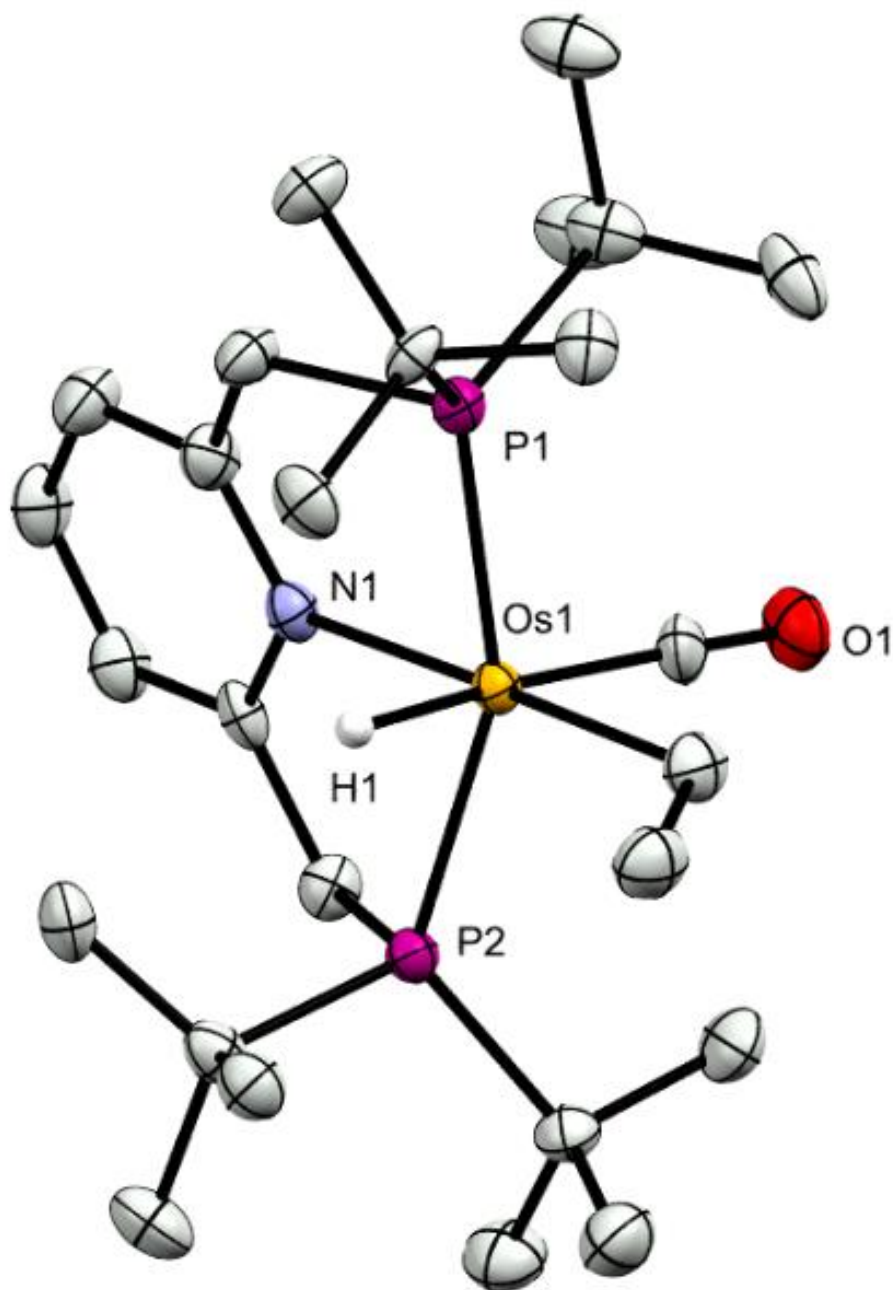
ORTEP representation (50% probability ellipsoids) of complex (<sup>t</sup>BuPNP)OsH<sub>4</sub> (**1-H<sub>4</sub>**) determined by X-ray diffraction. H atoms other than hydrides omitted. Crystal data can be found in the following reference.<sup>65</sup>

Figure 3.49: Structural data for complex ( $t^{\text{Bu}}\text{PNP}$ )OsH<sub>2</sub>(C<sub>2</sub>H<sub>4</sub>) (**1-H<sub>2</sub>(C<sub>2</sub>H<sub>4</sub>)**)



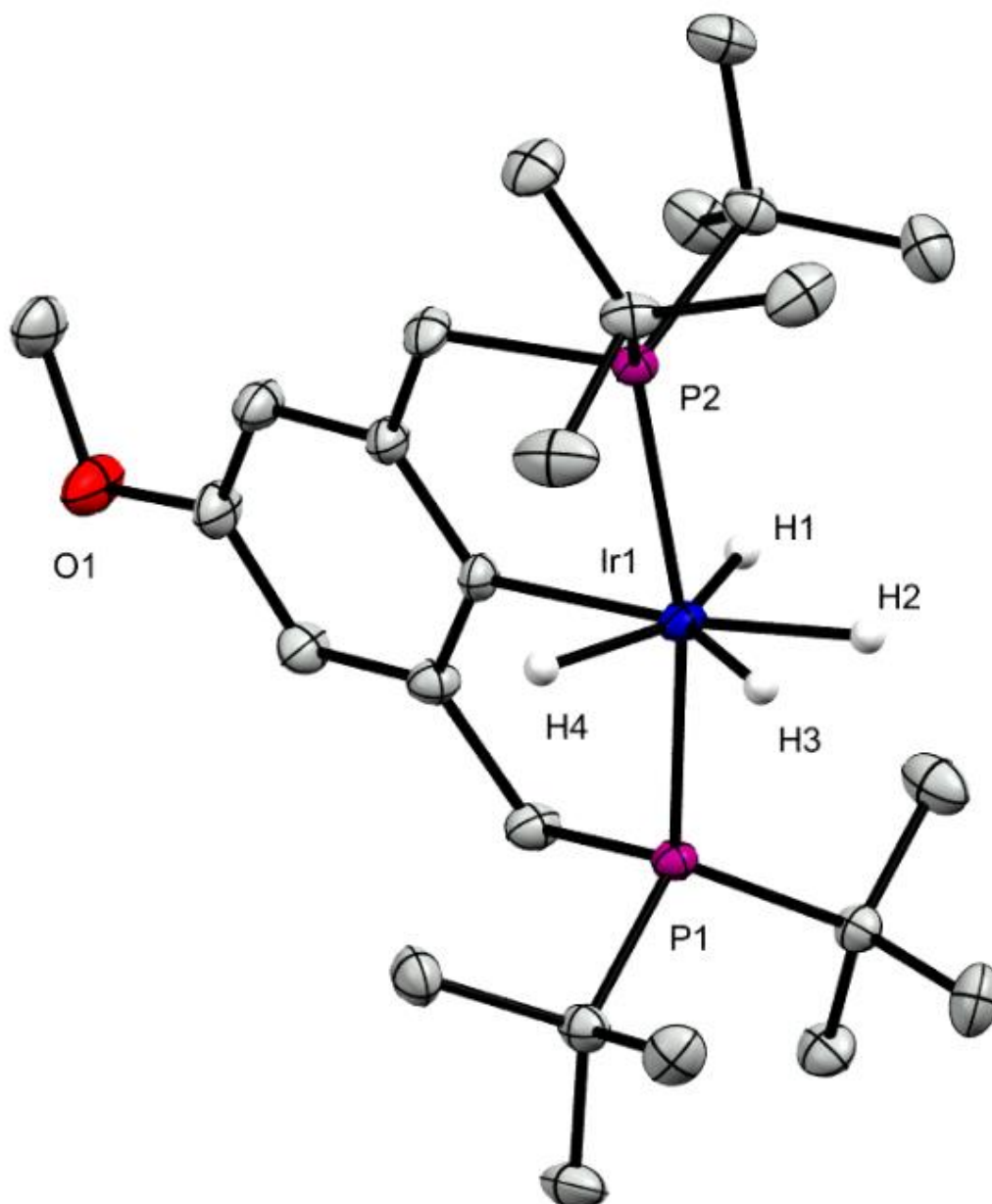
ORTEP representation (50% probability ellipsoids) of complex ( $t^{\text{Bu}}\text{PNP}$ )OsH<sub>2</sub>(C<sub>2</sub>H<sub>4</sub>) (**1-H<sub>2</sub>(C<sub>2</sub>H<sub>4</sub>)**) determined by X-ray diffraction. H atoms other than hydrides omitted for clarity. Crystal data can be found in the following reference.<sup>65</sup>

Figure 3.50: Structural data for complex (<sup>t</sup>BuPNP)Os(H)(Et)(CO) (**1-H(Et)(CO)**)



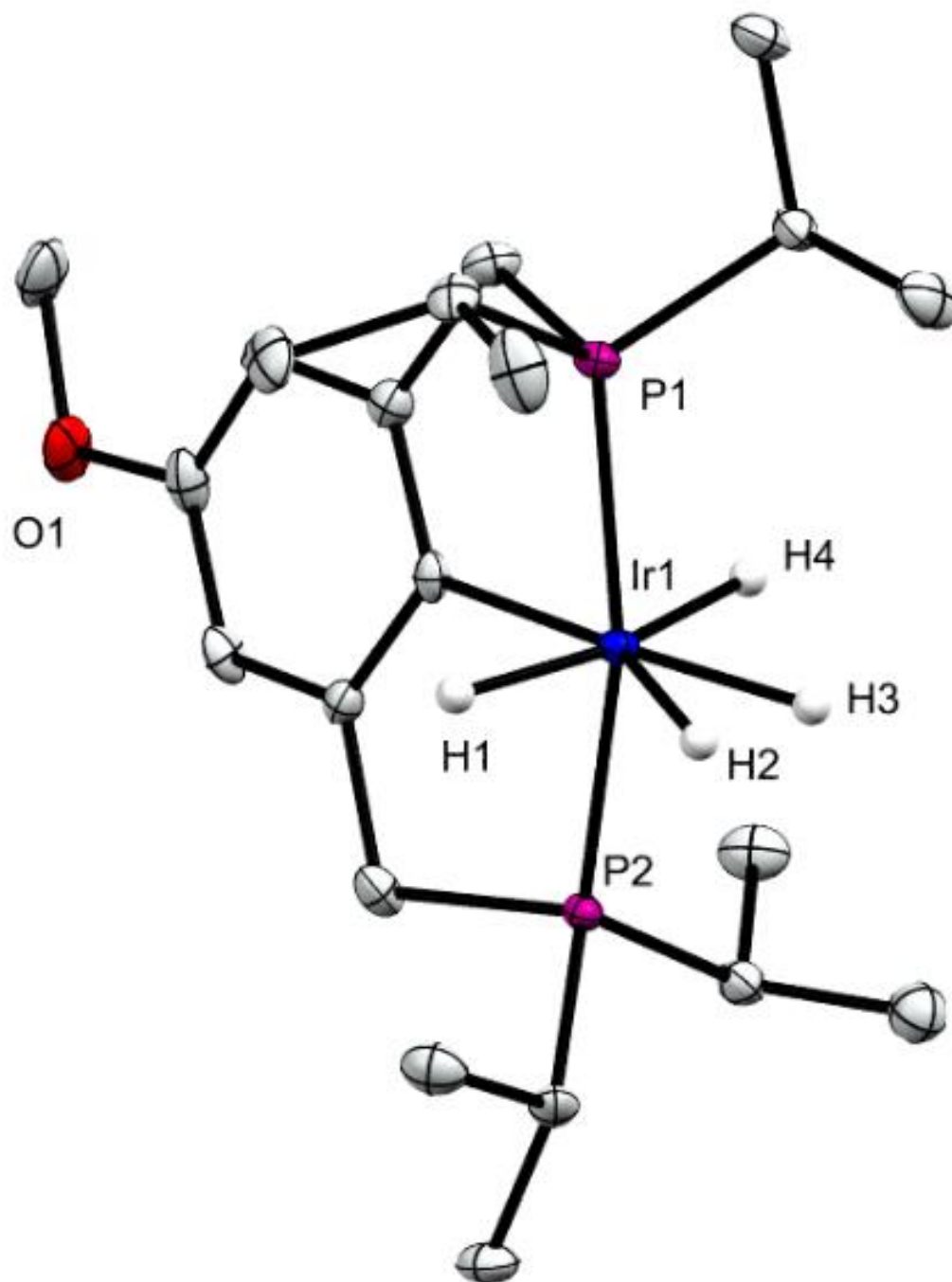
ORTEP representation (50% probability ellipsoids) of complex (<sup>t</sup>BuPNP)Os(H)(Et)(CO) (**1-H(Et)(CO)**) determined by X-ray diffraction. H atoms other than hydrides omitted for clarity. Crystal data can be found in the following reference.<sup>65</sup>

Figure 3.51: Structural data for complex  $(\text{MeO-}^t\text{BuPCP})\text{IrH}_4$



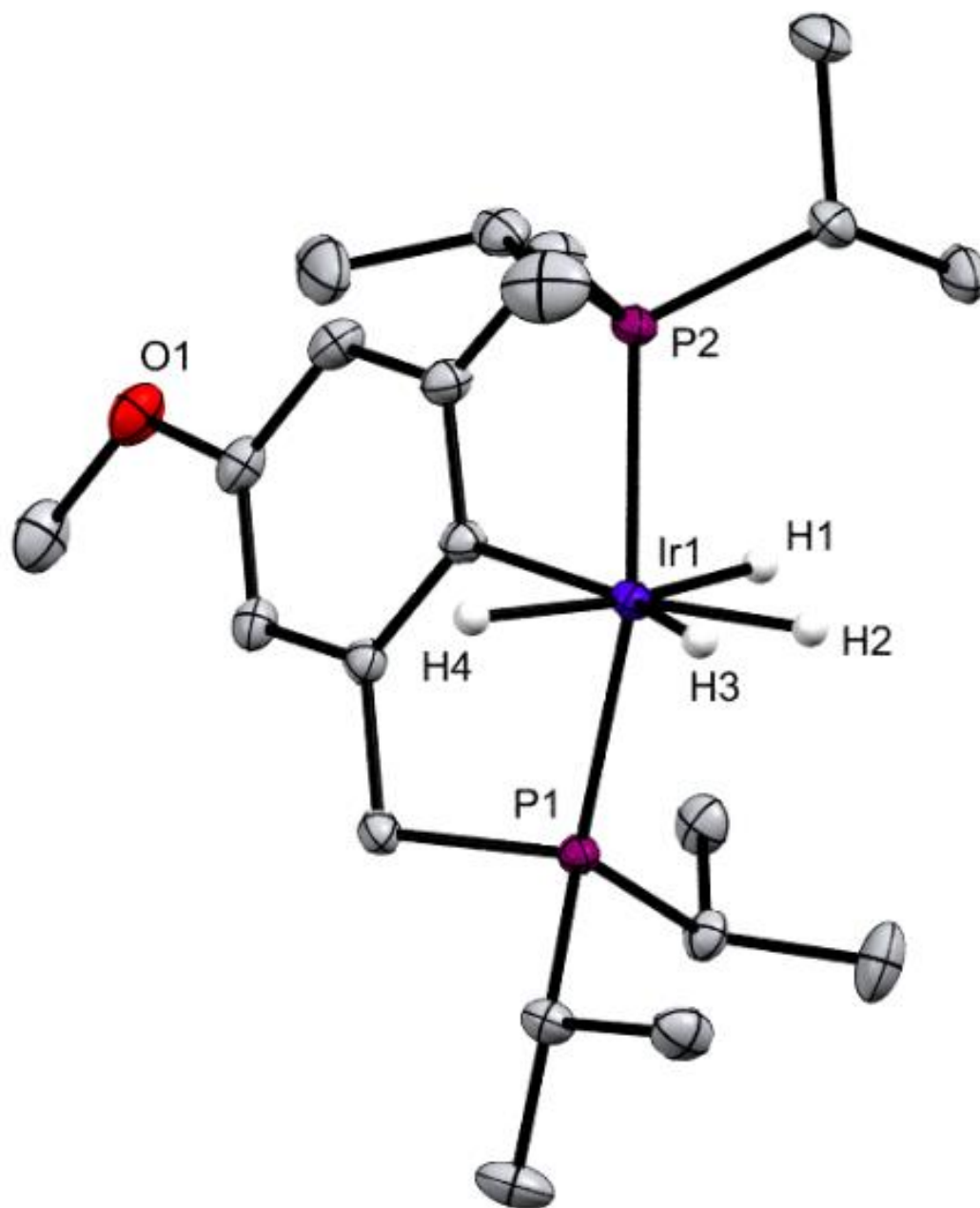
ORTEP representation (50% probability ellipsoids) of complex  $(\text{MeO-}^t\text{BuPCP})\text{IrH}_4$  determined by X-ray diffraction. H atoms other than hydrides omitted for clarity. Crystal data can be found in the following reference.<sup>65</sup>

Figure 3.52: Structural data for complex  $(\text{MeO-}^i\text{PrPCP})\text{IrH}_4$  (monoclinic)



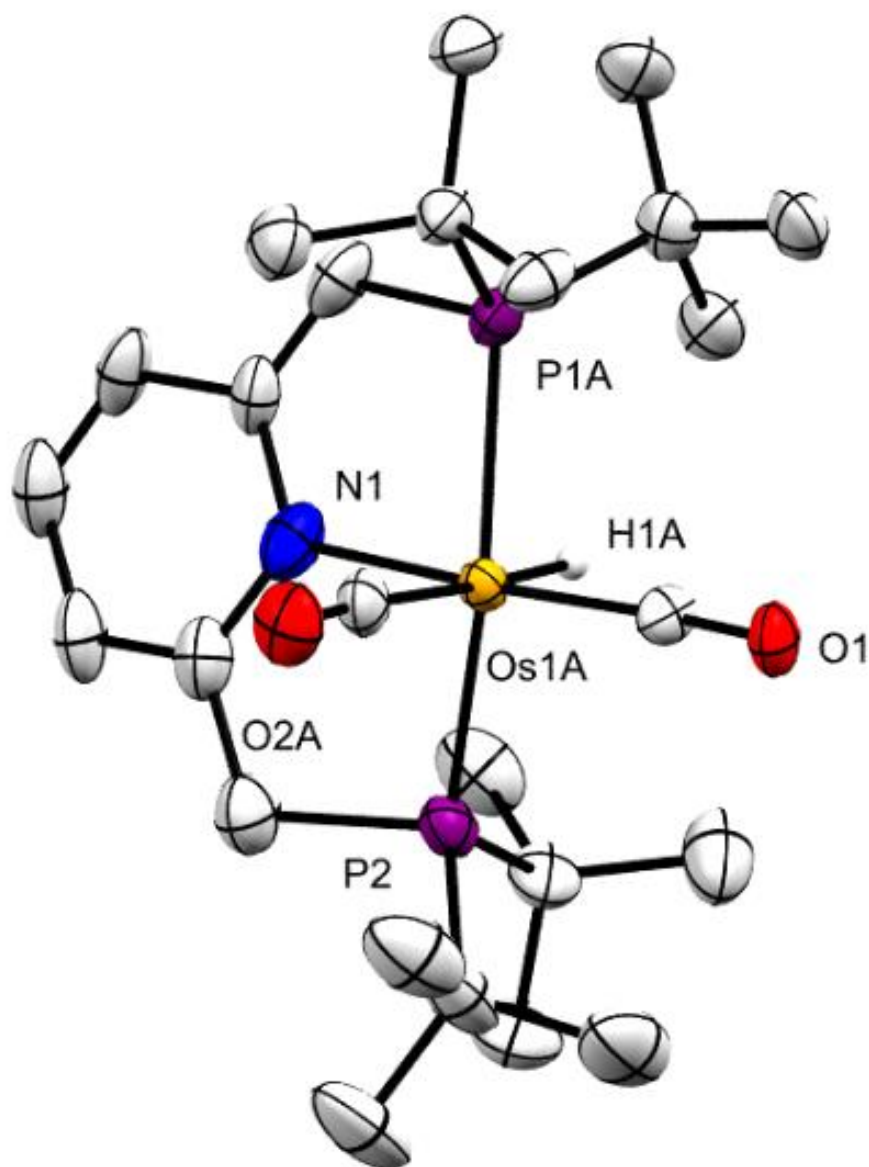
ORTEP representation (50% probability ellipsoids) of complex  $(\text{MeO-}^i\text{PrPCP})\text{IrH}_4$  (monoclinic) determined by X-ray diffraction. H atoms other than hydrides omitted for clarity. Crystal data can be found in the following reference.<sup>65</sup>

Figure 3.53: Structural data for complex  $(\text{MeO-}^i\text{PrPCP})\text{IrH}_4$  (triclinic)



ORTEP representation (50% probability ellipsoids) of complex  $(\text{MeO-}^i\text{PrPCP})\text{IrH}_4$  (triclinic) determined by X-ray diffraction. H atoms other than hydrides omitted for clarity. Crystal data can be found in the following reference.<sup>65</sup>

Figure 3.54: Structural data for complex (<sup>t</sup>BuPNP)Os(H)(CO)<sub>2</sub> (6-(H)(CO)<sub>2</sub>)



ORTEP representation (50% probability ellipsoids) of complex (**5-H(CO)<sub>2</sub>**) determined by X-ray diffraction. H atoms other than hydrides omitted for clarity.

Table 3.10. Crystal data and structure refinement for (tBuPNP)OsH(CO)<sub>2</sub>.

Identification code	(tBuPNP)OsH(CO) <sub>2</sub>	
Empirical formula	C <sub>25</sub> H <sub>43</sub> N O <sub>2</sub> Os P <sub>2</sub>	
Formula weight	641.74	
Temperature	100(2) K	
Wavelength	0.71073 Å	
Crystal system	Monoclinic	
Space group	P2 <sub>1</sub> /n	
Unit cell dimensions	a = 15.5621(17) Å	∠ = 90°.
	b = 11.5827(13) Å	∠ = 91.777(2)°.
	c = 30.000(3) Å	∠ = 90°.
Volume	5404.9(10) Å <sup>3</sup>	
Z	8	
Density (calculated)	1.577 Mg/m <sup>3</sup>	
Absorption coefficient	4.858 mm <sup>-1</sup>	
F(000)	2576	
Crystal size	0.380 x 0.080 x 0.040 mm <sup>3</sup>	
Theta range for data collection	1.358 to 29.139°.	
Index ranges	-21 ≤ h ≤ 21, -15 ≤ k ≤ 15, -40 ≤ l ≤ 41	
Reflections collected	61640	
Independent reflections	14545 [R(int) = 0.0770]	
Completeness to theta = 25.242°	99.9 %	
Absorption correction	Semi-empirical from equivalents	
Max. and min. transmission	0.2644 and 0.1735	
Refinement method	Full-matrix least-squares on F <sup>2</sup>	
Data / restraints / parameters	14545 / 1358 / 633	
Goodness-of-fit on F <sup>2</sup>	1.087	
Final R indices [I > 2σ(I)]	R1 = 0.0607, wR2 = 0.1174	
R indices (all data)	R1 = 0.0970, wR2 = 0.1296	
Extinction coefficient	n/a	
Largest diff. peak and hole	2.689 and -1.559 e.Å <sup>-3</sup>	



Table 3.11 Bond lengths [Å] and angles [°] for (tBuPNP)OsH(CO)<sub>2</sub>.

Os(1A)-C(24)	1.895(6)	Os(1B)-C(25B)	1.920(7)
Os(1A)-C(25A)	1.920(7)	Os(1B)-P(1B)	2.322(8)
Os(1A)-N(1)	2.150(6)	Os(1B)-H(1B)	1.601(10)
Os(1A)-P(2)	2.331(2)	C(25B)-O(2B)	1.173(9)
Os(1A)-P(1A)	2.391(3)	P(1B)-C(8B)	1.936(11)
Os(1A)-H(1A)	1.589(10)	P(1B)-C(12B)	1.947(11)
C(25A)-O(2A)	1.172(9)	C(8B)-C(11B)	1.504(15)
P(1A)-C(6)	1.816(8)	C(8B)-C(9B)	1.516(15)
P(1A)-C(12A)	1.901(9)	C(8B)-C(10B)	1.531(15)
P(1A)-C(8A)	1.908(9)	C(9B)-H(9D)	0.9800
C(8A)-C(11A)	1.509(12)	C(9B)-H(9E)	0.9800
C(8A)-C(9A)	1.527(12)	C(9B)-H(9F)	0.9800
C(8A)-C(10A)	1.528(12)	C(10B)-H(10D)	0.9800
C(9A)-H(9A)	0.9800	C(10B)-H(10E)	0.9800
C(9A)-H(9B)	0.9800	C(10B)-H(10F)	0.9800
C(9A)-H(9C)	0.9800	C(11B)-H(11D)	0.9800
C(10A)-H(10A)	0.9800	C(11B)-H(11E)	0.9800
C(10A)-H(10B)	0.9800	C(11B)-H(11F)	0.9800
C(10A)-H(10C)	0.9800	C(12B)-C(13B)	1.473(15)
C(11A)-H(11A)	0.9800	C(12B)-C(14B)	1.520(15)
C(11A)-H(11B)	0.9800	C(12B)-C(15B)	1.564(17)
C(11A)-H(11C)	0.9800	C(13B)-H(13D)	0.9800
C(12A)-C(13A)	1.481(13)	C(13B)-H(13E)	0.9800
C(12A)-C(14A)	1.521(13)	C(13B)-H(13F)	0.9800
C(12A)-C(15A)	1.571(15)	C(14B)-H(14D)	0.9800
C(13A)-H(13A)	0.9800	C(14B)-H(14E)	0.9800
C(13A)-H(13B)	0.9800	C(14B)-H(14F)	0.9800
C(13A)-H(13C)	0.9800	C(15B)-H(15D)	0.9800
C(14A)-H(14A)	0.9800	C(15B)-H(15E)	0.9800
C(14A)-H(14B)	0.9800	C(15B)-H(15F)	0.9800
C(14A)-H(14C)	0.9800	O(1)-C(24)	1.139(7)
C(15A)-H(15A)	0.9800	N(1)-C(5)	1.377(11)
C(15A)-H(15B)	0.9800	N(1)-C(1)	1.386(10)
C(15A)-H(15C)	0.9800	C(1)-C(6)	1.337(11)

C(1)-C(2)	1.435(10)	C(23)-H(23B)	0.9800
C(2)-C(3)	1.343(12)	C(23)-H(23C)	0.9800
C(2)-H(2)	0.9500	Os(2A)-C(49)	1.874(7)
C(3)-C(4)	1.401(13)	Os(2A)-C(50)	1.916(9)
C(3)-H(3)	0.9500	Os(2A)-N(2)	2.147(6)
C(4)-C(5)	1.382(11)	Os(2A)-P(3)	2.3569(18)
C(4)-H(4)	0.9500	Os(2A)-P(4)	2.3825(19)
C(5)-C(7)	1.500(12)	Os(2A)-H(2A)	1.600(10)
C(6)-H(6)	0.9500	P(3)-C(31)	1.829(8)
C(7)-P(2)	1.837(9)	P(3)-C(37)	1.874(8)
C(7)-H(7A)	0.9900	P(3)-C(33)	1.898(7)
C(7)-H(7B)	0.9900	P(4)-C(32)	1.773(8)
P(2)-C(20)	1.886(9)	P(4)-C(41)	1.896(8)
P(2)-C(16)	1.907(9)	P(4)-C(45)	1.903(9)
C(16)-C(19)	1.446(14)	O(3)-C(49)	1.160(8)
C(16)-C(18)	1.539(12)	O(4)-C(50)	1.160(9)
C(16)-C(17)	1.543(14)	N(2)-C(26)	1.363(9)
C(17)-H(17A)	0.9800	N(2)-C(30)	1.404(9)
C(17)-H(17B)	0.9800	C(26)-C(27)	1.387(11)
C(17)-H(17C)	0.9800	C(26)-C(31)	1.491(11)
C(18)-H(18A)	0.9800	C(27)-C(28)	1.396(12)
C(18)-H(18B)	0.9800	C(27)-H(27)	0.9500
C(18)-H(18C)	0.9800	C(28)-C(29)	1.368(11)
C(19)-H(19A)	0.9800	C(28)-H(28)	0.9500
C(19)-H(19B)	0.9800	C(29)-C(30)	1.413(10)
C(19)-H(19C)	0.9800	C(29)-H(29)	0.9500
C(20)-C(22)	1.524(11)	C(30)-C(32)	1.390(10)
C(20)-C(23)	1.546(13)	C(31)-H(31A)	0.9900
C(20)-C(21)	1.552(12)	C(31)-H(31B)	0.9900
C(21)-H(21A)	0.9800	C(32)-H(32)	0.9500
C(21)-H(21B)	0.9800	C(33)-C(36)	1.503(11)
C(21)-H(21C)	0.9800	C(33)-C(34)	1.544(13)
C(22)-H(22A)	0.9800	C(33)-C(35)	1.545(11)
C(22)-H(22B)	0.9800	C(34)-H(34A)	0.9800
C(22)-H(22C)	0.9800	C(34)-H(34B)	0.9800
C(23)-H(23A)	0.9800	C(34)-H(34C)	0.9800

C(35)-H(35A)	0.9800	C(42)-H(42A)	0.9800
C(35)-H(35B)	0.9800	C(42)-H(42B)	0.9800
C(35)-H(35C)	0.9800	C(42)-H(42C)	0.9800
C(36)-H(36A)	0.9800	C(43)-H(43A)	0.9800
C(36)-H(36B)	0.9800	C(43)-H(43B)	0.9800
C(36)-H(36C)	0.9800	C(43)-H(43C)	0.9800
C(37)-C(38)	1.518(11)	C(44)-H(44A)	0.9800
C(37)-C(39)	1.537(10)	C(44)-H(44B)	0.9800
C(37)-C(40)	1.547(11)	C(44)-H(44C)	0.9800
C(38)-H(38A)	0.9800	C(45)-C(48)	1.514(13)
C(38)-H(38B)	0.9800	C(45)-C(46)	1.520(13)
C(38)-H(38C)	0.9800	C(45)-C(47)	1.521(11)
C(39)-H(39A)	0.9800	C(46)-H(46A)	0.9800
C(39)-H(39B)	0.9800	C(46)-H(46B)	0.9800
C(39)-H(39C)	0.9800	C(46)-H(46C)	0.9800
C(40)-H(40A)	0.9800	C(47)-H(47A)	0.9800
C(40)-H(40B)	0.9800	C(47)-H(47B)	0.9800
C(40)-H(40C)	0.9800	C(47)-H(47C)	0.9800
C(41)-C(44)	1.492(12)	C(48)-H(48A)	0.9800
C(41)-C(42)	1.528(12)	C(48)-H(48B)	0.9800
C(41)-C(43)	1.533(11)	C(48)-H(48C)	0.9800
C(24)-Os(1A)-C(25A)	93.1(3)	P(1A)-Os(1A)-H(1A)	80.3(2)
C(24)-Os(1A)-N(1)	173.6(3)	O(2A)-C(25A)-Os(1A)	175.7(6)
C(25A)-Os(1A)-N(1)	93.1(3)	C(6)-P(1A)-C(12A)	106.8(4)
C(24)-Os(1A)-P(2)	99.50(15)	C(6)-P(1A)-C(8A)	104.4(4)
C(25A)-Os(1A)-P(2)	98.51(17)	C(12A)-P(1A)-C(8A)	110.2(5)
N(1)-Os(1A)-P(2)	81.22(19)	C(6)-P(1A)-Os(1A)	99.3(3)
C(24)-Os(1A)-P(1A)	96.52(15)	C(12A)-P(1A)-Os(1A)	118.3(3)
C(25A)-Os(1A)-P(1A)	97.67(17)	C(8A)-P(1A)-Os(1A)	115.8(3)
N(1)-Os(1A)-P(1A)	81.0(2)	C(11A)-C(8A)-C(9A)	110.6(8)
P(2)-Os(1A)-P(1A)	156.49(8)	C(11A)-C(8A)-C(10A)	106.6(7)
C(24)-Os(1A)-H(1A)	91.3(3)	C(9A)-C(8A)-C(10A)	109.6(7)
C(25A)-Os(1A)-H(1A)	175.3(4)	C(11A)-C(8A)-P(1A)	107.0(6)
N(1)-Os(1A)-H(1A)	82.4(3)	C(9A)-C(8A)-P(1A)	109.4(6)
P(2)-Os(1A)-H(1A)	82.3(2)	C(10A)-C(8A)-P(1A)	113.7(7)

C(8A)-C(9A)-H(9A)	109.5	C(12A)-C(15A)-H(15A)	109.5
C(8A)-C(9A)-H(9B)	109.5	C(12A)-C(15A)-H(15B)	109.5
H(9A)-C(9A)-H(9B)	109.5	H(15A)-C(15A)-H(15B)	109.5
C(8A)-C(9A)-H(9C)	109.5	C(12A)-C(15A)-H(15C)	109.5
H(9A)-C(9A)-H(9C)	109.5	H(15A)-C(15A)-H(15C)	109.5
H(9B)-C(9A)-H(9C)	109.5	H(15B)-C(15A)-H(15C)	109.5
C(8A)-C(10A)-H(10A)	109.5	C(25B)-Os(1B)-P(1B)	99.0(3)
C(8A)-C(10A)-H(10B)	109.5	C(25B)-Os(1B)-H(1B)	168.4(5)
H(10A)-C(10A)-H(10B)	109.5	P(1B)-Os(1B)-H(1B)	84.0(3)
C(8A)-C(10A)-H(10C)	109.5	O(2B)-C(25B)-Os(1B)	174.1(11)
H(10A)-C(10A)-H(10C)	109.5	C(8B)-P(1B)-C(12B)	103.6(8)
H(10B)-C(10A)-H(10C)	109.5	C(8B)-P(1B)-Os(1B)	117.7(8)
C(8A)-C(11A)-H(11A)	109.5	C(12B)-P(1B)-Os(1B)	111.8(8)
C(8A)-C(11A)-H(11B)	109.5	C(11B)-C(8B)-C(9B)	113.0(15)
H(11A)-C(11A)-H(11B)	109.5	C(11B)-C(8B)-C(10B)	106.6(13)
C(8A)-C(11A)-H(11C)	109.5	C(9B)-C(8B)-C(10B)	110.9(13)
H(11A)-C(11A)-H(11C)	109.5	C(11B)-C(8B)-P(1B)	105.4(9)
H(11B)-C(11A)-H(11C)	109.5	C(9B)-C(8B)-P(1B)	109.1(11)
C(13A)-C(12A)-C(14A)	111.6(9)	C(10B)-C(8B)-P(1B)	111.7(13)
C(13A)-C(12A)-C(15A)	108.6(8)	C(8B)-C(9B)-H(9D)	109.5
C(14A)-C(12A)-C(15A)	106.5(8)	C(8B)-C(9B)-H(9E)	109.5
C(13A)-C(12A)-P(1A)	111.4(7)	H(9D)-C(9B)-H(9E)	109.5
C(14A)-C(12A)-P(1A)	111.9(7)	C(8B)-C(9B)-H(9F)	109.5
C(15A)-C(12A)-P(1A)	106.5(7)	H(9D)-C(9B)-H(9F)	109.5
C(12A)-C(13A)-H(13A)	109.5	H(9E)-C(9B)-H(9F)	109.5
C(12A)-C(13A)-H(13B)	109.5	C(8B)-C(10B)-H(10D)	109.5
H(13A)-C(13A)-H(13B)	109.5	C(8B)-C(10B)-H(10E)	109.5
C(12A)-C(13A)-H(13C)	109.5	H(10D)-C(10B)-H(10E)	109.5
H(13A)-C(13A)-H(13C)	109.5	C(8B)-C(10B)-H(10F)	109.5
H(13B)-C(13A)-H(13C)	109.5	H(10D)-C(10B)-H(10F)	109.5
C(12A)-C(14A)-H(14A)	109.5	H(10E)-C(10B)-H(10F)	109.5
C(12A)-C(14A)-H(14B)	109.5	C(8B)-C(11B)-H(11D)	109.5
H(14A)-C(14A)-H(14B)	109.5	C(8B)-C(11B)-H(11E)	109.5
C(12A)-C(14A)-H(14C)	109.5	H(11D)-C(11B)-H(11E)	109.5
H(14A)-C(14A)-H(14C)	109.5	C(8B)-C(11B)-H(11F)	109.5
H(14B)-C(14A)-H(14C)	109.5	H(11D)-C(11B)-H(11F)	109.5

H(11E)-C(11B)-H(11F)	109.5	C(4)-C(3)-H(3)	119.7
C(13B)-C(12B)-C(14B)	111.2(15)	C(5)-C(4)-C(3)	118.2(8)
C(13B)-C(12B)-C(15B)	109.9(14)	C(5)-C(4)-H(4)	120.9
C(14B)-C(12B)-C(15B)	106.8(14)	C(3)-C(4)-H(4)	120.9
C(13B)-C(12B)-P(1B)	112.2(12)	N(1)-C(5)-C(4)	122.0(8)
C(14B)-C(12B)-P(1B)	110.6(12)	N(1)-C(5)-C(7)	117.2(7)
C(15B)-C(12B)-P(1B)	105.9(12)	C(4)-C(5)-C(7)	120.8(8)
C(12B)-C(13B)-H(13D)	109.5	C(1)-C(6)-P(1A)	118.6(6)
C(12B)-C(13B)-H(13E)	109.5	C(1)-C(6)-H(6)	120.7
H(13D)-C(13B)-H(13E)	109.5	P(1A)-C(6)-H(6)	120.7
C(12B)-C(13B)-H(13F)	109.5	C(5)-C(7)-P(2)	112.1(6)
H(13D)-C(13B)-H(13F)	109.5	C(5)-C(7)-H(7A)	109.2
H(13E)-C(13B)-H(13F)	109.5	P(2)-C(7)-H(7A)	109.2
C(12B)-C(14B)-H(14D)	109.5	C(5)-C(7)-H(7B)	109.2
C(12B)-C(14B)-H(14E)	109.5	P(2)-C(7)-H(7B)	109.2
H(14D)-C(14B)-H(14E)	109.5	H(7A)-C(7)-H(7B)	107.9
C(12B)-C(14B)-H(14F)	109.5	C(7)-P(2)-C(20)	105.2(4)
H(14D)-C(14B)-H(14F)	109.5	C(7)-P(2)-C(16)	103.7(4)
H(14E)-C(14B)-H(14F)	109.5	C(20)-P(2)-C(16)	109.3(4)
C(12B)-C(15B)-H(15D)	109.5	C(7)-P(2)-Os(1A)	99.0(3)
C(12B)-C(15B)-H(15E)	109.5	C(20)-P(2)-Os(1A)	117.8(3)
H(15D)-C(15B)-H(15E)	109.5	C(16)-P(2)-Os(1A)	119.1(3)
C(12B)-C(15B)-H(15F)	109.5	C(19)-C(16)-C(18)	108.2(8)
H(15D)-C(15B)-H(15F)	109.5	C(19)-C(16)-C(17)	106.0(9)
H(15E)-C(15B)-H(15F)	109.5	C(18)-C(16)-C(17)	109.0(9)
C(5)-N(1)-C(1)	120.0(7)	C(19)-C(16)-P(2)	112.3(7)
C(5)-N(1)-Os(1A)	120.2(6)	C(18)-C(16)-P(2)	111.9(6)
C(1)-N(1)-Os(1A)	119.8(5)	C(17)-C(16)-P(2)	109.2(6)
C(6)-C(1)-N(1)	121.2(7)	C(16)-C(17)-H(17A)	109.5
C(6)-C(1)-C(2)	121.2(8)	C(16)-C(17)-H(17B)	109.5
N(1)-C(1)-C(2)	117.6(7)	H(17A)-C(17)-H(17B)	109.5
C(3)-C(2)-C(1)	121.4(8)	C(16)-C(17)-H(17C)	109.5
C(3)-C(2)-H(2)	119.3	H(17A)-C(17)-H(17C)	109.5
C(1)-C(2)-H(2)	119.3	H(17B)-C(17)-H(17C)	109.5
C(2)-C(3)-C(4)	120.6(8)	C(16)-C(18)-H(18A)	109.5
C(2)-C(3)-H(3)	119.7	C(16)-C(18)-H(18B)	109.5

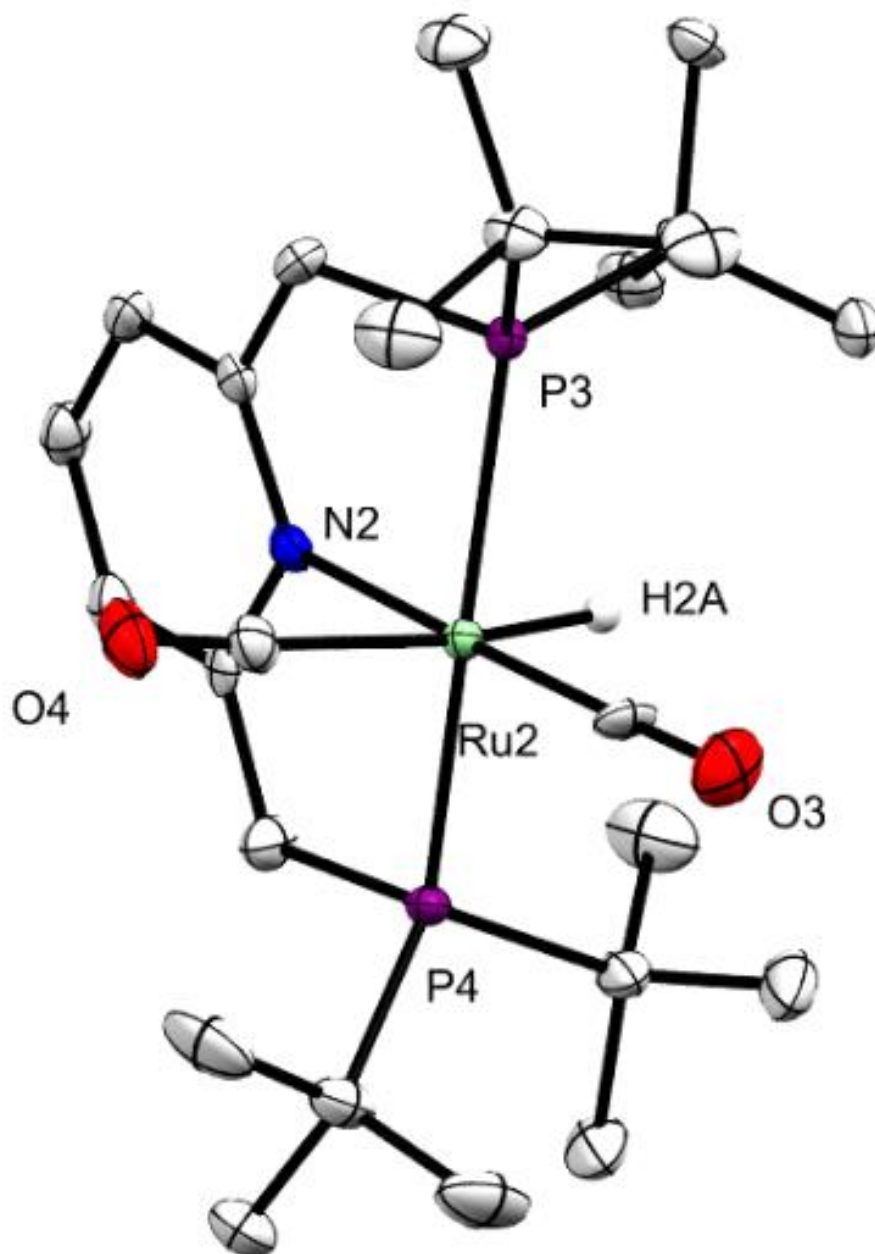
H(18A)-C(18)-H(18B)	109.5	C(49)-Os(2A)-N(2)	176.7(3)
C(16)-C(18)-H(18C)	109.5	C(50)-Os(2A)-N(2)	85.3(3)
H(18A)-C(18)-H(18C)	109.5	C(49)-Os(2A)-P(3)	99.6(2)
H(18B)-C(18)-H(18C)	109.5	C(50)-Os(2A)-P(3)	95.2(2)
C(16)-C(19)-H(19A)	109.5	N(2)-Os(2A)-P(3)	80.34(17)
C(16)-C(19)-H(19B)	109.5	C(49)-Os(2A)-P(4)	97.2(2)
H(19A)-C(19)-H(19B)	109.5	C(50)-Os(2A)-P(4)	98.9(2)
C(16)-C(19)-H(19C)	109.5	N(2)-Os(2A)-P(4)	81.91(17)
H(19A)-C(19)-H(19C)	109.5	P(3)-Os(2A)-P(4)	156.24(9)
H(19B)-C(19)-H(19C)	109.5	C(49)-Os(2A)-H(2A)	93.2(3)
C(22)-C(20)-C(23)	104.1(7)	C(50)-Os(2A)-H(2A)	168.8(4)
C(22)-C(20)-C(21)	107.0(7)	N(2)-Os(2A)-H(2A)	83.5(3)
C(23)-C(20)-C(21)	110.6(8)	P(3)-Os(2A)-H(2A)	81.7(2)
C(22)-C(20)-P(2)	116.0(6)	P(4)-Os(2A)-H(2A)	80.7(2)
C(23)-C(20)-P(2)	107.6(6)	C(31)-P(3)-C(37)	105.5(4)
C(21)-C(20)-P(2)	111.2(6)	C(31)-P(3)-C(33)	104.4(4)
C(20)-C(21)-H(21A)	109.5	C(37)-P(3)-C(33)	109.7(4)
C(20)-C(21)-H(21B)	109.5	C(31)-P(3)-Os(2A)	99.1(3)
H(21A)-C(21)-H(21B)	109.5	C(37)-P(3)-Os(2A)	115.2(2)
C(20)-C(21)-H(21C)	109.5	C(33)-P(3)-Os(2A)	120.5(3)
H(21A)-C(21)-H(21C)	109.5	C(32)-P(4)-C(41)	106.2(4)
H(21B)-C(21)-H(21C)	109.5	C(32)-P(4)-C(45)	106.5(4)
C(20)-C(22)-H(22A)	109.5	C(41)-P(4)-C(45)	109.4(4)
C(20)-C(22)-H(22B)	109.5	C(32)-P(4)-Os(2A)	99.4(3)
H(22A)-C(22)-H(22B)	109.5	C(41)-P(4)-Os(2A)	119.0(3)
C(20)-C(22)-H(22C)	109.5	C(45)-P(4)-Os(2A)	114.8(3)
H(22A)-C(22)-H(22C)	109.5	C(26)-N(2)-C(30)	119.6(6)
H(22B)-C(22)-H(22C)	109.5	C(26)-N(2)-Os(2A)	121.4(5)
C(20)-C(23)-H(23A)	109.5	C(30)-N(2)-Os(2A)	118.9(5)
C(20)-C(23)-H(23B)	109.5	N(2)-C(26)-C(27)	121.5(7)
H(23A)-C(23)-H(23B)	109.5	N(2)-C(26)-C(31)	117.2(7)
C(20)-C(23)-H(23C)	109.5	C(27)-C(26)-C(31)	121.3(7)
H(23A)-C(23)-H(23C)	109.5	C(26)-C(27)-C(28)	119.8(8)
H(23B)-C(23)-H(23C)	109.5	C(26)-C(27)-H(27)	120.1
O(1)-C(24)-Os(1A)	177.2(5)	C(28)-C(27)-H(27)	120.1
C(49)-Os(2A)-C(50)	98.0(3)	C(29)-C(28)-C(27)	119.0(7)

C(29)-C(28)-H(28)	120.5	C(33)-C(36)-H(36B)	109.5
C(27)-C(28)-H(28)	120.5	H(36A)-C(36)-H(36B)	109.5
C(28)-C(29)-C(30)	121.6(8)	C(33)-C(36)-H(36C)	109.5
C(28)-C(29)-H(29)	119.2	H(36A)-C(36)-H(36C)	109.5
C(30)-C(29)-H(29)	119.2	H(36B)-C(36)-H(36C)	109.5
C(32)-C(30)-N(2)	119.4(6)	C(38)-C(37)-C(39)	109.4(6)
C(32)-C(30)-C(29)	122.4(7)	C(38)-C(37)-C(40)	107.9(7)
N(2)-C(30)-C(29)	118.2(7)	C(39)-C(37)-C(40)	106.6(6)
C(26)-C(31)-P(3)	111.8(6)	C(38)-C(37)-P(3)	111.0(5)
C(26)-C(31)-H(31A)	109.2	C(39)-C(37)-P(3)	113.5(5)
P(3)-C(31)-H(31A)	109.2	C(40)-C(37)-P(3)	108.2(5)
C(26)-C(31)-H(31B)	109.2	C(37)-C(38)-H(38A)	109.5
P(3)-C(31)-H(31B)	109.2	C(37)-C(38)-H(38B)	109.5
H(31A)-C(31)-H(31B)	107.9	H(38A)-C(38)-H(38B)	109.5
C(30)-C(32)-P(4)	119.3(6)	C(37)-C(38)-H(38C)	109.5
C(30)-C(32)-H(32)	120.4	H(38A)-C(38)-H(38C)	109.5
P(4)-C(32)-H(32)	120.4	H(38B)-C(38)-H(38C)	109.5
C(36)-C(33)-C(34)	107.6(8)	C(37)-C(39)-H(39A)	109.5
C(36)-C(33)-C(35)	106.8(7)	C(37)-C(39)-H(39B)	109.5
C(34)-C(33)-C(35)	110.7(7)	H(39A)-C(39)-H(39B)	109.5
C(36)-C(33)-P(3)	108.5(5)	C(37)-C(39)-H(39C)	109.5
C(34)-C(33)-P(3)	110.5(6)	H(39A)-C(39)-H(39C)	109.5
C(35)-C(33)-P(3)	112.5(6)	H(39B)-C(39)-H(39C)	109.5
C(33)-C(34)-H(34A)	109.5	C(37)-C(40)-H(40A)	109.5
C(33)-C(34)-H(34B)	109.5	C(37)-C(40)-H(40B)	109.5
H(34A)-C(34)-H(34B)	109.5	H(40A)-C(40)-H(40B)	109.5
C(33)-C(34)-H(34C)	109.5	C(37)-C(40)-H(40C)	109.5
H(34A)-C(34)-H(34C)	109.5	H(40A)-C(40)-H(40C)	109.5
H(34B)-C(34)-H(34C)	109.5	H(40B)-C(40)-H(40C)	109.5
C(33)-C(35)-H(35A)	109.5	C(44)-C(41)-C(42)	107.5(8)
C(33)-C(35)-H(35B)	109.5	C(44)-C(41)-C(43)	106.4(7)
H(35A)-C(35)-H(35B)	109.5	C(42)-C(41)-C(43)	110.5(7)
C(33)-C(35)-H(35C)	109.5	C(44)-C(41)-P(4)	109.3(6)
H(35A)-C(35)-H(35C)	109.5	C(42)-C(41)-P(4)	110.9(6)
H(35B)-C(35)-H(35C)	109.5	C(43)-C(41)-P(4)	112.0(6)
C(33)-C(36)-H(36A)	109.5	C(41)-C(42)-H(42A)	109.5

C(41)-C(42)-H(42B)	109.5	C(47)-C(45)-P(4)	112.9(6)
H(42A)-C(42)-H(42B)	109.5	C(45)-C(46)-H(46A)	109.5
C(41)-C(42)-H(42C)	109.5	C(45)-C(46)-H(46B)	109.5
H(42A)-C(42)-H(42C)	109.5	H(46A)-C(46)-H(46B)	109.5
H(42B)-C(42)-H(42C)	109.5	C(45)-C(46)-H(46C)	109.5
C(41)-C(43)-H(43A)	109.5	H(46A)-C(46)-H(46C)	109.5
C(41)-C(43)-H(43B)	109.5	H(46B)-C(46)-H(46C)	109.5
H(43A)-C(43)-H(43B)	109.5	C(45)-C(47)-H(47A)	109.5
C(41)-C(43)-H(43C)	109.5	C(45)-C(47)-H(47B)	109.5
H(43A)-C(43)-H(43C)	109.5	H(47A)-C(47)-H(47B)	109.5
H(43B)-C(43)-H(43C)	109.5	C(45)-C(47)-H(47C)	109.5
C(41)-C(44)-H(44A)	109.5	H(47A)-C(47)-H(47C)	109.5
C(41)-C(44)-H(44B)	109.5	H(47B)-C(47)-H(47C)	109.5
H(44A)-C(44)-H(44B)	109.5	C(45)-C(48)-H(48A)	109.5
C(41)-C(44)-H(44C)	109.5	C(45)-C(48)-H(48B)	109.5
H(44A)-C(44)-H(44C)	109.5	H(48A)-C(48)-H(48B)	109.5
H(44B)-C(44)-H(44C)	109.5	C(45)-C(48)-H(48C)	109.5
C(48)-C(45)-C(46)	109.2(8)	H(48A)-C(48)-H(48C)	109.5
C(48)-C(45)-C(47)	105.8(8)	H(48B)-C(48)-H(48C)	109.5
C(46)-C(45)-C(47)	109.9(7)	O(3)-C(49)-Os(2A)	179.0(6)
C(48)-C(45)-P(4)	106.9(6)	O(4)-C(50)-Os(2A)	176.5(7)
C(46)-C(45)-P(4)	111.9(7)		



Figure 3.55: Structural data for complex ( $t^{\text{Bu}}\text{PNP}$ )RuH(CO)<sub>2</sub> (**7-H**)(CO)<sub>2</sub>)



ORTEP representation (50% probability ellipsoids) of complex ( $t^{\text{Bu}}\text{PNP}$ )RuH(CO)<sub>2</sub> (**7-H**)(CO)<sub>2</sub>) determined by X-ray diffraction. H atoms other than hydrides omitted for clarity.

Table 3.12 Crystal data and structure refinement for (t<sup>Bu</sup>PNP)RuH(CO)<sub>2</sub>

Identification code	(t <sup>Bu</sup> PNP)RuH(CO) <sub>2</sub>	
Empirical formula	C <sub>25</sub> H <sub>43</sub> N O <sub>2</sub> P <sub>2</sub> Ru	
Formula weight	552.61	
Temperature	100(2) K	
Wavelength	0.71073 Å	
Crystal system	Monoclinic	
Space group	P2 <sub>1</sub> /n	
Unit cell dimensions	a = 15.562(2) Å	β = 90°.
	b = 11.5615(16) Å	γ = 91.585(3)°.
	c = 29.835(4) Å	α = 90°.
Volume	5365.9(13) Å <sup>3</sup>	
Z	8	
Density (calculated)	1.368 Mg/m <sup>3</sup>	
Absorption coefficient	0.724 mm <sup>-1</sup>	
F(000)	2320	
Crystal size	0.380 x 0.080 x 0.040 mm <sup>3</sup>	
Theta range for data collection	1.366 to 28.281°.	
Index ranges	-20 ≤ h ≤ 20, -15 ≤ k ≤ 15, -39 ≤ l ≤ 31	
Reflections collected	42465	
Independent reflections	13197 [R(int) = 0.0626]	
Completeness to theta = 25.242°	99.8 %	
Absorption correction	Semi-empirical from equivalents	
Max. and min. transmission	0.7461 and 0.6679	
Refinement method	Full-matrix least-squares on F <sup>2</sup>	
Data / restraints / parameters	13197 / 1050 / 602	
Goodness-of-fit on F <sup>2</sup>	1.135	
Final R indices [I > 2σ(I)]	R1 = 0.0615, wR2 = 0.1206	
R indices (all data)	R1 = 0.0799, wR2 = 0.1273	
Extinction coefficient	n/a	
Largest diff. peak and hole	1.437 and -1.328 e.Å <sup>-3</sup>	

Table 3.13 Bond lengths [ $\text{\AA}$ ] and angles [ $^\circ$ ] for  $(^t\text{BuPNP})\text{RuH}(\text{CO})_2$ 

Ru(1A)-C(24)	1.876(4)	C(7)-H(7A)	0.9900
Ru(1A)-C(25A)	1.948(4)	C(7)-H(7B)	0.9900
Ru(1A)-N(1)	2.149(3)	C(8)-C(11)	1.525(6)
Ru(1A)-P(2)	2.3379(11)	C(8)-C(10)	1.542(6)
Ru(1A)-P(1)	2.3887(11)	C(8)-C(9)	1.544(6)
Ru(1A)-H(1A)	1.559(8)	C(9)-H(9A)	0.9800
C(25A)-O(2A)	1.138(5)	C(9)-H(9B)	0.9800
Ru(1B)-C(24)	1.878(5)	C(9)-H(9C)	0.9800
Ru(1B)-C(25B)	1.950(7)	C(10)-H(10A)	0.9800
Ru(1B)-P(1)	2.179(4)	C(10)-H(10B)	0.9800
Ru(1B)-N(1)	2.261(5)	C(10)-H(10C)	0.9800
Ru(1B)-P(2)	2.538(4)	C(11)-H(11A)	0.9800
Ru(1B)-H(1B)	1.653(8)	C(11)-H(11B)	0.9800
C(25B)-O(2B)	1.138(7)	C(11)-H(11C)	0.9800
C(25B)-C(15)	1.82(4)	C(12)-C(13)	1.514(7)
O(2B)-C(15)	1.91(3)	C(12)-C(14)	1.539(6)
P(1)-C(6)	1.756(4)	C(12)-C(15)	1.551(7)
P(1)-C(12)	1.890(4)	C(13)-H(13A)	0.9800
P(1)-C(8)	1.897(4)	C(13)-H(13B)	0.9800
P(2)-C(7)	1.842(4)	C(13)-H(13C)	0.9800
P(2)-C(20)	1.886(4)	C(14)-H(14A)	0.9800
P(2)-C(16)	1.892(4)	C(14)-H(14B)	0.9800
N(1)-C(5)	1.361(5)	C(14)-H(14C)	0.9800
N(1)-C(1)	1.383(5)	C(15)-H(15A)	0.9800
C(1)-C(6)	1.375(6)	C(15)-H(15B)	0.9800
C(1)-C(2)	1.436(5)	C(15)-H(15C)	0.9800
C(2)-C(3)	1.358(6)	C(16)-C(19)	1.500(7)
C(2)-H(2)	0.9500	C(16)-C(17)	1.535(7)
C(3)-C(4)	1.402(6)	C(16)-C(18)	1.536(6)
C(3)-H(3)	0.9500	C(17)-H(17A)	0.9800
C(4)-C(5)	1.368(6)	C(17)-H(17B)	0.9800
C(4)-H(4)	0.9500	C(17)-H(17C)	0.9800
C(5)-C(7)	1.505(6)	C(18)-H(18A)	0.9800
C(6)-H(6)	0.9500	C(18)-H(18B)	0.9800

C(18)-H(18C)	0.9800	C(28)-H(28)	0.9500
C(19)-H(19A)	0.9800	C(29)-C(30)	1.429(5)
C(19)-H(19B)	0.9800	C(29)-H(29)	0.9500
C(19)-H(19C)	0.9800	C(30)-C(32)	1.391(5)
C(20)-C(22)	1.533(6)	C(31)-H(31A)	0.9900
C(20)-C(23)	1.538(6)	C(31)-H(31B)	0.9900
C(20)-C(21)	1.540(6)	C(32)-H(32)	0.9500
C(21)-H(21A)	0.9800	C(33)-C(36)	1.515(6)
C(21)-H(21B)	0.9800	C(33)-C(34)	1.520(6)
C(21)-H(21C)	0.9800	C(33)-C(35)	1.546(6)
C(22)-H(22A)	0.9800	C(34)-H(34A)	0.9800
C(22)-H(22B)	0.9800	C(34)-H(34B)	0.9800
C(22)-H(22C)	0.9800	C(34)-H(34C)	0.9800
C(23)-H(23A)	0.9800	C(35)-H(35A)	0.9800
C(23)-H(23B)	0.9800	C(35)-H(35B)	0.9800
C(23)-H(23C)	0.9800	C(35)-H(35C)	0.9800
C(24)-O(1)	1.139(5)	C(36)-H(36A)	0.9800
Ru(2)-C(49)	1.858(4)	C(36)-H(36B)	0.9800
Ru(2)-C(50)	1.961(4)	C(36)-H(36C)	0.9800
Ru(2)-N(2)	2.131(3)	C(37)-C(39)	1.535(5)
Ru(2)-P(3)	2.3536(10)	C(37)-C(40)	1.539(6)
Ru(2)-P(4)	2.3712(11)	C(37)-C(38)	1.540(6)
Ru(2)-H(2A)	1.535(7)	C(38)-H(38A)	0.9800
P(3)-C(31)	1.828(4)	C(38)-H(38B)	0.9800
P(3)-C(37)	1.880(4)	C(38)-H(38C)	0.9800
P(3)-C(33)	1.892(4)	C(39)-H(39A)	0.9800
P(4)-C(32)	1.756(4)	C(39)-H(39B)	0.9800
P(4)-C(41)	1.889(4)	C(39)-H(39C)	0.9800
P(4)-C(45)	1.899(4)	C(40)-H(40A)	0.9800
N(2)-C(26)	1.370(5)	C(40)-H(40B)	0.9800
N(2)-C(30)	1.396(5)	C(40)-H(40C)	0.9800
C(26)-C(27)	1.375(6)	C(41)-C(44)	1.506(7)
C(26)-C(31)	1.507(6)	C(41)-C(42)	1.524(6)
C(27)-C(28)	1.404(6)	C(41)-C(43)	1.538(6)
C(27)-H(27)	0.9500	C(42)-H(42A)	0.9800
C(28)-C(29)	1.365(6)	C(42)-H(42B)	0.9800

C(42)-H(42C)	0.9800	P(1)-Ru(1A)-H(1A)	80.0(2)
C(43)-H(43A)	0.9800	O(2A)-C(25A)-Ru(1A)	176.6(4)
C(43)-H(43B)	0.9800	C(24)-Ru(1B)-C(25B)	110.8(12)
C(43)-H(43C)	0.9800	C(24)-Ru(1B)-P(1)	104.7(2)
C(44)-H(44A)	0.9800	C(25B)-Ru(1B)-P(1)	89.0(11)
C(44)-H(44B)	0.9800	C(24)-Ru(1B)-N(1)	151.9(3)
C(44)-H(44C)	0.9800	C(25B)-Ru(1B)-N(1)	95.7(12)
C(45)-C(48)	1.530(7)	P(1)-Ru(1B)-N(1)	83.95(16)
C(45)-C(47)	1.533(6)	C(24)-Ru(1B)-P(2)	91.4(2)
C(45)-C(46)	1.542(7)	C(25B)-Ru(1B)-P(2)	100.3(11)
C(46)-H(46A)	0.9800	P(1)-Ru(1B)-P(2)	157.3(2)
C(46)-H(46B)	0.9800	N(1)-Ru(1B)-P(2)	74.62(15)
C(46)-H(46C)	0.9800	C(24)-Ru(1B)-H(1B)	82.4(3)
C(47)-H(47A)	0.9800	C(25B)-Ru(1B)-H(1B)	166.7(12)
C(47)-H(47B)	0.9800	P(1)-Ru(1B)-H(1B)	88.7(3)
C(47)-H(47C)	0.9800	N(1)-Ru(1B)-H(1B)	71.0(3)
C(48)-H(48A)	0.9800	P(2)-Ru(1B)-H(1B)	77.5(3)
C(48)-H(48B)	0.9800	O(2B)-C(25B)-C(15)	77(2)
C(48)-H(48C)	0.9800	O(2B)-C(25B)-Ru(1B)	169(3)
C(49)-O(3)	1.155(5)	C(15)-C(25B)-Ru(1B)	112.9(16)
C(50)-O(4)	1.136(5)	C(25B)-O(2B)-C(15)	68(2)
		C(6)-P(1)-C(12)	105.7(2)
C(24)-Ru(1A)-C(25A)	95.27(17)	C(6)-P(1)-C(8)	106.8(2)
C(24)-Ru(1A)-N(1)	172.41(15)	C(12)-P(1)-C(8)	109.8(2)
C(25A)-Ru(1A)-N(1)	92.32(15)	C(6)-P(1)-Ru(1B)	99.97(18)
C(24)-Ru(1A)-P(2)	97.94(12)	C(12)-P(1)-Ru(1B)	104.0(2)
C(25A)-Ru(1A)-P(2)	98.06(12)	C(8)-P(1)-Ru(1B)	128.3(2)
N(1)-Ru(1A)-P(2)	80.97(10)	C(6)-P(1)-Ru(1A)	99.43(15)
C(24)-Ru(1A)-P(1)	97.22(12)	C(12)-P(1)-Ru(1A)	117.98(15)
C(25A)-Ru(1A)-P(1)	98.62(12)	C(8)-P(1)-Ru(1A)	115.42(15)
N(1)-Ru(1A)-P(1)	81.59(10)	C(7)-P(2)-C(20)	104.8(2)
P(2)-Ru(1A)-P(1)	156.26(4)	C(7)-P(2)-C(16)	103.7(2)
C(24)-Ru(1A)-H(1A)	90.8(3)	C(20)-P(2)-C(16)	109.3(2)
C(25A)-Ru(1A)-H(1A)	173.9(3)	C(7)-P(2)-Ru(1A)	98.66(15)
N(1)-Ru(1A)-H(1A)	81.6(3)	C(20)-P(2)-Ru(1A)	116.55(14)
P(2)-Ru(1A)-H(1A)	81.7(2)	C(16)-P(2)-Ru(1A)	120.91(16)

C(7)-P(2)-Ru(1B)	104.30(17)	C(10)-C(8)-P(1)	114.2(3)
C(20)-P(2)-Ru(1B)	102.65(18)	C(9)-C(8)-P(1)	110.4(3)
C(16)-P(2)-Ru(1B)	129.80(18)	C(8)-C(9)-H(9A)	109.5
C(5)-N(1)-C(1)	120.9(3)	C(8)-C(9)-H(9B)	109.5
C(5)-N(1)-Ru(1A)	120.7(3)	H(9A)-C(9)-H(9B)	109.5
C(1)-N(1)-Ru(1A)	118.4(3)	C(8)-C(9)-H(9C)	109.5
C(5)-N(1)-Ru(1B)	127.5(3)	H(9A)-C(9)-H(9C)	109.5
C(1)-N(1)-Ru(1B)	109.9(3)	H(9B)-C(9)-H(9C)	109.5
C(6)-C(1)-N(1)	120.8(4)	C(8)-C(10)-H(10A)	109.5
C(6)-C(1)-C(2)	122.3(4)	C(8)-C(10)-H(10B)	109.5
N(1)-C(1)-C(2)	116.9(4)	H(10A)-C(10)-H(10B)	109.5
C(3)-C(2)-C(1)	121.1(4)	C(8)-C(10)-H(10C)	109.5
C(3)-C(2)-H(2)	119.5	H(10A)-C(10)-H(10C)	109.5
C(1)-C(2)-H(2)	119.5	H(10B)-C(10)-H(10C)	109.5
C(2)-C(3)-C(4)	120.3(4)	C(8)-C(11)-H(11A)	109.5
C(2)-C(3)-H(3)	119.9	C(8)-C(11)-H(11B)	109.5
C(4)-C(3)-H(3)	119.9	H(11A)-C(11)-H(11B)	109.5
C(5)-C(4)-C(3)	118.3(4)	C(8)-C(11)-H(11C)	109.5
C(5)-C(4)-H(4)	120.9	H(11A)-C(11)-H(11C)	109.5
C(3)-C(4)-H(4)	120.9	H(11B)-C(11)-H(11C)	109.5
N(1)-C(5)-C(4)	122.5(4)	C(13)-C(12)-C(14)	110.6(4)
N(1)-C(5)-C(7)	117.1(4)	C(13)-C(12)-C(15)	108.2(4)
C(4)-C(5)-C(7)	120.4(4)	C(14)-C(12)-C(15)	105.5(4)
C(1)-C(6)-P(1)	119.5(3)	C(13)-C(12)-P(1)	111.6(3)
C(1)-C(6)-H(6)	120.3	C(14)-C(12)-P(1)	112.5(3)
P(1)-C(6)-H(6)	120.3	C(15)-C(12)-P(1)	108.1(3)
C(5)-C(7)-P(2)	111.7(3)	C(12)-C(13)-H(13A)	109.5
C(5)-C(7)-H(7A)	109.3	C(12)-C(13)-H(13B)	109.5
P(2)-C(7)-H(7A)	109.3	H(13A)-C(13)-H(13B)	109.5
C(5)-C(7)-H(7B)	109.3	C(12)-C(13)-H(13C)	109.5
P(2)-C(7)-H(7B)	109.3	H(13A)-C(13)-H(13C)	109.5
H(7A)-C(7)-H(7B)	107.9	H(13B)-C(13)-H(13C)	109.5
C(11)-C(8)-C(10)	106.4(4)	C(12)-C(14)-H(14A)	109.5
C(11)-C(8)-C(9)	109.5(4)	C(12)-C(14)-H(14B)	109.5
C(10)-C(8)-C(9)	109.4(4)	H(14A)-C(14)-H(14B)	109.5
C(11)-C(8)-P(1)	106.7(3)	C(12)-C(14)-H(14C)	109.5

H(14A)-C(14)-H(14C)	109.5	C(16)-C(19)-H(19B)	109.5
H(14B)-C(14)-H(14C)	109.5	H(19A)-C(19)-H(19B)	109.5
C(12)-C(15)-C(25B)	112.9(6)	C(16)-C(19)-H(19C)	109.5
C(12)-C(15)-O(2B)	148.3(6)	H(19A)-C(19)-H(19C)	109.5
C(25B)-C(15)-O(2B)	35.4(6)	H(19B)-C(19)-H(19C)	109.5
C(12)-C(15)-H(15A)	109.5	C(22)-C(20)-C(23)	107.3(4)
C(25B)-C(15)-H(15A)	136.7	C(22)-C(20)-C(21)	108.9(4)
O(2B)-C(15)-H(15A)	102.0	C(23)-C(20)-C(21)	106.6(4)
C(12)-C(15)-H(15B)	109.5	C(22)-C(20)-P(2)	115.5(3)
C(25B)-C(15)-H(15B)	63.8	C(23)-C(20)-P(2)	107.6(3)
O(2B)-C(15)-H(15B)	61.4	C(21)-C(20)-P(2)	110.5(3)
H(15A)-C(15)-H(15B)	109.5	C(20)-C(21)-H(21A)	109.5
C(12)-C(15)-H(15C)	109.5	C(20)-C(21)-H(21B)	109.5
C(25B)-C(15)-H(15C)	47.4	H(21A)-C(21)-H(21B)	109.5
O(2B)-C(15)-H(15C)	54.5	C(20)-C(21)-H(21C)	109.5
H(15A)-C(15)-H(15C)	109.5	H(21A)-C(21)-H(21C)	109.5
H(15B)-C(15)-H(15C)	109.5	H(21B)-C(21)-H(21C)	109.5
C(19)-C(16)-C(17)	106.7(4)	C(20)-C(22)-H(22A)	109.5
C(19)-C(16)-C(18)	106.9(4)	C(20)-C(22)-H(22B)	109.5
C(17)-C(16)-C(18)	110.4(4)	H(22A)-C(22)-H(22B)	109.5
C(19)-C(16)-P(2)	109.9(3)	C(20)-C(22)-H(22C)	109.5
C(17)-C(16)-P(2)	110.0(3)	H(22A)-C(22)-H(22C)	109.5
C(18)-C(16)-P(2)	112.8(3)	H(22B)-C(22)-H(22C)	109.5
C(16)-C(17)-H(17A)	109.5	C(20)-C(23)-H(23A)	109.5
C(16)-C(17)-H(17B)	109.5	C(20)-C(23)-H(23B)	109.5
H(17A)-C(17)-H(17B)	109.5	H(23A)-C(23)-H(23B)	109.5
C(16)-C(17)-H(17C)	109.5	C(20)-C(23)-H(23C)	109.5
H(17A)-C(17)-H(17C)	109.5	H(23A)-C(23)-H(23C)	109.5
H(17B)-C(17)-H(17C)	109.5	H(23B)-C(23)-H(23C)	109.5
C(16)-C(18)-H(18A)	109.5	O(1)-C(24)-Ru(1A)	176.9(4)
C(16)-C(18)-H(18B)	109.5	O(1)-C(24)-Ru(1B)	164.0(4)
H(18A)-C(18)-H(18B)	109.5	C(49)-Ru(2)-C(50)	99.58(18)
C(16)-C(18)-H(18C)	109.5	C(49)-Ru(2)-N(2)	176.30(16)
H(18A)-C(18)-H(18C)	109.5	C(50)-Ru(2)-N(2)	84.10(15)
H(18B)-C(18)-H(18C)	109.5	C(49)-Ru(2)-P(3)	99.45(13)
C(16)-C(19)-H(19A)	109.5	C(50)-Ru(2)-P(3)	94.30(11)

N(2)-Ru(2)-P(3)	80.50(9)	C(30)-C(29)-H(29)	119.7
C(49)-Ru(2)-P(4)	96.97(13)	C(32)-C(30)-N(2)	119.8(3)
C(50)-Ru(2)-P(4)	99.87(11)	C(32)-C(30)-C(29)	121.7(4)
N(2)-Ru(2)-P(4)	82.00(9)	N(2)-C(30)-C(29)	118.5(4)
P(3)-Ru(2)-P(4)	156.17(4)	C(26)-C(31)-P(3)	112.0(3)
C(49)-Ru(2)-H(2A)	93.0(3)	C(26)-C(31)-H(31A)	109.2
C(50)-Ru(2)-H(2A)	167.2(3)	P(3)-C(31)-H(31A)	109.2
N(2)-Ru(2)-H(2A)	83.3(3)	C(26)-C(31)-H(31B)	109.2
P(3)-Ru(2)-H(2A)	81.3(2)	P(3)-C(31)-H(31B)	109.2
P(4)-Ru(2)-H(2A)	80.7(2)	H(31A)-C(31)-H(31B)	107.9
C(31)-P(3)-C(37)	105.12(19)	C(30)-C(32)-P(4)	119.1(3)
C(31)-P(3)-C(33)	104.5(2)	C(30)-C(32)-H(32)	120.5
C(37)-P(3)-C(33)	109.58(18)	P(4)-C(32)-H(32)	120.5
C(31)-P(3)-Ru(2)	98.90(13)	C(36)-C(33)-C(34)	107.3(4)
C(37)-P(3)-Ru(2)	115.18(13)	C(36)-C(33)-C(35)	106.8(4)
C(33)-P(3)-Ru(2)	121.03(14)	C(34)-C(33)-C(35)	110.0(4)
C(32)-P(4)-C(41)	106.9(2)	C(36)-C(33)-P(3)	108.1(3)
C(32)-P(4)-C(45)	105.8(2)	C(34)-C(33)-P(3)	110.8(3)
C(41)-P(4)-C(45)	108.7(2)	C(35)-C(33)-P(3)	113.6(3)
C(32)-P(4)-Ru(2)	99.76(14)	C(33)-C(34)-H(34A)	109.5
C(41)-P(4)-Ru(2)	119.43(15)	C(33)-C(34)-H(34B)	109.5
C(45)-P(4)-Ru(2)	114.73(14)	H(34A)-C(34)-H(34B)	109.5
C(26)-N(2)-C(30)	119.0(3)	C(33)-C(34)-H(34C)	109.5
C(26)-N(2)-Ru(2)	122.2(3)	H(34A)-C(34)-H(34C)	109.5
C(30)-N(2)-Ru(2)	118.7(2)	H(34B)-C(34)-H(34C)	109.5
N(2)-C(26)-C(27)	123.0(4)	C(33)-C(35)-H(35A)	109.5
N(2)-C(26)-C(31)	115.9(3)	C(33)-C(35)-H(35B)	109.5
C(27)-C(26)-C(31)	121.1(4)	H(35A)-C(35)-H(35B)	109.5
C(26)-C(27)-C(28)	118.5(4)	C(33)-C(35)-H(35C)	109.5
C(26)-C(27)-H(27)	120.7	H(35A)-C(35)-H(35C)	109.5
C(28)-C(27)-H(27)	120.7	H(35B)-C(35)-H(35C)	109.5
C(29)-C(28)-C(27)	120.1(4)	C(33)-C(36)-H(36A)	109.5
C(29)-C(28)-H(28)	120.0	C(33)-C(36)-H(36B)	109.5
C(27)-C(28)-H(28)	120.0	H(36A)-C(36)-H(36B)	109.5
C(28)-C(29)-C(30)	120.7(4)	C(33)-C(36)-H(36C)	109.5
C(28)-C(29)-H(29)	119.7	H(36A)-C(36)-H(36C)	109.5



H(36B)-C(36)-H(36C)	109.5	H(42B)-C(42)-H(42C)	109.5
C(39)-C(37)-C(40)	107.0(3)	C(41)-C(43)-H(43A)	109.5
C(39)-C(37)-C(38)	109.5(3)	C(41)-C(43)-H(43B)	109.5
C(40)-C(37)-C(38)	107.7(3)	H(43A)-C(43)-H(43B)	109.5
C(39)-C(37)-P(3)	113.5(3)	C(41)-C(43)-H(43C)	109.5
C(40)-C(37)-P(3)	108.4(3)	H(43A)-C(43)-H(43C)	109.5
C(38)-C(37)-P(3)	110.6(3)	H(43B)-C(43)-H(43C)	109.5
C(37)-C(38)-H(38A)	109.5	C(41)-C(44)-H(44A)	109.5
C(37)-C(38)-H(38B)	109.5	C(41)-C(44)-H(44B)	109.5
H(38A)-C(38)-H(38B)	109.5	H(44A)-C(44)-H(44B)	109.5
C(37)-C(38)-H(38C)	109.5	C(41)-C(44)-H(44C)	109.5
H(38A)-C(38)-H(38C)	109.5	H(44A)-C(44)-H(44C)	109.5
H(38B)-C(38)-H(38C)	109.5	H(44B)-C(44)-H(44C)	109.5
C(37)-C(39)-H(39A)	109.5	C(48)-C(45)-C(47)	106.7(4)
C(37)-C(39)-H(39B)	109.5	C(48)-C(45)-C(46)	108.5(4)
H(39A)-C(39)-H(39B)	109.5	C(47)-C(45)-C(46)	109.4(4)
C(37)-C(39)-H(39C)	109.5	C(48)-C(45)-P(4)	107.9(3)
H(39A)-C(39)-H(39C)	109.5	C(47)-C(45)-P(4)	113.1(3)
H(39B)-C(39)-H(39C)	109.5	C(46)-C(45)-P(4)	111.0(3)
C(37)-C(40)-H(40A)	109.5	C(45)-C(46)-H(46A)	109.5
C(37)-C(40)-H(40B)	109.5	C(45)-C(46)-H(46B)	109.5
H(40A)-C(40)-H(40B)	109.5	H(46A)-C(46)-H(46B)	109.5
C(37)-C(40)-H(40C)	109.5	C(45)-C(46)-H(46C)	109.5
H(40A)-C(40)-H(40C)	109.5	H(46A)-C(46)-H(46C)	109.5
H(40B)-C(40)-H(40C)	109.5	H(46B)-C(46)-H(46C)	109.5
C(44)-C(41)-C(42)	107.0(4)	C(45)-C(47)-H(47A)	109.5
C(44)-C(41)-C(43)	105.2(4)	C(45)-C(47)-H(47B)	109.5
C(42)-C(41)-C(43)	110.3(4)	H(47A)-C(47)-H(47B)	109.5
C(44)-C(41)-P(4)	108.9(3)	C(45)-C(47)-H(47C)	109.5
C(42)-C(41)-P(4)	112.5(3)	H(47A)-C(47)-H(47C)	109.5
C(43)-C(41)-P(4)	112.5(3)	H(47B)-C(47)-H(47C)	109.5
C(41)-C(42)-H(42A)	109.5	C(45)-C(48)-H(48A)	109.5
C(41)-C(42)-H(42B)	109.5	C(45)-C(48)-H(48B)	109.5
H(42A)-C(42)-H(42B)	109.5	H(48A)-C(48)-H(48B)	109.5
C(41)-C(42)-H(42C)	109.5	C(45)-C(48)-H(48C)	109.5
H(42A)-C(42)-H(42C)	109.5	H(48A)-C(48)-H(48C)	109.5

H(48B)-C(48)-H(48C)	109.5
O(3)-C(49)-Ru(2)	179.1(4)
O(4)-C(50)-Ru(2)	175.5(4)

### 3.11 References:

1. Hartwig, J.F. *Organotransition Metal Chemistry: From Bonding to Catalysis*; University Science Books: Sausalito, CA, 2010.
2. Ogino, Y.; Chen, H.; Kwong, H.; Sharpless, K.B. *Tetrahedron Letters*. **1991**, 32, 3965.
3. Vaska, L. *Inorg. Nucl. Chem. Let.* **1965**, 1, 89.
4. Mitchell, T.R.B. *J. Chem. Soc.* **1970**, B, 823.
5. Bell, B.; Chatt, J.; High, G.J. *J. Chem. Soc., Dalton Trans.* **1977**, 997.
6. (a) Dobson, A.; Robinson, S.D. *Inorg. Chem.* **1977**, 16, 137. (b) Dobson, A.; Moore, D.S.; Robinson, S.D.; Hursthouse, M.B.; New, L. *Polyhedron*. **1985**, 4, 1119.
7. Schlünken, C.; Esteruelas, M. A.; Lahoz, F. J.; Oro, L. A.; Werner, H. *Eur. J. Inorg. Chem.* **2004**, 2477.
8. Baratta, W.; Ballico, M.; Del Zotto, A.; Siega, K.; Magnolia, S.; Rigo, P. *Chem. Eur. J.* **2008**, 14, 2557.
9. Baratta, W.; Ballico, M.; Chelucci, G.; Siega, K.; Rigo, P. *Angew. Chem. Int. Ed.* **2008**, 47, 4362.
10. Bertoli, M.; Choualeb, A.; Lough, A. J.; Moore, B.; Spasyuk, D.; Gusev, D. G. *Organometallics*. **2011**, 30, 3479.
11. Vega, E.; Lastra, E.; Gamasa, M. P. *Inorg. Chem.* **2013**, 52, 6193.
12. Gusev, D.G.; Dolgushin, F.M.; Antipin, M.Y. *Organometallics*. **2001**, 20, 1001.
13. Ingleson, M.J.; Pink, M.; Fan, H.; Caulton, K.G. *J. Am. Chem. Soc.*, 2008, 130, 4262.
14. Asensio, G.; Cuenca, A.B.; Esteruelas, M.A.; Medio-Simon, M.; Olivan, M.; Valencia, M. *Inorg. Chem.* **2010**, 49, 8665.
15. Gruver, B.C.; Adams, J.J.; Arulsamy, N.; Roddick, D.M. *Organometallics*. **2013**, 32, 6468.
16. Hermann, D.; Gandelman, M.; Rozenberg, H.; Shimon, L. J. W.; Milstein, D. *Organometallics* **2002**, 21, 812-818.
17. Gunanathan, C.; Milstein, D. *Chem. Rev.* **2014**, 114, 12024-12087.
18. Zell, T.; Milstein, D. *Acc. Chem. Res.* **2015**, 48, 1979-1994.
19. Anaby, A.; Feller, M.; Ben-David, Y.; Leituss, G.; Diskin-Posner, Y.; Shimon, L. J. W.; Milstein, D. *J. Am. Chem. Soc.* **2016**, 138, 9941-9950.
20. Feller, M.; Gellrich, U.; Anaby, A.; Diskin-Posner, Y.; Milstein, D. *J. Am. Chem. Soc.* **2016**, 138, 6445-6454.
21. Feller, M.; Ben-Ari, E.; Iron, M. A.; Diskin-Posner, Y.; Leituss, G.; Shimon, L. J. W.; Konstantinovski, L.; Milstein, D. *Inorg. Chem.* **2010**, 49, 1615-1625.
22. (a) Zaoying, L.; Chiming, C.; Chungkwong, P. *Wuhan Univ. J. Nat. Sci.* **1996**, 1, 230-234. (b) Jia, G.; Lee, H. M.; Williams, I. D.; Lau, C. P.; Chen, Y. *Organometallics* **1997**, 16, 3941-3949. (c) Liu, S. H.; Lo, S. T.; Wen, T. B.; Zhou, Z. Y.; Lau, C. P.; Jia, G. *Organometallics* **2001**, 20, 667-672.
23. (a) Chase, P. A.; Gossage, R. A.; van Koten, G. In *The Privileged Pincer-Metal Platform: Coordination Chemistry & Applications*; van Koten, G., Gossage, R. A., Eds.; Springer International Publishing: Cham, 2016, p 1-15. (b) Asay, M.; Morales-Morales, D. In *The Privileged Pincer-Metal Platform: Coordination Chemistry & Applications*; van Koten, G., Gossage, R. A., Eds.; Springer International Publishing:

- Cham, 2016, p 239-268. (c) van Koten, G. In *Organometallic Pincer Chemistry*; van Koten, G., Milstein, D., Eds.; Springer Berlin Heidelberg: Berlin, Heidelberg, 2013, p 1-20. (d) Poverenov, E.; Milstein, D. In *Organometallic Pincer Chemistry*; van Koten, G., Milstein, D., Eds.; Springer Berlin Heidelberg: Berlin, Heidelberg, 2013, p 21-47. (e) Roddick, D. M. In *Organometallic Pincer Chemistry*; van Koten, G., Milstein, D., Eds.; Springer Berlin Heidelberg: Berlin, Heidelberg, 2013, p 49-88. (f) St. John, A.; Goldberg, K. I.; Heinekey, D. M. In *Organometallic Pincer Chemistry*; van Koten, G., Milstein, D., Eds.; Springer Berlin Heidelberg: Berlin, Heidelberg, 2013, p 271-287. (g) Gelman, D.; Romm, R. In *Organometallic Pincer Chemistry*; van Koten, G., Milstein, D., Eds.; Springer Berlin Heidelberg: Berlin, Heidelberg, 2013, p 289-317.
24. (a) Kumar, A.; Goldman, A. S. In *The Privileged Pincer-Metal Platform: Coordination Chemistry & Applications*; van Koten, G., Gossage, R. A., Eds.; Springer International Publishing: Cham, 2016, p 307-334. (b) Choi, J.; MacArthur, A. H. R.; Brookhart, M.; Goldman, A. S. *Chem. Rev.* **2011**, *111*, 1761-1779.
  25. Choi, J.; Goldman, A. S. In *Iridium Catalysis*; Andersson, P. G., Ed.; Springer Berlin Heidelberg: Berlin, Heidelberg, 2011, p 139-167.
  26. Probably the most successful example of osmium-complex-catalyzed alkane dehydrogenation chemistry has been reported by Roddick. In contrast with the approach considered in this work, catalysis in that case was proposed to proceed via C-H addition to the four-coordinate Os(II) species ( $\text{CF}_3\text{PCP}$ )OsH: Gruver, B. C.; Adams, J. J.; Arulsamy, N.; Roddick, D. M. *Organometallics* **2013**, *32*, 6468-6475.
  27. (a) Bright, D.; Ibers, J. A. *Inorg. Chem.* **1969**, *8*, 1078-1083. (b) Demadis, K. D.; El-Samanody, E.-S.; Meyer, T. J.; White, P. S. *Polyhedron* **1999**, *18*, 1587-1594.
  28. Asensio, G.; Cuenca, A. B.; Esteruelas, M. A.; Medio-Simon, M.; Olivan, M.; Valencia, M. *Inorg. Chem.* **2010**, *49*, 8665-8667.
  29. Osmium tetrahydride complexes supported by other pincer ligands have been reported: (a) Bertoli, M.; Choualeb, A.; Gusev, D. G.; Lough, A. J.; Major, Q.; Moore, B. *Dalton Trans.* **2011**, *40*, 8941-8949. (b) Esteruelas, M. A.; Honczek, N.; Olivan, M.; Onate, E.; Valencia, M. *Organometallics* **2011**, *30*, 2468-2471. (c) Alos, J.; Bolano, T.; Esteruelas, M. A.; Olivan, M.; Onate, E.; Valencia, M. *Inorg. Chem.* **2013**, *52*, 6199-6213. (d) Schendzielorz, F. S.; Finger, M.; Volkmann, C.; Würtele, C.; Schneider, S. *Angew. Chem., Intl. Ed.* **2016**, *55*, 11417-11420.
  30. gNMR, 4.0.1.; Cherwell Scientific Publishing Limited: Oxford, United Kingdom, 1995.
  31. Desrosiers, P. J.; Cai, L.; Lin, Z.; Richards, R.; Halpern, J. *J. Am. Chem. Soc.* **1991**, *113*, 4173-4184.
  32. Hart, D. W.; Bau, R.; Koetzle, T. F. *J. Am. Chem. Soc.* **1977**, *99*, 7557-7564.
  33. Hebden, T. J.; Goldberg, K. I.; Heinekey, D. M.; Zhang, X.; Emge, T. J.; Goldman, A. S.; Krogh-Jespersen, K. *Inorg. Chem.* **2010**, *49*, 1733-1742.
  34. Gupta, M.; Hagen, C.; Kaska, W. C.; Cramer, R. E.; Jensen, C. M. *J. Am. Chem. Soc.* **1997**, *119*, 840-841.
  35. Krogh-Jespersen, K.; Czerw, M.; Zhu, K.; Singh, B.; Kanzelberger, M.; Darji, N.; Achord, P. D.; Renkema, K. B.; Goldman, A. S. *J. Am. Chem. Soc.* **2002**, *124*, 10797-10809.

36. Zhu, K.; Achord, P. D.; Zhang, X.; Krogh-Jespersen, K.; Goldman, A. S. *J. Am. Chem. Soc.* **2004**, *126*, 13044-13053.
37. Renkema, K. B.; Kissin, Y. V.; Goldman, A. S. *J. Am. Chem. Soc.* **2003**, *125*, 7770-7771.
38. (a) Göttker-Schnetmann, I.; White, P. S.; Brookhart, M. *Organometallics* **2004**, *23*, 1766-1776. (b) Findlater, M.; Cartwright-Sykes, A.; White, P. S.; Schauer, C. K.; Brookhart, M. *J. Am. Chem. Soc.* **2011**, *133*, 12274-12284. (c) Haibach, M. C.; Guan, C.; Wang, D. Y.; Li, B.; Lease, N.; Steffens, A. M.; Krogh-Jespersen, K.; Goldman, A. S. *J. Am. Chem. Soc.* **2013**, *135*, 15062-15070.
39. (a) Bartlett, K. L.; Goldberg, K. I.; Borden, W. T. *J. Am. Chem. Soc.* **2000**, *122*, 1456-1465. (b) Goldman, A. S.; Goldberg, K. I. In *Activation and Functionalization of C-H Bonds*; Goldberg, K. I., Goldman, A. S., Eds. 2004; Vol. ACS Symposium Series 885, p 1-43.
40. When **1-H<sub>4</sub>** was allowed to react with C<sub>2</sub>D<sub>4</sub> at 85 °C, <sup>1</sup>H NMR and <sup>2</sup>H NMR of the resulting isotopomer of **1-H<sub>2</sub>(C<sub>2</sub>H<sub>4</sub>)** showed extensive H/D scrambling between ethylene and hydride protons.
41. (a) Göttker-Schnetmann, I.; Brookhart, M. *J. Am. Chem. Soc.* **2004**, *126*, 9330-9338. (b) Adams, J. J.; Arulsamy, N.; Roddick, D. M. *Organometallics* **2011**, *30*, 697-711. (c) Kundu, S.; Choi, J.; Wang, D. Y.; Choliy, Y.; Emge, T. J.; Krogh-Jespersen, K.; Goldman, A. S. *J. Am. Chem. Soc.* **2013**, *135*, 5127-5143. (d) Bezier, D.; Brookhart, M. *ACS Catal.* **2014**, *4*, 3411-3420. (e) Kumar, A.; Zhou, T.; Emge, T. J.; Mironov, O.; Saxton, R. J.; Krogh-Jespersen, K.; Goldman, A. S. *J. Am. Chem. Soc.* **2015**, *137*, 9894-9911. (f) Kovalenko, O. O.; Wendt, O. F. *Dalton Trans.* **2016**, *45*, 15963-15969. (g) Press, L. P.; Kosanovich, A. J.; McCulloch, B. J.; Ozerov, O. V. *J. Am. Chem. Soc.* **2016**, *138*, 9487-9497.
42. (a) Felkin, H.; Fillebeen-Khan, T.; Holmes-Smith, R.; Lin, Y. *Tetrahedron Lett.* **1985**, *26*, 1999-2000. (b) Burk, M. J.; Crabtree, R. H. *J. Am. Chem. Soc.* **1987**, *109*, 8025-8032.
43. Cheng, C.; Kim, B. G.; Guironnet, D.; Brookhart, M.; Guan, C.; Wang, D. Y.; Krogh-Jespersen, K.; Goldman, A. S. *J. Am. Chem. Soc.* **2014**, *136*, 6672-6683.
44. (a) Baroudi, A.; El-Hellani, A.; Bengali, A. A.; Goldman, A. S.; Hasanayn, F. *Inorg. Chem.* **2014**, *53*, 12348-12359. (b) Wang, D. Y.; Choliy, Y.; Haibach, M. C.; Hartwig, J. F.; Krogh-Jespersen, K.; Goldman, A. S. *J. Am. Chem. Soc.* **2016**, *138*, 149-163.
45. Ben-Ari, E.; Gandelman, M.; Rozenberg, H.; Shimon, L. J. W.; Milstein, D. *J. Am. Chem. Soc.* **2003**, *125*, 4714-4715.
46. Kloek, S. M.; Heinekey, D. M.; Goldberg, K. I. *Organometallics* **2006**, *25*, 3007-3011.
47. We located two distinct energy minima for the product of H<sub>2</sub> addition to **4-H<sub>2</sub>**, namely **4-H<sub>4</sub>** for which the shortest H-H distance (H<sub>endo</sub>-H<sub>endo</sub>) is 1.62 Å, and **4-(H<sub>2</sub>)H<sub>2</sub>**, which has a dihydrogen ligand located cis to N with d<sub>H-H</sub> = 0.90 Å. Although the dihydrogen complex **4-(H<sub>2</sub>)H<sub>2</sub>** is calculated to be lower in free energy, the difference is too small to be considered very meaningful (ΔH° = -0.6 kcal/mol, ΔG° = -1.2 kcal/mol). Since **4-H<sub>4</sub>** is isostructural with **1-H<sub>4</sub>** and structurally much closer to **2-H<sub>4</sub>** than is **4-(H<sub>2</sub>)H<sub>2</sub>**, for purposes of this discussion we will refer only to **4-H<sub>4</sub>** and not **4-(H<sub>2</sub>)H<sub>2</sub>**.

48. Holmes, A. J.; Rayner, P. J.; Cowley, M. J.; Green, G. G. R.; Whitwood, A. C.; Duckett, S. B. *Dalton Trans.* **2015**, 44, 1077-1083.
49. (a) Reed, A. E.; Weinstock, R. B.; Weinhold, F. *J. Chem. Phys.* **1985**, 83, 735-746. (b) Reed, A. E.; Curtiss, L. A.; Weinhold, F. *Chem. Rev.* **1988**, 88, 899-926. (c) NBO 5.G; Glendening, E. D.; Badenhoop, J. K.; Reed, A. E.; Carpenter, J. E.; Bohmann, J. A.; Morales, C. M.; Weinhold, F. (Theoretical Chemistry Institute, University of Wisconsin, Madison, WI, 2001); <http://www.chem.wisc.edu/~nbo5>
50. Crabtree, R. H.; Quirk, J. M. *J. Organomet. Chem.* **1980**, 199, 99-106.
51. Reductive addition of H<sub>2</sub> to cationic Ir(I) was first proposed by Crabtree in 1980 (reference 36). An alternative interpretation, perhaps more conservative, is that the second H<sub>2</sub> addition is relatively much more oxidative than the first, thereby avoiding designations of "oxidative" and "reductive" in an absolute sense which may be very method-dependent. In this context we note that substituent effects have been interpreted to indicate that H<sub>2</sub> addition to neutral Ir(I) analogues of (PNP)Ir<sup>+</sup> is approximately neutral with respect to oxidation/reduction (reference 30b).
52. (a) Jean, Y.; Eisenstein, O. *Polyhedron* **1988**, 7, 405-407. (b) Rachidi, I. E. I.; Eisenstein, O.; Jean, Y. *New J. Chem.* **1990**, 14, 671-677.
53. Isoelectronic and structurally similar (<sup>t</sup>Bu<sub>4</sub>PCP)Ir(III) complexes have also been shown to yield irreversibly cyclometallated products: (a) Mohammad, H. A. Y.; Grimm, J. C.; Eichele, K.; Mack, H.-G.; Speiser, B.; Novak, F.; Quintanilla, M. G.; Kaska, W. C.; Mayer, H. A. *Organometallics* **2002**, 21, 5775-5784. (b) Mohammad, H. A. Y.; Grimm, J. C.; Eichele, K.; Mack, H.-G.; Speiser, B.; Novak, F.; Kaska, W. C.; Mayer, H. A. *ACS Symposium Series* **2004**, 885, 234-247.
54. Chelucci, G.; Baldino, S.; Baratta, W. *Acc. Chem. Res.* **2015**, 48, 363.
55. Jansen, A.; Pitter, S. *Monatshefte für Chemie*. **1999**, 130, 783.
56. Wilklow-Marnell, M.; Li, B.; Zhou, T.; Krogh-Jespersen, K.; Brennessel, W.W.; Emge, T.J.; Goldman, A.S.; Jones, W.D. *J. Am. Chem. Soc.* **2017**, 139, 8977.
57. Ghosh, R.; Kanzelberger, M.; Emge, T.J.; Hall, G.S.; Goldman, A.S. *Organometallics*. **2006**, 25, 5668.
58. Morris, R. *Inorg. Chem.* **1992**, 31, 1471
59. Ben-Ari, E.; Leituss, G.; Shimon, L.J.W.; Milstein, D. *J. Am. Chem. Soc.* **2006**, 128, 15390.
60. (a) Simler, T.; Braunstein, P.; Danopoulos, A.A. *Organometallics*. **2016**, 35, 4044. (b) Nerush, A.; Vogt, M.; Gellrich, U.; Leituss, G.; Ben-David, Y.; Milstein, D. *J. Am. Chem. Soc.* **2016**, 138, 6985. (c) Feller, M.; Gellrich, U.; Anaby, A.; Diskin-Posner, Y. Milstein, D. *J. Am. Chem. Soc.* **2016**, 138, 6445.
61. Gnanaprakasam, B.; Zhang, J.; Milstein, D. *Angew. Chem. Int. Ed.* **2010**, 49, 1468-1471.
62. Hermann, D.; Gandelman, M.; Rozenberg, H.; Shimon, L. J. W.; Milstein, D. *Organometallics* **2002**, 21, 812.
63. Klok, S. M.; Heinekey, D. M.; Goldberg, K. I. *Organometallics* **2006**, 25, 3007.
64. Dorta, R.; Goikhman, R.; Milstein, D. *Organometallics*. **2003**, 22, 2806.
65. Lease, N.; Pelczar, E.M.; Zhou, T.; Malakar, S.; Emge, T.J.; Hasanayn, F.; Krogh-Jespersen, K.; Goldman, A.S. *Organometallics*. **2018**, 37, 314-326.

## Chapter 4

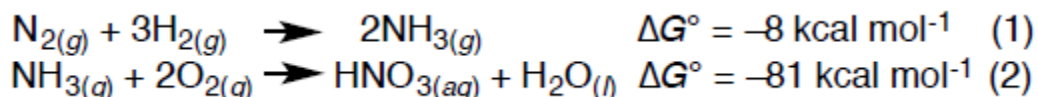
### Synthesis of Pincer-Ligated Metal Complexes for Nitrogen Reduction to Ammonia

#### Abstract:

Current industrial methods for the reduction of dinitrogen to ammonia are highly inefficient, requiring high temperatures ( $>300^{\circ}$ ) and high pressure of  $\text{N}_2$  and  $\text{H}_2$  ( $>125$  bar). This process, the Haber-Bosch process, consumes about 2% of the world's energy annually. Due to the high energy costs of this process, the reduction of dinitrogen to ammonia in an energy efficient manner is one of the most important chemical reactions being studied today. One possible solution would be an electrochemical reduction of dinitrogen using an electrode as the electron source and an acid as the proton source. These sources are cheap, abundant, and can be run with a significantly smaller amount of energy than the Haber-Bosch process. In order to perform this electrochemical reduction a complex capable of splitting dinitrogen is required. Recent work has shown that pincer-ligated complexes with Mo, Re, and Os can split dinitrogen to form the corresponding metal nitrides. Herein we report the synthesis of pincer-ligated Re and Mo chloride complexes and study their reactivity to split dinitrogen.

## 4.1 Introduction

The fixation of nitrogen to synthesize ammonia is one of the most important chemical reactions currently under investigation and is at the nexus of the food, water and energy industries. Ammonia is used in nearly all synthetic fertilizers, which is estimated to support half of the world's population. Ammonia is produced by the hydrogenation of dinitrogen using the Haber-Bosch process (eq. 1).<sup>1,2</sup> Ammonia and ammonia products, such as ammonium nitrate synthesized by the Oswald process<sup>3,4</sup> (eq. 2) are key additives to synthetic fertilizers.

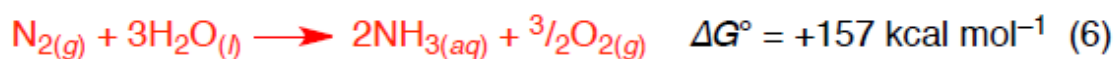
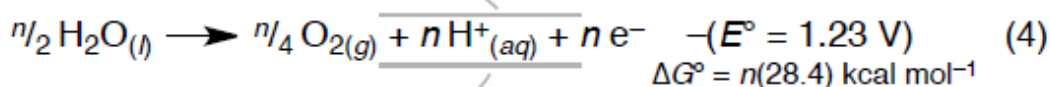


While incredibly important, fertilizers are very extremely energy intensive to produce mainly due to the production of ammonia. Manufacturing of ammonia is estimated to require 6 EJ of fossil fuel derived energy or about 2% of the world's total energy use.<sup>5</sup> The production of H<sub>2</sub> gas from methane or other fossil fuels represents the major energy requiring component, with the high pressures (>125 atm), high temperatures (>300°C) and low per pass conversion (ca 15%).<sup>6</sup>

The energy demands of the Haber-Bosch process also have environmental effects. The fixation of nitrogen to produce ammonia is one of the leading causes of CO<sub>2</sub> gas emissions which have shown to have a direct link to climate change.<sup>7-14</sup> Alternative methods for ammonia production are needed to lower the overall cost, energy demand and environmental impact of current industrial nitrogen fixation.



The electrocatalytic reduction of dinitrogen using  $\text{H}^+$  and  $\text{e}^-$  is seen as a viable alternative for ammonia synthesis. In this electrochemical approach the protons and electrons would be produced by the oxidation of water (equation 4).



When you combine equations 3 and 4 you get the true energetic cost of the reduction of nitrogen to ammonia. The energetic cost of the Haber-Bosch process from the equation can be misleading as it does not account for the energy needed to make  $\text{H}_2$ . The thermochemistry shown is in aqueous solution. Nevertheless, we have demonstrated that the reduction of nitrogen to ammonia can also be done in organic solvents.<sup>15</sup>

Nitrogen can be reduced according to a few possible mechanisms as seen in Scheme 4.1. In nature, multimetallic FeS clusters of nitrogenase enzymes reduce  $\text{N}_2$  from  $\text{H}^+$  (from water) and  $\text{e}^-$  (-0.4 V from ATP hydrolysis).<sup>16-18</sup> Work reported by Yandulov and Schrock in 2003 demonstrated the first molecular catalyst capable of reducing  $\text{N}_2$  to  $\text{NH}_3$  using acid as the proton source and a chemical reductant as the

electron source.<sup>19,20</sup> Peters<sup>21-23</sup> and Nishibayashi<sup>24-29</sup> has also expanded on this work focusing on iron and molybdenum based complexes.

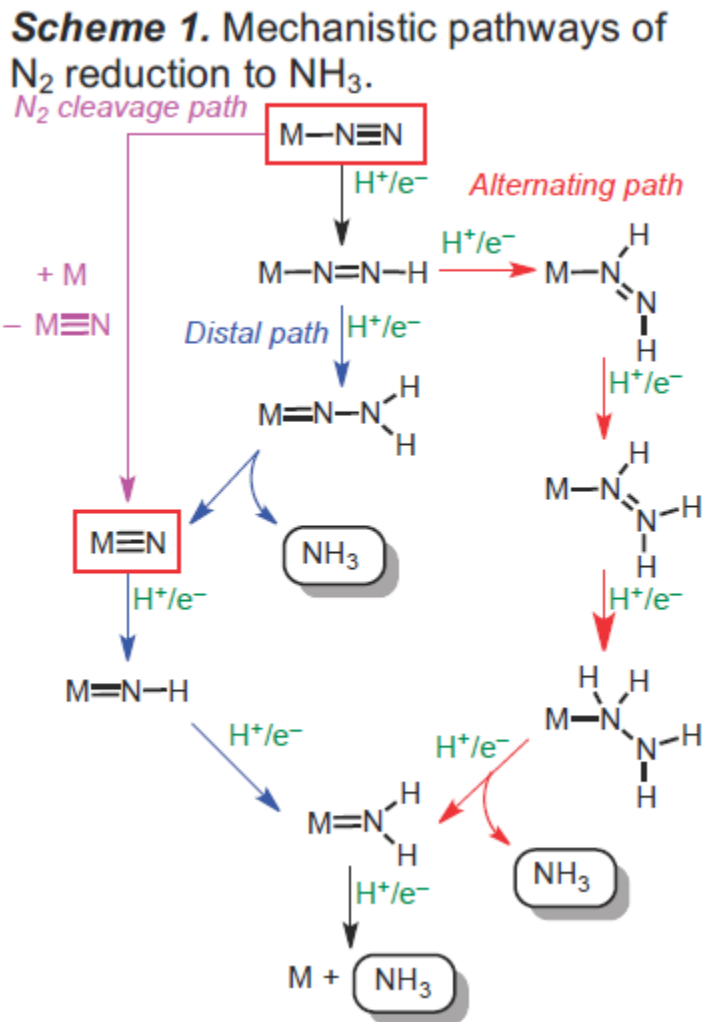
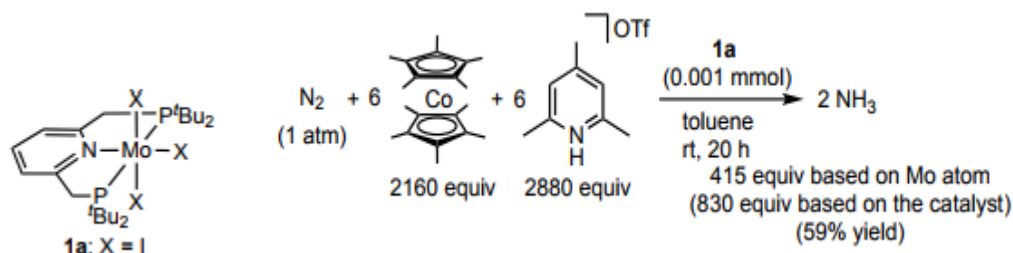


**Figure 4.1:** Alternative pathways for dinitrogen reduction to ammonia

Computational and mechanistic work by Schrock and Peters has demonstrated the reduction of nitrogen can go through the distal pathway (blue Figure 4.1). In this pathway the mechanism goes through the high energy diazenido ( $M-NNH$ ) and hydrazido ( $M-NNH_2$ ) intermediates, of which both Schrock and Peters isolated. Initial reports of nitrogen reduction by Schrock suffered from low turnovers of ammonia even

with adjustments of the acid reductant pairs. In addition the side reaction of acid and reductant to form  $H_2$  was a concern. Recent work Nishibayashi<sup>30</sup> has demonstrated complexes capable of up to 450 turnovers of ammonia per metal center, a dramatic increase over the previous record held by Peters with 63 turnovers.<sup>21-23</sup>



**Scheme 4.1:** Reduction of dinitrogen to ammonia using PNPMo complexes (Nishibayashi)

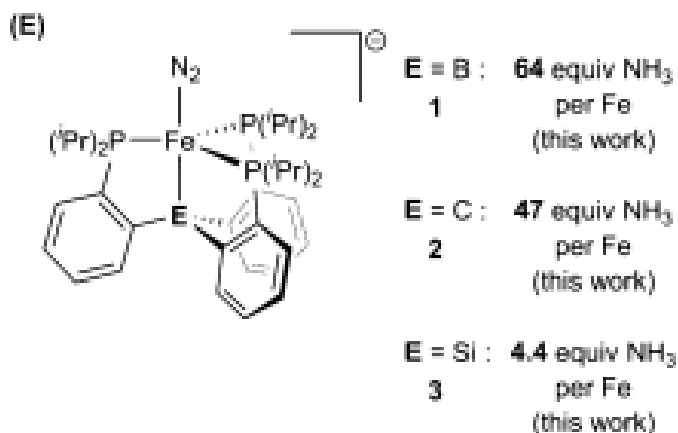
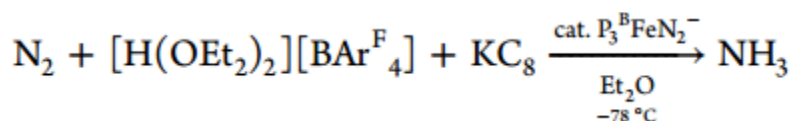


**Figure 4.2:** Reduction of dinitrogen by iron based complexes (Peters)

In hopes of improving the ability of molecular catalysts to reduce  $N_2$  to ammonia we have decided to use an electrode as our source of electrons. There have been

reports of electrocatalytic heterogeneous reduction of  $N_2$  using nano- $Fe_2O_3$  in molten KOH/NaOH at 250°C at -1.1 V with 35% faraday efficiency.<sup>31</sup> In addition, there have been examples of heterogeneous complexes with molecular surface species that can perform nitrogen fixation chemistry. These reports include complexes such as a Fe(phthalocyanine) system that had a 1.6% faraday efficiency for 10 min.<sup>32-33</sup> However, these systems do have some issues such as strong overpotentials and they not mechanistically understood.<sup>34-35</sup>

Currently, there are significantly less reports using molecular complexes to reduce nitrogen electrocatalytically. In 1985, Pickett reported that  $N_2$  could be converted to ammonia at -2.7 V per ferrocene, however the tungsten complex used could only perform the reductive steps stepwise because the W- $N_2$  complex needed to be protonated by a strong acid.<sup>36-37</sup> In 2012, Schrock also studied his molybdenum complexes electrocatalytically however, protonation of the ligand prevents any activity.<sup>38</sup> Lastly in 2016, Peters reported some evidence that his complexes can undergo stoichiometric formation of ammonia at -45° at -2.6 V vs. ferrocene.<sup>39</sup> The challenges of using electrochemical means to reduce nitrogen have been reviewed<sup>40-41</sup> and still no molecular catalyst has been reported to reduce nitrogen to ammonia catalytically using electrochemical means.

In contrast to previous work, the focus of this project is on the nitrogen cleavage pathway in Scheme 4.1, the pink pathway. With this pathway we envision the splitting of nitrogen to form metal nitrides that can then undergo proton coupled electron transfer (PCET) steps to reduce the nitride to ammonia. This pathway avoids the high

energy diazenido and hydrazido intermediates lowering the overall potentials needed for the reaction which should help us avoid the side reaction of  $\text{H}_2$  formation.

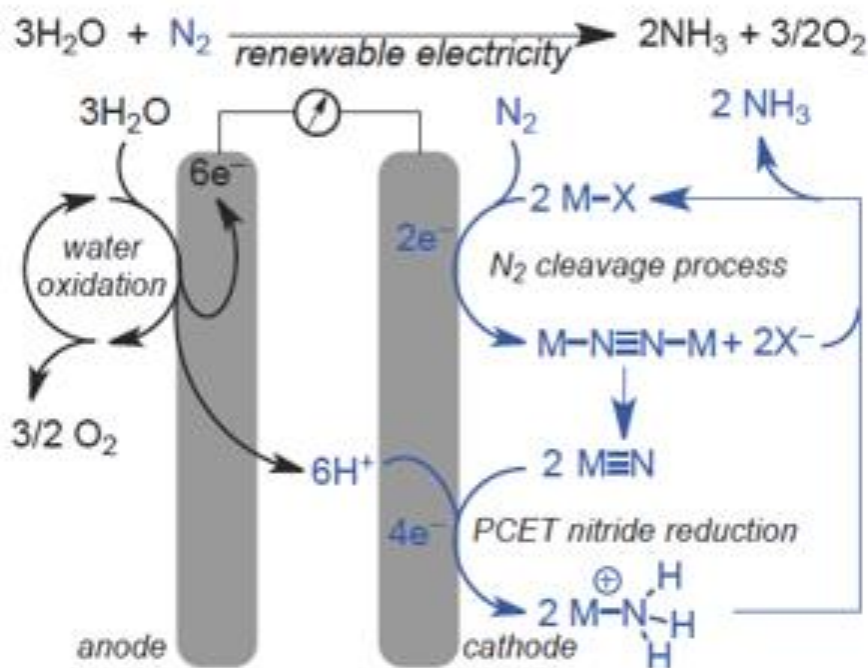


**Figure 4.3:** Electrochemical  $\text{N}_2$  splitting approach

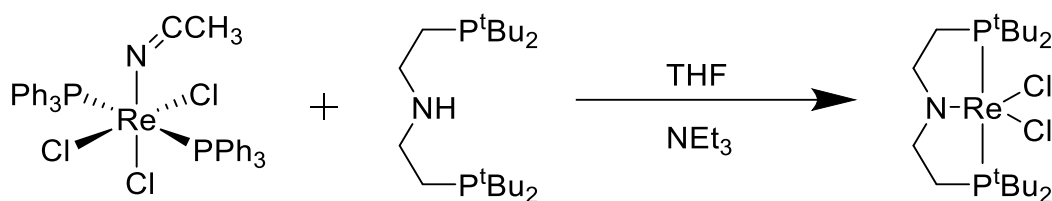
Each step in the reductive approach of nitrogen fixation has some precedent but a complete catalytic cycle from nitrogen cleavage to nitride reduction has not been reported. We envision that pincer ligated metal complexes can perform this nitrogen cleavage followed by reduction of the metal nitride electrocatalytically.

## 4.2 Synthesis of Pincer-Ligated Rhenium Complexes

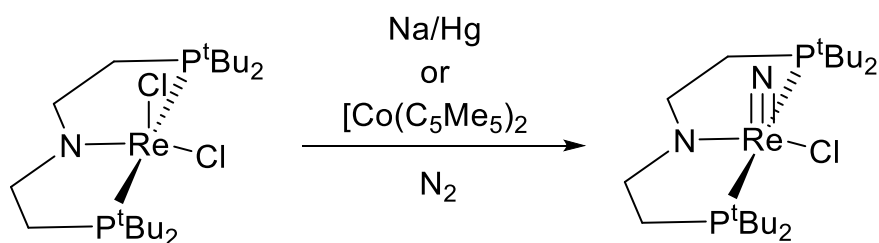
The first step of our proposed catalytic cycle is the formation of the metal nitride via the splitting of  $\text{N}_2$ . Metal nitrides are well studied and have been synthesized with many different metals and ligand frameworks. While a lot of metal nitrides are

synthesized by reaction of metal with a reactive azide species, reports of the direct formation of metal nitrides from  $N_2$  is much more limited.

Recently the Schneider group has reported that MACHO-ligated PNP rhenium species can split  $N_2$  to form the rhenium nitride.<sup>42</sup> Schneider first synthesized the MACHO (<sup>t</sup>BuPNP)Re dichloride species by reacting MACHO ligand with base and a phosphinated rhenium source. Then under a  $N_2$  atmosphere and reducing conditions the (PNP)Re(II) monochloride is formed which can then homolytically cleave dinitrogen to form the rhenium nitrides.



**Scheme 4.2:** Synthesis of MACHO rhenium pincer complex (Schneider)



**Scheme 4.3:** Reduction of MACHO Re complex followed by  $N_2$  cleavage

Based on the work by the Schneider group we looked at a range of PCP and PNP ligated complexes with Ir, Rh, Ru, Os, Mo and Re in order to see if any had promise to split  $N_2$ . Computational analysis suggested that iridium and rhodium would not be good candidates for  $N_2$  splitting as the dinitrogen complexes are too stable. Osmium and

ruthenium have extremely high barriers for N<sub>2</sub> cleavage, ruling them out as well.

Complexes using technetium look the most promising by computational analysis;

however, the handling of technetium is complicated due to radioactive isotopes making them less than ideal. Complexes with rhenium have very favorable thermodynamics for formation of the metal nitrides. In fact, our collaborators at UNC and Yale have observed that the rhenium nitrides might be too stable for oxidation or reduction. The calculations for these metals can be seen in the table below (for the full table see the experimental section).

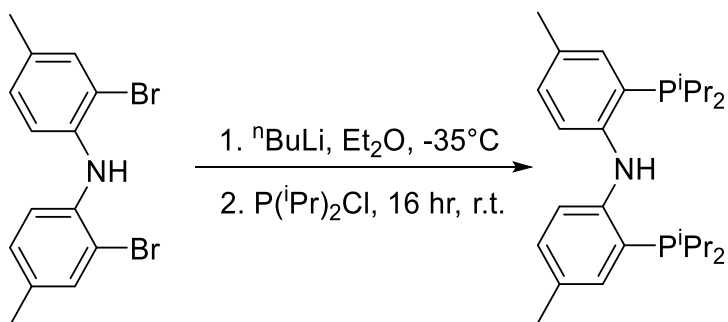
**Table 4.1:** Computational analysis for the N<sub>2</sub> cleavage using various pincer ligands and metals

<b>G(2M+2N<sub>2</sub>)=0.0</b>						
<b>SPECIES</b>	n	Ox. state	d e-'s	2* M-N <sub>2</sub>	2 MN + N <sub>2</sub>	Rxn: 2 M- N <sub>2</sub> = 2 MN + N <sub>2</sub>
(tBuPOCOP)MoI	0	2	4	3.4	-32.0	-35
(tBuPOCOP)MoI <sup>-</sup> anion	-1	1	5	-15.4	-56.2	-41
(tBuPONOP)MoI	0	1	5	-6.8	-49.0	-42
(MACHO)Ru	0	1	7	-41.2	8.0	49
(MACHO)Os	0	1	7	-50.2	-20.8	29
(MACHO)TcCl	0	2	5	5.8	-24.0	-30
(MACHO)ReCl	0	2	5	-13.4	-56.6	-43
(tBuPCP)Ru	0	1	7	-47.0	30.8	78
(tBuPCP)Os	0	1	7	-49.6	6.8	56
(tBuPCP)TcCl	0	2	5	9.4	-14.6	-24
(tBuPCP)ReCl	0	2	5	-5.2	-53.0	-48
(Phebox)Ru	0	1	7	-3.6	48.2	52
(Phebox)Os	0	1	7	-31.8	23.8	56
(Phebox)TcCl	0	2	5	-8.0	-20.0	-12

(Phebox)ReCl	0	2	5	-17.2	-39.2	-22
(MACHO-H <sup>+</sup> )Ru	1	1	7	-48.4	12.6	61
(MACHO-H <sup>+</sup> )Os	1	1	7	-63.4	-27.8	36
(MACHO-H <sup>+</sup> )TcCl	1	2	5	10.8	-16.4	-27
(MACHO-H <sup>+</sup> )ReCl	1	2	5	-5.4	-48.0	-43

From the computational analysis we decided to synthesize some rhenium complexes to see if nitrogen splitting was as favorable as computed. Additionally altering the ligand system could lead to more reactive nitrides that could react electrochemically.

The first ligand system we chose to look at was another PNP ligand similar to the one used by the Schneider lab but instead of alkyl linkers we chose one with aryl linkers. This ligand was first reported by Ozerov<sup>43</sup> and has been used to metallate various metals including iridium and rhodium. The ligand was synthesized according to literature procedure<sup>43</sup>.

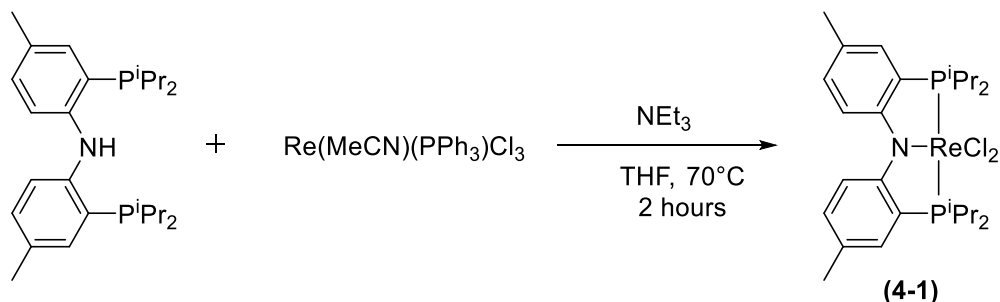


**Scheme 4.4:** Synthesis of ( $\text{iPr}$ PNP) ligand (Ozerov ligand)

The reaction to make the aryl (PNP) $\text{ReCl}_2$  complex was run in an analogous way to the complex reported by the Schneider group. Reaction of the ligand with



triphenylphosphine bound rhenium precursor in the presence of base yielded a dark purple solution with what appeared to be salt formation.



**Scheme 4.5:** Attempted synthesis of (<sup>i</sup>PrPNP)ReCl<sub>2</sub> (4-1)

While the appearance of the solution was consistent with the MACHO ligated (<sup>t</sup>BuPNP)ReCl<sub>2</sub> the NMR data was not. <sup>31</sup>P-NMR of the solution showed free triphenylphosphine and no new signals, which is consistent with a paramagnetic species. Conversely the MACHO complex has a clear diamagnetic signal in the <sup>31</sup>P-NMR.

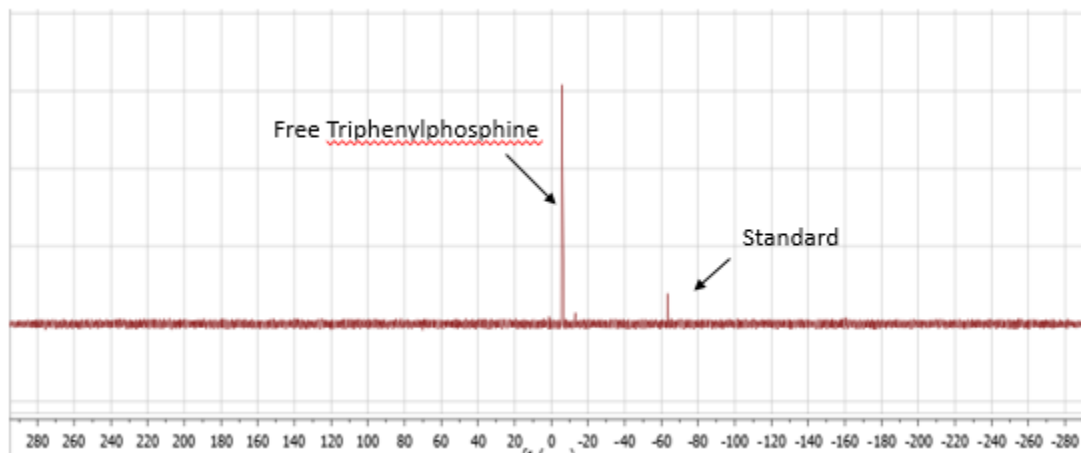


**Figure 4.4:** <sup>31</sup>P-NMR: Attempted synthesis of (<sup>i</sup>PrPNP)ReCl<sub>2</sub> (4-1)

The <sup>1</sup>H-NMR had signals as far down field as 60 ppm, with multiple signals outside the standard 0-12 ppm range, also consistent with a paramagnetic complex. The number of

signals was far greater than what one would suspect even from a paramagnetic complex. It is hypothesized that the smaller steric bulk of the isopropyl groups when compared to the *t*-butyl's of the MACHO ligand could lead to dimerization or other paramagnetic side products. The (<sup>i</sup>PrPNP)ReCl<sub>2</sub> complex could not be isolated.

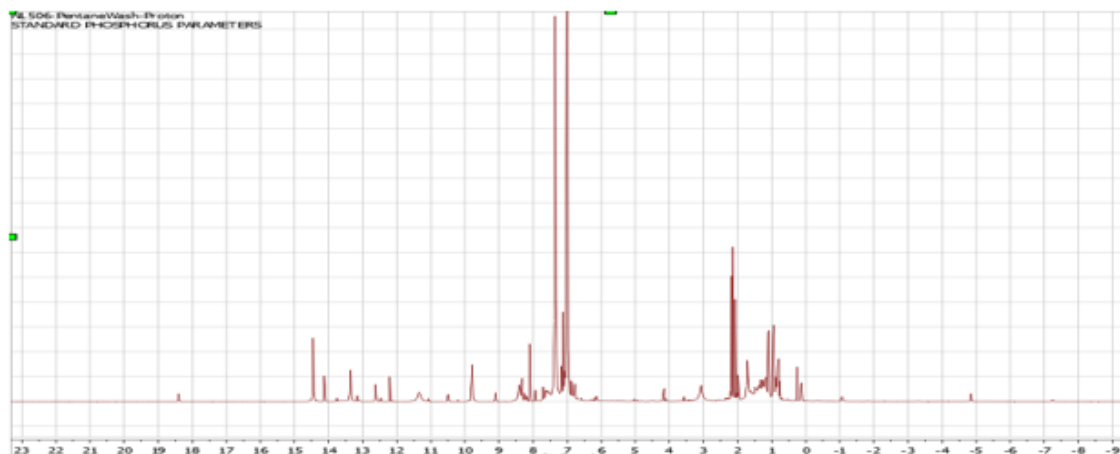
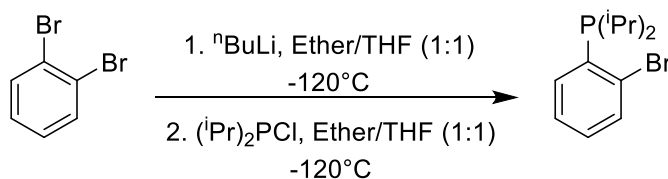
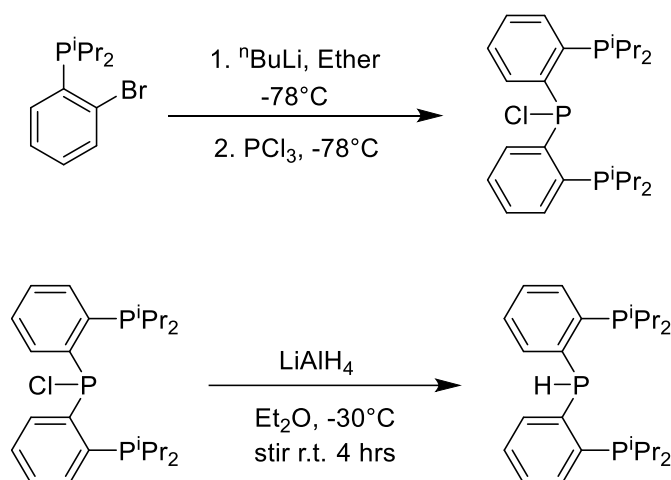


**Figure 4.5:** <sup>1</sup>H-NMR: Attempted synthesis of (<sup>i</sup>PrPNP)ReCl<sub>2</sub> (**4-1**)

With the unsuccessful formation of the (<sup>i</sup>PrPNP)ReCl<sub>2</sub> alternative ligand systems were tested. The next ligand selected interchanged the anionic nitrogen center donor for an anionic phosphorus center atom. This ligand was originally reported by the Peters group in 2005.<sup>44</sup> Yet not much other work has been described for this ligand and no rhenium complexes have been reported.

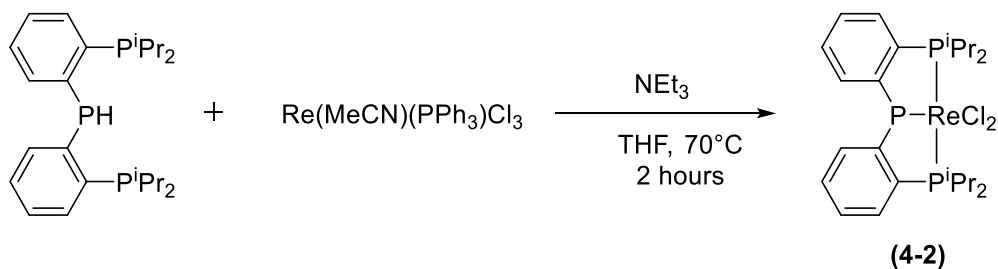


**Scheme 4.6:** Synthesis of PPP ligand arm (Ozerov)



**Scheme 4.7:** Synthesis of PPP ligand (Peters)

Reaction of the ( $i\text{Pr}$ PPP) ligand with triphenylphosphine rhenium precursor in the presence of base resulted in a pinkish solution with visible salt formation.



**Scheme 4.8:** Attempted synthesis of ( $i\text{Pr}$ PPP) $\text{ReCl}_2$  (**4-2**)

Unlike the previous situation with the ( $i\text{Pr}$ PNP) ligand visible signals were observed in the  $^{31}\text{P}$ -NMR for this reaction. In addition to free triphenylphosphine four new signals were observed with three of the new signals integrating 1:1:1.

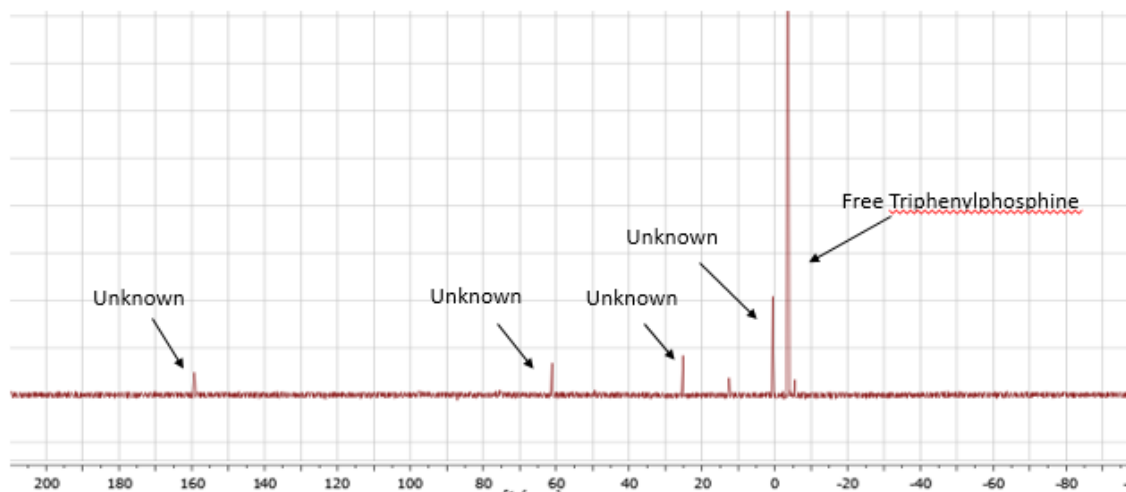


**Figure 4.6:**  $^{31}\text{P}$ -NMR: Attempted synthesis of  $(^{\text{iPr}}\text{PPP})\text{ReCl}_2$  (4-2)

When looking at the  $^1\text{H}$ -NMR signals that would be attributable to a paramagnetic complex are observed (58 and 51 ppm). Similar to the previous  $(^{\text{iPr}}\text{PNP})$  ligand example the number of signals in the proton NMR were more than expected. This most likely is due to the formation of multiple complexes (possible dimerization) or isomers. No one species could be isolated cleanly to be fully characterized.

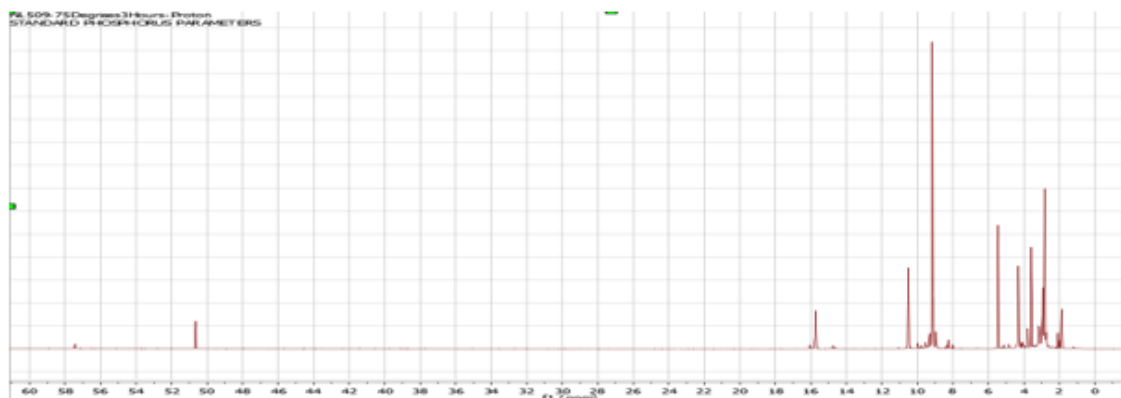
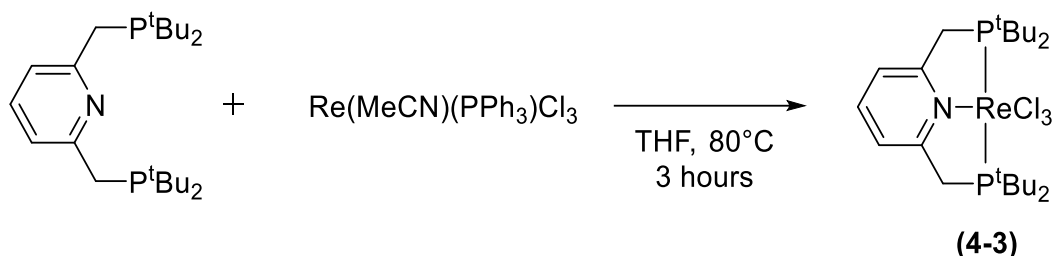


**Figure 4.7:**  $^1\text{H}$ -NMR: Attempted synthesis of  $(^{\text{iPr}}\text{PPP})\text{ReCl}_2$  (4-2)

Due to the possibility of dimerization caused by using isopropyl based ligands we decided to switch to more bulky ligands using tert-butyl groups. The first ligand looked at was the pyridine based <sup>t</sup>BuPNP ligand first synthesized by the Milstein group<sup>45</sup> and one we have used extensively with osmium. Reaction of ligand with triphenylphosphine rhenium precursor in THF lead to the formation of the (<sup>t</sup>BuPNP)ReCl<sub>3</sub> complex.



**Scheme 4.9:** Synthesis of (<sup>t</sup>BuPNP)ReCl<sub>3</sub> (**4-3**)

Single crystal analysis of this complex was obtained showing formation a near octahedral structure with ligand angles (N-Re-P) of 79.2°. Additionally the structure had Re-Cl distances of 2.35 and 2.43 Å. MALDI TOF mass spectroscopy confirmed the structure with a parent peak at 542 and the correct isotope splitting pattern. Comparing the MS data to a mass spec simulations shows strong similarities suggesting the correct product was identified.

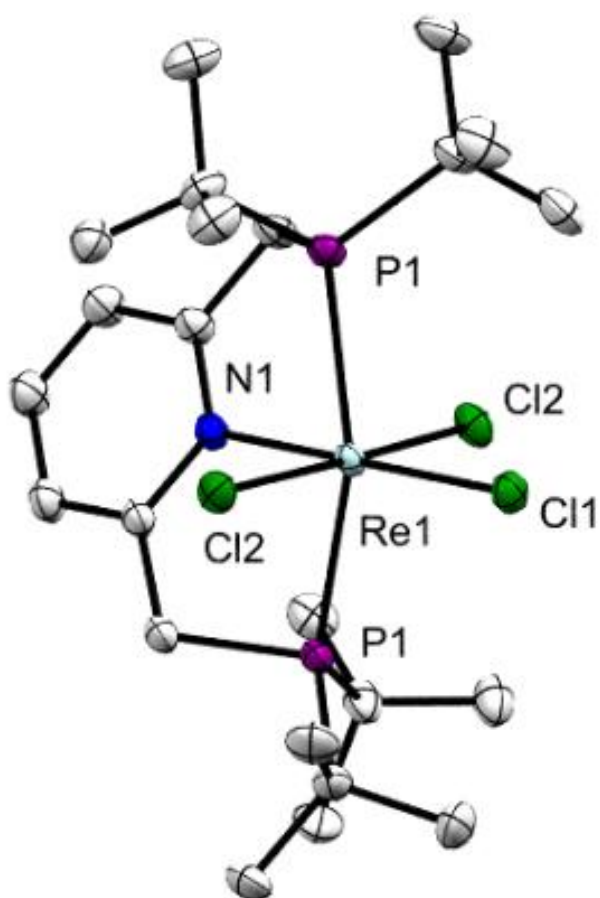


**Figure 4.8** ORTEP representation (50% probability ellipsoids) of the structure of **(4-3)** determined by X-ray diffraction; hydrogen atoms omitted for clarity.

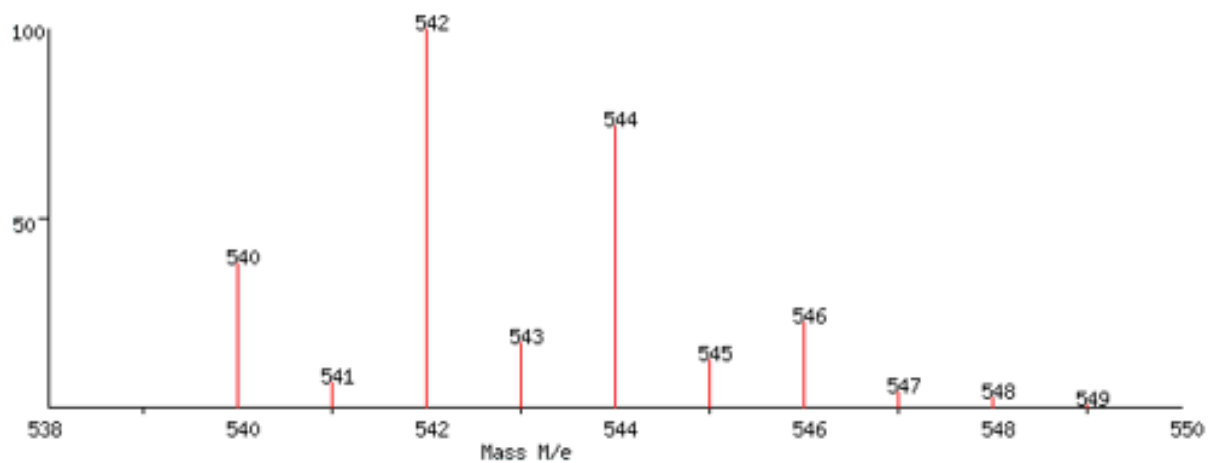


**Figure 4.9** Mass spectroscopy simulation data for (4-3)

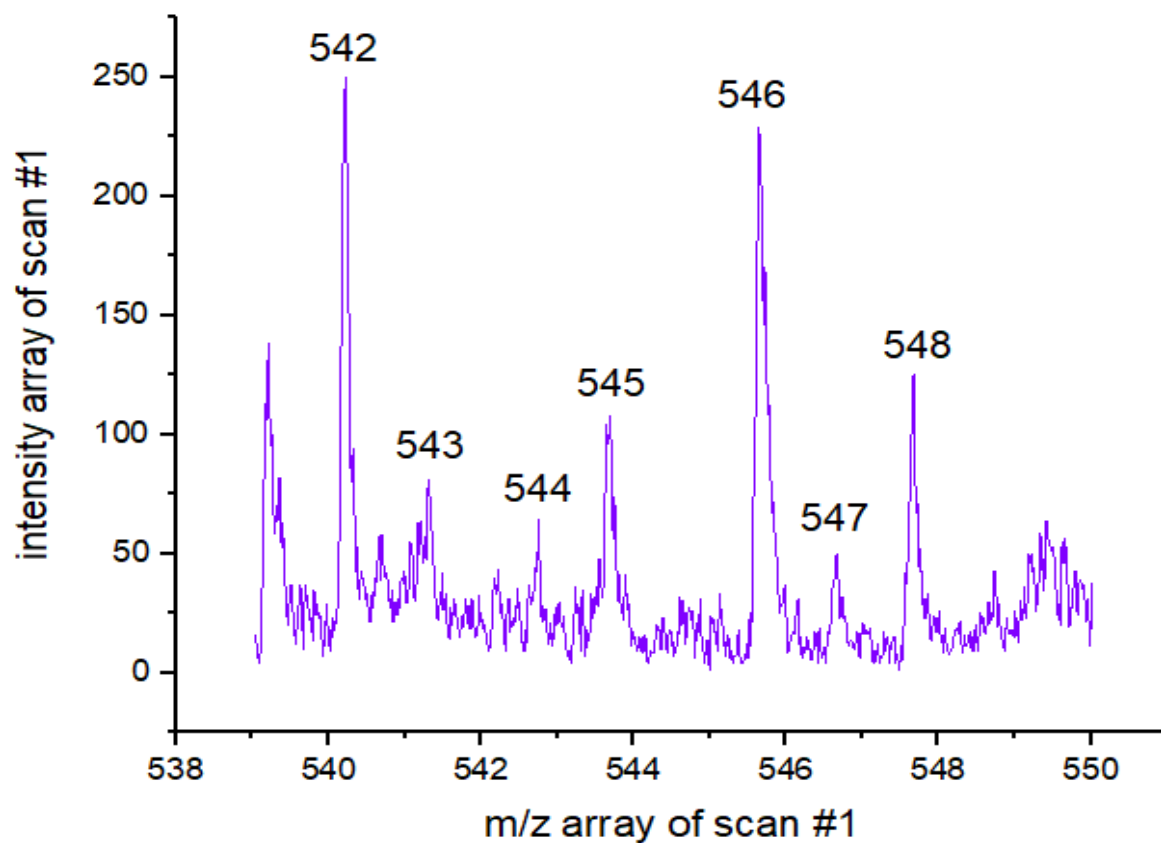


**Figure 4.10** Mass spectroscopy data for (4-3)

$^{31}\text{P}$ -NMR spectroscopy of the  $(^t\text{BuPNP})\text{ReCl}_3$  complex shows free triphenylphosphine with no new signals consistent with the formation of a paramagnetic  $\text{Re(III)}$  complex. The  $^1\text{H}$ -NMR is consistent with a paramagnetic species, showing a very broad peak at about 7 ppm integrating to 36 H atoms of the tert-butyl groups. All other signals for the ligand can be seen in the NMR with the proper integrations.

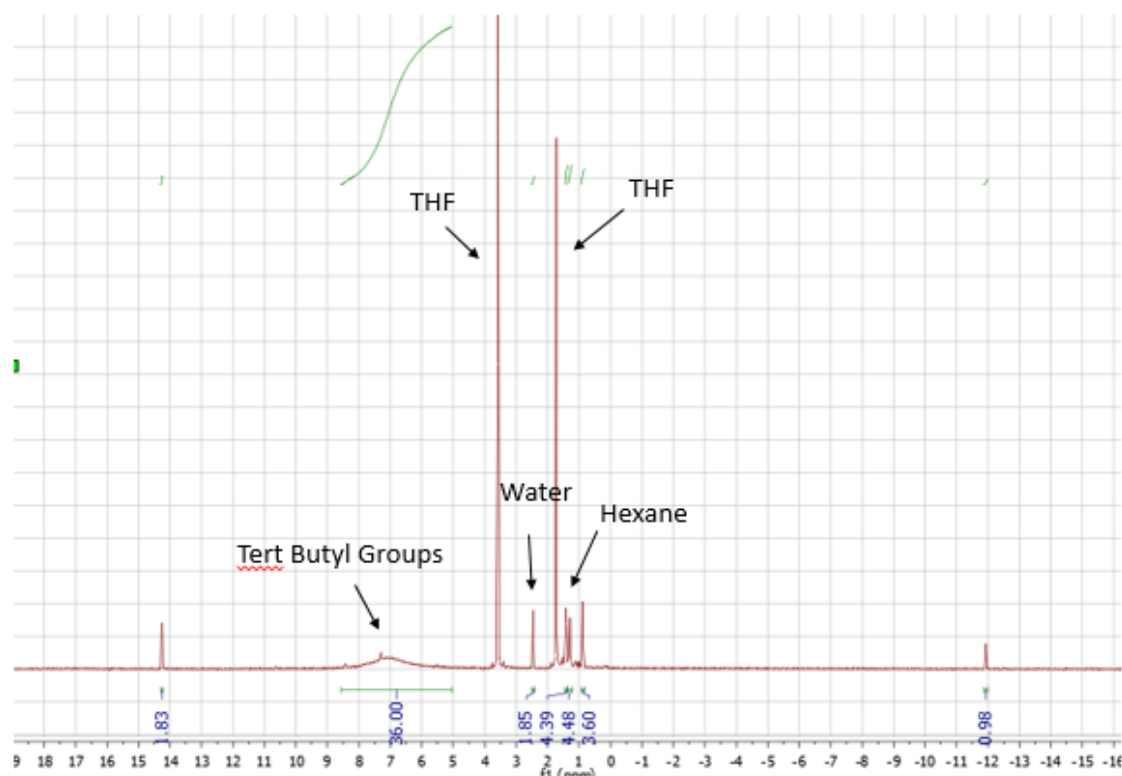
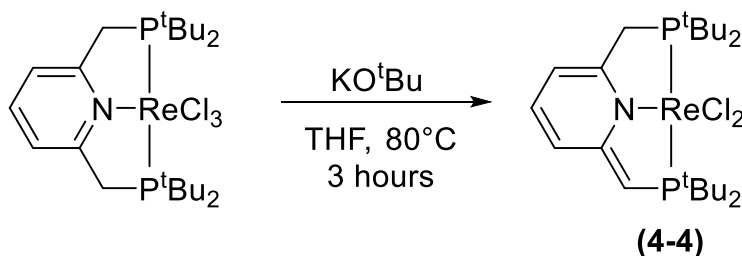


**Figure 4.11:**  $^1\text{H}$ -NMR spectra of  $(^t\text{BuPNP})\text{ReCl}_3$  (4-3)

As we have demonstrated with  $(^t\text{BuPNP})\text{Os}$  complexes discussed in the previous chapter the pyridine based PNP ligand can dearomatize moving the double bond to the ligand arm. This dearomatization of  $(^t\text{BuPNP})$  ligand is reported with a variety of metal complexes and is most notable used with ruthenium reported by Milstein as a



hydrogenation catalyst <sup>46</sup>. Dearomatization of the (<sup>t</sup>BuPNP)ReCl<sub>3</sub> complex would yield a complex similar to the MACHO ligand used by the Schneider group. Seeing as the MACHO PNPReCl<sub>2</sub> complex was very good at splitting dinitrogen we attempted to synthesize the dearomatized (<sup>t</sup>BuPNP)ReCl<sub>2</sub>.



**Scheme 4.10:** Synthesis of dearomatized (<sup>t</sup>BuPNP)ReCl<sub>2</sub> (**4-4**)

Reaction of (<sup>t</sup>BuPNP)ReCl<sub>3</sub> with sodium tert-butoxide resulted in a color change from a brown/reddish color to a deep red along with what looked like salt formation. <sup>31</sup>P-NMR still showed no signals suggesting a paramagnetic product. Nevertheless this data could not distinguish if starting material reacted. By <sup>1</sup>H-NMR we can see new paramagnetic signals different from those in the starting material. The signals seen at 4.6 and 3.2 ppm integrate 1:2 most likely corresponding to the aryl protons. In the region between 1.6 and 2.0 ppm a doublet and two sets of doublet of doublets can be seen. These splitting patterns correspond with the dearomatized structure proposed. Integration of these peaks are not reliable as a large broad peak can be seen underlying the signals from 1.2 to 1.8 ppm. This is proposed to be the tert-butyl groups unfortunately without integration it is hard to confirm.

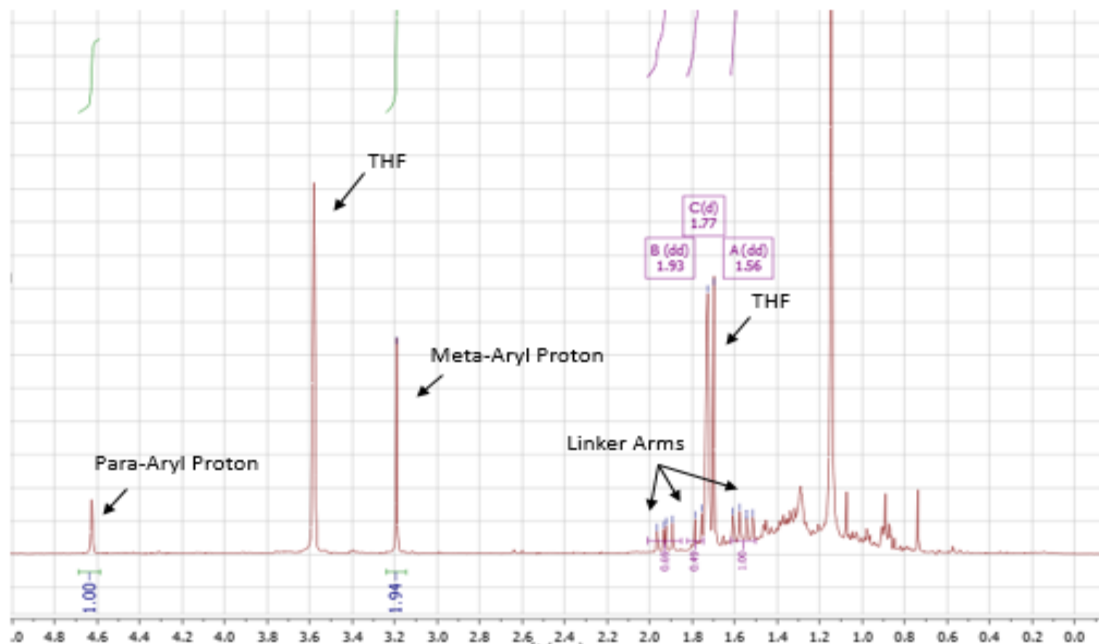
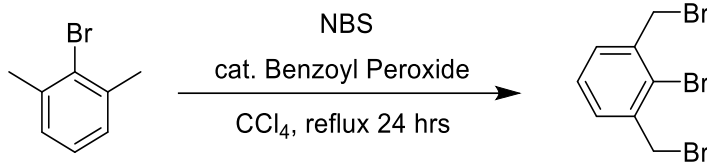


**Figure 4.12:**  $^1\text{H}$ -NMR spectra of  $(^t\text{BuPNP})\text{ReCl}_3$  (**4-4**)

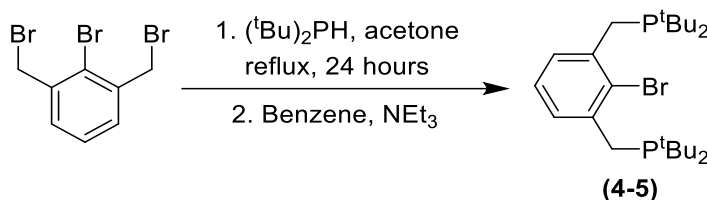
Unfortunately this complex was unable to be isolated due to what appeared to be reactivity with most solvents. Our hypothesis is that advantageous water or any easily accessible proton source could re-protonate the ligand. This was observed when the solvent was removed from the resulting solution leaving the product residue. Upon adding solvent again the signals previously observed in the  $^1\text{H}$ -NMR were lost.

Another ligand that is commonly used in our lab is the  $(^t\text{BuPCP})$  pincer which has never been reported with rhenium. The commonly used  $(^t\text{BuPCP})$  pincer could not be used as the C-H activated required when using this ligand is unlikely occur with rhenium. Instead synthesis of a  $(^t\text{BuPCP})$  pincer ligand with the center aryl position brominated would allow for a synthetic route to the rhenium complex. This was done by initial formation of the dibenzylbromo-bromobenzene complex in Scheme 4.10 using a literature reported synthesis.<sup>47</sup>



**Scheme 4.11:** Synthesis of 2-bromo-1,3-bis(bromomethyl)benzene

In order to synthesize the brominated (<sup>t</sup>BuPCP) ligand the tribromide synthesized was treated first with di-tertbutyl-phosphine followed by a work up with base. The synthesis yielded a white powder that had a single peak in the <sup>31</sup>P-NMR at 33.6 ppm which is about 0.5 ppm away from the non-brominated (<sup>t</sup>BuPCP) ligand. <sup>1</sup>H-NMR showed all of the ligand signals with all the signals in expected positions. The only noticeable change was the slight downfield shift of the meta-protons on the backbone.



**Scheme 4.12:** Synthesis of ((2-bromo-1,3-phenylene)bis(methylene))bis(di-tert-butylphosphane)

(4-5)

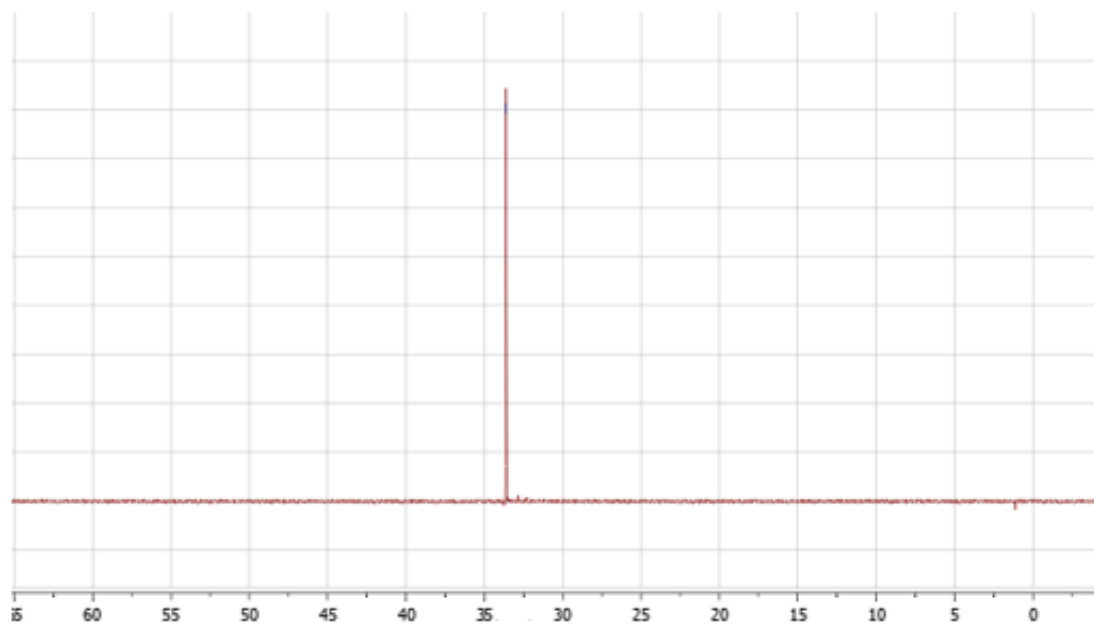


Figure 4.13:  $^{31}\text{P}$ -NMR: spectra of (4-5)

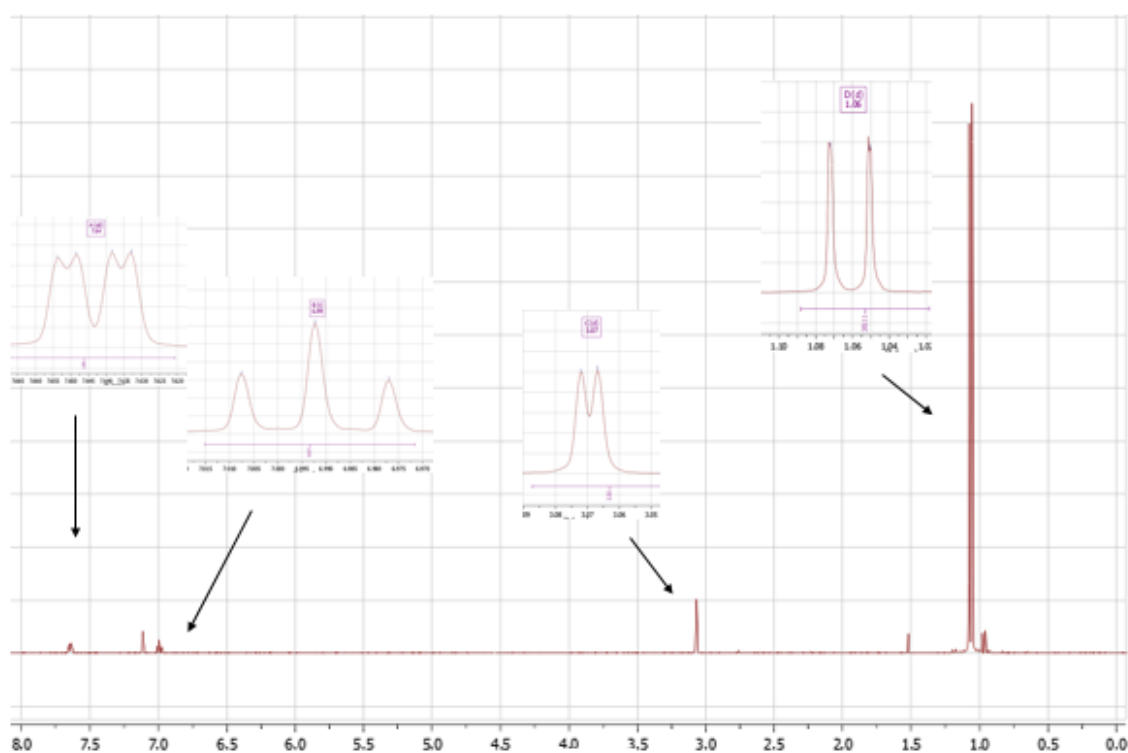
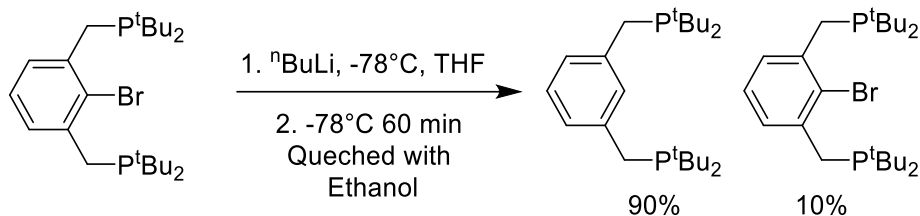


Figure 4.14:  $^1\text{H}$ -NMR spectra (4-5)

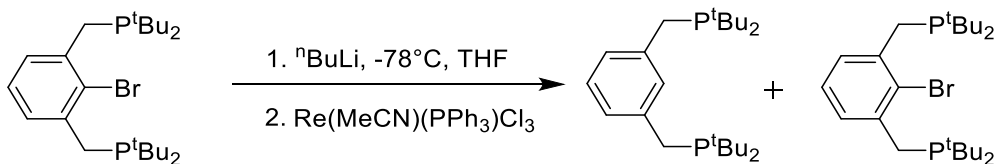
With the ligand synthesized, the next step would be metalation with rhenium.

The synthetic plan was lithiation of the ligand with *n*-butyl lithium followed by addition of rhenium precursor. In order to optimize the lithiation reaction the ligand was treated with *n*-butyl lithium and quenched with degassed ethanol. Initial reactions were run using diethyl ether as the solvent, unfortunately insolubility of the ligand in the solvent led to no reaction being observed. Changing the solvent to THF lead to lithiation of the ligand.



**Scheme 4.13** Lithiation optimization reaction

With the optimized conditions for the lithiation reaction the synthesis of the  $(^t\text{BuPCP})\text{ReCl}_2$  complex was attempted. Reaction of the brominated  $(^t\text{BuPCP})$  ligand with *n*-BuLi was followed by addition of the rhenium precursor used previously.



**Scheme 4.14:** Lithiation of (4-5) followed by treatment with rhenium precursor

The results of the reaction yielded only unreacted starting material and free  $(^t\text{BuPCP})$  ligand. The only viable proton source would be the free acetonitrile released from the rhenium precursor. Literature reports show that the deprotonation of acetonitrile is

viable<sup>48</sup> and is likely the source of free ligand observed in this experiment. An alternative rhenium source would be needed in hopes of synthesizing the (<sup>t</sup>BuPCP)ReCl<sub>2</sub>.

### 4.3 Synthesis of pincer-ligated molybdenum complexes

Computational analysis suggested that rhenium pincer complexes would be able to split nitrogen to form metal nitrides. Another metal that had favorable calculated energies for N<sub>2</sub> cleavage was molybdenum. Molybdenum is one of the most studied metals for the reduction of dinitrogen to ammonia and currently a molybdenum complex has the record for highest equivalents of ammonia generated.<sup>30</sup>

The Schrock and Nishibayashi groups have reported ground breaking work for nitrogen reduction using molybdenum complexes. In 2003, the Schrock group demonstrated the first nitrogen reduction using molybdenum with a tren-based triamidoamine(3-) ligand ([N(CH<sub>2</sub>CH<sub>2</sub>N- (HIPT))<sub>3</sub>]<sup>3-</sup> ([HIPTN<sub>3</sub>N]<sup>3-</sup>) where HIPT = 3,5-(2,4,6- triisopropylphenyl)C<sub>6</sub>H<sub>3</sub>).<sup>19</sup> It was proposed that this process goes through the distal pathway (Figure 4.1) and eight of the intermediates were isolated and characterized.<sup>49</sup> The Schrock group also demonstrated molybdenum's ability to cleave dinitrogen directly using a pincer based molybdenum POCOP species.<sup>50</sup> This work firmly established that molecular complexes can perform nitrogen fixation in a similar way to those proposed in nature.

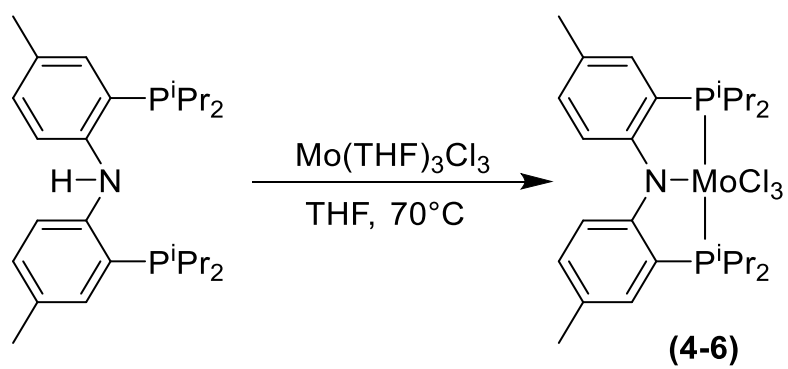
Nishibayashi has multiple reports demonstrating pincer based molybdenum complexes ability to reduce dinitrogen to ammonia, starting with his initial report using a PNP molybdenum complex.<sup>24-29</sup> His group has gone on to report pincer ligated

molybdenum nitrides that can undergo catalytic reduction under  $N_2$  to form ammonia. This includes their most current report where they use  $(^{tBu}PNP)MoX_3$  complexes cleave dinitrogen to form the corresponding metal nitrides followed by reduction to ammonia. This system holds the current record for ammonia produced.<sup>51</sup>

Finally the Schneider lab has also recently reported that pincer-ligated MACHO molybdenum complexes were capable of splitting dinitrogen to form metal nitrides.<sup>52</sup> In all these cases discussed strong reducing agent (cobaltacene, chromocene,  $KC_8$  or sodium amalgam) and acid (lutadinium triflate or  $H(Et_2O)_2Barf$ ) were used as the source of electrons and protons.

Based on computational and literature precedent we chose to synthesize some molybdenum complexes in the hope they would split dinitrogen. We chose to start with the diaryl-PNP (Ozerov) ligand discussed before seeing as PNP ligated molybdenum complexes have been shown to fixate nitrogen well. In addition the center binding nitrogen atom has potential as a proton shuttle if the pincer-ligated molybdenum nitride can be synthesized.

The Ozerov ligand was treated with  $Mo(THF)_3Cl_3$  in THF (brown suspension) and heated for 2 hours at  $70^\circ C$ . The solution turned dark blue upon heating with stirring needed to mix the insoluble starting material.  $^{31}P$ -NMR showed loss of the free ligand signal with a single broad new signals observed at  $\delta$  45 ppm.  $^1H$ -NMR showed broad singlets in the range of  $\delta$  -30 and 70 ppm. Single crystal X-ray diffraction of the sample confirmed formation of the  $(^{iPr}PNP)MoCl_3$  complex.



**Scheme 4.15:** Synthesis of (<sup>i</sup>PrPNP)MoCl<sub>3</sub> (**4-6**)

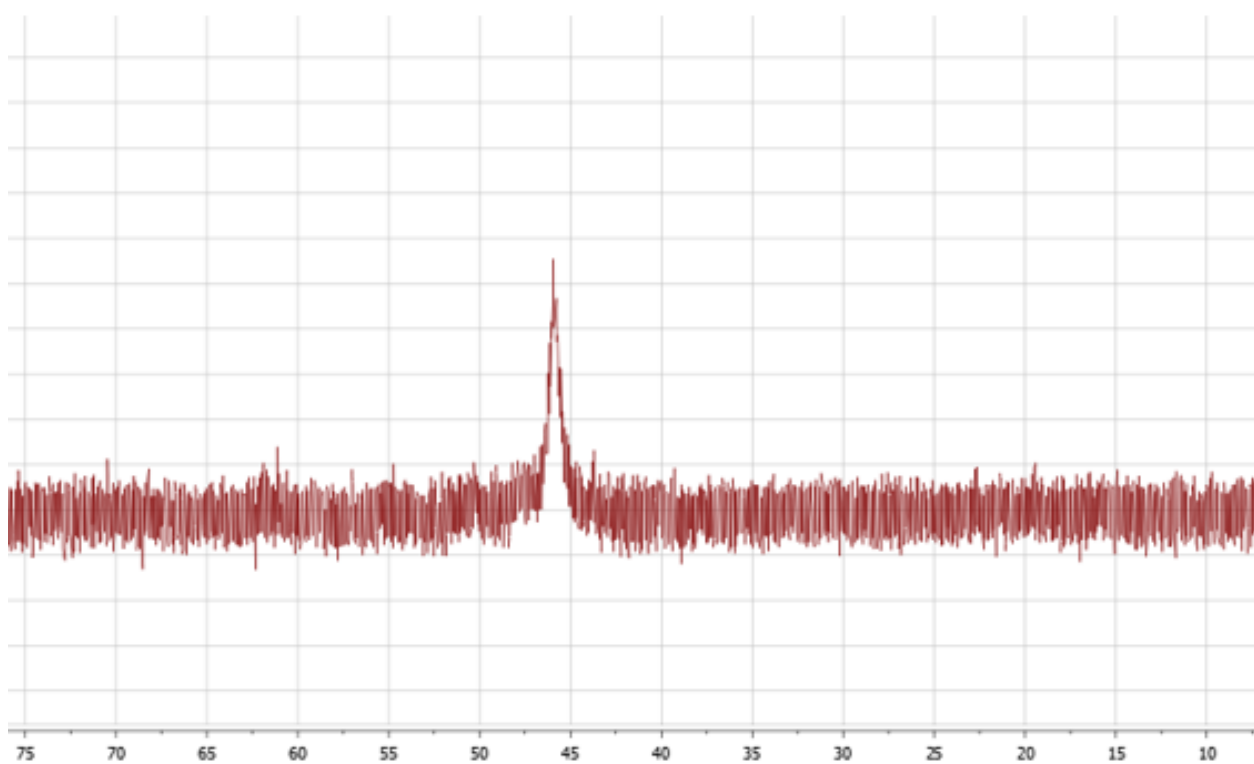


**Figure 4.15:** <sup>31</sup>P-NMR spectra of (**4-6**)



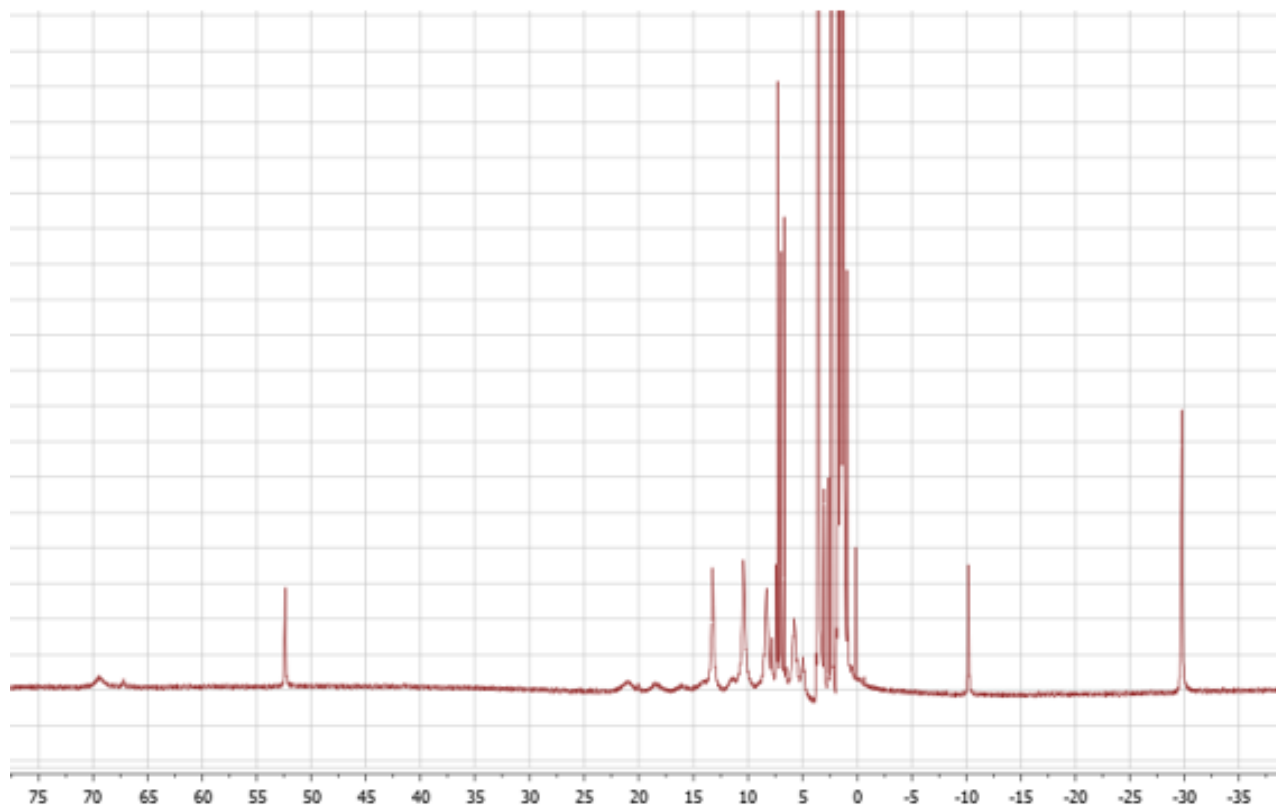


**Figure 4.16:** <sup>1</sup>H-NMR spectra of (4-6)

The loss of the proton on the ligand was not expected as no base was added to the reaction mixture. This could be explained by upon coordination a hydrogen atom is lost from the ligand. This could then couple with another hydrogen atom releasing H<sub>2</sub> from the reaction. The full mechanism of this proposed pathway has not been explored as of yet.

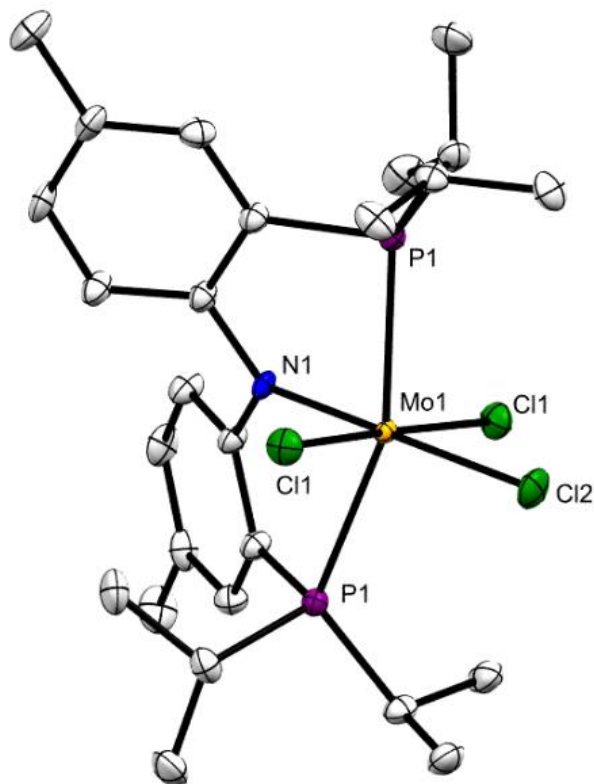


**Figure 4.17** ORTEP representation (50% probability ellipsoids) of the structure of **(4-6)** determined by X-ray diffraction; hydrogen atoms omitted for clarity.

Single crystal X-Ray diffraction studies confirmed the structure of the (*i*PrPNP)Mo(IV) complex. The Mo-Cl bonds were found to be 2.38 and 2.4 Å. The loss of the hydrogen atom on the ligand is consistent with the structure observed. The C-N-C angle is a 118.6° consistent with the two C-N bonds and the N-Mo bond being in the same plane in a trigonal planar geometry. A protonated nitrogen would cause the geometry around the nitrogen atom to be tetrahedral, thus those three bonds would not be in the same plane.

## 4.4 Experimental

### 4.4.1 General Information

All procedures involving organometallic compounds were conducted under an argon atmosphere using standard glovebox and Schlenk techniques. Solvents were purchased as anhydrous grade and purged with argon before use. Deuterated solvents (*p*-xylene- $d_{10}$ , toluene- $d_8$ , benzene- $d_6$ , THF- $d_8$ ) were degassed via freeze-pump-thaw cycles and dried over activated  $Al_2O_3$  and stored on 3 Å molecular sieves prior to use. Ethylene, Nitrogen and carbon monoxide was purchased from various suppliers in the highest purity available and used as received.  $^1H$  and  $^{31}P$  NMR spectra were recorded on 400 MHz and 500 MHz Varian spectrometers. Chemical shifts are reported in ppm.  $^1H$  NMR signals are referenced to the residual solvent signals, and  $^{31}P$  NMR signals are referenced to an external standard of 85%  $H_3PO_4$ . X-Ray diffraction was obtained from an oil coated crystal mounted on a glass fiber. The  $^{tBu}_4PNP$  ligand was synthesized according to a method published by Milstein.<sup>45</sup> Ozerov ( $^{iPr}PNP$ ) and Peters ( $^{iPr}PPP$ ) ligands were synthesized following literature procedure.<sup>43-44</sup> 2-bromo-1,3-bis(bromomethyl)benzene was synthesized following literature procedure.<sup>47</sup>

For all complexes, X-ray diffraction data were collected on a Bruker Smart APEX CCD diffractometer with graphite mono-chromatized  $MoK\alpha$  radiation ( $\lambda = 0.71073\text{\AA}$ ) at a temperature of 100 K or 120 K. Crystals were immersed in Paratone oil and placed on a glass needle or nylon loop. The data were corrected for Lorentz effects, polarization, and absorption, the latter by a multiscan (SADABS) method.<sup>51</sup> The structures were solved by

direct methods (SHELXS86).<sup>S2</sup> All non-hydrogen atoms were refined (SHELXL97)<sup>3</sup> based upon  $F_{\text{obs}}$ .<sup>S3</sup> All hydrogen atom coordinates were calculated with idealized geometries (SHELXL97). Scattering factors ( $f_0$ ,  $f'$ ,  $f''$ ) are as described in SHELXL97.

#### 4.4.2 Computational analysis of N<sub>2</sub> cleavage: Thermodynamics

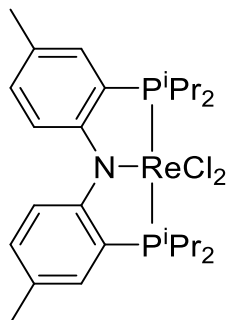
**Table 4.2: Full Table**

<b>G(2M+2N<sub>2</sub>)=0.0</b>						
<b>SPECIES</b>	<b>n</b>	<b>Ox. state</b>	<b>d e-'s</b>	<b>2* M-N<sub>2</sub></b>	<b>2 MN + N<sub>2</sub></b>	<b>Rxn: 2 M-N<sub>2</sub> = 2 MN + N<sub>2</sub></b>
( <sup>t</sup> BuPOCOP)MoI	0	2	4	3.4	-32.0	-35
( <sup>t</sup> BuPOCOP)MoI <sup>-</sup> anion	-1	1	5	-15.4	-56.2	-41
( <sup>t</sup> BuPONOP)MoI	0	1	5	-6.8	-49.0	-42
(MACHO)Ru	0	1	7	-41.2	8.0	49
(MACHO)Os	0	1	7	-50.2	-20.8	29
(MACHO)TcCl	0	2	5	5.8	-24.0	-30
(MACHO)ReCl	0	2	5	-13.4	-56.6	-43
( <sup>t</sup> BuPCP)Ru	0	1	7	-47.0	30.8	78
( <sup>t</sup> BuPCP)Os	0	1	7	-49.6	6.8	56
( <sup>t</sup> BuPCP)TcCl	0	2	5	9.4	-14.6	-24
( <sup>t</sup> BuPCP)ReCl	0	2	5	-5.2	-53.0	-48
(Phebox)Ru	0	1	7	-3.6	48.2	52
(Phebox)Os	0	1	7	-31.8	23.8	56
(Phebox)TcCl	0	2	5	-8.0	-20.0	-12
(Phebox)ReCl	0	2	5	-17.2	-39.2	-22
(MACHO-H <sup>+</sup> )Ru	1	1	7	-48.4	12.6	61
(MACHO-H <sup>+</sup> )Os	1	1	7	-63.4	-27.8	36
(MACHO-H <sup>+</sup> )TcCl	1	2	5	10.8	-16.4	-27
(MACHO-H <sup>+</sup> )ReCl	1	2	5	-5.4	-48.0	-43
(MACHO-H <sup>•</sup> )Ru	0	1	7	-67.0	14.2	81
(MACHO-H <sup>•</sup> )Os	0	1	7	-73.4	-7.8	66
(MACHO-H <sup>•</sup> )TcCl	0	2	5	-24.4	-6.8	18
(MACHO-H <sup>•</sup> )ReCl	0	2	5	-39.4	-49.4	-10
(imine-PNP)Ru	1	1	7	-47.0	22.4	69

(imine-PNP)Os	1	1	7	-58.4	-13.6	45
(imine-PNP)TcCl	1	2	5	9.2	-10.4	-20
(imine-PNP)ReCl	1	2	5	-5.2	-40.6	-35
(PpyNP)Ru	0	0	8	-36.0	44.0	80
(PpyNP)Os	0	0	8	-37.2	18.6	56
(PpyNP)TcCl	0	1	6	7.2	-21.2	-28
(PpyNP)ReCl	0	1	6	-7.6	-51.8	-44
(macho-PPP)Ru	0	1	7	-31.4	50.8	82
(macho-PPP)Os	0	1	7	-31.6	18.8	50
(macho-PPP)TcCl	0	2	5	26.0	-11.0	-37
(macho-PPP)ReCl	0	2	5	-0.6	-43.4	-43
(macho-PPP-H+)Ru	1	1	7	-27.0	60.8	88
(macho-PPP-H+)Os	1	1	7	-32.2	35.8	68
(macho-PPP-H+)TcCl	1	2	5	5.2	-5.2	-10
(macho-PPP-H+)ReCl	1	2	5	-8.8	-36.0	-27
(macho-PPP-H)Ru	0	0	8	-39.0	62.0	101
(macho-PPP-H)Os	0	0	8	-43.6	35.4	79
(macho-PPP-H)TcCl	0	1	6	-	-	-
(macho-PPP-H)ReCl	0	1	6	-55.4	-34.4	21
(Meeks)Ru	1	1	7	-	33.4	-
(Meeks)Os	1	1	7	-45.2	11.8	57
(Meeks)TcCl	1	2	5	15.8	-22.0	-38
(Meeks)ReCl	1	2	5	-3.0	-56.6	-54
(Oz-PNP)OsCl <sub>2</sub>	0	3	5	-14.5	39.3	54

#### 4.4.3 Synthesis of pincer-ligated metal halides

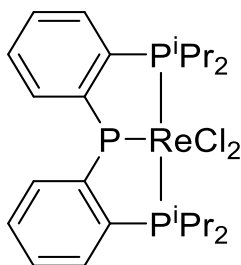
##### Attempted Synthesis of diaryl (<sup>i</sup>PrPNP)ReCl<sub>2</sub> (4-1)



(<sup>i</sup>PrPNP) Ligand (0.0057 g, 0.013 mmol) and Re(MeCN)(PPh<sub>3</sub>)Cl<sub>3</sub> (0.011 g, 0.013 mmol) were dissolved in THF (0.5 mL) resulting in an orange/yellow suspension which was transferred to a J. Young tube. Next trimethylamine (5.0 μL) was added and the solution began to turn purple. The solution was then heated to 70°C for 2 hours in which it turned dark purple and salt formation was observed. The solution was filtered and the solvent was removed leaving a purple residue.

<sup>1</sup>H-NMR (400 MHz, THF-d<sub>8</sub>) : Greater than 18 paramagnetic broad signals were observed between δ 0 and 80 ppm. <sup>31</sup>P-NMR{<sup>1</sup>H} (121 MHz, toluene-d<sub>8</sub>): δ No signals observed

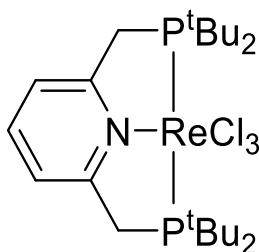
##### Attempted synthesis of (<sup>i</sup>PrPPP)ReCl<sub>2</sub> (4-2)



(<sup>i</sup>PrPPP) Ligand (0.0048 g, 0.011 mmol) and Re(MeCN)(PPh<sub>3</sub>)Cl<sub>3</sub> (0.010 g, 0.012 mmol) were dissolved in THF (0.5 mL) resulting in an orange/yellow suspension which was transferred to a J. Young tube. Next trimethylamine (5.0 μL) was added and the solution began to turn pinkish/red. The solution was then heated to 70°C for 2 hours in which salt formation and a color change to pinkish/red was observed. The solution was filtered and the solvent was removed leaving a red residue.

<sup>1</sup>H-NMR (400 MHz, THF-d<sub>8</sub>): Greater than 15 paramagnetic broad signals observed. <sup>31</sup>P-NMR{<sup>1</sup>H} (121 MHz, toluene-d<sub>8</sub>): δ No signals observed

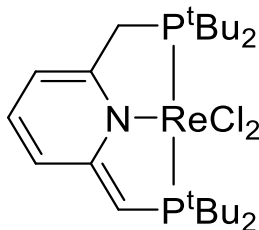
#### Synthesis of (<sup>t</sup>BuPNP)ReCl<sub>3</sub> (4-3)



(<sup>t</sup>BuPNP) Ligand (0.123g, 0.31 mmol) and Re(MeCN)(PPh<sub>3</sub>)Cl<sub>3</sub> (0.264 g, 0.31 mmol) were dissolved in THF (20 mL) resulting in an orange/yellow suspension. The suspension was then refluxed overnight giving a greenish/red solution. After cooling to room temperature the solvent was removed and the residue was redissolved in a small amount of CH<sub>2</sub>Cl<sub>2</sub> (2 mL). Next 15 mL of hexane was added crashing out a reddish/green solid. The solid was filtered and washed with hexane and then dried under vacuum.  
Yield 0.160 g (75%)

$^1\text{H-NMR}$  (400 MHz,  $\text{THF-d}_8$ ):  $\delta$  14.26 (d,  $J = 7.8$ , 2H, *m*-py), 7.04 (broad singlet, 36H, *t*-butyl), 0.89 (t,  $J = 6.8$ , 4H,  $\text{CH}_2\text{-P}$ ), 1.85 (m, 4H, isopropyl C-H), -11.94 (t,  $J = 7.7$ , 1H, *p*-py).

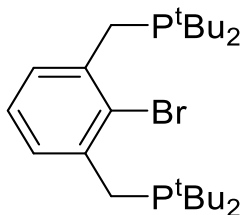
#### Synthesis of dearomatized ( $^t\text{BuPNP}$ ) $\text{ReCl}_2$ (4-4)



( $^t\text{BuPNP}$ ) $\text{ReCl}_3$  (0.054 g, 0.07 mmol) was dissolved in THF (0.5 mL) resulting in a rust red colored solution. Potassium tert-butoxide (0.0088 g, 0.07 mmol) was added, resulting the solution turning to a purple change. The solution was allowed to stir at room temperature for 3 hours. The solvent was then removed and the residue was redissolved in a small amount of  $\text{THF-d}_8$ .

$^1\text{H-NMR}$  (400 MHz,  $\text{THF-d}_8$ ):  $\delta$  4.63 (broad singlet, 1H, *p*-py), 3.19 (s, 1H, *t*-butyl), 1.93 (dd,  $J = 16.4$ , 12.5, 1H,  $\text{CH}_2\text{-P}$ ), 1.77 (d,  $J = 12.4$ , 1H,  $\text{CH-P}$ ), 1.56 (dd,  $J = 25.1$ , 12.2, 1H,  $\text{CH}_2\text{-P}$ ), 1-1.4 (broad signal, tert-butyl).

#### Synthesis of brominated $^t\text{BuPCP}$ ligand (4-5)

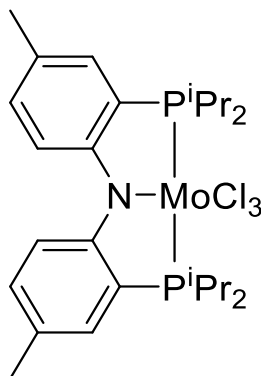




First, 2-bromo-1,3-bis(bromomethyl)benzene (0.256 g, 0.747 mmol) was dissolved in acetone (15 mL). Next di-tertbutylphosphine (0.27 mL, 1.49 mmol) was added to the clear solution dropwise. The solution was refluxed overnight with powdery white precipitate formed during the heating. The solution was cooled to room temperature and the solvent was removed. The white solid was then dissolved in benzene (15 mL) and trimethylamine (0.250 mL) was added. The solution was stirred for 3 hours and upon stirring formation of a crystalline solid was observed. The solution was filtered through a celite pad and the solvent was removed leaving a white powder. Yield 0.320 grams (90.8%).

$^1\text{H-NMR}$  (400 MHz, toluene- $d_8$ ):  $\delta$  7.69 (dd,  $J = 7.8, 2.7$ , 2H, *m-aryl*), 7.04 (t,  $J = 7.6$ , 1H, *p-aryl*), 3.12 (d,  $J = 2.6$ , 4H,  $\text{CH}_2$ ), 1.11 (d,  $J = 10.6$ , 36H, tert-butyl).  $^{31}\text{P-NMR}\{^1\text{H}\}$  (121 MHz, toluene- $d_8$ ):  $\delta$  33.6 (s,  $\text{P}^t\text{Bu}_2$ )

#### Synthesis of Ozerov-( $i\text{Pr}$ PNP) $\text{MoCl}_3$ (4-6)



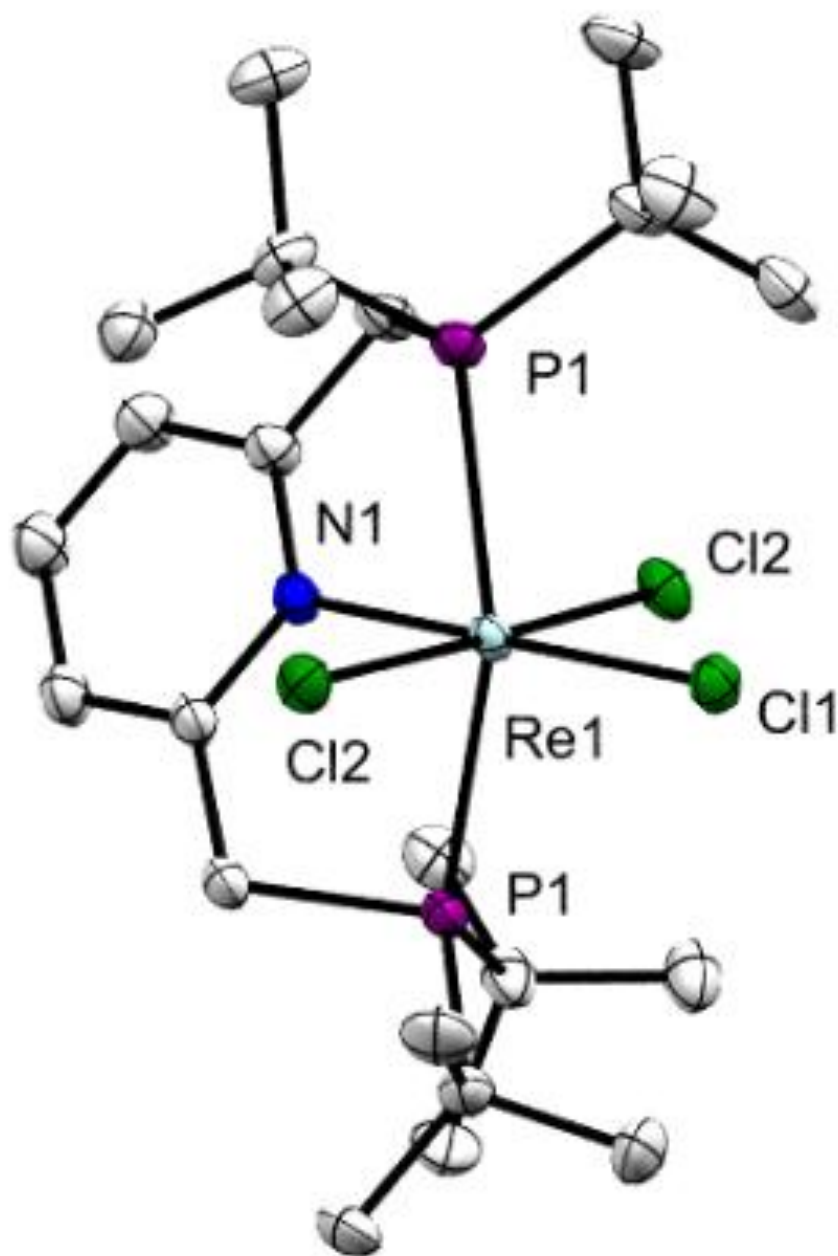
Ozerov-( $i\text{Pr}$ PNP) ligand (0.0104 g, 0.0264 mmol) was added to a J.Young tube and dissolved in 0.5 mL of THF (clear solution). Next  $\text{MoCl}_3(\text{THF})_3$  (0.0101 g, 0.0241 mmol) was added and the solution turned pink with some pink solid still visible in the tube. The

solution was then heated to 70°C for 1.5 hours resulting in the solution turning dark green/blue with some solid still visible. The solution was filtered through celite and the solid was washed with pentane and dried. A dark greenish/blue solid was obtained.

$^1\text{H}$ -NMR (400 MHz, THF- $\text{d}_8$ ): Complex was paramagnetic making identification of all signals difficult. Characteristic signals were as follows  $\delta$  69.3 (broad s), 52.4 (s), -10.2 (s), -29.8 (s).  $^{31}\text{P}$ -NMR{ $^1\text{H}$ } (121 MHz, THF- $\text{d}_8$ ):  $\delta$  45.9 (broad s,  $\text{P}^t\text{Bu}_2$ )

#### 4.4.4 Crystal Data

Figure 4.18: Structural data for complex  $(^t\text{BuPNP})\text{ReCl}_3$  (**4-3**)



ORTEP representation (50% probability ellipsoids) of complex  $(^t\text{BuPNP})\text{ReCl}_3$  (**4-3**) determined by X-ray diffraction. H atoms other than hydrides omitted.

Table 4.3. Crystal data and structure refinement for (<sup>t</sup>BuPNP)ReCl<sub>3</sub> (**4-3**)

Identification code	nick3cm_0m_a	
Empirical formula	C <sub>26.33</sub> H <sub>51</sub> Cl <sub>3</sub> N <sub>2</sub> Re	
Formula weight	736.17	
Temperature	120(2) K	
Wavelength	0.71073 Å	
Crystal system	Hexagonal	
Space group	P6 <sub>1</sub> 22	
Unit cell dimensions	a = 16.170(3) Å	a = 90.00(3)°.
	b = 16.170(3) Å	b = 90.00(3)°.
	c = 19.883(4) Å	g = 120.00(3)°.
Volume	4502.1(19) Å <sup>3</sup>	
Z	6	
Density (calculated)	1.629 Mg/m <sup>3</sup>	
Absorption coefficient	4.439 mm <sup>-1</sup>	
F(000)	2232	
Crystal size	0.410 x 0.090 x 0.080 mm <sup>3</sup>	
Theta range for data collection	1.454 to 32.610°.	
Index ranges	-24 ≤ h ≤ 24, -24 ≤ k ≤ 15, -29 ≤ l ≤ 30	
Reflections collected	53677	
Independent reflections	5496 [R(int) = 0.0604]	
Completeness to theta = 25.242°	99.9 %	
Absorption correction	Semi-empirical from equivalents	
Max. and min. transmission	0.7464 and 0.4873	
Refinement method	Full-matrix least-squares on F <sup>2</sup>	
Data / restraints / parameters	5496 / 148 / 224	
Goodness-of-fit on F <sup>2</sup>	1.093	
Final R indices [I > 2σ(I)]	R1 = 0.0217, wR2 = 0.0522	
R indices (all data)	R1 = 0.0242, wR2 = 0.0531	
Absolute structure parameter	-0.006(3)	
Extinction coefficient	n/a	
Largest diff. peak and hole	0.998 and -0.589 e.Å <sup>-3</sup>	

Table 4.4. Bond lengths [ $\text{\AA}$ ] and angles [ $^\circ$ ] for  $(^t\text{BuPNP})\text{ReCl}_3$  (**4-3**)

Re(1)-N(1)	2.108(3)	C(10)-H(10B)	0.9800
Re(1)-Cl(2)#1	2.3523(8)	C(10)-H(10C)	0.9800
Re(1)-Cl(2)	2.3523(8)	C(11)-H(11A)	0.9800
Re(1)-Cl(1)	2.4316(12)	C(11)-H(11B)	0.9800
Re(1)-P(1)#1	2.4700(10)	C(11)-H(11C)	0.9800
Re(1)-P(1)	2.4700(10)	C(12)-H(12A)	0.9800
P(1)-C(4)	1.851(3)	C(12)-H(12B)	0.9800
P(1)-C(9)	1.902(3)	C(12)-H(12C)	0.9800
P(1)-C(5)	1.908(4)	C(21)-C(24)#2	0.81(7)
N(1)-C(1)#1	1.367(3)	C(21)-C(24)#3	0.81(7)
N(1)-C(1)	1.367(4)	C(21)-C(25)#3	1.22(7)
C(1)-C(2)	1.383(5)	C(21)-C(25)#2	1.22(7)
C(1)-C(4)	1.506(5)	C(21)-C(22)	1.561(13)
C(2)-C(3)	1.382(4)	C(21)-C(22)#4	1.561(13)
C(2)-H(2)	0.9500	C(22)-C(25)#2	0.75(7)
C(3)-H(3)	0.9500	C(22)-C(24)#3	1.25(10)
C(4)-H(4A)	0.9900	C(22)-C(24)#2	1.51(5)
C(4)-H(4B)	0.9900	C(22)-C(23)	1.547(13)
C(5)-C(6)	1.531(5)	C(22)-C(23)#3	1.80(11)
C(5)-C(8)	1.537(5)	C(22)-C(23)#2	1.95(2)
C(5)-C(7)	1.538(5)	C(22)-C(22)#4	2.02(11)
C(6)-H(6A)	0.9800	C(23)-C(25)#2	1.34(6)
C(6)-H(6B)	0.9800	C(23)-C(24)	1.550(14)
C(6)-H(6C)	0.9800	C(23)-C(25)#5	1.69(9)
C(7)-H(7A)	0.9800	C(24)-C(25)#5	0.77(12)
C(7)-H(7B)	0.9800	C(24)-C(24)#5	1.28(14)
C(7)-H(7C)	0.9800	C(24)-C(25)	1.565(13)
C(8)-H(8A)	0.9800	C(24)-C(25)#2	2.01(4)
C(8)-H(8B)	0.9800	C(25)-C(25)#6	1.83(16)
C(8)-H(8C)	0.9800	C(31)-C(34)#2	0.88(5)
C(9)-C(10)	1.528(6)	C(31)-C(35)#2	1.03(7)
C(9)-C(12)	1.528(5)	C(31)-C(34)#6	1.31(5)
C(9)-C(11)	1.544(5)	C(31)-C(31)#6	1.41(10)
C(10)-H(10A)	0.9800	C(31)-C(32)	1.554(14)

C(31)-C(32)#6	1.60(5)	N(1)-C(1)-C(4)	118.3(3)
C(31)-C(33)#2	1.69(7)	C(2)-C(1)-C(4)	121.2(3)
C(32)-C(32)#6	0.68(11)	C(3)-C(2)-C(1)	120.2(3)
C(32)-C(33)	1.562(13)	C(3)-C(2)-H(2)	119.9
C(32)-C(33)#2	1.96(3)	C(1)-C(2)-H(2)	119.9
C(33)-C(34)#7	1.556(13)	C(2)#1-C(3)-C(2)	119.0(4)
C(33)-C(34)	1.556(13)	C(2)#1-C(3)-H(3)	120.5
C(34)-C(34)#7	0.45(5)	C(2)-C(3)-H(3)	120.5
C(34)-C(35)	1.542(13)	C(1)-C(4)-P(1)	110.3(2)
C(34)-C(35)#2	1.975(19)	C(1)-C(4)-H(4A)	109.6
		P(1)-C(4)-H(4A)	109.6
N(1)-Re(1)-Cl(2)#1	88.18(2)	C(1)-C(4)-H(4B)	109.6
N(1)-Re(1)-Cl(2)	88.18(2)	P(1)-C(4)-H(4B)	109.6
Cl(2)#1-Re(1)-Cl(2)	176.36(4)	H(4A)-C(4)-H(4B)	108.1
N(1)-Re(1)-Cl(1)	180.0	C(6)-C(5)-C(8)	106.9(3)
Cl(2)#1-Re(1)-Cl(1)	91.82(2)	C(6)-C(5)-C(7)	108.3(3)
Cl(2)-Re(1)-Cl(1)	91.82(2)	C(8)-C(5)-C(7)	108.5(3)
N(1)-Re(1)-P(1)#1	79.922(19)	C(6)-C(5)-P(1)	108.9(2)
Cl(2)#1-Re(1)-P(1)#1	90.46(3)	C(8)-C(5)-P(1)	112.7(3)
Cl(2)-Re(1)-P(1)#1	88.90(3)	C(7)-C(5)-P(1)	111.4(2)
Cl(1)-Re(1)-P(1)#1	100.08(2)	C(5)-C(6)-H(6A)	109.5
N(1)-Re(1)-P(1)	79.921(19)	C(5)-C(6)-H(6B)	109.5
Cl(2)#1-Re(1)-P(1)	88.90(3)	H(6A)-C(6)-H(6B)	109.5
Cl(2)-Re(1)-P(1)	90.46(3)	C(5)-C(6)-H(6C)	109.5
Cl(1)-Re(1)-P(1)	100.079(19)	H(6A)-C(6)-H(6C)	109.5
P(1)#1-Re(1)-P(1)	159.84(4)	H(6B)-C(6)-H(6C)	109.5
C(4)-P(1)-C(9)	105.97(15)	C(5)-C(7)-H(7A)	109.5
C(4)-P(1)-C(5)	101.88(16)	C(5)-C(7)-H(7B)	109.5
C(9)-P(1)-C(5)	109.61(18)	H(7A)-C(7)-H(7B)	109.5
C(4)-P(1)-Re(1)	93.63(11)	C(5)-C(7)-H(7C)	109.5
C(9)-P(1)-Re(1)	120.35(13)	H(7A)-C(7)-H(7C)	109.5
C(5)-P(1)-Re(1)	120.63(12)	H(7B)-C(7)-H(7C)	109.5
C(1)#1-N(1)-C(1)	119.7(4)	C(5)-C(8)-H(8A)	109.5
C(1)#1-N(1)-Re(1)	120.13(19)	C(5)-C(8)-H(8B)	109.5
C(1)-N(1)-Re(1)	120.13(18)	H(8A)-C(8)-H(8B)	109.5
N(1)-C(1)-C(2)	120.5(3)	C(5)-C(8)-H(8C)	109.5

H(8A)-C(8)-H(8C)	109.5	C(24)#2-C(21)-C(22)#4	53(7)
H(8B)-C(8)-H(8C)	109.5	C(24)#3-C(21)-C(22)#4	71(4)
C(10)-C(9)-C(12)	107.2(3)	C(25)#3-C(21)-C(22)#4	28(3)
C(10)-C(9)-C(11)	107.5(3)	C(25)#2-C(21)-C(22)#4	95(6)
C(12)-C(9)-C(11)	110.4(3)	C(22)-C(21)-C(22)#4	81(5)
C(10)-C(9)-P(1)	109.9(3)	C(25)#2-C(22)-C(24)#3	35(7)
C(12)-C(9)-P(1)	107.8(3)	C(25)#2-C(22)-C(24)#2	80(5)
C(11)-C(9)-P(1)	114.0(3)	C(24)#3-C(22)-C(24)#2	54(6)
C(9)-C(10)-H(10A)	109.5	C(25)#2-C(22)-C(23)	60(5)
C(9)-C(10)-H(10B)	109.5	C(24)#3-C(22)-C(23)	93(3)
H(10A)-C(10)-H(10B)	109.5	C(24)#2-C(22)-C(23)	136(3)
C(9)-C(10)-H(10C)	109.5	C(25)#2-C(22)-C(21)	50(4)
H(10A)-C(10)-H(10C)	109.5	C(24)#3-C(22)-C(21)	31(3)
H(10B)-C(10)-H(10C)	109.5	C(24)#2-C(22)-C(21)	30(3)
C(9)-C(11)-H(11A)	109.5	C(23)-C(22)-C(21)	106.9(13)
C(9)-C(11)-H(11B)	109.5	C(25)#2-C(22)-C(23)#3	70(10)
H(11A)-C(11)-H(11B)	109.5	C(24)#3-C(22)-C(23)#3	58(4)
C(9)-C(11)-H(11C)	109.5	C(24)#2-C(22)-C(23)#3	96(6)
H(11A)-C(11)-H(11C)	109.5	C(23)-C(22)-C(23)#3	88(3)
H(11B)-C(11)-H(11C)	109.5	C(21)-C(22)-C(23)#3	87(4)
C(9)-C(12)-H(12A)	109.5	C(25)#2-C(22)-C(23)#2	131(5)
C(9)-C(12)-H(12B)	109.5	C(24)#3-C(22)-C(23)#2	99(4)
H(12A)-C(12)-H(12B)	109.5	C(24)#2-C(22)-C(23)#2	51.4(6)
C(9)-C(12)-H(12C)	109.5	C(23)-C(22)-C(23)#2	167(3)
H(12A)-C(12)-H(12C)	109.5	C(21)-C(22)-C(23)#2	82(3)
H(12B)-C(12)-H(12C)	109.5	C(23)#3-C(22)-C(23)#2	102(3)
C(24)#2-C(21)-C(24)#3	105(10)	C(25)#2-C(22)-C(22)#4	83(9)
C(24)#2-C(21)-C(25)#3	38(8)	C(24)#3-C(22)-C(22)#4	48(4)
C(24)#3-C(21)-C(25)#3	99(7)	C(24)#2-C(22)-C(22)#4	38(4)
C(24)#2-C(21)-C(25)#2	99(7)	C(23)-C(22)-C(22)#4	139(4)
C(24)#3-C(21)-C(25)#2	38(8)	C(21)-C(22)-C(22)#4	50(3)
C(25)#3-C(21)-C(25)#2	117(9)	C(23)#3-C(22)-C(22)#4	61(3)
C(24)#2-C(21)-C(22)	71(4)	C(23)#2-C(22)-C(22)#4	54(3)
C(24)#3-C(21)-C(22)	53(7)	C(25)#2-C(23)-C(22)	29(3)
C(25)#3-C(21)-C(22)	95(6)	C(25)#2-C(23)-C(24)	88(4)
C(25)#2-C(21)-C(22)	28(3)	C(22)-C(23)-C(24)	107.6(13)

C(25)#2-C(23)-C(25)#5	73(5)	C(24)#5-C(24)-C(25)#2	152(7)
C(22)-C(23)-C(25)#5	85(4)	C(22)#8-C(24)-C(25)#2	121(4)
C(24)-C(23)-C(25)#5	27(4)	C(23)-C(24)-C(25)#2	42(3)
C(25)#2-C(23)-C(22)#3	87(7)	C(25)-C(24)-C(25)#2	149(3)
C(22)-C(23)-C(22)#3	88(4)	C(22)#8-C(25)-C(24)#5	111(10)
C(24)-C(23)-C(22)#3	43(4)	C(22)#8-C(25)-C(21)#8	102(3)
C(25)#5-C(23)-C(22)#3	24(3)	C(24)#5-C(25)-C(21)#8	40(6)
C(25)#2-C(23)-C(22)#8	137(4)	C(22)#8-C(25)-C(23)#8	91(7)
C(22)-C(23)-C(22)#8	153(3)	C(24)#5-C(25)-C(23)#8	151(10)
C(24)-C(23)-C(22)#8	49(2)	C(21)#8-C(25)-C(23)#8	154(10)
C(25)#5-C(23)-C(22)#8	69(3)	C(22)#8-C(25)-C(24)	72(3)
C(22)#3-C(23)-C(22)#8	65(3)	C(24)#5-C(25)-C(24)	54(10)
C(25)#5-C(24)-C(21)#8	102(10)	C(21)#8-C(25)-C(24)	31(3)
C(25)#5-C(24)-C(22)#3	34(6)	C(23)#8-C(25)-C(24)	154(8)
C(21)#8-C(24)-C(22)#3	96(9)	C(22)#8-C(25)-C(23)#5	86(10)
C(25)#5-C(24)-C(24)#5	96(10)	C(24)#5-C(25)-C(23)#5	66(7)
C(21)#8-C(24)-C(24)#5	37(6)	C(21)#8-C(25)-C(23)#5	104(6)
C(22)#3-C(24)-C(24)#5	73(8)	C(23)#8-C(25)-C(23)#5	99(7)
C(25)#5-C(24)-C(22)#8	127(10)	C(24)-C(25)-C(23)#5	98(6)
C(21)#8-C(24)-C(22)#8	79(3)	C(22)#8-C(25)-C(25)#6	110(9)
C(22)#3-C(24)-C(22)#8	94(7)	C(24)#5-C(25)-C(25)#6	92(10)
C(24)#5-C(24)-C(22)#8	53(3)	C(21)#8-C(25)-C(25)#6	130(7)
C(25)#5-C(24)-C(23)	87(7)	C(23)#8-C(25)-C(25)#6	63(3)
C(21)#8-C(24)-C(23)	157(6)	C(24)-C(25)-C(25)#6	141(9)
C(22)#3-C(24)-C(23)	79(6)	C(23)#5-C(25)-C(25)#6	45(5)
C(24)#5-C(24)-C(23)	121(3)	C(22)#8-C(25)-C(24)#8	124(7)
C(22)#8-C(24)-C(23)	79(2)	C(24)#5-C(25)-C(24)#8	101(10)
C(25)#5-C(24)-C(25)	123(10)	C(21)#8-C(25)-C(24)#8	131(5)
C(21)#8-C(24)-C(25)	51(5)	C(23)#8-C(25)-C(24)#8	50.5(13)
C(22)#3-C(24)-C(25)	94(6)	C(24)-C(25)-C(24)#8	155(7)
C(24)#5-C(24)-C(25)	29(6)	C(23)#5-C(25)-C(24)#8	67(4)
C(22)#8-C(24)-C(25)	28(2)	C(25)#6-C(25)-C(24)#8	23(4)
C(23)-C(24)-C(25)	106.7(13)	C(34)#2-C(31)-C(35)#2	107(8)
C(25)#5-C(24)-C(25)#2	65(10)	C(34)#2-C(31)-C(31)#6	141(10)
C(21)#8-C(24)-C(25)#2	161(6)	C(35)#2-C(31)-C(31)#6	47(2)
C(22)#3-C(24)-C(25)#2	81(5)	C(34)#6-C(31)-C(31)#6	146(9)



C(34)#2-C(31)-C(32)	137(6)	C(34)#7-C(34)-C(35)	162(10)
C(35)#2-C(31)-C(32)	111(3)	C(31)#8-C(34)-C(35)	40(5)
C(34)#6-C(31)-C(32)	130(4)	C(31)#6-C(34)-C(35)	154(7)
C(31)#6-C(31)-C(32)	65(2)	C(34)#7-C(34)-C(33)	81.7(9)
C(32)#6-C(32)-C(31)	81(3)	C(31)#8-C(34)-C(33)	83(5)
C(32)#6-C(32)-C(33)	117(7)	C(31)#6-C(34)-C(33)	72(3)
C(31)-C(32)-C(33)	106.4(12)	C(35)-C(34)-C(33)	107.0(12)
C(32)#6-C(32)-C(31)#6	74(5)	C(34)#7-C(34)-C(35)#2	14(10)
C(31)-C(32)-C(31)#6	53(4)	C(31)#8-C(34)-C(35)#2	151(10)
C(33)-C(32)-C(31)#6	65(2)	C(31)#6-C(34)-C(35)#2	28(3)
C(34)#7-C(33)-C(34)	16.6(19)	C(35)-C(34)-C(35)#2	164(2)
C(34)#7-C(33)-C(32)	90(3)	C(33)-C(34)-C(35)#2	88.9(7)
C(34)-C(33)-C(32)	105.9(12)	C(31)#8-C(35)-C(34)	33(3)
C(32)#7-C(33)-C(32)	164(3)	C(31)#7-C(35)-C(34)	113.3(19)
C(34)#7-C(33)-C(31)#6	31(2)	C(31)#8-C(35)-C(34)#7	37(2)
C(34)-C(33)-C(31)#6	47.2(17)	C(31)#7-C(35)-C(34)#7	116.1(18)
C(32)#7-C(33)-C(31)#6	137(2)	C(34)-C(35)-C(34)#7	4(5)
C(32)-C(33)-C(31)#6	58.7(15)	C(34)#9-C(35)-C(34)#7	148.0(17)
C(34)#7-C(34)-C(31)#6	15(10)	C(34)#8-C(35)-C(34)#7	152(3)
C(31)#8-C(34)-C(31)#6	154(8)		

---

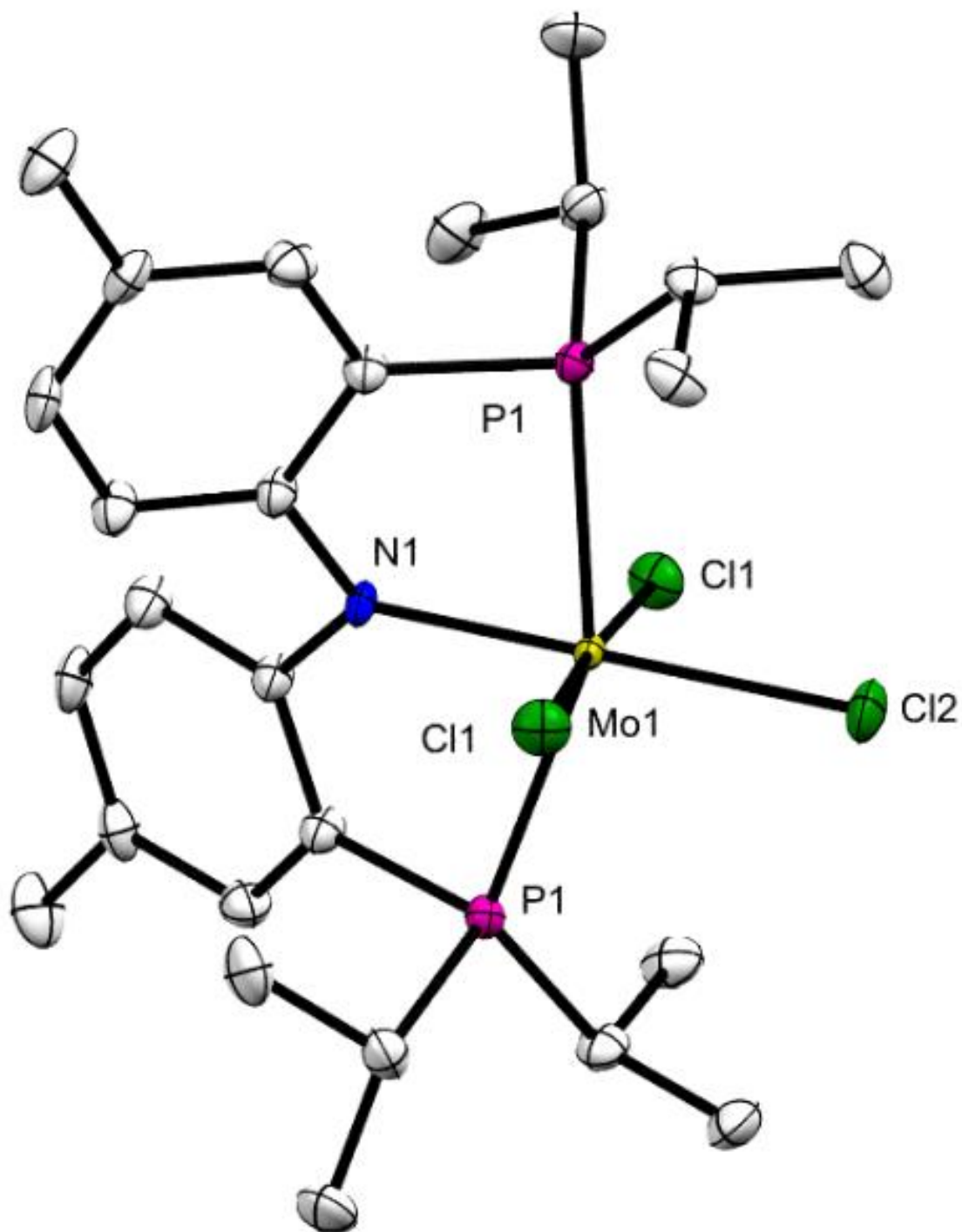
Symmetry transformations used to generate equivalent atoms:

#1 -x+y,y,-z+3/2 #2 y-1,-x+y,z-1/6 #3 x,x-y+2,-z+7/6

#4 x-y+1,-y+2,-z+1 #5 y-1,x+1,-z+4/3 #6 -x+y-1,y,-z+3/2

#7 -x,-x+y,-z+5/3 #8 x-y+1,x+1,z+1/6 #9 -y+1,-x+1,-z+11/6

Figure 4.19: Structural data for complex Ozerov-(<sup>t</sup>BuPNP)MoCl<sub>3</sub> (**4-6**)



ORTEP representation (50% probability ellipsoids) of complex Ozerov-(<sup>i</sup>PrPNP)MoCl<sub>3</sub> (**4-6**) determined by X-ray diffraction. H atoms other than hydrides omitted.

Table 4.5. Crystal data and structure refinement for (*i*PrPNP)MoCl<sub>3</sub> (4-6)

Identification code	nickblack_P21n_a	
Empirical formula	C <sub>26</sub> H <sub>40</sub> Cl <sub>3</sub> Mo N P <sub>2</sub>	
Formula weight	630.82	
Temperature	120(2) K	
Wavelength	0.71073 Å	
Crystal system	Monoclinic	
Space group	P2/n	
Unit cell dimensions	a = 11.4519(7) Å	a = 90°.
	b = 9.5946(6) Å	b = 98.8120(10)°.
	c = 13.0527(8) Å	g = 90°.
Volume	1417.25(15) Å <sup>3</sup>	
Z	2	
Density (calculated)	1.478 Mg/m <sup>3</sup>	
Absorption coefficient	0.875 mm <sup>-1</sup>	
F(000)	652	
Crystal size	0.250 x 0.120 x 0.050 mm <sup>3</sup>	
Theta range for data collection	2.123 to 30.034°.	
Index ranges	-16 ≤ h ≤ 16, -13 ≤ k ≤ 13, -18 ≤ l ≤ 18	
Reflections collected	14658	
Independent reflections	4152 [R(int) = 0.0822]	
Completeness to theta = 25.242°	100.0 %	
Absorption correction	Semi-empirical from equivalents	
Max. and min. transmission	0.7460 and 0.6133	
Refinement method	Full-matrix least-squares on F <sup>2</sup>	
Data / restraints / parameters	4152 / 0 / 155	
Goodness-of-fit on F <sup>2</sup>	1.049	
Final R indices [I > 2σ(I)]	R1 = 0.0510, wR2 = 0.1127	
R indices (all data)	R1 = 0.0687, wR2 = 0.1202	
Extinction coefficient	n/a	
Largest diff. peak and hole	1.570 and -0.941 e.Å <sup>-3</sup>	

Table 4.6. Bond lengths [Å] and angles [°] for (*i*PrPNP)MoCl<sub>3</sub>.

Mo(1)-N(1)	2.000(4)	C(11)-C(12)	1.537(5)
Mo(1)-Cl(1)	2.3761(8)	C(11)-H(11)	1.0000
Mo(1)-Cl(1)#1	2.3761(8)	C(12)-H(12A)	0.9800
Mo(1)-Cl(2)	2.4015(12)	C(12)-H(12B)	0.9800
Mo(1)-P(1)	2.5308(8)	C(12)-H(12C)	0.9800
Mo(1)-P(1)#1	2.5308(8)	C(13)-H(13A)	0.9800
P(1)-C(2)	1.821(3)	C(13)-H(13B)	0.9800
P(1)-C(8)	1.844(3)	C(13)-H(13C)	0.9800
P(1)-C(11)	1.853(3)		
N(1)-C(1)	1.437(4)	N(1)-Mo(1)-Cl(1)	91.78(2)
N(1)-C(1)#1	1.437(4)	N(1)-Mo(1)-Cl(1)#1	91.78(2)
C(1)-C(6)	1.392(5)	Cl(1)-Mo(1)-Cl(1)#1	176.44(4)
C(1)-C(2)	1.406(4)	N(1)-Mo(1)-Cl(2)	180.0
C(2)-C(3)	1.395(4)	Cl(1)-Mo(1)-Cl(2)	88.22(2)
C(3)-C(4)	1.398(5)	Cl(1)#1-Mo(1)-Cl(2)	88.22(2)
C(3)-H(3)	0.9500	N(1)-Mo(1)-P(1)	78.12(2)
C(4)-C(5)	1.386(5)	Cl(1)-Mo(1)-P(1)	89.50(3)
C(4)-C(7)	1.512(5)	Cl(1)#1-Mo(1)-P(1)	91.23(3)
C(5)-C(6)	1.406(5)	Cl(2)-Mo(1)-P(1)	101.88(2)
C(5)-H(5)	0.9500	N(1)-Mo(1)-P(1)#1	78.12(2)
C(6)-H(6)	0.9500	Cl(1)-Mo(1)-P(1)#1	91.23(3)
C(7)-H(7A)	0.9800	Cl(1)#1-Mo(1)-P(1)#1	89.50(3)
C(7)-H(7B)	0.9800	Cl(2)-Mo(1)-P(1)#1	101.88(2)
C(7)-H(7C)	0.9800	P(1)-Mo(1)-P(1)#1	156.24(4)
C(8)-C(10)	1.513(5)	C(2)-P(1)-C(8)	109.19(15)
C(8)-C(9)	1.535(5)	C(2)-P(1)-C(11)	104.39(15)
C(8)-H(8)	1.0000	C(8)-P(1)-C(11)	105.12(16)
C(9)-H(9A)	0.9800	C(2)-P(1)-Mo(1)	94.83(11)
C(9)-H(9B)	0.9800	C(8)-P(1)-Mo(1)	122.18(11)
C(9)-H(9C)	0.9800	C(11)-P(1)-Mo(1)	118.88(12)
C(10)-H(10A)	0.9800	C(1)-N(1)-C(1)#1	118.6(3)
C(10)-H(10B)	0.9800	C(1)-N(1)-Mo(1)	120.70(17)
C(10)-H(10C)	0.9800	C(1)#1-N(1)-Mo(1)	120.70(17)
C(11)-C(13)	1.520(5)	C(6)-C(1)-C(2)	119.4(3)

C(6)-C(1)-N(1)	122.4(3)	C(8)-C(9)-H(9B)	109.5
C(2)-C(1)-N(1)	118.1(3)	H(9A)-C(9)-H(9B)	109.5
C(3)-C(2)-C(1)	119.8(3)	C(8)-C(9)-H(9C)	109.5
C(3)-C(2)-P(1)	125.0(3)	H(9A)-C(9)-H(9C)	109.5
C(1)-C(2)-P(1)	115.2(2)	H(9B)-C(9)-H(9C)	109.5
C(2)-C(3)-C(4)	121.5(3)	C(8)-C(10)-H(10A)	109.5
C(2)-C(3)-H(3)	119.2	C(8)-C(10)-H(10B)	109.5
C(4)-C(3)-H(3)	119.2	H(10A)-C(10)-H(10B)	109.5
C(5)-C(4)-C(3)	117.8(3)	C(8)-C(10)-H(10C)	109.5
C(5)-C(4)-C(7)	120.9(3)	H(10A)-C(10)-H(10C)	109.5
C(3)-C(4)-C(7)	121.3(3)	H(10B)-C(10)-H(10C)	109.5
C(4)-C(5)-C(6)	122.0(3)	C(13)-C(11)-C(12)	109.7(3)
C(4)-C(5)-H(5)	119.0	C(13)-C(11)-P(1)	111.2(2)
C(6)-C(5)-H(5)	119.0	C(12)-C(11)-P(1)	113.7(3)
C(1)-C(6)-C(5)	119.4(3)	C(13)-C(11)-H(11)	107.3
C(1)-C(6)-H(6)	120.3	C(12)-C(11)-H(11)	107.3
C(5)-C(6)-H(6)	120.3	P(1)-C(11)-H(11)	107.3
C(4)-C(7)-H(7A)	109.5	C(11)-C(12)-H(12A)	109.5
C(4)-C(7)-H(7B)	109.5	C(11)-C(12)-H(12B)	109.5
H(7A)-C(7)-H(7B)	109.5	H(12A)-C(12)-H(12B)	109.5
C(4)-C(7)-H(7C)	109.5	C(11)-C(12)-H(12C)	109.5
H(7A)-C(7)-H(7C)	109.5	H(12A)-C(12)-H(12C)	109.5
H(7B)-C(7)-H(7C)	109.5	H(12B)-C(12)-H(12C)	109.5
C(10)-C(8)-C(9)	111.2(3)	C(11)-C(13)-H(13A)	109.5
C(10)-C(8)-P(1)	113.6(2)	C(11)-C(13)-H(13B)	109.5
C(9)-C(8)-P(1)	107.8(2)	H(13A)-C(13)-H(13B)	109.5
C(10)-C(8)-H(8)	108.0	C(11)-C(13)-H(13C)	109.5
C(9)-C(8)-H(8)	108.0	H(13A)-C(13)-H(13C)	109.5
P(1)-C(8)-H(8)	108.0	H(13B)-C(13)-H(13C)	109.5
C(8)-C(9)-H(9A)	109.5		

---

Symmetry transformations used to generate equivalent atoms:

#1 -x+1/2,y,-z+1/2

#### 4.5 References:

1. Erisman, J.W.; Sutton, M.A.; Galloway, J.; Klimont, Z.; Winjwarter, W. "How a Century of Ammonia Synthesis Changed the World" *Nat. Geosci.* **2008**, *1*, 636
2. Smil, V. *Enriching the Earth: Fritz Haber, Carl Bosch, and the Transformation of World Food Production*; MIT Press: Cambridge, MA, 2004
3. Ashcraft, R.W.; Raman, S.; Green, W.H. "Ab Initio Aqueous Thermochemistry: Application to the Oxidation of Hydroxylamin in Nitric Acid Solution" *J. Phys. Chem. B.* **2007**, *111*, 11968.
4. Argonne National Laboratories ATcT enthalpies of formation based on version 1.118 of the Thermochemical Network, <http://atct.anl.gov/Thermochemical Data/version 1.118/index.php>
5. Peplow, M. "A fixation with nitrogen" *Chemistry World*, *48*, April 18, 2013. <http://www.rsc.org/chemistryworld/2013/04/nitrogen-fixation-ammonia-synthesis-haber-bosch>
6. Appl, M. "Ammonia" In *Ullmann's Encyclopedia of Industrial Chemistry*; Wiley-VCH Verlag GmbH & Co. KGaA, 2000 [http://dx.doi.org/10.1002/14356007.a02\\_143.pub2](http://dx.doi.org/10.1002/14356007.a02_143.pub2)
7. IPCC, 2014: Summary for Policymakers. In: *Climate Change 2014: Impacts, Adaptation and Vulnerability. Part A: Global and Sectoral Aspects. Contribution of Working Group 11 to the Fifth Assessment Report of the Intergovernmental Panel on Climate Change* Field, C.B., V.R. Barros, D.J. Jokken, K.J. Mach, M.D. Mastrandrea, T.E. Bilir, M. Chatterjee, K.L. Ebi, Y.O. Estrada, R.C. Genova, B. Girma, E.S. Kissel, A.N. Levy, S. MacCracken, P.R. Mastrandrea, and L.L. White, eds. Cambridge University Press, Cambridge. United Kingdom and New York, NY, USA, pp. 1-32.
8. Min, S-K.; Zhang, X.; Zwiers, F.W.; Hegerl, G.C. "Human contribution to more-intense precipitation extremes" *Nature* **2011**, *470*, 378-381.
9. Trenberth, K.E. "Changes in precipitation with climate change" *Clim. Res.* **2011**, *47*, 123.
10. Coumou, D.; Rahmstorf, S. "A decade of weather extremes" *Nature Clim. Change* **2012**, *2*, 491.
11. Dai, A. "Increasing drought under global warming in observations and models" *Nature Clim. Change* **2013**, *3*, 52-58.
12. Marvel, K.; Bonfils, C. "Identifying external influences on global precipitation" *Proc. Natl. Acad. Sci.* **2013**, *110*, 19301-19306.
13. Trenberth, K.E.; Dai, A.; van der Schrier, G.; Jones, P.D.; Barichivich, J.; Briffa, K.R.; Sheffield, J. "Global warming and changes in drought" *Nature Clim. Change* **2014**, *4*, 17-22.
14. "Climate Change and Agriculture in the United States: Effect and Adaptation" 2012. *Climate Change and Agriculture in the United States: Effects and Adaptation*. USDA Technical Bulletin. 1935. Washington, DC. 186 pages.
15. Lindley, B.M.; Appel, A.M.; Krogh-Jespersen, K.; Mayer, J.M.; Miller, A.J.M. "Evaluating the Thermodynamics of Electrocatalytic N<sub>2</sub> Reduction in Acetonitrile" *ACS Energy Letters* **2016**, 698-704.

16. Seefeldt, L.C.; Hoffman, B.M.; Dean, D.R. "Electron transfer in nitrogenase catalysis" *Curr. Op. Chem. Biol.* **2012**, *16*, 19-25.
17. *The Metal-Driven Biogeochemistry of Gaseous Compounds in the Environment*; Kroneck, P.M.H.; Sosa Torres, M.E., Eds.; Springer: Dordrecht, 2014.
18. Holland, P.L. "Nitrogen Fixation" In *Comprehensive Coordination Chemistry II*, McCleverty, J.; Meyer, T.J., Eds.: Elsevier, Oxford, 2004; Vol. 8, 569-599.
19. Yandulov, D.V.; Schrock, R.R. *Science* **2003**, *301*, 76-78.
20. Schrock, R.R. *Chem. Commun.* **2003**, 2389-2391.
21. Anderson, J.S.; Rittle, J.; Peters, J.C. *Nature* **2013**, *501*, 84-87.
22. Creutz, S.E.; Peters, J.C. *J. Am. Chem. Soc.* **2014**, *136*, 1105-1115.
23. Anderson, J.S.; Cutsail, G.E.; Rittle, J.; Connor, B.A.; Gunderson, W.A.; Zhang, L.; Hoffman, B.M.; Peters, J.C. *J. Am. Chem. Soc.* **2015**, *137*, 7803-7809.
24. Arashiba, K.; Miyake, Y.; Nishibayashi, Y. *Nature Chem.* **2011**, *3*, 120-125.
25. Kuriyama, S.; Arashiba, K.; Nakajima, K.; Tanaka, H.; Kamaru, N.; Yosizawa, K.; Nishibayashi, Y. *J. Am. Chem. Soc.* **2014**, *136*, 9719-9731.
26. Tanaka, H.; Arashiba, K.; Kuriyama, S.; Sasada, A.; Nakajima, K.; Yoshizawa, K.; Nishibayashi, Y. *Nat. Commun.* **2014**, *5*, 3737-3737.
27. Nishibayashi, Y. *Inorg. Chem.* **2015**, *54*, 9234-9247.
28. Arashiba, K.; Kinoshita, E.; Kuriyama, S.; Eizawa, A.; Nakajima, K.; Tanaka, H.; Yoshizawa, K.; Nishibayashi, Y. *J. Am. Chem. Soc.* **2015**, *137*, 5666-5669.
29. Tanaka, H.; Nishibayashi, Y.; Yoshizawa, K. *Acc. Chem. Res.* **2016**, *49*, 987-995.
30. Arashiba, K.; Eizawa, A.; Tanaka, H.; Nakajima, K.; Yoshizawa, K.; Nishibayashi, Y. *Bull. Chem. Soc. Jpn.* **2017**, *90*, 1111-1118.
31. Licht, S.; Cui, B.C.; Wang, B.H.; Li, F.F.; Lau, J.; Liu, S.Z. *Science* **2014**, *345*, 637-640.
32. Furuya, N.; Yoshiba, H. *J. Electroanal. Chem. Interfacial Electrochem.* **1989**, *263*, 171-174.
33. Furuya, N.; Yoshiba, H. *J. Electroanal. Chem. Interfacial Electrochem.* **1989**, *272*, 263-266.
34. Kordali, V.; Kyriacou, G.; Lambrou, C. *Chem. Commun.* **2000**, 1673-1674.
35. Pospisil, L.; Bulickova, J.; Hromadova, M.; Gal, M.; Civis, S.; Cihelka, J.; Tarabek, J. *Chem Commun.* **2007**, 2270-2272.
36. Pickett, C.J.; Talarmin, J. *Nature* **1985**, *317*, 652-653.
37. Pickett, C.J.; Talarmin, J. *J. Chem. Soc., Dalton Trans.* **1986**, 1453-1457.
38. Munisamy, T.; Schrock, R.R. *Dalton Trans.* **2012**, *41*, 130-137.
39. Del Castillo, T.J.; Thompson, N.B.; Peters, J.C. *J Am. Chem. Soc.* **2016**, *138*, 5341-5350.
40. Van der Ham, C.J.M.; Koper, M.T.M.; Hetterscheid, D.G.H. *Chem. Soc. Rev.* **2014**, *43*, 5183-5191.
41. Rosca, V.; Duca, M.; DeGroot, M.T.; Koper, M.T.M. *Chem. Rev.* **2009**, *109*, 2209-2244.
42. Klopsch, I.; Finger, M.; Würtele, C.; Milde, B.; Werz, D.B.; Schneider, S. *J. Am. Chem. Soc.* **2014**, *136*, 6881.
43. Lei, F.; Foxman, B.M.; Ozerov, O.V.; *Organometallics*, **2004**, *23*, 326.
44. Mankad, N.P.; Rivard, E.; Harkins, S.B.; Peters, J.C. *J. Am. Chem. Soc.*, **2005**, *127*, 16032.

45. Dominik, H.; Gandelman, Mark.; Haim, R.; Shimon, L.J.W.; Milstein, D. *Organometallics*. **2002**, 21, 812.
46. Ben-Ari, E.; Leitus, G.; Shimon, L.J.W.; Milstein, D. *J. Am. Chem. Soc.* **2006**, 128, 15390.
47. Akira, S.; Takuro, O.; Risa, Y.; Matsujiro, A.; Kazuaki, I. *Organic Letters* **2011**, 13, 892-895.
48. Kolthoff, I.M.; Chantooni Jr., M.K. *J. Am. Chem. Soc.* 1968, 90:13, 3320.
49. (a) Thimm, W.; Gradert, C.; Broda, H.; Wennmohs, F.; Neese, F.; Tuczek, F. *Inorg. Chem.* **2015**, 54, 9248-9255. (b) Schenk, S.; Le Guennic, B.; Kirchner, B.; Reiher, M. *Inorg. Chem.* **2005**, 44, 9640-9642. (d) Schenk, S.; Le Guennic, B.; Kirchner, B.; Reiher, M.; *Inorg. Chem.* **2008**, 47, 3634. Hinrichsen, S.; Broda, H.; Gradert, C.; Soncksen, L.; Tuczek, F. *Annu. Rep. Prog. Chem., Sect. A: Inorg. Chem.* **2012**, 108, 17.
50. Hebden, T.J.; Schrock, R.R.; Takase, M.K.; Müller, P. *Chem. Commun.*, 2012, **48**, 1851–1853.
51. Kinoshita, E.; Arashiba, K.; Kuriyama, S.; Eizawa, A.; Nakajima, K.; Nishibayashi, Y. *Eur. J. Inorg. Chem.* **2015**, 1789–1794.
52. Silantyev, G.A.; Förster, M.; Schluschaß, B.; Abbenseth, J.; Würtele, C.V.; Holthausen, M.C.; Schneider, S. *Angewandte Chemie*. **2017**, 56, 5872.



## Chapter 5

### Synthesis of pincer-ligated metal complexes for alkane dehydrogenation

#### Abstract:

(<sup>R4</sup>PCP)Ir complexes are some of the most active complexes for alkane dehydrogenation. In order to improve the activity or regioselectivity for alkane dehydrogenation new complexes with alternative metals and new ligand designs are being synthesized. The three approaches used to improve catalytic activity in this chapter were addition of a cationic group into the central arene ring at the para position, using ligands that can participate in metal ligand cooperativity and use of new metals with reported ligand frameworks. Herein we reported the synthesis of new pincer-ligated metal complexes and study their reactivity for alkane dehydrogenation.

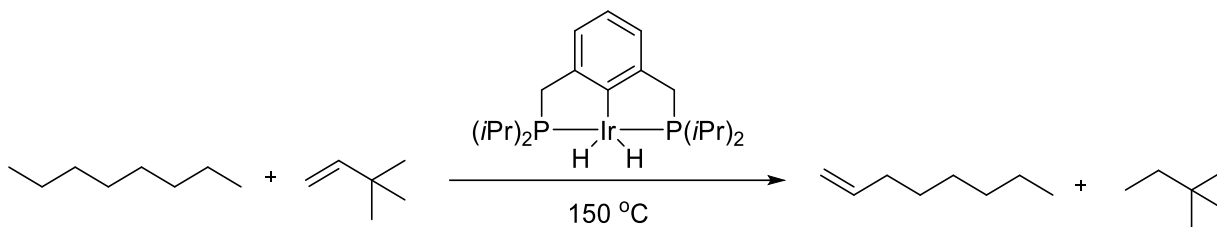
## 5.1 Introduction

Since the seminal report by Moulton and Shaw<sup>1</sup> pincer-ligated metal complexes have shown an exceedingly large range of chemical applications primarily in the field of C-H activation. Alkenes are a valuable chemical commodity and are a versatile feedstock in the chemical community. Alkanes while much more abundant than alkenes do not have as many applications. Heterogeneous catalysts have been reported to dehydrogenate alkanes, unfortunately they suffer poor selectivity and thus are only used on simple substrates such as ethylene and ethylbenzene where only a single product can be synthesized.<sup>2-6</sup> Homogenous alkane dehydrogenation was first reported by Crabtree<sup>7-9</sup> and Felkin<sup>10-12</sup> who used tert-butylethylene (TBE) as a sacrificial hydrogen acceptor making the reaction thermosneutral.

Pincer-ligated iridium complexes have been reported as some of the most active catalysts for alkane dehydrogenation.<sup>13</sup> The first use of iridium pincer complexes for alkane dehydrogenation was by Kaska and Jensen who reported the dehydrogenation of cyclooctane using TBE acceptor.<sup>14</sup> Goldman then reported that the dehydrogenation of n-octane could also be performed using the (<sup>i</sup>PrPCP)Ir complex. Interestingly Goldman found that these complexes were selective for formation of alpha olefins.

Decreasing the steric bulk of the catalyst (substituting t-butyl groups for isopropyls on the phosphorus) yielded increased reaction rates for the dehydrogenation of cyclooctane and n-octane while preserving selectivity for the terminal olefin.<sup>15</sup> While

these complexes did have high stabilities prolonged heating above 200°C (key for acceptorless alkane dehydrogenation) lead to decomposition of the catalyst.



**Scheme 5.1:** Transfer dehydrogenation of n-octane by  $(^{\text{iPr}}\text{PNP})\text{IrH}_2$

Modifications to the pincer structure can improve stability as well as reactivity of the complex. Replacing the benzene based backbone with an anthrophos supported backbone imparted improved stability with lower reactivity.<sup>16</sup> Substituting the tert-butyl groups for adamantyl groups on the (PCP)Ir complex improved stability of the catalysts and increased total turnover numbers for acceptorless dehydrogenation of cyclodecane.<sup>17</sup> Replacing the  $\text{CH}_2$  linkers of the (PCP)Ir complex with oxygens ((POCOP)Ir complexes) yielded complexes with improved reactivity for the dehydrogenation of cyclooctane. This increase in reactivity was attributed to the decreased steric bulk around the metal center of the POCOP vs. PCP complexes.<sup>18</sup>

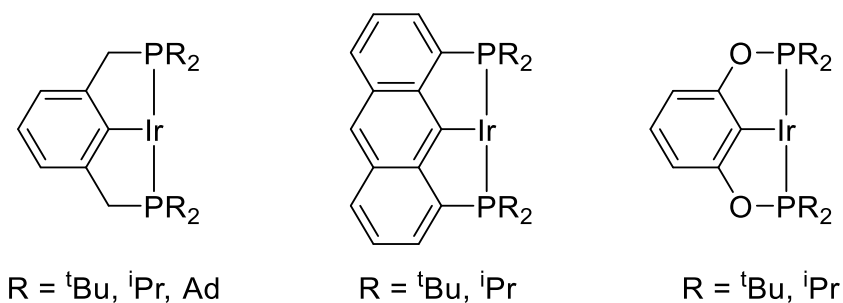


**Figure 5.1:** Modified ligand complexes

Extensive work has been reported modifying and synthesizing new pincer ligand motifs. This work has included changing the center ligand atom (O, N, P) to alter the electronics of the complexes particularly through trans influence.<sup>19-21</sup>

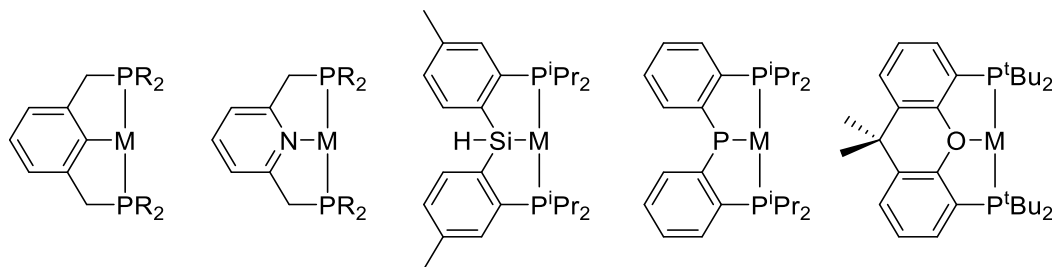


**Figure 5.2:** Tuning the trans-influence of pincer ligands

Improving the activity of pincer ligated complexes can also be done by using ligands capable of metal ligand cooperativity (MLC). Metal ligand cooperativity is when a ligand is non-innocent in a catalytic pathway and is key to the overall mechanism of action. MLC mechanisms have been reported for hydrogenation and dehydrogenation reactions using pincer ligands for a broad range of substrates.

Pincer ligands with a center nitrogen atom have shown a strong affinity for MLC type reactions due to importance of the metal-amine/metal-amide bond in many of these reactions. Aliphatic PNP iridium complexes have shown high reactivity for hydrogenation of ketones by a MLC outer sphere mechanism seen in Figure 5.3.<sup>22</sup>

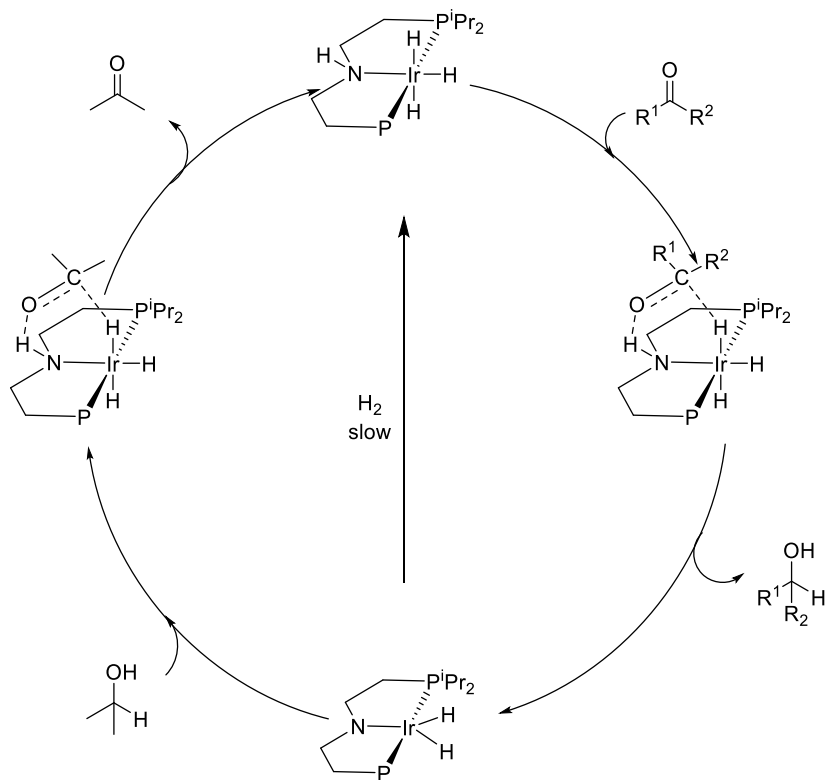
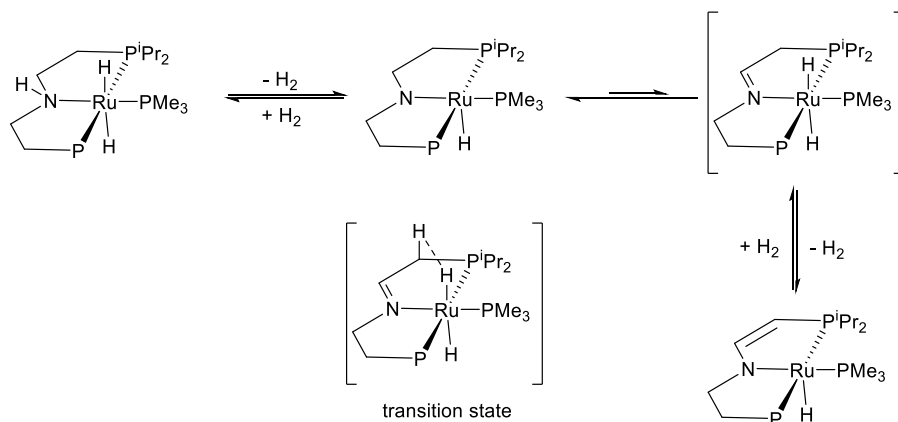


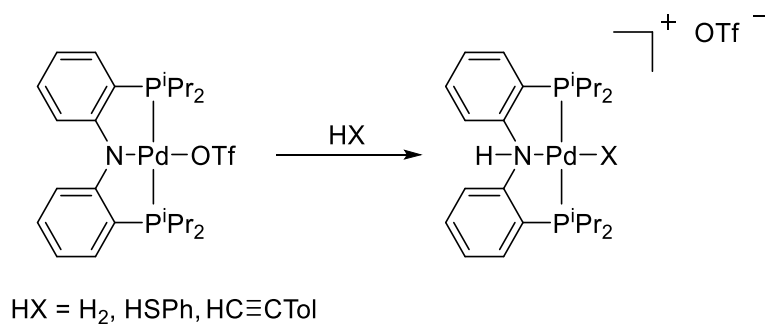
**Figure 5.3:** Outer sphere hydrogenation of ketone using MLC mechanism

MLC type behavior has also been observed though an inner sphere mechanism of aliphatic PNP complexes. Aliphatic PNP ruthenium complexes have been reported to lose  $H_2$  from a metal hydride and ligand proton to form the enamine bound ligand.<sup>23</sup>



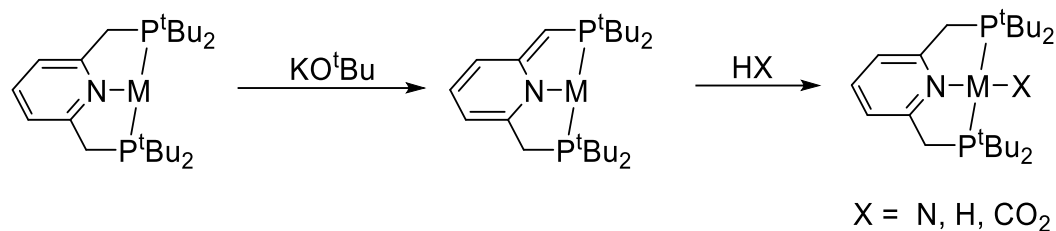
**Scheme 5.2:** Loss of  $H_2$  to form enamine pincer complex

Aryl PNP ligands while not as effective for MLC type reactivity has shown some promise in the activation of H-X bonds. Ozerov reported a PNP palladium complex that showed reactivity for addition of H-X ( $H_2$ , terminal alkyne and thiol) bonds across the N-Pd bond.<sup>24</sup> This type of reactivity has also been demonstrated using M-(O, S and B) bonds.



**Scheme 5.3:** Addition of HX across metal-ligand bond

MLC type reactions have also been studied extensively using lutidine based PNP ligands first reported by Milstein.<sup>25</sup> Milstein reported that dearomatization of these aryl pincers occurred readily in the presence of base modifying the center L ligand to an anionic X ligand. Upon dearomatization addition across the metal and deprotonated linker arm can be performed. N-H and  $CO_2$  bonds have all been reported to add across the metal/ligand of these dearomatized structures.<sup>26-27</sup>



**Scheme 5.4:** Dearomatization of PNP ligand followed by HX addition across metal/ligand

Following these literature examples we have proposed modifications to the pincer motif that we hypothesis will improve reactivity. We have taken the approach of using methods such as tuning the ligand to increase activity as well as using ligands capable of metal ligand cooperativity. Herein we report new pincer complexes and their reactivity towards small molecule activation.

## 5.2 Para-Nitrogen (<sup>t</sup>BuPCP)Ir synthesis and activity

### 5.2.1 Computational Analysis

Alkane dehydrogenation using pincer ligated iridium complexes tend to follow the same mechanism despite modifications of the ligand. However variations on the ligand motif have led to changes in selectivity for terminal olefins. For example when comparing (<sup>t</sup>BuPCP)Ir vs. (<sup>t</sup>BuPOCOP)Ir, the latter has shown to be the more active catalyst between the two. However (<sup>t</sup>BuPCP)Ir has shown to be the more selective catalyst for formation of terminal olefins vs. internal olefins. Our group has detailed the factors that effect this change in selectivity and they have found the major factors are electronic not steric<sup>28</sup>

As shown in Figure 5.4 the mechanism for dehydrogenation by pincer iridium complexes using TBE acceptor is first hydrogenation of a sacrificial olefin (TBE), which is followed by C-H activation of the alkane and finally  $\beta$ -hydride elimination and finally olefin dissociation. DFT analysis of this reaction using both ( $t^{\text{Bu}}$ PCP)Ir and ( $t^{\text{Bu}}$ POCOP)Ir shed some light on the observed difference of selectivity between the two catalysts.

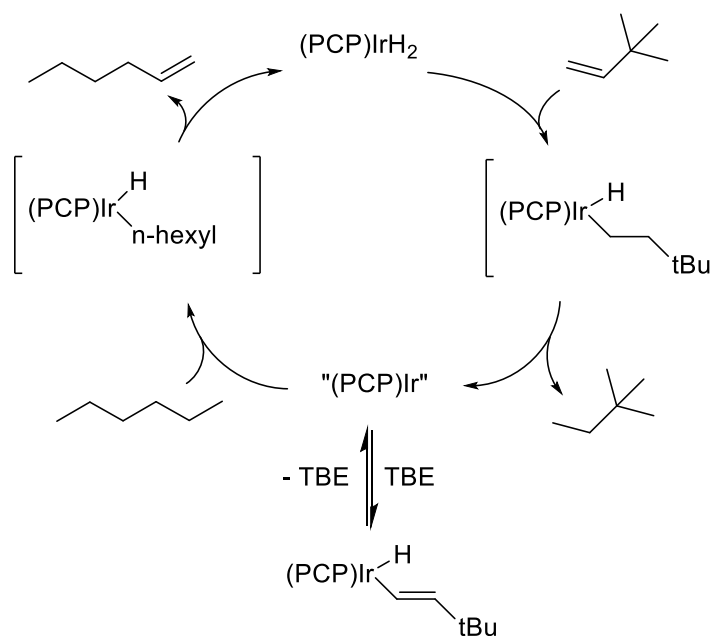


**Figure 5.4:** Mechanism of transfer alkane dehydrogenation



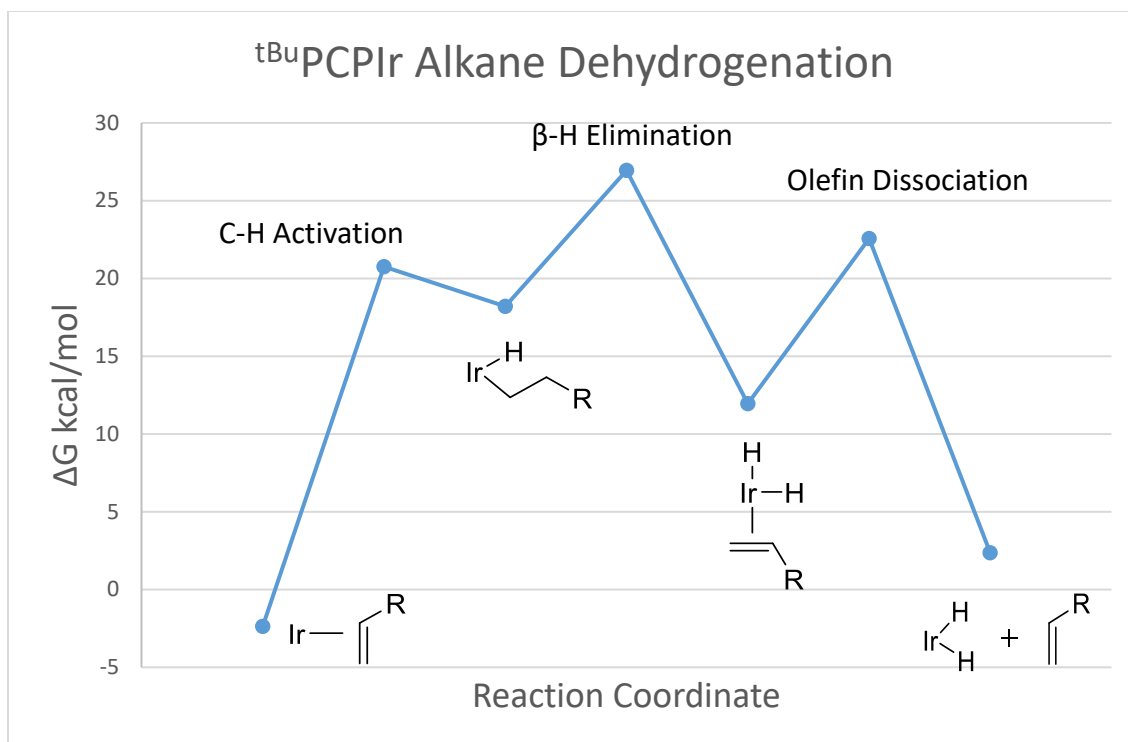


**Figure 5.5:** Free energy diagram for alkane dehydrogenation by (<sup>t</sup>BuPCP)Ir

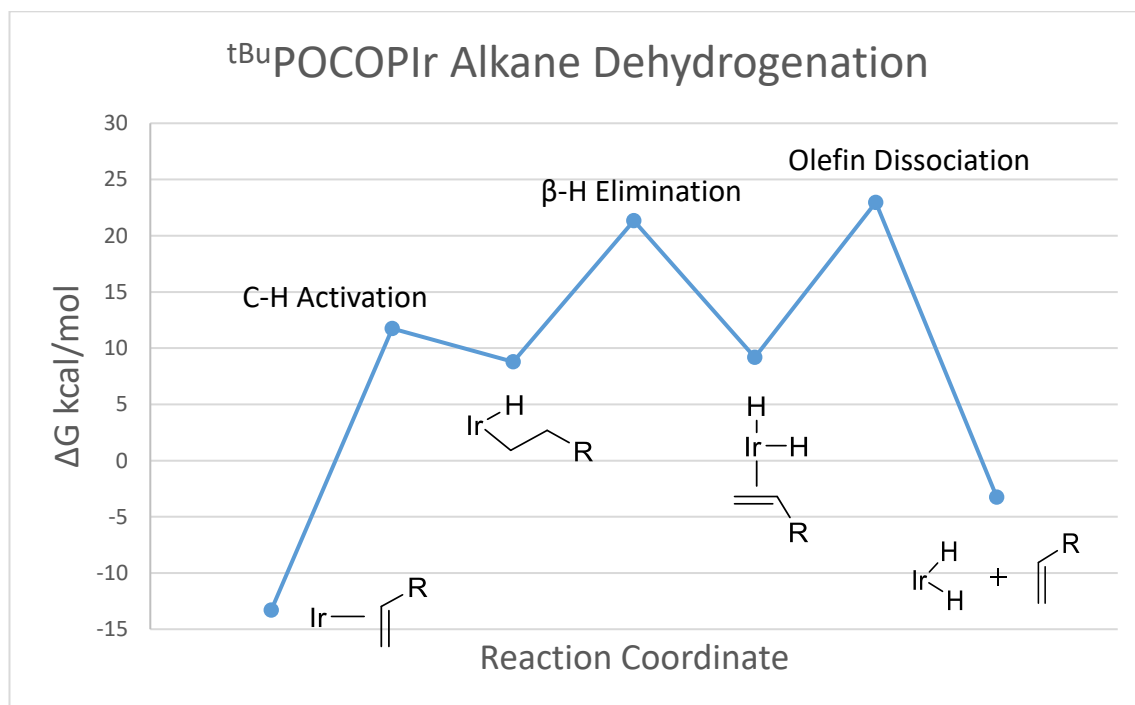


**Figure 5.6:** Free energy diagram for alkane dehydrogenation by (<sup>t</sup>BuPOCOP)Ir

The DFT calculations suggest that the rate determining step of alkane dehydrogenation is different when comparing  $(^t\text{BuPCP})\text{Ir}$  and  $(^t\text{BuPOCOP})\text{Ir}$ . The rate determining step for  $(^t\text{BuPCP})\text{Ir}$  is the  $\beta$ -hydride elimination and for  $(^t\text{BuPOCOP})\text{Ir}$  it is the olefin dissociation. It has been reported that pincer ligated iridium complexes can form internal olefins directly through initial formation of an iridium  $\eta_3$ -allyl species in addition to isomerization of terminal olefins.<sup>29-30</sup> Olefin dissociation from  $(^t\text{BuPCP})\text{Ir}$  is much quicker than compared to  $(^t\text{BuPOCOP})\text{Ir}$  thus lowering the possibility of formation of the  $\eta_3$ -allyl species. This is one possible explanation for the higher terminal olefin selectivity for  $(^t\text{BuPCP})\text{Ir}$  vs.  $(^t\text{BuPOCOP})\text{Ir}$ .

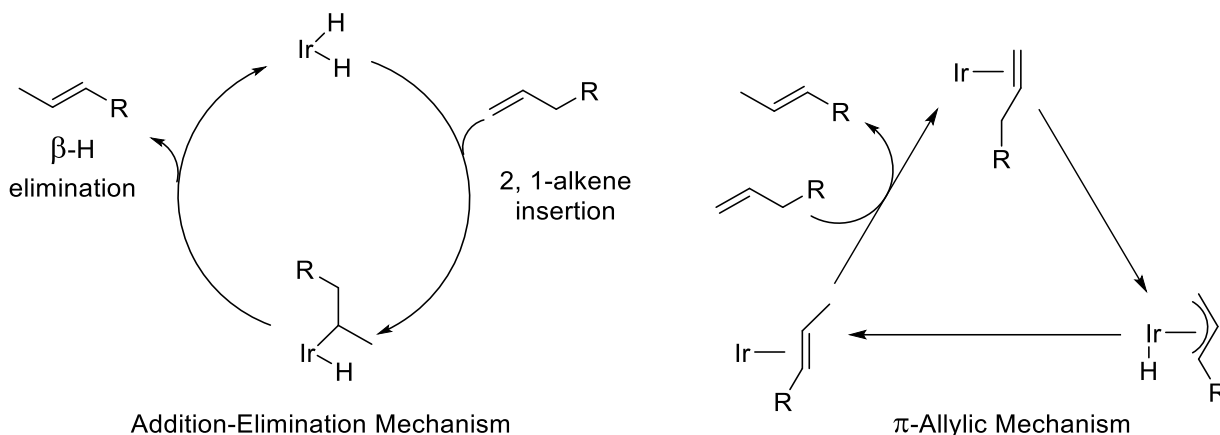


**Figure 5.7:** Mechanisms for alkene isomerization by pincer iridium complexes

In order to identify new potential catalysts for alkane dehydrogenation, DFT calculations were run modeling catalysts with differing electronic properties. Additionally, we were looking for catalysts that had the rate determining step be  $\beta$ -hydride elimination, suggesting better selectivity for terminal olefins.

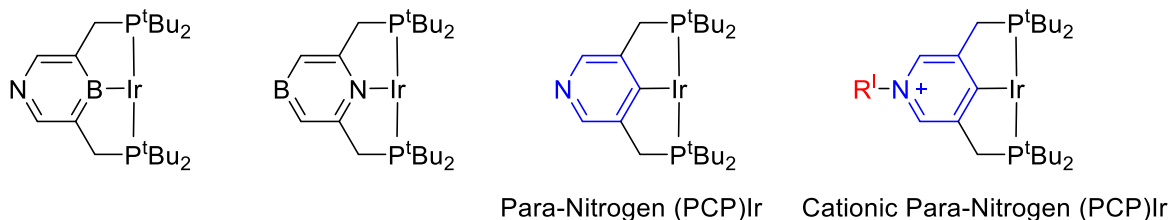


**Figure 5.8:** Model catalysts for charge incorporation into pincer ligand

Preliminary calculations began with studying complexes with aryl rings containing boron and nitrogen groups. While these complexes seemed viable computationally, no straight forward synthesis was apparent. Next complexes with only a para-nitrogen in the aryl ring of the ligand were examined. DFT results showed that having the para-nitrogen group in the ligand would have very similar energy barriers as the standard (<sup>t</sup>BuPCP)Ir complex. However upon protonation or methylation of the para-nitrogen the energy barriers of each of the steps of alkane dehydrogenation were lowered. Additionally it seems that this cationic species would also have a similar energy profile to standard (<sup>t</sup>BuPCP)Ir with β-hydride elimination being the rate determining step.

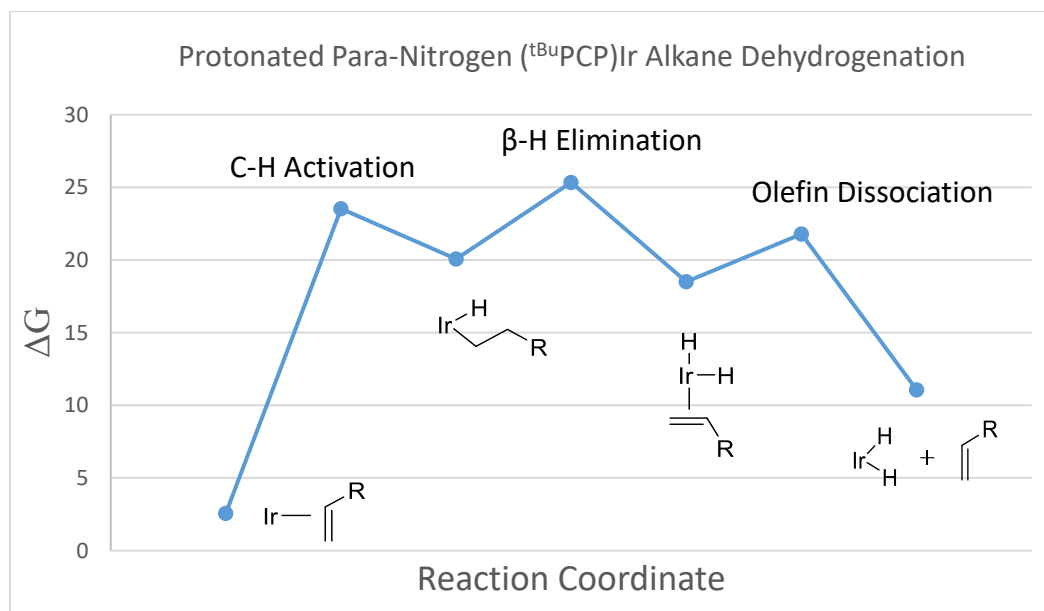


**Figure 5.9:** Free energy diagram for alkane dehydrogenation by para-nitrogen (<sup>t</sup>BuPCP)Ir

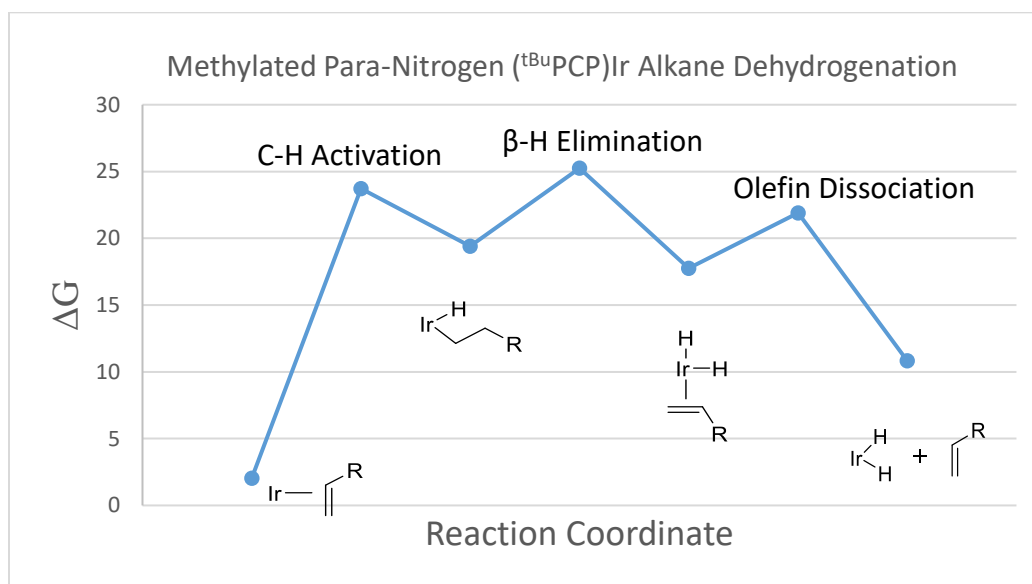


**Figure 5.10:** Free energy diagram- alkane dehydrogenation by alkylated para-nitrogen (<sup>t</sup>BuPCP)Ir

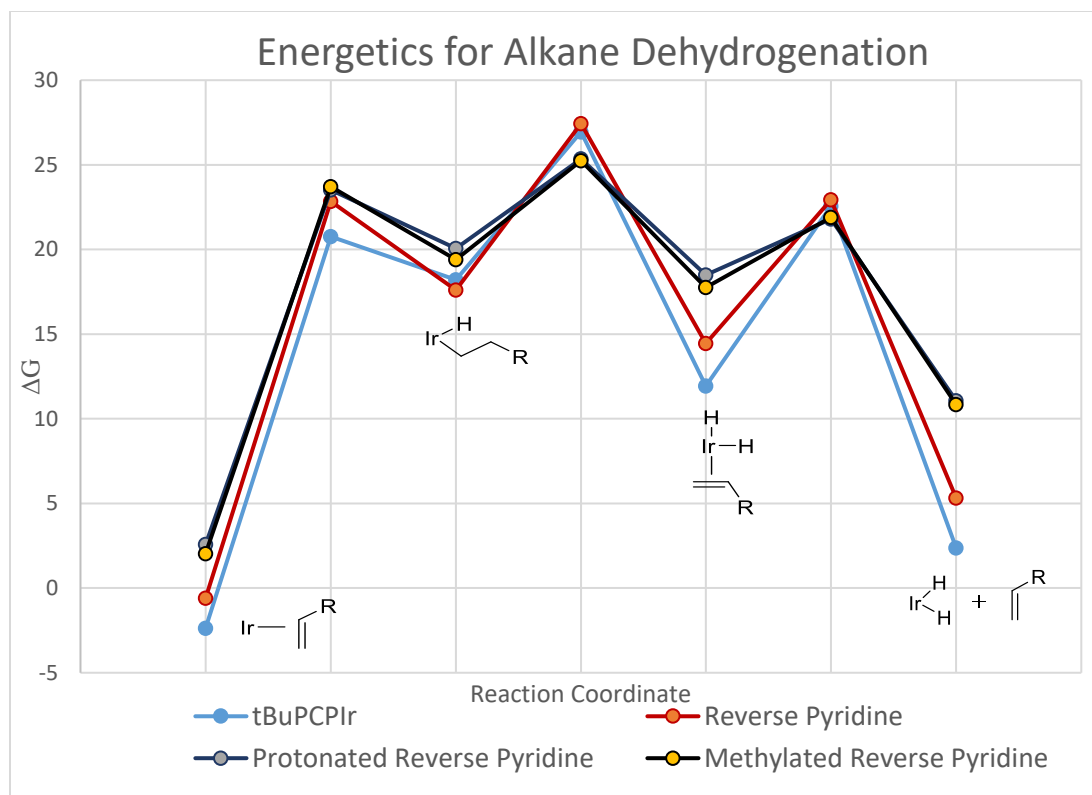


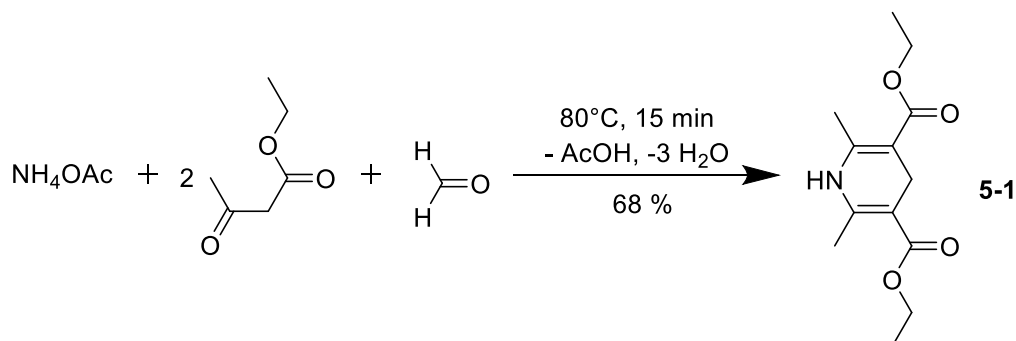
**Figure 5.11:** Comparative free energy diagram for alkane dehydrogenation

Similar results were reported by the Cundari group who computed the concerted metalation deprotonation mechanism of methane addition to Phebox ligated metal species. He reported that addition of a para nitrogen into the central ring of the system decreased the free energy of the methane addition.<sup>31</sup> Based on our computations and those by the Cundari group we believe that the cationic para-nitrogen (<sup>t</sup>BuPCP)Ir complex has potential to be a more active and selective catalyst for alkane dehydrogenation.

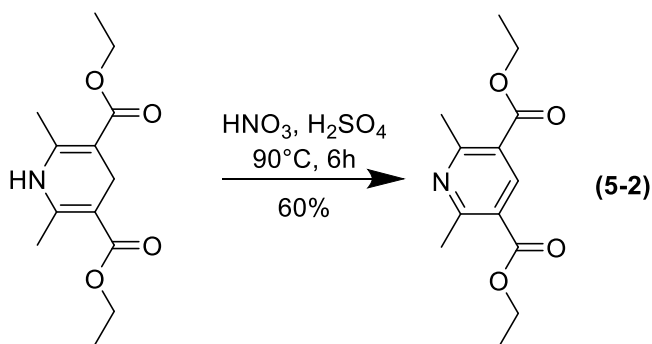
### 5.2.2 Synthesis of para-nitrogen (<sup>t</sup>BuPCP)Ir

Synthesis of the para-nitrogen catalyst began with a Hantzsch synthesis and oxidation.<sup>34</sup> This reaction takes a nitrogen source, an aldehyde and two  $\beta$ -keto esters to

form a nitrogen containing heterocycle. This is followed by an oxidation using nitric and sulfuric acids to form a pyridine ring. The dimethyl substituted aryl backbone for this ligand was chosen to prevent intermolecular reactions such as backbone pyridine coordination to an adjacent iridium metal center. Upon synthesizing the diester product it became commercially available and was purchased from that point forward.



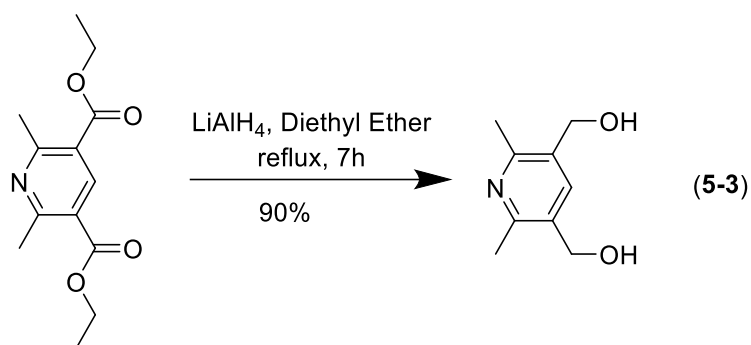
**Scheme 5.5:** Synthesis of diethyl 2,6-dimethyl-1,4-dihydropyridine-3,5-dicarboxylate (5-1)



**Scheme 5.6:** Synthesis of diethyl 2,6-dimethylpyridine-3,5-dicarboxylate (5-2)

The next step of the synthesis was reduction of the diester to form the diol. The reduction was done using lithium aluminum hydride. Formation of the product was successful however work up to separate the solution was difficult. The presence of the para-nitrogen in the backbone resulted in the polarity of the molecule to increase more

than expected. During the work up water was used to quench excess lithium aluminum hydride upon which the product solubilized in the water phase. Multiple solvents were used however none were successful in extracting the product. The water was evaporated off leaving a whitish powder which was then dissolved in acetonitrile crashed out a yellow oil which was discarded and removal of the solvent yielded the product.  $^1\text{H}$ -NMR in deuterated methanol showed the expected peaks with the O-H bond seen as a sharp triplet.



**Scheme 5.7:** Synthesis of (2,6-dimethylpyridine-3,5-diyl)dimethanol (**5-3**)

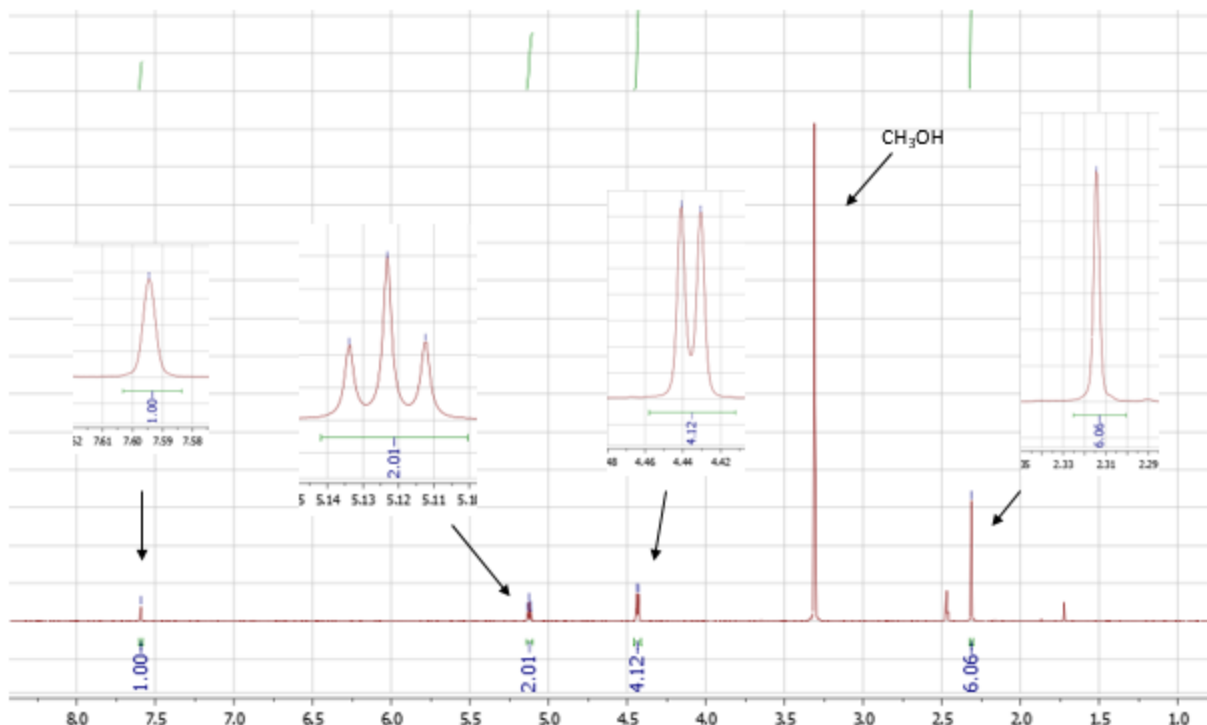
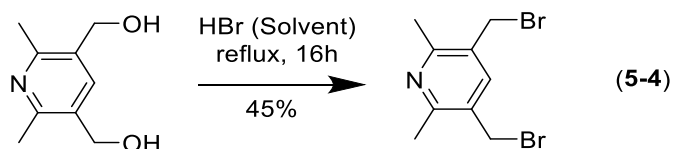


**Figure 5.12:**  $^1\text{H}$ -NMR spectra of **(5-3)**

The next step of the synthesis was the bromination of the diol. Bromination of alcohols are typically done with  $\text{Br}_2$ , however using that reagent was not successful in brominating the diol. Instead using aqueous hydrobromic acid as the source of bromine followed by quenching with sodium bicarbonate solution was very successful in forming the dibenzyl bromide product. Extracting the product into dichloromethane yielded the product in moderate yields.



**Scheme 5.8:** Synthesis of 3,5-bis(bromomethyl)-2,6-dimethylpyridine **(5-4)**



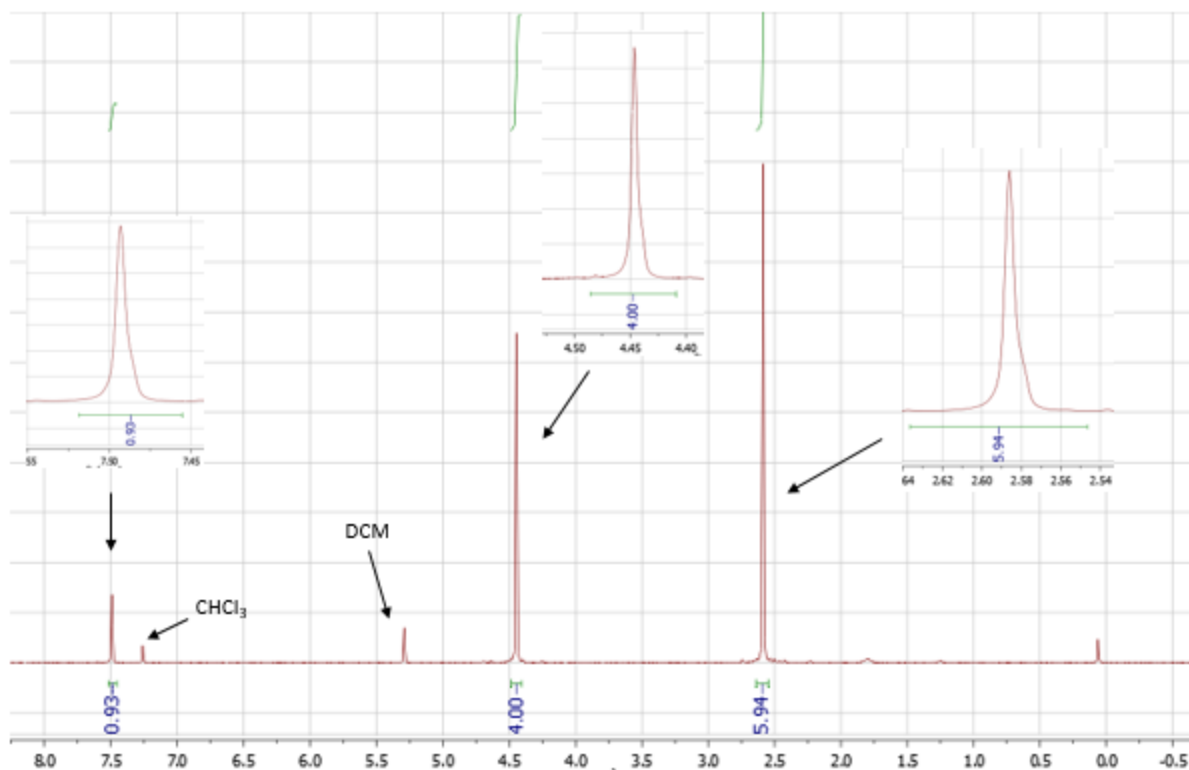
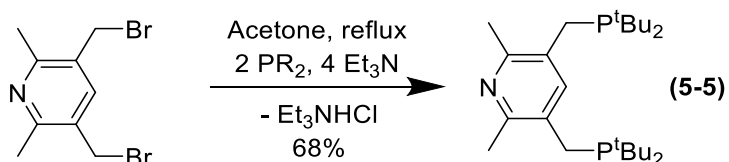


**Figure 5.13:**  $^1\text{H}$ -NMR spectra of **(5-4)**

Phosphination of the di-benzyl bromide was done using di-tertbutylphosphine with the bromide in acetone. This was followed by removal of the solvent and reaction of the phosphonium salt with base (trimethylamine) to generate the para-nitrogen ( $^t\text{BuPCP}$ ) ligand.  $^{31}\text{P}$ -NMR showed a single peak at 26 ppm with the  $^1\text{H}$ -NMR showing all the correct ligand signals.



**Scheme 5.9:** Synthesis of 3,5-bis((di-tert-butylphosphanyl)methyl)-2,6-dimethylpyridine **(5-5)**

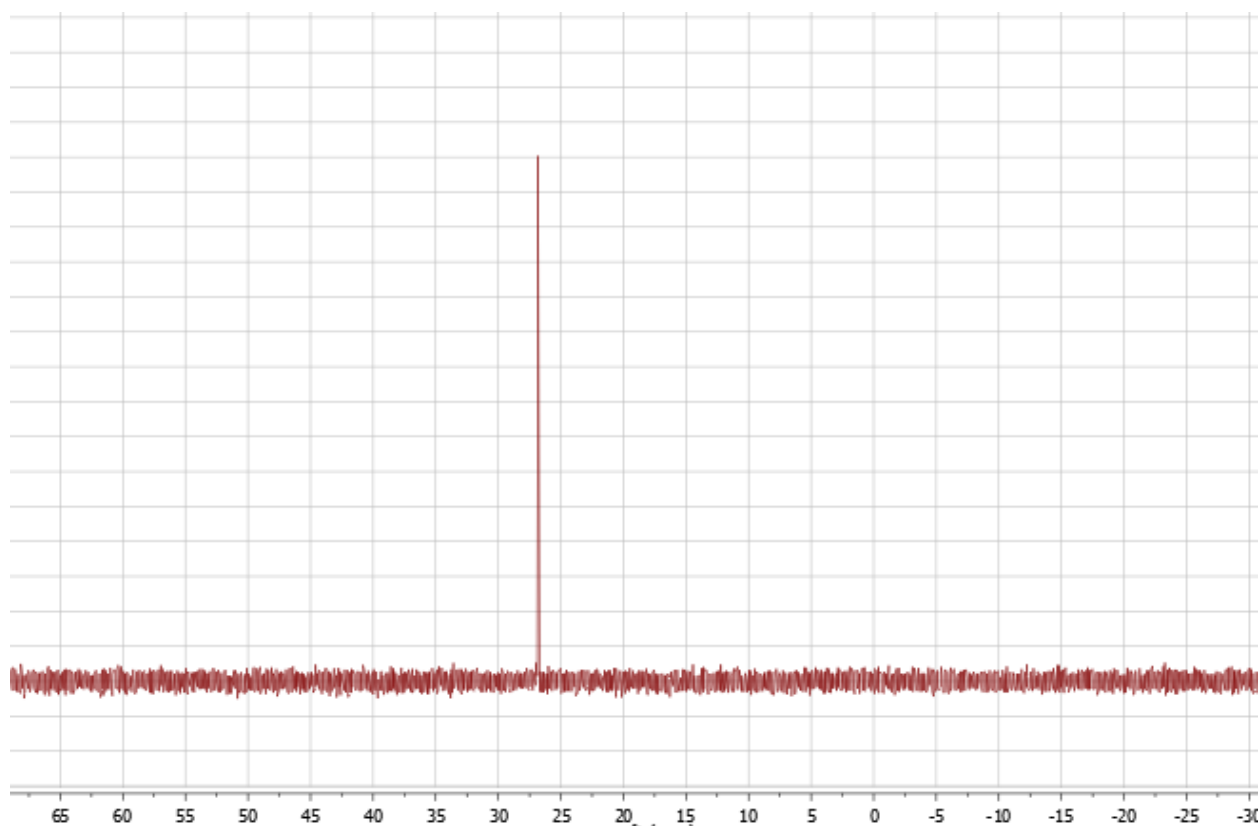


Figure 5.14:  $^{31}\text{P}$ -NMR spectra of (5-5)

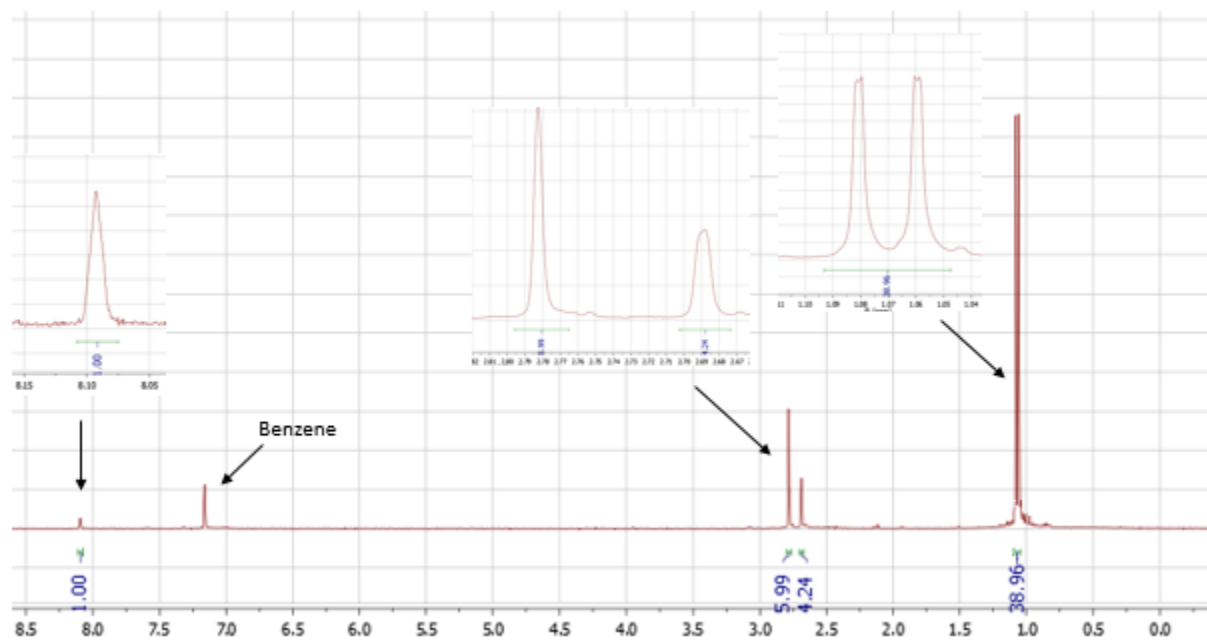
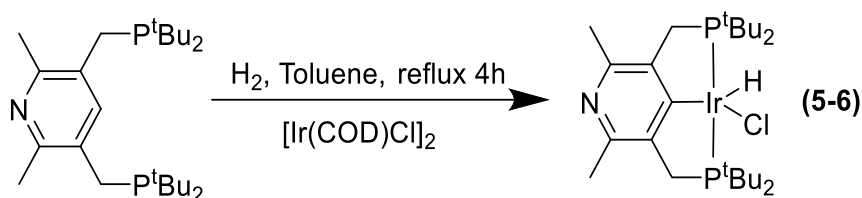
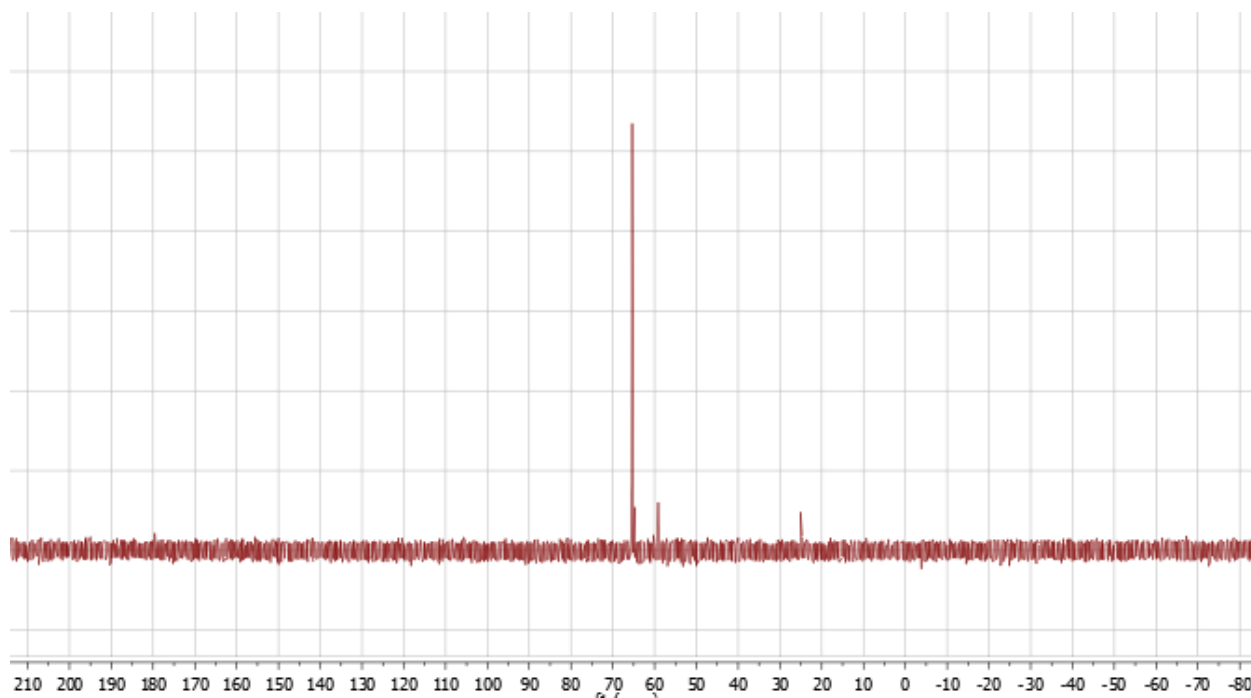


Figure 5.15:  $^1\text{H}$ -NMR spectra of (5-5)

Metalation of the para-nitrogen ligand was done using iridium cyclooctadiene chloride dimer under a hydrogen flow. Extraction of the product into pentane resulted in formation of a red powder with good yield.  $^{31}\text{P}$ -NMR of the product had a single new resonance peak at 66 ppm.  $^1\text{H}$ -NMR of the product showed all the correct corresponding ligand peaks in addition to a new hydride peak observed at -42 ppm.



**Scheme 5.10:** Synthesis of para-nitrogen ( $^t\text{BuPCP}$ )IrHCl complex (5-6)



**Figure 5.16:**  $^{31}\text{P}$ -NMR spectra of (5-6)

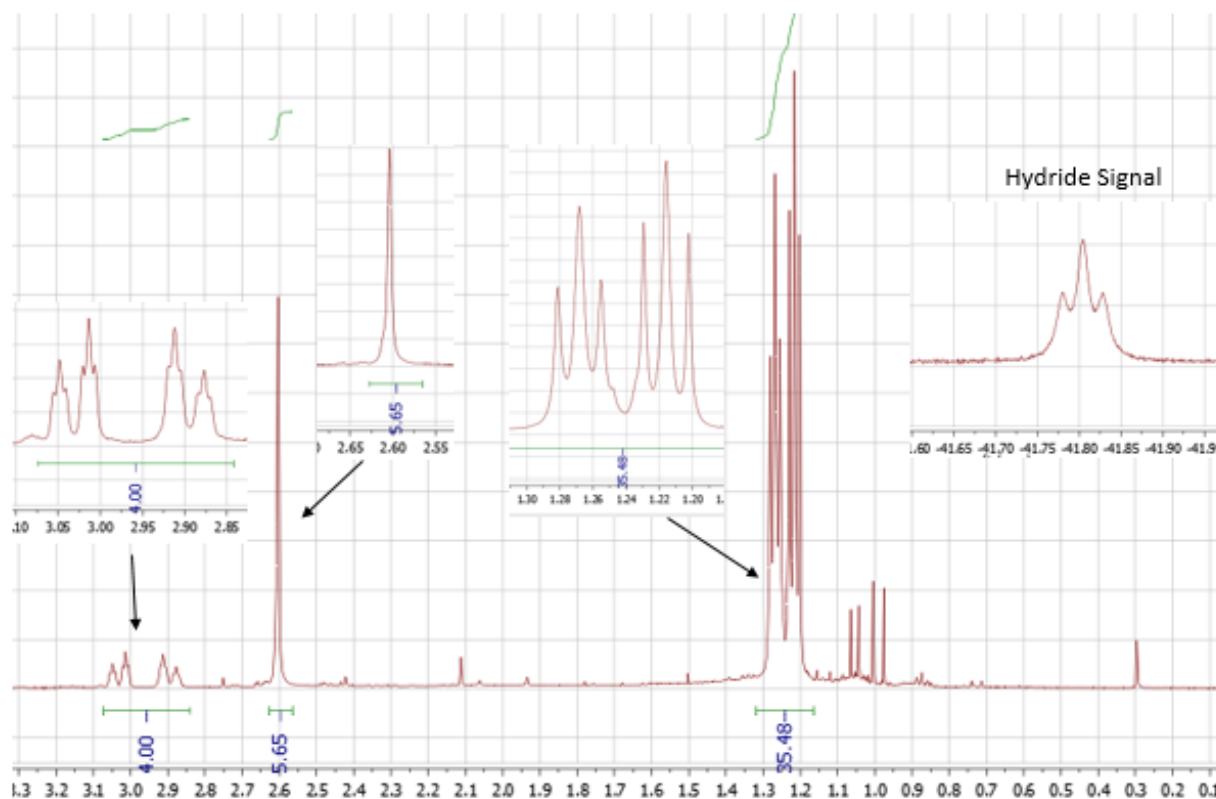
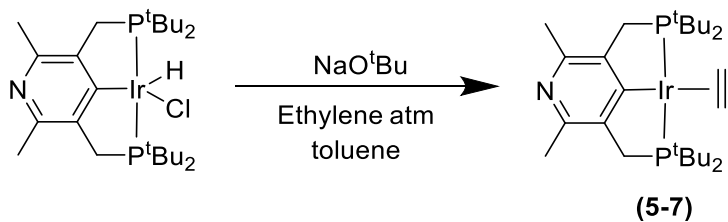


**Figure 5.17:**  $^1\text{H}$ -NMR spectra of (5-6)

Reaction of the para-nitrogen ( $^t\text{BuPCP}$ )IrHCl complex with base (sodium tert-butoxide) in the presence of ethylene lead to the formation of the four coordinate iridium olefin complex.  $^{31}\text{P}$ -NMR showed a single new resonance peak at 61.3 ppm and the  $^1\text{H}$ -NMR showed all the corresponding ligand peaks with the addition of a new peak integrating to four protons (coordinated ethylene).



**Scheme 5.11:** Synthesis of para-nitrogen ( $^t\text{BuPCP}$ )Ir( $\text{C}_2\text{H}_4$ ) complex (5-7)

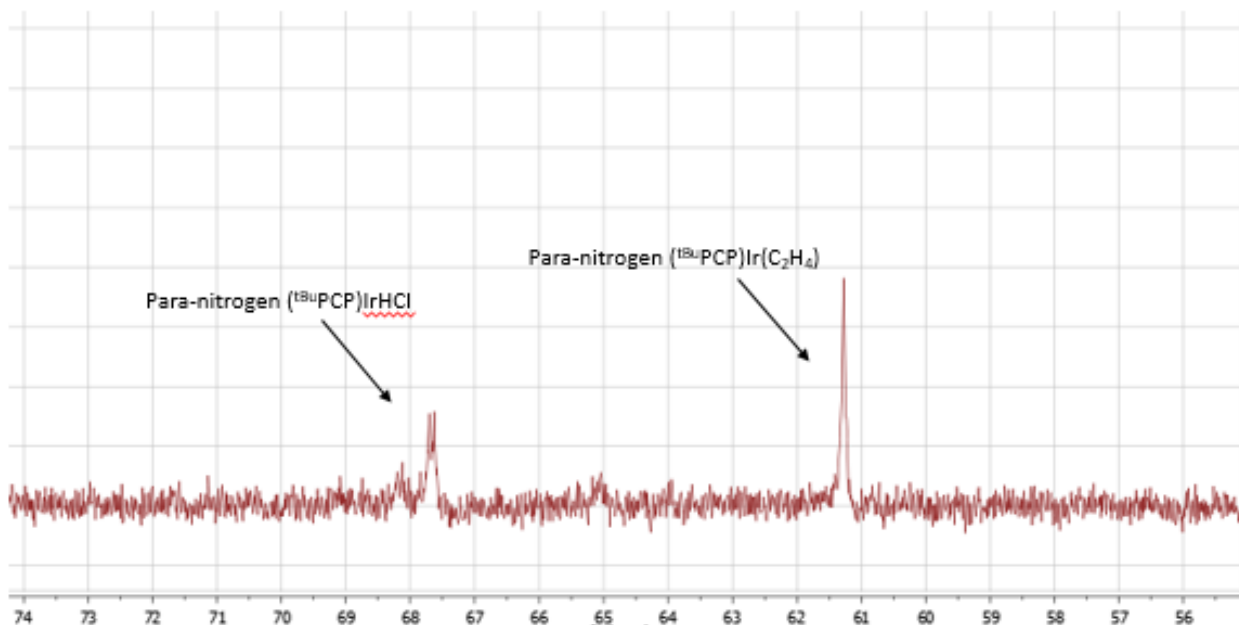
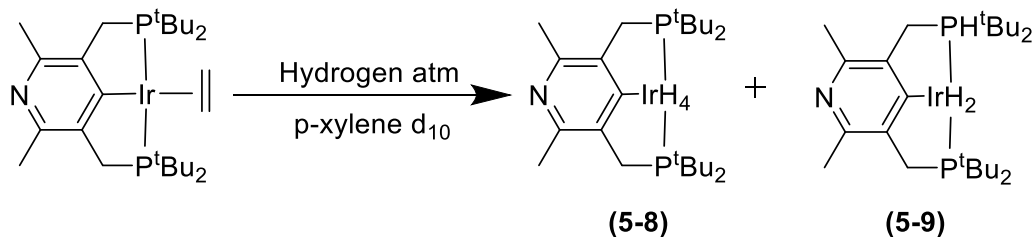


**Figure 5.18:**  $^{31}\text{P}$ -NMR spectra of (5-7)

Reaction of the para-nitrogen  $(^t\text{BuPCP})\text{Ir}(\text{C}_2\text{H}_4)$  complex with hydrogen lead to a color change from red/purple to orange/yellow. Additionally two new species were observed by NMR.  $^{31}\text{P}$ -NMR showed new signals at 74 and 88 ppm while the  $^1\text{H}$ -NMR showed ligand signals in addition to two new hydride peaks at -9 and -18 respectively.



**Scheme 5.12:** Synthesis of para-nitrogen  $(^t\text{BuPCP})\text{IrH}_4/\text{H}_2$  complexes (5-8, 5-9)

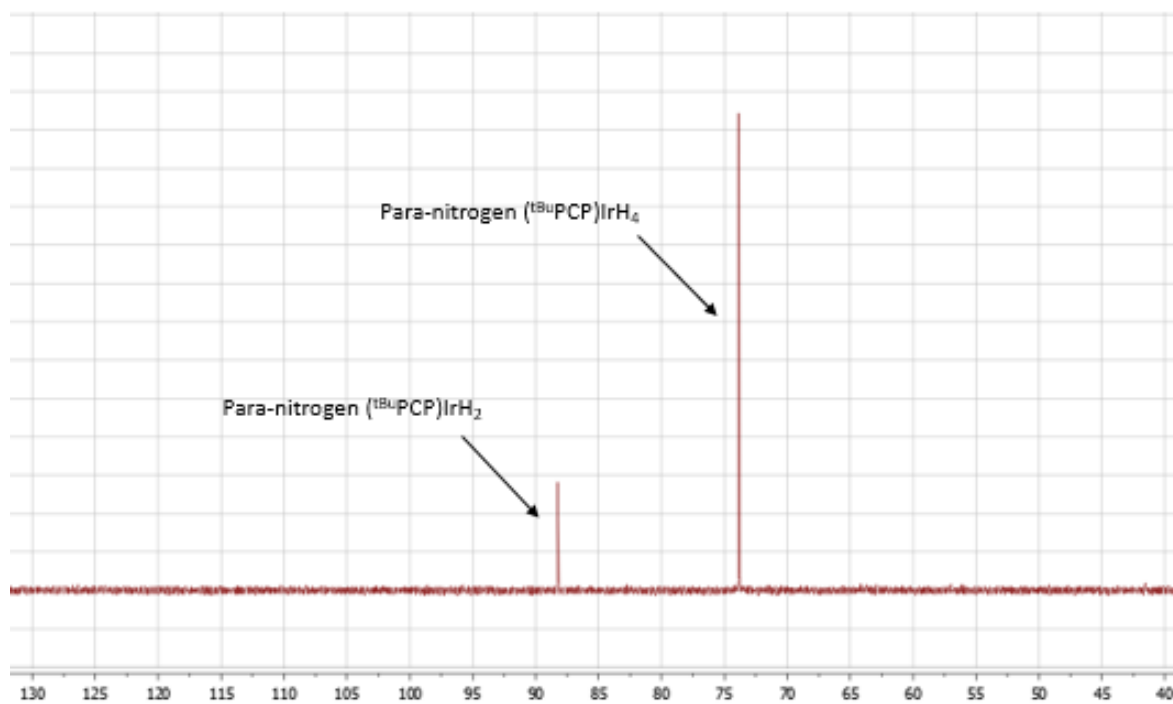


Figure 5.19:  $^{31}\text{P}$ -NMR spectra of (5-8, 5-9)

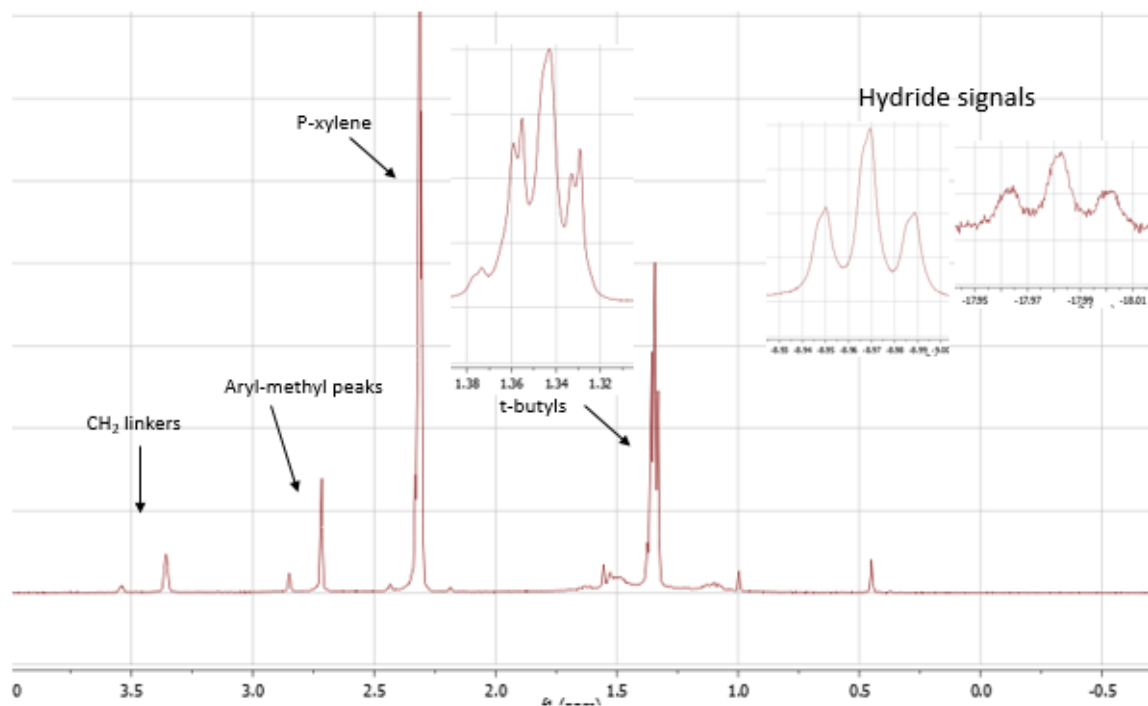
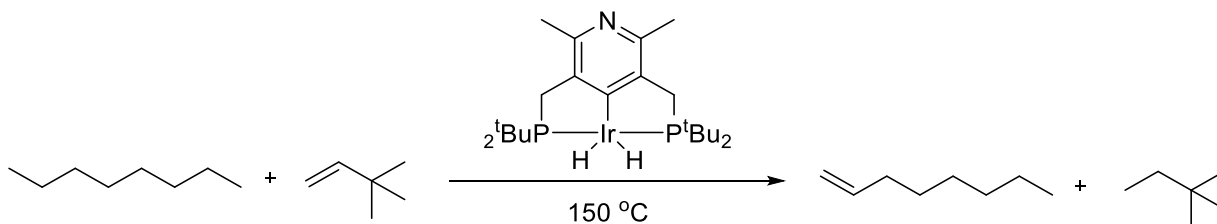


Figure 5.20:  $^1\text{H}$ -NMR spectra of (5-8, 5-9)

Having synthesized the precursors necessary, the para-nitrogen (<sup>t</sup>BuPCP)IrH<sub>x</sub> complex was tested for its activity for alkane dehydrogenation. The dehydrogenation of n-octane is a standard experiment to test if a complex is active for alkane dehydrogenation. Additionally use of octane as the reagent would give us insight into the selectivity of terminal olefin formation associated with this catalyst. Reaction of the para-nitrogen (<sup>t</sup>BuPCP)IrH<sub>x</sub> complex with n-octane and TBE as hydrogen acceptor was successful in forming 1-octene and internal octenes. The activity and selectivity for terminal olefins of this catalyst were very similar to results obtained when using standard (<sup>t</sup>BuPCP)IrH<sub>x</sub>. This agrees very well with our computational analysis that showed the two complexes have very similar energetic profiles.



**Scheme 5.13:** Transfer dehydrogenation of n-octane using (5-9)

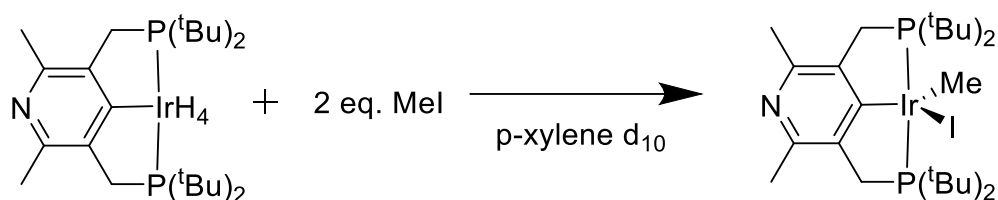
### 5.2.3 Formation of the cationic para-nitrogen (<sup>t</sup>BuPCP)Ir complex

The dehydrogenation results of para-nitrogen (<sup>t</sup>BuPCP)IrH<sub>x</sub> were very consistent with what was predicted by DFT calculations. This suggested that our DFT calculations that showed formation of the cationic para-nitrogen (<sup>t</sup>BuPCP)IrH<sub>x</sub> as a potentially superior catalyst had promise. Protonation of the backbone to form the cationic para-nitrogen (<sup>t</sup>BuPCP)IrH<sub>x</sub> did not seem as a viable option as we would suspect the fourteen

electron (PCP)Ir fragment would react intermolecular to remove the proton.

Methylation of the backbone however should form a more stable species and thus was our first target.

Initial attempts to methylate the backbone of the para-nitrogen complex were done by reacting para-nitrogen (<sup>t</sup>BuPCP)IrH<sub>x</sub> with one equivalent of methyl iodide. Allowing the reaction to stir overnight yielded two new products in a ratio of 1:7.5. Both new products appeared as singlets in the <sup>31</sup>P-NMR at 44.6 and 46.0 ppm. The <sup>1</sup>H-NMR showed loss of all hydride signals in addition to loss of symmetry among the tert-butyl groups. Upon addition of a second equivalent of methyl iodide full conversion to the product at 44.6 ppm was observed. The product is hypothesized to be the oxidative addition of methyl iodide to the iridium metal center. No methylation of the backbone could be observed by the NMR data.



**Scheme 5.14:** Reaction of (5-8) with methyl iodide



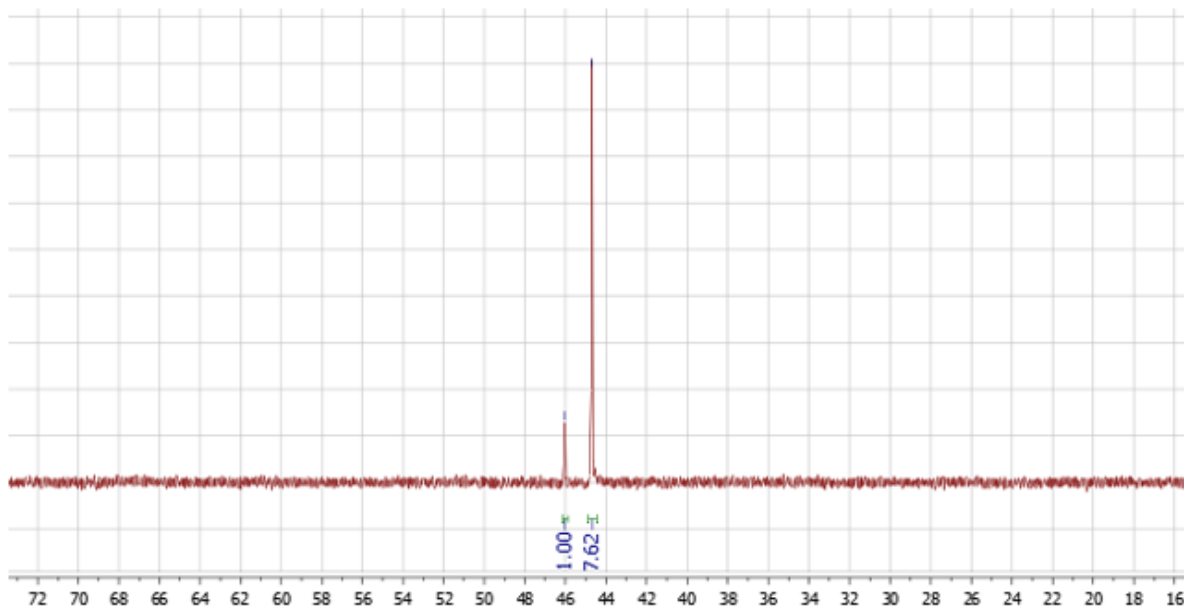


**Figure 5.21:**  $^{31}\text{P}$ -NMR of reaction of **(5-8)** with methyl iodide

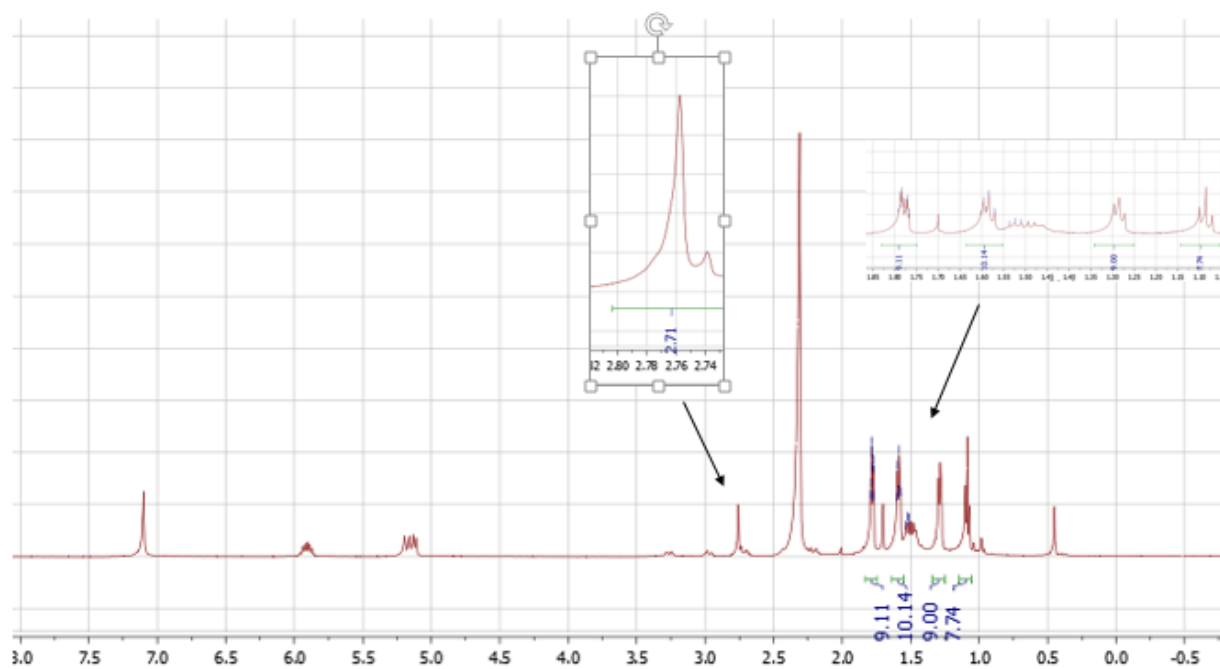
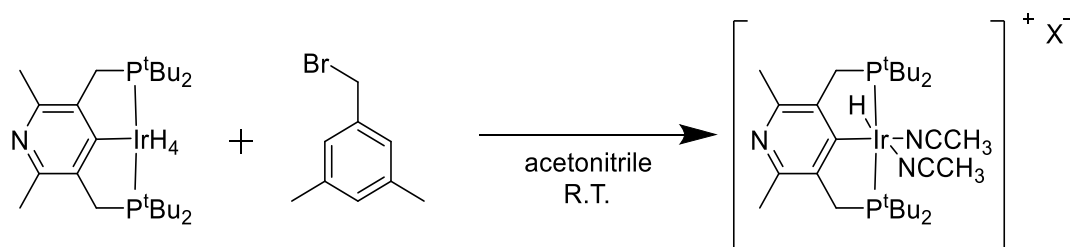


**Figure 5.22:**  $^1\text{H}$ -NMR of reaction of **(5-8)** with methyl iodide

The unsuccessful methylation lead to the investigation of other alkylation reagents. DFT calculations have shown that alkylation of the backbone would have the

same effect as simple methylation for lowering the transition states of dehydrogenation. The next substrate studied was a dimethyl-substituted benzyl bromide with the hopes the backbone nitrogen would undergo a  $\text{S}_{\text{N}}2$  substitution reaction. Knowing polar solvents aid in  $\text{S}_{\text{N}}2$  reactions the solvent used for this experiment was acetonitrile. Reaction of para-nitrogen ( $^{\text{tBu}}\text{PCP}$ ) $\text{IrH}_4$  with 3,5 dimethylbenzyl-bromide yielded two new products.  $^{31}\text{P}$ -NMR showed two new resonance signals at 58 and 52 ppm with the  $^1\text{H}$ -NMR showing a doublet of triplets in the hydride region at -20 ppm which appears to integrate to 1. No evidence of benzylation of the backbone was observed. One hypothesis for the product is formation of the iridium hydride di-acetonitrile complex.



**Scheme 5.15:** Reaction of **(5-8)** with 3,5 dimethylbenzyl bromide

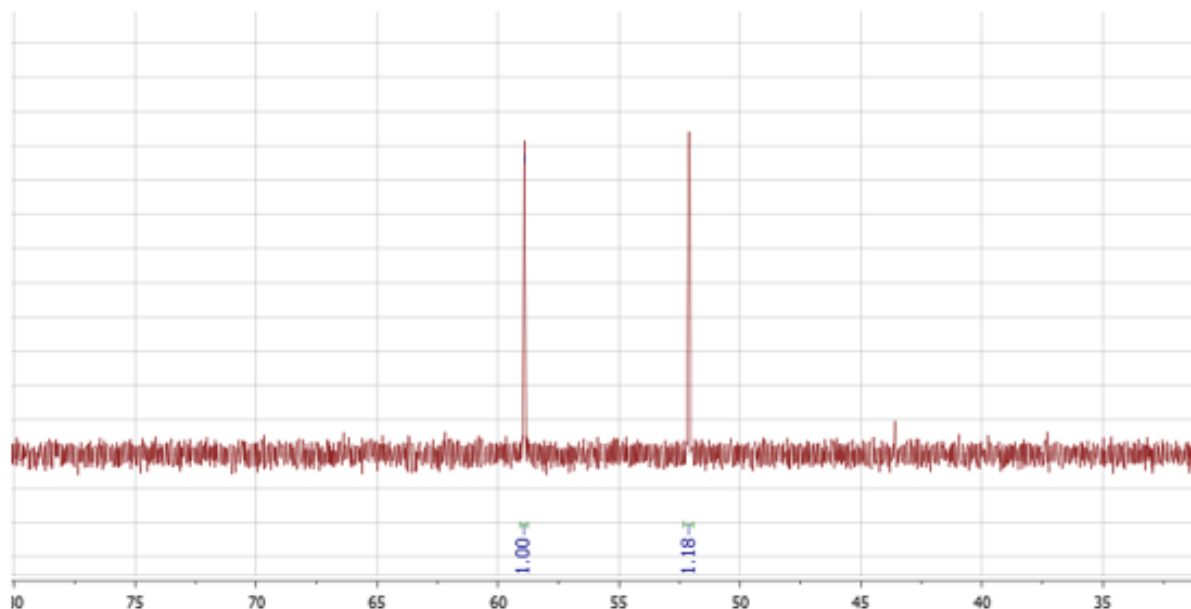


**Figure 5.23:**  $^{31}\text{P}$ -NMR of reaction of **(5-8)** with 3,5 dimethylbenzyl bromide

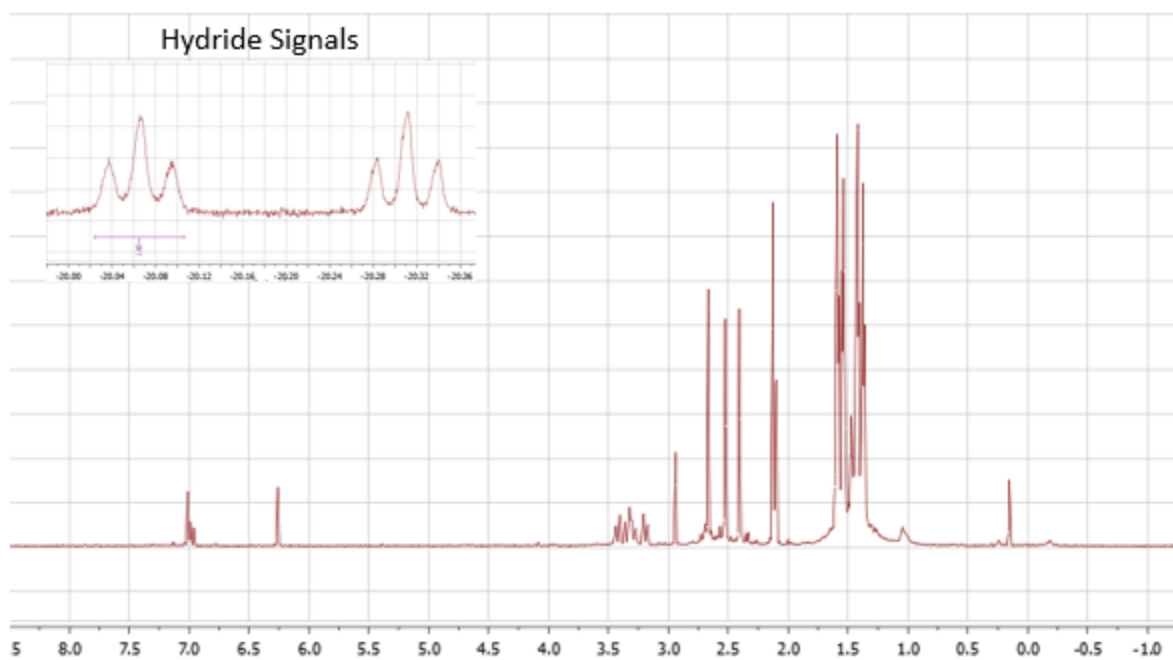
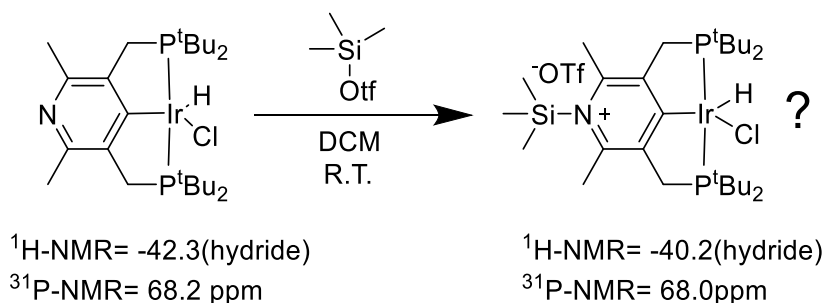


**Figure 5.24:**  $^1\text{H}$ -NMR of reaction of **(5-8)** with 3,5 dimethylbenzyl bromide

The observation that many of these alkylation reagents or solvents used for this reaction reacted with the iridium metal center suggested to us that using a more stable

metal center could be beneficial. The para-nitrogen (<sup>t</sup>BuPCP)IrHCl seemed like a good option as it had been well characterized and readily available. The tetrahydride complex could be easily converted to the IrHCl complex simply by quick heating in dichloromethane. The IrHCl complex could then be reacted with alkylating reagent.

In addition to alkylation of the backbone, DFT calculations suggested that silylation of the backbone would work as well in improving the catalytic activity. Reaction of para-nitrogen (<sup>t</sup>BuPCP)IrHCl with tert-butylchlorodimethylsilane did not yield any reaction even upon heating, possibly due to the reactivity of the Si-Cl bond or Cl being a poor counter-ion. To remedy some of these issues trimethylsilyl triflate was used instead. Treatment of para-nitrogen (<sup>t</sup>BuPCP)IrHCl with TMS triflate resulted in slight changes to the NMR peaks. Upon addition of TMS triflate the singlet in the <sup>31</sup>P-NMR shifted from 68.2 to 68.0 ppm relative to phosphorus standard. Additionally in the <sup>1</sup>H-NMR the hydride peak associated with the IrHCl complex shifted slightly from -42 to -40 ppm. These slight shifts could be consistent with silylation of the backbone as they should not affect the NMR signals greatly.



**Scheme 5.16:** Reaction of (5-6) with trimethylsilyl triflate

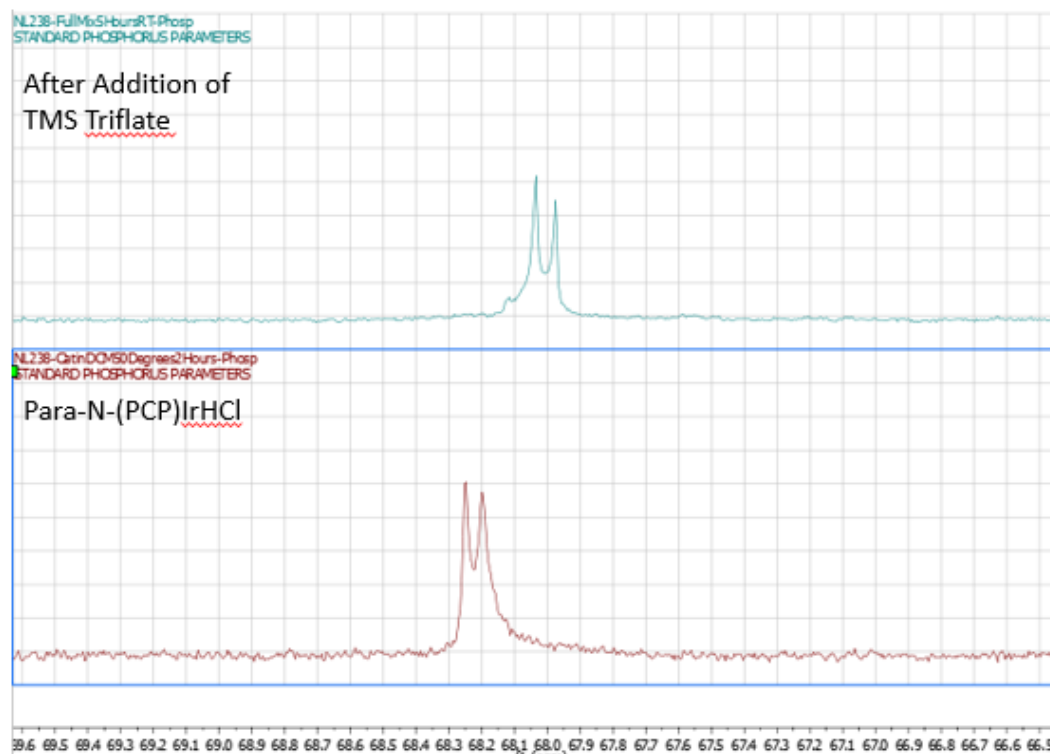


Figure 5.25:  $^1\text{H}$ -NMR: hydride shift upon reaction with trimethylsilyl triflate

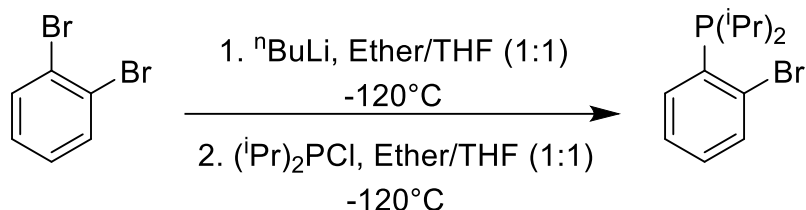
### 5.3 Synthesis of trisphosphine pincer-ligated iridium complexes

#### 5.3.1 Synthesis of ( $i\text{Pr}$ PPP)Ir complexes

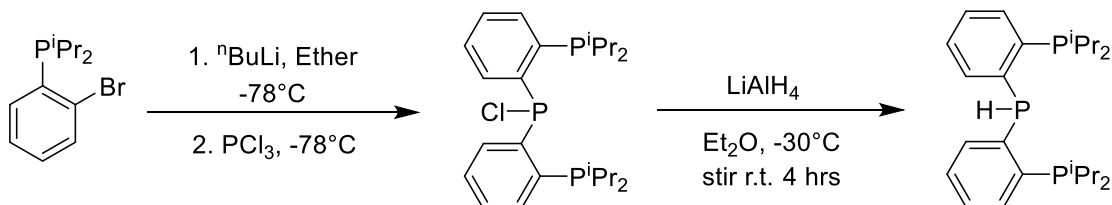
Transition metal complexes with polydentate-phosphine ligands are extremely common in the literature. Phosphine ligands come with a lot of advantages such as the ability to tune both the electronic and steric properties with ease. Additionally phosphine ligands have a tendency to bind strongly to late transition metals. With this in mind we decided to see if synthesis of triphosphine pincer ligands would aid in alkane dehydrogenation.

The ligand we chose to study was a tridentate phosphine with a diarylphosphine center linker with two alkyl phosphine arms. Synthesis of the ligand had been reported

as a two-step process with initial synthesis of the ligand arm followed by reaction with  $\text{PCl}_3$  to link the arms. Reduction of the phosphorus chloride bond with lithium aluminum hydride yielded the ligand.<sup>21</sup>

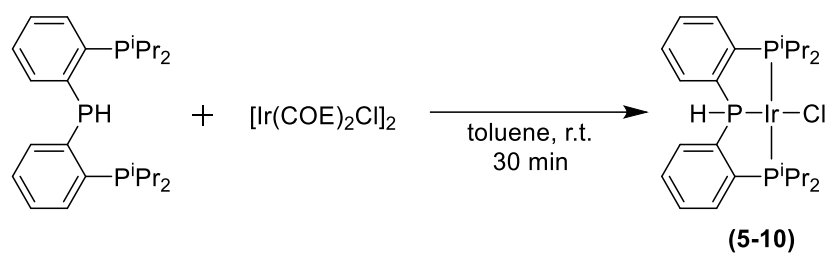


**Scheme 5.17:** Synthesis of ligand arm ((2-bromophenyl)diisopropylphosphane)



**Scheme 5.18:** Synthesis of  $(i\text{Pr})_3\text{PPP}$  ligand

Reaction of the ligand with iridium cyclooctene chloride dimer yielded a new product observed by NMR.  $^{31}\text{P}$ -NMR showed two new signals a double and triplet at 68 and 25 ppm respectively.  $^1\text{H}$ -NMR was consistent with the ligand being bound to the iridium center, observed in the loss of symmetry of the ligand isopropyl groups. Additionally signals attributable to a proton bound to the center phosphorus were observed as a doublet at 4.7 ppm with an unusually large coupling constant of about 350 Hz. The NMR data was consistent with the ligand binding to iridium center without P-H activation of the center ligand.



**Scheme 5.19:** Synthesis of (<sup>i</sup>PrPP<sup>H</sup>P)IrCl complex (5-10)

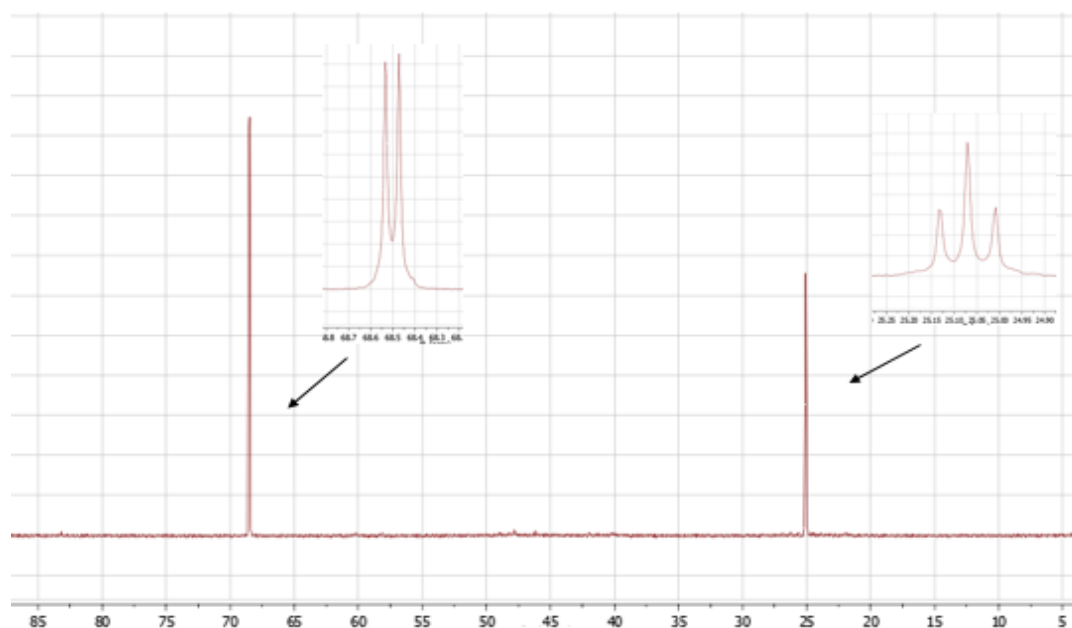


**Figure 5.26:** <sup>31</sup>P-NMR of (<sup>i</sup>PrPP<sup>H</sup>P)IrCl complex (5-10)

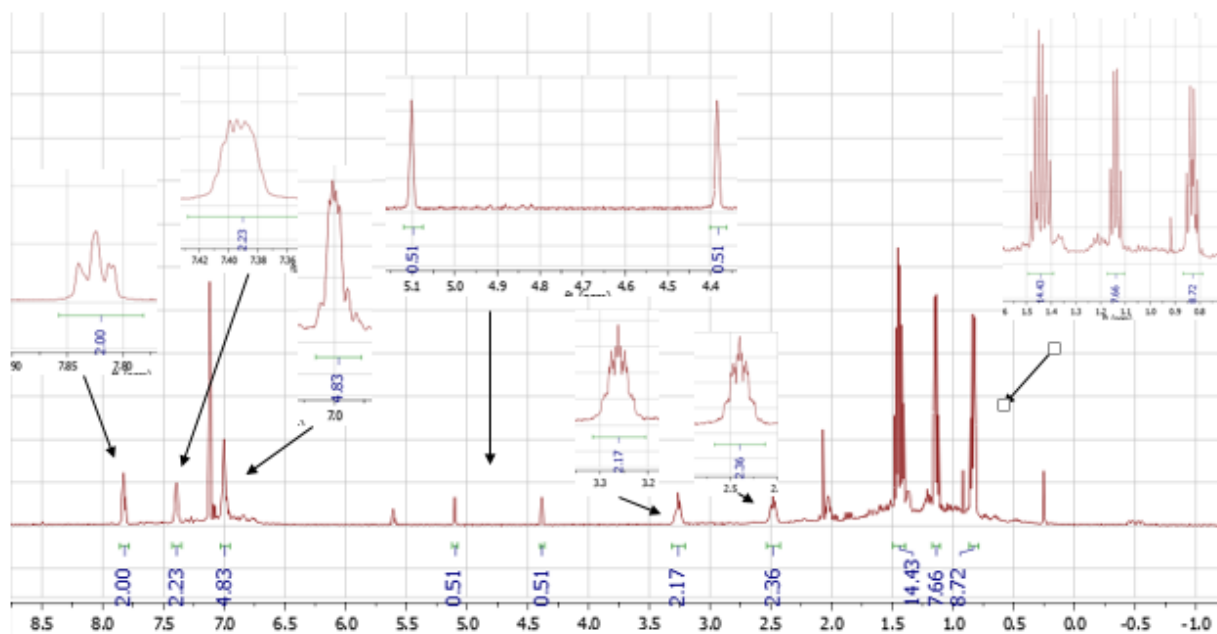


**Figure 5.27:**  $^1\text{H}$ -NMR of  $(i\text{PrPP}^{\text{H}}\text{P})\text{IrCl}$  complex (5-10)

The observation of the hydrogen atom bound to the phosphorous atom in the iridium species was not what was expected. Iridium activation of P-H bonds tend to occur readily however that was not the case here. Upon heating a sample of the  $(i\text{PrPP}^{\text{H}}\text{P})\text{IrCl}$  complex a new signals were observed in both the phosphorus and proton NMR's. The  $^{31}\text{P}$ -NMR showed multiple new signals making identification of any of the products difficult. Among the new peaks observed was a new hydride signal around -22 ppm appearing as a doublet of triplets. This splitting pattern would be consistent with activation of the P-H ligand bond forming the  $\text{IrHCl}$  complex.



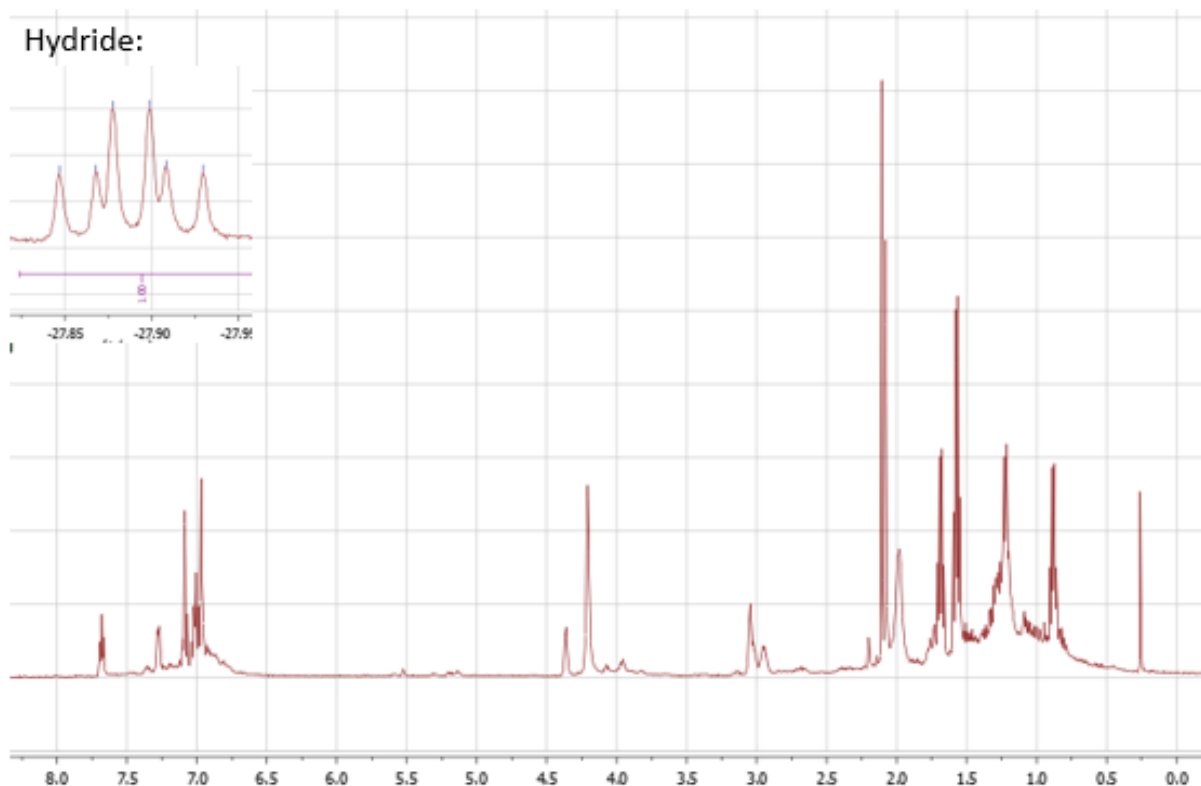
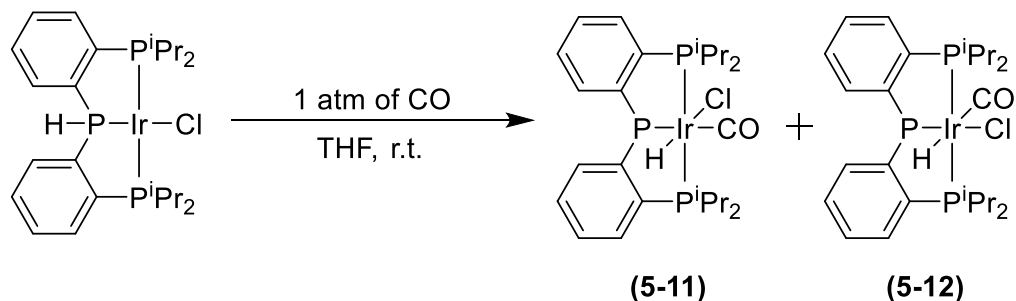


**Figure 5.28:**  $^1\text{H}$ -NMR of (5-10) heated to  $100^\circ\text{C}$  showing hydrogen migration

The ability of the hydrogen atom to move across the phosphorus iridium bond has potential to aid in hydrogenation and dehydrogenation through a metal ligand cooperation mechanism. The Milstein group has reported many examples of metal ligand cooperativity using the pyridine based ( $^t\text{BuPNP}$ ) ligand.<sup>26-29</sup> The potential to add hydrogen or other substrates across the Ir-P bond gave us hope for improved or unforeseen activity using the ( $^i\text{PrPP}^{\text{H}}\text{P}$ )IrCl complex.

In order to better observe this hydrogen transfer from phosphorus to iridium the ( $^i\text{PrPP}^{\text{H}}\text{P}$ )IrCl complex was treated with carbon monoxide. Upon addition of CO to a toluene solution of ( $^i\text{PrPP}^{\text{H}}\text{P}$ )IrCl a color change from orange to yellow was observed in addition to precipitate formation.  $^{31}\text{P}$ -NMR showed formation of multiple new signals all

which had weak intensity making splitting difficult to identify thus making identification of the products difficult. When the reaction was run in THF instead of toluene no precipitate was observed after the addition of CO. Again 8 signals were visible in the  $^{31}\text{P}$ -NMR, however the intensity of the signals was stronger in this case. Upon heating the reaction mixture to  $65^\circ\text{C}$  for 4 hours only 4 peaks were observable in the  $^{31}\text{P}$ -NMR.  $^1\text{H}$ -NMR showed two hydride signals both triplet of doublets at -9.5 and -18.5. This NMR data would be consistent with CO binding followed by P-Ir hydrogen transfer forming the cis and trans- $(^i\text{PrPPP})\text{IrHCl}(\text{CO})$  complexes.



**Scheme 5.20:** Treatment of (5-10) with carbon monoxide to form cis/trans  $(^i\text{PrPPP})\text{IrHCl}(\text{CO})$  complexes

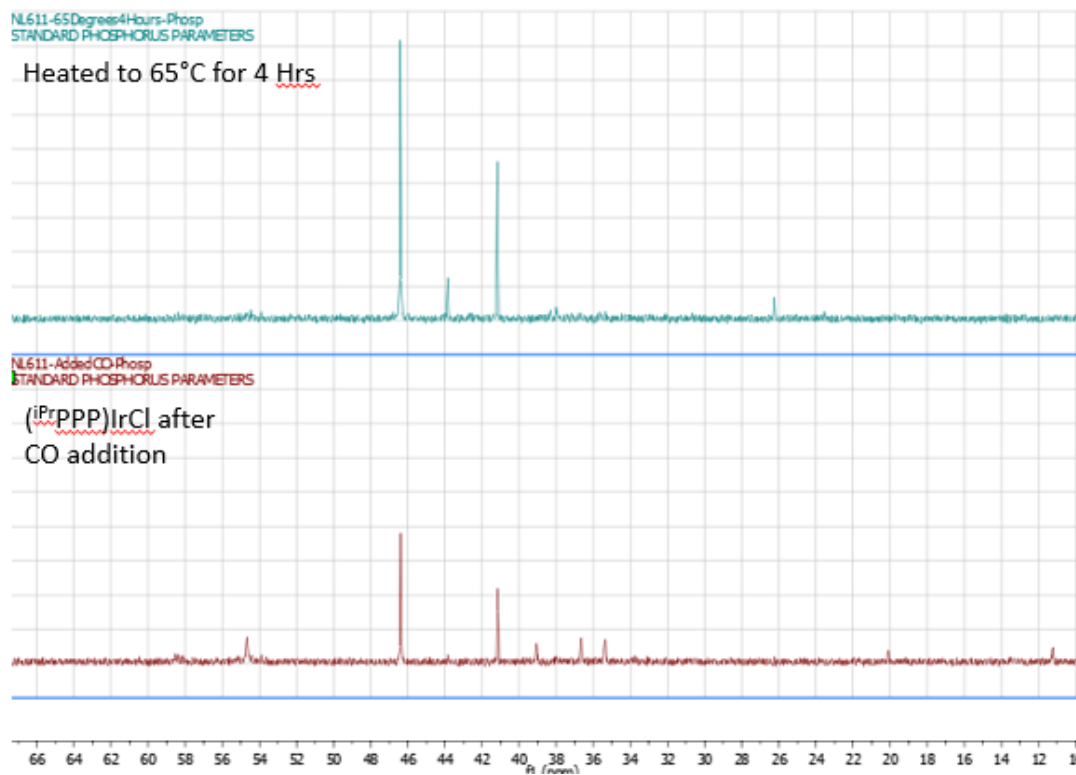


Figure 5.29:  $^{31}\text{P}$ -NMR of (5-11, 5-12) heated to 70°C

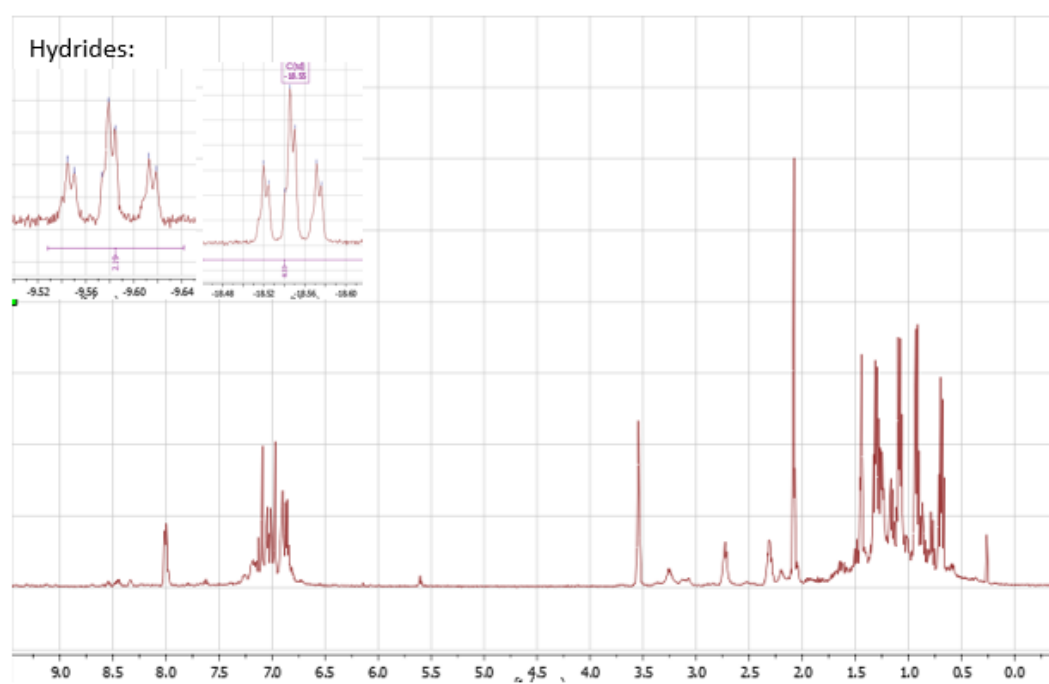
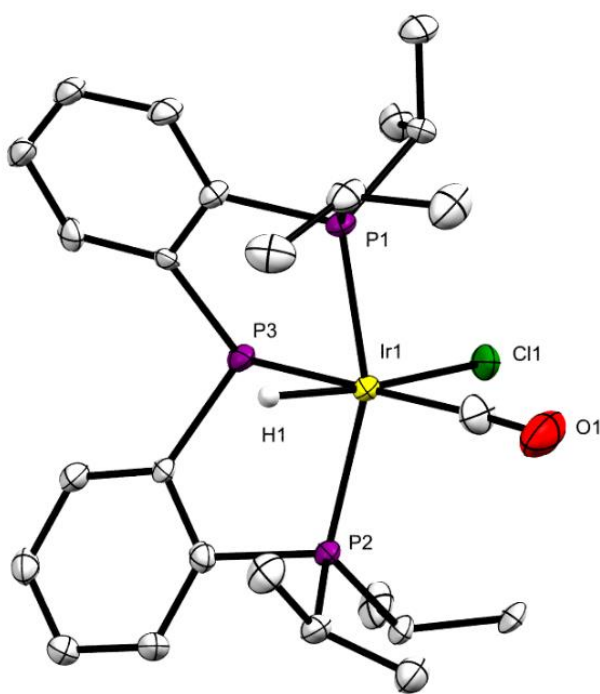


Figure 5.30:  $^1\text{H}$ -NMR of (5-11, 5-12) heated to 70°C

Single crystal analysis of the product confirmed the structure of the (<sup>i</sup>Pr<sub>3</sub>PPP)IrHCl(CO) complex. The crystal structure shows formation of the trans (H trans to Cl) product. The J coupling values for the two hydrides observed were (17 and 2.9 Hz) and (12.9 and 2.4 Hz) for the peaks at -9.5 and -18.5 ppm respectively. In both cases the phosphorus couplings (17 and 12.4 Hz) suggest cis phosphines to the hydride. This would be consistent with two structures with the hydride cis to all phosphines and either the chloride or the carbonyl trans to the hydride.

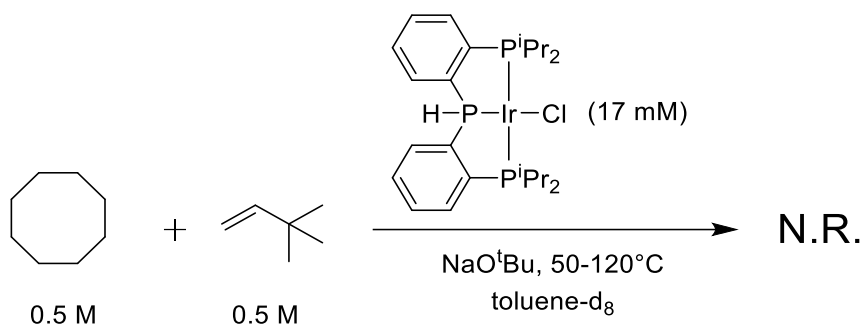


**Figure 5.31** ORTEP representation (50% probability ellipsoids) of the structure of **5-11** determined by X-ray diffraction; hydrogen atoms omitted for clarity.

Table 5.1: Selected Bond Lengths (Å) and angles (°) for (*i*PrPPP)IrHCl(CO)

Ir(1)-P(2)	2.323(3)	O(1)-C(25)	1.103(16)
Ir(1)-P(1)	2.327(3)	P(2)-C(19)	1.853(11)
Ir(1)-P(3)	2.376(3)	P(2)-C(22)	1.867(12)
Ir(1)-Cl(1)	2.503(3)	P(1)-C(16)	1.850(12)
Ir(1)-H(1)	1.599(15)	P(1)-C(13)	1.859(11)
P(2)-Ir(1)-P(3)	85.08(10)	C(2)-P(1)-Ir(1)	106.6(4)
P(1)-Ir(1)-P(3)	83.56(10)	C(12)-P(2)-Ir(1)	106.9(4)
P(2)-Ir(1)-P(1)	157.38(10)		

Potential catalytic activity of the (**5-10**) was assessed by running an alkane dehydrogenation reaction using COA (cyclooctane) as the substrate with TBE as the sacrificial hydrogen acceptor. A stock solution of COA and TBE in toluene- $d_8$  was prepared and (**5-10**) was added to the solution. Sodium tert-butoxide was added to initiate reactivity of the catalyst by deprotonation of the ligand backbone followed by loss of the chloride to form the active 14  $e^-$  species. Upon addition of the base a color change from orange to dark red was observed.  $^{31}\text{P}$ -NMR showed several signals suggesting formation of multiple species. The solution was heated to 50°C for 2 hours but no COE (cyclooctene) was observed. The solution was then heated to 90°C for 12 hours and still no COE was observed. Finally the solution was heated to 120°C for 24 hours and no reactivity was observed. During the course of heating the signals in the phosphorus NMR decreased. This could be due to catalyst decomposition or potential H/D exchange with the deuterated solvent.

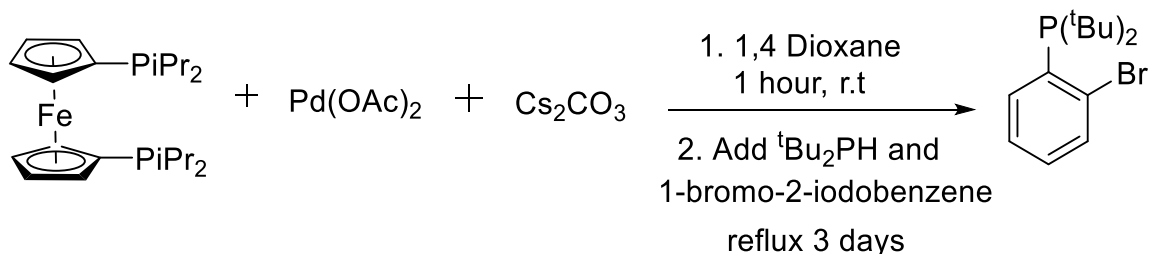


**Scheme 5.21:** COA transfer dehydrogenation using (5-10)

### 5.3.2 Synthesis of ( $^t\text{BuPPP}$ ) Ligand

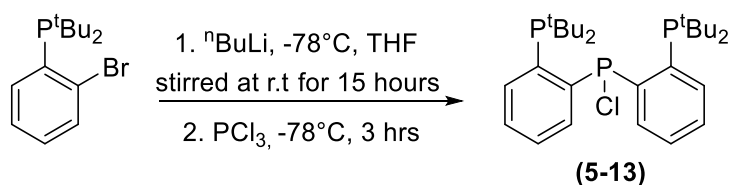
Reaction of ( $^i\text{PrPPP}$ )Ir complexes with base,  $\text{H}_2$  or CO lead to multiple new species observable in the phosphorus NMR. One possible explanation for this is formation of isomers due to the ligand binding in both the meridional and facial coordination phases. The facial coordination could be possible due to the low steric bulk on the phosphines due to the use of isopropyl groups. Tert-butyl phosphinated pincers are known to be more stable than isopropyl pincers<sup>34</sup> and the extra steric bulk of the *t*-butyl groups could prevent any possible facial coordination.

Synthesis of the ( $^t\text{BuPPP}$ ) ligand has not been reported, however the first intermediate towards making this ligand was published by Shimada in 2011.<sup>34</sup> They reported the synthesis of (2-bromophenyl)di-*tert*-butylphosphane using a Buchwald phosphine coupling reaction seen in Scheme 5.18.



**Scheme 5.22:** Buckwald type phosphine coupling to form ligand arm

Following the reported procedure (2-bromophenyl)di-tert-butylphosphane was synthesized and purified using an acid/base work up to remove residual iodo-bromobenzene. Following the synthetic pathway for the (<sup>i</sup>PrPPP) ligand, (2-bromophenyl)di-tert-butylphosphane was treated with n-BuLi followed by reaction with PCl<sub>3</sub>. Reaction conditions used for the lithiation reaction were the same as those for the (<sup>i</sup>PrPPP) ligand. Formation of the ligand was not successful as the <sup>31</sup>P-NMR of the product showed about 50% unreacted starting material. The other product observed was identified di-tert-butyl(2-(dichlorophosphanyl)phenyl)phosphane due to the characteristic phosphorus signal for the dichloroarylphosphine. The observation of unreacted starting material suggests that the lithiation reaction was not complete upon addition of PCl<sub>3</sub>. To remedy this situation the reaction mixture was allowed to stir at room temperature overnight after n-BuLi was added to ensure full lithiation. This was then followed by the addition of PCl<sub>3</sub> which yielded the (<sup>t</sup>BuPPClP) ligand.



**Scheme 5.23:** Synthesis of (<sup>t</sup>BuPP<sup>Cl</sup>P) ligand

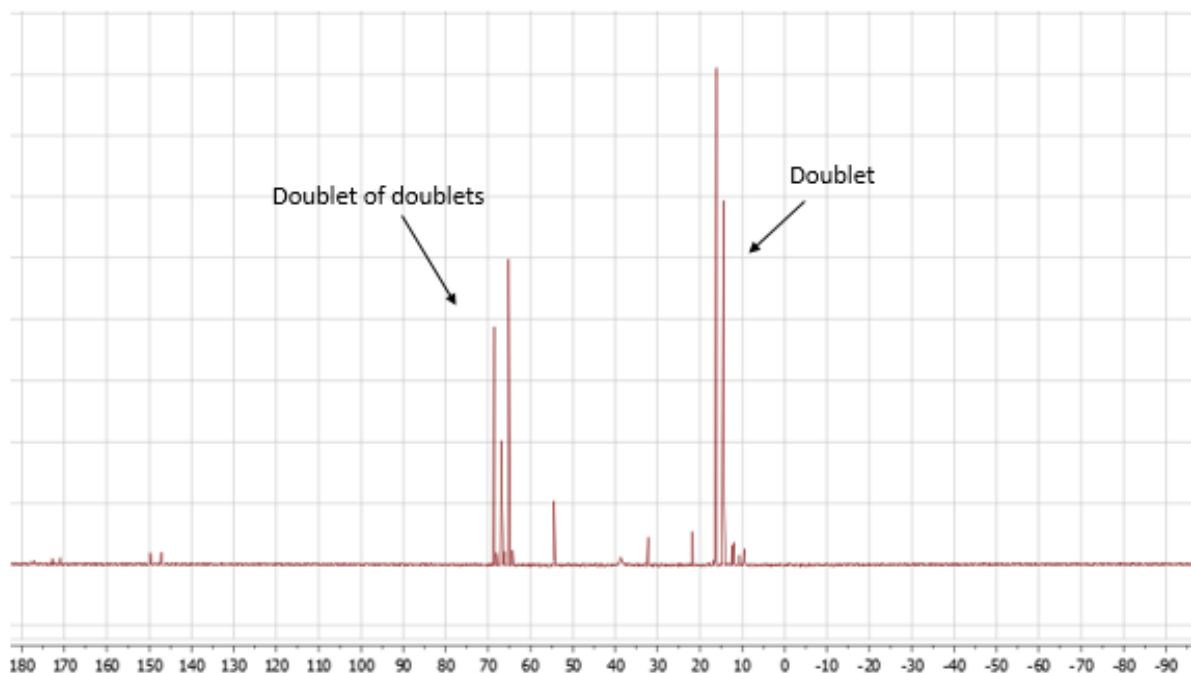
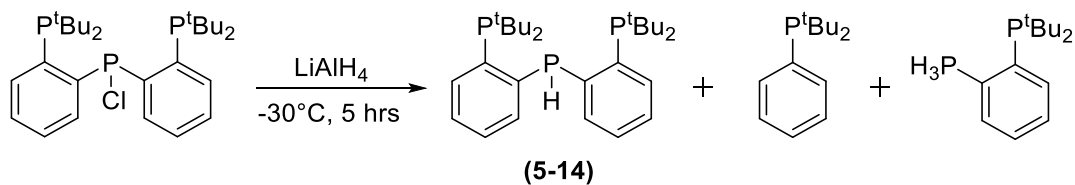


**Figure 5.32:** <sup>31</sup>P-NMR synthesis of (<sup>t</sup>BuPPP) ligand

With the (<sup>t</sup>BuPP<sup>Cl</sup>P) ligand synthesized the next step was to reduce the P-Cl bond to a P-H bond. To do this the (<sup>t</sup>BuPP<sup>Cl</sup>P) ligand was reacted with lithium aluminum hydride at -30°C and then stirred at room temperature for five hours. Upon work up of this reaction three products were observed by <sup>31</sup>P-NMR. The major product was the desired product the (<sup>t</sup>BuPP<sup>H</sup>P) ligand. The other two products were determined to be di-tert-butyl(phenyl)phosphane and di-tert-butyl(2-phosphanylphenyl)phosphane. These two products are most likely caused by aryl C-P cleavage of the ligand.





**Scheme 5.24:** Synthesis of (<sup>t</sup>BuPP<sup>H</sup>P) ligand

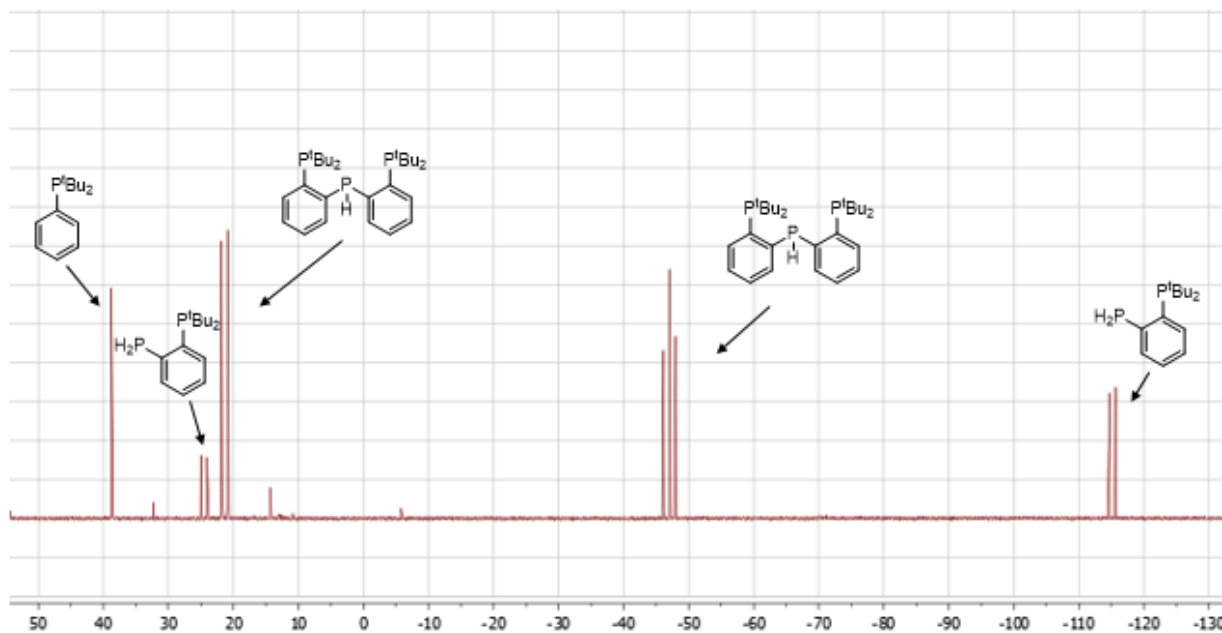
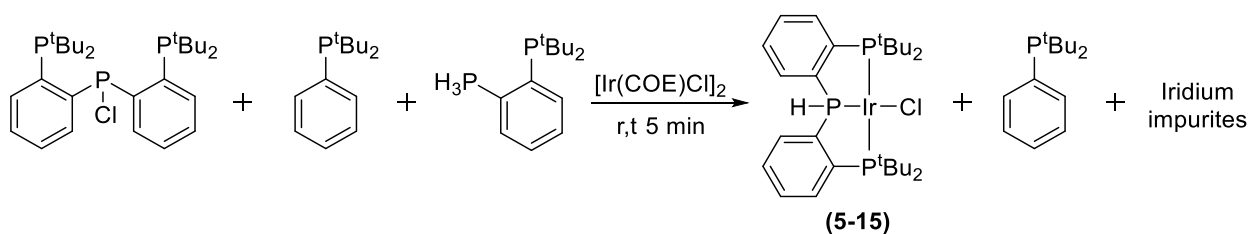


**Figure 5.33:** <sup>31</sup>P-NMR synthesis of (<sup>t</sup>BuPP<sup>H</sup>P) ligand

This side products of this reaction were difficult to remove as all the products are of similar structure. Filtering the mixture with benzene through a silica pad seemed to reduce the percentage of the side products. Further purification by column chromatography is one option the other is rerunning the reaction using a more mild reducing agent to hopefully prevent this C-P cleavage.

To see if this ligand would react with iridium in the same fashion as the (<sup>i</sup>PrPP<sup>H</sup>P) ligand, the impure mixture was treated with [Ir(COE)Cl]<sub>2</sub> (2:0.7 ligand to iridium ratio). Upon mixing the ligand mixture with the iridium source the solution turned ruby red immediately. <sup>31</sup>P-NMR revealed a doublet (74 ppm) and a triplet (26 ppm) both of which correspond with the formation of (<sup>t</sup>BuPP<sup>H</sup>P)IrCl. This assessment was supported by the

$^1\text{H}$ -NMR, wherein a doublet of triplets (4.15 and 5.10 ppm) with a coupling constant of 365 Hz was observed. This is consistent with what was observed with the ( $i\text{PrPP}^{\text{H}}\text{P}$ ) ligand, a coordinated iridium product with the center P-H bond still intact. Side products were observed most likely from iridium reacting with di-tert-butyl(2-phosphanlyphenyl)phosphane while the di-tert-butyl(phenyl)phosphane did not seem to react.



**Scheme 5.25:** ( $t\text{BuPP}^{\text{H}}\text{P}$ ) ligand reacted with  $[\text{Ir}(\text{COE})\text{Cl}]_2$

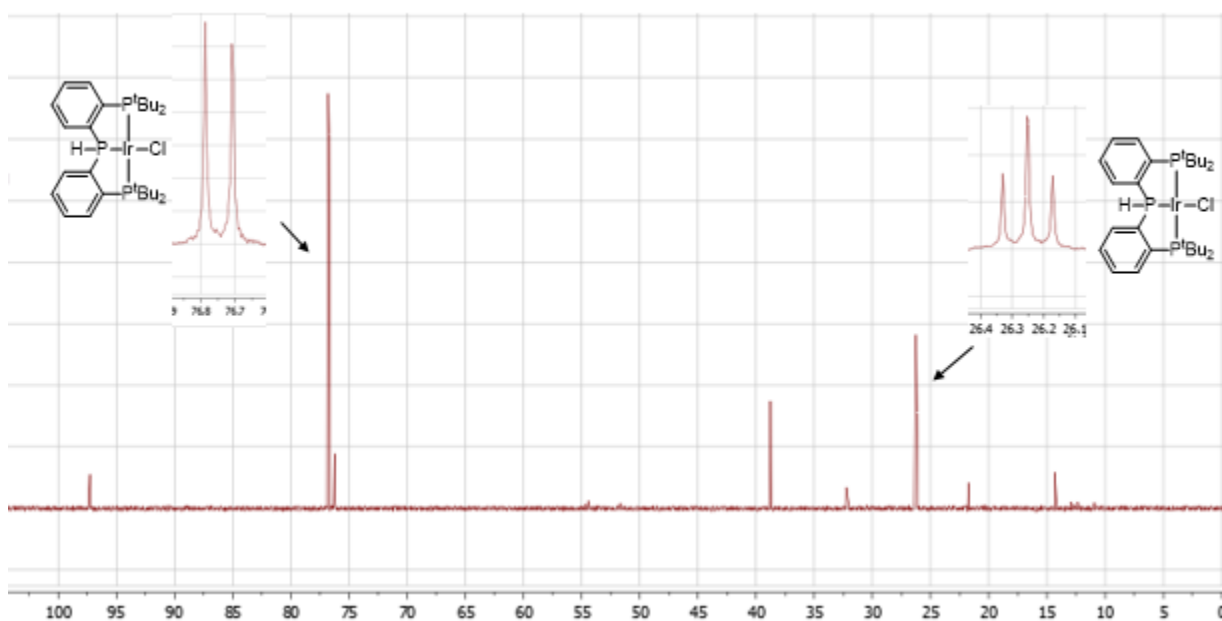


**Figure 5.34:**  $^{31}\text{P}$ -NMR of  $[\text{Ir}(\text{COE})\text{Cl}]_2$  reacted with ( $t\text{BuPP}^{\text{H}}\text{P}$ ) ligand

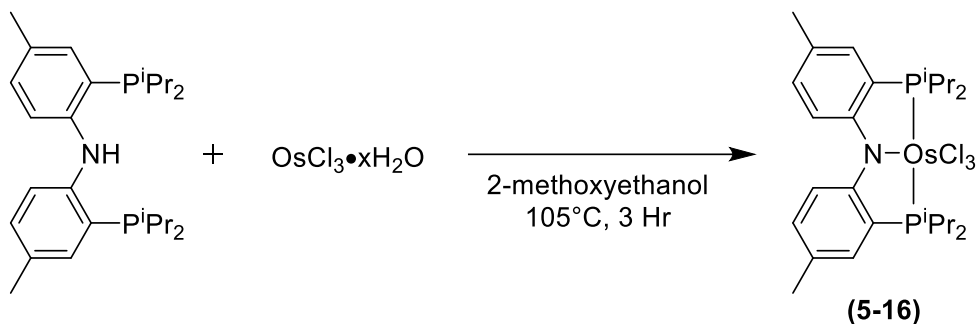
Upon heating this solution to 50°C for one hour, the  $^{31}\text{P}$ -NMR signals corresponding to the  $(^t\text{BuPP}^{\text{H}}\text{P})\text{IrCl}$  complex disappeared. All other signals previously observed were remained. Additionally multiple new signals were observed between 45 and 55 ppm. The loss of  $^{31}\text{P}$ -NMR signals and the appearance of multiple signals in the 50 ppm range is consistent with what was observed when heating **(5-10)**. It appears that the added bulk did not stabilize the complex as hypothesized. One possible reason for the degradation could be cyclometalation of the alkyl group on the phosphorus. Altering the substituents on the phosphorus to ones that cannot C-H activate might alleviate this issue.

#### 5.4 Pincer-ligated osmium complexes

As discussed in chapter 3 the use of osmium complexes for alkane dehydrogenation is very limited. PNP ligated osmium complexes are isoelectronic to PCP iridium complexes which are well known alkane dehydrogenation catalysts. Our studies using pyridine based  $(^t\text{BuPNP})\text{Os}$  complexes for alkane dehydrogenation were not successful due to unfavorable thermodynamics for hydrogenation of sacrificial hydrogen acceptors. Alternatively concerns over the stability of the catalyst arose as heating the solution to high temperatures lead to decomposition products.

Use of alternative PNP ligands could potentially alter the reactivity we observed with  $(^t\text{BuPNP})\text{Os}$ , in addition to providing better stability. We chose to study the previously discussed diaryl-PNP (Ozerov ligand) for use with osmium. We believed that making the ligand a LXL vs a LLL ligand would impart stronger stability to the complex.

Synthesis of the Ozerov ( $i^{\text{Pr}}\text{PNP}$ )OsCl<sub>3</sub> complex was done by reacting free ligand with OsCl<sub>3</sub>•xH<sub>2</sub>O in THF. Heating of the suspension resulted in the formation of a very dark green solution. <sup>31</sup>P-NMR showed a new resonance signal at about -120 ppm which was not expected as the product was anticipated to be paramagnetic. Single crystal analysis identified the product as the Ozerov ligand ( $i^{\text{Pr}}\text{PNP}$ )OsCl<sub>3</sub> in which the backbone nitrogen has been deprotonated. This was unexpected as no base was added to the solution however it is possible some of the osmium starting material could have deprotonated the complex. This deprotonation was similarly observed when reacting the ligand with MoCl<sub>3</sub>(THF)<sub>3</sub> as discussed in chapter 4.



**Scheme 5.26:** Synthesis of Ozerov ( $i^{\text{Pr}}\text{PNP}$ )OsCl<sub>3</sub> (**5-16**)

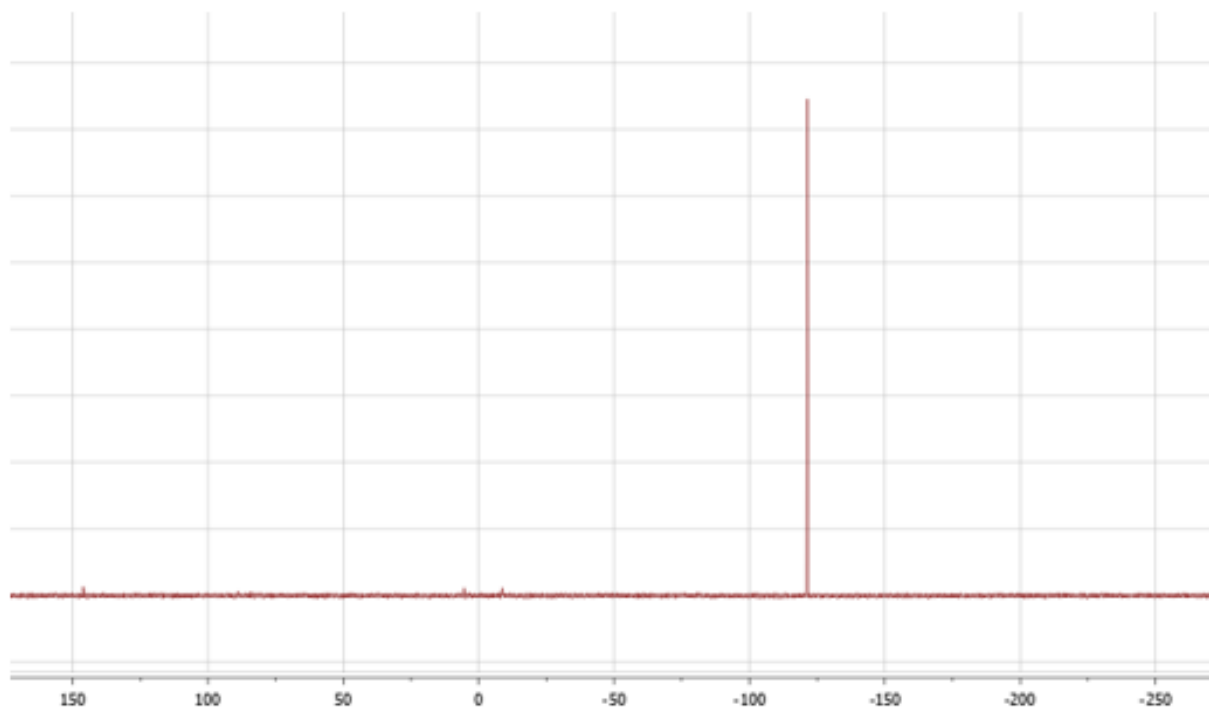


Figure 5.35:  $^{31}\text{P}$ -NMR spectra of (5-16)

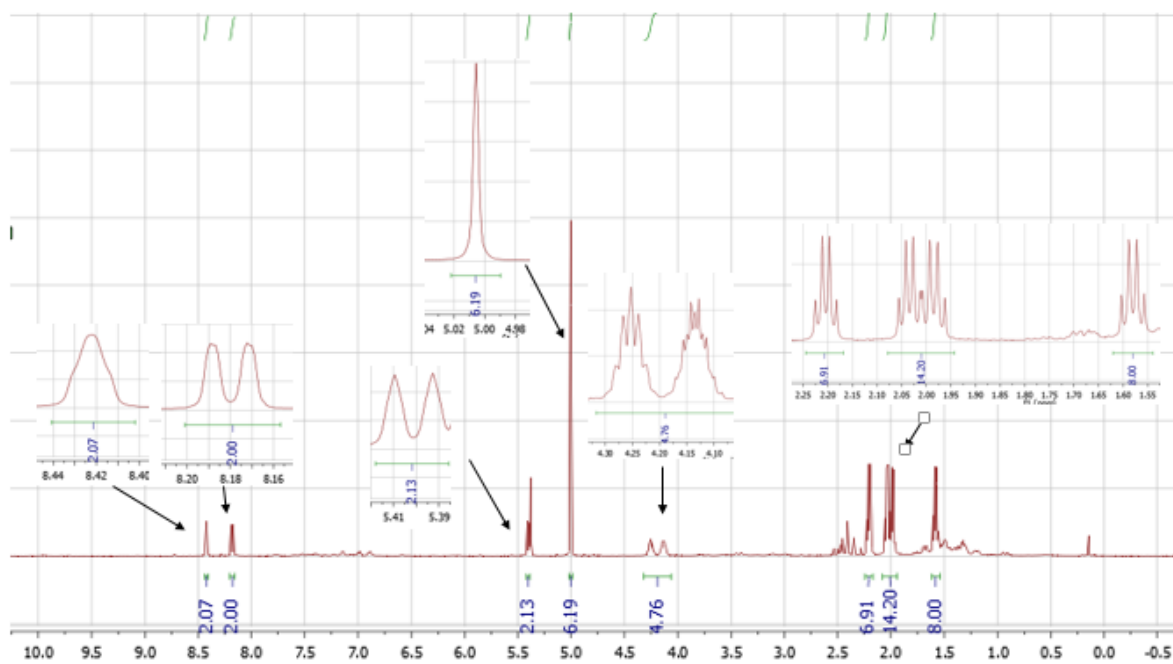
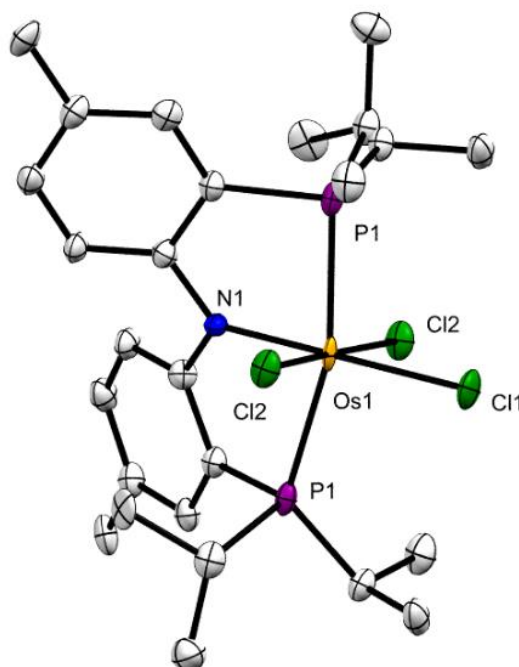


Figure 5.36 :  $^1\text{H}$ -NMR spectra of (5-16)

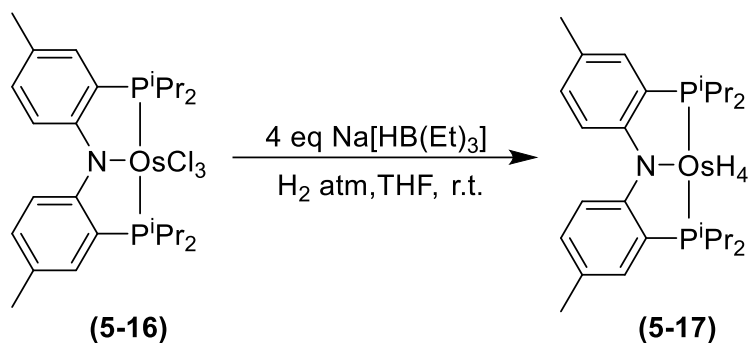


**Figure 5.37** ORTEP representation (50% probability ellipsoids) of the structure of **(5-16)** determined by X-ray diffraction; hydrogen atoms omitted for clarity.

**Table 5.2:** Selected Bond Lengths (Å) and angles (°) for (*i*PrPNP)OsCl<sub>3</sub> **(5-13)**

Os(1)-N(1)	1.943(16)	Os(1)-Cl(1)	2.381(5)
Os(1)-P(1)	2.375(4)	Os(1)-Cl(2)	2.355(4)
Os(1)-P(1)#1	2.375(4)	P(1)-C(2)	1.835(15)
N(1)-Os(1)-Cl(2)	91.31(9)	N(1)-Os(1)-Cl(1)	180.0
N(1)-Os(1)-P(1)#1	81.54(9)	C(1)-N(1)-Os(1)	120.5(8)

Having synthesized the trichloride osmium precursor the next step was the reduction to the tetrahydride a more viable alkane dehydrogenation starting material. Treatment of the (*i*PrPNP)OsCl<sub>3</sub> with 4 equivalents of sodium triethylborohydride in THF yielded a single new product.



**Scheme 5.27:** Synthesis of Ozerov (<sup>i</sup>PrPNP)OsH<sub>4</sub> (5-17)

<sup>31</sup>P-NMR showed a broad new singlet resonance signals at 57 ppm and <sup>1</sup>H-NMR showed a new broad hydride resonance at -12 ppm. The broad hydride signal is consistent with previously made pincer ligated osmium tetrahydride complexes. Correct integration of the hydride could not be obtained as once solvent was removed (in order to remove triethylborohydride) a color change from yellow to dark orange was observed. NMR of the product after solvent was removed showed no sign of the previous product. Instead new signals were observed in the <sup>31</sup>P-NMR in the region of 30 ppm and no hydride signals were seen in the <sup>1</sup>H-NMR. The isolation of the tetrahydride complex so far has not been successful.

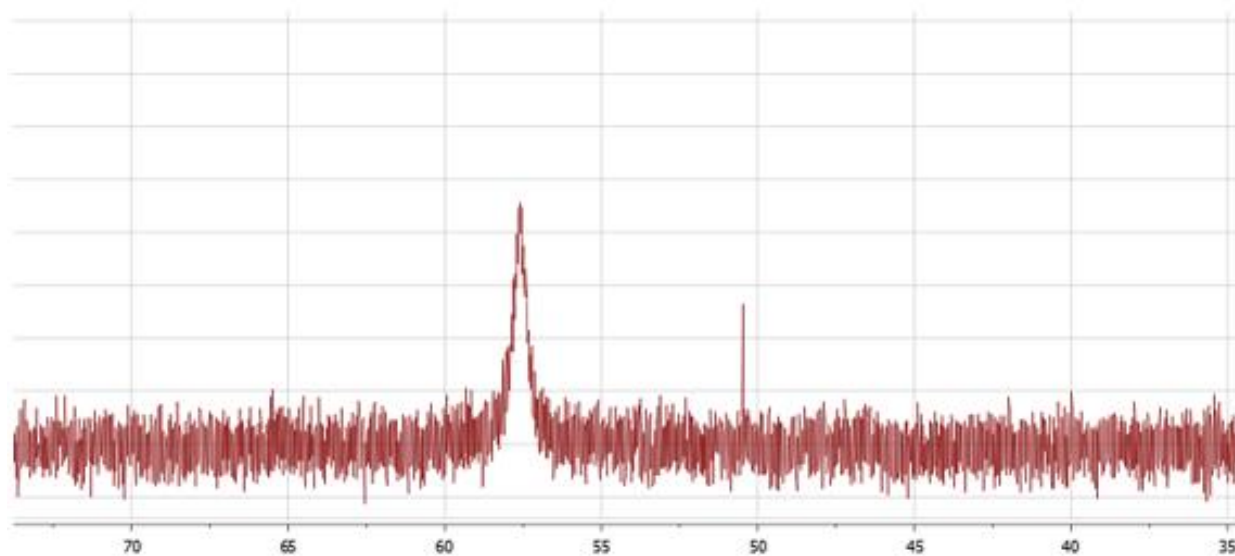


**Figure 5.38:**  $^{31}\text{P}$ -NMR spectra of (5-17)

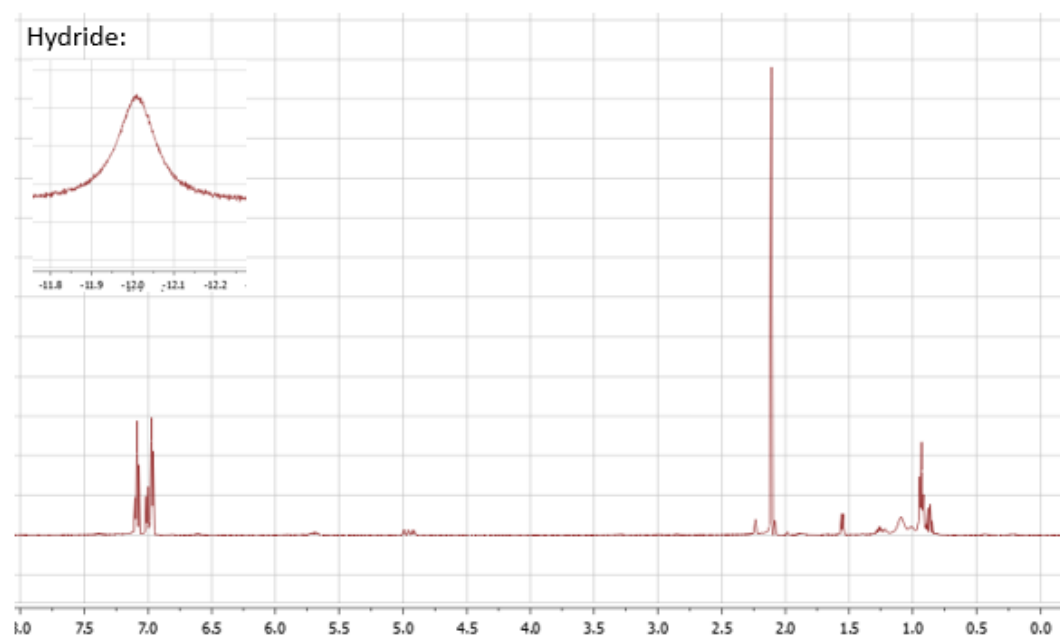


**Figure 5.39:**  $^{31}\text{P}$ -NMR spectra of (5-17)



## 5.5 Experimental

### 5.5.1 General Information

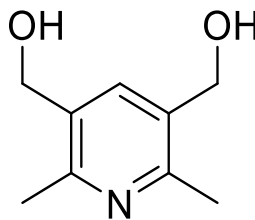
All procedures involving organometallic compounds were conducted under an argon atmosphere using standard glovebox and Schlenk techniques. Solvents were purchased as anhydrous grade and purged with argon before use. Deuterated solvents (*p*-xylene- $d_{10}$ , toluene- $d_8$ , benzene- $d_6$ , THF- $d_8$ ) were degassed via freeze-pump-thaw cycles and dried over activated  $Al_2O_3$  and stored on 3 Å molecular sieves prior to use. Ethylene, Nitrogen and carbon monoxide was purchased from various suppliers in the highest purity available and used as received.  $^1H$  and  $^{31}P$  NMR spectra were recorded on 400 MHz and 500 MHz Varian spectrometers. Chemical shifts are reported in ppm.  $^1H$  NMR signals are referenced to the residual solvent signals, and  $^{31}P$  NMR signals are referenced to an external standard of 85%  $H_3PO_4$ . X-Ray diffraction was obtained from an oil coated crystal mounted on a glass fiber. Peters ( $iPr$ PPP) ligands were synthesized following literature procedure.<sup>21</sup>

For all complexes, X-ray diffraction data were collected on a Bruker Smart APEX CCD diffractometer with graphite mono-chromatized  $MoK\alpha$  radiation ( $\lambda = 0.71073\text{\AA}$ ) at a temperature of 100 K or 120 K. Crystals were immersed in Paratone oil and placed on a glass needle or nylon loop. The data were corrected for Lorentz effects, polarization, and absorption, the latter by a multiscan (SADABS) method.<sup>51</sup> The structures were solved by direct methods (SHELXS86).<sup>52</sup> All non-hydrogen atoms were refined (SHELXL97)<sup>3</sup> based

upon  $F_{\text{obs}}$ . All hydrogen atom coordinates were calculated with idealized geometries (SHELXL97). Scattering factors ( $f_o$ ,  $f'$ ,  $f''$ ) are as described in SHELXL97.

### 5.5.2 Synthesis pincer-ligated metal complexes

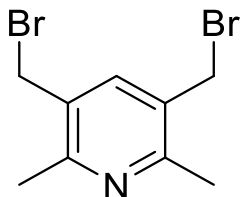
#### Synthesis of diethyl (2,6-dimethylpyridine-3,5-diyl)dimethanol (5-3)



Diethyl 2,6-dimethylpyridine-3,5-dicarboxylate (1.80 g, 7.17 mmol) was dissolved in diethyl ether (40 mL) forming a light green solution. In a second flask lithium aluminium hydride (1.36 g, 35.8 mmol) was dissolved in diethyl ether (60 mL) forming a gray suspension. The lithium aluminum hydride suspension was cooled to 0°C and the ester solution was cannula transferred in resulting in green colored suspension. Next a reflux condenser was attached to the flask and the solution was heated to 40°C for 7 hours where the color of the solution turned gray. The solution was then cooled to 0°C and 70 mL of water was added (very slowly) to quench the solution (2 layers formed, one with cloudy white solid). The solvent was removed leaving a white solid. The solid was dissolved in acetonitrile and then the solvent was removed leaving a yellow solid. Acetonitrile was added again this time solid crashed out. The acetonitrile solution was separated and the solvent was removed leaving a white powder. Yield 0.531 g (44.3%)

$^1\text{H-NMR}$  (400 MHz,  $\text{CD}_3\text{OD}$ ):  $\delta$  7.59 (s, 1H *aryl-H*), 5.13 (t,  $J = 5.3$ , 2H, O-H), 4.44 (d,  $J = 5.1$ , 4H,  $\text{CH}_2\text{-P}$ ), 2.31 (s, 6H, methyl).

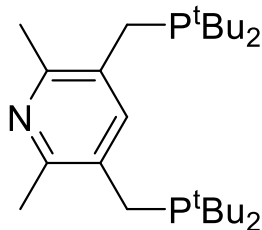
#### Synthesis of 3,5-bis(bromomethyl)-2,6-dimethylpyridine (5-4)



(2,6-dimethylpyridine-3,5-diyl)dimethanol (1.0 g, 5.98 mmol) was dissolved in 48% HBr aqueous solution (added very slowly as the addition is exothermic) resulting in a light brown solution. The solution was refluxed ( $100^\circ\text{C}$ ) for 19 hours upon which the solution turned a slightly darker brown. The solution was cooled to room temperature and then 10% wt solution of  $\text{NaCO}_3$  was added (added slowly as formation of  $\text{CO}_2$  is rapid).  $\text{NaCO}_3$  solution was added until solid crashed out of solution. The solution was filtered and the solid was collected and dissolved in  $\text{CH}_2\text{Cl}_2$ . The solution was then extracted with water 3 times. The  $\text{CH}_2\text{Cl}_2$  solution was then dried over  $\text{MgSO}_4$  and the color of the solution went from light brown to clear. The solution stirred for 30 min and then was filtered. The solvent was then removed leaving a white powder. Yield 0.80 g (45.6%).

$^1\text{H-NMR}$  (400 MHz,  $\text{CDCl}_3$ ):  $\delta$  7.50 (s, 1H *aryl-H*), 4.45 (s, 4H,  $\text{CH}_2\text{-P}$ ), 2.59 (s, 6H, methyl).

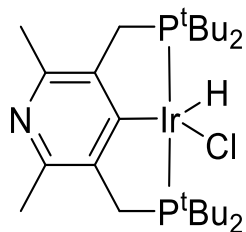
### Synthesis of 3,5-bis((di-tert-butylphosphanyl)methyl)-2,6-dimethylpyridine (5-5)



3,5-bis(bromomethyl)-2,6-dimethylpyridine (0.314 g, 1.07 mmol) was dissolved in acetone (15 mL) resulting in a clear solution. Next di-tertbutylphosphine (0.4 mL, 2.14 mmol) was added dropwise to the solution. The solution was then heated to reflux for 24 hours upon which the solution turned cloudy white. The solution was allowed to cool to room temperature and then the solvent was removed leaving a white powder. Benzene (25 mL) was added to dissolve the white powder followed by the addition of trimethylamine (0.4 mL). The solution was stirred at room temperature for 3 days during which a crystalline precipitate formed. The solution was removed by cannula filtration and the residue was washed with benzene (10 mL x 2). The solvent was removed leaving a white powder. Yield 0.425 g (93.5%).

$^1\text{H-NMR}$  (400 MHz, benzene- $\text{d}_6$ ):  $\delta$  8.09 (s, 1H *aryl-H*), 2.78 (s, 6H, *methyl*), 2.69 (broad singlet, 4H,  $\text{CH}_2\text{-P}$ ), 1.07 (dd,  $J = 10.7, 1.1$ , 36H, *tert-butyl*).  $^{31}\text{P-NMR}\{^1\text{H}\}$  (121 MHz, toluene- $\text{d}_8$ ):  $\delta$  26.8 (s,  $\text{P}^t\text{Bu}_2$ )

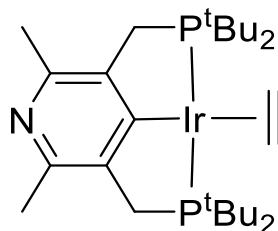
### Synthesis of para-nitrogen (<sup>t</sup>BuPCP)IrHCl (5-6)



3,5-bis((di-tert-butylphosphanyl)methyl)-2,6-dimethylpyridine (0.43 g, 1.01 mmol) and [Ir(COD)Cl]<sub>2</sub> (0.34 g, 0.506 mmol) were dissolved in toluene (50 mL) forming an orange solution. The solution was refluxed for 3 days under a flow of H<sub>2</sub> gas. Over the course of the reflux the solution turned red in color. The solution was allowed to cool to room temperature and the solvent was removed leaving a red solid. The solid was extracted with pentane (25 mL x 5) and the fractions were combined. The solvent was removed leaving the red solid product. Yield 0.640 grams (97%).

<sup>1</sup>H-NMR (400 MHz, benzene-d<sub>6</sub>): δ 2.96 (ddt, J = 65.8, 17.5, 3.9 Hz, 4H CH<sub>2</sub>-P), 2.60 (s, 6H, *methyl*), 1.24 (dt, J = 26.4, 6.7, 36H, *tert*-butyl), -41.8 (t, J = 12.3, 1H, Ir-H). <sup>31</sup>P-NMR{<sup>1</sup>H} (121 MHz, toluene-d<sub>8</sub>): δ 66.3 (s, P<sup>t</sup>Bu<sub>2</sub>)

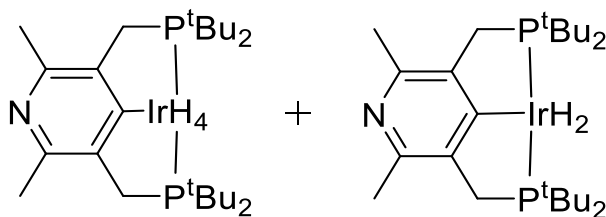
### Synthesis of para-nitrogen (<sup>t</sup>BuPCP)Ir(C<sub>2</sub>H<sub>4</sub>) (5-7)



Para-nitrogen (<sup>t</sup>BuPCP)IrHCl (0.143 g, 0.223 mmol) and sodium tert-butoxide (0.021 g, 0.223 mmol) were dissolved in toluene (15 mL). Next the solution was bubbled with ethylene and then allowed to stir at room temperature for 3 hours under an ethylene flow. Over the course of stirring the solution turned dark purple. The solution was then cannula filtered and the solvent was removed leaving a dark purple solid. Yield 0.120 g (82.9%)

<sup>1</sup>H-NMR (400 MHz, p-xylene-d<sub>10</sub>): δ 2.96 (ddt, J = 65.8, 17.5, 3.9 Hz, 4H CH<sub>2</sub>-P), 2.60 (s, 6H, *methyl*), 1.24 (dt, J = 26.4, 6.7, 36H, tert-butyl), -41.8 (t, J = 12.3, 1H, Ir-H). <sup>31</sup>P-NMR{<sup>1</sup>H} (121 MHz, toluene-d<sub>8</sub>): δ 61.3 (s, P<sup>t</sup>Bu<sub>2</sub>)

#### Synthesis of para-nitrogen (<sup>t</sup>BuPCP)IrH<sub>4</sub>/H<sub>2</sub> (5-8, 5-9)



Para-nitrogen (<sup>t</sup>BuPCP)Ir(C<sub>2</sub>H<sub>4</sub>) (0.100 g, 0.734 mmol) was dissolved in toluene (15 mL). Next the solution was bubbled with hydrogen and then allowed to stir at room temperature for 2 hours under a hydrogen flow. Over the course of stirring the solution turned yellow/orange. The solvent was then removed leaving an orange solid. NMR showed formation of two products the dihydride and tetrahydride. Yield 0.075 g (79.7%).

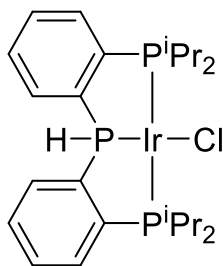
Dihydride:  $^1\text{H}$ -NMR (400 MHz, p-xylene- $\text{d}_{10}$ ):  $\delta$  3.53 (broad singlet, 4H  $\text{CH}_2\text{-P}$ ), 2.84 (broad singlet, 6H, *methyl*), 1.33 (dt,  $J = 6.5$ , 36H, tert-butyl), -18.0 (t,  $J = 9.5$ , 1H, Ir-H).

$^{31}\text{P}$ -NMR $\{^1\text{H}\}$  (121 MHz, toluene- $\text{d}_8$ ):  $\delta$  88.2 (s,  $\text{P}^t\text{Bu}_2$ )

Tetrahydride:  $^1\text{H}$ -NMR (400 MHz, p-xylene- $\text{d}_{10}$ ):  $\delta$  3.34 (broad singlet, 4H  $\text{CH}_2\text{-P}$ ), 2.70 (broad singlet, 6H, *methyl*), 1.33 (dt,  $J = 6.5$ , 36H, tert-butyl), -8.98 (t,  $J = 9.8$ , 1H, Ir-H).

$^{31}\text{P}$ -NMR $\{^1\text{H}\}$  (121 MHz, toluene- $\text{d}_8$ ):  $\delta$  73.8 (s,  $\text{P}^t\text{Bu}_2$ )

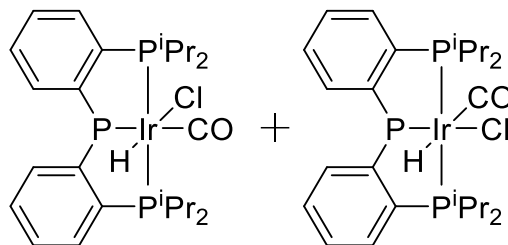
### Synthesis of ( $i\text{PrPP}^{\text{H}}\text{P}$ )IrCl (5-10)



( $i\text{PrPP}^{\text{H}}\text{P}$ ) ligand (0.307 g, 0.152 mmol) and  $[\text{Ir}(\text{COE})_2\text{Cl}]_2$  were dissolved in toluene (10 mL) forming an orange solution. The solution was stirred at room temperature for 1 hour. The solvent was removed leaving a brown solid. Yield 0.405 g (85.4%).

$^1\text{H}$ -NMR (400 MHz, benzene- $\text{d}_6$ ):  $\delta$  7.82 (td,  $J = 7.5, 6.9, 2.4$  Hz, 2H, aryl CH ortho to  $\text{P}^{i\text{Pr}}$ ), 7.39 (m, 2H, aryl C-H), 7.00 (m, 4H, aryl C-H), 4.74 (dt,  $J = 358, 2$  Hz, 1H, P-H), 3.26 (m, 2H,  $\text{CH}(\text{CH}_3)$ ), 2.48 (m, 2H,  $\text{CH}(\text{CH}_3)$ ), 1.44 (dq,  $J = 15.5, 7.5$  Hz, 12H,  $\text{CH}(\text{CH}_3)$ ), 1.14 (q,  $J = 7.0$  Hz, 6H,  $\text{CH}(\text{CH}_3)$ ), 0.83 (q,  $J = 7.0$  Hz, 6H,  $\text{CH}(\text{CH}_3)$ ).  $^{31}\text{P}$ -NMR $\{^1\text{H}\}$  (121 MHz, benzene- $\text{d}_6$ ):  $\delta$  20.1 (t,  $J = 12.7$ , P-H), 63.5 (d,  $J = 12.4$ ,  $\text{P}^{i\text{Pr}}_2$ )

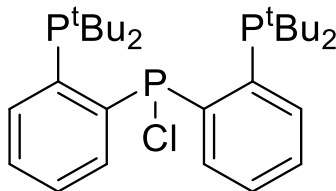
### Synthesis of (*i*PrPP<sup>H</sup>P)IrHCl(CO) (5-11 and 5-12)



(*i*PrPP<sup>H</sup>P)IrCl (**5-10**) (0.008 g, 0.011 mmol) was dissolved in THF (0.5 mL) forming a light brown solution. The solution was transferred to a J. Young tube and then charged with 1 atm of carbon monoxide. Upon addition of carbon monoxide the color of the solution went from light brown to yellow. The tube was then heated to 70°C for 1 hour.

<sup>1</sup>H-NMR (400 MHz, toluene-*d*<sub>8</sub>): Due to mixture of products accurate proton assignments could not be made except for hydride signals: trans-product δ -18.6 (td, *J* = 12.9, 2.4 Hz, Ir-H), cis-product δ -9.58 (td, *J* = 17.0, 2.9 Hz, Ir-H). <sup>31</sup>P-NMR{<sup>1</sup>H} (121 MHz, toluene-*d*<sub>8</sub>): trans (H to Cl) major product δ 54.66 (d, *J* = 3.5, P<sup>*i*</sup>Pr<sub>2</sub>), 49.40 (s, HP-diaryl), cis (H to Cl) minor product δ 52.10 (s, P<sup>*i*</sup>Pr<sub>2</sub>), 34.84 (s, HP-diaryl).

### Synthesis of (<sup>*t*</sup>BuPP<sup>Cl</sup>P) Ligand (5-13)



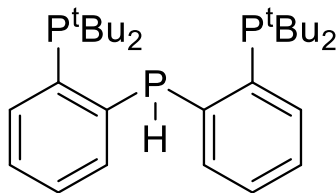
(2-bromophenyl)di-tert-butylphosphane (0.484 g, 1.61 mmol) was dissolved in diethyl ether (20 mL) forming a clear/yellowish solution. The solution was cooled down -70°C, upon which *n*-BuLi (0.65 mL, 1.63 mmol) was added dropwise. The solution stirred at -



70°C for approximately ten minutes and then was taken out of the cold bath and allowed to warm to room temperature. The solution was then allowed to stir overnight sealed under argon (approximately 15 hours) upon which it turned light yellow. Next the solution was again cooled down to -70°C and  $\text{PCl}_3$  (0.070 mL, 0.80 mmol) was added dropwise. The solution was then taken out of the cold bath and allowed to warm to room temperature and stir for 3 hours. After three hours a yellow solution with white precipitate was observed. The solvent was then removed by vacuum and the resulting solid was dissolved in benzene and cannula filtered (cannula filter must be very dry leave in oven overnight). The solvent was then removed leaving a yellowish solid. Yield 0.25 grams (61.4%)

$^1\text{H}$ -NMR (400 MHz, benzene- $\text{d}_6$ ):  $\delta$  7.93 (m, 2H, aryl C-H), 7.67 (m, 2H, aryl C-H), 7.08 (m, 4H, aryl C-H), 1.24 (d,  $J = 11.6$  Hz, 18H,  $\text{C}(\text{CH}_3)_3$ ), 1.14 (d,  $J = 11.6$  Hz, 18H,  $\text{C}(\text{CH}_3)_3$ ).  $^{31}\text{P}$ -NMR $\{^1\text{H}\}$  (121 MHz, benzene- $\text{d}_6$ ):  $\delta$  66.8 (dd,  $J = 280$  and 8 Hz, P-Cl), 15.4 (dd,  $J = 283$  and 4.5 Hz,  $\text{P}^t\text{Bu}_2$ )

#### Synthesis of ( $^t\text{BuPP}^t\text{P}$ ) Ligand (5-14)

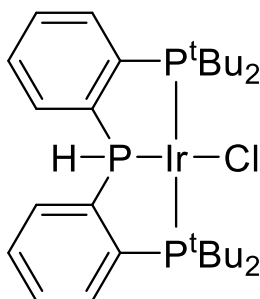


Two solutions were prepared, the first being  $\text{LiAlH}_4$  (0.060 g, 1.58 mmol) dissolved in diethyl ether (10 mL) and the other being the ( $^i\text{PrPP}^{\text{Cl}}\text{P}$ ) ligand (0.250 g, 0.49 mmol) dissolved in diethyl ether (10 mL). The ligand solution did not fully dissolve leaving a sort

of suspension. The solution with  $\text{LiAlH}_4$  was then cooled to  $-30^\circ\text{C}$  and the ligand solution was cannula transferred into the cooled down flask (some smoking in the flask was observed). To ensure full transfer of ligand to reducing agent, 10 mL of ether was put in the ligand flask and transferred to the cooled down flask. The combined solution was then warmed to room temperature and stirred for 6 hours. The solution was then filtered through silica (slowly as the  $\text{LiAlH}_4$  reacts exothermically with silica) resulting in a pale yellowish oil. NMR revealed the expected product with two side products from P-C cleavage. Side products are approximately 30% of the yield.

$^1\text{H}$ -NMR (400 MHz, benzene- $\text{d}_6$ ): Due to mixture of products could not determine proton NMR  $^{31}\text{P}$ -NMR $\{^1\text{H}\}$  (121 MHz, benzene- $\text{d}_6$ ): **Desired product**  $\delta$  21.4 (d,  $J = 154.4$ ,  $\text{P}^t\text{Bu}_2$ ), -47.1 (d,  $J = 154.0$ , HP-diaryl). **di-tert-butyl(2-phosphanylphenyl)phosphane**  $\delta$  24.5 (d,  $J = 147.4$ ,  $\text{P}^t\text{Bu}_2$ ), -115.2 (d,  $J = 146.9$ ,  $\text{PH}_2$ ). **di-tert-butyl(phenyl)phosphane**  $\delta$  38.8 (s,  $\text{P}^t\text{Bu}_2$ ).

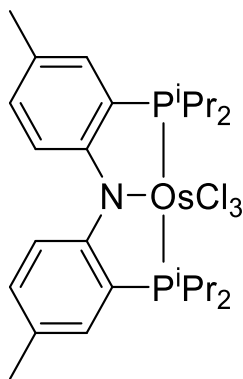
#### Synthesis of ( $^t\text{BuPP}^{\text{H}}\text{P}$ )IrCl Ligand (5-15)



( $^t\text{BuPP}^{\text{H}}\text{P}$ ) ligand mixture (0.012 g, 0.025 mmol) was dissolved in benzene  $\text{d}_6$  (0.5 mL). To this  $[\text{Ir}(\text{COE})_2\text{Cl}]_2$  (0.012 g, 0.017 mol) was added to the J. Young tube resulting in the solution to turn ruby red. The solution was then allowed to stir for 30 min.

$^1\text{H-NMR}$  (400 MHz, benzene- $\text{d}_6$ ): Due to mixture of products could not determine proton  
 $\text{NMR } ^{31}\text{P-NMR}\{^1\text{H}\}$  (121 MHz, benzene- $\text{d}_6$ ):  $\delta$  26.3 (t,  $J = 12.7$ , P-H), 76.6 (d,  $J = 12.8$ ,  
 $\text{P}^t\text{Bu}_2$ )

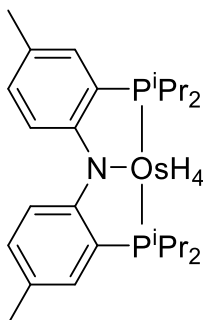
#### Synthesis of Ozerov-( $i^{\text{Pr}}$ PNP) $\text{OsCl}_3$ (5-16)



( $i^{\text{Pr}}$ PNP) ligand (0.050 g, 0.117 mmol) and osmium trichloride hydrate (0.041 g, 0.117 mmol) were dissolved in dried 2-methoxyethanol (3 mL) forming a brown colored suspension. The solution was heated to  $105^\circ\text{C}$  for 4 hours upon which the solution turned dark forest green. The solution was cooled to room temperature and the solvent was removed leaving a dark green solid. Yield 0.080 g (94.7%).

$^1\text{H-NMR}$  (400 MHz,  $\text{CD}_2\text{Cl}_2$ ):  $\delta$  8.42 (dt,  $J = 2.8, 2.8$ , 2H aryl-H), 8.18 (dd,  $J = 8.4, 1.7$  Hz, 2H, aryl-H), 5.40 (d,  $J = 8.5$ , 2H aryl-H), 5.40 (m, 2H aryl-H), 2.20 (dt,  $J = 7.1, 7.1$  Hz, 36H, tert-butyl), 2.03 (dt,  $J = 7.4, 7.4$  Hz, 36H, tert-butyl), 1.99 (dt,  $J = 7.1, 7.1$  Hz, 36H, tert-butyl), 1.58 (dt,  $J = 7.7, 7.7$  Hz, 36H, tert-butyl).  $^{31}\text{P-NMR}\{^1\text{H}\}$  (121 MHz, toluene- $\text{d}_8$ ):  $\delta$  -121.5 (s,  $\text{P}^t\text{Bu}_2$ )

### Synthesis of Ozerov-(<sup>i</sup>PrPNP)OsH<sub>4</sub> (5-17)



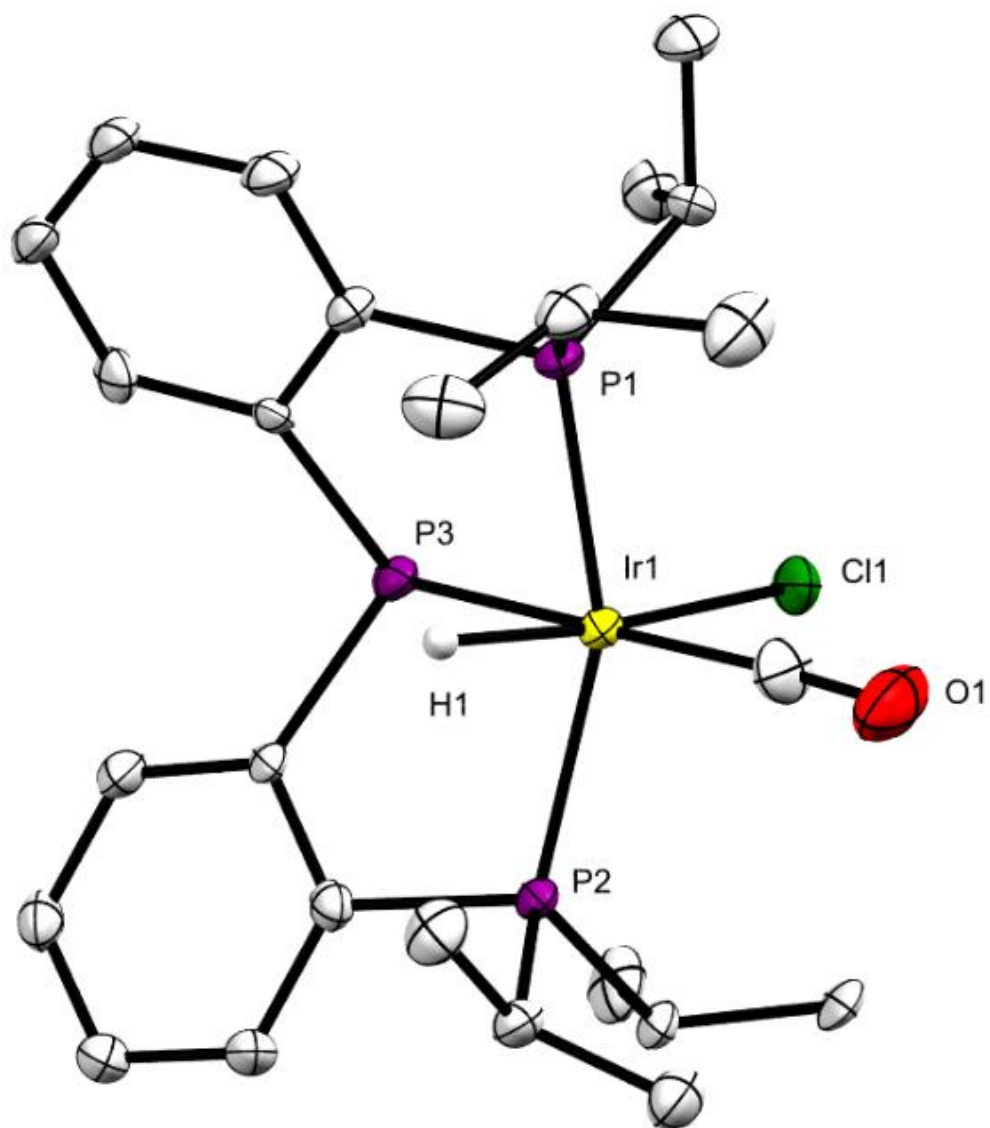
(<sup>i</sup>PrPNP)OsCl<sub>3</sub> (0.0072 g, 0.0099 mmol) was dissolved in 0.5 mL of THF (green solution).

The solution was bubbled with H<sub>2</sub> for 10 min and then left under a H<sub>2</sub> flow. The solution was then treated with 4 eq. of sodium triethylborohydride which caused the color of the solution to turn yellow with some green precipitate still visible upon complete addition of reducing agent. The solution was allowed to stir overnight under a H<sub>2</sub> atmosphere. The solution was now yellow with crystalline salt visible. Upon removal of solvent the color of the sample changed from yellow to brown.

<sup>1</sup>H-NMR (400 MHz, toluene-d<sub>8</sub>): Unable to obtain proton NMR as the compound decomposed upon removal of the reaction solvent and upon filtering through celite. <sup>31</sup>P-NMR{<sup>1</sup>H} (121 MHz, toluene-d<sub>8</sub>): δ 57.6 (s, P<sup>t</sup>Bu<sub>2</sub>)

### 5.5.3 Single crystal X-Ray diffraction data.

Figure 5.40: Structural data for complex (*i*<sup>Pr</sup>PPP)IrHCl(CO) (**5-11**)



ORTEP representation (50% probability ellipsoids) of complex (*i*<sup>Pr</sup>PPP)IrHCl(CO) (**5-11**) determined by X-ray diffraction. H atoms other than hydrides omitted.

Table 5.3. Crystal data and structure refinement for (*i*PrPPP)IrHCl(CO)

Identification code	irppp_P21_c	
Empirical formula	C <sub>25</sub> H <sub>37</sub> Cl Ir O P <sub>3</sub>	
Formula weight	674.10	
Temperature	120(2) K	
Wavelength	0.71073 Å	
Crystal system	Monoclinic	
Space group	P2 <sub>1</sub>	
Unit cell dimensions	a = 8.310(2) Å	a = 90.000(8)°.
	b = 14.492(3) Å	b = 105.949(8)°.
	c = 11.410(3) Å	g = 90.000(9)°.
Volume	1321.2(6) Å <sup>3</sup>	
Z	2	
Density (calculated)	1.695 Mg/m <sup>3</sup>	
Absorption coefficient	5.352 mm <sup>-1</sup>	
F(000)	668	
Crystal size	0.440 x 0.180 x 0.090 mm <sup>3</sup>	
Theta range for data collection	1.856 to 26.369°.	
Index ranges	-10 ≤ h ≤ 10, -18 ≤ k ≤ 18, -14 ≤ l ≤ 14	
Reflections collected	12185	
Independent reflections	5400 [R(int) = 0.0380]	
Completeness to theta = 25.242°	100.0 %	
Absorption correction	Semi-empirical from equivalents	
Max. and min. transmission	0.7463 and 0.3464	
Refinement method	Full-matrix least-squares on F <sup>2</sup>	
Data / restraints / parameters	5400 / 463 / 291	
Goodness-of-fit on F <sup>2</sup>	1.017	
Final R indices [I > 2σ(I)]	R1 = 0.0420, wR2 = 0.1037	
R indices (all data)	R1 = 0.0448, wR2 = 0.1055	
Absolute structure parameter	-0.029(11)	
Extinction coefficient	n/a	
Largest diff. peak and hole	3.152 and -2.185 e.Å <sup>-3</sup>	

Table 5.4 Bond lengths [ $\text{\AA}$ ] and angles [ $^\circ$ ] for  $(i\text{PrPPP})\text{IrHCl}(\text{CO})$ 

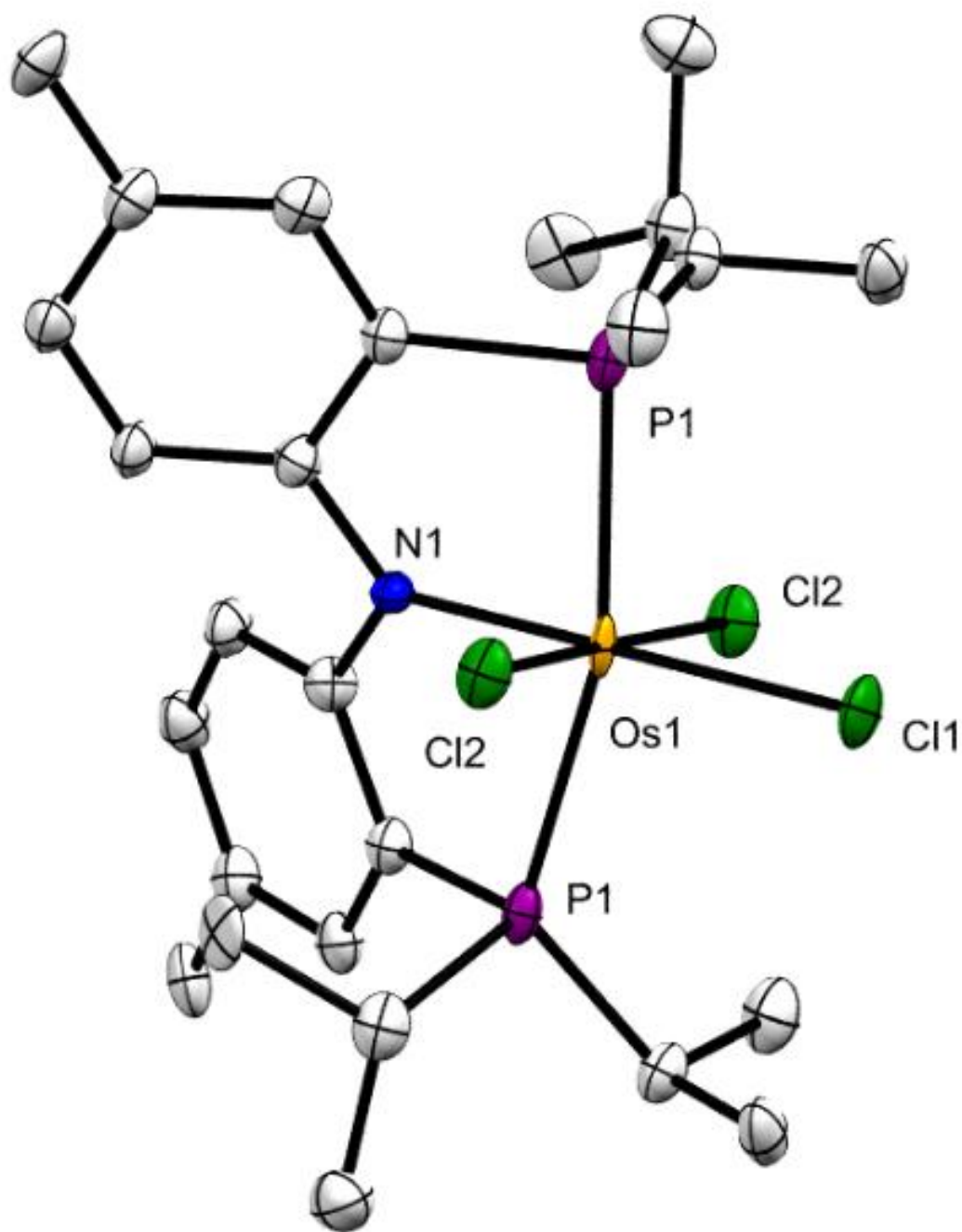
Ir(1)-C(25)	1.956(13)	C(11)-H(11)	0.9500
Ir(1)-P(2)	2.323(3)	C(13)-C(14)	1.517(15)
Ir(1)-P(1)	2.327(3)	C(13)-C(15)	1.539(17)
Ir(1)-P(3)	2.376(3)	C(13)-H(13)	1.0000
Ir(1)-Cl(1)	2.503(3)	C(14)-H(14A)	0.9800
Ir(1)-H(1)	1.599(15)	C(14)-H(14B)	0.9800
P(1)-C(2)	1.842(11)	C(14)-H(14C)	0.9800
P(1)-C(16)	1.850(12)	C(15)-H(15A)	0.9800
P(1)-C(13)	1.859(11)	C(15)-H(15B)	0.9800
P(2)-C(12)	1.844(11)	C(15)-H(15C)	0.9800
P(2)-C(19)	1.853(11)	C(16)-C(18)	1.527(18)
P(2)-C(22)	1.867(12)	C(16)-C(17)	1.529(18)
P(3)-C(1)	1.847(10)	C(16)-H(16)	1.0000
P(3)-C(7)	1.853(10)	C(17)-H(17A)	0.9800
O(1)-C(25)	1.103(16)	C(17)-H(17B)	0.9800
C(1)-C(6)	1.405(15)	C(17)-H(17C)	0.9800
C(1)-C(2)	1.421(15)	C(18)-H(18A)	0.9800
C(2)-C(3)	1.398(15)	C(18)-H(18B)	0.9800
C(3)-C(4)	1.385(17)	C(18)-H(18C)	0.9800
C(3)-H(3)	0.9500	C(19)-C(20)	1.536(15)
C(4)-C(5)	1.387(18)	C(19)-C(21)	1.546(18)
C(4)-H(4)	0.9500	C(19)-H(19)	1.0000
C(5)-C(6)	1.409(15)	C(20)-H(20A)	0.9800
C(5)-H(5)	0.9500	C(20)-H(20B)	0.9800
C(6)-H(6)	0.9500	C(20)-H(20C)	0.9800
C(7)-C(8)	1.409(16)	C(21)-H(21A)	0.9800
C(7)-C(12)	1.410(16)	C(21)-H(21B)	0.9800
C(8)-C(9)	1.394(17)	C(21)-H(21C)	0.9800
C(8)-H(8)	0.9500	C(22)-C(23)	1.530(16)
C(9)-C(10)	1.371(17)	C(22)-C(24)	1.530(16)
C(9)-H(9)	0.9500	C(22)-H(22)	1.0000
C(10)-C(11)	1.389(17)	C(23)-H(23A)	0.9800
C(10)-H(10)	0.9500	C(23)-H(23B)	0.9800
C(11)-C(12)	1.397(15)	C(23)-H(23C)	0.9800

C(24)-H(24A)	0.9800	C(2)-C(1)-P(3)	117.5(8)
C(24)-H(24B)	0.9800	C(3)-C(2)-C(1)	120.7(10)
C(24)-H(24C)	0.9800	C(3)-C(2)-P(1)	121.7(9)
		C(1)-C(2)-P(1)	117.6(8)
C(25)-Ir(1)-P(2)	94.7(4)	C(4)-C(3)-C(2)	120.5(11)
C(25)-Ir(1)-P(1)	98.2(4)	C(4)-C(3)-H(3)	119.7
P(2)-Ir(1)-P(1)	157.38(10)	C(2)-C(3)-H(3)	119.7
C(25)-Ir(1)-P(3)	175.2(5)	C(3)-C(4)-C(5)	120.1(11)
P(2)-Ir(1)-P(3)	85.08(10)	C(3)-C(4)-H(4)	119.9
P(1)-Ir(1)-P(3)	83.56(10)	C(5)-C(4)-H(4)	119.9
C(25)-Ir(1)-Cl(1)	89.2(5)	C(4)-C(5)-C(6)	120.0(10)
P(2)-Ir(1)-Cl(1)	100.62(10)	C(4)-C(5)-H(5)	120.0
P(1)-Ir(1)-Cl(1)	98.06(10)	C(6)-C(5)-H(5)	120.0
P(3)-Ir(1)-Cl(1)	86.12(10)	C(1)-C(6)-C(5)	121.0(10)
C(25)-Ir(1)-H(1)	106.9(7)	C(1)-C(6)-H(6)	119.5
P(2)-Ir(1)-H(1)	79.3(3)	C(5)-C(6)-H(6)	119.5
P(1)-Ir(1)-H(1)	79.2(3)	C(8)-C(7)-C(12)	117.6(9)
P(3)-Ir(1)-H(1)	77.7(5)	C(8)-C(7)-P(3)	122.4(8)
Cl(1)-Ir(1)-H(1)	163.8(6)	C(12)-C(7)-P(3)	118.9(8)
C(2)-P(1)-C(16)	104.6(5)	C(9)-C(8)-C(7)	120.7(11)
C(2)-P(1)-C(13)	106.7(5)	C(9)-C(8)-H(8)	119.6
C(16)-P(1)-C(13)	104.9(5)	C(7)-C(8)-H(8)	119.6
C(2)-P(1)-Ir(1)	106.6(4)	C(10)-C(9)-C(8)	120.7(11)
C(16)-P(1)-Ir(1)	115.3(4)	C(10)-C(9)-H(9)	119.6
C(13)-P(1)-Ir(1)	117.8(4)	C(8)-C(9)-H(9)	119.6
C(12)-P(2)-C(19)	104.0(5)	C(9)-C(10)-C(11)	120.1(11)
C(12)-P(2)-C(22)	103.0(5)	C(9)-C(10)-H(10)	120.0
C(19)-P(2)-C(22)	104.7(5)	C(11)-C(10)-H(10)	120.0
C(12)-P(2)-Ir(1)	106.9(4)	C(10)-C(11)-C(12)	120.0(10)
C(19)-P(2)-Ir(1)	120.1(4)	C(10)-C(11)-H(11)	120.0
C(22)-P(2)-Ir(1)	116.3(4)	C(12)-C(11)-H(11)	120.0
C(1)-P(3)-C(7)	106.1(5)	C(11)-C(12)-C(7)	120.8(10)
C(1)-P(3)-Ir(1)	104.3(4)	C(11)-C(12)-P(2)	120.5(8)
C(7)-P(3)-Ir(1)	104.7(4)	C(7)-C(12)-P(2)	118.1(8)
C(6)-C(1)-C(2)	117.6(9)	C(14)-C(13)-C(15)	110.0(10)
C(6)-C(1)-P(3)	124.2(8)	C(14)-C(13)-P(1)	115.2(9)



C(15)-C(13)-P(1)	109.7(7)	C(21)-C(19)-P(2)	110.7(8)
C(14)-C(13)-H(13)	107.2	C(20)-C(19)-H(19)	108.1
C(15)-C(13)-H(13)	107.2	C(21)-C(19)-H(19)	108.1
P(1)-C(13)-H(13)	107.2	P(2)-C(19)-H(19)	108.1
C(13)-C(14)-H(14A)	109.5	C(19)-C(20)-H(20A)	109.5
C(13)-C(14)-H(14B)	109.5	C(19)-C(20)-H(20B)	109.5
H(14A)-C(14)-H(14B)	109.5	H(20A)-C(20)-H(20B)	109.5
C(13)-C(14)-H(14C)	109.5	C(19)-C(20)-H(20C)	109.5
H(14A)-C(14)-H(14C)	109.5	H(20A)-C(20)-H(20C)	109.5
H(14B)-C(14)-H(14C)	109.5	H(20B)-C(20)-H(20C)	109.5
C(13)-C(15)-H(15A)	109.5	C(19)-C(21)-H(21A)	109.5
C(13)-C(15)-H(15B)	109.5	C(19)-C(21)-H(21B)	109.5
H(15A)-C(15)-H(15B)	109.5	H(21A)-C(21)-H(21B)	109.5
C(13)-C(15)-H(15C)	109.5	C(19)-C(21)-H(21C)	109.5
H(15A)-C(15)-H(15C)	109.5	H(21A)-C(21)-H(21C)	109.5
H(15B)-C(15)-H(15C)	109.5	H(21B)-C(21)-H(21C)	109.5
C(18)-C(16)-C(17)	112.3(11)	C(23)-C(22)-C(24)	109.6(10)
C(18)-C(16)-P(1)	112.6(8)	C(23)-C(22)-P(2)	114.9(8)
C(17)-C(16)-P(1)	111.8(9)	C(24)-C(22)-P(2)	112.9(8)
C(18)-C(16)-H(16)	106.5	C(23)-C(22)-H(22)	106.3
C(17)-C(16)-H(16)	106.5	C(24)-C(22)-H(22)	106.3
P(1)-C(16)-H(16)	106.5	P(2)-C(22)-H(22)	106.3
C(16)-C(17)-H(17A)	109.5	C(22)-C(23)-H(23A)	109.5
C(16)-C(17)-H(17B)	109.5	C(22)-C(23)-H(23B)	109.5
H(17A)-C(17)-H(17B)	109.5	H(23A)-C(23)-H(23B)	109.5
C(16)-C(17)-H(17C)	109.5	C(22)-C(23)-H(23C)	109.5
H(17A)-C(17)-H(17C)	109.5	H(23A)-C(23)-H(23C)	109.5
H(17B)-C(17)-H(17C)	109.5	H(23B)-C(23)-H(23C)	109.5
C(16)-C(18)-H(18A)	109.5	C(22)-C(24)-H(24A)	109.5
C(16)-C(18)-H(18B)	109.5	C(22)-C(24)-H(24B)	109.5
H(18A)-C(18)-H(18B)	109.5	H(24A)-C(24)-H(24B)	109.5
C(16)-C(18)-H(18C)	109.5	C(22)-C(24)-H(24C)	109.5
H(18A)-C(18)-H(18C)	109.5	H(24A)-C(24)-H(24C)	109.5
H(18B)-C(18)-H(18C)	109.5	H(24B)-C(24)-H(24C)	109.5
C(20)-C(19)-C(21)	109.2(10)	O(1)-C(25)-Ir(1)	173.9(14)
C(20)-C(19)-P(2)	112.6(8)		

Figure 5.41: Structural data for complex Ozerov-(*i*<sup>Pr</sup>PNP)OsCl<sub>3</sub> (5-13)



ORTEP representation (50% probability ellipsoids) of complex (*i*<sup>Pr</sup>PNP)OsCl<sub>3</sub> (**5-11**) determined by X-ray diffraction. H atoms other than hydrides omitted.

Table 5.5. Crystal data and structure refinement for (*i*PrPNP)OsCl<sub>3</sub>

Identification code	OsPPNCl3_P2n_a	
Empirical formula	C26 H40 Cl3 N Os P2	
Formula weight	725.08	
Temperature	120(2) K	
Wavelength	0.71073 Å	
Crystal system	Monoclinic	
Space group	P2/n	
Unit cell dimensions	a = 11.177(3) Å	a = 90°.
	b = 9.549(3) Å	b = 100.516(9)°.
	c = 13.078(4) Å	g = 90°.
Volume	1372.4(7) Å <sup>3</sup>	
Z	2	
Density (calculated)	1.755 Mg/m <sup>3</sup>	
Absorption coefficient	5.071 mm <sup>-1</sup>	
F(000)	720	
Crystal size	? x ? x ? mm <sup>3</sup>	
Theta range for data collection	1.584 to 24.398°.	
Index ranges	?<=h<=?, ?<=k<=?, ?<=l<=?	
Reflections collected	2394	
Independent reflections	2249 [R(int) = ?]	
Completeness to theta = 24.398°	99.8 %	
Absorption correction	Semi-empirical from equivalents	
Max. and min. transmission	0.7454 and 0.4225	
Refinement method	Full-matrix least-squares on F <sup>2</sup>	
Data / restraints / parameters	2249 / 216 / 158	
Goodness-of-fit on F <sup>2</sup>	1.001	
Final R indices [I>2sigma(I)]	R1 = 0.0837, wR2 = 0.2093	
R indices (all data)	R1 = 0.1030, wR2 = 0.2217	
Extinction coefficient	n/a	
Largest diff. peak and hole	5.022 and -3.022 e.Å <sup>-3</sup>	

Table 5.6. Bond lengths [Å] and angles [°] for (*i*PrPNP)OsCl<sub>3</sub>

Os(1)-N(1)	1.943(16)	C(11)-C(13)	1.52(2)
Os(1)-Cl(2)#1	2.355(4)	C(11)-H(11)	1.0000
Os(1)-Cl(2)	2.355(4)	C(12)-H(12A)	0.9800
Os(1)-P(1)#1	2.375(4)	C(12)-H(12B)	0.9800
Os(1)-P(1)	2.375(4)	C(12)-H(12C)	0.9800
Os(1)-Cl(1)	2.381(5)	C(13)-H(13A)	0.9800
P(1)-C(2)	1.835(15)	C(13)-H(13B)	0.9800
P(1)-C(11)	1.850(15)	C(13)-H(13C)	0.9800
P(1)-C(8)	1.867(16)		
N(1)-C(1)	1.423(16)	N(1)-Os(1)-Cl(2)#1	91.31(9)
N(1)-C(1)#1	1.423(16)	N(1)-Os(1)-Cl(2)	91.31(9)
C(1)-C(6)	1.35(2)	Cl(2)#1-Os(1)-Cl(2)	177.38(18)
C(1)-C(2)	1.42(2)	N(1)-Os(1)-P(1)#1	81.54(9)
C(2)-C(3)	1.39(2)	Cl(2)#1-Os(1)-P(1)#1	88.07(13)
C(3)-C(4)	1.40(2)	Cl(2)-Os(1)-P(1)#1	92.32(13)
C(3)-H(3)	0.9500	N(1)-Os(1)-P(1)	81.54(9)
C(4)-C(5)	1.37(2)	Cl(2)#1-Os(1)-P(1)	92.32(13)
C(4)-C(7)	1.50(2)	Cl(2)-Os(1)-P(1)	88.07(13)
C(5)-C(6)	1.39(2)	P(1)#1-Os(1)-P(1)	163.07(18)
C(5)-H(5)	0.9500	N(1)-Os(1)-Cl(1)	180.0
C(6)-H(6)	0.9500	Cl(2)#1-Os(1)-Cl(1)	88.69(9)
C(7)-H(7A)	0.9800	Cl(2)-Os(1)-Cl(1)	88.69(9)
C(7)-H(7B)	0.9800	P(1)#1-Os(1)-Cl(1)	98.46(9)
C(7)-H(7C)	0.9800	P(1)-Os(1)-Cl(1)	98.46(9)
C(8)-C(10)	1.53(2)	C(2)-P(1)-C(11)	109.3(7)
C(8)-C(9)	1.54(2)	C(2)-P(1)-C(8)	103.9(7)
C(8)-H(8)	1.0000	C(11)-P(1)-C(8)	103.6(7)
C(9)-H(9A)	0.9800	C(2)-P(1)-Os(1)	95.1(4)
C(9)-H(9B)	0.9800	C(11)-P(1)-Os(1)	124.6(5)
C(9)-H(9C)	0.9800	C(8)-P(1)-Os(1)	117.9(5)
C(10)-H(10A)	0.9800	C(1)-N(1)-C(1)#1	119.0(16)
C(10)-H(10B)	0.9800	C(1)-N(1)-Os(1)	120.5(8)
C(10)-H(10C)	0.9800	C(1)#1-N(1)-Os(1)	120.5(8)
C(11)-C(12)	1.51(2)	C(6)-C(1)-C(2)	117.9(13)

C(6)-C(1)-N(1)	125.7(13)	C(8)-C(9)-H(9B)	109.5
C(2)-C(1)-N(1)	116.4(13)	H(9A)-C(9)-H(9B)	109.5
C(3)-C(2)-C(1)	120.2(13)	C(8)-C(9)-H(9C)	109.5
C(3)-C(2)-P(1)	125.4(11)	H(9A)-C(9)-H(9C)	109.5
C(1)-C(2)-P(1)	114.4(10)	H(9B)-C(9)-H(9C)	109.5
C(2)-C(3)-C(4)	120.7(14)	C(8)-C(10)-H(10A)	109.5
C(2)-C(3)-H(3)	119.7	C(8)-C(10)-H(10B)	109.5
C(4)-C(3)-H(3)	119.7	H(10A)-C(10)-H(10B)	109.5
C(5)-C(4)-C(3)	117.8(14)	C(8)-C(10)-H(10C)	109.5
C(5)-C(4)-C(7)	121.2(14)	H(10A)-C(10)-H(10C)	109.5
C(3)-C(4)-C(7)	121.0(14)	H(10B)-C(10)-H(10C)	109.5
C(4)-C(5)-C(6)	121.5(14)	C(12)-C(11)-C(13)	111.4(13)
C(4)-C(5)-H(5)	119.3	C(12)-C(11)-P(1)	107.8(11)
C(6)-C(5)-H(5)	119.3	C(13)-C(11)-P(1)	113.3(11)
C(1)-C(6)-C(5)	121.9(14)	C(12)-C(11)-H(11)	108.1
C(1)-C(6)-H(6)	119.0	C(13)-C(11)-H(11)	108.1
C(5)-C(6)-H(6)	119.0	P(1)-C(11)-H(11)	108.1
C(4)-C(7)-H(7A)	109.5	C(11)-C(12)-H(12A)	109.5
C(4)-C(7)-H(7B)	109.5	C(11)-C(12)-H(12B)	109.5
H(7A)-C(7)-H(7B)	109.5	H(12A)-C(12)-H(12B)	109.5
C(4)-C(7)-H(7C)	109.5	C(11)-C(12)-H(12C)	109.5
H(7A)-C(7)-H(7C)	109.5	H(12A)-C(12)-H(12C)	109.5
H(7B)-C(7)-H(7C)	109.5	H(12B)-C(12)-H(12C)	109.5
C(10)-C(8)-C(9)	109.3(13)	C(11)-C(13)-H(13A)	109.5
C(10)-C(8)-P(1)	111.3(11)	C(11)-C(13)-H(13B)	109.5
C(9)-C(8)-P(1)	114.3(11)	H(13A)-C(13)-H(13B)	109.5
C(10)-C(8)-H(8)	107.2	C(11)-C(13)-H(13C)	109.5
C(9)-C(8)-H(8)	107.2	H(13A)-C(13)-H(13C)	109.5
P(1)-C(8)-H(8)	107.2	H(13B)-C(13)-H(13C)	109.5
C(8)-C(9)-H(9A)	109.5		

---

Symmetry transformations used to generate equivalent atoms:

#1 -x-1/2,y,-z-1/2

## 5.6 References:

1. Moulton, C. J.; Shaw, B. L. *J. Chem. Soc., Dalton Trans.* **1976**, 1020.
2. Weckhuysen, B. M.; Schoonheydt, R. A. *Catal. Today* **1999**, *51*, 223.
3. O'Connor, R. P.; Klein, E. J.; Henning, D.; Schmidt, L. D. *Appl. Catal., A* **2003**, *238*, 29.
4. Olsbye, U.; Virnovskaia, A.; Prytz, O.; Tinnemans, S. J.; Weckhuysen, B. M. *Catal. Lett.* **2005**, *103*, 143.
5. Adlhart, C.; Uggerud, E. *Chem.—Eur. J.* **2007**, *13*, 6883.
6. Jackson, S. D.; Stair, P. C.; Gladden, L. F.; McGregor, J. *Met. Oxide Catal.* **2009**, *2*, 595.
7. Baudry, D.; Ephritikhine, M.; Felkin, H.; Holmes-Smith, R. *J. Chem. Soc., Chem. Commun.* **1983**, 788.
8. Felkin, H.; Fillebeen-Khan, T.; Gault, Y.; Holmes-Smith, R.; Zakrzewski, J. *Tetrahedron Lett.* **1984**, *25*, 1279.
9. Felkin, H.; Fillebeen-Khan, T.; Holmes-Smith, R.; Lin, Y. *Tetrahedron Lett.* **1985**, *26*, 1999.
10. Burk, M. J.; Crabtree, R. H.; Parnell, C. P.; Uriarte, R. J. *Organometallics* **1984**, *3*, 816.
11. Burk, M. J.; Crabtree, R. H.; McGrath, D. V. *J. Chem. Soc., Chem. Commun.* **1985**, 1829.
12. Burk, M. J.; Crabtree, R. H. *J. Am. Chem. Soc.* **1987**, *109*, 8025.
13. (a) Kumar, A.; Goldman, A. S. In *The Privileged Pincer-Metal Platform: Coordination Chemistry & Applications*; van Koten, G., Gossage, R. A., Eds.; Springer International Publishing: Cham, 2016, p 307-334. (b) Choi, J.; MacArthur, A. H. R.; Brookhart, M.; Goldman, A. S. *Chem. Rev.* **2011**, *111*, 1761-1779.
14. Gupta, M.; Hagen, C.; Flesher, R. J.; Kaska, W. C.; Jensen, C. M. *Chem. Commun.* **1996**, 2083.
15. Liu, F.; Goldman, A. S. *Chem. Commun.* **1999**, 655.
16. Haenel, M. W.; Oevers, S.; Angermund, K.; Kaska, W. C.; HuaJun, Fan; Hall, M. B. *Angew. Chem., Int. Ed.* **2001**, *40*, 3596.
17. Punji, B.; Emge, T. J.; Goldman, A. S. *Organometallics* **2010**, *29*, 2702.
18. (a) G€ottker-Schnetmann, I.; White, P.; Brookhart, M. *J. Am. Chem. Soc.* **2004**, *126*, 1804. (b) G€ottker-Schnetmann, I.; Brookhart, M. *J. Am. Chem. Soc.* **2004**, *126*, 9330.
19. Morales-Morales, D.; Redon, R.; Yung, C.; Jensen, C.M. *Inorganica Chimica Acta.* **2004**, *357*, 2953
20. Gorgas, N.; Alves, L.G.; Stoeger, B.; Martins, A.M.; Veiros, L.F.; Kirchner, K. *J. Am. Chem. Soc.* **2017**, *139*, 8130.
21. Mankad, N.P.; Rivard, E.; Harkins, S.B.; Peters, J.C. *J. Am. Chem. Soc.*, **2005**, *127*, 16032.
22. a) Choualeb, A.; Lough, A.J.; Gusev, D.G. *Organometallics* **2007**, *26*, 5524; b) Bi, S.; Xie, Q.; Zhao, X.; Zhao, Y.; Kong, X. *Organomet. Chem.* **2008**, *693*, 633.
23. Friedrich, A.; Drees, M.; Kaess, M.; Herdtweck, E.; Schneider, S. *Inorg. Chem.* **2010**, *49*, 5482.
24. Gregor, L.C.; Chen, C.H.; Fafard, C.M.; Fan, L.; Guo, C.; Foxman, B.M.; Gusev, D.G.; Ozerov, O.V. *Dalton Trans.* **2010**, *39*, 3195

25. Hermann, D.; Gandelman, M.; Rozenberg, H.; Shimon, L. J. W.; Milstein, D. *Organometallics* **2002**, *21*, 812-818.
26. Khaskin, E.; Iron, M.A.; Shimon, L.J.W.; Zhang, J.; Milstein, D. *J. Am. Chem. Soc.* **2010**, *132*, 8542.
27. Feller, M.; Gellrich, U.; Anaby, A.; Diskin-Posner, Y.; Milstein, D. *J. Am. Chem. Soc.* **2016**, *138*, 6445-6454
28. Blessent, M. PhD. Dissertation, Rutgers University, 2016.
29. Biswas, S.; Brookhart, M.; Choliy, Y.; Goldman, A.; Huang, Z.; Krogh-Jespersen, K. Abstracts of Papers, 239th ACS National Meeting, San Francisco, CA, March 21-25, 2010; American Chemical Society: Washington, DC, 2010; INOR-674.
30. Liu, F.; Pak, E. B.; Singh, B.; Jensen, C. M.; Goldman, A. S. *J. Am. Chem. Soc.* 1999, *121*, 4086.
31. Pahls, D.R.; Allen, K.E.; Goldberg, K.I.; Cundari, T.R. *Organometallics* **2014**, *33*, 6413.
32. Choi, J.; MacArthur, A. H. R.; Brookhart, M.; Goldman, A. S. *Chem. Rev.* **2011**, *111*, 1761-1779.
33. Hantzsch, A. (1881). "Condensationprodukte aus Aldehydammoniak und Ketonartigen Verbindungen". *Chemische Berichte* **14** (2): 1637-8
34. Fang, H.; Choe, Y-K.; Li, Y.; Shimada, S. *Chem. Asian J.* **2011**, *6*, 2512.